Sixth International Conference on Geosynthetics

Conference Proceedings

25–29 March 1998
Atlanta, Georgia USA

Soil Reinforcement Applications
Geotechnical & Hydraulic Applications

Cooperating Organizations

GeoInstitute of ASCE (American Society of Civil Engineers)
Canadian Geotechnical Society
International Association of Geosynthetics Installers
EDANA (European Association for the Nonwovens Industry)
Geosynthetic Institute

Organized under the auspices of the International Geosynthetics Society Sponsored by the Industrial Fabrics Association International and the North American Geosynthetics Society

Table of Contents: Volume 2

Table of Contents: Volume 2

Table of Contents: Volume 2

Table of Contents: Volume 2

Deformations and Damage of Non-Woven Geotextiles in Road Construction

A. Watn
Senior Scientist, SINTEF Civil and Environmental Engineering, Norway

G. Eiksund
Research Scientist, SINTEF Civil and Environmental Engineering, Norway

Å. Knutson
Head of Division, Norwegian Public Road Administration, Road Research Laboratory, Norway

ABSTRACT: SINTEF Civil and Environmental Engineering have performed a research project in two phases on non-woven geotextiles in road constructions. The first phase was a large-scale laboratory test aimed to study the effect of non-woven geotextiles on road deformations at cyclic loading. The second phase was a field test aimed to study the resistance against damage of the geotextiles during construction. The project focused on the correspondence between properties from index tests and the observed behaviour. A clear correspondence was found between the initial tension stiffness of a geotextile and the deformation after cyclic loading. Low correlation was found between observed damage during construction and the evaluation criteria used for classification of geotextiles in Norway. To take into account these findings it is recommended a revision of the evaluation criteria. It is also proposed a survivability criterion based on a combination of deformation energy and stress-strain properties to cover the construction and lifetime requirements.

KEYWORDS: Geotechnical Engineering, soil, geotextile, damage.

1 INTRODUCTION

The criteria for evaluating strength and deformation properties for non-woven geotextiles used in separation and filtration in roads have been discussed for more than twenty years. The first systems for evaluation and classification of geotextiles for separation and filtration in roads were introduced by the Norwegian Road Research Laboratory (NRRL), (Alfheim and Sørli, 1977). Later several systems have been introduced but generally the classification requirements are mainly empirically based, and to some extent dependent on local conditions and experiences (Forschungsgesellscaft für straßen- und Verkehrswesen, 1994, Rathmayer, 1993, AASHTO, 1990). The evaluation criteria and the index test methods which are used, differ between the systems and a possible co-ordination between the systems have been discussed since their introduction.

1.1 The Norwegian classification system

Geotextiles for separation and filtration in roads are in Norway divided into four classes dependent on the type of material (maximum grain size) to be used against the geotextile:

Class 1: Generally not used
Class 2: Sand and gravel with max. diameter 50 mm
Class 3: Crushed stone with max. diameter 100 mm
Class 4: Blasted rock with max. diameter 2/3 of the layer thickness

The classification is based on an evaluation of results from the static puncture tests and the cone drop tests. The tested product will achieve points from the results in the tests referring to each criterion and the classification is then dependent on the total sum of points. For the static puncture test (CBR- test, ISO 12236:1996) the measured force and deformation are used to calculate a corresponding tension (force/mm) and strain (%). The classification criterion is based on the derived tension and strain, the maximum tension, the elongation strain at failure and the tension increase from 20 % to 70% strain (or until strain at failure if less than 70%). The average hole diameter is used as evaluation criterion for the cone drop test (Schalin 1995).

1.2 Relevant properties and test methods

There is a clear need for establishing a more fundamental understanding of the required characteristics of the geotextile to fulfil its functions (separation and filtration) in the road. The required properties must reflect the environmental loads imposed on the geotextile during the installation, construction and service lifetime. A theoretical sound correlation between the required properties and the corresponding required parameters found from index tests should be established. A combination of index tests, large scale performance tests, full scale field tests and collection of experiences from the field is believed to be the best way to establish such a correlation.

2 RESEARCH PROJECT

SINTEF Civil and Environmental Engineering have performed a research project on non-woven geotextiles in road constructions. The NRRL and has participated with observers and supervisors in the project. The project focused on the correspondence between geotextile properties found in index tests and the observed behaviour in laboratory and the field. The first project phase (SINTEF 1996) included index tests and large scale laboratory load test. This part aimed to study the effect of stress-strain properties on non-woven geotextiles on road deformations at cyclic loading. The second phase was a field test (SINTEF 1997) aiming to study the resistance against damage of the geotextiles during the construction. Non woven geotextiles with different production technology and area weight were used in the research projects.

2.1 Laboratory tests

2.1.1 Index tests

The index tests included cone drop tests, static puncture tests and wide width tensile tests. The tests were performed on virgin samples and on samples extracted after the load test. In addition the effect of thermal cycling and stress strain behaviour under frozen conditions were tested. Six different non-woven geotextiles were tested, three corresponding to class 2 and three corresponding to class 3. The geotextiles used in the laboratory tests corresponding to class 3 are listed in Table 1.

Table 1. Class 3 geotextiles used in the laboratory test.

Reference	Type of product	Nominal area weight (g/m^2)
SNP 3A	Staple fibre, needle punched, polypropylene	190
CNP 3B	Continuous filament, needle punched, polypropylene	160
CTP 3C	Continuous filament, thermally bonded, polypropylene	190

A summary of the results from the static puncture tests and the falling cone test on virgin samples for class 3 products is presented in Table 2.

Typical load displacement curves from the static puncture test are shown in Figure 2. Observe the differences in initial stiffness between the different geotextiles.

The thermal cycling had no significant effect on the results from the index test measurements.

Table 2 Results from initial index testing of the geotextiles.

Ref	Weight	Static Puncture test		Falling cone
	g/mm^2	Max force, N	Displ.at max. force , mm	Average hole diameter, mm
SNP 3A	197.8	2380	57	14
CNP 3B	171.5	2252	44	24.2
CTP 3C	190.8	1970	50.8	19.1

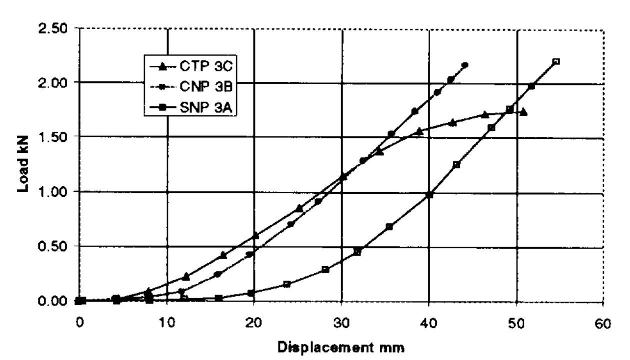

Figure 1. Typical load displacement curves for the class 3 geotextiles.

2.1.2 Large scale load test

The large scale laboratory testing was performed in a 12.5 m long and 1.8 m wide test bin filled with a 650 mm thick layer of soft clay with 2-3 kPa undrained shear strength. The geotextiles was placed on the clay and covered with 150 mm of crushed stone as shown in Figure 2. The geotextile test samples were 2 x 1.8 m. Cyclic and static load was then applied on a circular plate with diameter 250 mm on the bearing layer. The geotextiles used in the large scale laboratory test are listed in Table 1.

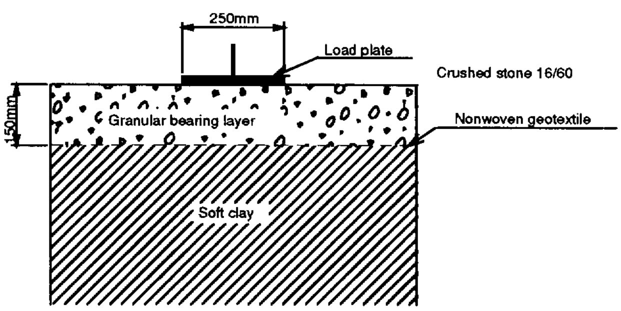

Figure 2. Bearing layer construction.

A cyclic load with frequency 1 Hz and amplitude 0-4 kN was applied on the load plate. A load of 4 kN corresponds to an average applied stress under the load plate of 81.5 kN/m^2. The gradually developing displacement on the geotextile beneath the load plate was measured during the test, the resulting deformation profiles after 1000 cycles are presented in Figure 3.

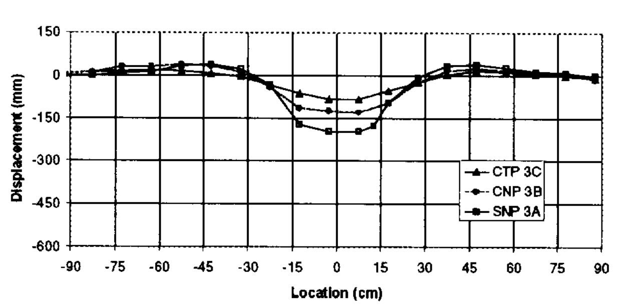

Figure 3. Measured vertical displacement profile of the geotextiles after completed load test.

2.1.3 Evaluation of results

There are considerable differences in the measured deformations and strains in the geotextile in the load test. The observed deformations correspond well with the load displacement relations, Figure 2, measured in the static puncture test. The average strain of the geotextiles was measured to be 10.3%, 4.6% and 1.4% for SNP 3A, CNP 3B and CTP 3C, respectively. Converted to displacement in the static puncture test these strains correspond 19 mm, 12 mm, and 7 mm displacement. Figure 4 shows that the load corresponding to the strain levels is approximately 0.08 kN for all the three geotextiles. In the same figure, the area under the load displacement curve, named as the deformation energy, is shaded. Note that the deformation energy based on these results is about the same for all the tested geotextiles, even with large differences in the strain level.

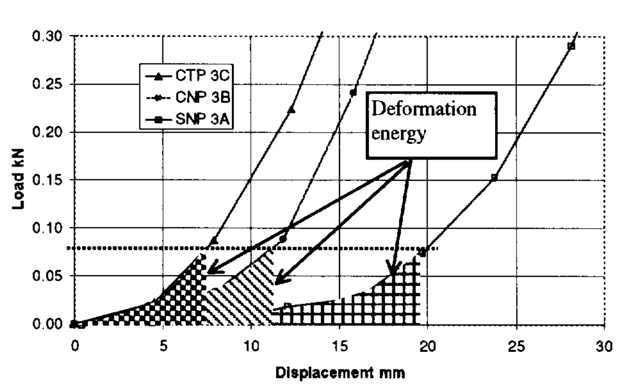

Figure 4. Force-strain relationship related to measured strain for the geotextiles in the load test

This test shows that the strain developing at a typical cyclic loading is strongly dependent of the initial stiffness. A criterion that is aimed to cover the need for remaining strength after construction should include the effect of initial stiffness.

2.2 Full scale field tests

2.2.1 Test set up

The test was performed outdoor on frozen uneven ground. The material in the ground consists of fill masses with silt, sand, clay and occasional stones. Due to rainfall just before and under the installation the upper 50-100 mm of the underground was saturated and muddy during the installation. As the temperature was decreasing during the test, this upper layer was frozen at the time of the extraction. Geotextiles used in the field test are listed in table 3.

Table 3. Geotextiles involved in the testing.

Reference	Type of product	Nominal area weight (g/m2)
CNP 4A	Continuous filament, needle punched, polypropylene	320
SNP 4B	Staple fibre, needle punched, polypropylene	330
SNP 4C	Staple fibre, needle punched, polypropylene	320
CTP 4D *)	Continuous filament, thermally bonded, polypropylene	350
SNP 4E	Staple fibre, needle punched, calendered on one side, polypropylene	300
CTP 4F **)	Continuous filament, thermally bonded, polypropylene and polyethylene	350

*) Not previously classified in class 4 in Norway
**) Tested in a separate field test

The geotextile CTP 4F was tested in a separate test together with CTP 4D that was also tested together with the other products. The results for CTP 4D are used as reference basis for comparing the results. The field test also included five geotextiles from class 2 not reported in this paper. The results from the index tests on virgin material are presented in Table 4. The load deformation relation curves from the static puncture test are shown in Figure 5.

Table 4. Results from index tests on the class 4 geotextiles.

Ref	Measured area weight g/m^2	Strength increase 20 - 70% strain N/mm	Push through tension N/mm	Push through strain %	Hole diameter mm	Number of points acc. to the Norw. classif.	Corresp applic class
CNP 4A	310.7	18.94	34.32	60.86	15.90	35	3
SNP 4B	359.0	23.20	38.28	70.78	12.10	44	4
SNP 4C	314.4	17.17	26.17	87.08	10.10	44	4
CTP 4D	353.1	10.60	33.87	70.12	13.90	41	4
SNP 4E	302.3	19.13	28.44	85.46	13.10	44	4
CTP 4F	345.9	14.3	38.9	51.4	20.9	35	3

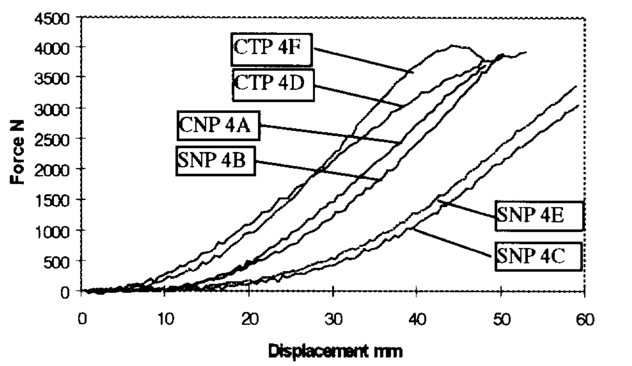

Figure 5. Measured force and displacement from the static puncture test.

The principle for the test fill is shown on Figure 6. The geotextiles were placed directly on the ground and then covered with fill material by the use of a pay loader. The covering was done sideways to ensure that each of the geotextiles was treated equally. For the class 4 material, blasted rock with a maximum diameter of 800 mm was used for the fill. The largest rock fragments were flaky shaped thus a fill height 500 mm was possible.

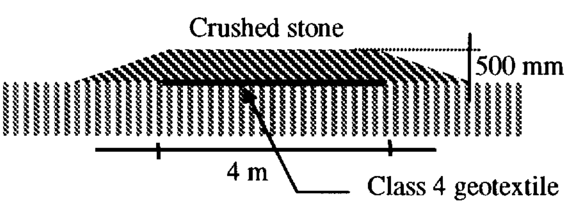

Figure 6. Principle for the test fill.

The fill material was compacted with a heavy vibrating roller with three overpasses along the centre line and on the shoulders on top of each fill. One week after the installation the fill material was removed. The top of the fill material was removed carefully with an excavator. The geotextile was then tied to the excavator and carefully lifted out.

2.2.2 Test results

The amount of damage and deformation of the geotextiles were observed during the extraction. By the visual inspection during extraction some damage in terms of holes could be seen on all the geotextiles. The degree of damage varied. The geotextiles SNP 4B and CTP 4D was less damaged than average, SNP 4C and CNP 4A average damaged while SNP 4E and CTP 4F most damaged. During the extraction it could be observed that the underground was more even under the products having a high initial stiffness compared to the others.

After extraction the samples were brought to the laboratory where the damages (number and size of holes) where counted and measured. The distribution of holes within different diameter ranges is shown in Figure 7.

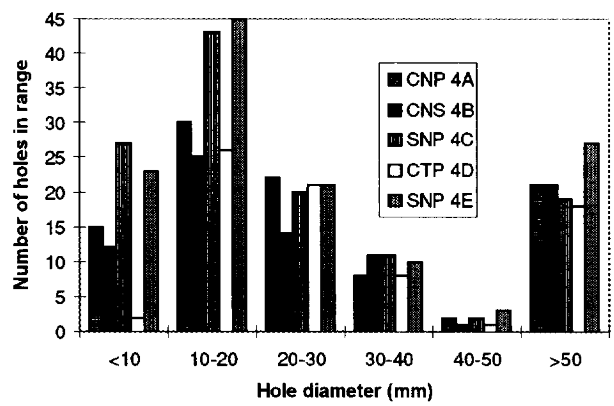

Figure 7. Distribution of holes.

2.2.3 Evaluation of results

In order to correlate the observed damage with index test results the degree of *Damage* on a geotextile is defined as the sum of the measured hole diameters. The *Resistance* *against damage* for one product can then be defined as the average damage divided by the damage on each geotextile as shown in Table 5, that is, the higher number the less damage. In the table the measured damage is normalised with respect to the average value for the five geotextiles, that is, a factor of 1.15 means 15 % less damage than the average.

Table 5. Resistance against damage.

Ref	*Damage* (Sum Of hole diameter)	*Resistance against damage* (Average damage)/ (damage)
CNP 4A	2793	1.07
SNP 4B	2613	1.15
SNP 4C	3157	0.95
CTP 4D	2655	1.13
SNP 4E	3759	0.80
CTP 4F	-	0.40*)

*) Based on a scaling of the results

As CTP 4F was tested in a separate test the results can not be compared directly with the others. The additional field test with the geotextiles CTP 4D and CTP 4F used a less heavy compaction equipment resulting in considerably less damage on CTP 4D compared with the first part of the test.

However, by using the results for CTP 4D as a reference basis a possible comparison of the degree of damage can be done. This way of scaling the degree of damage is quite uncertain since it is based on the damages on one geotextile only, but still it illustrates the much higher degree of damage found for CTP 4F compared to the other products tested.

The resistance against damage and the results from the index tests are used to evaluate the requirements in the classification system. The relevancy of an index test parameter for survivability of the geotextile is studied by correlating the parameter with the *resistance against damage* as defined above. The area weights are also included in the correlation. The results of the correlation are shown in Table 7. The test results from geotextile CTP 4F was not included in the correlation.

Table 6. Correlation between index test results and resistance against damage.

Parameter	Correlation
Weight/m^2	0.81
Strength incr. 20-70%	-0.11
Failure strength	0.84
Strain to failure	-0.77
1/(Cone drop hole diam)	-0.26
Number of points	-0.36

The parameters showing best correlation with the resistance against damage is the *push through strength* and the *area weight.* The criteria for *strength increase*, and *the number of points* shows poor correlation. The *strain to failure* and the *cone drop hole diameter* shows a fair negative correlation. The poor correlation for the number of points is remarkable. The low correlation is mainly caused by the fact that the two geotextiles with the most damage have full score based on the criteria in the index test.

The results from the index test do not point out an obvious candidate among the parameters that may explain why CTP 4F should be so severely damaged. In the primary tests the best correlation with the resistance against damage was found for the unit weight and the failure strength. This was not the case for CTP 4F that gives a high score on both unit weight and failure strength. Geotextile CTP 4F has, however, a relatively low value both for *strain to failure* and the *inverse of the cone drop hole diameter.* These low values may partly explain some of the higher degree of damage for the CTP 4F geotextile.

Both CTP 4D and CTP 4F are thermally bonded geotextiles, having a high initial stiffness. As shown in Figure 5, the force-displacement relations from the static puncture test are relatively similar for these to geotextiles compared to the other geotextiles tested. The large difference in degree of damage between CTP 4D and 4F is not reflected by similar differences in the index test results, with a possible exception for the deformation at failure. The damage on CTP 4F is therefore probably caused by material properties not measured in the index tests. A possible explanation may be the properties on the brittleness in the failure or the tear propagation for the geotextile.

3 CONCLUSIONS AND RECOMMENDATIONS

The project has provided useful information for evaluating relevant properties and requirements for geotextiles to be used for separation and filtration in roads. There are considerable differences in stress strain properties of the geotextiles that is also reflected in the behaviour in the field. Noticeable differences are found in the susceptibility for damage during installation. The criteria used in the existing systems for classification and specification do not seem to reflect properly the behaviour in the field. A revision of the criteria is therefore clearly needed.

The deformation of the geotextiles when subjected to loading, that is, in terms of rutting during installation and construction, is clearly linked to the initial stiffness of the geotextile. A criterion for geotextile survivability is clearly relevant, but has to reflect the behaviour during installation, construction and service lifetime. A criterion for geotextile survivability is suggested based on a combination of requirements for deformation energy and remaining stress and strain till failure. The principle is presented in Figure 8.

The deformation energy related to the installation and construction should be chosen with respect to the type of fill material, construction equipment and type of underground.

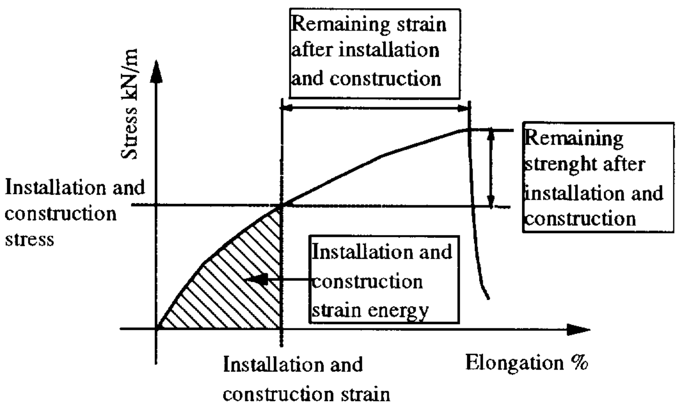

Figure 8. Survivability criterion principle.

The requirements for remaining strength and strain to failure should reflect the expected loads and deformations (settlement) for the service lifetime.

The final criteria should be based on a collection of data from laboratory and field tests correlated with long-term experiences from the field. The field experience should include different type of geotextiles, fill materials, subsoil conditions and construction equipment. This should preferably be done as joint project involving several countries, producers, public authorities and research organisations.

ACKNOWLEDGEMENT

The authors would like to thank Du Pont de Nemours (Luxembourg) S.A. for funding the work and the purchasers of non-woven geotextiles in Norway for providing free samples for testing. We would also like to thank Ingrid Sødergren from Vägverket, Sweden for participating as observer in the field test and for useful contribution to the discussion.

REFERENCES

AASHTO (1990): "Standard Specifications for Geotextiles". *American Association of State Highway and Transportation Officials,* M288-90, Washington DC.

Alfheim S.L., Sørlie A. (1977): " Testing and classification of fabrics for application in road constructions. *Intern. Conf. on the use of fabric in geotechnics* Paris 1977. Vol 2, pp 33-338.

CEN TC 189: "General and specific requirements for geotextiles and geotextile related products used in thr construction of roads and other trafficated areas" Preliminary draft.

Forschungsgesellscaft für straβen- und Verkehrswesen (1994): "Merkblatt für die Anwendung von Geotextilien und Geogittern im Erdbau des Straβaus".

Rathmayer, H (1993): "Nonwoven Geotextiles in Road constructions. Quality Requirements- The VTT-GEO Geotextile Specification". *Finnish National RoadAdministration,* FinnRA Reports 71/1993.

Rathmayer H. (1980) : "Long-term behaviour of geotextiles installed in road constructions in Finland since 1973. *Väg-och vattenbyggaren* 1980:7/8, pp 33 -36.

Schalin, L (1995): "A comparison among the Swedish, the Finnish and the Norwegian requirements for separation layers of geotextiles". *Norwegian Road Research Laboratory,* internal report nr 1786 (in Swedish).

SINTEF (1996): "Non-Woven Geotextiles in Road Constructions." Report.

SINTEF (1997): "Non-woven geotextiles - Field test on damage during installation." Report.

Rut Prediction for Roadways with Geosynthetic Separators

Wen-Sen Tsai, Moh and Associates, Inc., Taipei, Taiwan, Republic Of China

Robert D. Holtz
Professor, Department of Civil Engineering, University of Washington, Seattle, Washington, USA

ABSTRACT: Laboratory model tests that simulated field loading conditions were conducted to evaluate the performance of geotextiles separators. In the tests, rut depth was determined for various geotextiles, thickness of aggregate, subgrade soils, and the number of loading cycles. A rut prediction formulation for unpaved of roadways was developed, based on the Giroud and Noiray (1981) design procedure for unpaved roads. The prediction formula is verified by the rut measurement in a full scale field test.

KEY WORDS: geotextiles, separation, unpaved roads, model tests, rut prediction, design

1 INTRODUCTION

That geotextiles can markedly improve the performance of unpaved roadways constructed on soft foundation soils is well established. Although the primary geotextile function is separation, performance of unpaved roads is also significantly enhanced by the filtration, drainage, and reinforcement functions provided by the geotextile.

Ruts in the roadway surface are probably the most important indicator of roadway performance. Excessive or premature rutting is a good indication of either subgrade or aggregate failure, or both. Hence, the influence of geotextiles on the development of ruts can be used to evaluate their performance in unpaved roadway systems. Consequently, in this research, ruts were measured in laboratory scale model tests on subgrade-geotextile-aggregate systems. Cyclic plate load tests were conducted on three different thicknesses of base course aggregate, various types and weights of separator geotextiles, and two soft subgrade soils. The geotextiles investigated included heatbonded nonwovens, needlepunched nonwovens, and a woven silt-film. The results were used to develop a prediction equation for rut depths in unpaved roads. This rut prediction formula considers the base course thickness, subgrade strength, and number of loading cycles. The formula also predicted reasonably well the results of a full scale road test.

2 TEST SETUP, SOILS, GEOTEXTILES, AND PROCEDURES

Since the performance of geotextiles has been found to be strongly affected by the loading conditions, e.g. loading level and loading frequency, loading parameters used in this study modeled loading conditions experienced by separation geotextiles in the field. This was done by having stress levels applied to the geotextile due to a dynamic load in the test the same as in the field.

Furthermore, the boundary of the test apparatus did not interfere with the failure zone in the subgrade, when and if the subgrade experienced a shear failure under a dynamic load.

An 80 kN single axle load, termed the equivalent single axle load (ESAL), is used in the AASHTO pavement design method and a tire pressure of 620 kPa is common for loaded dump trucks. The contact area between the tire and pavement for this loading, expressed as a ratio of wheel load and tire pressure, was 0.0645 m^2.

A 0.416 m^3 steel drum, (Figure 1) contained layers of soils and was used to simulate a common roadway. The top layer was aggregate, which was under-lain by a layer of soft soil 300 mm thick. More details about the setup can be found in Tsai (1995) and Tsai and Holtz (1997).

2.1 Subgrade Soils and Aggregate

Two different soils, a silty (ML) soil and a clayey (CL) soil, were used as the subgrades in the study. The silty soil was a tailing material from washed crushed rock. The clayey soil was obtained by mixing the silty soil with 5% bentonite by weight. The crushed stone aggregate (GP) was similar to the base material used by The Washington State Department of Transportation (WSDOT) for pavements. Table 1 shows the basic properties of these three materials.

2.2 Geotextiles

Six different separator geotextiles, all polypropylene, were tested. Types and relevant properties and given in Table 2.

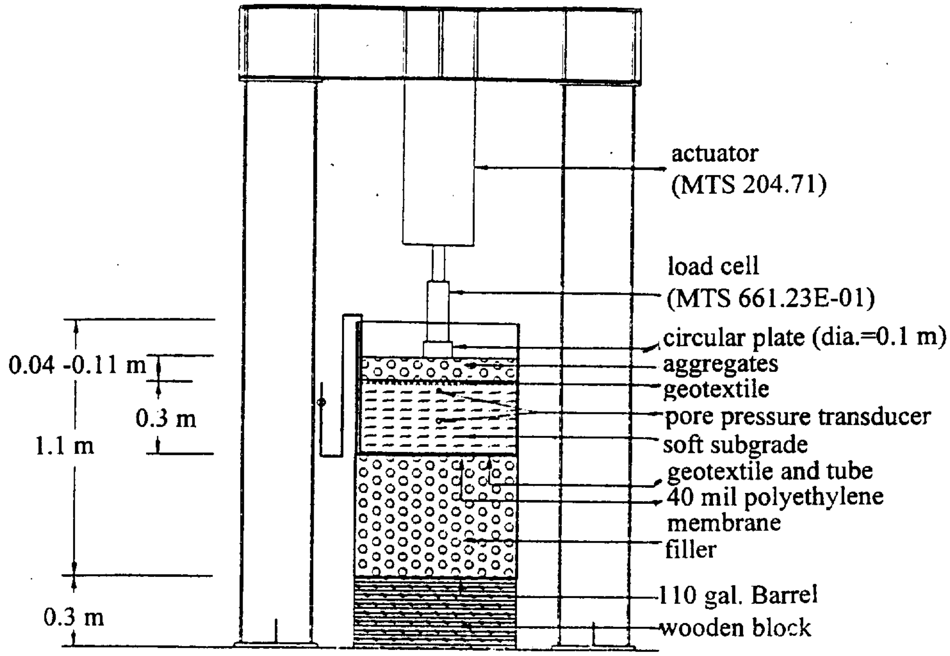

Figure 1. Experimental Setup

Table 1. Basic properties of the silty soil, the clayey soil and the aggregate.

Property	Silty Soil	Clayey Soil	Crushed Stone
% passing US No. 200 sieve	81	82	0
Coefficient of Uniformity	25	NA	3.6
Coefficient of Curvature	1	NA	1.3
Plastic Limit, %	27	24	NA
Liquid Limit, %	38	46	NA
Unified Soil Classification System	ML	CL	GP
Permeability, cm/sec	1.2×10-7	2.9×10-8	NA
Maximum Dry Density, kg/m3	1580	1622	1922
Optimum Moisture Content, %	20.5	20.3	NA

2.3 Test Procedure

Testing procedure reported by Tsai and Holtz (1994), Tsai (1995) and Tsai and Holtz (1997) was followed in all tests reported in this paper.

Table 2. Nominal physical and mechanical properties of geotextiles used in the study.

Geo-textile	Structure	Thickness	Mass per Unit Area	Grab Strength
		ASTM D 1777 mm	ASTM D 3776 g/m^2	ASTM D 4632 kN(%)
NP4	Nonwoven	1.3	142	0.511 (50)
NP6	Nonwoven	1.8	204	0.711 (50)
NP8	Nonwoven	2.3	268	0.933 (50)
HB4	Nonwoven	0.4	132	0.578 (100)
HB6	Nonwoven	0.5	197	1.000 (90)
SF4	Woven	NA	136	0.801 (15)

3 RUT MEASUREMENTS

In the model tests, the rut depths were determined based on the readings of a built-in LVDT in the MTS actuator that applied load to the circular plate.

A total of 19 tests were conducted in this study. Among the tests, three different aggregate base thicknesses, six different separators, two different subgrade soils, and four different subgrade strengths were used (Tsai, 1995; Tsai and Holtz, 1997).

Figure 2 shows a typical development of rut depth on the aggregate surface in a test where the geotextile was found to have survived. From this figure, we can see that

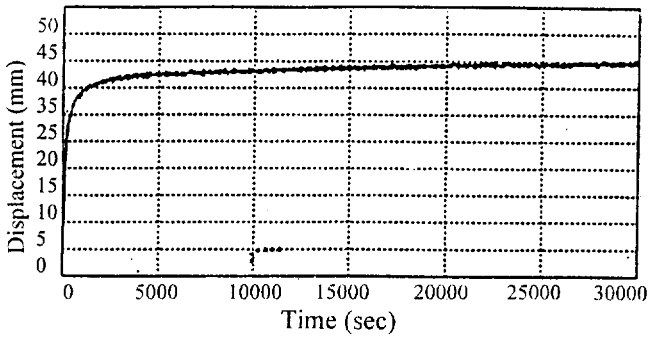

Figure 2. Typical development of rut depth on aggregate surface.

the rate of rut depth development was high initially, and then decreased with the number of cycles.

A summary of the measured ruts obtained in the tests are shown in Table 3. In this table, the notation of form A-B-C-D-E to identify each test. A is the thickness of the base course in mm; and B represents the type of separator used in the test. If it was a geotextile, then its mass per unit area (in oz/yd^2) is also given. NP represents a needlepunched nonwoven geotextile; HB is a heatbonded nonwoven, , and SF represents a slit-film woven geotextile. GF represents a graded granular filter separator, while MEM represents an impervious plastic membrane. Null means that no geotextile was used.

The subgrade soil type was represented by C, while D represents the subgrade strength in CBR. E represents the sequence of a test, if the test was repeated.

In some tests, local shear failure of the subgrades was experienced, especially the softer ones (40-NP4-Silt-0.5, 40-NP4-Silt-1, etc.). These tests generally had large ruts, some as deep as 147 mm. The ruts for these tests that failed were not used for rut prediction.

Note that the rut depth of Test 40-MEM-Silt-2 was greater than rut depths in tests with separators of lower moduli, e.g. 40-HB6-Silt-2, 40-NP4-Silt-2, 40-NP8-Silt-2. Similarly, the test with the clayey subgrade (Test 40-NP4-Clay-2) had a deeper rut (63 mm) than test 40-NP4-Silt-2 (45 mm) which had the same experimental parameters except subgrade soil type. This can be explained by the long-persisting high pore pressures in the clay, as discussed by Tsai and Holtz (1997). This high pore pressure reduced the modulus of the subgrade, and thus higher plastic subgrade deformation occurred.

The ruts discussed in this section are not equivalent to the ruts that would occur in the field, since the results are determined from scale model tests. Since a fixed wheel path is simulated in these test, the ruts obtained in laboratory tests are probably greater than in the field.

4 RUT PREDICTION BASED ON LABORATORY TEST RESULTS

Table 3. Ruts and depressions on subgrade surfaces after dynamic loading

Notation	Rut on Aggregate Surface (mm)	Depression Depth on Subgrade Surface (mm)	Depression Diameter on Subgrade Surface (mm)	Ratio of Depression Depth to Rut Depth (%)
110-HB4-Silt-2	18	14	229	78
110-NP4-Silt-2	20	9	152	45
110-SF4-Silt-2	18	6	165	33
110-Null-Silt-7	20	4	NA[a]	20
110-Null-Silt-2	49	30	203	61
110-Null-Silt-1	154	110	191	71
55-HB4-Silt-2[b]	130	203	140	156
40-GF-Silt-2	118	123	152	104
40-MEM-Silt-2	50	51	203	102
40-HB4-Silt-2	94	122	229	130
40-HB4-Clay-2	70	140	203	200
40-HB6-Silt-2	42	44	216	105
40-NP4-Silt-2a	45	44	191	98
40-NP4-Silt-2b	46	51	216	111
40-NP4-Clay-2	63	74	254	117
40-NP4-Silt-1	97	279	107	288
40-Np4-Silt-0.5	147	152	330	103
40-NP8-Silt-2	41	41	NA	100
40-SF4-Silt-2	46	64	191	139

a. Depression was very small and it was difficult to determine the depression zone.
b. The shaded rows indicate the tests where geotextiles were found to have failed.

The results from the laboratory model tests reported here can be used to predict the rut depths in the field with various subgrade strengths, base course thicknesses and geotextile separators. Then it may be possible to determine rut depths for given base course thicknesses using projected traffic loads during the road's service life. In 1981 Giroud and Noiray, proposed a design method for unpaved roads, both with and without geotextiles. In their procedure, the geotextile was used to increase the bearing capacity of the subgrade from elastic "bearing capacity", actually the maximum shear stress, or $N_c=\pi$ to ultimate bearing capacity $N_c=(\pi+2)$, due to the subgrade confinement and stress reduction on the subgrade surface provided by the geotextile. They also considered the effect of traffic load using empirical data presented by Hammit (1970) and Webster and Alford (1978). The design formula proposed by Giroud and Noiray is shown below.

$$h'_0 = \frac{119.24 \log N + 470.98 \log P - 279.01 r - 2283.34}{c_u^{0.63}} \quad (1)$$

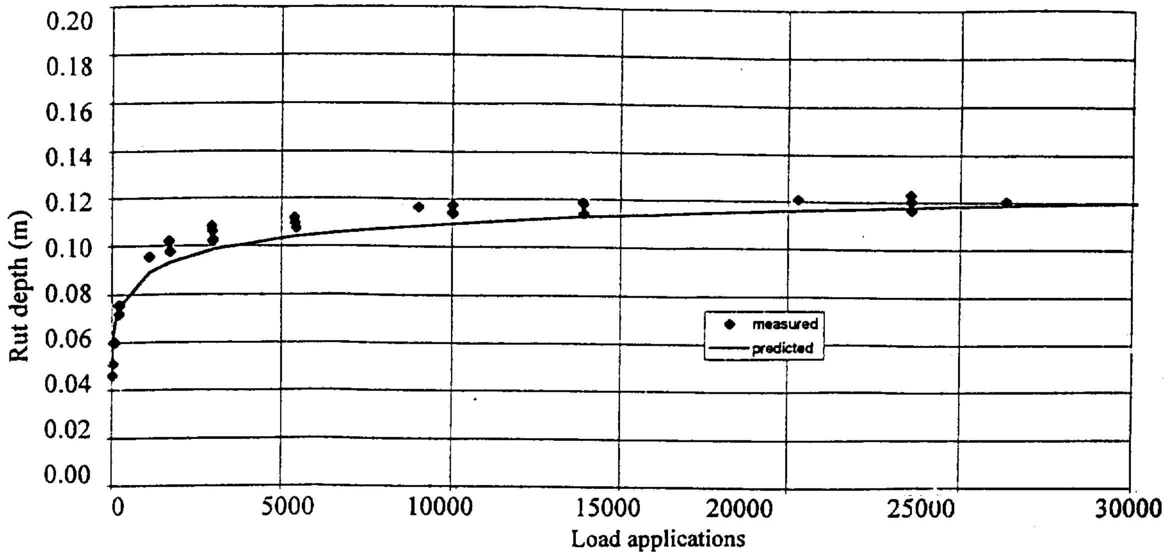

Figure 3. Measured and predicted ruts for Test 40-NP4-Silt-2

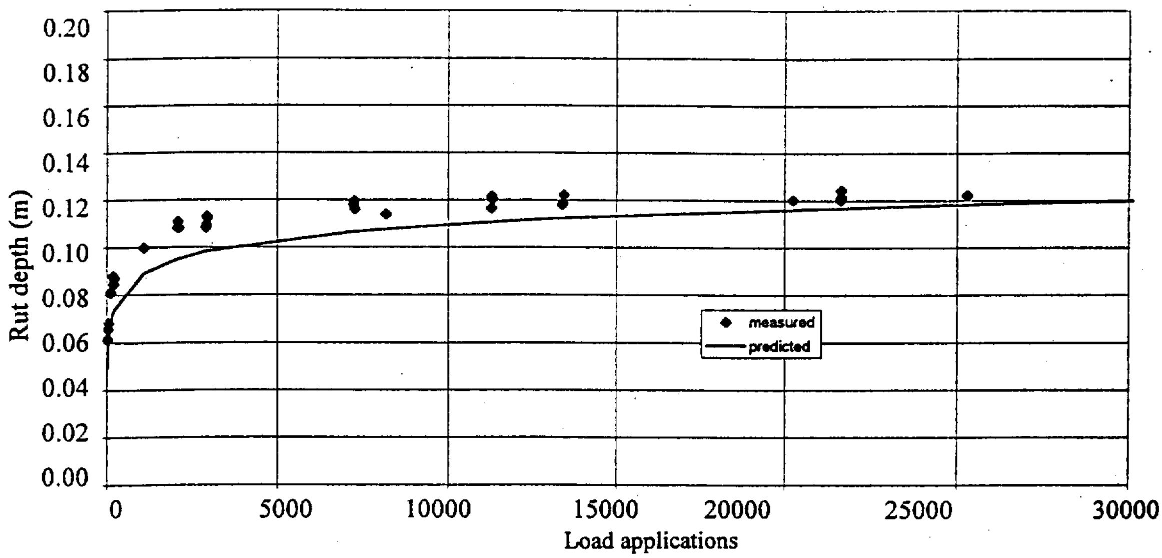

Figure 4. Measured and predicted ruts for Test 40-SF4-Silt-2

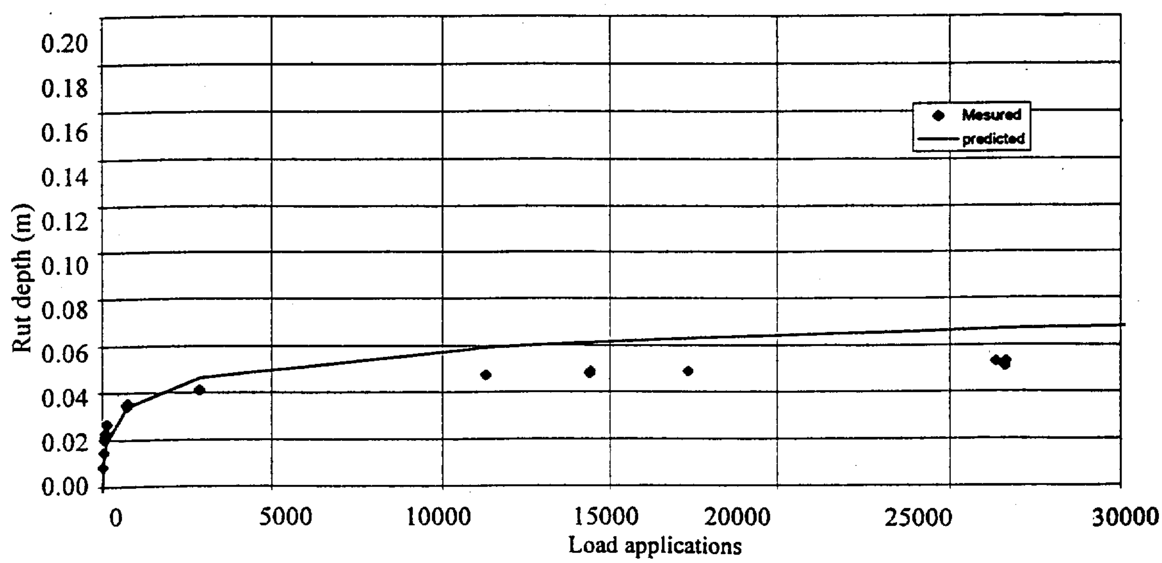

Figure 5. Measured and predicted ruts for Test 110-Null-silt-2

where

h'_0 = aggregate thickness (case without geotextile, when traffic is taken into account), in m
c_u = undrained cohesion of subgrade soil, in Pa
N =number of applications of load P
P =axle load, in N
r = rut depth, in m

Equation 1 can be rearranged to obtain:

$$r = -8.18 + 0.186 \log N - 0.00358\, c_u^{0.63}\, h'_o + 0.733 \log P \tag{2}$$

This equation is of the form:

$$r = A + B\log N + Cc_u^D H + E\left(\frac{k}{H}\right) \tag{3}$$

where A, B, C, D and E are parameters, and where H is aggregate thickness, in meters, for the case with or without geotextile.

The laboratory results (Tsai, 1995) showed that the presence of geotextiles can reduce ruts if the geotextile can survive during its service life. However, the tests also showed that geotextile type did not affect rut depth, probably because of the strength of the subgrade and the types of geotextiles tested. Thus Equation 3 does not include geotextile modulus but instead a term $E(k/H)$, where $k = 1$ if a geotextile is present, and $k = 0$ if no geotextile is present. Using the laboratory results obtained previously, a regression analysis was conducted. The model tests have a scale of 1:2.75. Therefore, the measured ruts in the laboratory tests were multiplied by 2.75 to reflect field rut depths.

A statistics program, *NLREG*, was used to perform a non-linear regression analysis on the results of the laboratory model tests which did not have a subgrade failure or a failed geotextile. In the regression analysis, the sample size was 330, and from these results, Equation 3 can be expressed as:

$$r = 0.260 + 0.009176\log N - 0.3935c_u^{0.1465}H - 0.01689\left(\frac{k}{H}\right) \tag{4}$$

The proportion of variance explained (R^2) and the standard error of estimate were 0.88 and 0.0128, respectively.

Equation 4 is used only with an equivalent single axle load (EASL or 80 kN), and N is the corresponding number of passages of ESAL. On the other hand, Equation 2 can be used for the design of unpaved roads without geotextiles and also applies for any axle loads besides ESAL. This is why the coefficients of Equation 4 are different from those of Equation 2. Figures 3, 4 and 5 illustrate the development of both measured ruts from some typical laboratory model tests and their predicted values based on Equation 4. These tests represent various loading conditions with respect to base course thickness, subgrade strength, and geotextile separators. From these figures, we can see that Equation 4 provides a reasonable prediction for these three tests. Other results in Tsai (1995) provide similar agreement.

5 USE OF THE RUT PREDICTION FORMULA FOR FULL SCALE ROAD TEST RESULTS

The results of the full scale road test described in Tsai et al. (1993) were used to verify the new rut prediction formula. In the full scale road test, ten wheel passes were applied using a loaded dump truck weighing 214 kN. The rear axle of the truck was a tandem axle and supported about two-thirds of the gross weight of the loaded dump truck, i.e. 143 kN. Based on Giroud and Noiray (1981), either single axle of the tandem axle carries an axle load equivalent to:

$$0.6 \times 143kN = 86kN \tag{5}$$

The equivalent number of the passages of the single axle load is:

$$2 \times N = 2 \times 10 = 20 \tag{6}$$

The number of the passages of the tandem axle thus can be expressed in equivalent single axle load (ESAL) and is shown below.

$$\mathrm{N} = 20 \times \left(\frac{86kN}{80kN}\right)^{3.95} = 27 \tag{7}$$

Equation 4 was used to calculate the ruts in the full scale road test. Figure 6 shows the values versus the measured values of the rut depths for the sections with 150 and 300 mm thick base courses in the full scale road tests (Tsai et al., 1993). Unfortunately, the subgrade strengths immediately below each location where the ruts were measured were not known. Hence, the mean values of subgrade strengths (shown in Tsai et al., 1993) in each section are used to predict the ruts. Figure 6 shows that many of the predicted values of the ruts are in the range of the measured values, so Equation 4 can be used to reasonably well predict the ruts with 150 and 300 mm base courses. Predictions are not made for the sections with 450 mm thick base course in the full scale road test, because the largest equivalent base course thickness in the laboratory model tests was only 300 mm. Therefore, some tests with thicker base course are needed to improve this equation for such cases.

6 CONCLUSIONS

By modifying Giroud and Noiray's (1981)design equations, a new rut prediction formula based on the results of laboratory tests on scale model subgrade-geotextile-aggregate systems was developed. The formula takes into account base course thickness, subgrade strength, type and weight of geotextile separators, and number of loading cycles. The ruts measured in typical laboratory model test, compared well with their predicted values. The results of full scale road tests were also used to verify the rut prediction formula, up to an equivalent base course thickness of 300 mm. The predicted values tended to be greater than the measured values.

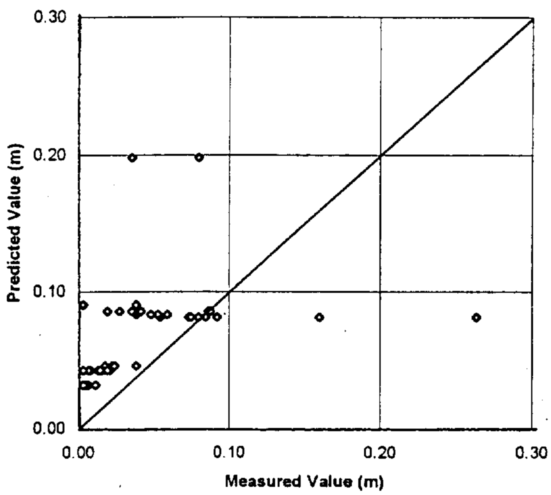

Figure 6. Predicted versus measured values of rut depths for the full scale road test

REFERENCES

Giroud, J.-P., and Noiray, L. (1981) "Geotextile-Reinforced Unpaved Road Design," *Journal of the Geotechnical Engineering Division*, ASCE, Vol. 107, No. GT9, pp. 1233--1254.

Hammit, G. (1970) "Thickness Requirements for Unsurfaced Roads and Airfield Bared Base Support," *Technical Report* S-70-5, United States Army Engineer Waterways Experiment Station, Vicksburg, Miss., July.

Tsai, W.-S. (1995) "Evaluation of Geotextiles as Separators in Roadways," *Ph.D. Thesis*, University of Washington, Seattle, Washington, pp. 173

Tsai, W.-S. and Holtz, R. D. (1994) "Performance of Geotextile Separators in Laboratory Model Tests", *Proceedings of the Fifth International Conference of Geotextiles, Geomembranes, and Related Products*, Singapore, Vol. 2, pp. 663-666.

Tsai, W.-S. and Holtz, R. D. (1997) "Laboratory Model Tests to Evaluate Geotextile Separators in Service", *Proceedings Geosynthetics '97 Conference*, Long Beach, Vol. 2, pp. 633-646.

Tsai, W.-S., Savage, M. B., Holtz, R. D., Christopher, B. R., and Allen, T. (1993) "Evaluation of Geotextiles as Separators in a Full Scale Road Test," *Proceedings Geosynthetics '93 Conference*, Vancouver, Canada, Vol. 1, pp. 35--48.

Webster, S. L., and Alford, S. J., (1978) "Investigation of Construction Concepts for Pavements Across Soft Ground," *Technical Report* S-78-6, United States Army Engineer Waterways Experiment Station, Vicksburg, Miss., July.

Quantifying the Separation Characteristic of Geosynthetics in Flexible Pavements

Imad L. Al-Qadi
Associate Professor, The Via Department of Civil Engineering, Virginia Tech, Blacksburg, VA

Brian J. Coree
Visiting Assistant Professor, The Via Department of Civil Engineering, Virginia Tech, Blacksburg, VA

Thomas L. Brandon
Associate Professor, The Via Department of Civil Engineering, Virginia Tech, Blacksburg, VA

Salman A. Bhutta,
Doctoral Candidate, The Via Department of Civil Engineering, Virginia Tech, Blacksburg, VA

Alexander K. Appea,
Graduate Student, The Via Department of Civil Engineering, Virginia Tech, Blacksburg, VA

ABSTRACT: A field experiment was conducted in which geosynthetics were used at the base/subgrade interface in instrumented sections of a flexible pavement on a rural highway in Bedford County, Virginia. The sections were monitored for two-and-one-half years under local traffic. In this paper, development of a transition layer (intermixing at the base course-subgrade interface) is hypothesized when geosynthetic is absent. An analysis of Falling Weight Deflectometer (FWD) data confirmed the hypothesis in the thinner base (100 mm) sections. The results so far obtained from thicker base sections (150 mm and 200 mm) are inconclusive.

KEYWORDS: Geotextiles, Geogrids, Pavements, Separation, Falling Weight Deflectometer.

1 INTRODUCTION

To examine the geosynthetic benefits in pavement system and validate an earlier laboratory investigation at Virginia Tech (Al-Qadi et al., 1996, Smith et al., 1995), a section of rural highway in Bedford County, Virginia, was selected in 1994 for an experimental project involving the use and evaluation of geosynthetic functions between a fine-grained subgrade and a granular base course. The experimental section comprised part of a route realignment project undertaken by the Virginia Department of Transportation (VDOT). It was hypothesized that under the action of traffic and environment the subgrade would, in the absence of a separation material, be pumped into the granular base and/or the base course material would penetrate into the subgrade thereby compromising the structural capacity of the pavement.

1.1 Site Description

Nine experimental sections, each of approximately 15 m in length, were constructed as part of the realignment of Route 616 in Bedford County, Virginia. The pavement construction comprised a nominal 90 mm hot-mix asphalt (HMA) wearing course surfacing over a granular base. The thickness of the base varied throughout the nine sections: 100 mm thick in sections 1 through 3, 150 mm in sections 4 through 6, and 200 mm in sections 7 through 9. The subgrade was a weak, reddish brown CH (AASHTO A-7-6) soil, except under sections 5 and 6 where it was identified as ML (AASHTO A-5). These materials were found to have soaked CBR values in the range 6 to 10% at in-situ moisture-density values.

Samples of all construction materials were taken from in-situ and tested in the Materials Laboratory at Virginia Tech. Conventional tests were performed on all recovered materials (HMA: Marshall parameters at 50-blows, asphalt extraction and aggregate gradation; base course: gradation, moisture content, moisture-density and CBR; subgrade: gradation, moisture content, moisture-density and CBR). Extra testing was undertaken on these materials to provide more fundamental material properties (HMA: resilient modulus and creep compliance; base and subgrade: resilient modulus).

The HMA had an asphalt content of about 6.2% by weight of mixture, an average air-void content of 4.6% and an average VMA of 17.9%. The average Marshall Stability and Flow values were 12.3 kN and 10 flow-units. The resilient modulus, M_R, of field specimens ranged from 3160 MPa at 5°C to 2620 MPa at 40°C. Creep compliance curves were obtained from all field and bulk samples.

The granular base material complied with VDOT specification for a type 21-B base. It classifies as a GW soil and has an optimum moisture of 6.1% at a density of 22.3 kN/m^3. Remolded samples were tested for resilient modulus, M_R, and can be expressed in terms of the bulk stress, θ, with an average result of:

$$M_R\,(\mathrm{MPa}) = 650\theta^{0.62} \tag{1}$$

Two types of geosynthetic materials were placed at the base/subgrade interface: a woven geotextile and a geogrid. Sections 1, 4, and 7 served as control sections with no geosynthetic at the base/subgrade interface, while the geotextile was placed in sections 2, 5, and 8. The geogrid was likewise installed in sections 3, 6, and 9. The experimental matrix is shown in Table 1. The pre-installation properties of the geosynthetics used are listed in Table 2. The geosynthetics were also tested after three years of field service to determine the installation, construction practice, environmental, and vehicular loading effects on these properties. A 0.6 m x 3.6 m (lane width) piece of each geosynthetic was obtained after excavating the pavement in October 1997. Both geosynthetics were found in excellent condition, and their properties are shown in Table 3. Analysis of changes in the geosynthetic properties and gradation of base and subgrade material after three years of service will be presented in a future publication.

Table 1. Experimental Matrix.

Section Type	Base Thickness		
	100 (mm)	150 (mm)	200 (mm)
Control	1*	4	7
Geosynthetic	2	5	8
Geogrid	3	6	9

* Denotes section number

Table 2. Characteristics and Properties of Geosynthetics Used (before testing).

Material	Direction	Ultimate	
		Strength (kN/m)	Elong. (%)
Geotextile	Warp	27	23.6
	Fill	25	9.9
Geogrid	Machine	19	8.9
	X-Mach	33	9.3

Construction started in April 1994 and was effectively completed by September 1994. This period included a significant amount of time and effort devoted to installing and checking the various instruments embedded in the pavement. The pavement was opened to traffic in September 1994 (Al-Qadi et al. 1996).

Table 3. Characteristics and Properties of Geosynthetics Used (after testing).

Material	Direction	Ultimate	
		Strength (kN/m)	Elong. (%)
Geotextile	Warp	18	14.8
	Fill	25	12.5
Geogrid	Machine	19	12.4
	X-Mach	32	14.1

1.2 Traffic

Traffic volume rates were recorded automatically by the installed instrumentation and varied from 300 vehicles per day in winter to more than 700 vehicles per day in summer.

Three calibration tests were run; a flat-bed truck was used at different axle loads, tire pressures and speeds. This was designed to provide a basis for calibration and validation of the installed instrumentation, and to yield a complete response matrix against which a mechanistic pavement design method, under development, could be validated.

1.3 Section Monitoring

Monitoring of the experimental sections was undertaken using two approaches. The first consisted of a series of embedded instrumentation designed to monitor and record traffic, temperature, moisture, pressure, and strains at various points within the pavement sections and on the geosynthetics. A data acquisition system was set up to collect all the appropriate readings from the instrumentation when triggered by the passage of a vehicle. Accumulated data was periodically transmitted electronically to the Materials Laboratory at Virginia Tech for storage and analysis. The second approach relied upon periodic, seasonal visits to the site to measure and record visible distress indicators, although only permanent deformation (rutting) was found to have occurred, to subject the test sections to Falling Weight Deflectometer (FWD) testing for structural evaluation, and, on occasion, to scan the sections using ground penetrating radar (GPR). This paper discusses the rutting and FWD test results

2 FIELD MONITORING

The test sections were periodically monitored to provide information relative to surface distresses (rutting) and to perform noninvasive, nondestructive structural evaluations of the different sections.

2.1 Rutting

Rutting was measured using a straight-edge method. Two readings were taken on each section during each visit. The magnitude of rutting was defined as the greatest gap between the straight-edge laid upon the pavement transverse to the direction of traffic and the pavement surface. This method would not distinguish between settlement or compaction rutting and plastic flow/heave rutting, however, it is noted that there was no indication of plastic flow/heave distortion of the pavement surfaces. Figures 1 and 2 summarize the development of rut depths during the monitoring period for sections 1 through 3 and 4 through 9, respectively.

From Figures 1 and 2, it is immediately apparent that the rutting histories of sections 1, 2, and 3 stand apart from those in sections 4 through 9, which are statistically identical. In these sections, the magnitude of rutting not only exceeds that in the others, but the rate at which it accumulated is seen to be increasing. Indeed, it has been observed that since about August 1996, the rutting measured in section 1 has exceed the maximum criterion of acceptability (25 mm), and the rate at which it is accumulating is accelerating.

The rutting that occurred during the first few months of traffic is mainly due to "normal' initial rutting from compaction under traffic. As can be noted, the rutting observed in the first four months is almost the same for all sections. The sharp increase in rutting (in all sections) just before October 1996 is due to the application of two weeks of heavy truck loading to accelerate rutting. The relatively low rutting in sections 4 through 6 was due to the greater wander in the area of the intersection.

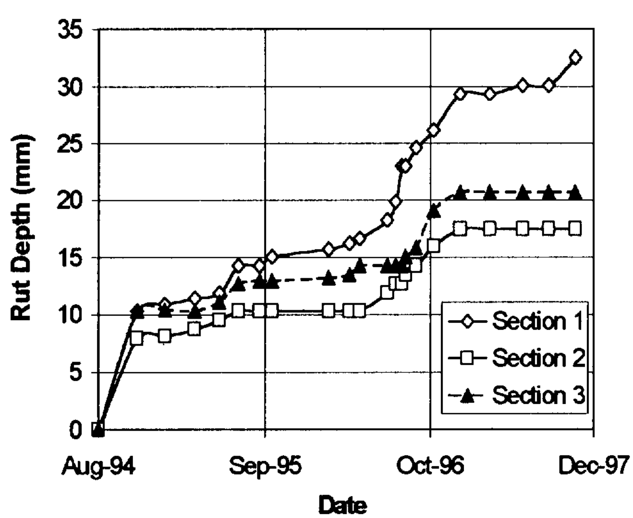

Figure 1. Rut Depth for Sections 1 through 3.

2.2 Falling Weight Deflectometer (FWD)

The Virginia Department of Transportation (VDOT) FWD was chosen to perform seasonal structural evaluations of the test sections. This device, which drops a calibrated mass onto a circular plate (radius 150 mm) in contact with the pavement surface, records the magnitude of the applied load, and the vertical deformation response of the pavement surface at the center of the loaded plate and a six locations offset from the loaded axis.

Two types of analysis may be performed on FWD data. The simplest and most direct analysis relies on computing a Surface Modulus, E_0, defined as the applied load divided by the measured axial deformation. This value is analogous to a spring constant (kN/mm), and provides a gross measure of the overall structural value of the pavement system, including the subgrade. A more sophisticated analysis is possible using various techniques of "back-calculation" which seek to match the observed pavement response to that returned by a mathematical model of a layered linear elastic half-space. This technique generally relies upon varying the linear elastic moduli of the component material layers until a satisfactory match to the observed surface deflection is achieved.

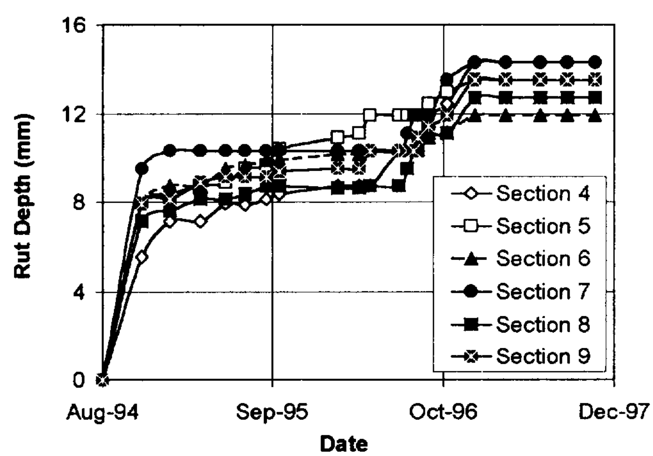

Figure 2. Rut Depth for Sections 4 through 9.

2.2.1 Surface Modulus (E_0)

The surface modulus of each section was computed for each of the seasonal site visits. This technique is simple because it requires that no assumptions be made relative to the thickness or elastic response of component layer materials. However, it is subject to modification in HMA surfaced pavement due to the effects of temperature upon the viscoelasticity of the asphalt bound materials, and can be further influenced by the presence of an effective rigid layer underlying the pavement at some depth. The results of these analyses are shown in Figure 3.

It can be seen from Figure 3 that the overall pavement responses of sections 1, 2, 3, and 9 stand out as being distinct from those in sections 4, 5, 6, 7, and 8 which are remarkably consistent. This apparent difference is ascribed to the details of the design of this road section, which was relocated to transform an intersection into a curve. Consequently, in spite of a significant excavation (mainly in sections 4 through 8), the sections at each end of the new construction are somewhat influenced at some depth by the presence of previously undisturbed and compacted subgrade materials. This will also explain the increased surface moduli observed in these sections; the authors believe that this is due not to stronger pavement sections, but to residual pre-compacted subgrade.

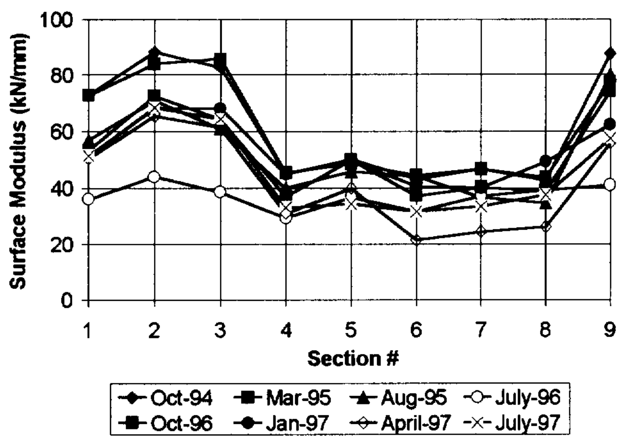

Figure 3. FWD-derived Surface Moduli (MPa).

Nonetheless, if the surface moduli for sections 1, 2 and 3 are closely examined, it will be seen that for all FWD tests, the surface modulus of section 2 (geotextile) exceeds that of section 3 (geogrid), which in turn exceeds that of section 1 (control). This pattern is also observed in sections 4, 5, and 6 (150 mm base) and in sections 7 and 8 (200 mm base), and would tend to indicate that the geotextile may contribute more to the structure than other sections (Al-Qadi et al. 1997).

2.2.2 Detailed FWD Analysis

FWD measured deflection profiles were plotted for different periods. The purpose of this exercise was to define any inconsistency, which might occur in the measurements taken by the geophones. Figures 4 and 5 are typical measured deflection basins for different load levels in July 1997 for sections 1 and 2.

The collected FWD field data was further analyzed using proprietary software, MODULUS version 5.0, developed by the Texas Department of Transportation (TxDOT) and the Texas Transportation Institute (TTI).

This package takes as input pavement responses recorded in the field and the thicknesses of each physical material layer. The elastic parameters (E, ν) of any layer except the subgrade may be either fixed or bounded within a range supplied by the user. The program then performs a search algorithm, varying the "slack" variables until an optimal match between the measured and computed deflection basins is found. The output from this program is the "optimal" set of layer moduli consistent with the measured values and the set layer property constraints.

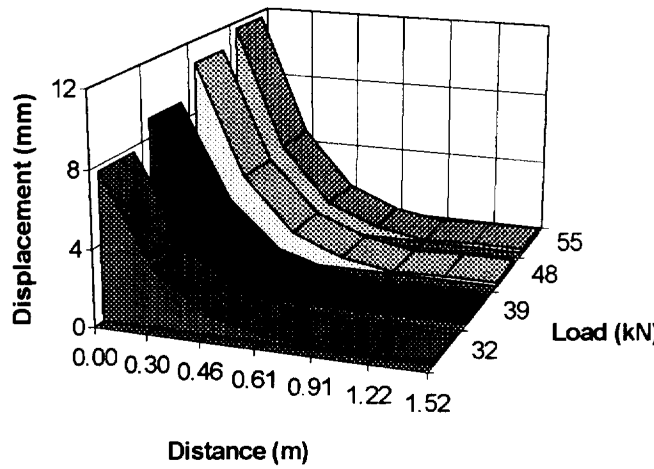

Figure 4. Deflection Basin Profile (July 1997), Section 1.

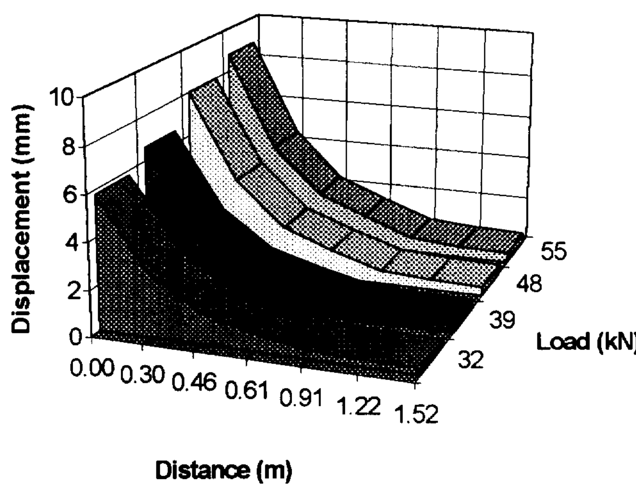

Figure 5. Deflection Basin Profile (July 1997), Section 2.

MODULUS uses an internal routine to detect the presence and depth of effective rigid layers deep within the pavement. This is important, and has been found to significantly influence the returned moduli. In this project, MODULUS did indeed detect an effective rigid bottom layer at a varying depth of 0.5-7.5 m (mostly above 2.0 m) below the pavement surface. Further data analysis indicates that the variation in depth to rigid bottom layer did not have any significant effect on the result pattern.

Due to the relatively thin HMA surfacing layer, the elastic properties of this layer were input and fixed by the authors based upon appropriate measured pavement temperatures and the laboratory resilient modulus characterization of specimens obtained form the field. The nominal elastic parameters of the granular base layer were also provided and fixed by the authors based upon laboratory measurements (Al-Qadi et al. 1996). The only parameter returned by MODULUS, therefore, was the subgrade modulus (Figure 6). This analysis confirms the differential response between the different treatments.

For most of the FWD results, the subgrade "apparent" resilient moduli of the sections with geotextile are greater than their corresponding control sections or geogrid stabilized/ reinforced sections. This may be attributed to a weaker base course layer in the latter sections as compared to the corresponding geotextile stabilized sections, which is consistent with the "pumping of subgrade fines into the base course layer and/or intermixing at the base-subgrade interface" hypothesis.

2.2.3 Base-Subgrade Interface Intermixing Model

One of the important functions of geosynthetics in pavements is stabilization, which is its ability to isolate and provide a barrier against the base course-subgrade intermixing (Koerner and Koerner 1994, Al-Qadi, et al., 1994, Jorenby and Hicks, 1986; Lair and Brau, 1986). The extent of contamination and the material properties of the intermixing layer are of critical importance in determing the performance of pavements. Although the concept of base course contamination has been realized for sometime (Yoder and Witczak, 1975), an estimate of its contribution to the reduction in pavement service life is still needed to be quantified. The following section details the approach adopted to determine the extent of contamination in this project.

The hypothesis put forth in the study was the development of a transition layer between the subgrade and base layer in the absence of a geotextile. To determine the transition layer thickness developed in control and (may be) geogrid stabilized reinforced sections, an independent layer of resilient modulus value between the base and subgrade was added and the "geotextile subgrade resilient modulus" was considered in the calculations as reference. After adding the transition layer with known properties to the control pavement system, a back-calculation procedure was adopted to determine the subgrade resilient modulus. This is an iterative process where the thickness of the transition layer is changed gradually to yield a subgrade resilient modulus approximately equal to that of the geotextile stabilized section.

For example, the subgrade resilient modulus, from the data collected in August 1995, for section 1 (100 mm control section) was 105 MPa, where the geotextile stabilized section had a subgrade resilient modulus of 110 MPa. A transition layer thickness of 13 mm at a resilient modulus of 138 MPa was needed to increase the subgrade resilient modulus to 110 MPa. Over the next 8 months the transition layer increased to 64 mm. The thickness further increased to 69 mm by October 1996 indicating asymptotic stabilization of intermixing layer versus time (see Figure 7). Further tests show insensitivity to greater contamination/ intermixing.

For the thicker base course sections (150 mm and 200 mm), the MODULUS program becomes insensitive to changes in transition layer thickness. This implied that the FWD back-calculation procedure could not estimate the contamination layer thickness accurately in the thicker base course sections (150 mm and 200 mm) at this time.

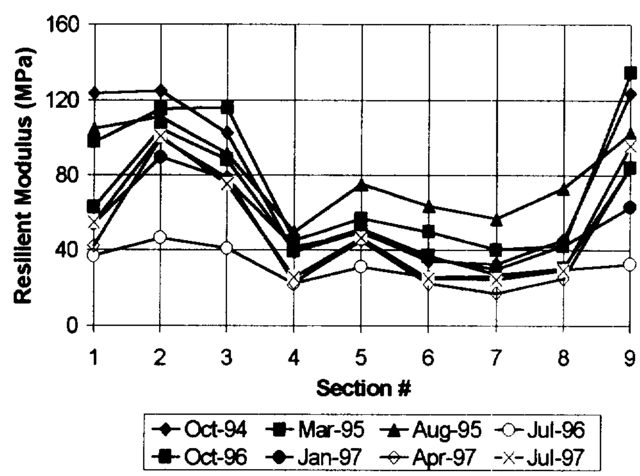

Figure 6. Apparent Subgrade Resilient Modulus Variation over Time.

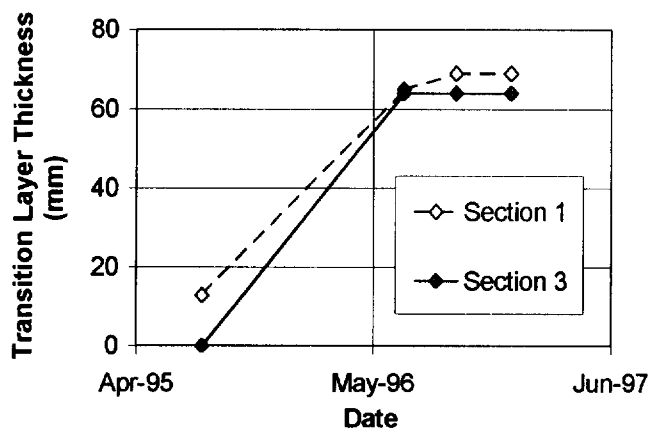

Figure 8. Development of Transition Layer.

3 CONCLUSIONS

The results of this field experiment and analysis of the data derived from non-destructive monitoring (rutting and FWD) suggest a clear difference in performance when geosynthetic is included in the pavement system; specially in the thinner base sections (1 through 3), while the short duration of the project prevent any clear distinctions being made in the thicker base sections (4 through 9) at his time. Within sections 1 through 3, the benefit of the geotextile is noted by comparison with the performance (rutting) of the control to the other sections; equally, a simple analysis of FWD data suggests that the degree of intermixing at the base-subgrade interface is a function of the geosynthetic used - no intermixing in the geotextile section, and delayed or reduced intermixing in the geogrid stabilized/reinforced section. MODOLUS program was used to obtain the extent of intermixing at the base course-subgrade interface in the 100 mm test sections over a period of 17 months (August 1995 to January 1997). It was found that the degree of intermixing can be quantified. However, for the thicker base course sections (150 mm and 200 mm) the back-calculation (so far) turns insensitive and the difference in performance between sections is within the numerical accuracy of the computer model.

4 ACKNOWLEDGEMENTS

The authors acknowledge the financial support by the Virginia Center for Innovative Technologies and the Amoco Fabrics and Fibers Company. The authors also acknowledge the VDOT support in providing the FWD testing for this study. The invaluable help by Barney Barnhart and Jeff Kesler of VDOT is greatly appreciated.

5 REFERENCES

Al-Qadi, I. L., Brandon, T. L., Smith, T. A., and Lacina, B. A. (1994) "How Do Geosynthetics Improve Pavement's Performance," *Proceedings of Material Engineering Conference*, San Diego, CA, USA, pp. 606-616.

Al-Qadi, I. L., Brandon, T. L., Bhutta, S. A., Appea, A. K., and Lacina, B. A. (1996) *Field Testing of Geosynthetically Stabilized Pavement Sections*, The Charles E. Via, Jr. Department of Civil Engineering, Virginia Tech, Blacksburg, VA, USA.

Al-Qadi, I. L., Brandon, T. L., and Bhutta, S. A. (1997) "Geosynthetically Stabilized Flexible Pavements," *Geosynthetics '97*, IFAI, Long Beach, CA, USA, pp. 647-662.

Brandon, T. L., Al-Qadi, I. L., Lacina B. A., and Bhutta S.A. (1996) "Construction and Instrumentation of Geosynthetically Stabilized Secondary Road Test Sections," *Transportation Research Record*, No. 1534, Washington, D.C., USA, pp. 55-57.

Jorenby, B. N. and Hick, R. G. (1986) "Base Course Contamination Limits," *Transportation Research Record*, No. 1095, Washington, D.C., USA, pp. 86-102.

Koerner, R. M. (1994) *Designing With Geosynthetics*, 3rd Edition, Prentice-Hall Inc., Englewood Cliffs, NJ, USA.

Koerner, R. M. and Koerner, G. R., (1994) *Separation: Perhaps The Most Underestimated Geotextile Function*, Geotechnical Fabrics Report, Industrial Fabrics Association International, St. Paul, MN, USA, pp. 4-10.

Laier, H. and Brau, G. (1986) "The Use of Geotextile in Road Construction under Intensive Dynamic Loading," *Third International Conference on Geotextiles*, Vienna, Austria, pp. 995-1000.

Smith, T. E., Brandon, T. L., Al-Qadi, I.L, Lacina, B. A., Bhutta, S.A., and Hoffman, S. (1995) *Laboratory Behavior of Geogrid and Geotextile Reinforced Flexible Pavements*, The Charles E. Via, Jr. Department of Civil Engineering, Virginia Tech, Blacksburg, VA, USA.

Yoder, E. J. and Witczak, M. K (1975) *Principles of Pavement Design*, 2nd Edition, John Wiley and Sons, Inc., New York, NY, USA.

Geosynthetic-Reinforced Pavements: Overview and Preliminary Results

S.W. Perkins
Assistant Professor, Department of Civil Engineering, Montana State University, Bozeman, Montana, 59717, U.S.A.

M. Ismeik
Postdoctoral Research Associate, Department of Civil Engineering, Montana State University, Bozeman, Montana, U.S.A.

M.L. Fogelsong, Y. Wang, E.V. Cuelho
Graduate Research Assistants, Department of Civil Engineering, Montana State University, Bozeman, Montana, U.S.A.

ABSTRACT: Montana State University (MSU), with support from the Montana Department of Transportation (MDT), has initiated a laboratory and analytical based research program to study and quantify the benefits derived by the addition of geosynthetics to the base course layer of flexible pavements, where the function of the geosynthetic is one of reinforcement. The objectives of the study are to verify previous work showing the positive benefit of using geosynthetics for base course reinforcement, to quantify the stress-strain response of laboratory-scale reinforced pavement test sections such that mechanisms of reinforcement can be more clearly understood and described, and to develop a comprehensive methodology for the design of such pavements. The purpose of this paper is to describe on-going research work at MSU, plans for laboratory testing and analytical modeling, and to present preliminary results from several completed test sections. Details of the test facility and instrumentation used to quantify behavior are presented.

KEYWORDS: Pavements, Base Course, Reinforcement, Laboratory Tests, Geogrids, Geotextiles

1 INTRODUCTION

Geogrids and geotextiles have been examined and used in practice for reinforcement of the base course layer of flexible pavements for over the past sixteen years, with both successes and failures having been reported. Early attempts using geotextiles (Brown et al., 1982; Ruddock et al., 1982; Halliday and Potter, 1984) indicated very little improvement in rut development characteristics that could be attributed to geotextile reinforcement. For studies involving both geogrids and geotextiles, Anderson and Killeavy (1989), Barksdale et al. (1989) and Cancelli et al. (1996) have demonstrated that geogrids are superior to geotextiles when used as a reinforcement member, while Al-Qadi et al. (1994) showed that superior performance was seen when a geotextile was used.

These studies involving both materials have provided insight into the importance of the roles of separation and filtration and the ensuing effect on reinforcement potential. The only study available where appreciable mixing of the base course and subgrade soils in control sections was noted (Al-Qadi et al., 1994) also corresponds to the one showing superior performance by the geotextile. Other studies exhibiting more moderate amounts of mixing, and indicative of conditions for which separation and filtration functions were not as critical (Anderson and Killeavy, 1989; Barksdale et al., 1989) indicate that improvement due to geogrid reinforcement can still be observed, but perhaps not to the extent had separation and filtration functions been incorporated into the section designs. On the other extreme, studies exhibiting no problems with mixing (Cancelli et al., 1996; Collin et al., 1996; Haas et al., 1988; Mirua et al., 1990; Moghaddas-Nejad and Small, 1996; Webster, 1993) have demonstrated significant improvement with geogrid reinforcement for properly designed sections.

Improvement in pavement performance has been observed in laboratory-scale experiments involving stationary circular plates to which a cyclic load has been applied (Cancelli et al., 1996; Haas et al., 1988; Miura et al., 1990), test tracks incorporating moving wheel loads (Barksdale et al., 1989; Collin et al., 1996; Moghaddas-Nejad and Small, 1996; Webster, 1993) and full-scale roads constructed with normal construction equipment (Anderson and Killeavy, 1989; Mirua et al., 1990). Improvement has been defined in terms of an extension of the life of the pavement, or the amount by which the base course layer could be reduced such that equivalent performance is seen. Reinforced pavements have been shown to have a life typically 3 to 10 times that of a similar unreinforced section, while a reduction of base thickness ranging from 22 to 50 % has been observed. Performance has typically been measured in terms of accumulated rut depth with increasing load cycle application.

Improvement has been seen for all levels of rut depth below that corresponding to an inoperable condition (25 mm). Measurement of strain on geogrid layers has shown that strain is developed immediately upon the first load application and well before any appreciable rut is developed in the pavement, provided the reinforcement was properly placed in the base layer. Strain measurements have indicated that these materials are engaged in a tensile capacity and that the level to which strain develops is closely related to the amount of improvement observed. These results indicate that this application is well suited for flexible pavements which cannot tolerate significant surface deformations and remain operational. Perkins and Ismeik (1997) have provided a more comprehensive review of studies addressing this application.

Despite the positive successes reported from field and laboratory based studies, this application has not been widely applied in practice and its use has been discouraged by a number of state departments of transportation. The overriding obstacle preventing the use of this application lies in the absence of an accepted design technique which accounts for the variables believed to control pavement performance. MSU, with support from the MDT and Federal Highway Administration, has initiated a laboratory and analytical based research program to study and quantify the benefits derived by the addition of geosynthetics to the base course layer of flexible pavements, where the function of the geosynthetic is one of reinforcement. The objectives of the study are to verify previous work showing the positive benefit of using geosynthetics for base course reinforcement, to quantify the stress-strain response of laboratory-scale reinforced pavement test sections such that mechanisms of reinforcement can be more clearly understood, and to develop a comprehensive methodology for the design of such pavements. The step from the observation of behavior in laboratory experiments to the development of a design solution will be accomplished through the development of a finite element model of a reinforced pavement. Once the model is shown to reasonably match the behavior observed in the laboratory experiments, the model will be used in a parametric study to evaluate the influence of variables thought to impact reinforced pavement performance. The purpose of this paper is to describe the on-going research work at MSU, the plans for laboratory testing and analytical modeling, and to present preliminary results from several completed laboratory test sections.

2 OVERVIEW OF RESEARCH PROGRAM

The MDT faces conditions in the eastern portion of the state where quality gravel sources for road construction are scarce and associated haul costs of such material are high. Subgrade conditions in this region consist of A-6 to A-7 soils, resulting in relatively low subgrade support values and relatively thick base course sections. Faced with these conditions, MDT has been interested in investigating the possible use of geosynthetics as reinforcement in the base course layer. MSU developed an early plan to construct a series of full-scale test sections along an existing or new roadway with these sections containing electronic instrumentation to measure pavement response. To investigate the suitability of proposed instrumentation and installation techniques, a pilot test section was constructed in the Summer of 1995 with results reported by Perkins and Lapeyre (1996, 1997).

The results of this instrumentation study indicated that excessive uncertainty existed in the installation and operation of instrumentation in an outdoor, field-scale test site and that successful completion of the originally planned approach was questionable. An alternate approach was then proposed where similar instrumentation used in the pilot test section would be used along with new devices to monitor the behavior of test sections constructed in a laboratory setting. This facility is described in this paper and essentially consists of a large reinforced concrete box in which pavement test sections are individually constructed and loaded with a 40 kN load cyclically applied to a 305 mm diameter circular plate resting on the pavement surface. The pavement test sections contain an extensive array of instruments to measure stress, strain, moisture content and temperature. Stress and strain response is measured in the pavement layers both during a dynamic load cycle and between load cycles to monitor the accumulated response with increasing load cycle.

It is anticipated that between 10-15 sections will be constructed and loaded over the course of the study. Geosynthetic type (geogrid versus geotextile), geosynthetic position within the base layer, subgrade type and strength and stiffness characteristics, and base and asphalt concrete (AC) thickness are anticipated as variables to be included in the study. The variables included in these sections are not intended to cover all possible pavement configurations but rather are intended to provide a description of response for a representative cross section of variables. The modeling portion of the study is intended to be used to supplement the experimental data by providing analytical predictions of behavior for those conditions not physically tested.

In conjunction with the experimental portion of the study, a finite element model of the laboratory-scale pavement sections is being developed. The model is being developed to match the stress, strain and deflection response observed in the 10-15 experimental test sections. Once confidence in the model is developed by this step, the model can be used to predict response of a wide range of pavement configurations for which experimental data is not available. Results from this parametric study will then be combined to form a design methodology suitable for use by flexible pavement designers. The form of this design methodology has not been defined at this point, but will most likely consist of simple equations and design charts which account for the variables found to be most influential on reinforced pavement response.

The modeling portion of the study is being accomplished through the use of a commercial finite element program and user defined material constitutive laws. Haas et al. (1988) and Miura et al. (1990) showed that in a similar test arrangement, tensile strains as great as 1.8 % were observed in geogrid reinforcement for surface rut depths less than 25 mm. Cyclic tension tests performed by Bathurst and Cai (1994) and preliminary tests performed by the authors indicate that for strains of this magnitude, simple isotropic linear elastic material models are inadequate. In anticipation of the need to predict strains of this magnitude, a series of monotonic, cyclic and sustained load tests are being performed on the geogrid and geotextile being used in this study. The monotonic load tests are being used to define the orthotropic elastic-plastic properties of the materials, where the in-plane shear modulus is thought to be particularly important in defining pavement response. Sustained load tests will provide intrinsic creep properties of the geosynthetics. Cyclic tension tests will be used to calibrate a non-linear, combined isotropic/kinematic hardening model which will model the ratchetting effect observed in repeated load tests. Ratchetting refers to the accumulation of plastic strain with increasing load cycle number for cyclic tests performed under constant load amplitude.

Ratchetting effects are also observed under compressive deviatoric loads in soil materials and will be modeled through the use of a bounding surface plasticity model. An interface model will be used between the base soil and the geosynthetics and will consist of a simple elastic-plastic Coulomb type friction law. It is anticipated that the elastic stiffness response will need to be normal stress dependent. The interface model will be calibrated from pull-out tests where the pull-out arrangement will be modeled as a boundary-value problem using the finite element model being developed. A standard viscoelastic model will be used for the asphalt concrete.

The research approach of collecting data from experimental test sections, using a model to match the observed behavior, using the model in a parametric study to examine the influence of a wide range of variables and using these results to establish a design solution to the problem is being applied to laboratory-scale experiments under stationary load conditions. Part of the reason for first exercising this approach in the laboratory is to establish its feasibility. Recognizing that different behavior is to be expected under conditions of a moving wheel load, if this approach is found to be successful, the authors intend to pursue an additional phase to the project where experiments are conducted in a test-track facility where more realistic loads can be applied to the pavement. The same research approach can then be applied, with the resulting design solution reflecting the moving wheel load case.

The remainder of this paper describes the laboratory test facility developed to evaluate reinforced flexible pavements under idealized load conditions. Preliminary results from a geogrid reinforced section and an unreinforced section are presented. These results are preliminary in that the primary function of the sections was to examine the performance of the proposed instrumentation and installation techniques. For this reason, the full array of instruments planned for subsequent sections was not included. While care was taken to make the two sections as comparable as possible, minor differences as noted existed.

3 LABORATORY TEST FACILITY

3.1 Test Box and Loading Arrangement

Laboratory-scale pavement test sections are being constructed in a reinforced concrete box having inside dimensions of 2 m by 2 m in plan and 1.5 m in height. The box consists of four sides having an open bottom and with the concrete laboratory floor serving as the bottom face. The front face of the box is removable to facilitate excavation of the test section.

Two I-beams were set into the wall forms prior to the placement of wet concrete. The I-beams were placed parallel to each other along opposite walls perpendicular to the front wall. The upper flanges of each I-beam act as rails for the load frame to move along.

The load frame consists of an additional two I-beams which span between the two I-beams embedded in the concrete wall. The ends of the load frame I-beams are attached to a carriage assembly allowing the load frame to roll from the front to the back of the box. Attached to the two load frame I-beams is a second carriage assembly upon which the load actuator is mounted. This second carriage assembly allows the load actuator to roll along the load frame I-beams, hence allowing the load actuator to move from side to side in the box. The two carriage assemblies allow the load actuator to be positioned at any point along the plan dimensions of the box. Figure 1 shows a photograph of the box and load frame.

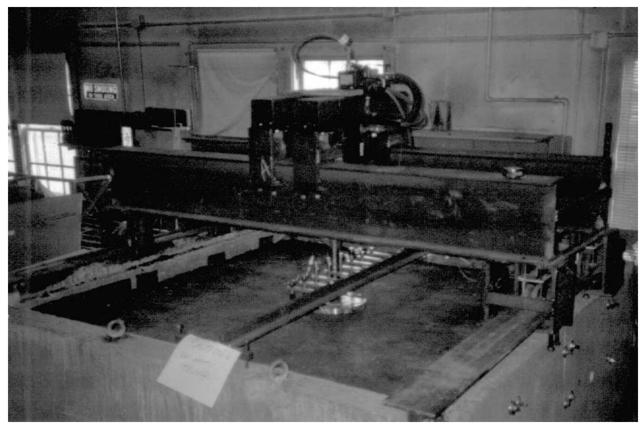

Figure 1. Test box and load frame.

The load actuator consists of a 305 mm diameter bore pneumatic cylinder with a 75 mm stroke. The threaded end of the actuator's piston is attached to a load cell having a range of 90 kN. A 55 mm diameter steel rod is attached to the other side of the load cell and extends down to and rests on a 305 mm diameter steel plate having a thickness of 25 mm. The end of the rod resting on the steel plate is rounded and sits inside a similar shaped recess in the plate, thus allowing the plate to rotate during loading. A waffled rubber pad 4 mm in thickness is placed between the steel plate and the AC surface to aid in providing a uniform pressure distribution on the AC surface.

A pneumatic binary regulator is used to control the time-history of air pressure supplied to the load cylinder. The pneumatic regulator is in turn controlled by a computer which sends a series of binary signals to the regulator's four solenoid valves allowing the division of the single inlet pressure into any one of fifteen equally spaced outlet pressures. Control of the binary signals is provided by the same software used for data acquisition.

Inlet pressure to the binary regulator is controlled and monitored by a standard gage and regulator. The binary regulator allows for any shaped load pulse to be specified and approximated by fifteen points for each of the ascending and descending portions of the pulse. Due to the limited number of points available for approximating load pulse curves, a simple triangular pulse with a linear rise time, a hold time at peak load, a linear fall time and a pause time between pulses has been specified. Two pulse durations of 0.5 and 1 Hz have been used, with times for the periods described above being 0.6, 0.3, 0.6 and 0.5 s for the 0.5 Hz pulse and 0.3, 0.2, 0.3 and 0.2 s for the 1 Hz pulse. Inlet pressure to the binary regulator has been set to give a peak load of 40 kN, corresponding to a load plate pressure of 550 kPa.

Two types of loads were applied to the pavement. The first type consisted of the application of a single load pulse at 25 different locations within the box. Application of these loads allowed for the careful examination of response from the different sensors. The second type of load consisted of a series of repeated loads when the load plate was placed at the center of the box. The 1 Hz load pulse was used for the repeated cycle tests for both sections 1 and 2 and the single pulse tests for section 2. The 0.5 Hz pulse was used for the single pulse tests for section 1.

3.2 Pavement Layer Materials and Thickness

The preliminary test sections reported in this paper used a slow curing cold mix asphalt concrete. This material was used due to the unavailability of hot mix asphalt during the time period in which the preliminary test sections were constructed. Hot mix asphalt is being used for subsequent test sections. The cold mix was heated in a mobile trailer-mounted oven prior to placement and compaction. Compaction was accomplished by a hand-operated vibratory plate compactor. Compacted thickness of the AC layer for sections 1 and 2 were 70 and 75 mm, with bulk density values of 21 and 22 kN/m^3, respectively. Results of laboratory tests on the cold mix asphalt are given in Table 1. A grain size distribution of the aggregate used in the mix is given in Figure 2.

A crushed stone base course meeting the MDT specifications for crushed top surfacing, type A, grade 3 is being used for all test sections. The grain size distribution for the material is shown in Figure 2, where it is seen that 100 % of the material passes the 19 mm sieve.

Sections 1 and 2 contained a compacted base section thickness of 200 mm. The material was compacted at a water content ranging between 5 to 6.5 %, resulting in dry density values of 21 kN/m^3. Measurement of dry density and water content during excavation of the sections indicated that the water content dropped to 4.5 to 5 % with the dry density remaining essentially unchanged.

A fine silty sand consisting of the fines trapped in the baghouse of a hot mix plant were used for the subgrade. The material has 40 % fines with a liquid limit of 18 % and a plastic limit of nearly the same value, classifying the material

Table 1. Cold mix asphalt concrete properties.

Property	Section	
	1	2
Marshall stability, lb (T-245)	9620	9620
Marshall flow (T-245)	15	15
Density, g/cm^3 (T-245)	2.31	2.31
Asphalt content, % (T-164)	5.0	5.0
Rice specific gravity (T-209)	2.48	2.48
Air voids, %	17.9	13.8
Penetration (T-49)	51	51
Kinematic viscosity (T-201)	554	554
Specific gravity of aggregate	2.61	2.61

Note: T designations refer to AASHTO test specifications

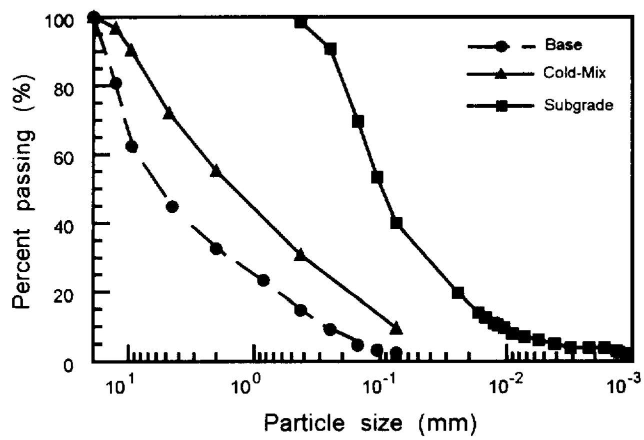

Figure 2. Grain size distributions of AC aggregate, base and subgrade.

as a SM or A-4. A grain size distribution of the material is given in Figure 2. Modified Proctor compaction tests indicate that the material has a maximum dry density of 18.2 kN/m^3 occurring at a water content of 11.5 %. The material was compacted in the box at a water content of 14.5 % and at an average dry density of 17.5 kN/m^3. Laboratory CBR tests on this material at this water content and dry density and in-situ Dynamic Cone Penetration (DCP) tests indicate a CBR of approximately 15. This material was not replaced between sections 1 and 2. Only the asphalt concrete, base and geogrid were removed between sections 1 and 2.

Section 1 contained an extruded, polypropylene, biaxial geogrid placed in the base course at a level of 40 mm above the base course - subgrade interface. The geogrid has a mass per unit area of 215 g/m^2, an aperture size of 25 by 33 mm in the machine and cross-machine directions, respectively, and a wide-width ultimate tensile strength of 13 and 20 kN/m in the machine and cross-machine directions, respectively. Section 2 was unreinforced.

The remaining test program will use hot mix asphalt for all sections. A second subgrade consisting of a highly plastic clay will be used for approximately one-half of the program with the silty sand being used for the other half. The clay will be prepared at a water content to produce a weak subgrade having a CBR of approximately 3-4. A woven geotextile will also be incorporated into the test program. Other variables to be included are base course and asphalt concrete thickness, and geosynthetic position.

3.3 Instrumentation

The two preliminary test sections described in this paper contained a limited number of instruments compared to sections which are currently being constructed with hot mix asphalt. The primary purpose of these preliminary test sections was to examine the performance and installation procedures of instruments to be used in later sections. The two sections discussed in this paper contained one asphalt concrete strain gage, 12 soil pressure cells, 8 soil strain gages and four foil strain gages mounted to the geogrid specimen in section 1. In addition, 8 LVDT's were used to monitor surface deformation of the asphalt concrete layer and the load cell was used to monitor applied load.

The single AC strain gage was used only in section 2. The strain gage was a H-type gage marketed by Dynatest. The gage was placed at the bottom of the AC layer. The stress cells placed in the base course and subgrade were also marketed by Dynatest and have a diameter of 68 mm and a thickness of 13 mm. Cells having two different ranges of 200 and 825 kPa were used. Four stress cells were placed in the base course layer, two being oriented to measure vertical stress and two to measure stress in the horizontal direction. The centerline of the stress cells was 120 mm below the top of the base course layer and were placed at a radius of 400 mm from the center of the box. The two cells measuring horizontal stress were oriented to measure stress in the radial direction when the load was placed in the middle of the box. Four stress cells were also placed in the upper portion of the subgrade at a distance of 130 mm below the top of the subgrade (level 1) and in a similar configuration as those contained in the base. Two additional cells were placed at levels of 430 mm (level 2) and 705 mm (level 3) below the top of the subgrade. At each level, one cell was placed at a radius of 400 mm to measure vertical stress while the other was placed to measure radial stress at this same radius.

Strain in the base and subgrade soils was measured using a LVDT mounted between rectangular end plates measuring 15 by 50 mm and 5 mm thick. The gage length between the end plates was nominally 80 mm. Four LVDT's were placed in the base course and four in the top layer of the subgrade in a similar configuration to the stress cells placed at these two levels.

On the geogrid used in section 1, four bonded resistance (foil) strain gages were placed on ribs located at a radius of 400 mm from the center of the box. Two gages were placed to measure radial strain in the machine direction of the geogrid while the other two were placed to measure radial strain in the cross-machine direction when the load was placed in the center of the box. The geogrid was placed 40 mm above the bottom of the base.

Data acquisition and control has been established to control the time-history of the load application and to trigger the collection of data. Two types of tests were performed on each section. After the construction of a section, the load frame was moved to 25 different points within the box to apply a single pulse of load. The full time history of each sensor was collected for each of the 25 locations. Once these tests were completed, the load plate was moved to the center of the box where a repeated load was applied. During the application of this repeated load, the peak and baseline reading of each instrument was measured and collected for the majority of the applied load cycles. The baseline reading corresponds to a time when no load was applied to the pavement and represents a permanent response corresponding to that particular load cycle, while the peak reading corresponds to a time when the peak load was applied. In addition to this data, the full time history of each sensor was measured for specified load cycle numbers.

4 EXPERIMENTAL RESULTS

4.1 Transient Response To A Single Load Pulse

At each of the 25 load locations, three separate single pulse load tests were conducted. Figure 3 illustrates three load traces from one of the 25 load locations for sections 1 and 2, where the shape of the load pulse curve is identical for each of the three applications. The spike on the descending branch of the curve is due to some small feedback in the binary control valve. Figure 4 illustrates the time-history response of stress cells located in the base and subgrade for sections 1 and 2 when the load was applied directly above the sensor. The data shows that in the base the vertical stress was slightly higher in the reinforced section, while in the subgrade the stress was slightly less. Figure 5 shows the time-history of radial stress in the base and subgrade when the load was applied at a radius of 310 mm from the sensor.

The peak response of stress cells located in the base layer and oriented to measure vertical, radial and tangential stress were recorded from various time-history records as the load was applied at different locations. Figure 6 illustrates the variation in these peak measurements with respect to the lateral distance from the load plate to the sensor, where positive stresses correspond to compression. For each stress parameter and at each lateral location, three data points are given corresponding to the three tests performed at that location. Figure 6 illustrates the reproducibility of the results.

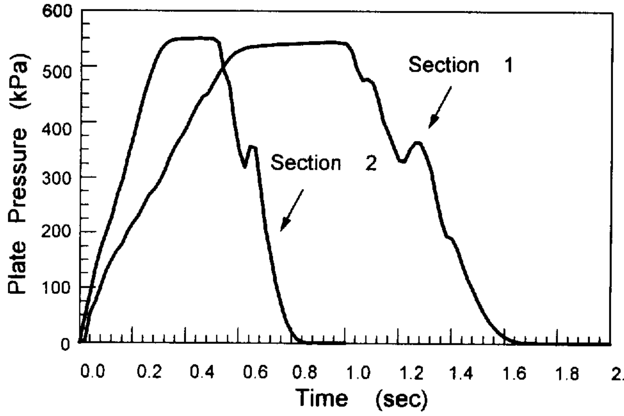

Figure 3. Load pulse time-history.

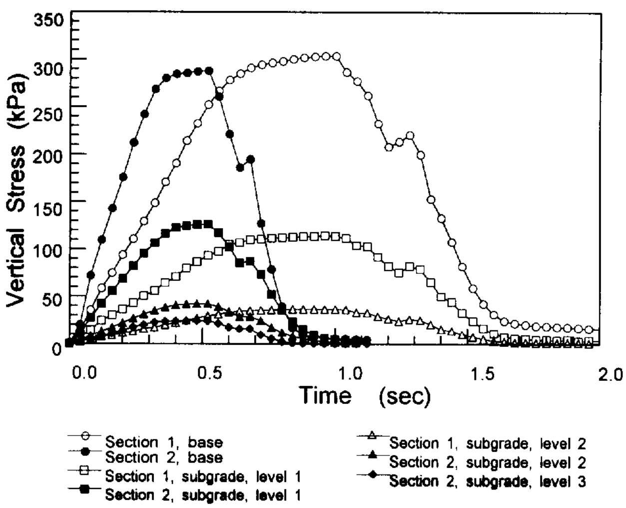

Figure 4. Vertical stress time-history in base and subgrade.

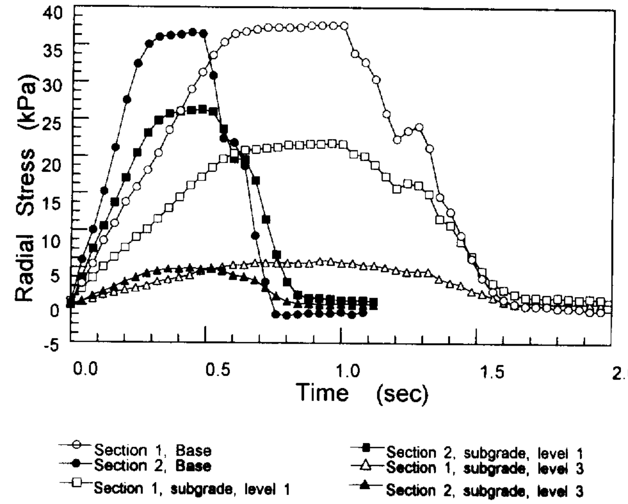

Figure 5. Radial stress time-history in base and subgrade.

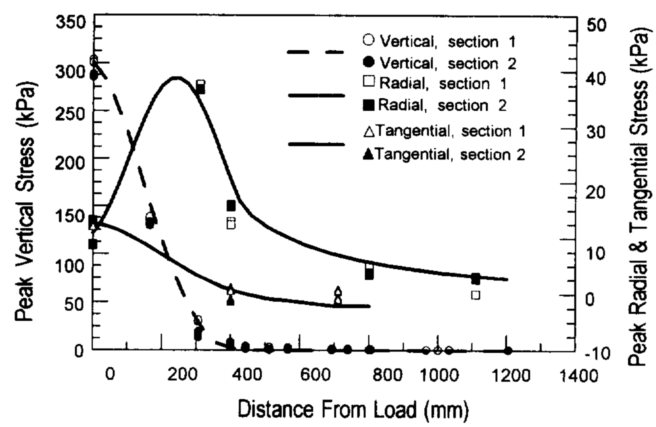

Figure 6. Peak vertical, radial and tangential stress in base.

The curves shown in Figure 6 correspond to general trends sketched to match the available data points and were not developed from rigorous analyses. This is also true for the curves shown in Figures 7 and 8.

Figure 7 shows results of vertical, radial and tangential strain in the base in a similar fashion as Figure 6, where positive strain corresponds to contraction. Figure 7 shows more scatter than Figure 6 and is due mainly to the influence of compaction induced during the first and second load applications on the subsequent load applications at that same location.

Figure 8 illustrates radial and tangential strain induced in the geogrid in section 1 due to single load pulses applied at various locations, where positive strains correspond to tension. The results indicate that as much as 0.17 % tensile strain is induced in the geogrid immediately below the centerline the load. Radial tensile strains quickly vanish to zero at a radius of approximately 200 mm, which is 50 mm greater than the radius of the load plate. Beyond this region strains become compressive, reaching a peak compressive strain at a radius of approximately 300 mm, whereafter they approach zero. In the tangential direction, the strains are seen to be in tension for all points away from the load and approach zero at a radius of 800 mm.

The results shown in Figure 8 have the same trend as the results for radial and tangential strain in the base shown in Figure 7, indicating that in regions where the base experiences extensional strains, the base interacts with the geogrid to transfer tension to the reinforcement. These results indicate that the primary function of the geogrid is in preventing lateral spread of the base course and that anchorage of the geogrid is not needed in such an application.

4.2 Transient and Permanent Response to Multiple Load Cycles

Upon completion of the single pulse tests, the load plate and frame were moved to the center of the box where a repeated load was applied. The mean and standard deviation of the

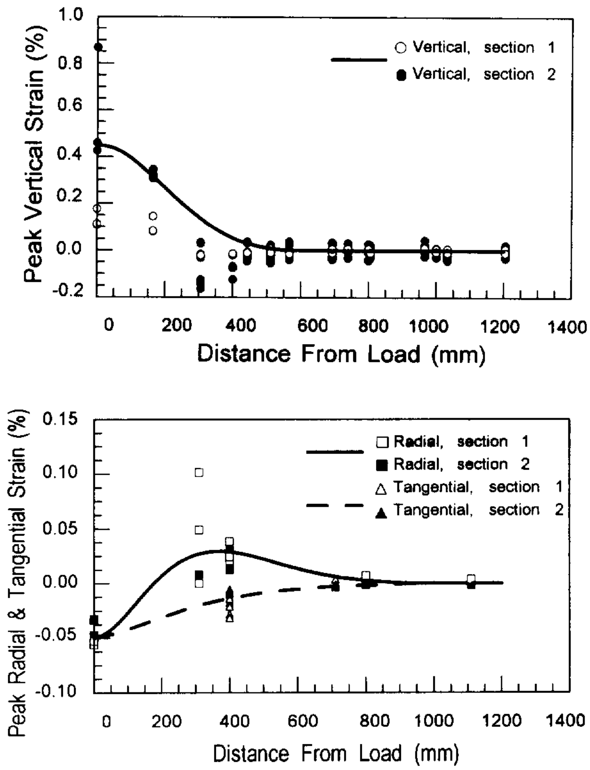

Figure 7. Peak vertical, radial and tangential strain in base.

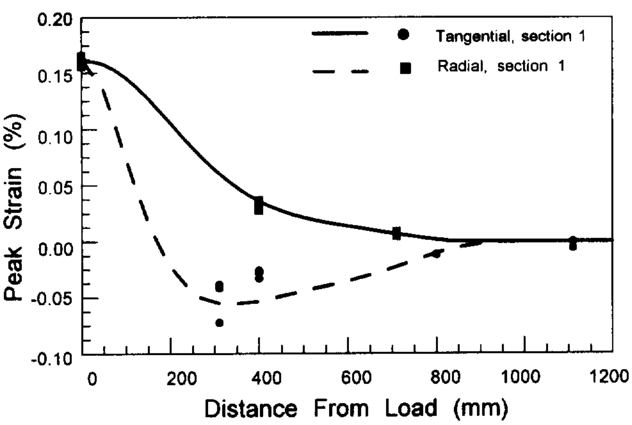

Figure 8. Peak radial and tangential strain in geogrid.

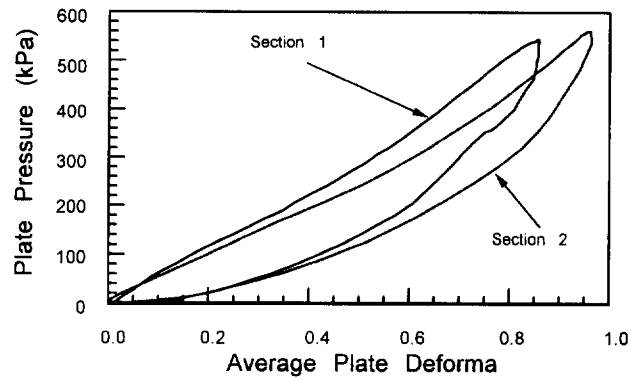

Figure 9. Load versus deformation for first cycle.

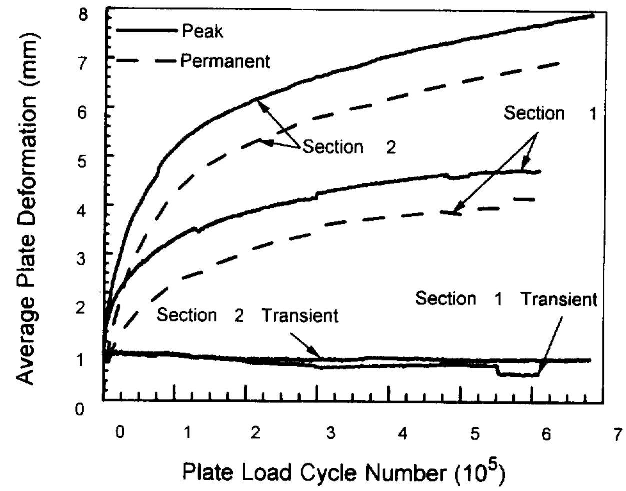

Figure 10. Deformation versus cycle number.

applied pressure was 548 and 4.0, and 550 and 4.3 for sections 1 and 2, respectively. Figure 9 shows the plate pressure versus average plate deformation observed during the first load application for sections 1 and 2. Figure 10 shows the development of surface deformation with load cycle number, where for each section three curves provided. The "peak" curve corresponds to the average plate deformation measured at the point in time where the applied load reached a maximum for that cycle. The "permanent" curve corresponds to the deformation immediately prior to when the load was applied. The "transient" curve corresponds to the difference between the "peak" and "permanent" curves and represents the dynamic or transient deformation for each load cycle. Figure 9 indicates that the dynamic stiffness of section 1 is slightly greater than section 2 for the first load cycle. The transient response Figure 10 shows that both sections become slightly more stiff with increasing load cycle, with section 1 experiencing a slightly greater increase in stiffness for load cycle numbers greater than 250,000 as compared to section 2. Section 2 shows a more rapid rate of rut depth than section 1, while section 1 appears to have reached a plateau when the rut depth in section 2 continues to increase linearly with cycle number.

Visual inspection of the asphalt from sections 1 and 2 indicated that the asphalt in section 1 was more stiff and less susceptible to flow than that in section 2 even though the laboratory results, including the Marshall and penetration tests, indicate that the materials were identical and the density and thickness in section 2 were greater than section 1. Temperature of the asphalt prior to compaction was not measured, but it is believed that this is the main difference between the materials causing the behavior observed. Thus it is not clear if the geogrid in section 1 is responsible for the improvement in behavior observed or if the improvement is due to the difference in asphalt. The additional sections being constructed as part of this project will clarify this point.

5 CONCLUSION

Preliminary results from a study designed to examine the reinforcement function of geosynthetics in flexible pavements have indicated the compatibility between extensible strains in the base and the development of tensile strain in the geogrid, indicating the reinforcement function of the material. The comparison of stress and strain measures in the soil layers indicated only slight differences between a reinforced and unreinforced section for the application of a single load pulse. This is to be contrasted against the significant difference observed in rut development for repeated cycle tests, indicating that examination and modeling of repeated load behavior is necessary to understand the mechanisms of reinforcement. Additional work being performed by the authors will help illustrate these mechanisms for pavement variables believed to influence performance.

ACKNOWLEDGMENTS

The authors gratefully acknowledge the financial support of the Federal Highway Administration and the Montana Department of Transportation through contract number 8106 and the Tensar Corporation for the donation of geogrid material.

REFERENCES

Al-Qadi, I.L., Brandon, T.L., Valentine, R.J., Lacina, B.A. and Smith, T.E. (1994) "Laboratory Evaluation of Geosynthetic Reinforced Pavement Sections" *Transportation Research Record* 1439, Washington DC., USA, pp. 25-31.

Anderson, P. and Killeavy, M. (1989) "Geotextiles and Geogrids: Cost Effective Alternate Materials for Pavement Design and Construction", *Proceedings of the Conference Geosynthetics '89* , San Diego, CA, USA, pp. 353-360.

Barksdale, R. D., Brown, S. F. and Chan, F. (1989) "Potential Benefits of Geosynthetics in Flexible Pavement Systems", *National Cooperative Highway Research Program Report No. 315* , Transportation Research Board, National Research Council, Washington DC, USA.

Bathurst, R.J. and Cai, Z. (1994) "In-Isolation Cyclic Load-Extension Behavior of Two Geogrids", *Geosynthetics Intentional*, Vol. 1, No. 1, pp. 1-19.

Brown, S.F., Jones, C.P.D. and Brodrick, B.V. (1982) "Use of Non-Woven Fabrics in Permanent Road Pavements", *Proceedings of the Institution of Civil Engineers*, London, UK, Part 2, Vol. 73, pp. 541-563.

Cancelli, A., Montanelli, F., Rimoldi, P. and Zhao, A. (1996) "Full Scale Laboratory Testing on Geosynthetics Reinforced Paved Roads", *Proceedings of the International Symposium on Earth Reinforcement*, Fukuoka/Kyushu, Japan, November, Balkema, pp.573-578.

Collin, J. G., Kinney, T. C. and Fu, X. (1996) "Full Scale Highway Load Test of Flexible Pavement Systems With Geogrid Reinforced Base Courses", *Geosynthetics Intentional*, Vol. 3, No. 4, pp. 537-549.

Haas R., Wall, J., and Carroll, R.G. (1988) "Geogrid Reinforcement of Granular Bases in Flexible Pavements," *Transportation Research Record* 1188, Washington DC, USA, pp. 19 - 27.

Halliday, A.R. and Potter, J.F. (1984) "The Performance of a Flexible Pavement Constructed on a Strong Fabric", *Transport and Road Research Laboratory, Report 1123*, Crowthorne, Berkshire, UK, 15 p.

Miura, N., Sakai, A., Taesiri, Y., Yamanouchi, T. and Yasuhara, K. (1990) "Polymer Grid Reinforced Pavement on Soft Clay Grounds", *Geotextiles and Geomembranes*, Vol. 9, pp. 99-123.

Moghaddas-Nejad, F, and Small, J. C. (1996) "Effect of Geogrid Reinforcement in Model Track Tests on Pavements", *Journal of Transportation Engineering*, Vol. 122, No.6, pp. 468-474.

Perkins, S.W. and Lapeyre, J.A. (1996) "*In-Field Performance of Geosynthetics Used To Reinforce Base Layers; Phase I: Instrumentation Selection and Verification*", Report No. FHWA/MT-96/8126-1, U.S. Department of Transportation, Federal Highway Administration, Washington, DC, USA, 160p.

Perkins, S.W. and Ismeik, M. (1997) "A Synthesis and Evaluation of Geosynthetic Reinforced Base Layers in Flexible Pavements: Experimental Work", *Geosynthetics International*, Vol.4, No.6.

Perkins, S.W. and Lapeyre, J.A. (1997) "Instrumentation of a Geosynthetic - Reinforced Flexible Pavement System", *Transportation Research Record* 1596, Washington, DC, USA.

Ruddock, E.C., Potter, J.F. and McAvoy, A.R. (1982) "A Full-Scale Experiment on Granular and Bituminous Road Pavements Laid on Fabrics", *Proceedings of the Second International Conference on Geotextiles*, Las Vegas, Nevada, USA, Vol. 2, pp. 365-370.

Webster, S. L. (1993) "Geogrid Reinforced Base Courses For Flexible Pavements For Light Aircraft, Test Section Construction, Behavior Under Traffic, Laboratory Tests, and Design Criteria", *Technical Report GL-93-6*, USAE Waterways Experiment Sta., Vicksburg, MS, USA, 86 p.

Cost Versus Reinforcing Effectiveness of Geotextiles in Pavement Works in Greece

A.G. Kokkalis
Assistant Professor, Democretus University of Thrace, Civil Engineering Department, 67100 Xanthi, Greece

ABSTRACT: Geotextile reinforced pavements might be both economically and technically advantageous over their conventional counterparts, especially under poor subgrade conditions. In this paper a systematic method of estimating possible cost implications of including a geotextile in the subgrade-subbase interface are discussed. The cost evaluations are obtained on the basis of the thickness of the aggregate layer which can be replaced by the geotextile been laid in the pavement-subgrade interface, so that the two structure have identical load-deformation behavior. The load-deformation behavior is evaluated by regression formulas, which have been derived from pavement finite element analysis and verified through field experiments. Reinforced pavements might provide numerous others indirect savings and conveniences, such as a more solid roadbed, a shorter construction time, ease in construction methods, savings in maintenance costs, higher factors of safety, acceptability of marginal materials etc. These factors were not included in this economic evaluation and all promote the reinforced alternative. The results obtained have been verified in several case studies.

KEYWORDS: Geotextiles, Reinforcement, Pavements, Unpaved roads, Road construction

1 INTRODUCTION

Geotextiles have already a 25-years history of successful applications in many fields of geotechnical engineering. A field of particular interest is that of highway and pavement works. In Greece the first relevant application of geotextiles took place in a highway in Peloponnese in 1977. Since then geotextiles established a widespread use in pavement engineering works. Nowadays, they are systematically used in most major highway schemes, like the Patra-Athens-Thessaloniki-Border and the Egnatia motorways. This constantly increasing application rate urged for a systematic analysis of the effectiveness of geotextile inclusion in a pavement system and the cost implications this involves.

A research activity concerning the reinforcing and other beneficial actions of geotextiles been laid in the pavement-subgrade interface was run at the Aristotle University of Thessaloniki since 1985 and at the Democretus University of Thrace lately.

2 REINFORCING ACTION OF GEOTEXTILES

A geotextile been laid at the subgrade-subbase interface fulfills any one of the actions of reinforcement, separation, filtration and in few cases drainage. It should be mentioned that in most cases more than one of the above functions act simultaneously. Of interest for this paper is the reinforcement function. This function is expressed, as a rule, in a dual manner, i.e. lateral restraint and membrane action. Membrane action is the most obvious one: as the pavement is deformed by the loads, the geotextile been laid on the top of the subgrade is also deformed. Assuming that no slip occurs the geotextile is strained. The vertical constituent of the stresses developed balance part of the applied load. At the cost of substantial displacement and ignoring the parameter of creep relaxation, the ultimate loading of the system can markedly increase (Sellmeijer 1993; Espinoza 1994). However, it has become obvious that the membrane effect mechanism fails to accurately predict the benefits that can be obtained from the inclusion of geotextiles at low deformations (Little 1992; Milligan et al. 1989). Non-woven products with relatively low stiffness is unlikely to produce any benefit at all if included in any membrane effect analysis. Nevertheless, experience has shown that there is a clear improvement to the performance of the pavement with the inclusion of low stiffness geotextiles. This improvement is mainly attributed to lateral restraint i.e. the stretched geotextile inhibits the lateral displacements of the aggregates. Another positive effect is that the subgrade just outside the traffic loading area is also loaded more or less vertically, through the stressed geotextile, which ensures maximum bearing capacity of the system. Furthermore, the aggregate layer acts like a beam spreading the load over a larger area. (Sellmeijer 1990, 1993). Finally, the separation and filtration functions, which the geotextile simultaneously performs, ensure the integrity, purity and stiffens of the aggregate layer which mobilize a plastic stress-strain state with higher factors of safety (Little 1992). The exact value of all these mechanisms is hard to evaluate analytically.

There are a profusion of methods for estimating the reinforcing effectiveness of geotextiles in pavements, ranging from the purely empirical to the use of finite elements models. It is the author's opinion that the latter methods, through calibration by full-scale experiments, permit any type of reinforcing action to be evaluated and included.

A finite element program was used herein to calculate the stress-strain fields in a great variety of weak pavements (which can also be considered as subbases of typical pavements) either reinforced or not with geotextiles. The program analyses the pavement-subgrade system as a three-dimensional axially symmetric multi-layered problem (Snaith et al. 1980). The wheel load is specified as a uniformly distributed pressure over a circular contact area. The boundary conditions of the system are: horizontal restrain at the lateral boundaries and both horizontal and vertical restrain at the base boundary. Material properties are specified for each layer of the system. The resilient modulus of each layer may be either linear or dependent on any number of stress regimes. The elastic analysis employs a successive over-relaxation technique to obtain the stress in each element of the finite element grid. When the elastic analysis is completed a non-iterative procedure makes use of the computed stress values and suitable creep equations to calculate the vertical permanent strain for each element. The strains are then converted to deformations and summed for each column of the grid to yield the overall surface permanent deformation profile.

The fabric has been modeled using a layer of its approximate thickness (for typical non-woven heat-bonded geotextiles their typical thickness has been taken as 1 mm). Since in practice local reinforcement of the soil structure occurs in the vicinity of the fabric, two transitional layers have been introduced, one above and one below the fabric layer having similar thickness as the geotextile itself. Thus, the abrupt change in resilient modulus between the fabric and its adjacent layers has been reduced, since these transition layers have intermediate characteristics between the fabric and the adjacent layers themselves.

A large number of the independent variables i.e. resilient modulus of geotextile, resilient modulus of subgrade and thickness of aggregate layer are then combined. Not taking into account the various numbers of load repetitions, 567 combinations as a total have been solved.

Characteristic permanent deformation profiles obtained from these pavement models are compared with those measured in the field from full scale experiments made in similar pavements. Although the deformation predicted were consistent with those measured, weighting factors were, as a rule, necessary, so that the computed values coincide with those observed in the field experiments. These calibration factors were specified for each layer.

The purpose of the field experiments involved was the determination of the load-deformation characteristics of subbases, either reinforced or not with geotextiles. Cycled plate bearing tests were carried out on the various model pavements. Model pavements were 4 by 4 meters in plan and founded on generally weak subgrades. Loads were applied through a rigid 0.3 meters diameter plate to approximate wheel load contact area. Loads also have magnitudes approximating standard wheel load and were applied on variable thickness granular pavements either reinforced or not with geotextiles. The geotextile anchorage was sufficient to ensure that no lateral slip would occur.

The results were subsequently statistically analyzed so that prediction formulas were developed through which the thickness of the granular layer could be obtained. This procedure, although it introduces inevitable inaccuracies, is preferable, since applying a prediction formula is considerably simpler than formulating and solving the finite element program for any new set of data. Additionally, it helps the study of the economic consequences of pavement geotextile reinforcement. However, it should be constantly kept in mind, (Palmeira and Cunha 1993; Douglas and Valsangar 1991) that it is difficult to predict geotextile reinforced pavement deformation by simple relationships. More detailed information for the whole procedure is given in Kokkalis, (1990).

The regression formulas obtained are, for pavements without geotextile reinforcement:

$$e_{pl} = 13.0\frac{1}{E_{SG}^{0.70}} + 18.5\frac{1}{H_{ag}^{0.63}} + 1.1(\log N)^{0.88} +$$

$$+2.2\frac{(\log N)^{1.21}}{E_{ag}^{0.88}} - 3.4, \ (R = 0.991) \tag{1}$$

$$\text{where: } E_{ag} = 0.19 H_{ag}^{0.45} E_{SG} \tag{2}$$

and in the case of geotextile reinforced pavements:

$$e_{pl} = 13.0\frac{1}{E_{SG}^{0.70}} + 18.5\frac{1}{H_{ag}^{0.63}} + 1.1(\log N)^{0.88} +$$

$$+5.1\frac{1}{E_{g}^{0.21}} + 2.2\frac{(\log N)^{1.21}}{E_{ag}^{0.88}} - 6.2, \ (R = 0.978) \tag{3}$$

$$\text{where: } E_{ag} = 0.12(\log E_g) H_{ag}^{0.45} E_{SG} \tag{4}$$

where: e_{pl} is the permanent deformation of the whole structure measured in mm, E_{SG} and E_{ag} are the resilient modulus of the subgrade and the aggregate layer respectively measured in MPa and E_g is the resilient modulus of the geotextile measured in KPa, H_{ag} is the thickness of the aggregate layer expressed in cm for equations (1) and (3) and in mm for equations (2) and (4) and N is the number of standard load repetitions applied to the pavement.

Care has been taken so that equations (1) and (3) yield consistent results.

The limitations of the formulas obtained are: $E_{SG} < 50$ MPa and $H_{ag} < 60$ cm.

A sensitivity analysis conducted on the derived formulas showed, as expected, that the single most important parameter affecting the required pavement thickness is the deformation behavior of the subgrade. Of most interest for this research is the sensitivity of the design equation to the thickness of the granular layer of the pavement and to the resilient modulus of the geotextile: permanent deformation is four times more sensitive to the parameter ''thickness of aggregate layer'' than to the parameter ''modulus of the geotextile''.

Apart from the field experiments, the whole procedure involved laboratory experiments for the determination of the interactional characteristics between the geotextile and the surrounding material, the determination of the stress-strain relationship of geotextiles when acting in isolation and when they are confined in the soil-aggregate environment of the project It is this confined resilient modulus (E_g) that has been used in the analysis. To obtain E_g a large shear box (30 X 30 cm) has been properly modified so that it could include and stress a geotextile specimen. The specimen was kept in contact with representative soil been laid underneath and graded aggregate been laid on top of the specimen. The geotextile specimen in this soil-geotextile-aggregate system was subsequently stressed whilst been compressed by loads equivalent to the traffic and dead loads which really apply to the system. Apart from few difficulties which arose and easily confronted this procedure of determining the confined stress-strain behavior of geotextiles could be regarded as successful (Kokkalis and Papacharisis 1989). From the derived stress-strain diagram, the values of E_g used were those corresponding to the actual strain the geotextile develops in situ.

3 COST IMPLICATIONS OF GEOTEXTILE INCLUSION

Geotextile reinforced pavements, apart from offering certain technical advantages, may consist an economically competent alternative as well. Numerous factors are affecting the relevant economic analysis, so that a generalized solution is unattainable. Each case study has its own prevailing economic parameters. It should be mentioned herein that, from a literature review it can be concluded, that in cases of soft subgrades, geotextile reinforced pavements usually present economic advantages.

The economic analysis of the reinforcing action of geotextile is based on the obvious fact that the stronger the geotextile, the greater the thickness of the subbase layer which could be replaced so that the two structures have identical load-permanent deformation behavior.

Apart from the substitution of part of the aggregate layer, geotextiles been laid on soft subgrades might also indirectly affect certain cost items by:

1. speeding up the construction,
2. creating a more solid working surface,
3. facilitating construction practice,
4. extending working periods,
5. reducing maintenance cost,
6. reducing vehicle operating cost,
7. making marginally rejected soil materials acceptable,
8. attaining higher factors of safety and
9. making the removal of soft surface layers not necessary.

It worth's mentioning for item 5., that maintenance cost for Greek secondary roads amounts up to 60% of the original construction cost over the whole design life of the road (Nikou 1988).

As it has been previously reported, all the above potential indirect savings are very difficult to be included in an economic analysis. In the analysis presented herein three cost items are taken into account, i.e. purchase cost of geotextiles and aggregate, transport cost and application cost. It should be commented that the application of geotextiles does not demand any specific machinery which should otherwise be included as a cost item. These three cost items have been applied to a number of pavement construction projects in Greece, where there were a geotextile inclusion. It is obvious that the range of unit costs is broad, whilst they are simultaneously critical for the results of the evaluation. Typical unit costs used are (1 ecu = 1.15 U.S. dollars):

1. purchase and transport cost of geotextiles: 1.0 ecu/m^2,
2. application cost of geotextiles: 0.1 ecu/m^2,
3. supply cost of aggregates: 0.08 ecu/m^2/cm of layer thickness,
4. transport cost of aggregates: 0.001 ecu/km/cm of layer thickness,
5. construction cost of aggregate layer: 0.02 ecu/m^2/cm of layer thickness,

From the above figures and through the equations (1) and (3) it can be derived that, assuming the mean transportation distance of aggregates as being 10 km, the reinforced pavement would be cost-effective if the geotextile could replace more than 10 cm of the thickness of the aggregate layer. This is the case when $E_{SG} < 40$ Mpa. If $E_{SG} < 25$ Mpa then the reinforced pavement becomes less expensive even if there is an adjacent source of aggregates. It is obvious that as the subgrade becomes softer, (in which case geotextile inclusion becomes more effective) and as acceptable aggregates can be only obtained from sources being farther away, geotextile reinforcement becomes economically advantageous. The economic influence of the resilient modulus of geotextile can hardly assessed, since it means both higher purchase cost and higher replacement potential. The quotation of the cases where geotextile reinforced pavements are cost effective can not be farther described, since the result depends on each specific data set.

Woven geotextiles possess much higher resilient modulus and are simultaneously more expensive. It would have been interesting to evaluate the cost efficiency of their application on the base that they, obviously, could replace a thicker layer of aggregates. However, the amount of bond that a geotextile can develop with the surrounding soil sets limits to the exploitation of very high modulus. In relevant full scale trials slip surfaces evidently developed for large deformations. It is accepted (Palmeira and Cunha 1993) that, in the long term, the use of a highly frictional medium modulus (like non-woven geotextiles) reinforcements may be capable of producing greater overall cost savings than the use of high modulus geotextiles.

4 CONCLUSIONS

The main conclusion drawn is that the cost implications of geotextile inclusion in pavements depend on the specific conditions of each project. In general, the thickness of the unbound subbase, which the geotextile could replace, costs as much as the supply and application of the geotextile itself, provided that a non-woven product is selected. Woven geotextiles present certain problems which, combined with their higher supply cost, make their application rather expensive.

The most important parameter affecting the economic analysis is the load-deformation behavior of the subgrade. As the subgrade becomes softer the geotextile inclusion solution becomes cost-effective. Availability of acceptable aggregate material is the next important parameter. The economic influence of the resilient modulus of geotextile can be hardly assessed, since it means both higher purchase cost and higher replacement potential.

It should be mentioned that the analysis is limited in the direct construction cost elements of the pavement. If other indirect savings and conveniences, such as providing a more solid roadbed, a shorter construction time, facilitation in construction methods, savings in maintenance and vehicle operating costs, increased factors of safety, acceptability of marginal materials, were included in the analysis, the economic supremacy of geotextile reinforced pavements over weak subgrades is expected to become evident.

ACKNOWLEDGEMENTS

The author is indebted to KEDE (Central Laboratory of the Ministry of Public Works) which supported the experimental procedure providing the necessary equipment and personnel. The author also wants to express its gratitude to the Civil Engineering Laboratories of the Aristotle University of Thessaloniki in which a series of experiments have also been performed.

REFERENCES

Douglas, R.A. and Valsangar, A.J. (1991) "Unpaved Geosynthetic Built Resource Access Roads: *Stiffness* Rather than *Rut Depth* as a Key Design Criterion", *Geotextiles and Geomembranes*, No. 10, Elsevier Science Limited, pp. 45-59.

Espinoza, R.D. (1994) "Soil-Geotextile Interaction: Evaluation of Membrane Support", *Geotextiles and Geomembranes*, No. 13, Elsevier Science Limited, pp. 281-293.

Kokkalis, A.G. and Papacharisis, N. (1989) "A Simple Laboratory Method to Determine In-Soil Behavior of Geotextiles", *Geotextiles and Geomembranes*, No. 8, Elsevier Science Limited, pp. 281-293.

Kokkalis, A.G. (1990) "A Theoretical and Experimental Approach to the Reinforcement of Secondary Roads", Ph.D. Thesis, *Aristotle University of Thessaloniki, Civil Engineering Department*, Thessaloniki, Greece, 560 p.

Little, P.H. (1992) "A Review of Two European Design Methods for Geotextile Reinforced Unpaved Roads", *Highways and Transportation*, Vol. 39, No. 8, Institution of Highways and Transportation, England, pp. 19-22.

Milligan, G.W.E., Jewel, R.A., Houlsby, G.T. and Burd, H.T. (1989) "A New Approach to the Design of Unpaved Roads", *Ground Engineering*, April, pp. 25-29.

Nikou, N. (1988) "A Proposal for Forest Roads Design Standards", Ph.D. Thesis, *Aristotle University of Thessaloniki, Civil Engineering Department*, Thessaloniki, Greece, 560 p.

Palmeira, E.M. and Cunha, M.G. (1993) "A Study of the Mechanics of Unpaved Roads with Reference to the Effects of Surface Maintenance", *Geotextiles and Geomembranes*, No. 12, Elsevier Science Limited, pp. 109-131.

Sellmeijer, J.B. (1990) "Design of Geotextile Reinforced Paved Roads and Parking Areas", *Forth International Conference on Geotextiles, Geomembranes and Related Products*, The Hague, Volume 1, pp. 177-182.

Sellmeijer, J.B. (1993) "MGEOT: A Low-Volume Road Designer", *Geotextiles and Geomembranes*, No. 12, Elsevier Science Limited, pp. 471-477.

Snaith, M.S., McMullen, D., Freer-Hewish, R.J. and Shein, A. (1980) "Flexible Pavement Analysis", Final Technical Report, *European Research Office*, Grant No DAERO-78-G-125, 203p.

A Study on Preventing And Repairing Road Frost Boiling by Applying Geotextile in Daqing Area

Jingan Cao
General Engineer, Daqing Oil Field Construction Design And Research Institute, Daqing, Heilongjiang Province, China

Zizhong Huang
Civil Engineer, Daqing Oil Field Construction Design And Research Institute, Daqing, Heilongjiang Province, China

Diangou Zhao
Engineer, Road Engineering Corporation of Daqing Oil Administration Bureau, Daqing, Heilongjiang Province, China

Jing Dai
Engineer, Road Engineering Corporation of Daqing Oil Administration Bureau, Daqing, Heilongjiang Province, China

ABSTRACT: This paper reports on the achievements in test research of applying needle-punched geotextile to prevent and repair road frost boiling and its application and dissemination in Daqing. The indoor simulated tests and outdoor road repairing tests have been begun since 1990. By these tests and analysis of gained data, the key technical question for preventing and repairing the road frost boiling have been solved and a complete set of design and construction methods also have been summed up. Theory and facts have proved that it is the ideal method by applying geotextile to prevent and repair road frost boiling in the seasonal freezing zone. This method is convenient for construction, excellent effect and notable economic and social benefits.

KEYWORDS: Freeze/thaw Behavior, Geotextiles, Geomembranes, Road Construction, Separation

1 INTRODUCTION

Daqing Oil Field is situated in the middle of Songnen plain in China, which is a seasonal freezing zone. During spring thawing period, under harmful factors, frost boiling becomes so severe that about 20 km road needs to be repaired in Daqing annually.

Many methods were tried to prevent and repair road frost boiling for many years, but its effects are all unsatisfactory. In 1990, a new way was found for preventing and repairing road frost boiling, which is to employ geotextile. Facts have proved that it is of excellent effect and notable economic benefit to apply geotextile to prevent and repair road frost boiling.

2 REASONS AND PREVENTIVE METHOD OF ROAD FROST BOILING

Road frost boiling is a peculiar phenomenon in the seasonal freezing zone . Frost effect increases the water content in subgrade in winter, and the extra water can not be drained off during spring thawing period, which makes subgrade be over-moistured, and reduces its load-bearing capacity. Under the load of running trucks, there appears springing, chapping, bulging and mud pouring, then the whole road is destroyed.

Frost boiling results from the comprehensive effect of 5 factors such as water, soil, temperature, pavement, and the load of running trucks. According to several years experience on repairing road frost boiling, it is believed that water is the major factor of 5 factors. In Daqing the water in the subgrade mainly comes from underground water, so the key of preventing road frost boiling is to cut off the ascent of capillary underground water. In order to solve this problem, the test research of applying geosynthetics to prevent and repair road frost boiling was carried out .

3 INDOOR TESTS

Two kinds of material, geotextile and geomembrane, were used in the indoor tests.

3.1 Separating Water and Isolated Heat Tests

The selected soil sample was a clay with medium liquid limit, a typical soil in Daqing. Its water content was 18.5% and its dry density before test was 1.68 g/cm^3. The soil sample was put into five round freezing containers(shown in Figure 1). Then the freezing containers were sent into

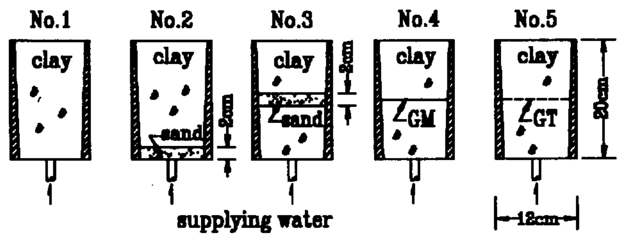

Figure 1. Sample model type.

freeze room. The samples were froze from the top of freezing containers while supplying enough water to the bottom of samples. Freezing continued 310 hours simulating the soil sample's natural state. At last, the test ended when the whole samples were frozen. All the measured data is listed in Table 1.

Table 1. The measured data of sample.

Content	Sample for comparison			Geo-membrane	Geo-textile
	No.1	No.2	No.3	No.4	No.5
	Measured value				
	Frost heaving amount				
	(mm)	(mm)	(mm)	(mm)	(mm)
Upper 10cm	9.0	11.7	11.6	3.4	1.7
Under 10cm	17.1	12.8	8.1	14.9	12.0
	Water content after freezing				
	(%)	(%)	(%)	(%)	(%)
Upper 10cm	26.6	26.6	20.5	13.9	16.7
Under 10cm	29.9	31.6	27.8	34.8	30.8
	Temperature in the middle of samples				
	(°C)	(°C)	(°C)	(°C)	(°C)
At the beginning	12.7	12.8	13.0	A.M. 13.2 B.M. 13.7	A.T. 12.5 B.T. 13.6
Temperature at top is -1	1.4	1.4	1.1	A.M.-1.1 B.M.-1.5	A.T. 1.1 B.T. 2.0
Air temperature is -9	-3.5	-3.2	-2.7	A.M.-2.1 B.M.-0.9	A.T. -2.6 B.T. -1.0
At the end of test	-1.0	-1.7	-1.1	A.M.-1.1 B.M.-0.8	A.T. -1.1 B.T. -0.8

Note: A.M. is the abbreviation for above the membrane; B.M. is the abbreviation for below the membrane; A.T. is the abbreviation for above the textile; B.T. is the abbreviation for below the membrane.

From Table 1 it can be seen that, after freezing under the condition of saturation water, the water content of the upper layer soil sample in container No. 4 and 5 is evidently less than that of the samples for comparison, and the frost heaving amount decreases more than 60%, while the temperature under the geomembrane and the geotextile is clearly higher than that of samples for comparison. Therefore, geomembrane and geotextile are rather effective to separate water, and geotextile can particularly isolate heat to a certain degree.

3.2 Freeze-thaw Resistance and Corrosion Resistance Tests

A freeze -thaw test was carried out under the temperature from -20°C to 10°C. After dipped into water, polyester geotextile was made to undergo 300 freeze-thaw cycles. Its tensile strength only decreased 21% as much as the original tensile strength, which mean polyester is good at freeze-thaw resistance.

In the corrosion resistance test(resisting acid and alkali), the polyester geotextile was soaked into the water solution of different pH values, and measured its strength which is listed in Table 2. The polyester textile was also dug out, which was buried in soil (pH = 9) for two years, and its measured strength only decreased 1.9%. The above tests proved that the polyester textile has a certain corrosion resistance .

Table 2. Measured strength of polyester textile in corrosion resistance test.

Soaking time (days)	pH value				
	1.54	4.24	7.00	9.26	11.81
	Tensile strength (N/5 cm)				
90	775	877	805	786	723
180	738	795	787	786	649
Strength decrease after 180 days (%)	7.8	0.7	1.7	1.9	19.0

Notes: The original tensile strength of geotextile (500 g/m^2) is 801 N/5 cm.

4 TEST ROAD

The test road section is on an Oil Field main line which is 10 m wide in subgrade and 7 m wide on bituminous concrete pavement. Most of the road sections are wet or over-wet because of the high underground water level and the water beside the road all the year. Moreover, a busy traffic of heavy trucks can be found on the road. There was always frost boiling since the road was built up in 1984. Up to 1989, the severe frost boiling stopped traffic. It was determined to repair this road thoroughly and to build a test road in the road section where frost boiling was most severe. The test road was began to build in June 1990, and was completed in July. To meet test conditions, there was no drain beside the road, and the height of subgrade embankment was less than the standard so that the road was over-wet.

4.1 Test Plans

In view of the reason of road frost boiling, three tests by sealing, separating and replacement were carried out.

4.1.1 Sealing in this plan

Ice gathering zone in subgrade was wrapped with impermeable geomembrane in order to form a water-tight zone for water in the vertical direction, to protect this zone from water on the ground, to cut off the ascent of capillary underground water, to cut down the height of ice gathering zone, to lighten the freeze and subsidence of subgrade, to improve the whole strength of subgrade and prevent frost boiling.

4.1.2 Separation in this plan

Separation, drain filtration and reinforcement characteristics of the geotextile were introduced to prevent road from frost boiling.

During spring thawing period, the water content of the subgrade is high and the strength is low. Under the repeatedly load of running trucks, base course material is easily pressed into the subgrade soil, while the mud is easily squeezed upwards. With these two acting together, then there appears frost boiling. After geotextile has being laid, there is no frost boiling. Having dug the road, it can been seen that base course material does not mix with the subgrade soil. It is the geotextile that plays the role of separation.

The test road was dug to be observed the water content of subgrade soil during spring thawing period. The result is there was less ice grains in the soil above geotextile than below it, and the water content in the latter was 1.1 times that of the former. Both indoor test and field observation prove that geotextile can cut off the ascent of capillary underground water from positive temperature zones to negative temperature zones.

Geotextile can drain water away in both vertical and horizontal directions. The measured coefficient of permeability of the soil and the geotextile in the test road were respectively 1.98×10^{-4} cm/s and 5.5×10^{-1} cm/s, the latter being more than 2700 times of the former. Thus water can be drained away along the cross slope through geotextile when the water content of the soil below the geotextile is high. In addition, geotextile laid between structural layers and it can bear load together with road surface and subgrade, and spread stress. Therefore, geotextile reinforces the road.

4.1.3 Replacement method

Replacement method, an usual method, is to replace the frozen subgrade soil with non-freeze or weak freeze material in order to reduce the water content of the subgrade, prevent subgrade from freezing and subsiding, keep the stability of subgrade and protect road from frost boiling.

4.2 Sections of Test Road and Pavement Structure

Based on the severity and contrast condition, the 550 m long test road was equally divided into 11 sections in which 4 sections were for sealing test, 4 sections for separating test and the other for replacement test.

The pavement structure was designed along with the 3rd class road standard. The structural composition and thickness were determined referring to the requirement of strength and freeze-thaw resistance, see Table 3.

4.3 The Selection of Geosynthetics

4.3.1 Geomembrane

The geomembrane is made of polyvinyl chloride(PVC), whose density is 200 g/m^2.

4.3.2 Geotextile

The selection of the geotextile is the key of the separating plan. Geotextile should play roles of separation, drainage, filtration and reinforcement, so its effective opening size(EOS) and strength are very important.

Table 3. Test road pavement structure.

Thickness of the base course	Structural type						
	Sealing		Separation		Replacing embankment		
	I-1 (cm)	I-2 (cm)	II-1 (cm)	II-2 (cm)	III-1 (cm)	III-2 (cm)	III-3 (cm)
Slag lime soil	15	15	20	15	20	20	20
Gravel lime soil	-	-	-	-	15	15	-
Lime soil	15	15	30	15	20	40	30
Soil wrapped by geomembrane	20	40	-	-	-	-	-
Soil	-	-	-	30	-	-	-
Geotextile	-	-	One layer		-	-	-
Sand and gravel	-	-	-	-	20	-	-

Note: The road surface course is 9 cm thick bituminous concrete; the allowable rebound deflection of pavement is 0.57 mm (The standard axial loading is 60 kN).

The mechanism of separation is similar to filtration mechanism in irrigation works, requiring the effective opening size of geotextile matches the grain diameter of subgrade soil in order to protect soil from capillary rising and drain water off without blocking. Then the following formulation should be satisfied:

$$d_{15}<O_{90}<d_{85} \quad (1)$$

where: O_{90}, the effective opening size of geotextile; d_{15} and d_{85} are respectively diameter of protected soil grain with 85% and 15% passing on standard screen.

Strength according to reference, the tensile strength should satisfy following formulation:

$$0.75<\frac{\text{transverse tensile strength}}{\text{longitudinal tensile strength}}<1.25 \quad (2)$$

The selected geotextile should meet strength requirements, and should be durable enough to resist aging and erosion by acid and alkali. Considering the widespread saline soil in Daqing, on the basis of indoor tests, field observation and relevant references on polyester geotextile, the polyester geotextile was selected as working geosynthetics.

4.4 The Determination of Location of Geosynthetics

Another key in both sealing and separating plans is to determine the location of the geomambrane and geotextile in the road cross section. We believe geosynthetics should be laid in the place with the most water content in the subgrade. Referring to the geological reference, the location is 0.6~0.8 m below the road surface, which was also proved by field test. The detailed direction in construction is shown in Figure 2.

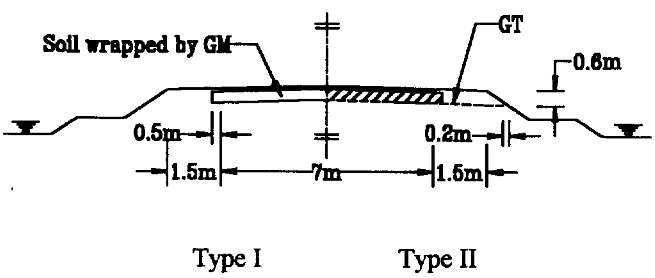

Figure 2. Road cross-sectional profile.

5 TEST EFFECT AND ECONOMIC BENEFIT

5.1 Test Effect

From the completion of the test road up to the end of 1996, most of the sections worked well except some damaged parts of the road surface on a few sections of sealing plan, though the real traffic volume was 45% more than the designed traffic volume. Since this road was built, two year systematic observation and three year detailed observation on road surface strength, evenness, crack, freeze-thaw, subgrade water content and freeze depth at 527 observing places have been carried out , and more than 20,000 data have been obtained . The measured rebound deflection during spring thawing period which is one of the major effect factors on the road, is listed in Table 4.

Table 4. The measured rebound deflection of road surface.

Type	III-1	II-1	I-2
Mileage	250m~300m (mm)	300m~350m (mm)	350m~400m (mm)
1990 Oct.	0.094	0.129	0.160
1991 Apr.	0.395	0.352	0.481
1992 Apr.	0.391	0.418	0.556
1993 May	0.350	0.378	0.556
1994 Apr.	0.365	0.509	0.793
1995 May	0.409	0.545	0.973
1996 May	0.388	0.494	0.845

The sealing plan resulted in a low road surface strength and a large rebound deflection, which were far from the design requirement. Especially the rebound deflection of type I-1 road section during spring thawing period in 1994 reached 1.1 mm , and a 5 m^2 local part on road surface was damaged. In addition, there were many underground pipelines across road in the Oil Field. The geomembrane will be destroyed when these underground pipelines are dug out. So, the sealing plan is unsuitable for using in Daqing Oil Field.

The replacement method resulted in a thick pavement structure layer and a greater reduction of strength. The rebound deflection during spring thawing period in 1995 was 12.1% more than that in 1994. Moreover, it had a too great amount of work and too much cost ($18 per square meter) to be adopted.

The separating plan met the designed strength requirement with a little reduction of strength. For example, the rebound deflection during spring thawing period in 1995 was only 7% more than that in 1994. Besides, it had a thin structural layer, little amount of work, low cost ($17 per square meter) and an excellent effect. Especially, structure of type II-1 is a structure with advanced technology and better economic benefit for preventing and improving road frost boiling in freeze area.

5.2 Economic Result

Referring to the settlement of test road, the separating plan saved $1 per square meter than the replacement method. Because the test road worked effectively during the first spring thawing period after its completion, this technique was disseminated in the same year, and the construction method was improved, so $1.3 per square meter was saved .

In the past seven years, more than 640,000 m^2 geotextile have been applied to 45 roads(total length 50 km), and saved $928,000 (direct expense). Besides, because preventing road from frost boiling and avoiding detours during the construction period, the transport efficiency was improved 54%, and $600,000 transport expense was saved annually. Therefore, both economic benefit and social benefit are notable.

6 CONCLUSION

Facts have proved that this is a new technique with convenient construction, excellent effect and notable economic benefit and social benefit, to apply geotextile to prevent and repair road frost boiling in severe cold area. We believe that the selection of textile and laying elevation are two keys of this technique. In Daqing, the suitable geotextile is polyester geotextile with 500 g/m^2, effective opening size being 0.08~0.1mm and laying elevation usually being about 0.7 m below the road surface.

REFERENCES

Hong,Y.W. (1992) *Geosynthetic in Engineering Practice*, 1st Edition, Heilongjiang Provincial Hydraulic Bureau, Harbin, Heilongjiang province, China.

Laboratory Study of the Dynamic Test System on Geogrid Reinforced Subgrade Soil

Dave Ta-Teh Chang
Associate Professor, Dept. of Civil Engineering, Chung Yuan University, Chung Li, Taiwan, R.O.C.

Wei-Jen Wang
Graduate Research Assistant, Dept. of Civil Engineering, Chung Yuan University, Chung Li, Taiwan, R.O.C.

Yao-Hung Wang
Research Assistant, Dept. of Civil Engineering, Chung Yuan University, Chung Li, Taiwan, R.O.C.

ABSTRACT : While geosynthetics were considered for pavement reinforcement, the R and CBR properties are no longer sufficient to govern the pavement thickness design. Resilient modulus testing has replaced static penetration testing as it more accurately simulates the in situ conditions on the pavement. Using geogrids of different types, this research studied their reinforcement effects on the subgrade, and the variation in reinforcement effects when geogrids were placed in varied depth during the application of repeated loadings. Repeated load test results show that geogrid reinforcement is highly effective as reflected in factors related to foundation stiffness and the amount of deformation associated with repeated addition of heavy loads. And it was found that improvement of the foundation stiffness is significantly related to the stiffness and initial modulus of the geogrid.

KEYWORDS: Bearing Capacity, Geogrids, Pavement, Reinforcement.

1 BACKGROUND

The function of geosynthetics in pavement reinforcement is to reduce the amount of deformation when a pavement is subject to loadings. Among various geosynthetics, geogrid is preferable for pavement reinforcement under high loadings. This is principally due to the interlocking between the geogrid and the soil. The fundamental properties of geogrid, such as light weight, resiliency, ease of installation, high modulus to strain resistance, acid resistance, and longer life span, make it an ideal geosynthetic for such applications.

Previously, the capacity of a reinforced pavement structure was determined by static penetration tests. However, the actual loadings by vehicles are dynamic, and such static tests may no longer meet today's requirements. In this study, the effects of geogrids in pavement reinforcement are examined under dynamic loadings. Dynamic tests of this type are not yet in common practice.

2 COEFFICIENT OF SUBGRADE REACTION

The coefficient of subgrade reaction was originally defined by Trezaghi (1955) :

$$k_s = \frac{q}{y} \tag{1}$$

in which k_s = coefficient of subgrade reaction, [KN/m^3] ; q = uniform loadings, Kpa ; y = deformation under static pressure [m].

Coefficient of subgrade reaction is frequently applied in foundation engineering for the computation of stiffness of subgrade. Upon actual application, this coefficient needs to be calibrated as provided by Terzaghi (1955).

For cohesive soil, then

$$k_s = k_p \times \frac{A_p}{A} \tag{2}$$

For cohesionless soil, then

$$k_s = k_p \left(\frac{A+1}{2A}\right)^2 \tag{3}$$

in which k_p = coefficient of subgrade reaction derived from the test ; A = area of foundation. ; A_p = area of plate ;

When the loading plate is of rectangular shape, then

$$k_s = k_p \left(\frac{m+0.5}{1.5}\right)^2 \tag{4}$$

in which m = size of the rectangular plate = L/B.(B: width of foundation)

Many indirect ways and/or empirical formula are available for calculating the coefficient of subgrade reaction. For example, from consolidation tests

$$k_s = \frac{1}{m_v \times H} \tag{5}$$

in which m_v = coefficient of volumetric compressibility ; H = 0.5B ~ 1.0B.(B: width of foundation), or by CBR and the like. From the above, it can be seen that size, shape and rigidity of plate, soil properties, and other variables can affect the coefficient of subgrade reaction.

3 BEARING CAPACITY RATIO (BCR)

For more suitable application in pavement reinforcement design , Bearing Capacity Ratio (BCR) is then suggested by Mandal and Sah (1992) as follows :

$$BCR = \frac{q_r}{q_{ur}} \qquad (6)$$

in which q_r= ultimate bearing capacity after reinforcement ; q_{ur}= ultimate bearing capacity before reinforcement.

Using this ratio, the effect of reinforcement by geosynthetics under static pressure can be determined.

4 MATERIALS

In this study, weathered mudstone is used to provide the soft subgrade layer for the testing. General properties of weathered mudstone are shown in Table 1.

Table 1 General properties of weathered mudstone

Properties	Values
Liquid limit, (%)	34.3
Plastic limit, (%)	21.6
Plastic Index	12.7
Maximum dry density, (g/cm^3)	1.68
Optimal Moisture Content O.M.C. (%)	17.5
Cohesion, (kg/cm^2)	0.5
Specific Gravity	2.7
Internal friction angle	17°

The specimen was prepared using 95% compaction and a moisture content of O.M.C.+2%, to the in situ condition.

As for geosynthetics, flexible geogrids of two different strength levels are used and are identified as the H-geogrid and the L-geogrid. Their general properties are shown in Table 2 below.

Table 2 General Properties of Geogrids

	H-Geogrid	L-Geogrid
Characteristic	flexible	flexible
Material	polyester	polyester
Size of opening	2cm × 2cm	2cm × 2cm
Elongation at breaking, %	14	17
Ultimate rib strength [kN/m]	232.0	107.9
Tensile modulus [kn/m]	1657.1	634.7

Notes : Rib tensile strength test was based on the method of GRI-GG1.

5 TESTING SYSTEM SETUP AND PROCEDURES

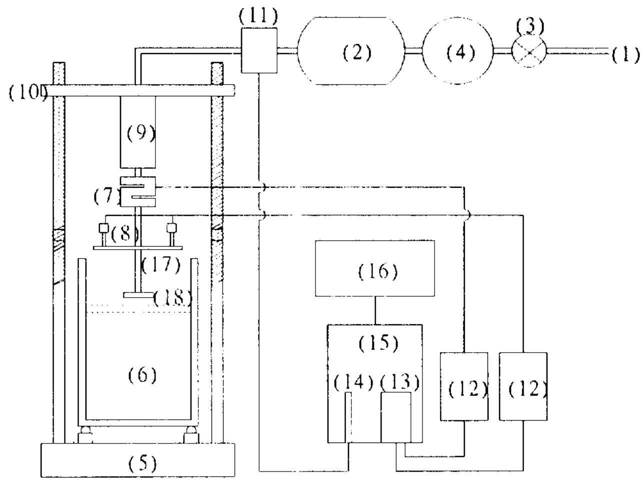

(1)Pneumatic system (2)Air tank (3)Valve (4)Pressure gauge (5)Platform (6)Test box (7)Load cell (8)LVDT (9)Pressure cylinder (10)Beam (11)Electromagnetic valve (12)Amplifier (13)AD/DA converter (14)Time control card (15)Computer (16)Laser printer (17) Rod (18)Loading Plate

Figure 1. Layout of test system

The testing system used in this study is arranged according to the resilient modulus testing device provided by Chang et al.(1991), and the layout is given in Figure 1. A metal box with a dimension of 0.457 m(length)× 0.457 m(width) × 0.762 m(height) is used for molding soil specimen. Newmark Charts (Newmark, N.M., 1942) were used to compute the transfer of stress below the circular plate. To enable the stress to decrease to the lowest level of 6% underneath the center of circular plate, the thickness of the soft specimen should be at least three times the width of plate. For a plate of 0.1016 m in diameter, the depth of mudstone computed in this test was 0.3 m.

To cope with the pneumatic system used in this test, plates of two different diameters 0.0508 m and 0.1016 m were used. The test was initially performed for each geogrid in four runs at 4 different embedded depths, which are 0.2, 0.4, 0.6 and 1.0 in terms of D/R (embedded depth/radius of plate).The determined best ratio was used for the rest of the tests.

AASHTO T274-82 (1983) method was followed to perform the dynamic loading with levels of 19.6(0.2), 39.2(0.4), 58.8(0.6), 78.4(0.8), 98.0(1.0), 117.6(1.2), 137.2(1.4), and 156.8(1.6) Kpa(kg/cm^2). As this test is related to the study of pavement reinforcement, the typical M_R Test details were followed in the selection of frequency of loading, contact interval, and loading waveform. In this case, the frequency is 0.33 Hz, the contact interval is 0.1 sec., and the loading is of triangular waveform.

6 RESULTS AND DISCUSSIONS

6.1 Effects of Stress Levels, Loading Numbers and Embedded Depth

Typical results are illustrated in Figure 2. A higher dynamic coefficient of subgrade reaction was observed under smaller stress, because smaller deformation resulted under the smaller stress. Under stress at the range between 19.6(0.2) to 117.6(1.2) Kpa(kg/cm^2), the dynamic coefficient decreased abruptly. When the stress is greater than 117.6(1.2) Kpa(kg/cm^2), the dynamic coefficient becomes constant. To demonstrate the trend of this curve, more tests have been performed using loading stresses of 29.4(0.3), 58.8(0.6), 88.2(0.9), 117.6(1.2), and 147.0(1.5) Kpa(kg/cm^2).

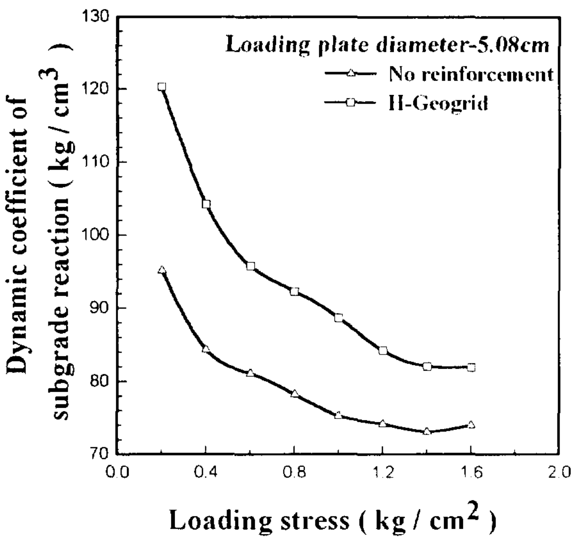

Figure 2. Responded dynamic coefficient of subgrade reaction with and without reinforcement

According to Chang et al (1991) study, in the first cycle (the first 200 loadings) of the test, the M_R values could vary in an irregular way. Several groups of tests have been conducted to verify this phenomenon, and the results are shown in Figure 3. Only H-geogrid, and 5.08cm-plate were used in these tests for determining number of loading for the rest of the program. It can be seen that during the first 200 loadings, the dynamic coefficient of subgrade reaction increases gradually, and after the first 200 loadings, the dynamic coefficient of subgrade reaction becomes stable although slight deviations are still observed. To neutralize these deviations, an averaged value was taken from loading no. 201 to loading no. 500 as the dynamic coefficient of subgrade reaction.

Regardless of whether the loadings are applied by the big plate or the small plate, during the first 200 loadings, the readings of the dynamic coefficient of subgrade reaction increase gradually. Reasons for this phenomenon could be that:①the plate was not in complete contact with the mudstone surface, resulting in a larger deformation at the beginning;②repeated loadings will compact the mudstone, and when the mudstone is compacted to a certain extent, the dynamic loading stress will transfer to a lower elevation in the mudstone. After 150~200 loadings, a certain degree of compaction will result, and the coefficient of subgrade reaction becomes stable accordingly. After 200 loadings, although the coefficient curve still shows some uncertainties, generally speaking, the value is close to a constant. The occurrence of uncertainties is relatively rare in the case of a large plate. This is because the effect of uneven compaction on a large plate is insignificant in comparison to that on a small plate.

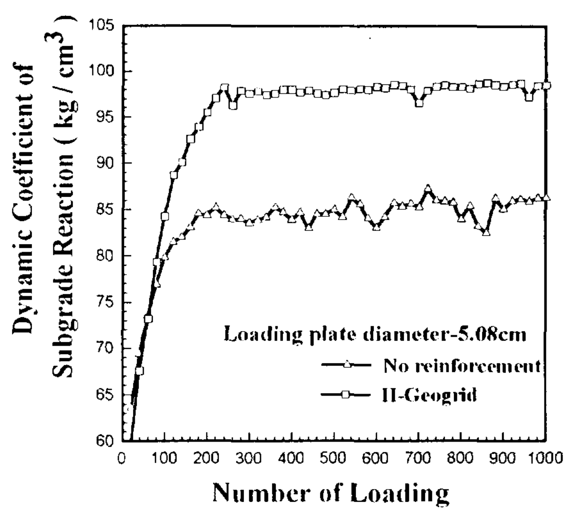

Figure 3. Significance of loading numbers for the performance

6.2 Effects of Geogrid Strength

Figure 4. indicates that the best reinforcement occurs when D/R = 0.2. The effects diminish for deeper embedded depth. For D/R ≥ 0.6, the effect of reinforcement becomes negligible. These findings are equivalent to the studies by Mandel and Sah (1992).

A series of tests were carried out at the best embedded depth (i.e., D/R = 0.2), to compare the effect of reinforcement by geogrids of different mesh sizes and plates of different dimensions. Findings indicate that the strength of H-geogrids is two times that of L-geogrids; whereas the dynamic coefficient of subgrade reaction after reinforcement by H-geogrids is more or less the same as that by L-geogrids (Fig.5 and Fig.6). It could be concluded that the effect of reinforcement is not directly related to the strength of geogrids but the tensile modulus (or stiffness) of the geogrid materials.

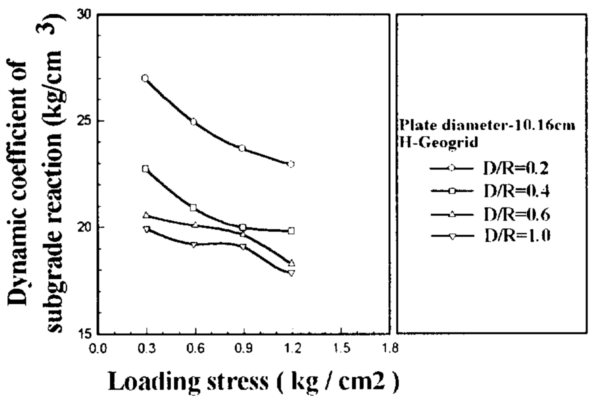

Figure 4. Effect of different embedded depth for 10.16cm diameter plate

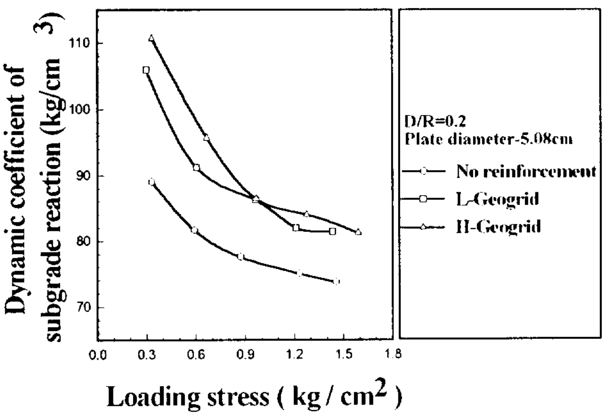

Figure 5. Dynamic coefficient of subgrade reaction with varied loading levels. (5.08cm-plate at D/R=0.2)

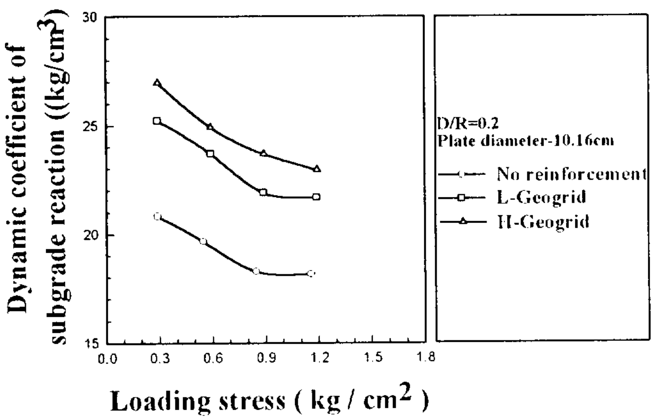

Figure 6. Dynamic coefficient of subgrade reaction with varied loading levels. (10.16cm-plate at D/R=0.2)

7 CONCLUSIONS

(1)The effect of geogrids in pavement reinforcement is confirmed.

(2)The best reinforcement occurs when D/R = 0.2. The effects diminish for deeper embedded depths. For D/R ≥ 0.6, the effect of reinforcement becomes negligible.

(3)Both the dynamic coefficient of subgrade reaction and the amount of permanent deformation can be used for the determination of the effect of reinforcement. The effect of reinforcement is not directly related to the strength of geogrids but to the stiffness of the geogrid materials.

(4)The level of the dynamic coefficient of subgrade reaction is related to the size of the plate, deformation of geogrids, and the interface properties between geogrid and mudstone (such as interlocking, friction).

REFERENCES

AASHTO, "Standard Method of Test for Resilient Modulus of Subgrade Soils.", 1983, AASHTO Designation, No.T274-82.

Chang, Dave Ta-Teh, Chen-En Chiang, and Chun-Young Chang, "Modified Testing Device to Evaluate MR Properties on Fly Ash Treated Subgrade Soil", pp 88~95, ASTM Geotechnical Testing Journal, March, 1991.

Mandal, J. N. and Sah, H. S. , November, 1992, "Bearing Capacity Tests on Geogrid-Reinforced Clay", Geotextiles and Geomembranes.

Newmark, N.M, 1942. "Influence Charts for Computation of Stresses in Elastic Soil", University of Illinois Engineering Experiment Station, Bulletin No.338.

Terzaghi, "Evaluation of Coefficients of Subgrade Reaction", Geotechnique, Vol.5, pp.297~326, 1955

Performance prediction model for asphalt overlays with geotextile interlayers on cracked pavements

R. M. Rodrigues
Associate Professor, Geotechnical Department, Instituto Tecnológico de Aeronáutica, São José dos Campos, Brazil

ABSTRACT: The paper presents the development of a mechanistic-empirical model for the prediction of reflective cracking on asphalt overlays with the use of a geotextile as interlayer, considering only the effect of traffic loads. The model is based on an interpretation of laboratory experimental data obtained by Majidzadeh et al (1984). The finite element method and concepts of fracture mechanics are used in this process. It is shown that different mechanisms for the reflective cracking process must be considered in function of the temperature and a proposition is made of a general model.

KEYWORDS: Reflective crack prevention, Pavements, Geotextiles, Finite element analysis, Asphalt overlay

1 INTRODUCTION

Reflective cracking in asphalt concrete overlays placed over cracked or jointed pavements is a major concern for design. The interface between the overlay and the cracked pavement is the best place to apply remedial measures, since it is at this location that the controlling stresses for the reflective cracking process occur. Geotextile-asphalt interlayers are an effective solution but a comprehensive design method is still lacking for cost-benefit evaluations. A model is suggested for practical application and it is the result of a mechanistic interpretation of laboratory test data obtained by Majidzadeh et al (1984).

2 EXPERIMENTAL DATA

Majidzadeh et al (1984) conducted repeated load tests on beams supported by elastic foundation (Figure 1) with the purpose of evaluating reflective cracking life of asphalt concrete overlays applied over cracked pavements. They performed tests with and without the presence of an asphalt impregnated geotextile membrane interlayer placed between the overlay and the cracked asphalt concrete (AC) or Portland cement concrete (PCC) layer. Tests were performed at two temperatures (4.4°C and 22.2°C). The asphalt concrete mix was a FAA P-401 with 5.9% in weight of AC-20 asphalt and 3.4% air voids. The existing crack was sawed to a width of 3.2 mm. Several combinations of layer thickness (h_1, h_2) and applied surface vertical pressure (q) were considered for each test configuration. Three geotextiles were considered and designated as being of low, medium and high tensile moduli. The performance of these geotextiles on the increase of reflective cracking life was nearly the same, with a slightly greater beneficial effect with the ones of higher moduli. For this reason, the analysis here performed employed the average of the test results for all geotextiles considered. According to Majidzadeh et al (1984), this result would be a consequence of the asphalt impregnation with different rates (from 0.3 to 0.9 l/m^2) of the three geotextiles, which tended to saturate them, leading to a more uniform behavior.

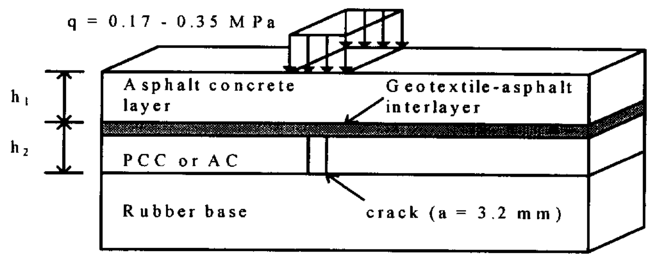

Figure 1. The experiment of Majidzadeh et al (1984).

3 ANALYSIS OF TEST RESULTS

Two dimensional finite element modeling (plane stress) was employed in the simulation of the test configuration of Figure 1. Only standard constant strain triangle elements were utilized for all materials, with a special mesh refinement at the crack tip. Each analysis had the objective of evaluating the stress state at the critical point in the asphalt concrete overlay. This point is situated immediately above the existing crack, on the underside of the overlay. The parameter chosen for this evaluation was the distortion energy density (U_d), which includes only the strain energy due to shear, leaving out the volumetric strains, since these latter strains are not related to fatigue cracking. Besides, this parameter is known to be less susceptible to suffer inaccuracies in the finite element method, when compared to stresses or strains. For these analyses, the asphalt-geotextile membrane interlayer was not included on the finite element mesh. So, even in the tests were the geotextile was present, the calculated values of U_d referred to a situation where the overlay was placed without the geotextile. The observed number of load cycles to a complete reflection of the crack (N_f) was correlated with the calculated values of U_d by:

$$N_f = A\left(\frac{1}{U_d}\right)^B \tag{1}$$

where A and B are material constants.

It was also analyzed the possible effect of the inclusion on this regression of the overlay thickness (h_1), in the form:

$$N_f = A\left(\frac{1}{U_d}\right)^B h_1^C \qquad (2)$$

Regression results are shown on Tables 1 and 2, together with the coefficient of determination (r^2) and the standard error of estimate (s). It can be seen that parameter U_d is strongly correlated with reflective cracking, independently of support conditions, applied load and overlay thickness. Besides, for T=22.2°C the inclusion of h_1 on the regression was significantly beneficial, while for T=4.4°C that is not the case. At 4.4°C the correlation between N_f and U_d is stronger than at 22.2°C and, for this latter temperature, it is highly desirable to include h_1 on the model. So, while U_d alone is sufficient to explain reflective cracking at 4.4°C, there is an effect at 22.2°C that is controlled by h_1. A possible interpretation for these results is that there is a stable crack progression through the overlay thickness with load repetitions after the occurrence of fracture at the bottom of layer, for the temperature of 22.2°C. At 4.4°C the asphalt concrete mixture would be a fragile material, making the crack progression to be of little importance in relation to the period necessary for fracture beginning at the critical point.

The inclusion of a geotextile-asphalt interlayer significantly increases reflective cracking life, specially for the lower temperature, as indicated by parameter A. At 4.4°C the influence of U_d on N_f is strongly affected by the inclusion of the geotextile interlayer, since the inclination of the $\log U_d \times \log N_f$ line changes from 1.883 to 0.8589. It is impossible, therefore, to consider geotextile action as of a Stress Absorbing Membrane Interlayer (SAMI) type, since there would not be a well defined reduction factor that could be applied to the calculated values of U_d for the case of overlay without geotextile in order to predict the greater reflective cracking life with the inclusion of the membrane. A definition of such reduction factor would require, instead, the use of a reduction function (a reduction factor varying with U_d), implying in a non linear SAMI action. This hypothesis must, however, be discarded, in light of the excellent correlation observed between N_f and the U_d values calculated without the inclusion of the geotextile interlayer on the finite element analyses.

Table 1. Overlay without geotextile interlayer (9 points).

	T = 4.4°C		T = 22.2°C	
	Eq. (1)	Eq. (2)	Eq. (1)	Eq. (2)
A	4.3616	9.2624	8.765	0.1514
B	1.883	2.119	2.051	1.8048
C	------	-0.9074	------	2.732
r^2	0.851	0.874	0.784	0.957
s	0.4606	0.4906	0.6413	0.3095

Table 2. Overlay with geotextile interlayer (6 points).

	T = 4.4°C		T = 22.2°C	
	Eq. (1)	Eq. (2)	Eq. (1)	Eq. (2)
A	1.178×10^4	1.307×10^4	15.87	0.2356
B	0.8589	0.8796	2.4193	1.6227
C	------	-0.0967	------	3.6547
r^2	0.964	0.965	0.728	0.874
s	0.1291	0.1476	0.871	0.641

4 OVERLAY WITHOUT GEOTEXTILE

Several studies have shown the validity of Paris' law for fatigue cracking prediction on asphalt concrete (Luther et al 1976). According to this law, crack progression can be predicted by a model of the form:

$$\frac{dc}{dN} = aK_I^b \qquad (3)$$

where c is the crack length, N is the number of cycles of the stress intensity factor K_I, and a and b are material properties. The stress intensity factor is a parameter that describes the stress field in the vicinity of a crack tip.

The irregular path followed by a crack that goes around aggregate particles puts doubts, however, as to the relevance of stress intensity factors calculations on this so heterogeneous material. The crack progression could be viewed, maybe, as a sequence of discrete ruptures of aggregate particles bonds along this irregular path. Besides, the results on Tables 1 and 2 indicate that reflective cracking life is controlled, to a high degree, by the distortion energy applied at the critical point on the underside of the overlay. Combining these two arguments, one could describe the process of consisting of two stages. During the first one, there would be happening the fracture under repeated loads of the aggregate bonds at the critical location. Conventional fatigue laws under controlled stress would be sufficient to predict duration of this stage. Tensile strength of the asphalt concrete is the major controlling factor in this case. The fracture occurrence would imply in the rupture of bonds of aggregate particles on the critical location and an initial length for this original crack would be on the order of magnitude of the maximum particle diameter (ϕ_{max}). After this, there begins a new mechanism were the crack thus formed serves as a means to redirection the dissipated energy to the formation of new free surfaces, resulting on the extension of the crack. A low speed for crack progression depends on the ability of the material to dissipate strain energy through plastic distortion rather than through formation of new free surfaces at the crack tip. Therefore, a fragile material will have a faster crack progression than a more ductile one.

These considerations can be expressed by the following model:

$$N_f = N_0(1 + F_{PT})^\beta \quad (4)$$

$$F_{PT} = \alpha(h_1 - \phi_{max}) \quad (5)$$

$$N_0 = M\left(\frac{1}{U_d}\right)^{n/2} \quad (6)$$

where: N_0 = number of load cycles for the fracture on the critical location of the overlay, where the distortion energy density is equal to U_d; F_{PT} = crack progression factor (≥ 0); α = mixture parameter related to crack progression under repeated loads; M and n = fatigue parameters of the asphalt concrete mixture.

This model implies in the fact that crack reflection life (N_f) is controlled by the fatigue life of the critical region on the underside of the asphalt concrete layer (N_0), and that the formed crack must propagate through the entire overlay thickness (h_l) from the initial fracture, whose length is of the order of magnitude of ϕ_{max}. Crack speed progression is controlled by parameter α, which is equal to zero when the material has a fragile behavior and increases from zero as the material becomes of a visco-elasto-plastic nature. If α=0 (crack propagation is unstable) the value of β has not any influence on N_f, but if $\alpha > 0$ the value of β will influence crack reflection life. Therefore, β is related to the stable crack progression process and has the meaning of a fracture material parameter, in the same sense as with the fracture parameters of Paris' Law.

Parameters M and n of equation (6) must be determined from stress controlled bending fatigue tests, which are well known to represent fracture formation at the critical zone and do not incorporate significant crack propagation effects. From analysis of several tests of this kind, the following relations can be stated:

$$N_0 = K\left(\frac{1}{\varepsilon}\right)^n \quad (7)$$

$$n = 1.813 - 0.1046\log_e K \quad (8)$$

where ε is the maximum tensile strain applied. Parameter n must be measured in repeated load or creep tests and parameter K can be calculated by equation (8). In the state of pure bending the following relation is valid:

$$\varepsilon = \left[\frac{3U_d}{E_R(1+\upsilon)}\right]^{\frac{1}{2}} \quad (9)$$

where E_R is the resilient modulus and ν is the Poisson's ratio. For the asphalt concrete employed, values of E_R are 10545 MPa at 4.4 °C and 3515 MPa at 22.2°C. Poisson's ratio was not measured and a typical value of 0.33 was adopted, as is usual in pavement analysis.

Therefore, the following correspondence can be established between equations (6) and (7):

$$M = K\left[\frac{E_R(1+\upsilon)}{3}\right]^{n/2} \quad (10)$$

Applying this relation to the values of M determined by regression of data from tests at 4.4°C without geotextile (Table 1, equation 1), results: $K = 6.8273 \times 10^{-9}$ and n=3.77. Substituting this value of K on equation (8) the predicted value for n is 3.78, which is nearly the same value determined from regression. This implies that $\alpha = 0$ for T=4.4°C. At this temperature the asphalt concrete mixture is, as expected, a fragile material.

Considering now the experimental data for T=22.2°C and overlay without geotextile, the fitting of the model was done varying α as the basic parameter and determining M, n and β by linear regression analysis. For any fixed value of α the model adjustment to the experimental data is the same (r^2=0.957 and s = 0.3095). The absolute error of estimate is the same as for the direct regression of equation (2). Results are shown on Table 3 were it can be seen that exponent n of the fatigue law is the same for all values of α and equal to 3.61. Only for α = 0.143 there is agreement between the value of M predicted by equations (8) and (10) and the value of M determined by regression to the experimental data, as can be seen at the rightmost column of Table 3. The resulting value of β is equal to 5.246.

Table 3 - Model fitting for T = 22.2°C.

α	M	n	β	K ($\times10^{-8}$)	K(eq. 8)/K
0.100	1.544	3.61	6.561	4.0731	1.178
0.120	1.428	3.61	5.833	3.7673	1.089
0.143	1.313	3.61	5.246	3.4587	1.000
0.150	1.278	3.61	5.103	3.3725	0.975
0.200	1.078	3.61	4.373	2.8446	0.822
0.500	0.494	3.61	3.054	1.3036	0.377

5 GEOTEXTILE EFFECT

The model for overlay without geotextile can be applied to help in the interpretation of the data for the tests with geotextile. The increase in reflective cracking life due to the geotextile inclusion is given by:

$$\Delta N = N_f - N_{OV} \quad (11)$$

where N_f is the reflective cracking life with geotextile and N_{OV} is the predicted reflective cracking life for the overlay without geotextile, as given by equation (4). Figure 2 shows the calculated values of ΔN for the tests conducted by Majidzadeh et al (1984), where it can be seen a clear dependence of ΔN with U_d, the distortion energy density at the crack tip on the overlay calculated without the inclusion of the geotextile.

There is a trend for convergence for low values of U_d of the relations between ΔN and U_d for the two temperatures considered, allowing the proposition of the following model:

$$\Delta N = 5.0 \times 10^5 \left(\frac{U_d}{1\text{kPa}} \right)^{\xi} \tag{12}$$

where: ξ = -0.677 for T = 4.4°C (with mean error of 16 %) and ξ = -2.10 for T = 22.2°C (with mean error of 27 %).

There are several experimental evidences showing that extension of reflective cracking life with the inclusion of geotextiles is a consequence of a crack arrest process, in which dissipated energy is deviated from the formation of new free surfaces at the critical zone on the overlay to propagation of a horizontal crack at the geotextile-pavement interface (Montestruque 1996). In this way, the possibility of writing equation (12) as an expression of experimental data would be a result from a stable horizontal crack progression, which could be described by a law analogous to Paris' Law:

$$\frac{dl}{dN} = AU_d^B \tag{13}$$

where l is the horizontal crack length, and A and B are fracture parameters for the geotextile-pavement bond. This hypothesis will be valid only if B > 0, since horizontal crack progression speed must increase with the distortion energy supply on the crack tip region. Integrating equation (13) and considering that U_d varies only slightly with horizontal crack extension (since this horizontal crack is of small length), one could write:

$$\Delta N = \frac{1}{A} \int_0^{l_{crit}} U_d^{-B} dl = \frac{l_{crit}}{A} U_d^{-B} \tag{14}$$

where l_{crit} is the critical length reached by horizontal crack, after which dissipated energy goes to the generation of new free surfaces at the crack tip on the overlay.

Comparing equations (12) and (14) one concludes that ξ=-B. Since ξ < 0 the condition B > 0 is satisfied, giving support to the hypothesis that increase in reflective cracking life can be interpreted as the result of a deviation of dissipated energy from the critical zone of the overlay to the

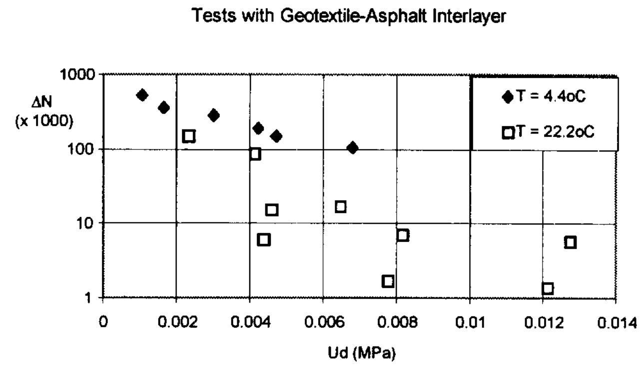

Figure 2. Increase in reflective cracking life with geotextile.

generation of a small localized rupture between geotextile and overlaid pavement. Parameter B influences the horizontal cracking process and is temperature dependent. Since the bond and the other materials involved are of asphaltic nature, this dependence is conceivable.

6 CONCLUSION

Reflective cracking life of asphalt overlays with the presence of an asphalt-geotextile membrane interlayer can be predicted by first estimating reflective cracking life without the interlayer (equation 4). This number of load cycles is then added to the delay predicted by equation (12). The model should be applied to field data in order to better evaluate it's consistency. Material parameters relevant for the model are: α (degree of fragile behavior in function of temperature), n, ϕ_{max} and E_R for the asphalt concrete, and ξ for the geotextile-pavement bond, at design temperature.

REFERENCES

Majidzadeh, K., Ilves, G., Sklyut, H. & Kumar, V.R. (1984) *Mechanistic Methodology for Airport Pavement Design with Engineering Fabrics. Volume I: Theoretical and Experimental Base*, Report No. DOT/FAA/PM-84/9,I, Federal Aviation Administration, Washington, D.C.,USA, 161 p.

Montestruque, G.E.V. (1996) "Estudo de Sistemas Anti-Reflexão de Trincas na Restauração de Pavimentos Asfálticos", MSc Thesis, Instituto Tecnológico de Aeronáutica, ITA, São José dos Campos, SP, Brasil, 141p.

Luther, M.S., Majidzadeh, K. & Chang, C.W. (1976) Mechanistic Investigation of Reflection Cracking of Asphalt Overlays. *Transportation Research Record 572*, p. 111-122, TRB, Washington, D.C.

EFFECTIVENESS OF SYNTHETIC INTERLAYERS IN BITUMINOUS PAVEMENTS

G. DONDI
D.I.S.T.A.R.T. DEPARTMENT
UNIVERSITY OF BOLOGNA, ITALY

ABSTRACT

The insertion of interlayers in bituminous pavements is quite widespread, although designers tend to use a wide range of synthetic interlayers, from nonwoven low-modulus to high strength polyester geotextiles, not always on the basis of their technical properties. This paper describes the results obtained in an experimental study carried out by our Department, based upon a series of dynamic tests. In order to simulate the road pavement, full-scale square samples were employed: in a steel box, partly filled with rubber, two bituminous concrete layers with different interlayers were placed. In some specimens, deep artificial grooves were made in order to examine a damaged existing pavement. The specimens were dynamically loaded up to failure, with the aim of achieving a simulation of fatigue failure, allowing to better understand sample behaviour. Static tests were carried out at intermediate stages during the dynamic loading. The results of the reinforced specimens, in terms of displacements and rut depths, demonstrated the advantages of interlayers insertion: geosynthetics appear to be able to delay the surface cracking due to reflection of fissures from the underlying layers. Failure cracking patterns can now be reported due to the completion of laboratory experimentation. Such patterns, which may be very different in the case of overlays standing on pre-fissured bases, show the benefits of interposing geosynthetics in pavements.

KEYWORDS: Pavements, Fatigue, Reinforcements, Reflection, Cracking , Prevention

1. INTRODUCTION

One of the main problems related to the durability of road pavements is represented by surface cracking, induced by fatigue, thermic effects and underlying cracking, i.e. for rehabilitation of cobbled roads (Fig. 1).

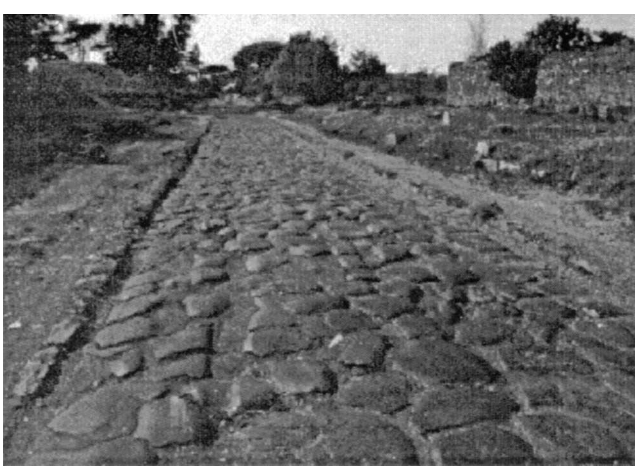

Figure 1. Cobbled surface of Via Appia, 2000 years old Roman road.

The interposition of geosynthetics as interlayers in asphalt pavements (often referred to as "reinforcement"), to prevent the mentioned phenomena, is quite widespread and has generally proved to be successful. Nevertheless, an overall accepted design method still does not exist. There are a lot of questions still pending regarding the best and worst type of interlayer (nonwoven geotextiles, geogrids, etc.), the appropriate position of installation and the opportunity of the insertion of interlayers also in new projects.

A reply has not yet been given to all these questions; however, with the laboratory experimentation described in this paper and the information obtained in situ with another experiment underway, an attempt has been made to contribute to the assessment of the behaviour of bituminous pavements containing synthetic interlayers. Only macro-reinforcement we will be considered in this article (Fig. 3); i.e., the interlayers that are well defined in the bituminous mix. This subject has already been studied in the past, from a theoretical point of view by our Department (Dondi and Righi, 1990), (Dondi, 1994) and, more recently, a large number of experiments were carried out. In an initial stage, for a preliminary static evaluation, some "three point bending" tests on asphalt beams: without interlayers (UR), with nonwoven geotextiles (GX) and with polyester (PET) geogrids (GG). Then created 24 specimens (1.4x1.4m) were created, having many different types of interlayers and degrees of disturbance (Fig. 2).

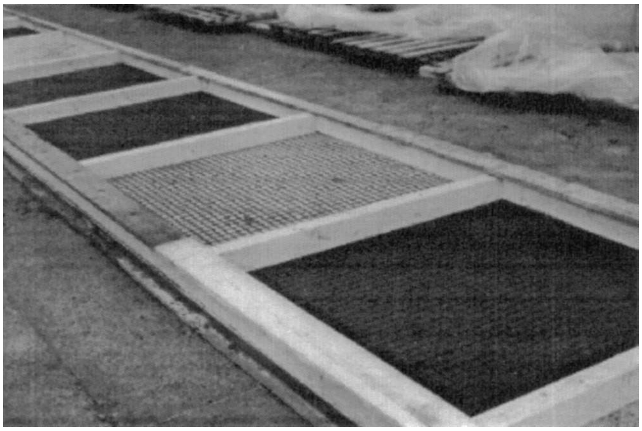

Figure 2. Sample preparation: in some, the longitudinal artificial cuttings can be seen.

It's well known that the reinforcement of asphalt requires high temperature resistant polymers: indeed, with modified binders, during compaction, the mix reaches high temperatures (140-150 °C and higher). For this reason, it was considered that the use of at least PP or PET geosynthetics would be necessary.

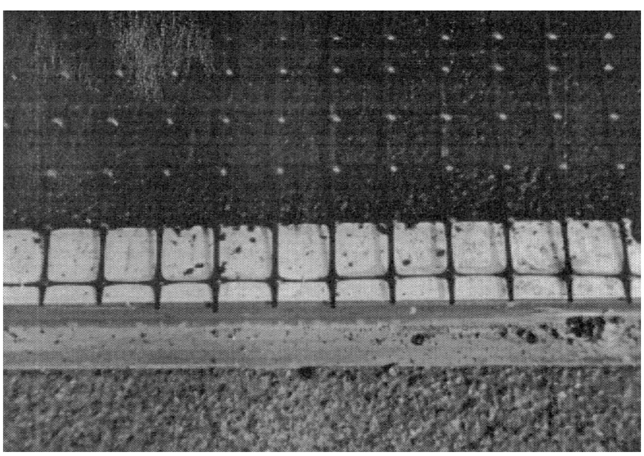

Figure 3. Detail of a polypropylene geogrid insertion in a specimen.

The insertion of nonwoven geotextiles in a flexible pavement generally causes a strength decrease, despite a better overall behaviour. For this reason, some stiffer geogrids or composites may be preferred. Furthermore, the latter theoretically appears to provide a better solution since it improves the linking with the upper bituminous layer also without any tack coat upon the interlayer surface.

2. PRELIMINARY PHASE

In the preliminary stage of the research, it was verified that, according to Judycki (1990), the best loading methodology was, for many reasons, the three point bending test since stresses and strains are more realistic. The samples were 100 mm wide, 85 or 100 mm high, and 600 mm long. The interlayer, when present, was placed 35 mm over the bottom of the sample. The rate of loading was approximately 50 mm/min', as also suggested by Kunst e Kirschner (1993) and all the tests were carried out using a bituminous mix, with a 5% of 80/100 penetration grade bituminous binder.

The grain size distribution curve of the aggregate is represented in Fig. 4, with the binder fuse of the Italian National Roads Administration.

As interlayers, we employed two geosynthetics currently used for road pavements: a nonwoven polypropylene geotextile (Grab Test, ASTM D-4632: 18 kN/m, ε_f=55%); and a polyester woven geogrid (Tensile strength: 60 kN/m). The tack coat was obtained with a cationic emulsion containing 70% of 80/100 bitumen, modified with 5 % Styrene-Butadyene-Styrene (SBS-R) modifier with radial structural arrangement.

Results showed that the most important improvement with interlayers was the increased capability of bearing high loads even after failure, i.e. a higher ductility.

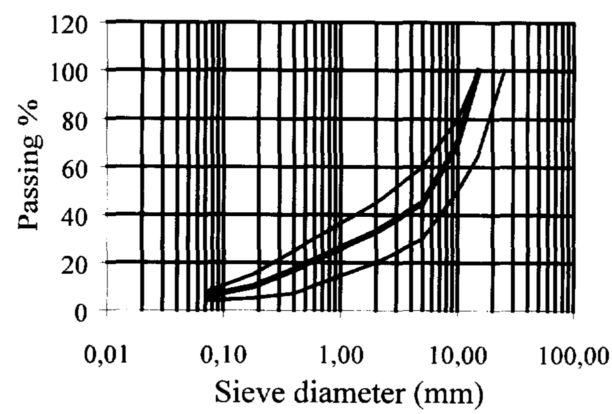

Figure 4. Grain size curve of the bituminous mix.

3. LABORATORY DYNAMIC TESTS

In a second stage described in this paper, we carried out more specific dynamic tests in order to better simulate traffic loads and boundary conditions (Dondi 1996). The first step of this research project consisted in a comparison of the results obtained with numerical models such as BISAR (De Jong 1973) and F.E.M. non linear models (Fig. 5), such as FENLAP (De Almeida 1993).

FENLAP is a computer program written in FORTRAN 77 language by J.R.de Almeida. This program performs a finite element calculation of an axi-symmetric solid and is designed for the structural analysis of pavements. It can run both on mainframe and on personal computers. FENLAP uses rectangular elements, distributed over a rectangular grid. A mesh with up to 23 columns and 23 rows, corresponding to a maximum of 484 elements (22 in each direction) may be analysed. The maximum number of layer which can be considered is 5. Due to the axi-symmetry, all nodes on the left side of the mesh are assumed to be on rollers, allowing vertical displacements but preventing radial ones. For the vertical boundary on the right side and for the lower boundary, several boundary conditions may be adopted as options. Nine different material models are given as an option for the stress-strain relationships of each layer; the main models and the corresponding elastic constants follow:

1) Linear elastic isotropic (all type of materials): 5 parameters, vertical Young's modulus E and Poisson's ratio ν;
2) Brown's (fine grained soils): 4 parameters, initial Young's modulus E_i, ν, A and B.

As non-linear models can be used in FENLAP, the program follows an iterative procedure in which the elastic properties are successively adjusted, for they depend on the values of stress computed. At each iterations, an error check is performed by comparing the new elastic moduli with the elastic ones determined in the previous iteration. If failure criteria are considered, the stresses are also compared with the values obtained in the previous iteration. When both errors fall below an admissible tolerance specified by the user, converge is said to be achieved and the iteration procedure is stopped.

In particular, we tried to establish the different behaviour of semi infinite and confined multilayered system with trial moduli. It was discovered that, in order to avoid significative boundary effects, the minimum dimension of square specimens was approximately 1.5x1.5 m.

Consequently, we created a bituminous concrete strip, approximately 36 m long, in two stages (two layers): after completion of the first one, artificial cuttings were also realised in some areas to represent the rehabilitation of a fractured pavement.

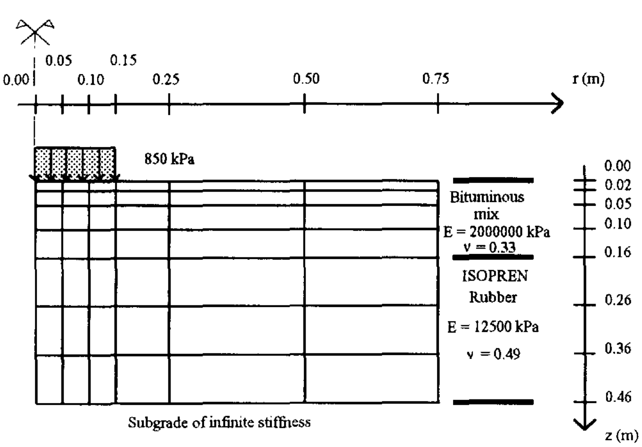

Figure 5. Numerical mesh (of the samples) for numerical analysis.

Various kinds of interlayers were then inserted; these specimens have the characteristics described in Table 1.

A steel box was then built to contain the asphalt specimens and the underlying layers (Fig. 6). The load was applied by means of a circular steel plate, with a diameter of 0.3 m standing on a rubber layer with the function of minimizing stress concentration related to plate stiffness.

To enhance only the behaviour of asphalt, and with the aim of reducing the uncertainties as much as possible, we decided to build the foundation bed with rubber.

This allows to minimise uncertainties related to resilient behaviour of granular materials and increases the reproducibility of the tests (Fig. 6).

Besides the traditional mechanical tests, other experiments were carried out in order to assess the complex modulus (E_c) and the phase shift angle (φ) of the asphalt specimens.

From the laboratory results of a simple static creep test, we obtained at a temperature of 25°C: E_c = 800 MPa and φ = 40°.

Table 1. Characteristics of specimens tested

a) Non Lesioned bituminous concrete (NL)
a.1) Unreinforced Specimen (UR);
a.2) Specimen with nonwoven geotextile interlayer (GX);
a.3) Specimen with bi-directional woven polyester (PET) geogrid (GG) interlayer;
a.4) Specimen with bi-directional polypropylene (PP) geogrid (RA) interlayer ;
a.5) Specimen with polypropylene (PP) geocomposite (GT=GX+GG) interlayer.
b) Lesioned bituminous concrete(LE)
b.1) Unreinforced Specimen (UR);
b.2) Specimen with nonwoven geotextile interlayer (GX);
b.3) Specimen with bi-directional woven polyester (PET) geogrid (GG) interlayer;
b.4) Specimen with bi-directional polypropylene (PP) geogrid (RA) interlayer;
b.5) Specimen with polypropylene (PP) geocomposite (GT=GX+GG) interlayer.
GX: tensile strength S_t = 18 kN/m (long.), 8 kN/m (trans.); yield strain ε_y = 55% (long.), 40% (trans.).
GG: tensile strength S_t = 60 kN/m (long.), 54 kN/m (trans.); yield strain ε_y = 14% (long.).
RA: tensile strength S_t = 20 kN/m (long.), 20 kN/m (trans.); yield strain ε_y = 13% (long.), 10% (trans.).
GT: tensile strength S_t = 20 kN/m (long.), 20 kN/m (trans.); yield strain ε_y = 13% (long.), 10% (trans.).

All the asphalt specimens, made outside in a single 36 meters long strip as described previously (see also Fig.2), were then cut away, brought in the laboratory, and placed directly on the rubber (settled down)in the steel box. Hence, as far as stiffness is concerned, , the rubber represents both the foundation and the subgrade layers. The asphalt specimens have a total thickness of 160 mm, arranged as follows (Fig. 6):

1. a 60 mm-thick asphalt layer bottom, in some cases fissured (indicated in the text as "LE", whereas the other non-fissured samples are referred to as "NL",) by cutting it with a steel tool to a depth of 50 mm;
2. the interlayer, when present, fixed with a cationic bituminous emulsion (1000 gr/m^2 approximately) tack coat;
3. a 100 mm-thick asphalt layer top.

In order to evaluate the minimum thickness of overlays, since some practical applications suggest that such a limit exists, we also realised some "REVERSE" samples (RE) in which the bottom asphalt layer was 100 mm thick (instead of 60 mm) and the overlay 60 mm thick (instead of 100 mm).

The load was applied with a hydraulic jack, controlled by the data acquisition system, at a frequency of 5 Hz. The shape of the loading wave is approximately sinusoidal and has an initial amplitude (ΔV_o) of 60 kN, in the range 5-65 kN. During the tests and in some cases with very high displacements, it was necessary to reduce this amplitude in order to maintain the original frequency.

Two reference grid patterns, 100x100 mm and 50x50 mm in the central portion, were sketched on the surface of the samples previously covered with white paint, to allow reporting the failure pattern vs. number of cycles.

Surface displacements, at different distances from the loading plate, were monitored with inductive transducers connected to an Instron data acquisition system (Fig. 6)

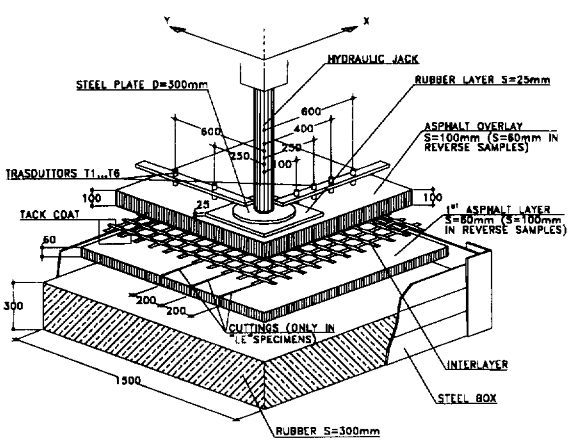

Figure 6. Sample composition.

In some tests, the acquisition of the temperature gradient to which the specimen is exposed during and after the test, by means of a temperature survey in several points and at various depths of the specimen, achieved by the installation of thermic probes with automatic data acquisition.

Figure 7. A specimen after 5x10^5 loading cycles

4. INTERPRETATION OF RESULTS

At the end of the tests (each one is approximately three days long), all the samples showed highly significant permanent displacements (Fig. 7), although the degree of damage was very different. Furthermore, cracks appeared later in specimens and their extension was much smaller than in samples without geosynthetics.

4.1 Cracking Pattern

As previously described, it is to be pointed out that the failure behaviour of the various types of samples differs substantially.

In non-lesioned samples (NL), cracking starts in radial directions on the free surface: this behaviour was previously observed by other authors (Kief et al., 1994, and therefore we could assume that this is normal for pavements whose unique factor of degradation is repetitive loading. In lesioned samples (LE), the cracking pattern, as shown in Fig. 9 for 5 x 10^5 cycles, follows the alignment of artificial cuttings.

The estimation of the benefit brought by the interlayers can be made by analysing the tables reported in this paragraph.

4.1.1 Normal Samples

The tables (Tab. 2 and Tab. 3) refer respectively to the specimens NL and LE.

These tables summarize the percentages of damaged surface (A_{les}) in comparison to the total area (A_t), and the decrease of cracking (ΔA_{les}) in the different situations (UR, GX, GG, GT and RA) in respect to the unreinforced the specimen (UR) at the end of every single test, after 5x10^5 loading cycles.

The surface under the loading plate was not included in the calculation of the total area.

Table 2. Percentages of the damaged surface in comparison to the total surface of the specimen (NL specimens).

Sample	NL-UR (%)	NL-GX (%)	NL-GG (%)	NL-GT (%)	NL-RA (%)
A_{les}/A_t	43	24	17	23	21
$\Delta A_{les}/A_t$	-	-44	-60	-47	-51

Table 3. Percentages of the damaged surface in comparison to the total surface of the specimen (LE specimens).

Sample	LE-UR (%)	LE-GX (%)	LE-GG (%)	LE-GT (%)	LE-RA (%)
A_{les}/A_t	38	13	10	9	17
$\Delta A_{les}/A_t$	-	-66	-74	-76	-55

The benefit had by the interlayer seems extremely high for all the type of interlayers and it is not excessively influenced by its modulus. In particular if we consider the NL specimens, we may observe a maximum improvement of 60 % (GG-PET and GT) while, for the remaining synthetic interlayer, the benefit proves to be quite steady at a range from 45% to 50%.

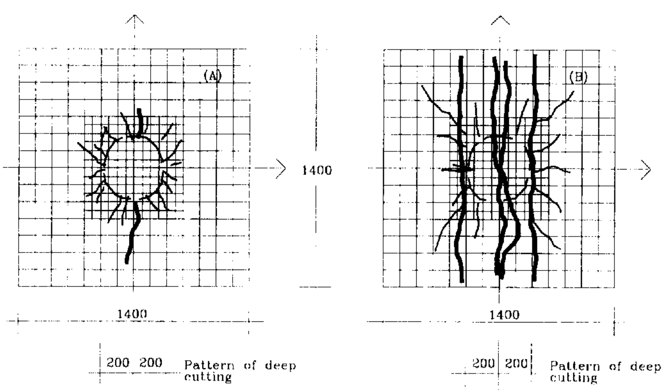

Figure 8. Cracking after 5 x 10^5 cycles in two samples: one, on the left, has an interlayer (NL -GX) and the other does not (NL -UR).

Instead, with regard to the LE series we obtain an maximum improvement of 74-76% (GT-PP and GG-PET) while, for the remaining materials, the improvement is sufficiently homogeneous with values between the 55% and the 66%.

Therefore, the improvement is more evident for the LE specimens although, also in this case, it is not strictly proportional to the strength of the interlayers.

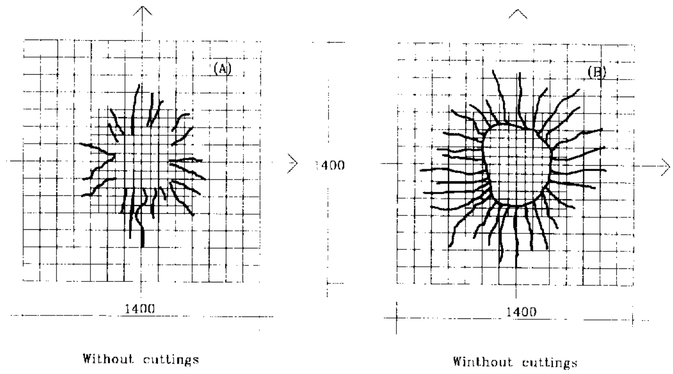

Figure 9. Cracking after 5 x 10^5 cycles in two samples: one, on the left, has an interlayer (LE -GX) and the other does not (LE -UR).

4.1.2 Reverse Samples

Also in these samples, characterised as previously specified by a thin overlay, the insertion of an interlayer reduces the cracking set, although the benefit is much more moderate than in the previous case.

Table 4. Results of "REVERSE" (RE-NL) specimens.

Sample	RE NL-UR (%)	RE NL-GX (%)	RE NL GG (%)	RE NL GT (%)	RE NL RA (%)
A_{les}/A_t	43	n.d.	31	28	34
$\Delta A_{les}/A_t$	-	n.d.	-28	-35	-21

The benefit achieved by the interlayer comes to a maximum improvement of 35 % (GT) while, for the remaining materials, the benefit proves to be quite steady at a range from 21% to 28%. Furthermore, with regard to the "reverse" series and unlike specimens with normal section, a very prominent, circular crack appears, at the edge of load mark, from which the previously mentioned radial cracks depart.

This confirms that the insertion of interlayers near the surface, as was foreseeable, must be taken into account with extreme caution.

4.2 Settlements

When analysing deformations settlement of non-fissured samples (NL), it is necessary to point out the difference between permanent deformations (visco-plastic deformation) and reversible ones (visco-elastic deformation).

4.2.1 Visco-plastic settlements

Permanent deformations, in the case there are no artificial cuttings, depend on the presence of interlayers, as is pointed out by Fig. 10. In this case, it appears evident that their extent is related to the modulus of the interlayer.

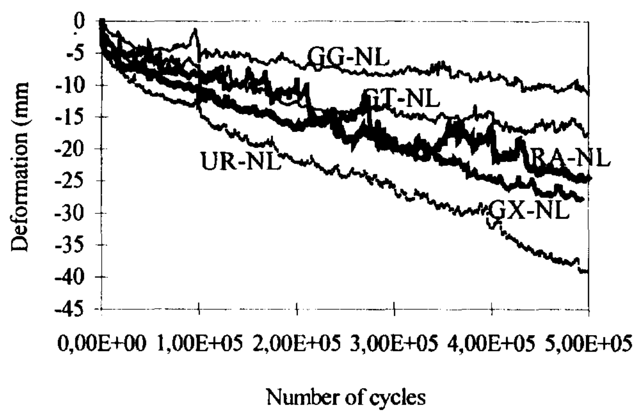

Figure 10. Permanent deformations under loading surface vs. N°. of cycles.

4.2.2 Visco-elastic settlements

Instantaneous deformations, with analogy to the previous case and in the same non lesioned condition, are also influenced by the presence of interlayers.

Hence, it's possible to assert that, when there are synthetic interlayers, NL specimens stiffness (not the resistance) increases in strict proportion to the modulus of interlayers. The improvement is made much more evident by increasing the number of loading cycles. This can be explained can be explained, order than by the fatigue behaviour, also by taking the specimens temperature into account. In fact, this conspicuously increases while the test is being carried out (Tab.5): this is due to the dissipation of the deformation energy, which is transmitted by the hydraulic jack.

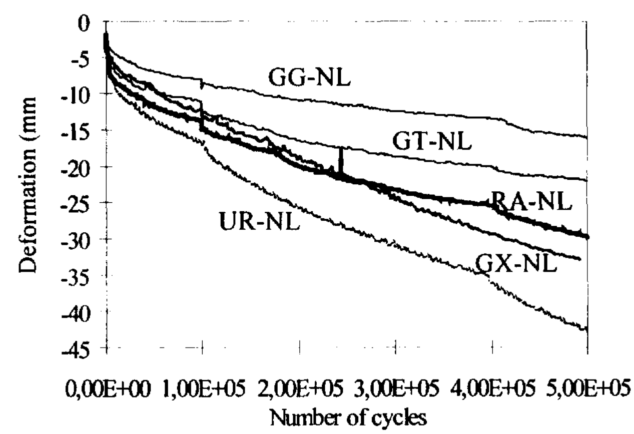

Figure 11 Instantaneous deformations under loading surface vs. N° of cycles.

It's also particular interesting to compare the details of the results obtained on two LE specimens, for which the behaviour appears significantly different in comparison with NL ones.

Table 5. Continuous logging of temperature in the specimen.

Load Cycle $x10^3$	Air Temp. C°	Probe 1 C°	Probe 2 C°	Probe 3 C°	Probe 4 C°
0	22.2	21.7	21.7	21.6	21.3
50	22.4	22.6	22.0	21.7	21.3
100	22.7	23.3	22.4	21.8	21.3
150	22.3	23.9	22.7	21.8	21.2
200	21.9	24.5	23.1	21.9	21.0
250	21.7	25.4	23.6	22.2	21.2
300	21.4	25.8	23.9	22.3	21.1
350	21.1	26.2	24.2	22.4	21.1
400	21.6	26.6	24.5	22.6	21.2
450	22.0	27.0	24.8	22.8	21.3
500	22.5	27.2	25.0	22.9	21.4

We now consider:

1. Lesioned specimen, without interlayers (LE-UR).
2. Lesioned specimen, with a nonwoven geotextile as interlayer (LE-GX).

In this case, maximum deformations (under loading) are surprisingly similar for specimens with (GX) and without interlayers (UR), while pseudo-elastic deformations follow a different behaviour: after 4 x 10^5 cycles, instantaneous settlements significantly increase in LE-UR specimens while they tend to be constant in the LE-GX specimen (see Fig. 12)

When analysing the total settlement of fissured specimens (see Fig. 12), the two curves for UR and GX samples are so close that no differences can be noticed.

So, contrarily to the NL case, we don't record any stiffness increase consequent to the introduction of a nonwoven geotextile in this case.

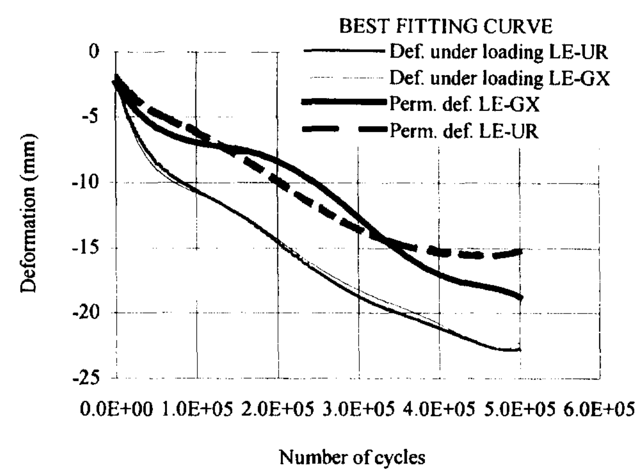

Figure 12. Settlement under loading surface vs. N° of cycles.

When taking into consideration the elastic fraction of the displacement, we can see that, prior to a certain number of cycles (i.e. approximately $4x10^5$, Fig. 12) the curves are quite similar. After this limit, there is a rapid increase of settlements in UR samples.

We can conclude that with LE specimens there is no reduction of permanent deformation but that the overall behaviour of LE-GX sample is better, considering the increase of pseudo-elastic stiffness.

5. IN SITU TESTS

In order to validate laboratory tests, we have created an experimental field by reproducing, in a lane of the Centro Padane Motorway S.p.A., A21 Piacenza-Cremona-Brescia (Fig.13), some sections very similar to those tested in the laboratory.

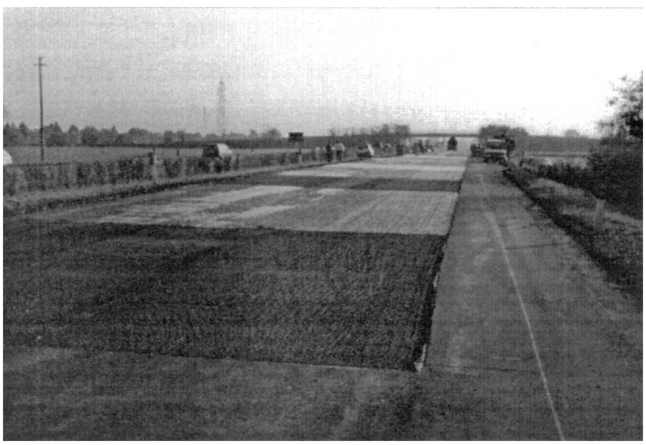

Figure 13. Experimental field in a motorway lane.

During rehabilitation works of the upper bituminous layer, deep cuttings were made (50-70 mm) in the binder layer (Fig. 14) between the edges of the road, in a 10 m wide and 120 m long area.

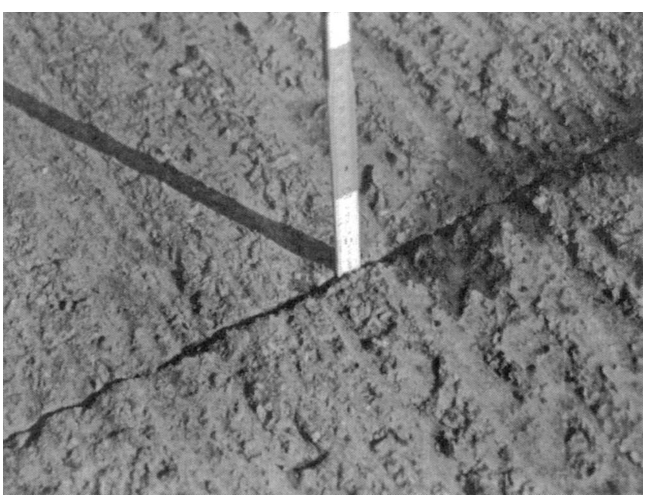

Figure 14. Detail of the groove.

These cuttings were regularly spaced at 500 mm to represent existing cracks (Fig. 15).

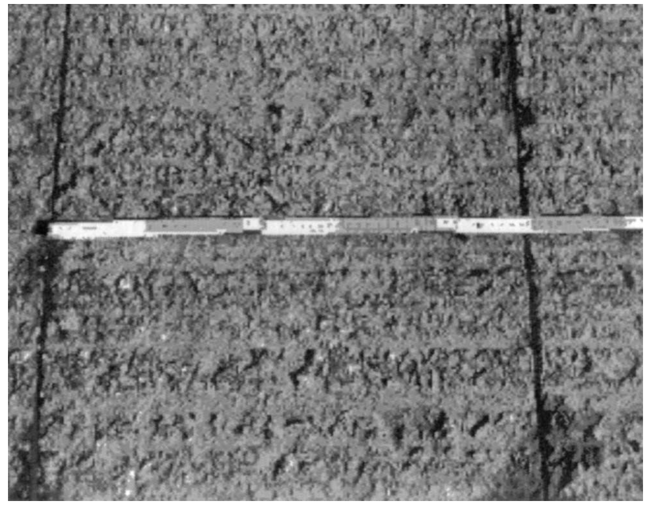

Figure 15. Detail of the distance between the grooves.

Then interlayers of different types, similar to those previously employed in laboratory tests, were laid down only on some parts of the lesioned field, on a bituminous tack coat (Fig. 16).

Finally, the lane was repaved with a layer of 90-100 mm thick asphalt. In order to evaluate the real traffic volume and composition, we also arranged in the vicinity a digital axles counter and an inductive load-measurement device.

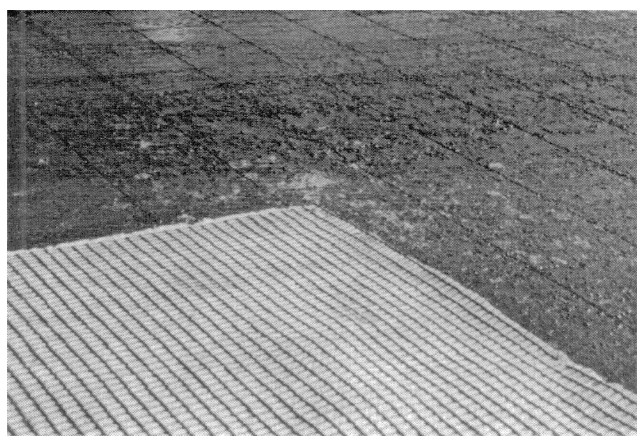

Figure 16. Detail of the reinforcement laying.

The experimental field, after nine months, performs well and there is no evidence of cracking reflection, neither in sections with deep cuttings and without interlayers, but the test is still continuing and we expect the results in next months.

6. CONCLUSIONS

The insertion of "high modulus" geosynthetics in upper bituminous layers requires a correct sequence of the following operations:

- thorough cleaning, through blowing and brushing, of the laying plane, or better through hydraulic jetting;
- sealing of the possible cracks through bituminous coat casting;
- laying of a first bituminous emulsion tack coat, possibly with elastomer;
- laying of the interlayer by means of a roller, equipped with clutch, able to provide low pretensioning stress;
- settlement of the surface by means of a clipper shearing machine for removing protrusions, resulting from a not perfectly homogeneous laying;
- laying of a second bituminous emulsion tack coat, possibly elastomer (it is not necessary if geogrids are used);
- laying and compaction of the subsequent asphalt layer.

When summarizing the achievable benefits, we may state that:

- advantages are particularly outstanding with geogrids and composites in critical conditions, such as heavy loads and for overlays of intensely fractured pavements;
- there is a significant improvement of the ductility of bituminous layers;
- with polyester geogrids, there is also a slight increase in ultimate strengths, without interlayer failure;
- in any case, also with nonwovens insertion with a good tack coat, the presence of an interlayer delays the cracking reflection and guarantees the durability for the overlays;
- the pseudo-elastic stiffness of the pavement is slightly increased and the degree of cracking is, in any case, much lower;
- with regard to the reduction of cracking ratio, the benefit brought by the interlayer seems extremely high for all types of interlayers and is not strongly influenced by the strengths and the moduli of this ratio. For the LE specimens and therefore with regard to the reflection of pre-existent cracking, the improvement is much more evident than for the NL specimens;
- it is absolutely unwary to place the interlayers too near the surface: the minimum coverage is 70 – 80 mm thick;
- recycling is allowed.

When designing a reinforcement, the following criteria should be followed.

When the geosynthetic is placed into the bituminous layers, it is necessary to observe some simple, but basic instructions during the laying of the interlayers: the laying stage is, in fact, fundamental, principally in order to guarantee a monolithic pavement. It's well-tested, in fact that an inadequate link between the layers, especially when geosynthetics with high bitumen absorption capacity are used, i.e. nonwovens and composites, can cause a quick failure of the pavement.

ACKNOWLEDGEMENTS

The Author wishes to thank Mr. Rimoldi, TENAX S.p.A., for laboratory facilities and Mr. Salvadori (Centro Padane Motorway S.p.A., A21 Piacenza-Cremona-Brescia, Italy) for his help for the realisation of in situ experimental field.

REFERENCES

De Almeida Rocha, J. C. G., (1993) "Analytical Techniques for the Structural Evaluation of Pavements", Thesis submitted to the University of Nottingham, Department of Civil Engineering, for the degree of Doctor of Philosophy.

De Jong, D.L., Peutz, M.G.F., and Korswagen, A.R. (1973) "Computer Program Bisar, Layered systems under normal and tangential surface loads".

Dondi, G., and Righi, P.V. (1990) "Rinforzo delle sovrastrutture stradali", Quaderno AIPCR: "L' Impiego dei geotessili e prodotti affini nelle opere stradali", XXI Convegno Nazionale Stradale, 11-15 giugno, Trieste, pagg, 9-18.

Dondi, G., (1994) "Three dimensional finite element analysis of a reinforced paved road", Proceedings of the 5th International Conference on Geotextiles, Geomembranes and Related Products, Sept., Singapore.

Dondi, G., (1995) "Le pavimentazioni flessibili rinforzate mediante geosintetici", Estratto dagli Atti del Convegno Naz.:"La ricerca nel settore delle infrastrutture interportuali e aeroportuali", 28-29 giugno, Trieste.

Dondi G., (1996). "Laboratory test on bituminous mixes reinforced by geosynthetics", 3rd International RILEM Conference on Reflective cracking in pavements, October 2-4, Maastricht, NL.

Dondi G., (1997) "Full scale dynamical testing on reinforced bituminous pavements", Geosynthetics '97 International Conference, 11-13 March, Long Beach, Cal., U.S.A.

Judycki, J., (1990) "Bending test of asphaltic mixture under statical loading", Proceedings of the fourth Intern. RILEM Symposium, October, Budapest.

Kunst, P.A.J.C., and Kirschner, R. (1993) "Comparative laboratory investigations on polymer asphalt inlays", Geosynthetics '93 Conference Proceedings, March, Vancouver, British Columbia.

Kief, O., Livneh, M., Ishai, I. and Altus, E. (1994) "Experimental and analytical approaches for studying reflective crack retardation", Proceedings of the 5th International Conference on Geotextiles, Geomembranes and Related Products, Sept., Singapore.

Geotextile Within Asphalt Overlay on a Brazilian Road: A 13-Year Case Study

P.R. Aguiar
MULTIGEO Eng. Associados, São Paulo, Brazil

C.E.L. Paiva
Professor, Geotechnical and Transport Enginnering Dept., Faculdade de Engenharia Civil, UNICAMP, São Paulo, Brazil

ABSTRACT: This paper examines the use of geotextile within an asphalt overlay on a rural road with medium traffic 13 years after application. Testing was carried out using four 300m long experimental sections of the road. Each one was further divided in two areas: a field test area with geotextile use and a control covered with ordinary asphalt. Different thicknesses of asphalt overlays were used. Data concerning the current pavement surface and structural stages are presented and compared with the original ones. Finally, some conclusions about the four sections are drawn and the concept of the technique employed is evaluated.

KEYWORDS: Asphalt overlay, geotextiles, pavements, rehabilitation, reflective crack prevention.

1 INTRODUCTION

The SP-52 in São Paulo, Brazil, carries medium traffic from the city of Cruzeiro to the boundary between the states of São Paulo and Minas Gerais. Local temperatures range from 10°C to 38°C.

In 1984 asphalt overlays were laid on the road in order to overcome severe pavement deformations. Four experimental sections with similar pavement structures were chosen for this study and each section was further divided in two areas: one of them received a geotextile reinforced overlay, while the second one was covered with conventional pavement for comparison.

The present work examines the current road surface conditions and compares deflection measurements carried out in 1984, in 1985 and in 1997, 13 years later.

2 PREVIOUS PAVEMENT CONDITIONS

The transversal section of the SP-52, built in 1967, consisted of a 0.03m thick asphalt concrete layer over a 0.15m thick wet-mix macadam granular base and a 0.20m thick sub-base reinforced with chosen soil, as shown in figure 1.

In 1981 the Average Daily Traffic (ADT) was 1121 vehicles, 29% of which were commercial (trucks and buses). In 1983 the pavement presented many surface deformations such as longitudinal cracking, alligator cracking, sinking, potholes, holes and localized patches. To solve these problems the pavement needed improvements in the base course and drainage system as well as repairs to the cracked surface course.

Figure 1: Previous pavement transversal section

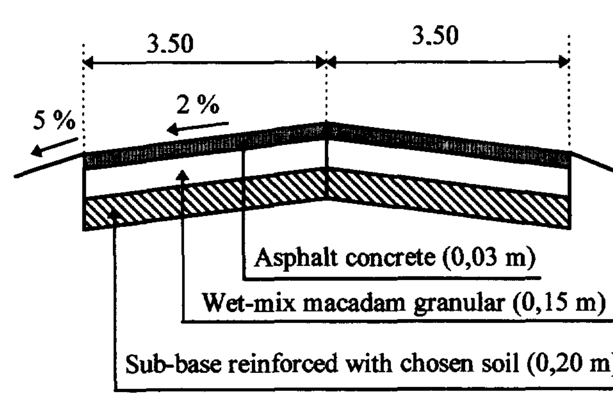

Four 300m long sections were chosen for the experimental design. Pavement structural conditions were done by means of Benkelman beam deflection measurements, taken in 1984 (before the overlay), in 1985 (4 months later) and in 1997 (13 years later). Figures 2 and 3 show the internal and external lane deflections, respectively.

Figure 2: Internal Lanes-Deflections

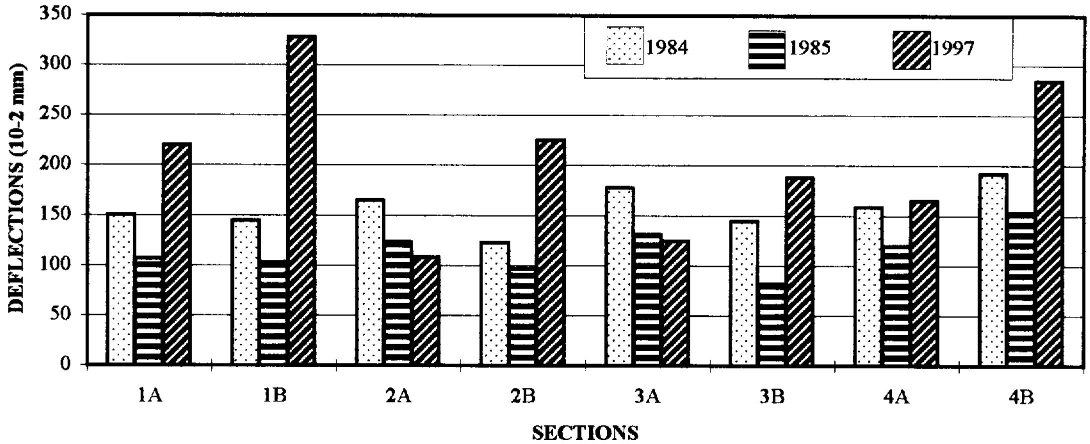

Figure 3: External Lanes-Deflections

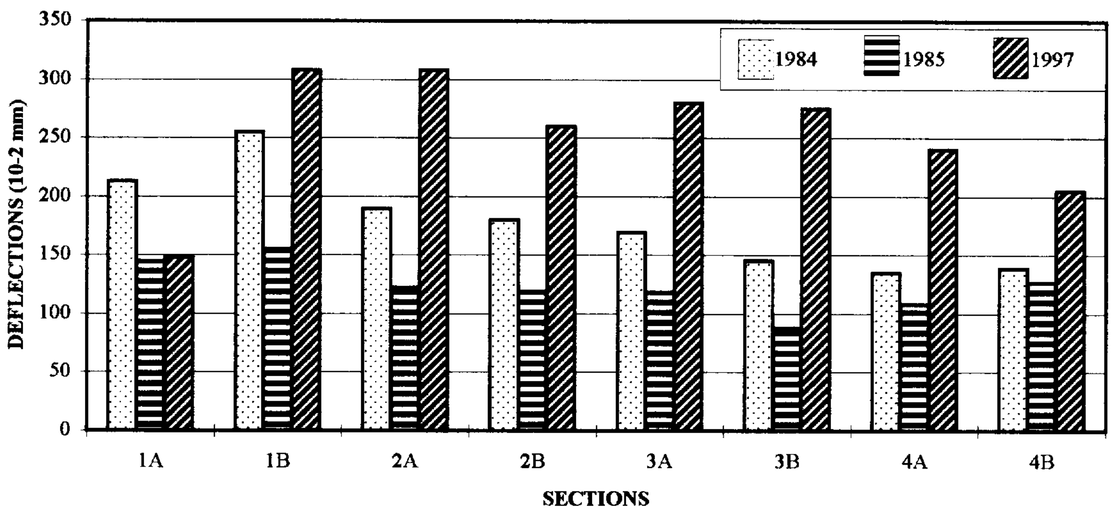

3 THE OVERLAY INSTALLATION

Since there were no project criteria considering geotextile reinforcement conditions in Brazil in 1984, the sections were designed according to the usual method based on USACE and thus ignoring the geotextile reinforcement properties.

Each 300m long section was divided in two areas with similar characteristics. The compositions of the pavement sections laid on each of them between May and June, 1984, are shown in figure 4.

A 100 % polyester non-woven continuous filament geotextile called BIDIM OP-20 (RHODIA-STER S/A) was employed (200 g/m2, 15 kN/m wide width tensile NF G-38014, 30-35% elongation). In the beginning and at the end of each section the geotextile was attached to the previous pavement with metallic staples in order to avoid sliding.

Table 1 summarises the main occurrences during installation (left and right sides of the road were named considering the São Paulo (Cruzeiro) - Minas Gerais direction), whereas figures 2 and 3 show deflection measurements done in 1985.

Figure 4: Overlays transversal sections

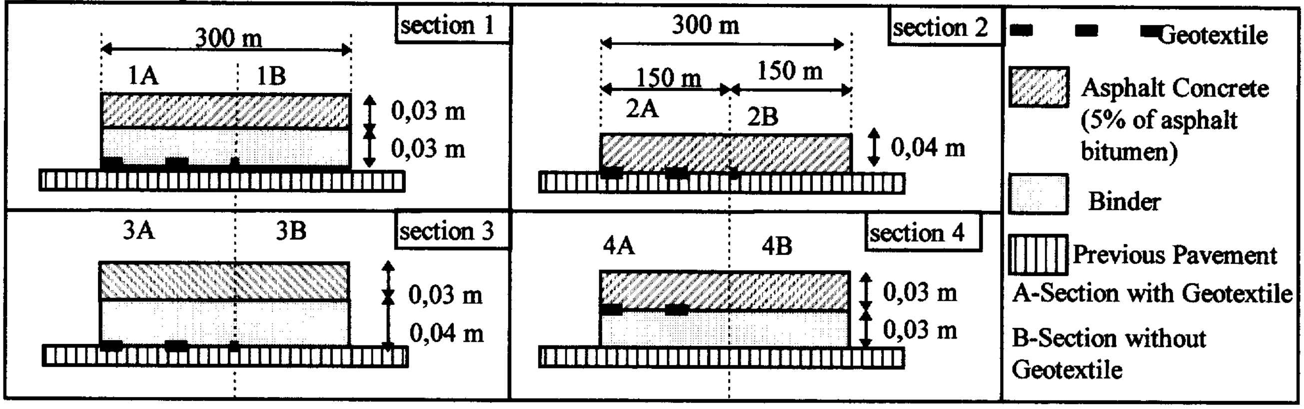

Table 1: Main Ocurrences during overlay installation.

Sections	Lane (*)	1ST Tack Coat (L/m^2) (**)	2ND Tack Coat (L/m^2) (**)	Observations
1.A	Right	0,90	0,50	Great number of wrinkles,some of them removed.
	Left	0,87	0,94	
2.A	Right	0,80	0,90	Right side without wrinkles; left side with few wrinkles,
	Left	0,70	0,62	eliminated by brushing; deteriorated base without any treatment.
3.A	Right	0,70	1,00	Section in curve, with ocurrence of wrinkles in its internal side.
	Left	0,60	0,90	The geotextile was cut and juxtaposed with prior pavement.
4.A	Right	0,50	1,40	Wrinkles removed by means of cutting and juxtaposing it with
	Left	0,70	0,90	prior pavement.

(*) São Paulo-Minas Direction
(**) Cationic Asphalt Emulsion

4 13 YEARS LATER

In 1995 an analysis made by the Department of Roads of São Paulo State (DER,1995) considered the pavement area to be good, with 14% of cracking, 0.05% of potholes and 0.30% of sinking. The ADT was then 1936 vehicles, 27% of which were commercial.

However, a more recent evaluation carried out in 1997 showed that there was an accelerated pavement damage in the last two years (figures 2 and 3). The current surface conditions were considered regular, with 32% of cracking severity, 5% of potholes and 30% of patches.

Table 2 summarises the observations during the 1997 evaluation.

5 CONCLUSIONS

The last deflection measurements presented in figures 2 and 3 as well as the surface deformations observed (table 2) lead to the conclusion that most of the analysed sections are at the end of their expected lifetime. These results differ somewhat from the ones obtained in 1995, when the pavement condition was considered good.

Comparing areas 1B to 1A and 2B to 2A one can conclude that the geotextile inlay acted as a reflective cracking barrier, albeit there were no significant differences either between areas 3A and 3B or between 4A and 4B.

Although sections 1 and 4 had the same asphalt concrete thickness, the former is very damaged while the latter is in good conditions. The reason for this disparity may lie on their positions on the road. Section 1 is located on a hill and immediately after a road police station, whereas section 4 presents no obstruction for free flow of commercial vehicles.

An intensive surface damage with alligator cracking was observed in a small segment of area 1A. Some small asphalt concrete pieces could be removed and it turned out that in the damaged area the course thickness was only 0.02m instead of the specified 0.03m. Therefore the asphalt concrete has come apart from the pavement after 10 years in operation.

Table 2: Conditions of the Sections in April 1997

Section	Lane	(MG-Cruzeiro)		(Cruzeiro-MG)		Observations	Concept
1A	Int	OK		TT	BI	Block cracking	Regular
	Ext	TB	AI	TL+TT	MI		
1B	Int.	TB	AI	TB	AI	Block cracking, alligator cracking	Regular
	Ext	J	MI	J	AI		
2A	Int	OK		TB	MI	Several segments in good state and others	Regular
	Ext	TL+T	BI	J	AI	in regular state with alligator cracking	
		T					
2B	Int	TL+T	MI	TL+TT	BI	Transversal and longitudinal cracking;	Regular
	Ext	T	AI	TL+TT	MI	few segments with alligator cracking	
		J					
3A	Int	TT	BI	OK		Segments in good state and others with	Regular
	Ext	OK		J	AI	alligator cracking	
3B	Int	TT+T	BI	OK	OK	Segments in good state and others with	Regular
	Ext	L	BI	TL+J	AI	alligator cracking	
		TT+T					
		L					
4A	Int	OK		OK		Good state	Good
	Ext	OK		TL	BI		
4B	Int	OK		OK		Good state	Good
	Ext	OK		OK			

TB: block cracking TL: longitudinal cracking AI: high intensity BI: low intensity Ext: External lane
J: alligator cracking TT: transversal cracking MI: medium intensity Int: Internal lane OK: Good
Regular: 25 to 50 % of surface defects; Surface cracking length lower than 3,5 m. PSI between 2,0 and 3,0.
Good: 5 to 25 % surface defects. PSI between 3,0 and 3,8.

Residual asphalt for geotextile impregnation was used in much smaller amounts than in the USA, in order to keep the geotextile drainage capacity and avoid the usual exudation that occurs in tropical countries.

There are still few overlays with geotextile in Brazil. A rise in such applications is expected, since some highways are now private and their owners take only high cost-benefit solutions. From our results it is thus possible to advise a 20% increase in the asphalt emulsion for the forthcoming geotextile applications.

ACKNOWLEDGMENTS

The authors would like to thank to the DER-Department of Roads of São Paulo, head and local offices, for the equipments and data of pavement system management of SP-52 road, and RHODIA-STER S/A by the data presented.

REFERENCES

Aguiar, P.R. (1984) "Relatório sobre a aplicação do geotêxtil BIDIM no recapeamento da rodovia SP-52", *RHODIA Report*, São Paulo, SP, Brazil.

Aguiar, P. R.(1985) "Avaliação e Planejamento da Aplicação BIDIM em Recapeamento Asfáltico" *RHODIA Report*, São Paulo, SP, Brazil.

DER-Departamento de Estradas de Rodagem do Estado de São Paulo (1995) "Levantamento de condições de pavimento - Rodovia SP-52", São Paulo, SP, Brazil.

Paiva, C.E.L, Aguiar, P.R. (1996) "Análise comparativa de algumas obras de recapeamento asfáltico com aplicação de geotexteis" *30ª Reunião Anual de Pavimentação*, ABPv, Salvador, BA, Brazil, pp 1458-1466.

UNICAMP- Universidade Estadual de Campinas (1997) "Levantamento de condições existentes do pavimento da rodovia SP-52", Campinas, SP, Brazil

Fracture Behaviour of Geosynthetics in Asphalt Layers

R. Lugmayr
Technical Consultant, Polyfelt Geosynthetics., Linz, Austria

ABSTRACT: The fracture behaviour of different overlay systems was determined due to a research from Tschegg et al (1998). Using a new wedge splitting procedure with deep notched drilling cores the fracture properties of the interfaces geosynthetic reinforcement - asphalt layers and the resistance to crack growth of reflection cracks in three different overly systems was determined in this paper. The test was carried out with a polypropylene needle-punched nonwoven geotextile, a flexible geocomposite interlayer consisting of polypropylene needle-punched nonwoven reinforced with high strength glass filaments and a stiff polypropylene geogrid with a nonwoven fixed on the junctions. The result of the research of Tschegg et al (1998) was evaluated and discussed in this paper from the practical engineers point of view.

KEYWORDS: Adhesion, Asphalt Overlay, Fractures, Geocomposites, Geogrids

1 INTRODUCTION

Formation and propagation of reflection cracks in bituminous pavements are unsolved problems in theory and practical application until today. It is necessary to characterize the fracture behaviour of the basic components in order to be able to calculate, model and simulate cracks. The fracture behaviour and bond strength of bonds between the asphalt layers, has to be determined.

The fracture behaviour of bituminous overlays and the bond strength was basically investigated due to the research at the Technical University in Vienna, Austria (Tschegg et al 1995a,b, 1997). In order to characterize the fracture behaviour of different overlay systems using typical geosynthetic products further research (Tschegg et al. 1998) was also done. The propagation of reflective cracks of the whole system and crack propagation of the interface was investigated. The determined results are of great scientifical and practical interest. The results are evaluated and discussed in this paper from the practical engineers point of view. Preliminary a short description of the research procedure (Wedge splitting test and experimental details) Tschegg and Co-worker (1998) is shown.

2 PRINCIPLE OF THE TESTING METHOD

In Figure 1 a core specimen of asphalt pavements with mounted loading device and displacement gauge is depicted. Specimens are placed on a narrow linear support in a compression testing machine.
The specimen has a rectangular groove with a starter notch at the bottom of the groove. For interface tests (fracture test of the adhesive bond) , the specimens are oriented in a way, that the interface is aligned in the plane defined by starter notch and linear support. In order to characterize the fracture mechanical properties of the crack propagation the Geosynthetic Interlayer is placed normal to the plane starter notch and linear support. A deep notch simulates the reflective crack up to the geosynthetic of the wearing course. A crack is forward to (through) the interface into the overlayer of the specimen during the fracture test due to the splitting force (loading condition: bending).

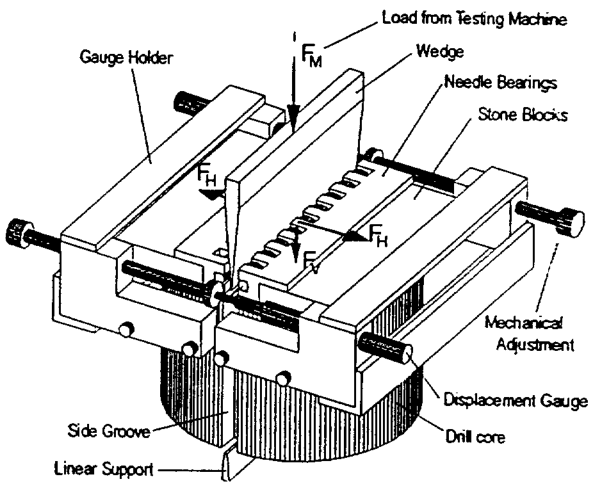

Figure 1: Test arrangement for drill core-specimen (according to Tschegg 1986)

Two load transmission pieces are placed in the groove and a wedge is inserted between them. The wedge transmits a force F_M from the testing machine to the specimen. The slender wedge exerts a large horizontal force component F_H and a small vertical force component F_V on the specimen. The force F_M is determined with a load cell in the testing machine. More details of the testing method is described in Tschegg et al 1995a and Tschegg 1997.

3 EXPERIMENTAL DETAILS

3.1 Material, specimen shape and size

From a bituminous base layer sample, of Austrian standard type BT I 16 (crushed aggregates, maximum grain size 16 mm, binder content 4.8-4.9 % of 100 pen-bitumen), plates of 70 - 80 mm thickness were produced. Compaction was performed with a vibration roller. Thus the asphalt aggregate mixture and production of the layer was similar to that, which is used in road construction. The plate surfaces were treated with a water jet until all binders and fine aggregates were removed from the surface. In this way a road with traffic was simulated.

Further drilling cores with a diameter of 200mm and a height of 120mm with and without interlayer were produced. In order to simulate a reflective crack the wearing course was then cut down of 10mm above the interlayer. Additionally two 50mm deep side notches were cut to eliminate border influences of the specimen. The ligament area has a dimension of 100x55mm and is large enough that the size effect has no influence on the test results. Two stone plates were glued onto the front face of the drilling core parallel to the starter notch. They act as a groove for taking up the loading device. In the case of the stiff geogrid interlayer it was distinguished between specimen with one and two bars (Fig. 2) in order to evaluate the influence of different bar number in the ligament area on the fracture behaviour.

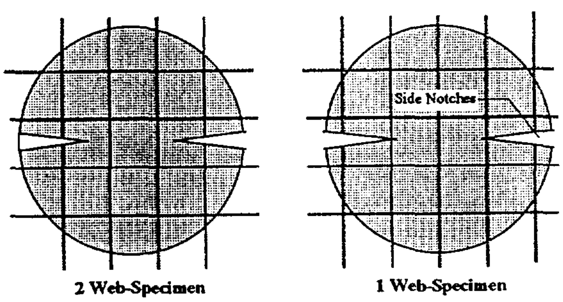

Figure 2 : One and two bar specimen

3.2 Testing conditions and evaluation

The vertical load of the testing machine is the transfered into the sample via a wedge ($\alpha/2=15°$) and two load transferring pieces. The load is applied over a roller bearing in order to eliminate any friction forces which would influence the results.
Testing was performed with a mechanical compression testing machine with a load capacity of 5 kN. Unstable crack growth was not observed in any of the tests. The cross-head velocity was 2 mm/min in all tests. Before testing, the specimens were stored in a cooling chamber with a control accuracy of +/- 0,5°C for approximately 24 hours. Testing temperatures were -10°C, 0°, and +10°C.

Investigated interlayers were installed according the producer recommendations. Used interlayer systems were:

A) Geotextile, flexible polypropylene needle-punched nonwoven ;
B) Geocomposite, polypropylene needle-punched nonwoven reinforced with flexible high strength glass fibers;
C) Geogrid, stiff pre-stressed deformation resistant polypropylene grid with nonwoven fixed on the junctions;
D) Control specimen without interlayer.

The complied load-displacement curves (in the following LDC) are characterizing the fracture behaviour fully, so this curves were used as a basis for the following test evaluation.

The fracture energy (energy which is necessary to split the specimen completely) describe the resistance against crack propagation. The area under the LDC is proportional to the fracture energy. The fracture energy can be obtained simply from the LDC. After dividing the established fracture energy with the area of fracture (projection) the specific fracture energy was obtained. This result is a parameter which is independent of shape and dimension of the specimen.

3.3 Interface fracture behaviour

The different fracture behaviour of the four interface types is best described by the shape of the post-peak section of the LDC in Fig.3. Without interlayer the curve drops very quickly after the maximum values has been reached, compared to geotextile interlayer. This means that with increasing crack mouth opening, without interlayer no more forces are transmitted, whereas with the fibers of the nonwoven geotextile probably bridge the crack and allow a transmission of forces (bridging effect). The surface structure of the geotextil interlayer and the geocomposite interlayer do not differ considerably. Therefore the geotextile shows a more shallow shape of the curve than geocomposite only in the very late post-peak section of the LDC. Due to the included glass fibers of the geocomposite the stiffness increased slightly and reduces insignificantly the bridging effect in the interface crack.

The nonwoven component fixed on the geogrid is extremely stiffened by the geogrid. The fibers are coarser, and the fiber structure is more dense, which results in a smoother and less felted surface of the nonwoven. With the geogrid, the binder cannot guarantee the bonding of the fibers to the base course. The bridging effect is thus small, as the nonwoven can be easily delaminated from the base course. This results in a much lower resistance against crack propagation compared to the other interlayer systems.

The area under the LDC represents the resistance against crack propagation. Figure 3 describe qualitative the high resistance against interface crack elongation of the "Geotextile and the flexible Geocomposite". The low resistance of the "Control and stiff Geogrid" specimen can be also obtained from Fig. 3.

3.4 Reflective Cracking Behaviour

The LDC of reflective cracking tests give the best overview of high resistance against crack propagation of interlayer systems. The fracture energy for the crack opening obtained from the LDC are determined till the crack meet the overlay surface.

The obtained specific fracture energies G_f is direct proportional to resistance against crack propagation. They are drawn up as G_f/G_{f0}, (G_{f0}=spec. fracture energy of specimen "Control") in figure 4. The figure point out very clear the excellent performance of geosynthetics to resistance of crack propagation at temperatures -10°C to +10°C. The "flexible Geocomposite" perform best of all investigated geocomposites. G_f -values of the "stiff geogrid" are not determined in the investigation Tschegg et al (1998) due to the low adhesion bonding of the interlayer. At temperatures 0°C and 10°C the adhesive bond strength is reduced due to the stiff geogrid. In fact, the specimen were detached during testing and the determination of LDC was not possible (Tschegg et al 1998).

For the long term behaviour of an asphalt wearing course the energy which is consumed at the beginning of the crack formation is decisive, where the cracked pavement can still fulfill its function. Therefore the specific fracture energies consumed up to a crack opening width of 4 mm at the testing temperature of -10C have been plotted in figure 5. This figure point out very clear the highest values of the consumed energy and the best resistance against crack opening of the flexible Geocomposites. This could be observed from small to large openings of cracks. Under equal conditions of loading the expected lifetime of the system with flexible Geocomposites versus the other tested systems is much longer.

More detailed information of increasing the resistance against crack propagation in asphalt overlayers can be found in the publication Tschegg et al (1998).

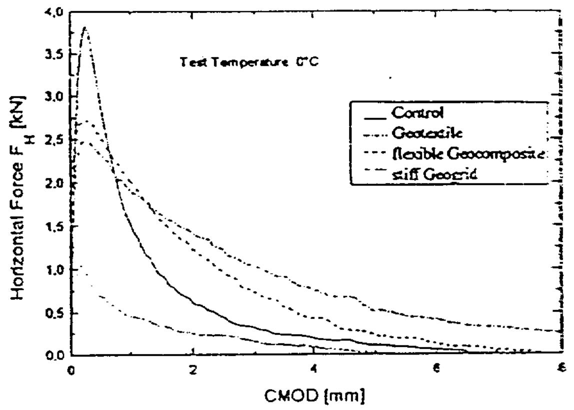

Figure 3 : Load-displacement-curve

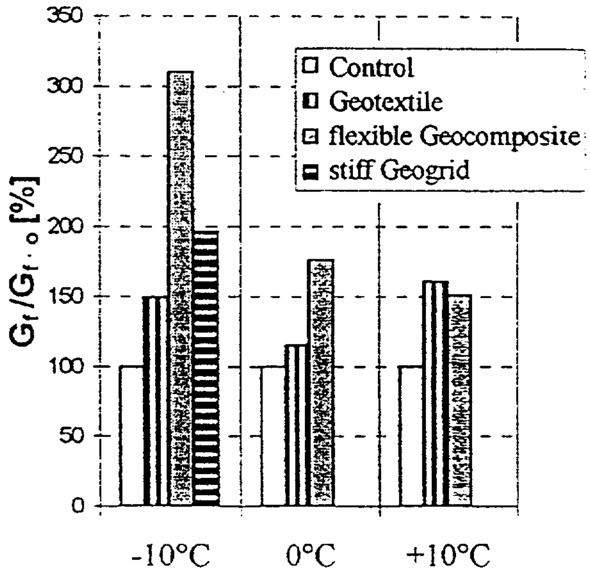

Figure 4: Specific fracture energy G_f/G_{f0}

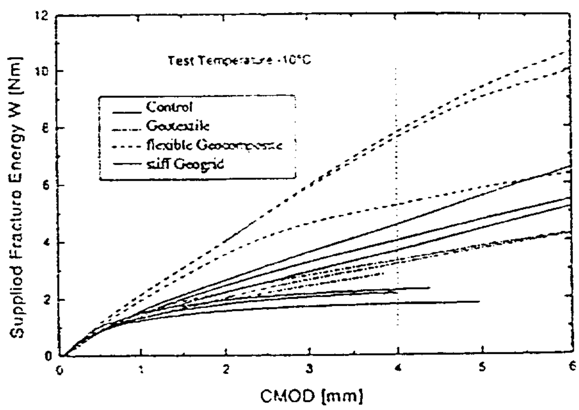

Figure 5: Supplied fracture energy acc. to Crack-opening-displacement

4 DISCUSSION AND CONCLUSION

The fracture mechanical parameters differ considerably for different interlayer systems. A high resistance against crack propagation is achieved by interlayers with flexible (low stiffness) and a good bonding to the asphalt layer by the polymermodified bituminous binder.

Maximum force values (F_{max}) from the LDC of the four investigated overlay systems (taken from Figure 3) considerable differences were found at 0°C. The F_{max} value is comparable with the values of the pull-of-test. Specimen without interlayer ("Control") show the highest values. However the highest resistance against crack propagation in the interface are achieved with Geotextile and flexible Geocomposite. The conclusion is that the adhesion bonding (calculated of max. strength) gives no statement of the fracture behaviour. Only the parameter G_f and a sound evaluation of the fracture behaviour results in a respectable statement of adhesive bond strength.

The normalized specific fracture energy G_f/G_{f0} (resistance against reflective crack propagation versus bonding without geosynthetics) shows the different fracture behaviour of overlay systems much more precisely than the strength values (calculated from F_{max}) taken from the LDC.

A high resistance against crack propagation was achieved with the flexible geocomposite interlayer with high strength glass fibers at temperatures of -10°C and 0°C. At higher temperatures, the differences were smaller.

The Load-displacement-curves show the consumption of energy during crack propagation as a function of Crack-mouth-opening-displacement and allow the judgement of the crack retarding effect of interlayers. The optimum performance is achieved by interlayers which consume most of the energy in the early post-peak section. If this effect starts at high Crack-mouth-opening-displacement values (i.e. in the late post-peak section) the overlay is already cracked and the interlayer has no significant beneficial effect.

It could be proven by the experiments (Tschegg et al 1998) that interlayers with good bonding to the asphalt show the highest resistance against reflective crack propagation.

5 SUMMARY

On different overlay systems, the fracture behaviour of the interface between interlayer and asphalt layer have been investigated with regard to reflection crack propagation using the wedge splitting method according to Tschegg.

The described wedge splitting method is suitable for the description of interface cracking and reflection cracking in overlay systems. Drill cores can be used as specimens, which are easy to be gained and handled, and need only slight modification. The testing procedure is simple and can be performed in a straight forward an inexpensive way.

For the practical engineer, this fracture test method can help to control and judge the construction quality of pavements with regard to crack formation.

With reference to the maximum splitting force F_{max} best performance is shown by the conventional homogeneous system without interlayer.

Due to the most inhomogeneous system the largest decrease is given with the stiff geogrid interlayer.

The best resistance against reflective crack propagation is illustrated by the flexible geocomposite interlayer and the geotextile interlayer.

REFERENCES

Tschegg, E.K. (1986), Equipment and appropriate specimen shapes for tests to measure fracture values (in German), patent AT- 390328.

Tschegg E.K., G. Kroyer, D.M. Tan, S.E. Stanzl-Tschegg and J. Litzka (1995b), Investigation of bonding between asphalt layers on road construction. ASCE J. of Transp. Eng., Vol. 121, No.4, pp 309-316

Tschegg E.K., (1997), An efficient Fracture Test Method for Bituminous Materials and Layer Bonds, in Proc. „Mechanical Test for Bituminous Materials", ed. By H.D. Benedetto and L. Francken, Of the fifth intern. RILEM symposium MTBM Lyon 97, France, pp 405-41.

Tschegg E.K., (1998) Fracture Behaviour of Geosynthetic Interlayers in Road Pavements, ASCE J. of Transp. Eng. in press 1998

Dondi G. (1996), Laboratory test on bituminous mixes reinforced by geosynthetics. Proc of RILEM Conf."Reflective Cracking in Pavements", Maastricht, pp 231-240

Jaecklin F.P. and J. Scherer (1996), Asphalt reinforcing using glass fibre grid "Glasphalt". Proc of RILEM Conf. "Reflective Cracking in Pavements", Maastricht, pp 268-277

Molenaar A.A.A.(1993). Evaluation of pavement structure with emphasis on reflecting cracking. State of the Art and Design Recommandations, Liege, March 1993

Polyfelt (1986) Design and Practice Manual for Geotextiles

Response Investigation and Design Guidelines for Asphalt Pavements with an EPS Geofoam Sub-base

M. Duškov
Consultant Pavement Engineering, Oranjewoud BV, Rotterdam, The Netherlands

L.J.M. Houben
Head of Road and Railroad Research Laboratory, Delft University of Technology, Delft, The Netherlands

A. Scarpas
Research Associate, Delft University of Technology, Delft, The Netherlands

ABSTRACT: The use of Expanded PolyStyrene (EPS) Geofoam instead of traditional "heavy" sand for pavement sub-base can reduce or even eliminate the additional load on the subsoil, thus decrease or eliminate the settlement of pavement structures on a compressible subsoil. The experiences with EPS geofoam are very promising but a uniform design procedure does not yet exist for this type of structure. Optimisation of the existing EPS pavement design guidelines and their improvement has demanded materials research on EPS, the use of three dimensional finite element pavement models and in situ full-scale measurement. Extensive materials research provided data for the stress-strain response of EPS under representative loading and environmental conditions. 3-D modelling enabled critical evaluation of existing design methodologies by analyzing pavements with different roadbases, different EPS types and different asphalt thicknesses. In situ measurements by means of built-in strain transducers in asphalt provided data for verification of the 3-D modelling.

KEYWORDS: Geofoam, Road Construction, Soft Soil, Finite element analysis, Material Tests

1 INTRODUCTION

This paper deals with the use of Expanded Polystyrene (EPS) Geofoam as a light-weight sub-base material in pavement structures. In comparison with other sub-base materials EPS has, besides an extremely low density and a low modulus of elasticity, a low water absorption and a low thermal conductivity. Through a substantial reduction of the pavement's weight, EPS as a sub-base material offers a major new solution for reduction of the settlements of new road structures and roads to be widened in areas with soils of poor load-bearing capacity. Such areas are present in the western and northern parts of the Netherlands. The application of EPS however affects the performance of the overlaying structure. To investigate, on one hand, to which extent the EPS characteristics influence the overall pavement behaviour and, on the other, the long term durability of EPS in relation to varying environmental conditions, materials research on EPS, in- situ measurements and numerical analyses of the structural behaviour of pavements with an EPS sub-base have been carried out. Based on the research findings the current Dutch design guidelines have been revised and optimized.

2 MATERIALS RESEARCH

The extensive testing of the EPS material involved the characterization of the elastic and permanent deformation behavior under both repetitive and static loadings, the water absorption of EPS, as well as the mechanical properties of EPS15 and EPS20 after water absorption and freeze-thaw cycles (Duškov 1997). Summarizing the experimental results it can be stated that:

- EPS absorbs water very slowly and to a limited extent. The maximum percentage of water, that EPS20 will absorb, is 2% v/v. The maximum percentage will rapidly increase, however, if EPS is overloaded and its cell structure is damaged.
- The dynamic E modulus of EPS20 under the loading conditions corresponding to the maximum expected values for pavement sub-base conditions, has the values which are somewhat larger than the value of 5 MPa which is normally used in pavement design procedures.
- The Poisson's ratio value of EPS20 of 0.10 seems to be appropriate for design purposes.
- Low temperatures, water absorption level and exposure to freeze-thaw cycles, separately or combined, have no negative influence on the mechanical behaviour of EPS.
- Under a static stress of about 20 kPa corresponding to the dead weight of the pavement toplayers, the creep of EPS20 amounts a few tenths of a percent. The practical consequence is a small additional permanent vertical deformation of the pavement structure caused by creep of the EPS sub-base layer. The main part of this creep however occurs during construction of the overlaying layers.
- The ultrasonic test method has potential to be used on site to determine the elastic modulus at various positions of EPS blocks for quality control purposes. Additional work has to be done, however, to validate the test procedure.

3 IN SITU MEASUREMENTS

In order to get an insight into the structural behaviour of flexible pavement structures with an EPS sub-base, asphalt strains and surface deflections have been measured on the Matlingeweg in Rotterdam. The considered pavement structure was of interest for investigation because of its sub-base, which consists of a 1.0 m thick EPS layer, combined with a heavy traffic loading. The measurements were carried out by means of the Falling Weight Deflectometer (FWD) and four strain transducers built-in at the bottom of the asphalt layer. Overlaying of the pavement structure has taken place much earlier than it was originally planned because severe cracking occurred at the pavement's surface within a few weeks after reconstruction.

The temperature dependent behaviour of the asphalt layer disables a direct comparison between the measured strain values. It implicates that those values have to be translated to a reference temperature before comparison. The back-calculated E-values in the pavement structure layers were used to transform the measured asphalt strain values to a reference temperature and to present the trend of the transformed strain values as a function of the pavement structure age.

The following conclusions and recommendations regarding the pavement condition in general (after 3 years in service) and the elasticity moduli of the pavement layers in particular are drawn:

- The back-calculated very low E-values for the sand capping layer (from 40 to 65 MPa) and the crushed masonry/concrete base (from 80 to 85 MPa) before overlaying highlight the inability of the EPS to provide a proper support to the roadbase in the considered pavement structure with a 130 mm thick asphalt layer. Correspondingly insufficient support of the roadbase to the asphalt layer resulted in a critically high asphalt strain of about 192 μm/m (T=20°C). Use of overestimated E-values for the roadbase materials was probably the main reason for the inappropriate pavement design.
- Open joints between the EPS blocks in a sub-base can have very serious consequences for the design life of pavement structures, and thus have to be avoided by all means. The joints between the blocks in various layers should not coincide with each other. Open joints are especially risky in the case of an EPS sub-base which consists of only one EPS layer. The longitudinal joints between the EPS blocks should not be close to a wheel track. An adequate (lateral) support of the blocks is necessary to prevent any movement of the blocks.
- The back-calculated E-value of the EPS sub-base ranges from 10.4 to 19.7 MPa, which is somewhat higher than the elasticity moduli found in literature for the EPS types under consideration (EPS25 and EPS30).
- The back-calculated E-value of the asphaltic concrete layer varied between 5,000 and 25,000 MPa, due to the temperature range of 0.2°C to 31.0°C, during the various FWD measurements. The E-modulus was about 10,500 MPa for the reference temperature T=20°C.
- The E-value of the crushed masonry/crushed concrete base ranged from 140 to 600 MPa after overlaying. The modulus found for the sand varied between 70 and 150 MPa. In some measurements the values found for the crushed masonry/concrete base were lower than could be expected for this unbound material. In order to design an appropriate pavement thickness on an EPS sub-base the E-values obtained in this study for the unbound base and sand layer are suggested to be used as input data in calculations of the design life.
- The asphalt strain remained more or less constant in the 3-year period after overlaying. The constant value of the strain is a sign of a good condition of the pavement structure. The maximum horizontal tensile asphalt strain amounts to about 85 μm/m at the reference asphalt temperature of 20°C.

4 3-D FINITE ELEMENT ANALYSIS

4.1 Modelled Pavement Structures

The three-dimensional (3-D) finite element analysis of pavement structures with an EPS sub-base layer is necessary since it allows modelling of the block structure in the EPS sub-base, in contrast with two-dimensional or axial symmetric pavement models. Three separate 3-D analyses were carried out. Firstly, a 3-D pavement structure model was developed with a single vertical interface layer next to the wheel load. Secondly, a polder road was analyzed; in this case a much more complex model was developed to analyze the effects of: *a)* different block patterns, *b)* various EPS types in the sub-base and *c)* a concrete capping layer, on the stress and strain values in the pavement layers. Finally, using experiences from the previous analyses, a model for a motorway pavement structure was designed with a simplified EPS block structure to investigate the consequences of implementation of EPS (instead of sand) on the behaviour of (Dutch) motorway pavement structures.

The analysis of single-joint pavement structure model was performed to investigate whether the existence of an open joint in the sub-base does affect the pavement behaviour. In this particular analysis one interface layer was used to model the vertical joint. The wheel load was placed just adjacent to the joint to enforce maximum shear forces in the layer above the EPS sub-base. Also the effects of using a concrete (capping) layer above the EPS sub-base and a somewhat different EPS type were determined.

The polder road analysis was carried out because in the western part of the Netherlands a great number of polder roads are located in areas with a low bearing capacity subsoil. These polder roads, constructed in the traditional way on soft, saturated subsoil, are subjected to (uneven) settlements. The use of EPS, particularly in the sub-base of these roads, is likely to offer a solution for the settlement problems by reducing the weight of the pavement structure. Once designed, the 3-D polder road model enabled the analysis of the effects of different block patterns in the sub-base on the pavement structure behaviour. The complexity of the model was defined by the need of modelling different block patterns by means of a single mesh.

The last finite element analysis was performed on a model for a motorway pavement structure with layer thicknesses corresponding to the usual values for Dutch motorways (see Figure 1). 3-D modelling of the heaviest loaded road type was done to determine to which extent building-in of EPS blocks in the sub-base influences its structural behaviour. The reference was an identical structure with a sand sub-base layer. Additionally, the effects of a concrete capping layer above the EPS blocks were investigated. Based upon the results of the previous analyses the motorway model was simplified compared to the polder road model. A single vertical joint was designed in the EPS layer and the axle load was placed next to that joint.

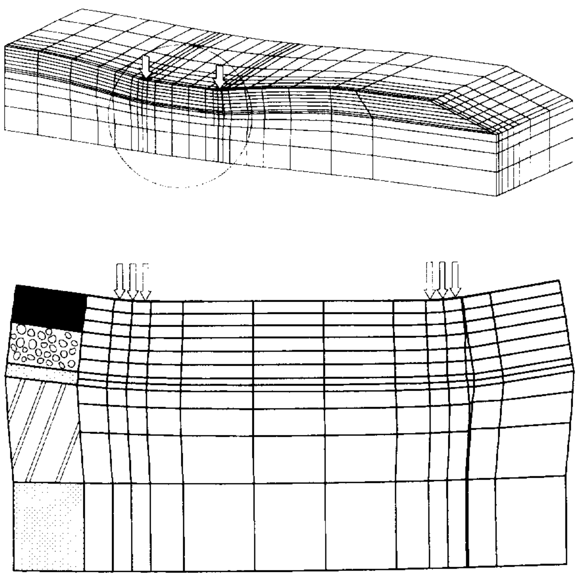

Figure 1. Resulting deformations due to a 100 kN axle load in a motorway pavement structure with an implemented EPS sub-base

All described models and analyses were realized by the means of the three-dimensional version of the finite element program CAPA (Computer Aided Pavement Analysis) (Scarpas 1995). The implemented interface elements allowed a flexible simulation of mechanisms in joint faces making this program one of the best of its kind.

4.2 Concluding Remarks on 3-D Finite Element Analyses

- Open joints between the EPS blocks in the sub-base significantly affect the behaviour of pavement structures with an unbound roadbase. The wide joints make it impossible to support properly the above-laid unbound base. This results in insufficient support of the roadbase to the asphalt layer. Consequently, higher stress and strain values occur in the asphalt layer under the wheel load with as final result a shorter life of the pavement structure.
- Implementation of a concrete capping layer above the EPS sub-base neutralizes the (negative) influence of the joints between the EPS blocks on the pavement behaviour. Such a capping layer ensures enough support to the unbound roadbase layers above this layer, also in the case of existing open joints between the EPS blocks.
- The maximum vertical stress values occurring in the EPS sub-base layers under the 100 kN standard axle load do not exceed the linear-elastic region experimentally determined for this material.
- Application of a denser (and more costly) EPS type with a somewhat higher elasticity modulus in the sub-base has only a very limited influence on the horizontal strain values at the bottom of the asphalt layer and, therefore, on the overall behaviour of pavement structures with an EPS sub-base.
- In the case of the polder roads the existence of open vertical joints in the EPS sub-base results into approximately 10% higher horizontal asphalt strains under the 100 kN standard axle load when a wheel load is located above such a joint. Accordingly, if longitudinal open joints coincide with a wheel track it could lead to a reduction of the pavement life with about 40%.
- EPS sub-bases where the blocks are laid in various patterns deform somewhat different under traffic load. Different sub-base behaviour occurs along the joints between the EPS blocks. However, the absolute deformation differences are so small that the effects on the structural pavement behaviour are of no practical importance.
- The (negative) influence of the division of the sub-base into two sublayers seems to be very limited. Still, building-in the EPS blocks in at least two sublayers in the sub-base is recommendable to avoid continuous vertical joints. Avoiding open joints between the EPS blocks demands accurate laying and in order to do this it is easier to use less thick blocks because block dimensions always deviate somewhat.
- In case of the polder road, pavement strengthening by increasing the asphalt layer thickness with 30% (extra 50 mm) or by building-in a 150 mm thick cement treated capping layer above the EPS sub-base appeared to be similarly beneficial with respect to the horizontal asphalt strain. The realized asphalt strain reduction amounts to approximately 30% resulting in a 6 times longer pavement life.

- ❑ The horizontal strain values at the bottom of the asphalt layer of the motorway pavement structure with the sand sub-base are approximately 40% lower than the corresponding values above an open joint in the EPS sub-base. As a result of this the reduction of the pavement life would amount to about 12 times if the EPS sub-base has been built-in with a wide joint exactly along the wheel track.
- ❑ The implementation of a concrete capping layer above the EPS sub-base enables the design and construction of light-weight pavement structures with an EPS sub-base, suitable for heavily loaded motorways. Its design life is even longer than that of the corresponding traditional structures with a sand sub-base.

5 DESIGN GUIDELINES

5.1 Current Dutch Design Guidelines

Generally speaking, the current Dutch design procedure for pavement structures with an EPS sub-base includes three steps. In the first step the list of requirements is being established by defining both the boundary conditions and the design starting points. In the next step it is checked whether the implemented light-weight sub-base assures sufficient reduction, if not elimination, of settlements without danger of upward movements due to buoyancy. Repeated calculations for different sub-base thickness values in the assumed pavement structure lead iteratively to the optimum EPS layer thickness. Finally the durability of the considered pavement structure and built-in materials is checked for the expected traffic loading during the design life. Based on these calculations the thickness of the upper pavement layers above the EPS sub-base has to be determined.

The boundary conditions are: in-situ subsoil conditions, groundwater level and traffic intensity. Important subsoil conditions are the geotechnical profile, the density and thickness of the layers, the sensitivity to settlements, the soil mechanical history (settlements in the past) etc. The starting points, i.e. arbitrarily defined preconditions, are: the pavement design life expressed as the number of 100 kN standard axle load repetitions, the street level, and pavement material characteristics of the previously selected type of pavement structure.

This design procedure differs to a certain extent from the Dutch design procedure that is followed in the case of application of a traditional sand sub-base. The differences regard the weight-balance and the buoyancy calculations. Both calculations serve the purpose of determining the proper thickness of the EPS sub-base. With "proper EPS sub-base thickness" is meant such a thickness that subsoil settlements are eliminated or reduced to an acceptable amount; water absorption in the EPS sub-base is taken into account in the subsoil stress calculation by assuming an EPS density of 100 kg/m^3. The excavation depth for the EPS material may be restricted by considering the buoyancy forces for the case of highest possible ground water level. Even if areas are flooded the upper pavement layers must be heavy enough to keep the EPS sub-base in position. In the buoyancy calculation the dry density of the EPS sub-base material is used. The minimum safety factor recommended for buoyancy calculations amounts to 1.1 (De Wijs and Hengeveld 1988).

Once the proper EPS layer thickness has been determined the design procedure continues with calculation of the pavement design life based on the Shell Pavement Design Manual (1978). This mechanistic procedure is the main pavement design method used in the Netherlands. The Shell Pavement Design Manual considers the horizontal tensile strain at the bottom of the asphalt layer and the vertical compressive strain at the top of the subgrade to be of critical importance for the design. The asphalt strain value has to be limited in order to prevent asphalt fatigue cracking while the limitation of the vertical strain serves to prevent excessive permanent deformation in the subgrade. In the Manual strain values are given as a function of the allowable number of load applications. So, by knowing the strain values, one is able to determine the pavement design life expressed as 'allowable number of 100 kN axle load repetitions'.

5.2 Shortcomings of Current Design Guidelines

The missing part in the discussed current design procedure for pavement structures with an EPS sub-base is a design criterion regarding the EPS material. There is no established maximum value for either strain or stress occurring in the EPS layer due to the traffic load, the limit value which should not be exceeded because of negative effects on the material behaviour.

The strain occurring in the EPS layer is a result of the dead weight of the upper pavement layers, on one hand, and the traffic loading, on the other. Generally speaking, the higher the (static) strain component due to the dead weight, the lower the (dynamic) component due to the traffic loading. The static strain due to the dead weight of a thin pavement structure (where a relatively high dynamic strain can be expected) amounts to about 0.2% (Duškov 1997).

Cyclic loading test results point out that EPS15 does not accumulate permanent deformations under combined static and cyclic stress of 15 kPa and 20 kPa respectively. The related total strain amounted to 0.6%. EPS20 resisted a cyclic stress component of 30 kPa, i.e. undergoing cyclically a total strain of about 0.7%, without permanent deformation.

Based on the results reviewed above it may be stated that as long as the elastic deformation in the EPS sub-base due to repeated (traffic) loads is limited to 0.4%, then permanent deformation of the EPS blocks is negligible and will have no influence on the pavement behaviour. Therefore, the design criterion for the EPS layer should be a maximum strain value of 0.4%.

In completed pavement structures the strains in the EPS sub-base due to the traffic loads are unlikely to be critical. More problems can be expected in the construction phase before all layers are built-in. If the EPS layer is overstressed by the construction traffic driving on (unbound) base layers, the effective EPS elasticity modulus is reduced and the water absorption increases.

Pavement analyses by means of both multi-layer (Duškov 1991) and finite element models (Duškov 1996) pointed out a negligible influence of the EPS thickness on the structural pavement behaviour. Due to the low elasticity modulus the EPS block layer simply does not contribute to the load distribution and functions only as a fill material.

Since the stress and strain values in the pavement layers are independent of the thickness of the EPS sub-base it is possible to determine the pavement design life before carrying out settlement and buoyancy calculations. As input value an unit EPS thickness, e.g. 0.5 m, could be applied. The advantage of such an approach is that the upper pavement layers can be designed first and their total weight thus is known before carrying out the weight-balance calculation and determining the thickness of the EPS layer.

5.3 Revised Design Guidelines

Based on the considerations given in the previous chapters the following guidelines for the design of pavements with an EPS sub-base are given.

- ⇨ In designing the pavement it must be realized that EPS20 blocks in contact with water will absorb about 2% v/v of water. EPS15 blocks will absorb more water, probably about 3% v/v. Although these volume percentages are low it means a considerable increase in weight which has to be taken into account when designing roads with EPS sub-bases. The usually assumed maximum density of saturated EPS of 100 kg/m^3 contains a high safety factor, a density of 50 kg/m^3 seems to be a more realistic value.

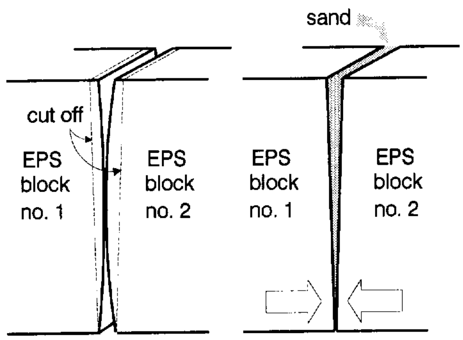

Figure 2. Filling up of joints between deviated blocks

- ⇨ During construction much attention should be paid to proper placement of the EPS blocks. All joints should be closed and load transfer across the joints should be promoted. As in the case with concrete block pavements, filling of the joints with jointing sand is strongly recommended. In order to be able to fill the joints a **V** type joint is recommended (Figure 2). Blocks with such joints can be easily made.
- ⇨ The EPS thickness has a negligible influence on the structural behaviour of the pavement. Therefore, first the upper pavement layers should be designed by using an unit EPS thickness, e.g. 0.5 m, and then, when the exact dead weight of the upper pavement layers is known, the weight-balance calculations should be performed and the proper EPS thickness determined. The revised design procedure, including the ϵ_{EPS} criterion, is shown in Figure 3.

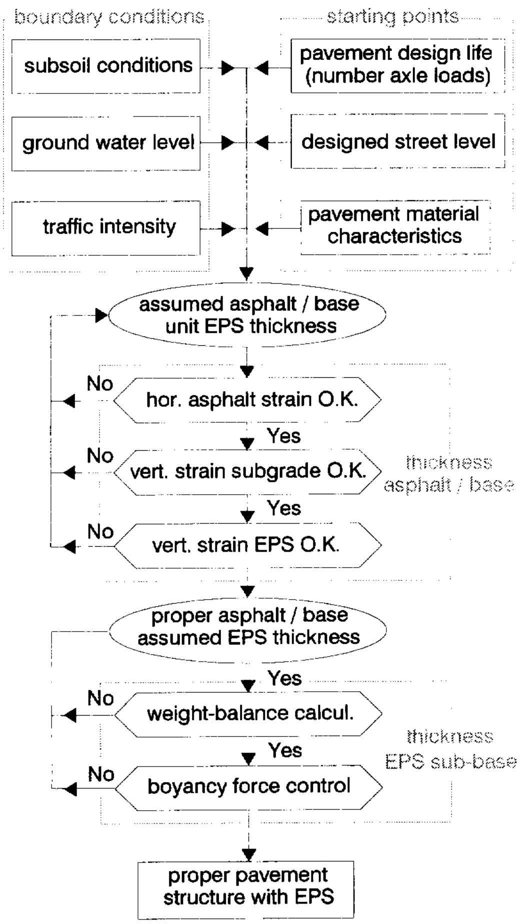

Figure 3. Flowchart of the revised Dutch design procedure (incl. EPS strain criterion) for flexible pavement structures with an EPS sub-base

- ➪ Longitudinal joints between EPS blocks must not coincide with a wheel track because it will result into a significant reduction of the pavement life. The EPS block pattern should be designed such that longitudinal joints are located between the wheel tracks.
- ➪ As long as the elastic deformation due to repeated (traffic) loads is limited to 0.4%, then permanent deformation of both EPS15 and EPS20 blocks is negligible and will have no influence on the pavement behaviour. Therefore, the vertical strain value of 0.4% should be used as the design criterion for the EPS layer.
- ➪ During the construction phase, which is the most critical phase, special measures (such as steel planking) should or could be taken to ensure that the maximum allowable EPS strain value of 0.4% is not exceeded. Overloading EPS results in a lower modulus of elasticity and a higher water absorption.
- ➪ The presence of an EPS sub-base in a pavement structure has a significant influence on the stress and strain development in the pavement. *If granular materials are placed immediately on top of the EPS layer* then the stiffness of such a layer is low and in fact much lower than is normally expected. Consequently, unbound material modulus values reduced up to 50% should be used as input data for design purposes.

  Unbound base materials that have the potential to develop a high stiffness do not pay off. Also relatively expensive self-cementing materials (e.g. blast furnace slags) seem to be not adequate above an EPS sub-base as cementing does not develop because of a significant amount of movement in the structure caused by the heavy traffic loads.
- ➪ For design purposes a minimum elastic modulus of 5 MPa can be adopted for EPS20. In the case of EPS15 a minimum modulus of 4 MPa should be used.
- ➪ Neither the modulus of EPS nor its other characteristics will deteriorate due to environmental influences like repeated wetting and freeze-thaw cycles.
- ➪ The application of denser (and more expensive) EPS types with a somewhat higher elasticity modulus has no significant effects on the overall pavement behaviour. The use of EPS15, the lightest EPS type, instead of EPS20 can reduce the material costs considerably. However, one has to realize that the vertical strains in EPS15 will be about 1.25 times greater than those in EPS20, while the criterion $\epsilon_{EPS} \leq 0.4\%$ is still valid.
- ➪ Application of a cement treated capping layer on top of the EPS sub-base has a tremendously beneficial effect on the performance of the pavements. Such a capping layer neutralizes the effects of open joints between the EPS blocks, guarantees sufficient support to overlaying unbound base material even under high traffic intensity and eliminates any restriction for use of cheaper low-density EPS types. A cement treated capping layer is therefore strongly recommended.
- ➪ Although additional work needs to be done to validate the test procedure modulus testing by means of the ultrasonic method is very promising for quality control of the blocks on site.

6 ACKNOWLEDGEMENT

Shell Nederland Chemie BV, Road and Hydraulic Engineering Division of the Ministry of Traffic, Public Works and Water Management (DWW-RWS), and Stybenex BV are greatfully acknowledged for sponsoring this research into EPS geofoam.

7 REFERENCES

Duškov, M. (1997) *EPS as a Light-Weight Sub-base Material in Pavement Structures*, PhD Thesis, Delft University of Technology, Delft, The Netherlands, p 251.

Duškov, M. (1996) *3-D Finite Element Analyses of Pavement Structures with an EPS Geofoam Sub-base*, Proc. Int. Symp. on EPS Construction Method, EPS TOKYO '96, Tokyo, Japan, pp. 48-57.

Duškov, M. (1991) *Use of Expanded Polystyrene Foam (EPS) in Flexible Pavements on Poor Subgrades*, Proc. Volume 1, Int. Conf. on Geotechnical Engineering for Coastal Development, Yokohama, Japan, pp. 783-788.

Scarpas, A. (1995). *CAPA Finite Elements System*, FEMA User's Manual, Faculty of Civil Engineering, Delft University of Technology, Delft , The Netherlands, p 55.

Shell Pavement Design Manual (1978), Shell International Petroleum Company Limited, London, UK.

Wijs de, W., Hengeveld, H. (1989) *Roads on Expanded Polystyrene Foam* (in Dutch), Foundation for Building Research, Rotterdam, The Netherlands, p. 101.

Particles Washout Associated With The Retention Of Broadly Graded Soils By Geotextiles

Jean Lafleur
Professor, Département de Génie Civil, Géologique et des Mines, Ecole Polytechnique de Montréal, Montréal, QC, Canada

ABSTRACT: Engineering sense suggests that the filtration opening size O_F of a filter does not need to be smaller than the smaller particles of a retained base to fulfill its function. Research on the filtration of broadly graded soils has shown however, that some finer particles are washed out in the process of soil filter bridge formation near the interface zone. The model proposed by Lafleur et al. (1989) relates the mass of washout and the associated setttlement to the retention ratio of the combination R_R (= O_F/d_I) and to the broadness coefficient of the retained soil C_B (= O_F/d_o). Compatibility tests between square mesh sieves and and three different broadly graded bases were made. The results have confirmed the validity of the existing model.

KEYWORDS: Filtration, piping, Gradient Ratio test, woven geotextiles, seepage control.

1 INTRODUCTION

The main function of a filter is to retain soil particles without altering the flow of water. Current selection criteria are based on geometric and hydraulic considerations supplemented by experimental evidence from which success or failure has been assessed. Success involves implicitly that there is no washout of soil particles. Giroud (1996) admits however, *that soil retention does not require that the migration of all soil particles be prevented. Soil retention simply requires that the soil behind the filter remains stable.* The amount of washout has been recognized as an important factor in the interpretation of compatibility tests (Austin et al., 1997, Fannin et al., 1994, Honjo et al., 1996, Lafleur et al., 1996, Bhatia et al., 1996). The overall performance of a drainage structure is related to the washout that produces two detrimental effects:

- formation of voids and caverns near the filter interface, that transmit uneven subsidence at the surface;
- filling and clogging of downstream water conveyance systems.

The severity of the loading is not the same for every application. For example, a dynamic environment such as beneath roads or erosion control applications is more agressive on the particles than a static, continuous flow. The consequences of washout may also vary. In dams, concentrated washout and piping lead to the formation of sinkholes at the crest. Austin et al. (1997) have demonstrated that a 150 mm diameter and 100 m. long drainage pipe with a 3% slope can be completely filled at the lowest point in the profile when washout is in the order of 0.25 kg/m^2.

2 PREDICTION OF WASHOUT

Before a filter/base combination attains equilibrium, apreciable washout can occur, especially in broadly graded soils. Lafleur et al. (1996) have shown that for nonwoven geotextiles, the particles migration is less than 2.5 kg/m^2 provided that for internally stable soils,

$$\boxed{R_R < 1}$$

where:
R_R = retention ratio = O_F/d_I
O_F = filtration opening size obtained from hydrodynamic sieving
d_I = base indicative size
= d_{85} for uniform soils ($C_u \le 6$)
= d_{50} for broadly ($C_u > 6$) linearly graded soils
= d_{30} for broadly concave upward graded soils
= d_G for broadly gap graded soils (d_G is the lowest size of the gap)

For internally unstable or suffosive soils, the filtration process is different. Suffosive soils are broadly graded with gradation curves that are markedly concave upward or that show a gap below 30% passing. It has been shown by Kenney and Lau (1985) that for such soils, finer particles can move within the coarser grains skeleton. These movable particles can form a cake near the base/filter interface if O_F is too small. This phenomenon is called blinding or external clogging. To avoid this risk, the filter must have a minimum opening size. At the other extreme, to avoid piping, O_F must be less than a given value, $d_I = d_{30}$ and

$$\boxed{1 < R_R < 5}$$

Lafleur et al. (1989) have studied the self-filtration or bridging that develops near the interface zone separating broadly graded soils from filters. They presented a model to evaluate the amount of base washout M_P induced in the process and the associated settlement ΔH. Some assumptions had to be made:

- the combination is compatible i.e. the retention ratio is smaller than 5;
- the soil near the interface is divided into m layers, with

$$m = \left\| \left(\frac{\log C_B}{\log R_R^{'}} \right) \right\| \quad \text{and } C_B = \text{broadness coefficient} = O_F/d_o$$

- all the fines smaller than the opening size of each upstream layer are washed out. The constriction size of the remaining particles is equal to their minimum grain size divided by the ratio $R_R^{'}$ taken equal to 9 (Sherard et al., 1984).

The induced settlement is given by

$$\Delta H = d_{100} \sum_{j=1}^{m} \left(\frac{P_j}{100} \right)$$

$P_j =$ percent in mass finer than $(O_F/R_R^{'})^i$ originally present in the jth layer and $i = j - 1$

The mass of washout is equal to

$$M_P = \rho_D \cdot \Delta H \qquad \text{where } \rho_D = \text{dry density of the base}$$

An extensive testing program was designed to bring some experimental support to the above model and to verify the accuracy of the assumptions.

3 TESTING PROGRAM

The program involved broadly graded soils with different gradations filtered by square mesh sieves. The filtrameter shown on Fig. 1 was used. Its diameter is 197 mm such as to minimize wall effects for samples containing coarse particles. Four lateral piezometers at distances of 55, 90, 130, 180 mm respectively from the filter, allowed the evaluation of the local permeabilities. Water was circulated downward at an overall gradient of 5 through the soils. The downstream part of the filtrameter was submerged to maintain positive pressure head throughout the samples. The sieve openings were 19.1, 9.52, 4.76 and 2.00 mm and the filters designated 19, 10, 5 and 2 respectively.

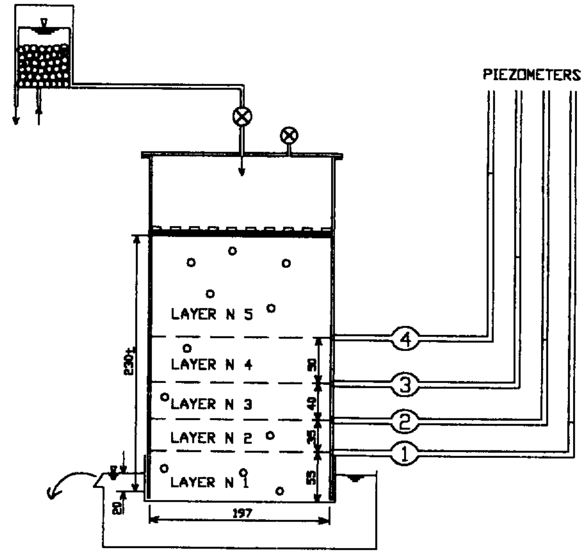

Fig. 1 Filtrameter for screen tests

The soils were reconstituted either from natural subrounded particles (G) or spherical glass beads (B) comprised between 0.1 and 19 mm in size. Their gradations are described on Fig. 2 and Table 1: rectilinear (R), gap-graded (D) and concave upward (C). They are internally stable and broadly graded. Although their coefficients of uniformity varies between 7 and 21, their coefficients of curvature do not lie beween 1 and 3, so they cannot be classified as "well-graded". Their indicative size d_I (arrows on Fig. 2) varies between 0.7 and 3.0 mm.

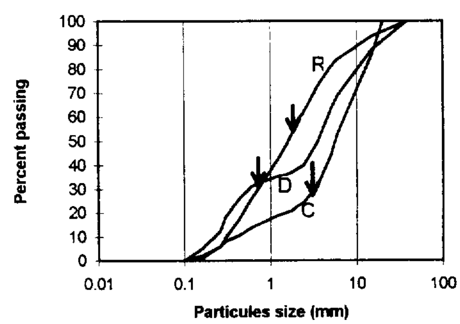

Fig. 2 Gradation curves of tested bases

Table 1 Base soil gradation properties

base	d_{10} mm	d_{85} mm	d_I mm	C_u	C_C
R	0.29	6.6	1.8	6.9	0.77
D	0.22	11.8	0.7	20.0	0.31
C	0.37	13.6	3.0	18.9	3.59

The tests lasted 150 minutes and vibrations were applied by tapping with a rubber hammer on the sides of the permeameter. Equilibrium was interpreted on the basis of the shape of the local permeability curves. At the end of the tests, the mass of passing particles was recorded and the samples were cut for gradation analyses into 5 slices, limited at the top and at the bottom of the sample and at the level of the piezometers.

4 RESULTS

The Table 2 gives an overview ot the test results. The retention ratio R_R of the combinations varies between 0.7 and 27 and those for which the model applies (R_R < 5), have been highlighted. One can apreciate the convergency between the model and the measurements, from the computed relative errors Δ. It appears that, although the measurements are in the same order of magnitude as the calculations, the model underestimates the amount of washout. The shape of the particles may have played a role since for a given opening size, the washout is nearly the double with the spherical grains (tests B). These are more mobile than the subrounded particles G and thereby, more susceptible to washout.

The Fig. 3 is a logarithmic plot of the mass of washout versus the retention ratio for all the tests of this program: M_P increases regularly with R_R. At the critical R_R-value of one, the plot indicates that M_P varies between 8 and 50 kg/m², which is more than the previously mentionned limit of 2.5 kg/m². This discrepancy can be related to the structure of the filter. The metallic mesh sieves used in the tests are similar to a woven geotextile and they have a large Percent Open Area (POA), varying between 62 and 75%. This is much more than the current woven geotextiles for which POA ranges between 1 and 20% (Mlynarek and Lombard, 1997). For purpose of comparison, the results of compatibility tests made by these authors (designated ML) have been reported on Fig. 3. They have been classified as low POA (≤ 10%) and high (40% > POA > 10%). The influence is obvious: for a R_R-value of one, M_P is equal to 0.24 kg/m² for POA <10 and to 0.92 kg/m² for POA > 10.

Physically, when the ratio between the solid retention structure (filaments) and the opening voids is higher, there is relatively more surface to retain particle so that bridging and retention are easily promoted. Giroud (1996) arrived at similar conclusions when he demonstrated that for nonwoven geotextiles with given thickness and fibres diameter, the opening size is smaller with lower porosity.

Table 2 Tests results and comparison

	R_R	ΔH (mm)			M_P (kg/m²)		
		meas	calc	Δ%	meas	calc	Δ%
GR19	10.6	137.0			201.0		
GR10	5.6	52.9			88.4		
GR5	2.8	15.5	13.4	-14	27.1	18.6	-31
GR2	1.1	5.1	11.3	+122	7.5	15.7	+109
BR19	10.6	-			394.8		
BR10	5.6	-			366.0		
BR5	2.8	23.9	9.4	-61	41.0	14.5	-65
BR2	1.1	6.8	7.3	+7	12.0	11.1	-8
GD19	27.1	76.0			128.8		
GD5	7.1	9.7			17.4		
GD2	2.8	6.8	6.7	-1	11.8	9.5	-19
BD19	27.1	-			393.7		
BD10	14.3	105.8			187.0		
BD5	7.1	18.5			34.0		
BD2	2.8	10.2	5.2	-49	19.4	8.4	-57
GC19	6.3	51.9			87.1		
GC10	3.3	13.3	5.1	-62	24.4	8.0	-67
GC5	1.7	4.8	4.4	-8	9.0	6.1	-32
GC2	0.7	2.2	3.8	+73	5.4	5.4	0
BC19	6.3	-			394.0		
BC10	3.3	126.6	4.9	-96	220.0	7.3	-97
BC2	0.7	6.7	2.6	-61	17.0	4.1	-76

Fannin et al. (1994) have performed modified Gradient Ratio tests on nonwoven geotextiles and different soils. Their results (FVS) have also been plotted on Fig. 3 separating uniform (U) and well-graded (WG) base soils. The shape of the M_P-R_R curve is different: for well graded soils it is gradual, for uniform soils, it shows a sharp quasi vertical break around $R_R = 1$.

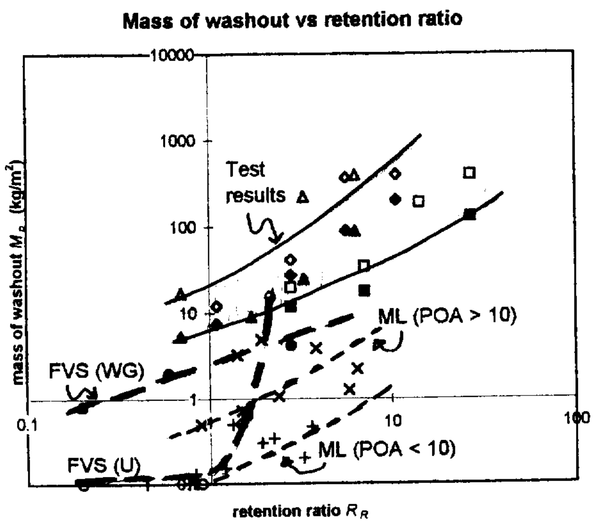

Fig. 3 Mass of washout versus retention ratio

5 DISCUSSION AND CONCLUSION

The amount of washout associated with the filtration of broadly graded soils was evaluated from screen tests using square conventional sieve mesh with different opening sizes.

The results have confirmed the validity of the approach suggested by Lafleur et al. (1989). The retention ratio R_R between the opening size of a filter and the indicative size of the base, is the most important factor intervening in the amount of washout. The experimental relationship between M_P and R_R is gradual for broadly graded soils while for uniform soils, it shows a marked bend around $R_R = 1$. The success or failure of a filter for broadly graded soils is therefore quite subjective because it depends on the amount of tolerable washout. Finally, the results have disclosed that the Percent Open Area and by extension, the porosity, play a role in the rearrangement of the particles near the interface. The lower the value, the lower the washout.

ACKNOWLEDGMENT

The author wishes to acknowledge the diligent work of Khaireddine Sakrani, who performed the tests as partial fulfilment for his M.Sc.A. degree and of Sebastien Lopez, who helped in the preparation of this paper.

REFERENCES

Austin, D.N., Mlynarek, J. & Blond, E. (1997). Expanded anti-clogging criteria for woven filtration geotextile. *Geosynthetics '97*, IFAI, Long Beach, CA, USA, Vol. 2, pp. 1123-1144.

Bhatia, S.K., Moraille, J., Keith, K. & Smith J.L. (1996). Comparative performance of granular vs. geotextile filters in the laboratory. *GEOFILTERS '96* edited by Lafleur & Rollin, Montréal, QC, Canada, pp. 449-460.

Fannin, R.J., Vaid, Y.P & Shi, Y.C. (1994) Filtration behaviour of nonwoven geotextiles. *Canadian Geotechnical Journal*. Vol. 31, No. 4, pp. 555-563.

Giroud, J.P. (1996). Granular filters and geotextile filters. *GEOFILTERS '96* edited by Lafleur & Rollin, Montréal, QC, Canada, pp. 565-680.

Honjo, Y., Haque, M.A. & Tsai, K.A. (1996). Self-filtration behaviour of broadly and gap-graded cohesionless soils. *GEOFILTERS '96* edited by Lafleur & Rollin, Montréal, QC, Canada, pp. 227-236.

Kenney, T.C. & Lau, D. (1985). Internal stability of granular filters. *Canadian Geotechnical Journal*, Vol. 22, No. 2, pp. 215-225.

Lafleur, J., Eichenauer, T. & Werner, G. (1996). Geotextile filter retention criteria for well graded cohesionless soils. *GEOFILTERS '96* edited by Lafleur & Rollin, Montréal, QC, Canada, pp. 429-438.

Lafleur J., Mlynarek J. & Rollin A.L. (1989). Filtration of Broadly Graded Cohesionless Soils. *Journal of Geotechnical Engineering*, ASCE, Vol.115, No.12, pp.1747-1768

Mlynarek, J.,& Lombard, G. (1997). Significance of percent open area (POA) in the design of woven geotextile filters. *Geosynthetics '97*, IFAI, Long Beach, CA, Vol. 2, pp. 1093-1107.

Sherard J.L., Dunnigan, L.P. & Talbot, J.R. (1984). Basic properties of sand and gravel filters. *Journal of Geotechnical Engineering*, ASCE, Vol. 110, No. 6. pp. 684-700.

Geotextile Characteristic Opening Size: The Influence of Some Test Parameters

Barroso, Madalena C. P.
Research Assistant, National Civil Engineering Laboratory (LNEC), Lisbon, Portugal

Lopes, Maria da Graça D. A.
Senior Research Officer, National Civil Engineering Laboratory (LNEC), Lisbon, Portugal

ABSTRACT: Designing a geotextile for filtration applications requires information on the characteristic opening size of the geotextile. Several techniques are available for measuring the characteristic opening size, but there is no one universally accepted. Three test methods are usually used: dry sieving, hydrodynamic sieving and wet sieving. The wet sieving test method was used to study the influence of some test parameters (soil granulometry, water flow rate and vertical amplitude) on the results of opening size measurement. For this purpose six nonwoven geotextiles were used. The results showed that the test conditions can indeed influence results of the measurement of characteristic opening size.

KEYWORDS: Geotextile, Wet sieving test method, Characteristic Opening Size

1 INTRODUCTION

Where geotextiles are used as filters they must perform two functions simultaneously. One is to retain fine soil particles and the other is to allow the seepage of water from the retained soil. The ability of the geotextile to filter is a function of the size and distribution of the pores and the porosity. However, the distribution of the pores within the geotextile is difficult to determine. As a result, several indirect test methods have been developed. Three techniques are used: dry sieving, standardised in the United States, United Kingdom, Belgium and the Netherlands; hydrodynamic sieving, standardised in Canada, France and Italy; and wet sieving, standardised in Germany, Austria and Switzerland. For a given geotextile the results obtained are dependent on the test method used (Bhatia & Smith, 1995).

In order to obtain a unified standard in Europe, the different existing national standards are being harmonised under the auspices of the European Committee for Standardisation (CEN). An index test has been developed based on the wet sieving technique. A specific parameter, the Characteristic Opening Size (COS also called O_{90}), indicates the size of the largest grain size particle that can pass through the geotextile.

A final draft European Standard was authored by Technical Committee 189 and was recently submitted for formal vote to the European countries (prEN ISO 12956). Before becoming a standard the test method was validated. It was necessary to clarify the influence of some specific parameters, in order to determine the best test conditions. During the work on standard harmonisation, intercomparision tests were performed in several countries. The results obtained have shown that O_{90} can be affected by test conditions, as reported by Faure (1996).

In this context, a test programme has been carried out in Portugal's National Civil Engineering Laboratory (LNEC), to study the influence of some test parameters, namely the soil granulometry, the vertical amplitude and the water flow rate.

2 DESCRIPTION OF THE TEST PROCEDURE

The tests were performed based on final draft of the European Standard prEN ISO 12956 (Geotextiles and geotextile related products–Determination of the characteristic opening size).

The principle of the test is to sieve a well graded granular material (usually soil) through a geotextile specimen. The specimens are soaked in water at laboratory temperature and leave it to saturate for at least twelve hours. Then they are placed in the clamping device on the sieving apparatus (figure 1). For each specimen, a soil mass of 7,0 kg per square meter of exposed sieving area is spread on the geotextile and watered by means of a spray nozzle. The water supply is open and it is adjusted by the operator in order to spray uniformly over whole specimen ensuring that all soil particles are wetted, but do not allow the water level to rise above the granular material. The amplitude of sieving is adjusted to a sufficient level to agitate the soil particles. During 10 minutes of sieving all water and soil passing through the specimen are collected. The passed soil is dried and weighed. The particle size distribution is plotted on a semi-logarithmic graph with sieve size on the horizontal axis and the cumulative percentage of the combined passed granular material on the vertical axis. The Characteristic Opening Size corresponds to the d_{90} of the particle size distribution curve (O_{90}=d_{90}).

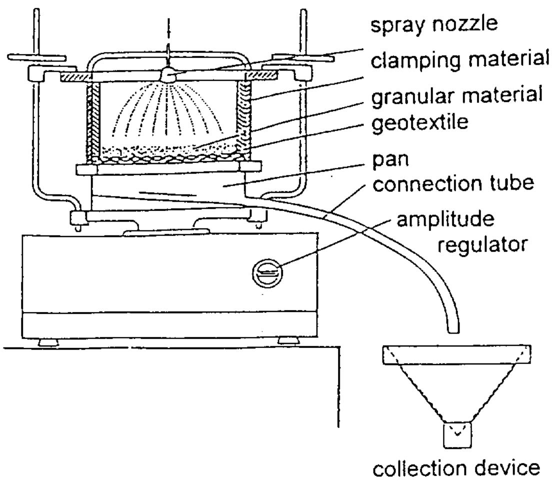

Figure 1. Example of apparatus.

3 MATERIALS TESTED

Six nonwoven geotextiles were used in this work. Table 1 presents the fabrics tested.

Table 1. Geotextiles tested.

Geot.	Manufacturing process	Polymer type	Mass per unit area (g/m^2)
A	Needlepunched nonwoven	Polyester	133
B	Needlepunched nonwoven	Polypropylene	242
C	Needlepunched nonwoven	Polypropylene	476
D	Heatbonded nonwoven	Polypropylene	139
E	Needlepunched nonwoven	Polyester	134
F	Needlepunched nonwoven	Polyester	293

4 TEST PROGRAMME

Before the experimental programme started, the repeatability of the test method was studied. Geotextile B was selected to evaluate the O_{90} of over forty-eight specimens. The tests were performed with a vertical amplitude of 0,75 mm and with an average water flow rate of 1,4 l/min (at a pressure of 200 kPa). The soil used was the Soil 2 (see figure 2). The O_{90} obtained was:

- average = 84 μm
- standard deviation (s) = 4,5μm
- coefficient of variation = 5,2 %

Based on these values the repeatability of the test method was judged to be good.

During the tests several problems occurred:

- the soil tended to agglomerate on the surface of some specimens, preventing the soil from passing through the geotextile. When this happened, the water flow rate was increased until the agglomerate was broken up;
- water accumulated above some specimens. In these cases, the water flow rate was reduced to avoid soil particle loss.

Following the repeatability tests, the O_{90} test conditions were studied. Firstly three geotextiles were tested with several soils. Then another three geotextiles were tested with different amplitudes and two water flow rates. Table 2 shows the parameters analysed and the geotextiles used.

Table 2. Parameters analysed.

Geotextile	Repeat-ability	Soil granul.	Amplitude	Water flow rate
A			•	•
B	•		•	•
C			•	•
D		•		
E		•		
F		•		

5 TEST RESULTS AND DISCUSSION

5.1 Influence of Soil Granulometry on O_{90}

Three soils were used (figure 2 a). According to the CEN draft test method, the soil used must fulfil the following requirements: it must be cohesionless; the uniformity coefficient (C_u) must be greater than 3 and smaller than 20; the soil must not be gap-graded; and the assumed O_{90} must be between d_{20} and d_{80}. Table 3 presents the features of the soils used.

Soil 1 was initially analysed using the ASTM series of sieves, which has fewer sieves than the ISO series. As result, the soil granulometry was not well defined for the particle sizes used to estimate O_{90}. Therefore, a new soil (Soil 2) was made up. The difference in particle size distribution obtained for Soils 1 and 2 (see figure 2 b) show how important it is to use a higher number of sieves, to define properly the soil granulometry.

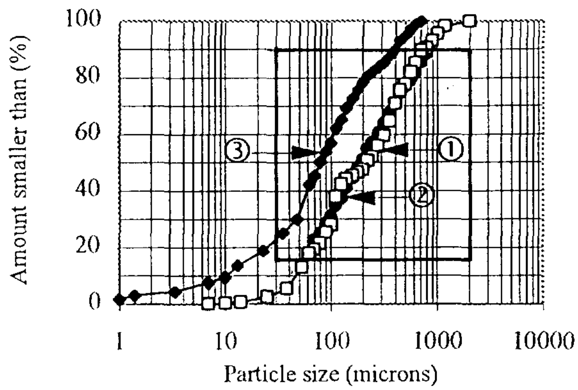

(a)

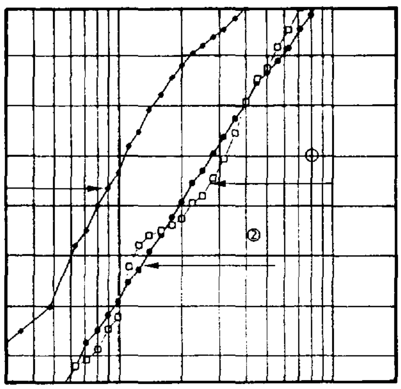

(b)

Figure 2: (a) Particle size distribution of the soils used; (b) detail on difference of Soil 1 and Soil 2.

Table 3. Characteristics of the soils.

Soil 1	Soil 2	Soil 3
C_u= 6,8	C_u= 5,9	C_u= 10,3
d_{20}= 75μm	d_{20}= 67 μm	d_{20}= 25 μm
d_{80}= 532 μm	d_{80}= 583 μm	d_{80}= 218 μm

The tests were performed with an average water flow rate of 1,8 l/min (at a pressure of 200 kPa). The amplitude selected was 0,75 mm. The results obtained are presented on table 4.

It seems that the O_{90} values are dependent on the soil used, especially for geotextiles with smaller mass per unit of area, since the one with higher mass per unit area only showed a slight difference in O_{90}.

Several problems occurred during the tests:

- water accumulated above some specimens of geotextile F when tested with Soil 1, and above some specimens of geotextiles D, E and F, when tested with Soil 3. The wet sieve pan outlet did not drain the water quickly enough. The solution adopted was to decrease inflow and the amplitude until the water drained;
- it was difficult to keep the amplitude constant for some specimens of geotextiles A, B and C tested with Soils 1 and 2. Changes occurred without any apparent cause. When this occurred, the operator had to adjust the amplitude manually.

Table 4. Variation of O_{90} with the soil granulometry.

Geotextile	Soil 1	Soil 2	Soil 3
	O_{90} (μm)	O_{90} (μm)	O_{90} (μm)
D	119	125	113
E	118	122	111
F	118	116	110

5.2 Influence of Amplitude on O_{90}

The tests started with geotextile B carried out with three vertical amplitudes of 0,75 mm, 1 mm, and 1,25 mm, keeping the water flow rate constant (2,4 l/min, at a pressure of approximately 200 kPa). Since the time available to perform the tests was very limited and because the results obtained with geotextile B showed a very small difference in O_{90} for amplitudes higher than 1 mm, the geotextiles A and C were tested only with amplitudes of 1 mm and 1,25 mm. Nevertheless, it is believed that the results for geotextiles A and C would also follow the same trend, thus producing similar results to those given by geotextile B for amplitudes bellow 1 mm.

Soil 2 was used in the tests. The overall results are presented in figure 3.

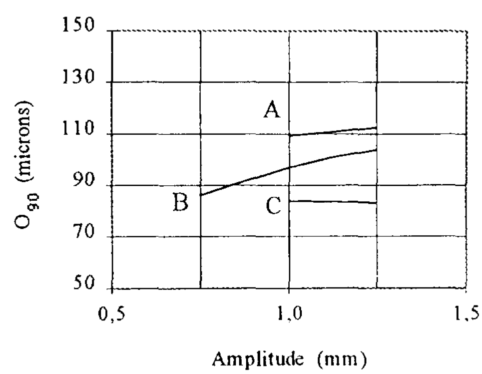

Figure 3. Variation of O_{90} with the amplitude.

The results showed only a slight variation in O_{90} with the increasing amplitude for amplitudes above 1 mm.

Several observations were made during the tests:
- the same problem with soil agglomeration on the surface of the geotextiles previously reported also occurred with some specimens of geotextiles A and C, when tested with the amplitude of 1 mm, and with some specimens of geotextile A at an amplitude of 1,25 mm. In these cases, the solution adopted was to increase the water flow rate until the agglomerate was broken up;
- the difficulty with accumulation of water, also occurred with some specimens of geotextile C, when tested with both amplitudes, and with some specimens of geotextile B during the tests performed with an amplitude of 1,25 mm; once more the water flow rate was reduced;
- it was difficult to keep the amplitude constant when some specimens of geotextile A were tested. It decreased without any explanation. When this occurred, the operator had to adjust the amplitude manually.

5.3 Influence of Water Flow Rate on O_{90}

The tests were performed with two water flow rates: 2,4 l/min (at a pressure of approximately 200 kPa) and 3,0 l/min (at a pressure of approximately 300 kPa), keeping the vertical amplitude constant (1 mm). Soil 2 was used in the tests. The results obtained are presented in figure 4.

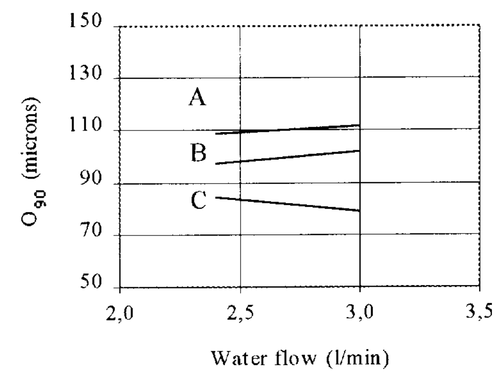

Figure 4. Variation of O_{90} with the water flow rate.

The results showed that there are no significant differences in O_{90} values obtained when water flow rate is varied, for the soil used.

During the tests several problems occurred:
- the soil tended to agglomerate on the surface of some specimens of the geotextiles A and C, preventing the soil from passing through the geotextiles. When this occurred the water flow was reduced once more. As tests progressed, soil agglomerates moved freely over the geotextile specimens;
- water accumulated above some specimens of the geotextile C, due to air that was trapped inside the top chamber. When this happened, the test was stopped and the water was allowed to flow through the inlet pipe, before the test was continued.

6 CONCLUSIONS

Based on the test results the following was concluded:
(1) for nonwoven geotextiles, soil granulometry seems only to influence O_{90} values for geotextiles with small mass per unit area. However, only a few geotextiles were tested, therefore, it is difficult to know if this influence may be attributed to the variability of the nonwoven geotextiles themselves;
(2) for nonwoven geotextiles, the O_{90} appeared not to be influenced by amplitude, when the amplitude was higher than 1 mm;
(3) for nonwoven geotextiles, the O_{90} seemed not to be affected by the water flow rate.

These conclusions must be seen in the light of the small number of tests that were performed, and the experimental difficulties encountered. The authors suggest that more tests should be carried out using different types of geotextiles.

ACKNOWLEDGEMENTS

The authors wish to thank to Programme Praxis XXI of Ministry for Science and Technology and to FEDER, for financial support under its Project 3/3.1/CEG/2598/95.

REFERENCES

Bhatia, S. K. & Smith, J. L. (1995) "Sieving techniques for measuring pore openings–an open question", *Proceedings of the Geosynthetics '95 Conference*, Nashville, Tennessee, USA, Vol. 1, pp. 281-295.

Faure, Y. H. (1996) "Characteristic opening size of geotextiles: European intercomparison tests for standardisation", *Proceedings of the 1st European Geosynthetics Conference*, Eurogeo, Maastricht, Netherlands, pp. 1047-1054.

prEN ISO 12956 (1996) Geotextiles and geotextiles related products - Determination of the characteristic opening size.

Permeability Requirements For Geotextile Filter Design

R.J. Fannin,
Assoc. Professor, Department of Civil Engineering, University of British Columbia, Vancouver, B.C., Canada

Y.C. Shi
Sembawang Engineering and Construction Pte Ltd., Singapore

Y.P. Vaid
Professor, Department of Civil Engineering, University of British Columbia, Vancouver, B.C., Canada

ABSTRACT: Inconsistencies in design of geotextile filters are reported, with reference to current regulatory guidance. Results of laboratory Gradient Ratio tests are then described, and used to illustrate the role of a unified approach to interpretation of soil-geotextile compatibility that accounts for hydraulic gradient, permeability, and excess water head (or porewater pressure) across the filter.

KEYWORDS: Filtration; Geotextiles; Gradient Ratio Tests; Permeability; Seepage Control

1. INTRODUCTION

Design requirements for a geotextile in filtration applications include soil retention, permeability and strength. The permeability requirements are intended to promote an unimpeded flow of water through the filtration zone. Approaches used in design are derived from empirical relationships comparing the permeability of the geotextile filter (k_F) to that of the soil (k_S). The USFHWA (Christopher and Holtz, 1985) and Canadian Foundation Engineering Manual (CGS, 1993) require that for filtration of fines in critical or severe applications:

$$k_F > 10\ k_S \qquad (1)$$

and for filtration of clean medium to coarse sands:

$$k_F > k_S \qquad (2)$$

More recently Giroud (1996) has proposed separate design criteria for the pore water pressure, to limiting value of 10% of the compressive stress, and for an excessive reduction in flow rate, to a limit of 10% of that in the soil without a filter. The limit values of 10% in the criteria, which are arbitrary and based on judgement, yield the following relationships:

$$k_F > 10\ k_S\ i_S \quad \text{(excessive pore water pressure)} \qquad (3)$$

$$k_F > k_S \quad \text{(excessive flow rate reduction)} \qquad (4)$$

In laboratory testing, the relative permeability of the soil and the permeability of the geotextile are evaluated to ensure compatibility. One example is the Gradient Ratio test (ASTM D5101) which allows the permeability of the soil-geotextile composite zone (k_{sg}) to be compared with that of the soil (k_S). Piping of material adjacent to the geotextile yields a value of $GR_{ASTM} < 1$, while in contrast clogging yields a value of $GR_{ASTM} > 1$, where ports 3, 5 and 7 define $GR_{ASTM} = i_{57}/i_{35}$ (see Fig. 1). The basis for a unified interpretation of the GR test was presented (Fannin et al., 1994a), in which the historic limiting criterion of $GR_{ASTM} < 3$ for compatibility of geotextile and soil was shown, from continuity of flow, to yield an implicit permeability ratio given by:

$$k_{57} > 0.33\ k_{35} \qquad (5)$$

This criterion for clogging, proposed by Haliburton and Wood (1982) and later adopted by regulatory agencies, differs markedly from the companion empirical criteria for permeability reported above, most notably that of Giroud (1996) for excessive pore water pressure. In this paper, results are presented to illustrate the development of this composite zone with time. The objective is to assess the implications of apparent contradictions in the permeability and clogging criteria advocated for filter design.

2. GRADIENT RATIO (GR) TEST RESULTS

A program of tests was performed on selected combinations of 10 soils (4 uniformly graded and 6

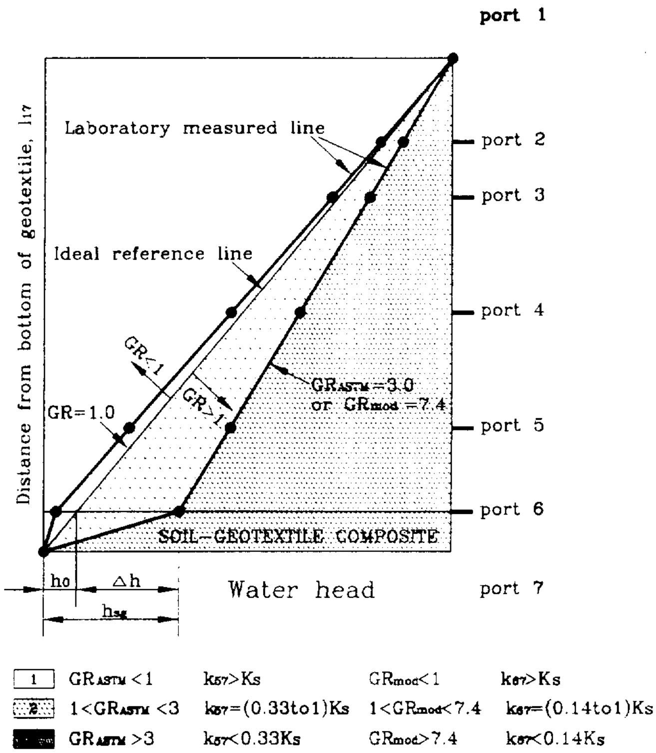

Fig. 1. Schematic unified interpretation of the gradient ratio test.

broadly graded) and 4 needle-punched nonwoven geotextiles (Shi, 1993; Fannin et al., 1994a). The GR permeameter was modified to include 3 ports in addition to those specified in the ASTM test method, as follows: port 6 is located only 8 mm above the top surface of the geotextile specimen, port 4 is located midway between ports 3 and 5, and port 2 is located 13 mm above port 3.

Measurements were taken of the water head at each port, and the resulting flow rate, at four values of imposed system hydraulic gradient in the range i_{17} = 1 to 10.

Values of permeability in the soil (k_{35}) and in the very thin soil-geotextile composite zone (k_{67}) were then deduced, together with a GR_{mod} given by k_{35}/k_{67} (= i_{67}/i_{35}). A similar approach has been reported by Austin et al. (1997).

Results are reported for two of the broadly graded soils (BML74 and BML90) with one nonwoven needle punched geotextile, for which material properties are reported in Tables 1 and 2. The variation of permeability with time, see Fig. 2, shows a permeability in the composite zone which is greater than of the soil for BML90 (a silt with trace of sand) but less than that of the soil for BML74 (a sandy silt). The behaviour appears independent of system gradient. The stable response over time is attributed in part to the technique used in sample preparation, which ensures full saturation of the soil and geotextile (Fannin et al., 1994b).

Table 1 Properties of the soils

Description	Code	D_{85} (μm)	D_{50} (μm)	D_{15} (μm)	Cu[a]	K_{35}[b] (m/s)
Silt with sand	BML74	246	43	12	5.5	1×10^{-6}
Silt	BML90	57	22	9	4.1	1×10^{-6}

[a]Coefficient of uniformity (D_{60}/D_{10})
[b]Typical value

Table 2 Properties of the nonwoven geotextile

FOS (μm)	Thickness (mm)	Mass/unit area (g/m^2)	Grab strength (N) MD/CMD[a]	Elongation (%) MD/CMD
150	1.6	199	677/720	53/102

[a]MD = Machine direction; CMD = Cross-machine direction

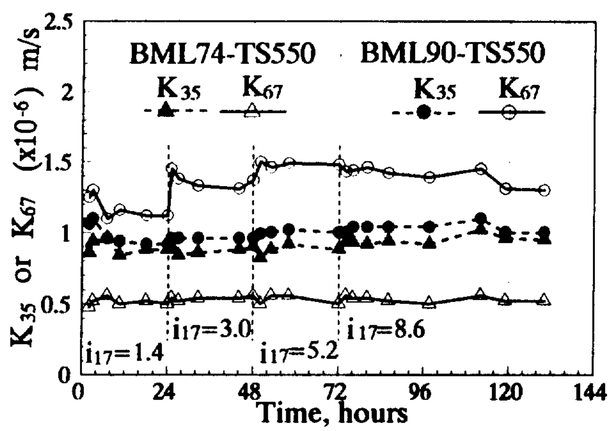

Fig. 2. Permeability of soil and soil-geotextile composite.

3. EXCESS WATER HEAD LOSS

A relationship for excess water head loss Δh was presented by Shi et al (1996), where with reference to Fig. 1:

$$\Delta h = h_{sg} - h_0 \tag{6}$$

from which it can be shown that:

$$\Delta h = \frac{10 i_{17} \left(GR_{mod} - 1\right)\left(\ell_{17} - 10\right)}{10\left(GR_{mod} - 1\right) + \ell_{17}} \qquad (7)$$

and all dimensions are in millimeters.

It is almost independent of the thickness of the upstream soil (ℓ_{17}) when ℓ_{17} exceeds 1000 mm, see Fig. 3(a), however, it is proportional to GR_{mod} and i_{17}, see Figs. 3(b and c).

Typical values of the hydraulic gradient equivalent to i_{17} are reported after Giroud (1996) and Luettich et al (1992) in Table 3. Assuming that ℓ_{17} = 1000 mm, the water head loss is calculated for GR_{mod} = 7.4; the losses do not exceed 120 mm for hydraulic gradients less than 2.0. An excess water head loss of 596 mm is predicted for an hydraulic gradient of 10.

Table 3 Typical hydraulic gradients and corresponding excess water head loss (ℓ_{17} = 1000 mm, $GR_{mod} = k_{35}/k_{67}$ = 7.4).

Application	Typical hydraulic gradient	Excess water head loss Δh (mm)
Standard dewatering trench	1.0	60
Inland channel protection	1.0	60
Pavement edge drain	1.0	60
Vertical wall drain	1.5	89
Landfill leachate collection / detection removal system	1.5	89
Landfill leachate collection removal system	1.5	89
Dam toe drains	2	119
Dam clay cores	3 to >10	178 to 596
Shoreline protection	10	596
Liquid impoundment with clay liners	>10	>596

Notes: Typical hydraulic gradients developed after Giroud (1988) and Luettich et al (1992), critical applications may require designing for higher gradients than those given.

Values of Δh determined for the two Gradient Ratio tests described above are reported in Table 4. Given the average gradient ratio (GR_{mod}) of 1.7 developed in testing soil BML74 with the geotextile, Δh is found to be in the range 8 to 10 mm, for a system hydraulic gradient (i_{17}) of 1.4 and ℓ_{17} varying from 100 to 10,000 mm. The range is 50 to 60 mm when i_{17} = 8.6. The losses are associated with a partial clogging of the geotextile filter zone.

In contrast, an average gradient ratio (GR_{mod}) of 0.8 developed for soil BML90 with the geotextile. A gradient

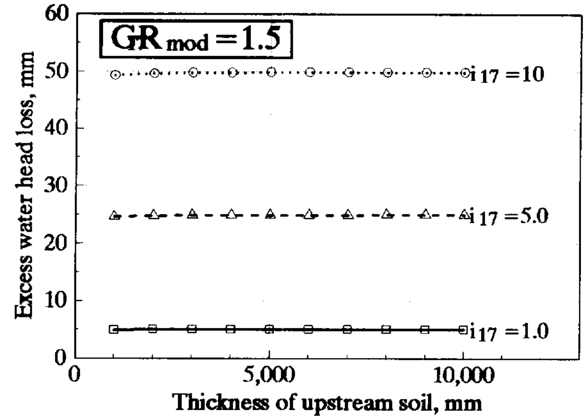

(a)

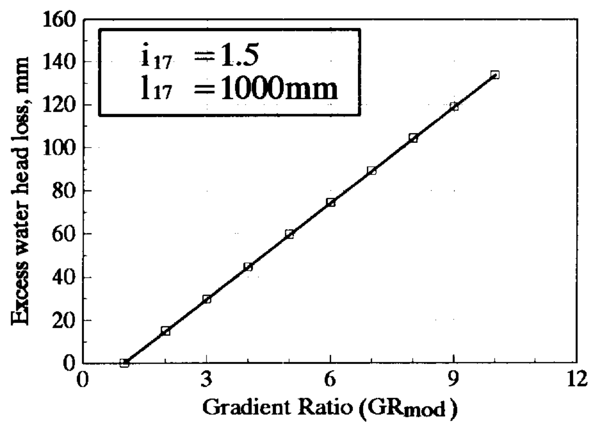

(b)

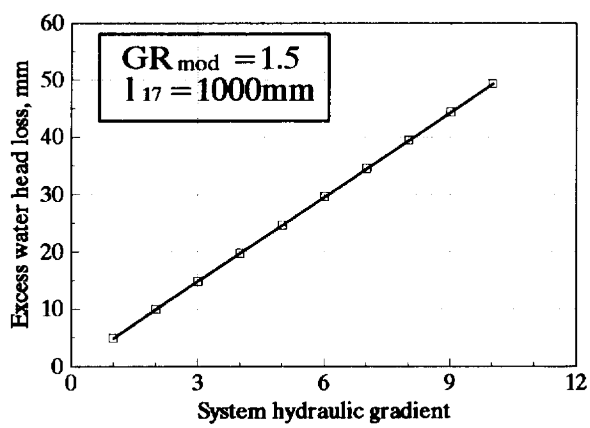

(c)

Fig. 3. Variation of excess water head (from eqn. 7).

ratio less than unity indicates the soil-geotextile composite is more permeable than soil being retained, yielding negative values of Δh.

Table 4 Excess water head loss for soils BML74 and BML90 with TS550 (mm)

ℓ_{17}	BML74	-TS550	BML90	-TS550
(mm)	$i_{17} = 1.4$	$i_{17} = 8.6$	$i_{17} = 1.4$	$i_{17} = 8.6$
100	8.2	50.6	-2.6	-15.8
1000	9.6	59.2	-2.8	-17.1
10,000	9.8	60.1	-2.8	-17.2

4. CONCLUDING REMARKS

1. The gradient ratio test provides a means of evaluating the compatibility of a soil and geotextile with reference to permeability of the soil being retained.
2. The excess head loss (Δh) in the soil-geotextile composite zone is shown from theoretical analysis to be almost independent of thickness of the upstream soil, but proportional to the system hydraulic gradient (i_{17}) and gradient ratio (GR).
3. A series of trial calculations indicates the value of excess water head loss (Δh) induced by a GR > 1 is relatively small for applications governed by a system hydraulic gradient between 1 and 2, and gradient ratio $GR_{mod} < 7.4$ and therefore $GR_{ASTM} < 3$.
4. There is a need to better link design criteria for k_F and k_S, with laboratory performance data from Gradient Ratio tests yielding values of k_{sg}. It is proposed that excess water head loss (Δh), which can be used in design assessments of performance and related stability analyses, is the most appropriate parameter.

ACKNOWLEDGEMENTS

The research was funded by the Natural Sciences and Engineering Research Council of Canada (NSERC). The Ontario Ministry of Transportation supplied the geotextile materials.

REFERENCES

ASTM D5101-96 Standard Test Method for measuring the soil-geotextile system clogging potential by the gradient ratio, Annual Book of ASTM Standards, ASTM Philadelphia.

Austin, D.N., Mlynarek, J. and Blond, E. (1997). Expanded anticlogging criteria for woven filtration geotextiles. Geosynthetics '97, pp. 1123-1144, IFAI, St. Paul, MN.

Canadian Geotechnical Society, Canadian Foundation Engineering Manual, 3rd edition, Vancouver, B.C.

Christopher, B.R. and Holtz, R.D. (1985), Geotextiles Engineering Manual, U.S. Federal Highway Administration, Report FHWA-TS-86/203, pp. 1044.

Fannin, R.J., Vaid, Y.P. and Shi, Y.C. (1994a), Filtration behaviour of nonwoven geotextiles, Canadian Geotechnical Journal, Vol. 31, No. 4, pp. 555-563

Fannin, R.J., Vaid, Y.P. and Shi, Y.C. (1994b), A critical evaluation of the gradient ratio test, ASTM Geotech. Testing Journal, 17: 35-42.

Giroud, J.P. (1996), Granular and geotextile filters, Proceedings of Geofilters'96, Montreal, Quebec, 29-31 May, pp. 565-680.

Haliburton, T.A. and Wood, P.D. (1982), Evaluation of U.S. Army Corps of Engineers gradient ratio test for geotextiles performance, Proceedings of the second international conference on geotextiles, Las Vegas.

Luettich, S.M., Giroud, J.P. and Bachus, R.C. (1992), "Geotextile filter design guide", Geotextiles and Geomembranes, Special Issue on Geosynthetics in Filtration, Drainage and Erosion, Vol. 11, Nos. 4-6, pp. 433-441.

Shi, Y.C., Fannin, R.J. and Vaid, Y.P. (1996), Evaluation of geotextile filter behaviour using the Gradient Ratio test, Proceedings of Geofilters'96, Montreal, Quebec, 29-31 May, 469-480.

Shi, Y.C. (1993), Filtration behaviour of nonwoven geotextiles in the gradient ratio test, M.A.Sc. thesis, Univ. of British Columbia, Vancouver, Canada.

Geotextiles Filter Design by Probabilistic Analysis

Urashima, Denise C.
Student, Department of Geotechnique, Aeronautical Institute of Technology, São José dos Campos, São Paulo, Brazil

Vidal, Delma
Professor, Department of Geotechnique, , Aeronautical Institute of Technology, São José dos Campos, São Paulo, Brazil

ABSTRACT: A methodology to obtain the parameters to design needle-punched nonwoven geotextiles filters based upon probabilistic analysis and in-suspension filtration tests is proposed. The superposition of theoretical pore size distribution curve and that obtained by in-suspension filtration tests allows one to estimate the distance between confronts, essential to use the probabilistic theory. This paper presents tests results and analysis for thin geotextiles (mass per unit area less than 200 g/m^2) and a design procedure that shows the versatility of this method.

KEYWORDS: Design, Filtration, Geotextiles, Nonwoven Fabrics, Probability

1 INTRODUCTION

The good performance of geotextiles in filtration functions has been reported in practical engineering thus becoming one of the most popular geosynthetics applications in the world. In recent years, research has been conducted at several laboratories in order to obtain a better knowledge of mechanisms and parameters associated with filtration problems.

Filter design is usually based on Terzaghi's proposition, empirically or semi-empirically adapted by different authors. However, these design procedures don't allow a complete understanding of the filtration phenomena. It is impossible to estimate the filter thickness needed to retain the soil particles.

Silveira(1965) proposed a probabilistic analysis to study the carrying of soil particles in a filter. This analysis gives us the filter thickness needed to retain the soil particles, if the filter pore size distribution curve and the average distance between confrontation particle/filter voids are known.

This paper presents a procedure to obtain the necessary parameters to design thin needle-punched nonwoven geotextiles filter (mass per unit area less than 200 g/m^2), combining Gourc's(1982) and Silveira's(1965,1993) propositions, to estimate the distance between confronts. Some results are presented and examples discussed to show the relevance of the adopted procedure.

2 THEORETICAL ANALYSIS

From a probabilistic analysis of carrying spherical particles through a protective filter, Silveira(1965) proposes to establish the necessary filter thickness to retain a determined diameter soil particle.

This proposition analyses the particle path through the filter. Taking the confidence level as P', the probability, P, of a defined diameter particle, d, to be retained by a pore size smaller than it, before a number N of voids confronts, assuming that each confrontation is a independent event, necessary to satisfy the condition:

$$P' \equiv 1 - P^N \qquad (1)$$

In other words, it is possible to determine the number of pore confronts necessary to warrant the particle retention when it tries to cross the filter thickness by:

$$N \equiv \log(1 - P') / \log P \qquad (2)$$

Considering the average distance between confronts as s, the total filter thickness, t_{GT}, necessary to retain a defined particle diameter is given by:

$$t_{GT} = s\ N \qquad (3)$$

Therefore, to carry out this analysis it is necessary to know the average distance between confronts and the probability of the particle finding a pore size smaller than itself, represented by the pore size distribution curve. Both these parameters are difficult to obtain.

The filter pore size distribution curve has been evaluated by several experimental methods. Several of them are discussed by Bathia et al.(1994) and Fisher et al.(1993). Some are very complex, others are not compatible with geotextiles.

Silveira(1993) proposed to realise in-suspension filtration tests with different filters thickness and to evaluate the pore size distribution curve by retro-analysis using his probabilistic theory. In this case, it is necessary to estimate the average distance between confronts.

For the granular filters, the average distance between confronts can be evaluated in function of granular filter particle diameters. In the case of geotextiles, this supposition can not be used because the geotextiles fibres are not necessarily in contact, and the Silveira(1993) proposition can not be directly applied.

To solve this problem, the Silveira's proposition was combined with a theoretical analysis to obtain the filter pore size distribution curve for needle-punched nonwoven geotextiles, proposed by Gourc(1982) in which case the accumulated probability, Q, of finding a pore size smaller than a defined diameter, d, is obtained by the expression:

$$Q = 1 - \exp [- (\eta \pi d^2 / 4 + \lambda \ d / 2) / n_{GT}] \qquad (4)$$

where n_{GT} is the geotextile porosity and the parameters η and λ can be calculated from the fibre diameter, d_f, by:

$$\eta = 8 (1 - n_{GT}) / (\pi^2 \ d_f^2) \qquad (5)$$

$$\lambda = (2 + 4 / \pi) \ (1 - n_{GT}) / d_f \qquad (6)$$

3 TESTS AND MATERIALS

To carry out this work the authors analysed several fabrics available in Brazil. This paper presents results obtained with thin fabrics, usually employed in filtration functions, and separated into three groups, each one having the same production characteristics, as shown in Table 1.

Table 1. Needle-punched nonwoven geotextiles group characteristics

product	filament	polymer	d_f (mm)
A	continuous	PET	0.022
B	staple	PP	0.030
C	staple	PP	0.026

All fabrics were analysed for their physical characteristics: thickness, mass per unit area, and fibre diameter. Specimens with 150 mm diameter and having physical characteristics close to the average value were selected and submitted to a special in-suspension filtration tests described in Urashima and Vidal(1997).

These tests, illustrated on Figure 1, were conducted to evaluate the bigger particle passing across the filter on the first one seepage front, under severe flow conditions (the particles are been transported by flow). These results can be compared to the hydrodynamic opening size tests results, where the particles are submitted to several seepage front (2000 cycles).

The soil particle used in these tests were obtained from a granite powder, selected after analysis in repeated sieving tests, compounded from uniform single fractions (105/88, 88/75, 75/66, 66/53, 53/44, 44/37, <37 μm).

4 RESULTS

Physical characteristics of the geotextiles are presented in Table 2. The theoretical pore size distribution curves obtained from Gourc(1982) are presented in Figure 2.

Some results of the in-suspension filtration tests are presented on Figure 3.

Table 3 presents an abstract of experimental and analytical values. $O_{95,sf}$ is the 95 % opening size measured in suspension filtration tests. The distances between confronts presented were obtained considering a confidence level, P' = 98 %, and theoretical pore size distribution curves in Figure 1.

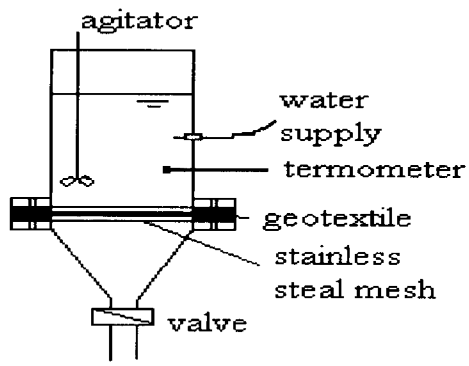

Figure 1. The test apparatus scheme.

Table 2. Geotextiles physical characteristics

geotextile	M_A (g/m^2)	C.V. (%)	t_{GT} (mm)	C.V. (%)	n_{GT} (%)
AA	158	7.7	1.33	7.4	91.4
AB	181	6.3	1.55	5.3	91.5
BA	167	3.9	1.67	5.4	88.9
BB	198	5.9	1.86	3.7	88.2
CA	129	8.9	0.93	8.3	85.6
CB	135	8.0	1.00	5.8	85.0

Table 3. Experimental and analytical results

geotextile	thickness (mm)	$O_{95,sf}$ (mm)	distance between confronts (mm)
AA	1.33	0.070	0.459
AB	1.55	0.059	0.448
BA	1.67	0.044	0.234
BB	1.86	0.041	0.219
CA	0.93	0.062	0.345
CB	1.00	0.054	0.347

These results show that the adopted methodology provides a very close evaluation of distances between confronts, for fabrics with same production characteristics.

Fabrics with mass per unit area greater than 200 g/m^2

present distances between confronts increasing with thickness. For example, to the BC geotextile (t_{GT} = 2.28mm) and CC (t_{GT} = 1.74mm) this distance was 0.367 and 0.518, respectively. Their analysis has been improved to confirm and comprehend this tendency.

5 CALCULATIONS

The procedure to specify geotextiles satisfying retention criteria, can take several paths:

a) Defining a soil particle diameter to retain (for example, d_{85} in well graded soil or d_{50} or an other value in function of soil characteristics), and choosing a geotextile (pore size distribution curve, distance between confronts and thickness known) to obtain the retention confidence level of this diameter;
b) Defining a soil particle diameter to retain, to determine the necessary thickness to retain this diameter with a given confidence level, for each geotextile group (for example, A, B or C);
c) For a chosen geotextile with pore distribution curve, distance between confronts and thickness known, to verify the soil particle to be retained with a specified confidence level;

With the retention or clogging criteria verified, it is necessary to analyse the permeability and survival criteria to complete the geotextile specification.

A well graded soil with d_{85} equivalent to 0.11 mm can be used to demonstrate a case of needle-punched nonwoven geotextile filter design, satisfying the retention criteria.

In this case, if it is possible to consider that this soil particle diameter can retain the soil particles smaller than itself, two attitudes can be adopted:

a) to determine the thickness necessary to retain d_{85} particle diameter for the geotextiles groups analysed,
b) to determine the retention confidence level of this particle diameter for a specified geotextile.

From equations 2, 3 and 4:

$$t_{GT} = s \log (1 - P')/\log (1 - Q) \qquad (7)$$

for a confidence level P' equal to 99.9 %, Q obtained from Figure 1 or equation 4 and s obtained from Table 3, we have for:

- geotextiles group A: $t_{GT} > 1.38$ mm
- geotextiles group B: $t_{GT} > 0.84$ mm
- geotextiles group C: $t_{GT} > 0.75$ mm

and the geotextiles AB, BA and CA can be adopted.

If the geotextile AA (t_{GV} = 1.35 mm) is available, the retention confidence level to retain the d_{85} soil particle, determined from equations 2, 3 and 4 is 99.88%.

Comparing these results with a traditional retention criteria like the one proposed by the French Geotextiles and Geomembranes Committee (CFGG), considering the best soil condition, the geotextile hydrodynamic opening size needs to be lower than 0.138mm. In this case, the geotextiles of the group A can not be adopted (AA - $O_{95,H}$ =0.21 mm, AB - $O_{95,H}$ =0.17 mm).

It is necessary to remember that Silveira's proposition takes into consideration the most critical situation, i.e. the particles are been transported by flow.

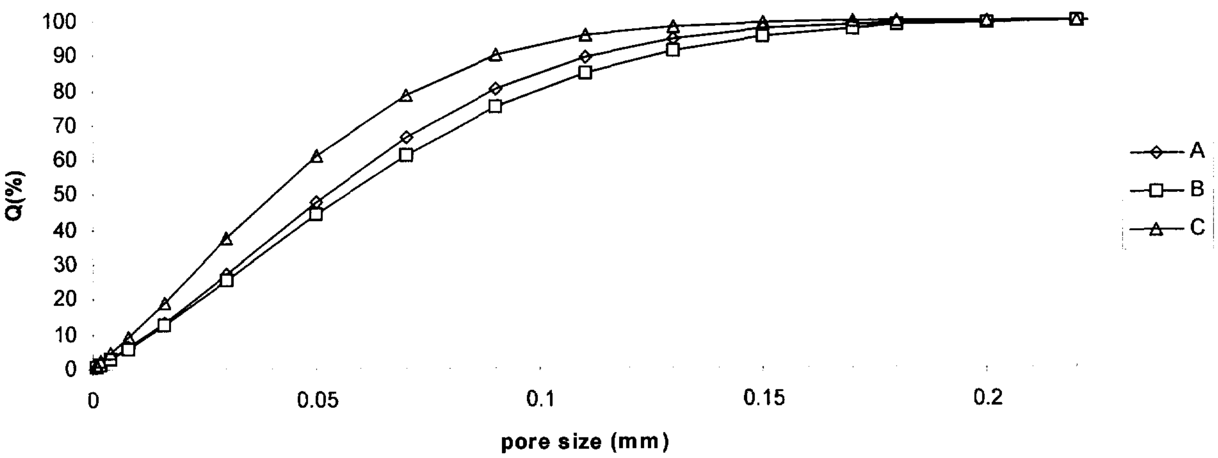

Figure 2. Theoretical pore size distribution for the analysed geotextiles groups.

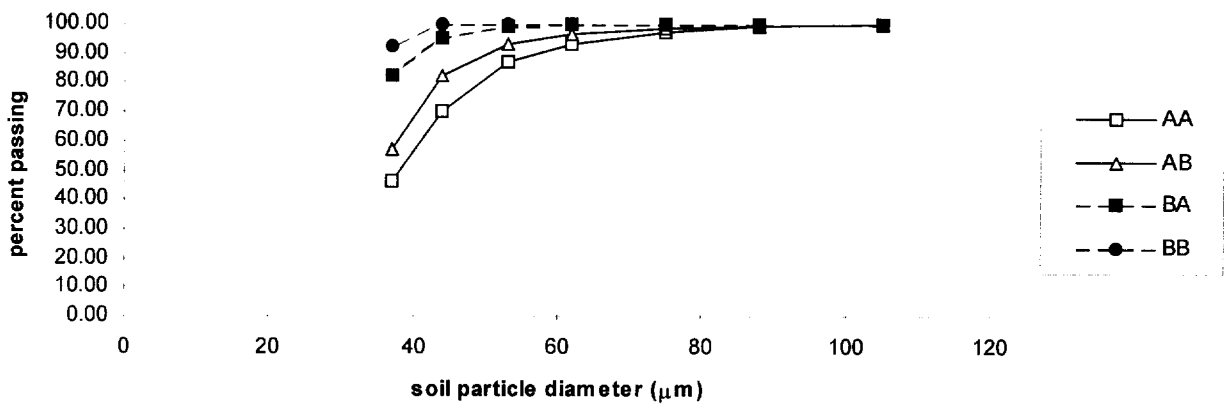

Figure 3. Grain size distribution curves of the soil passant mass observed in some in-suspension filtration tests.

6 COMMENTS

Although Silveira's(1993) procedure can not allow us to determine directly the pore size distribution curve of geotextiles because the average distance between confronts are not known and we do not have several fabric thicknesses with the same production characteristics (each fabric thickness represents one point of the curve), his proposition is interesting to evaluate the average distance between confrontations, if the pore size distribution curve can be obtained by an other method.

From the results of in-suspension filtration tests, conducted according to the probabilistic theory suppositions, and the theoretical pore size distribution curve proposed by Gourc(1982), it is possible to evaluate the average distance between confronts.

Each geotextile or group of fabrics that presents the same production characteristics can be analysed and have their filtration parameters evaluated.

To define a production line (group of geotextiles presenting the same fabric filtration characteristics) it is necessary to have a good technological control of the production procedure that warrants the same characteristics. The nonwoven geotextiles are very sensitive to a variation of the needle intensity. Anyway, the analysis of in-suspension filtration tests results can detect the fabric variations.

Fabrics with mass per unit area greater than 200 g/m^2 need to be better studied to verify if the observed variation on the average distance between confronts with apparently the same production characteristics is a function of the in-suspension filtration tests methodology adopted, or intrinsic fabric variation. Tests with larger specimens are been carried out to improve our knowledge.

The superposition of the theoretical pore size distribution curve and in-suspension filtration tests results looks to be an applicable proposition for thin geotextiles.

ACKNOWLEDGEMENTS

This research was partially supported by FAPESP (São Paulo Research Support Foundation).

REFERENCES

Bhatia, S.K., Smith, J.L., Christopher, B.R. (1994). Interrelationship between pore openings of geotextiles and methods of evaluation. *Fifth International Conference on Geotextiles, Geomembranes and Realted Products*, Singapore, pp. 705-710.

Fischer, G.D., Holtz, R.D., Chistopher, B.R. (1993) A critical review of geotextile pore size measurement methods. *Geofilters'93 - International Conference on Filters and Filtration Phenomena in Geotechnical Engineering*, Karlsrule, Germany, pp 83-90.

Gourc, J.P. (1982) Quelques aspects du comportement des géotextiles en mécanique des sols, *Université Scientifique et Médicale de Grenoble, Institut Polytechnique de Grenoble*, Grenoble, France.

Silveira, A (1965) An analysis of the problem of washing through in protective filters. *VI International Conference on Soil Mechanics and Foundation Engineering*. Montreal, Canada, pp 551-555.

Silveira, A (1993) A method for determining the void size distribution curve for filter materials, *International Conference on Filters and Filtration Phenomena in Geotechnical Engineering*. Karslrule, Germany, pp.71-73.

Urashima, D.C., Vidal, D. (1997) Filtration opening size by in suspension tests. *Symp. on Recent Developments in Soil and Pavement Mechanics*, Rio de Janeiro, Brazil, 25-27 jun.

Filter behaviour of hydraulically and mechanically damaged geotextiles

YH Faure, Y. Kehila

LIRIGM, University Joseph Fourier, Grenoble, France

ABSTRACT : In this paper, a geotextile filter is considered hydraulically « damaged » when it is clogged by soft soil and mechanically damaged when it is punched or torn by gravels during installation. Specific tests were performed to damage hydraulically non-woven filters by filtration of fine soil in suspension (critical conditions for clogging). Physical properties and filtration characteristics of filters like filtration opening size are analysed to show their influence on velocity of clogging. Clogging occurs when the filtration opening size is smaller than the dmax of the fine soil and the velocity of clogging is very sensitive to the geotextile density (or porosity). Three levels of damage action were applied to damage filters mechanically. A lot a perforations are necessary to produce variation of filtration opening size when it is determined by sieving method (wet sieving or hydrodynamic sieving). A very deformable geotextile is less damaged than a rigid one.

KEYWORDS : Filtration, Degradation, Clogging Tests, Non-woven fabrics

1 INTRODUCTION

A lot of studies have been carried out in the past in order to analyse geotextile filter behaviour and, in general, clean undamaged specimens are tested. However, during on-site installation, geotextiles are laid mostly on a soft, saturated fine soil and, as a result, filter pollution (or clogging) occurs when operatives walk on the geotextile. Moreover, when the gravel layers are subsequently placed on the filter, mechanical damage may occur, such as punctures or tears. In both cases, the geotextile filter is considered to be hydraulically or mechanically damaged.

This paper presents the experiments carried out and the results obtained, indicating the filter behaviour of different textile structures.

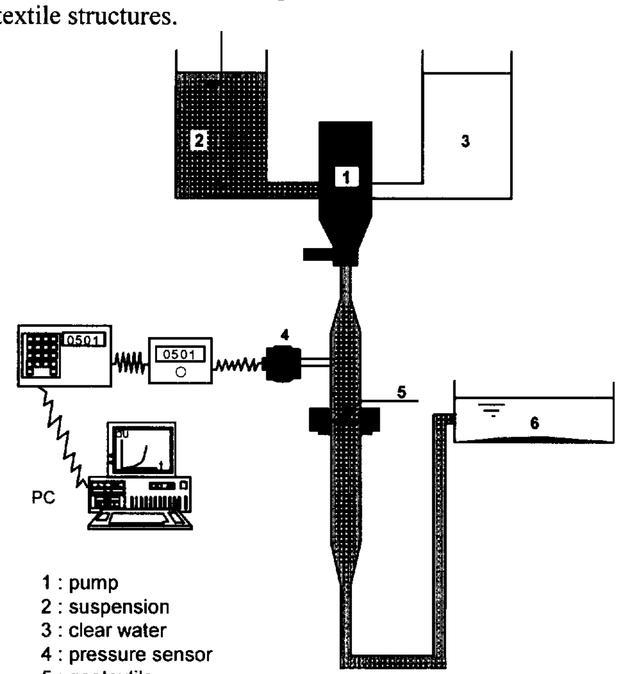

Figure 1: Diagram of the test assembly used for filtering soils in suspension

2 HYDRAULIC DAMAGE: FILTRATION OF WATER LOADED WITH SOIL IN SUSPENSION

In order to study the effect of hydraulic damage, a filtration test was performed on a sample of water loaded with soil in suspension. This test, presented in a previous paper by Faure et al. (1993), reproduces the critical conditions encountered when installing the geotextile on site: the soil in the trench is often very muddy and the geotextile must filter the soil carried in suspension in the water without clogging. Then, when the soil has consolidated and is in close contact with the filter, the water is no longer charged with particles in suspension, or contains only very little (on condition that the internal stability of the soil to be filtered is established). It is necessary to check that the clogging level during the initial stage is not too high, and it would be beneficial if the circulating clear water could help unclog the geotextile, thereby ensuring better subsequent operation of the system.

2.1 Description of the filtration test

The test assembly consists of the following components -
- two upstream reservoirs, one for supplying water loaded: with soil particles in suspension, and one constant-level reservoir to ensure the circulation of clear water (a three-way valve is used to switch instantaneously from one reservoir to the other),
- a constant discharge pump to provide a constant solid and liquid flow when clogging is not too high,
- a sample holder (effective diameter: 50 mm),
- a constant-level downstream reservoir.

A pressure sensor is connected to the circuit 0.15 m upstream of the geotextile. This sensor monitors the time-dependent increase in pressure due to filter clogging.

2.2 Soil used

The retention criteria for geotextiles filters are based on the characteristic "geotextile filtration opening" size, O_f. If the value of O_f has been correctly chosen, the granular skeleton of the soil is retained (Giroud, 1996) and the risk of clogging during the initial operating period of the filter is due only to the fine elements in the soil. This is the reason why the retention criterion of the CFG (French Geosynthetics Committee) requires a filtration opening O_f greater than 80 µm, in the case of coherent soils, to allow particles smaller than 80 µm to pass through the geotextile.

For the filtration tests on loaded water, a clayey soil was used with upper particle size limited to 80 µm. The particle size range of this pottery-type clay (Figure 2) was measured without deflocculant because, during the test, it is used without deflocculant.

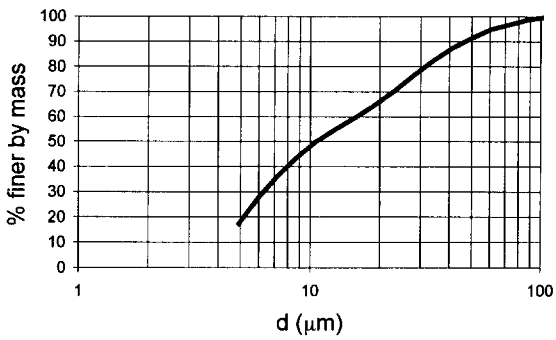

Figure 2: Particle size range of the soil for filtration tests of soil in suspension

2.3 Characteristics of geotextiles tested

All the geotextiles are made of non-woven polypropylene. The distinguishing parameters (cf. Table 1) are mass per unit area μ_g, thickness T_g and fibre diameter d_f. Porosity can be then calculated by mean of:

$$n = 1 - \frac{\mu_g}{\rho_f T_g}$$ where ρ_f is the density of the fibres.

The density of the geotextile is : $\rho_g = \frac{\mu_g}{T_g}$

SF geotextiles are made with short fibres while CF materials are made with continuous filaments. The HB geotextiles are heat-bonded.

2.4 Test procedure

After installing the test sample and saturating the system, soil particles are tipped into the reservoir filled with water (capacity 25 *l*). The concentration Co of the suspension is 0.5, 1 or 2 g/l. A mechanical stirrer ensures that the suspension remains homogeneous at all times. The flow rate is imposed by the pump with a speed of 40 mm/s. When the particles come into contact with the filter, recording of the pressure « u » starts. This pressure gradually increases Then, when the clogging level is too high, the pressure suddenly increases at a much faster rate until the safety valve is tripped. (Figure 3). Overpressure is defined by the difference : $u - u_o$ (u_o is the measured value of u at the beginning of the test with clear water).

2.5 Influence of geotextile structure

Figure 3 shows that the mass per unit area is not the main parameter governing the clogging rate: when O_f is greater than d_{max} of the soil (cf. CF300b and SF300), no clogging occurs: the pressure has hardly increased after all the water has flowed through. On the other hand, with a filtration opening size $O_f < d_{max}$, clogging occurs all the faster as the porosity is lower (HB300 and CF300a).

The density ρ_g (= μ_g / T_g) was calculated for each geotextile sample. This parameter gives an indication of the compactness of the fibrous medium (like the porosity).

Table 1: Characteristics of geotextiles tested (mean values)

Géotextile Lirigm name	Structure	μ_g g/m2	T_g mm	d_f mm	n %	O90 (Hyd. S) µm
CF130a	nw-needlepunched.	126	1.1	26	87.5	85
CF130b	nw-needlepunched.	127	1.3	37	89.4	155
HB130	heatbonded	137	0.5	42	70.2	140
SF130	nw-needlepunched.	134	2.5	31	94.2	175
CF300a	nw-needlepunched.	292	2.6	26	87.8	65
CF300b	nw-needlepunched.	286	2.8	37	88.9	105
HB300	heatbonded	294	0.8	42	60.1	65
SF300	nw-needlepunched.	269	3.9	31	92.5	100
CF400a	nw-needlepunched.	400	3.45	26	87.4	61
CF600a	nw-needlepunched.	633	4.5	26	84.7	59
CF600b	nw-needlepunched.	617	4.4	37	84.8	50
CF800a	nw-needlepunched.	816	5.9	26	85.0	60
SF1100	nw-needlepunched.	1119	7.8	49	84.7	101

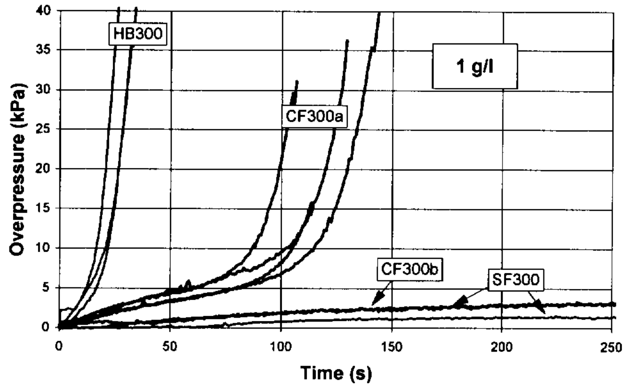

Figure 3: Influence of geotextile structure 2.6 Influence of geotextile density (or porosity)

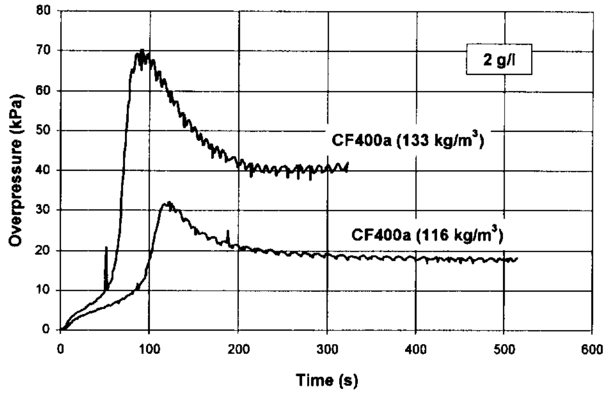

Figure 4: Clogging - Unclogging curves

To study the clogging phenomenon, the clogging rate was defined by the slope of the straight line tangent to the clogging pressure curve before the "elbow" ($Vc = \Delta u / \Delta t$)

Figure 5 shows the variation in Vc / Co (to compare tests conducted with different concentrations Co) as a function of ρ_g for CFa geotextiles of the same fibre diameter and same needle-punched structure. Despite the dispersion, the compactness (or the porosity) would indeed seem to be the parameter most influencing the filter clogging rate, regardless of the weight per unit area. Clogging therefore occurs mainly on the surface or in the first layers of fibres.

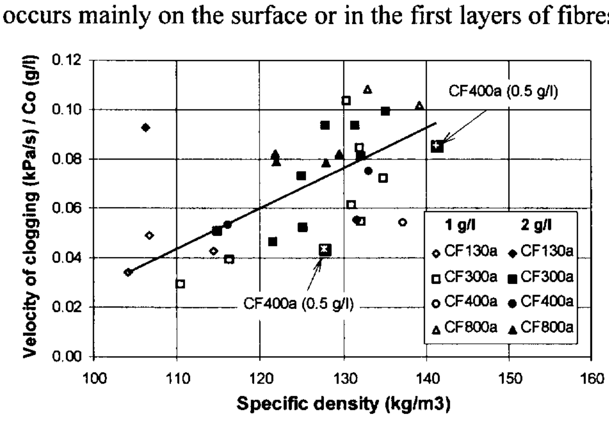

Figure 5: Determining role of geotextile density

2.7 Unclogging

The ease with which a geotextile is likely to become clogged is controlled by the injection of clear water, always with a flow speed of 40 mm/s, as soon as the pressure reaches 10 kPa. The graphs in Figure 4 illustrate this phenomenon and clearly show the role of compactness (for CF400a filters). A high density filter remains less permeable than a low density filter although its clogging level was the same as the low density filter.

3 MECHANICAL DAMAGE:

If a geotextile incurs mechanical damage, during the installation procedure (punctures, tears), its filtration characteristics, permeability and filtration opening size are modified: the permeability increases and the filtration opening size as well. The question is to know whether these variations will disturb the filtering behaviour of the geotextile and, if so, in what proportions, and is it still operational after this damaging action?

- The permeability increases: this is a positive effect with regard to the permeability condition required by the filter criteria. However, a permeability test after a damaging action enables the level of filter damage to be estimated.
- The filtration opening size increases: the geotextile is now not so efficient at retaining the soil. To estimate the damage incurred on a geotextile, is the transmission observation method objective?

Damaging action tests were conducted with three stress levels and the filtration opening size of the damaged samples was then measured by wet sieving and by hydrodynamic sieving

3.1 Levels of damaging actions

Level 1: Tests were carried out according to the draft European Standard Procedure for simulating site damage. A geotextile specimen is laid between two gravel layers (corundum SD 5-10 mm) and subjected to cyclic loading of 900 kPa with a frequency of 1 Hz for 200 s (Figure 6).

Level 2: The test device used is the same as before. The damage is produced by a 230 mm square plate with 57 ASTM punches (ASTM D 5494 standard), Figure 7. The point of each punch has a pyramidal shape and the base is circular (25 mm diameter). Together, they form a triangular arrangement with a side length of 25 mm. The geotextile is laid on an 80 mm thick layer of sand (0-2 mm). The cross-section of the cell containing the sample is small (250 x 250 mm), slightly larger than the punch plate. The punches are in direct contact with the geotextile. A load of 380 kPa is applied (i.e. 0.35 kN per punch), for 200 cycles at 1 Hz.

Level 3: The punches consist of 23 mm high cones with an apex angle of 40° (Figure 8). 19 cones are fixed on a support plate in a triangular arrangement with a 60 mm side length. A load of 0.60 kN per cone, or an equivalent pressure of 150 kPa, is applied at 1 Hz for 200 cycles.

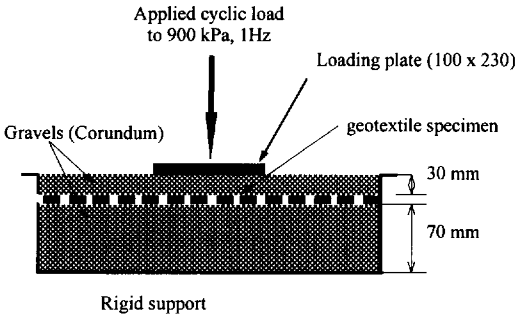

Figure 6: Test device for the level 1 damage test

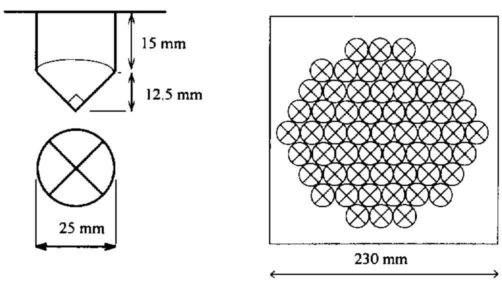

Figure 7: ASTM punches for the level 2 damage test

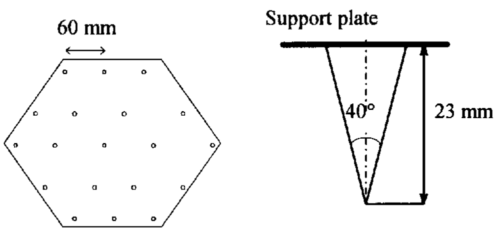

Figure 8: Cones for the level 3 damage test

3.2 Results (Figure 9)

Not all the geotextiles were systematically subjected to the same stress levels. Depending on the results obtained, a higher or lower level was not necessarily applied. For example, when the HB130 geotextile suffered considerable damage at level 2, it was not considered necessary to apply level 3.

Level 1 : With level No 1 damaging action, only the HB130 geotextile would appear to have suffered any damage: many of the filaments are broken and perforation marks are visible. However, measurement of the O90 opening by the wet sieving test shows only a slight increase in O90: from 117 to 142µm.

For the other geotextiles no damage was observed or measured.

Level 2 : With level 2, of the 130 g/m2 geotextiles, only the SF130 kept the same O90 value, although it suffered considerable strain. The heavier geotextiles (300 g/m2), despite showing the marks of the punches after the test, have suffered only minor damage and their O90 value has hardly increased, even for HB300.

Level 3 : With the stress applied at level 3, all the geotextiles are perforated: cone holes are clearly visible by shining a light through the sample, although the size of the holes varies depending on the geotextile.

For the highly deformable SF300 and SF1100, the cone hole diameters are much smaller than those of the CF300a, in which the holes are more like cuts. However, it is worth noting that although the holes are several millimetres in size, the values of O90 remain well under 1 mm. There are two reasons for this:

- after the damage test, with the samples at rest, the perforations and cuts in the needle-punched material tend to close with time, a feature that is not found in heat-bonded geotextiles,
- the number of perforations (only 7) inside the sample (200 mm diameter) tested by wet sieving or hydrodynamic sieving is not sufficient. During sieving, a small quantity of soil passes through the holes and the proportion of large particles is insufficient.

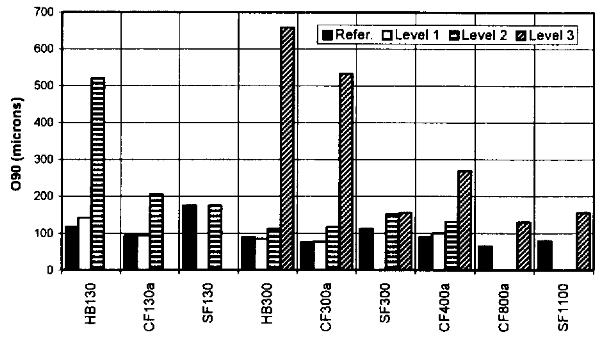

Figure 9: O90 histogram after the damaging action

4 CONCLUSION

This study of the hydraulic behaviour of geotextile filters after incurring hydraulic or mechanical damage has highlighted the role played by characteristic parameters.

Hydraulic damage (water loaded with soil particles in suspension): filter clogging is delayed when the filtration opening size is greater than the d_{max} value of the soil in suspension. With an Of value equal to or slightly lower than the value of d_{max} of the tested soil in suspension (here d_{max} = 80 µm), the risk of clogging increases when the filter porosity is smaller.

Mechanical damage: the filtration opening size of geotextile filters is not modified at level 1. In order for the filtration opening size test to be sensitive to the filter damage, the number of perforations must be sufficiently great like with the level 2 damage test.

REFERENCES

Faure, YH., Elamir, A., Farkouh, B., Gendrin, P., Reisinger, P. (1993) « Geotextile filter behaviour with critical filtration conditions » *Proc. 1st Int. Conf. Geo-Filters*, Karlsruhe, pp 209-116.

Giroud, JP. (1996) « Granular filters and geotextile filters » *Proc. 2nd Int. Conf. Geo-Filters*, Montreal, pp 565-680.

Large-scale Performance Tests to Evaluate Filtration Processes

Th. Kossendey
LGA-Geotechnical Institute, Nuremberg, Germany

G. Karam
Du Pont de Nemours, Luxembourg, Luxembourg

ABSTRACT: The long-term filter performance of 5 geotextiles differing in permittivity, thickness, mass per unit area and type of polymer was studied experimentally in large permeameters supplied with three different soils. In three test series, the geotextile samples of 500 mm diameter were submitted to steady state seepage under different hydraulic gradients for 6 to 24 months. In the first two performance tests, the water flow was in the direction of gravity. The third test series simulated the case of upward water flow. Although the geotextiles differed in their parameters, their filter performance exhibited very similar characteristics and satisfied the requirements for stable filter performance. A detailed microscopic investigation into the soil structure directly above the geotextiles confirmed that the geotextiles formed an internal soil filter with a bridging network.

KEYWORDS: Long-Term Filtration, Clogging tests, Performance Evaluation, Microstructure

1 INTRODUCTION

Geotextile filters function adequately when they retain a majority of the soil particles at the interface between a finer and a coarser soil and permit the flow of water through the pores of the soils and the geotextile filter without any water pressure build up upstream of the filter. Many investigations were carried out to obtain reliable criteria for the design of geotextile filters, but it is difficult to predict the long-term filter behaviour. The long-term performance of geotextile filters depends primarily on the following factors:

- the properties of the filter,
- the properties of the soils,
- the type of water flow.

Since these major factors are variable, it is not possible at the present time to predict the long-term filter performance of different geotextiles quantitatively on a theoretical basis. The long-term filter performance can only be evaluated correctly on the basis of either field experience or large scale performance tests under well defined boundary conditions which can be related to the in-situ situation.

2 TESTING PROGRAMME

2.1 Soils used for the performance tests

According to the geotextile filter criteria currently applied in Germany (FGSV 1994), a soil is called a "problem soil" regarding the geotextile filtration, if any one of the following criteria applies:

a) $C_u = d_{60}/d_{10} < 15$ and the soil contains some fines < 0.06 mm
b) > 50 % content of the grain size fraction $0.02 \text{ mm} < d < 0.1$ mm
c) $I_p < 15$ % (if not available: content of clay / content of silt < 0.5)

The fine-grained silt used for long-term filtration test was a loess from a road construction site in the Central Hesse area, about 30 km north of Frankfurt/Main.

The soils A and B were blended from different quartz fractions. Thus, it was possible to design cohesionless soils with gradation curves which met the above-mentioned criteria for a "problem soil" with respect to geotextile filtration.

The soils used in the permeation tests fully satisfied all criteria for a "problem soil". The grain size distributions are shown on Figure 1. Details of the soil parameters used in the tests are given by Kossendey et al. (1996b).

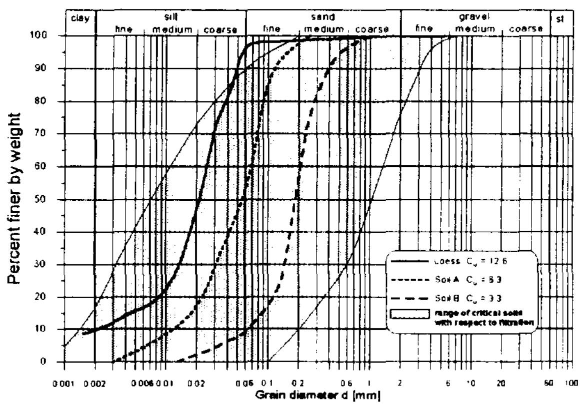

Figure 1. Grain size distributions of the soils used in the long-term permeation tests

2.2 Geotextiles

5 different nonwovens (3 heat-bonded, PP and 2 needle-punched, PET) geotextiles were selected for the long-term performance tests. They comprised geotextiles of various polymers and different manufacturing technologies in a wide range of their properties. Details of the selected geotextiles are given in table 1. Their properties were determined by index tests at the laboratory of the LGA-Geotechnical Institute. The results of these tests served as reference data for the evaluation of changes in the geotextile properties after the long-term permeation.

2.3 Permeameter circuit

The test equipment used in these test series consists of 3 supply containers and 4 permeameters per circuit arranged radially around the supply container. They have a diameter of 50 cm and a height of 167.5 cm. A detailed description of the permeameters was given previously by Gartung et al. (1994) and Kossendey et al. (1996b).

2.4 Test conditions

In total, three long-term filtration test series differing in their boundary conditions were carried out. For the first two test series, a mesh was placed upon the conical bottom plate with a discharge opening at the centre in each of the permeameters. The geotextile sample was installed above the mesh and attached to the permeameter by a fixing ring. The soil layer was placed on the geotextile. The first long-term test series was carried out under a hydraulic gradient of i=3 regarding the soil layer above the geotextiles. This hydraulic gradient falls into the range of typical hydraulic gradients for drainage applications under steady-state flow conditions, as noted by Davindenkoff (1976) and Luettich et al. (1992). During the second test series the hydraulic gradient was selected as i = 12 to observe the permeation behaviour under higher hydraulic gradients. The permeation of the tests was in direction of gravity. In order to examine the filtration behaviour of a system geotextile/soil under conditions of upward permeation against the direction of gravity, a third test series was implemented with a hydraulic gradient i = 2,5 (figure 2). The soil layers of each test implementation were only slightly compacted to test the filtration behaviour for the worst case.

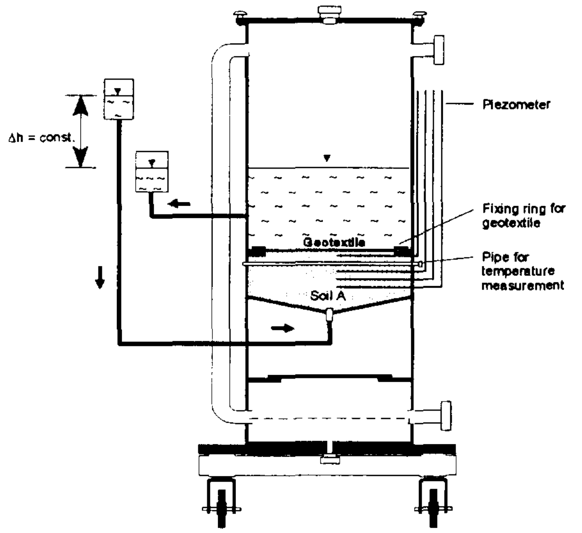

Figure 2. Schematic sketch of the test with upward permeation

The test liquid (tap water) permeated uniformly through the system geotextile/soil. The determined values of dissolved oxygen in the different circuits were between 4.2 ppm and 5.5 ppm. Following the definition of de-aired water (maximum at 6 ppm), the criterion for the oxygen content of de-aired water was met in the filtration tests.

2.5 Analysis of the microstructure

In order to analyse the microstructure at the interface geotextile/soil influenced by the interaction between geotextile and soil, microscopic sections were prepared. The undisturbed soil samples taken after the end of the tests were saturated by a resin in the same way as by water in the filtration tests to prevent the soil samples from any disturbance. The viscosity of the resin was similar the water that permeated the system geotextile/ soil.

3 TEST RESULTS

3.1 Performance tests with a hydraulic gradient i = 3

During an initial period of approximately four weeks, an increase in the system permeability of the permeameters with the loess soil was observed. In spite of the increase in permeability, no soil particles were detected by the collecting glass. After about four weeks, the permeability of all permeameters began to decrease. With increasing test duration, the permeameters showed only small differences in the system permeabilities. They followed the same trend towards constant values. The system permeabilities of the permeameters are given in Figure 3. The coefficient of permeability of the loess soil tested by small scale index test was $1.2 \cdot 10^{-8}$ m/s. The observed permeabilities of the large scale system geotextile/soil never fell below this value, so the permeabilities of the system soil / geotextile were higher than that of the small soil sample at all times. The reason for the discrepancy may be local variations in the density of the large permeameter sample, and associated inhomogeneities in the distributions of the coefficient of hydraulic conductivity.

The behaviour of the system permeabilities in the permeameters with soil A and soil B are similar to the results of the tests described by Kossendey et al. (1996a, 1996b). In permeameter with geotextile NP1 an additional load of 20 kPa was applied. The system permeabilities began to increase in all permeameters. In contrast to the test with the loess soil, the initial period of increasing permeabilities lasted only a few days.

Except for a slight cloudiness of the test liquid which could not be quantified, no particle migration was observed in the test circuit with soil A at the beginning of the tests. Although the geotextile HB1 was not dimensioned with respect to the criteria of FGSV, it satisfied the requirements for a sufficient filter performance. The greatest amount of migrated soil particles of NP1 was detected during the first 2 hours. With increasing test duration, the geotextile showed a stabilization like in the other permeameters. The reason for the higher amount might be details in the filling procedure of the permeameter. The cumulative amount of the migrated soil particles is given in table 1.

Table 1. Cumulative amount of migrated soil

Geotextile	Amount of migrated soil [g/m²]	Soil
HB 1	19.02	A
HB 2	14.80	A
HB 3	5.97	A
NP 1*	78.38	A
HB 1	24.27	B
HB 2	9.15	B

* with 20 kPa load

After that initial period, the flow rates became consistent and the various permeameters showed only very small differences. As a result of higher compaction of the soil layer, the measured permeabilities in the permeameters with geotextiles NP1 and HB2 (soil A) were lower. The system permeabilities of the permeameters with soils A and B stabilized to equilibrium conditions after 100 days, and then they varied only in a very small range for the remainder of the test period. Like in the test with the loess soil, there were no discernible differences in the performance between the types of geotextile. The system permeabilities are given also on figure 3.

The permeameters which were filled with soil B and the permeameter with the geotextile HB 1 and soil A showed a slight decrease in their permeabilities after 300 days, while all of the other permeameters were constant in their permeabilities. After the monthly addition of a disinfectant against microbiological growth, an immediate increase in the permeabilities of the treated permeameters was observed. Although a biofilm of algae was not observed at the surface of the soil layer, probably a microbial growth within the pores of the soil had to lead to a reduction of the system permeabilities. The measured permeabilities of the dismantled geotextiles were smaller than those of the virgin geotextiles by a factor of 10 at maximum, but they never fell below the permeability of the test soils.

3.2 Performance test with a hydraulic gradient i = 12

Two heat-bonded and two needle-punched nonwovens were selected for a second test series to evaluate the filter performance under a hydraulic gradient of i = 12. In a first step, a layer of soil A with 5 cm thickness installed without compaction in the permeameters was permeated.

The development of the permeabilities of both tests under the hydraulic gradient i = 12 was similar to the results of the first test series. After an initial period of increase, the permeabilities began to decrease slightly. The measured amount of migrated soil was higher than in the test with a hydraulic gradient i = 3, but after 2 hours permeation no measurable amounts of soil were detected. After a test duration of 85 days, the soil layer in the permeameters was brought into suspension to simulate the extreme case of the destruction of the internal soil filter. Like in the first test, there were no discernible differences in the performance between the geotextile types. The measured amounts of migrated soil were higher than the results before the disturbance, but piping of the soil stopped within 3 hours. A distinct trend of a better performance of thicker products regarding the retention of particles was not observed. The system permeabilities and the cumulative amount of migrated soil particles are given on Figures 4 and 5.

3.3 Performance tests with upward permeation

Four nonwovens (two heat-bonded and two needle-punched) were selected for a third test series to evaluate the filter performance with upward permeation under a hydraulic gradient i = 2.5. The behaviour of the permeabilities was similar to the results of the two test series mentioned above. During an initial period of about 10 days, the permeabilities showed a nonuniform permeation behaviour. After that initial period, the permeabilities in all permeameters adjusted to constant flow rates. In order to simulate the frequent case of interrupted water flow in a subsurface drainage system, the upward permeation of the test system was stopped after 40 days. After the renewed start of the permeation, following an initial period of instability, the system permeabilities remained again relatively constant with time. The system permeabilities are given on Figure 6.

Table 2. Geosynthetics used in the long-term permeation tests

	Geotextile	Polymer	Mass per unit area [g/m²]	Thickness (2 kPa) [mm]	$O_{90,w}$ [mm][1]	k_v (20 kPa) [m/s][2]	Permittivity (20 kPa) [s^{-1}][2]
heat-bonded	HB 1	PP	113	0.44	0.18	$4.0 \cdot 10^{-4}$	1.34
	HB 2	PP	195	0.56	0.13	$2.4 \cdot 10^{-4}$	0.55
	HB 3	PP	300	0.82	0.09	$3.2 \cdot 10^{-4}$	0.42
needle-punched	NP 1	PET	250	2.97	0.10	$2.2 \cdot 10^{-3}$	0.83
	NP 2	PET	365	4.02	0.09	$2.3 \cdot 10^{-3}$	0.55

1 measured by wet sieving (draftDIN 60500-6)
2 related to 10° Celsius and 1 geotextile layer, surcharge loads are given in brackets

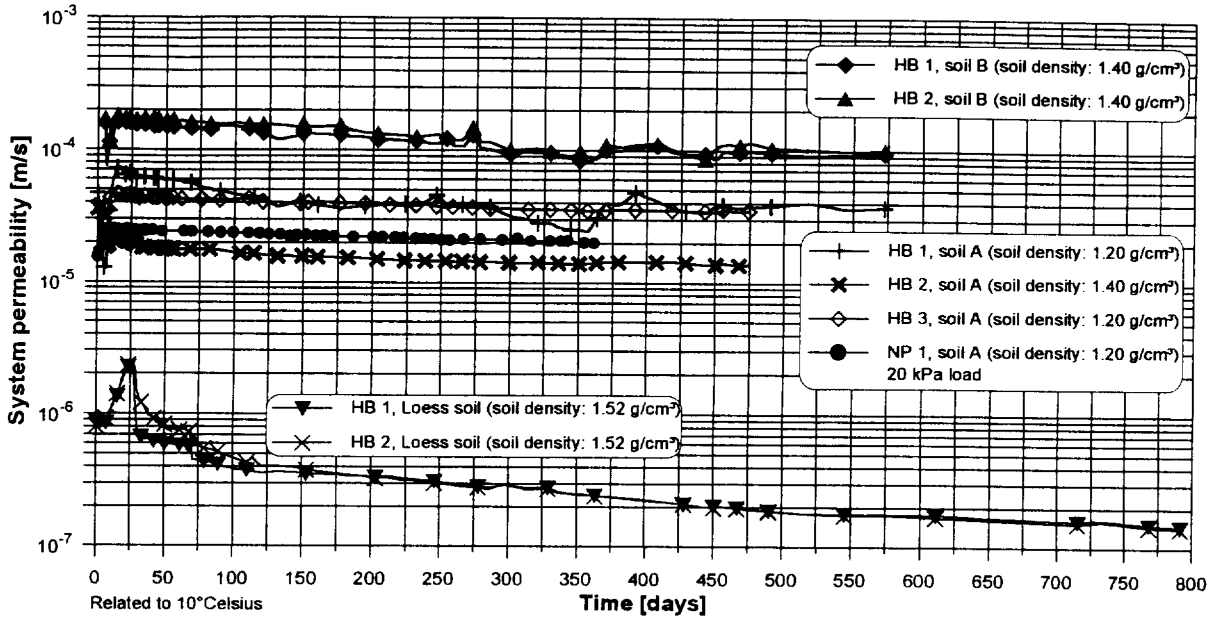

Figure 3. Permeabilities of the different systems of geotextile/soil (downward permeation, hydraulic gradient i=3)

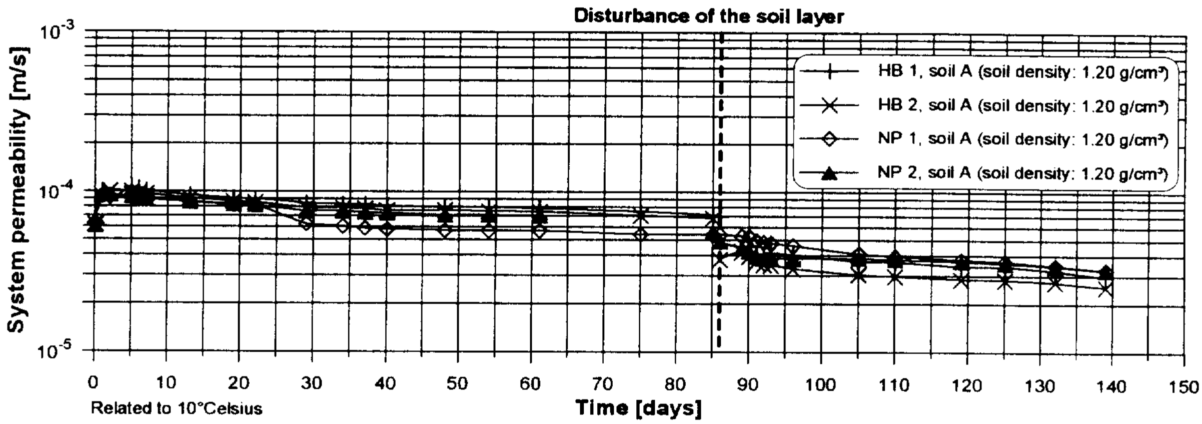

Figure 4. Permeabilities of the system of geotextile/soil A (downward permeation, hydraulic gradient i=12)

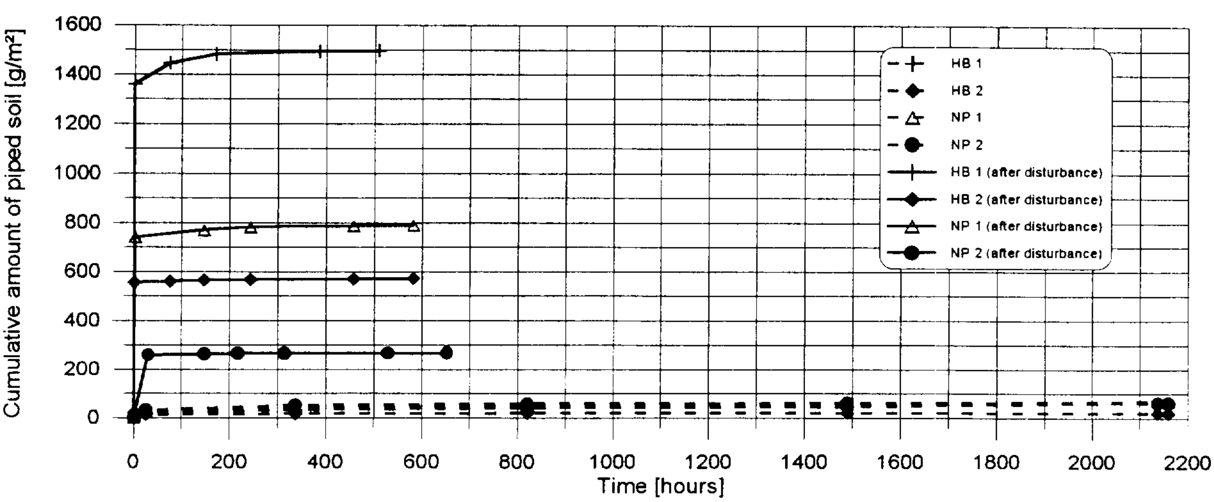

Figure 5. Cumulative amounts of piped soil (hydraulic gradient i=12)

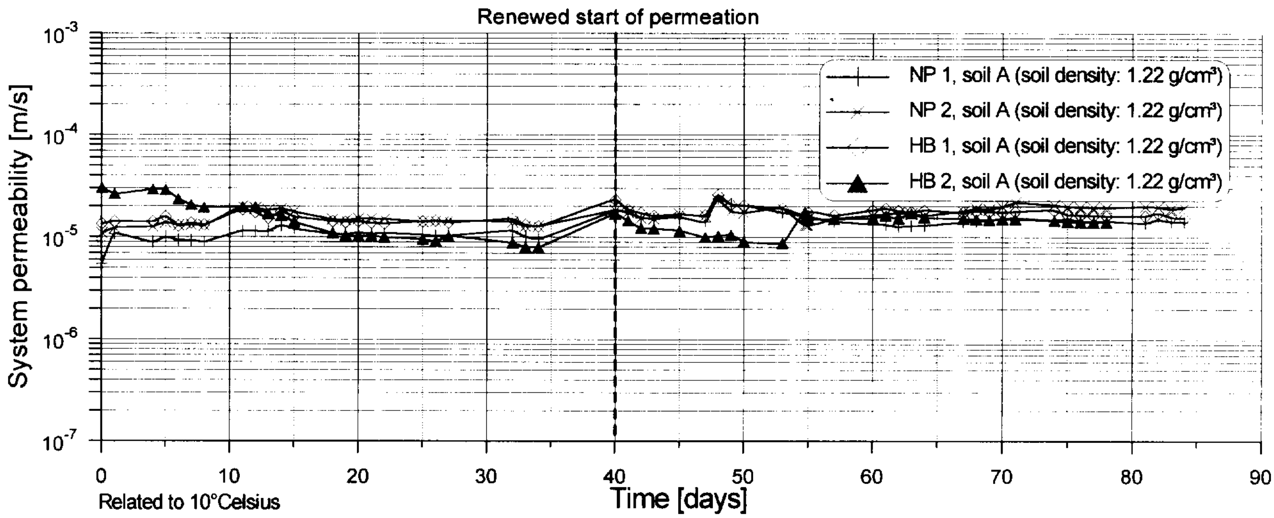

Figure 6. Permeabilities of the system of geotextile/soil A (upward permeation, hydraulic gradient i=2.5)

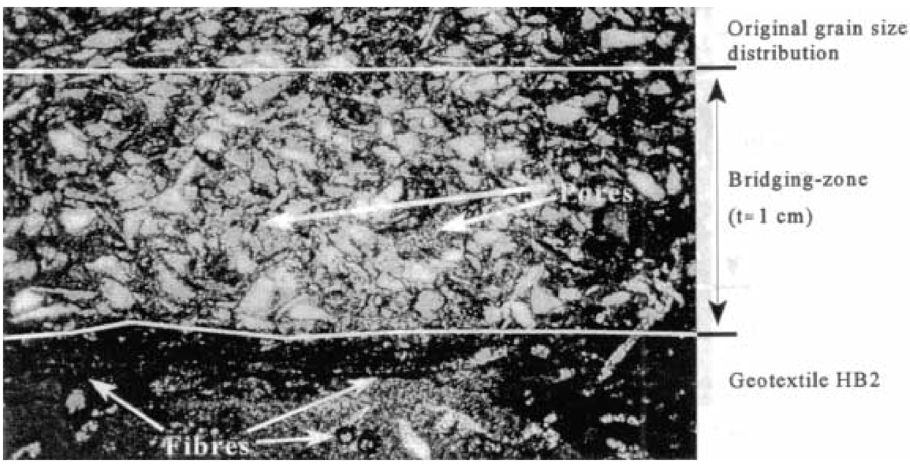

Figure 7. Microstructure at the interface Geotextile HB2/ Soil A (2nd Test series; hydraulic gradient i=12)

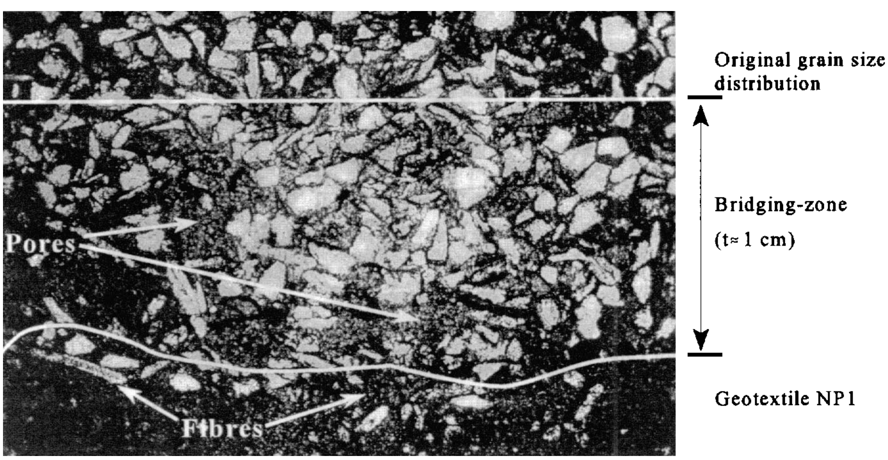

Figure 8. Microstructure at the interface Geotextile NP1/ Soil A (2nd Test series; hydraulic gradient i=12)

4 MICROSTRUCTURAL ANALYSES

During the dismantling of permeameters of the test series permeated downward, undisturbed geotextile/soil samples were prepared for microscopic analyses. In all analysed microscopic sections, it was observed that soil particles formed an internal soil filter in the form of a bridging network above the geotextiles. The geotextile filter layers acted as a catalyst for the formation of this internal filter system of the soil. The thickness of the bridging-zone was dependent on the hydraulic gradient. The thickness of the bridging-zone observed in the tests under the hydraulic gradient i = 3 was 5 mm at maximum and about 1 cm in the tests under a hydraulic gradient i = 12. A trapping of finer soil particles by the filter layer was noticed only in tests with the needle-punched geotextiles. However, the penetration was about 0.5 mm, so that the phenomena of deep filtration discussed by Heerten (1993) was not observed. The microstructures of soil A and the geotextiles HB2 and NP1 are given on figures 7 and 8.

5 CONCLUSION

Although the tested geotextiles differed in their material parameters, their filter performance exhibited essentially the same characteristics. They satisfied the requirements of stable permeation conditions. A review of the test results published by Kisskalt (1992), by Gartung et al. (1994) and by Kossendey et al. (1996a, 1996b), revealed that this observation applies to the geotextiles and test soils studied by Kisskalt and by Kossendey et al. as well. The test duration of up to 800 days and the large scale of the test equipment admit the application of these findings to conditions which are encountered in engineering practice (steady-state-flow conditions and lower hydraulic gradients). The opening size $O_{90,w}$ (measured by the wet sieving method) of most of the recently obtainable nonwovens falls into the region from 0.07 to 0.13 mm. Following the obtained test results, it has to be assumed that geotextiles which meet the retention criterion based on $O_{90,w}$, will perform successfully under these boundary conditions.

Along with the results of previous research investigations (Kisskalt 1992 and Kossendey et al., 1996a, 1996b), the findings of these long-term studies in filtration with 25 different geotextiles and 6 critical soils regarding filtration are a wide basis for the assessment of the long-term filter performance. All results confirmed that the thickness of a geotextile layer is not a relevant criterion for filtration under steady-state-flow conditions and the retention criterion based on $O_{90,w}$, has proved to be a reliable basis for the dimensioning of geotextile filter layers. Field examinations of geotextiles installed up to 15 years ago (Rollin et al.,1994 and Mylnarek et al., 1994) confirm the results with respect to the long-term performance.

The test results of the long-term test series reported in the present paper and compared to results of previous test series carried out at the LGA-Geotechnical Institute can be summarized as follows:

- all permeameters showed the same flow behaviour with increasing test duration
- stable flow conditions were obtained in all permeameters
- the system permeability was independent of the type of geotextile
- the thickness of a geotextile filter layer had definitely not any influence on the filtration behaviour under test conditions described above
- the microscopic analyses indicated that the geotextile filter acts as a catalyst for the formation of an internal soil filter based on a bridging network
- the phenomenon of deep filtration was not observed
- no measurable migration of soil particles occurred after 48 h, stable hydraulic conditions were obtained in all permeameters
- even relatively openly designed geotextiles performed successfully
- no failure of the geotextile filter by clogging was found during the performance tests

6 REFERENCES

Davidenkoff, R. (1976) "Anwendung von Filtern im Wasserbau", W. Ernst & Sohn, Berlin, Germany.

draftDIN 60500-4 (1997) "Prüfung von Geotextilien.- Bestimmen des Wasserdurchlässigkeitsbeiwertes $k_{v,konst.}$ senkrecht zur Geotextilebene unter Auflast bei konstantem hydraulischen Höhenunterschied"

draftDIN 60500-6 (1994) "Bestimmung der Öffnungsweite D_w (O_{90})"

FGSV Forschungsgesellschaft für Straßen- und Verkehrswesen (1994) "Merkblatt für die Anwendung von Geotextilien und Geogittern im Erdbau des Straßenbaus", FGSV, Cologne, Germany, 72 p.

Gartung, E., Kossendey, Th. & Murray, H. R.(1994) "Long-term filter function of nonwovens: large scale performance tests", *5. Int. Conf. on Geotextiles*, Singapore, Vol 2, pp. 729-732

Heerten, G. (1993) "A contribution to the improvement of dimensioning analogies for grain filters and geotextile filters", Geofilters'92, Balkema, Karlruhe, Germany, pp. 121-128.

Kisskalt, J. (1992) "Kunststoffe in der Geotechnik - Deponiebau mit Geokunststoffen-", *Veröffentlichungen des Grundbauinstitutes der Landesgewerbeanstalt Bayern*, Vol. 68, LGA, Nuremberg, Germany, 405 p.

Kossendey, Th., Gartung, E. & Lawson, C.R. (1996a) "Long-term performance tests for verification of current geotextile filter criteria", *Geofilters'96*, Bitech Publishers Ltd., Montreal, Canada, pp. 275-284

Kossendey, Th. & Karam, G. (1996b) "A Critical Review of the Current Filter Criteria on the Basis of Long-Term Performance Tests" , *EuroGeo 1*, Balkema, Maastricht, The Netherlands, pp. 961 - 968

Luettich, S. M., Giroud, J. P. & Bacchus, R. C. (1992) "Geotextile filter design guide", *Geotextiles and Geomembranes*, Vol. 11, Special issue 1992: 355-370. Barking: Elsevier Science Publisher

Mlynarek, J., Bonnell, R. B., Broughton, R. S. & Rollin, A. L. (1994) "Long-term effectiveness of subsurface agricultural drainage systems", *5. Int. Conf. on Geotextiles*, Singapore, Vol 2, pp. 725-728

Rollin, A. L., Mlynarek, J., Hoekstra, S. E. & Berkhout, H. C. (1994) "Geotextile thickness: A relevant filter design criterion", *5. Int. Conf. on Geotextiles*, Singapore, Vol 2, pp. 795-698

The Performance of a Geotextile Filter in Tropical Soil

M.G. Gardoni
Civil Engineer, University of Brasilia, Brasília, Brazil

E.M. Palmeira
Associate Professor, University of Brasília, Brasília, Brazil

ABSTRACT: Problems with granular filters in residual soils from quartzite is well known by the Federal District Highway Department, Brasilia, Brazil. These soils are structurally formed by clusters of fine particles. However, geotextile filters have been used successfully under these conditions. This paper investigates a geotextile drain in residual soil from quartzite that have been performing well for the last 10 years. Soil and geotextile samples were collected from the drain and tested in the laboratory. Chemical and microscopic analyses were performed on the residual soil and on samples of the geotextile. Current filter criteria were also used and the results obtained suggest that the accuracy of a criterion prediction may be a function of the procedure used to obtain grain size distribution of the soil and on cluster resistance to high gradients. In general the drain is in good operational conditions.

KEYWORDS: nonwoven geotextile, filter, residual soil, geotextile permeability, filter criteria.

1. INTRODUCTION

Geotextile draining systems have consistently performed well in highways around Brasilia, Federal District, Brazil. In several similar situations granular filters have clogged when in contact with residuals soils from quatzite, which is very common in the region. Besides, local government environmental agencies have been very strict on the exploitation and use of natural materials such as sand and gravels. This causes these materials having to be transported from distant places for drain construction, which increases significantly the cost of granular drains in comparison to synthetic drains. Because of these reasons geotextile drains have become increasingly competitive in comparison to natural drains and the Federal District Highway Department has increased the acceptance of geotextile drainage systems in the region.

This paper presents a study of a 10 years old geotextile drain built in the BR-020 highway, close to Brasilia, in a region of residual soils from quartzite. The study involved the inspecion of the geotextile in situ, collection of geotextile, soil and water samples for laboratory tests.

2. CHARACTERISTCS OF THE DRAIN, MATERIALS AND EQUIPMENTS USED

2.1 Drain characteristcs

The drain in the BR-020 highway was constructed in a region of residual soil and weathered rock from quartzite, with the presence of meta-siltstone and meta-claystone. The drain is 400 m long at each side of the road and was constructed in a 0.6 m wide and 1.5 m deep trench. Figure 1 shows schematically the drain geometrical characteristcs.

2.2 Soil, water and geotextile characteristics

A trench was excavated alongside the drain to collect soil and geotextile samples for testing. Undisturbed soil samples as well as geotextile samples on the side and on the top of the drain were collected. Visual inspection showed that the geotextile layer was in good state not being observed any damage that might have been inflicted to the geotextile during construction. The drain, as a whole, was in very good operational conditions. At this stage it was also very clear the greater contamination of gravel material not protected by the geotextile. Water samples were also collected for analyses.

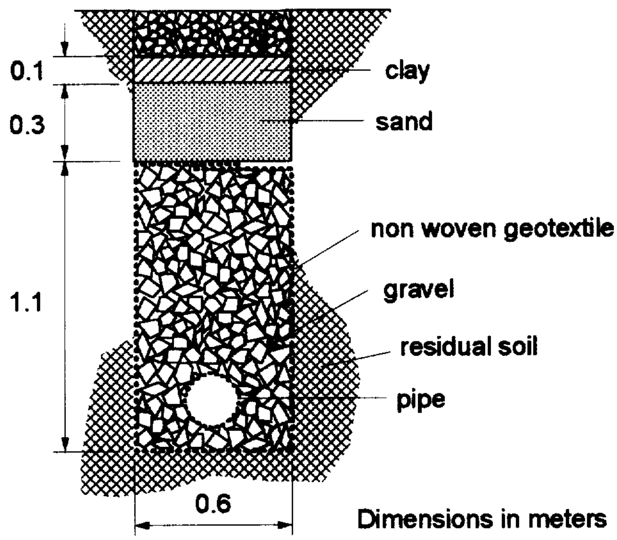

Figure 1. Drain characteristics.

Standard laboratory tests were performed on the residual soil samples for the determination of grain size distribution, void ratio, moisture content, etc. Table 1 summarizes the main characteristcs of the soil. The soil is a fine sand (83% of sand particles) and its grain size distribution is shown in Figure 2. Two curves for the grain size distribution of the residual soil are presented in this figure. One is the curve obtained with the sedimentation test using deflocculant (standard procedure) and the other is the result with the sedimentation test without the use of deflocculant. The reason for the latter type of sedimentation test is due to the fact that soils in this region are commonly structurally composed of clusters of soil particles, forming strong larger grains, which may be loosened by the action of the deflocculating agent used in the tests but not necessarily by water flow in a drain or in filtration tests. Therefore, for the use of filtration criteria, the grain size curve obtained without the use of deflocculant may be the appropriate one under these circumstances. Figure 2 shows a marked difference between results of sedimentation tests with and without the use of deflocculant.

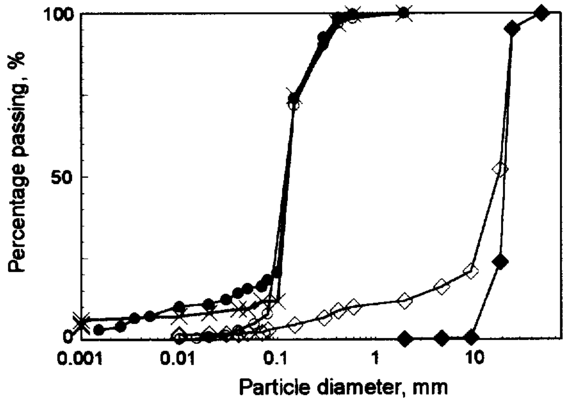

Figure 2. Grain size distributions of the soils.

Table 1. Soil properties.

Natural moisture content, %	11.4
Specific gravity (in situ), kN/m^3	22.6
Void ratio	0.33
Density of the soil particles	2.71
Permeability coefficient, cm/s	80 x 10^{-4}

It is important to note that depending on the grain size distribution choosen for filter design the values of grain diameters obtained can be significantly different. The same applies to the value of the coefficient of non-uniformity of the soil (CU) which may be 1.4 or 19, depending on the curve used. The latter value suggests that if the pack of grains is destroyed by the action of the water the soil can be highly sensitive to suffusion .

Chemical and mineralogical tests were also performed in the residual soil such as methylene blue and X-rays diffractometry. These tests yielded to results of coefficient of activity for the fine fraction of the soil equal to 6.88 g/g, specific surface of 7.35 m^2/g and cations exchange capacity of 0.8 meq/100. Results of the chemical analysis are presented in Table 2. The soil can be then classified as a low activity lateritic soil. This was confirmed by the presence of kaolinite as the predominant clay mineral in the soil fine fraction in X-rays diffractometry tests.

Table 2. Chemical composition of the soil.

Substance	Percentage (%)
SiO_2	89.10
Fe_2O_3	1.12
Al_2O_3	2.53
CaO	0.13
MgO	0.06

Tests with samples of the underground water in the region revealed a pH equal to 7.95 and low values of turbidity (0.7 NTU) and iron content (0.23 mg/l). These values are close to the values observed for distilled water.

A nonwoven needle punched geotextile, made of polyester, comercially available under the name Bidim OP20, was used to envelope the gravel material (Fig. 1). Table 3 presents the main characteristics of the geotextile used.

Table 3. Geotextile characteristics.

FOS, mm	0.130
AOS, mm	0.12-0.21
t_{GT}, mm	2.2
k_n, cm/s	0.55

Notes: FOS - filtration opening size (AFNOR G 38017); AOS - apparent opening size (ASTM D4751-87); t_{GT} - geotextile thickness; k_n - geotextile permeability coefficient normal to its plane (ASTM D4491-89).

2.3 Experimentals

Filtration tests with undisturbed soil samples and the same type of geotextile used in the drain were performed in the laboratory as well as geotextile permeability tests with geotextile samples exhumed from the drain. A permeameter similar to the one presented by Calhoun (1972) was employed for the filtration tests, which is composed of a pvc cell that can accomodate 100 mm diameter soil samples. A total system gradient of 2 was adopted for the filtration tests. The equipment also allows the execution of gradient ratio tests. However, for the present case the definition of gradient ratio may be irrelevant due to the fact that undisturbed samples, rather than reconstituted samples, were tested. So, heterogeneities in the undisturbed soil mass can affect the value of the gradient ratio obtained. Nevertheless, the general procedure recommended by ASTM (1991) for gradient ratio tests (ASTM D 5101-90) was followed in the present case.

For the conformance of the cylindrical external face of the soil sample to the cylindrical internal surface of the permeameter cell the soil sample side was covered by a layer of paraffin which was then trimmed appropriately to achieve a satisfactory match between soil and cell diameters. The internal wall of the permeameter cell was greased to avoid any preferential flow along the soil-cell interface. Filtration tests with durations as long as 2500 hours (≅ 3.5 months) were performed.

Distilled water was used in the laboratory tests and its composition after having crossed the soil sample was monitored during the test to assess variations in pH, turbidity, total iron and electrical conductivity.

To assess the loss of permeability of the geotextile in the drain after 10 years of operation the carefully exhumed geotextile samples were subjected to permeability tests in the laboratory. The equipment in this case is similar to the one presented in ASTM (1991) for the determination of the permeability of geotextiles normal to its plane (ASTM D 4491-89).

Investigations of the state of the exhumed samples of geotextile were also carried out using electronic microscopy. For this analysis samples of exhumed geotextile were firstly totaly impregnated by polyesterene resin under vacuum. Slices of these samples could then be cut for the analysis by an electronic microscope.

Additional information on materials, equipments and methodologies can be found in Gardoni (1995).

3. RESULTS OBTAINED

3.1 Filtration test

Figure 3 shows the result of a filtration test with an undisturbed residual soil sample and the same geotextile used in the drain. Approximately 2000 hours were necessary for the stabilization of water flow conditions.

At the end of the long term filtration test the soil mass close to the geotextile (one third of the original sample height) was tested for void ratio determination. It was observed that the void ratio increased from 0.33 to 0.53 in that region. This suggests that some level of suffusion occurred during the long term filtration test. This can be also inferred from the grain size distribution of the soil sample close to the geotextile after the filtration test, which is also presented in Figure 2 (grain size analysis with the use of deflocculant). This indicates that the mobility or dispersion of soil clusters may be dependent of the gradient used in the test.

Figure 2 also shows the grain size distributions of the gravel materials enveloped by the geotextile and on top of the drain (Fig. 1). It can be observed that the unprotected gravel was significantly contaminated by the fines from the residual soil while the gravel inside the drain was clean.

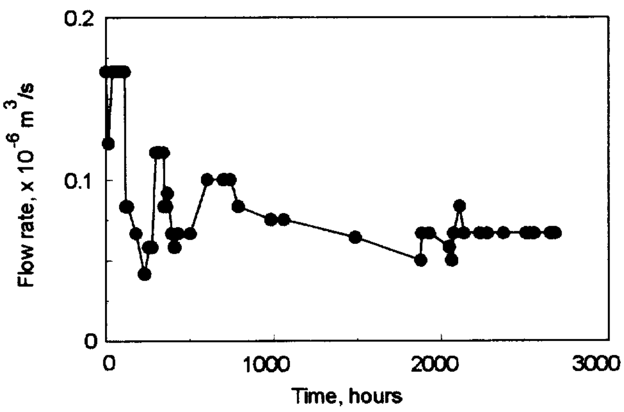

Figure 3. Flow rate versus time in a filtration test.

The analysis of the water that passed through the soil sample in comparison to the standard distilled water showed high values of turbidity and increases on iron content and pH, as shown in Table 4. These results suggest that there was iron precipitation under laboratory conditions.

Table 4. Water composition at the entrance and at the exit of the soil sample (end of the test).

Stage	ph	(1)	(2)	(3)	(4)
Entrance	6.8	0.028	0.38	3.10	1.8
Exit	7.1	2.22	82	10.6	7.4

Notes:
(1) - total iron (mg/l); (2) - turbidity (NTU); (3) electrical conductivity (μS/cm) and (4) - total dissolved solids (mg/l).

3.2 Geotextile permeability

The geotextile samples taken from the drain side and top as well as the sample used in the filtration test discussed above were tested to assess their loss of permeability under field and laboratory conditions. Firstly, for this comparison, a series of geotextile permeability tests were performed on virgin samples of the same geotextile in order to determine its average permeability coefficient and the scatter of test results. As the mass per unit area of thin geotextiles can vary markedly along the geotextile layer, several samples of varying mass per unit area were tested. The results of normal geotextile permeability of virgin samples versus geotextile mass per unit area are presented in Figure 4 where a rather constant average normal permeability with mass per unit area can be observed as well as a significant scatter of test results.

The results of permeability tests with geotextile samples from the drain and from the filtration test are also presented in Figure 4 and in Table 5. A reduction of geotextile permeability of 50 to 60% with respect to the average permeability of the virgin samples can be observed for the exhumed geotextile samples. The geotextile sample used in the filtration test retained only about 5% of its original normal permeability. These results suggest that much more severe conditions occurred in the laboratory filtration test than in the field (larger gradient, for instance). Nevertheless, the values of permeability coefficient or geotextile permittivity are still significantly high for practical purposes, as shown in Table 5.

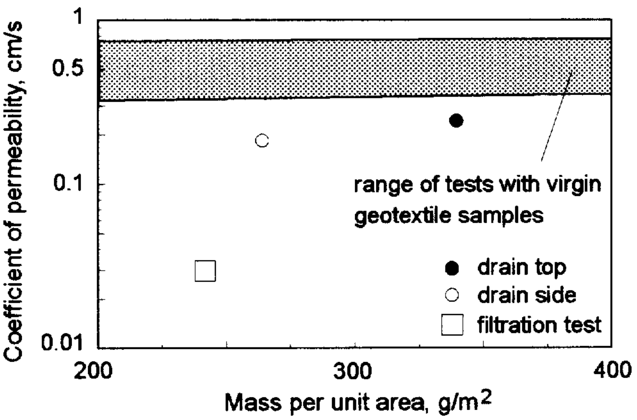

Figure 4. Geotextile permeability test results.

Table 5. Geotextile permeability tests results.

Geotextile specimen	t_{GT} (mm)	M_A (g/m^2)	k_n (cm/s)	ψ (s^{-1})
Drain top	1.6	340	0.24	1.50
Drain side	1.6	264	0.19	1.19
Filtration test	2.0	242	0.03	0.15

Notes: t_{GT} = geotextile thickness, M_A = geotextile mass per unit area, k_n = geotextile coefficient of permeability and ψ = geotextile permittivity.

3.3 Evaluation of filter criteria

As mentioned earlier in this work, for a proper application of filter criteria the grain size characteristics of the soil in contact with the geotextile have to be well determined. In the case of the residual soil investigated in the present work the value of relevant grain diameters depend on the use or not of deflocculant in the sedimentation test. Because the soil mass is mainly composed of coarse "grains" composed of clusters of particles that may or may not be dispersed by water flow or migrate through the soil mass, the designer has to decide which grain size distribution curve should be used for design purposes. The aim of this section is to evaluate the results obtained by some design criteria available in the literature for the drain under investigation. The following filter criteria were employed: French Committee on Geotextiles and Geomembranes (CFGG, 1986), Canadian Geotechnical Society (CGS, 1992), Carroll (1983), Christopher and Holtz (1985), Giroud (1982), IRIGM (Grenoble)/Ecole Politechnique de Montreal (Faure et al, 1986), Mlynarek et al (1990), Ontario Ministry of Transportation (OMT, 1992), University of British Columbia - UBC (Fannin et al, 1994), United States Federal Highway Administration (USFHWA, Christopher and Holtz, 1985) and United States Army Corp of Engineers (USACE, 1977). Table 6 summarises the results of filter criteria evaluation. It can be observed that most of the criteria would lead to the acceptance of the use of geotextile while only two would reject its use as filter for the residual soil. It is interesting to note that the criterion presented by Giroud (1982) would not be entirely applicable for the grain size distribution curve obtained in the sedimentation test with deflocculant because to some extent the soil could be considered as a gap graded soil by that criterion. Nevertheless, if the criterion was also applied in this case the geotextile would have failed to meet filter requirements. The geotextile may fail or not by the criterion presented in Mlynarek et al (1990) depending on the value of the apparent opening size used for the geotextile (maximum or minimum value in Table 3).

Table 6. Evaluation of filter criteria

Criterion	Grain Size Analysis	
	Without deflocculant	With deflocculant
CFGG (1986)	F	F
CGS	P	P
Carroll (1983)	P	P
Christopher & Holtz (1985)	P	P
Giroud (1982)	P	NA/F
Mlynarek et al (1990)	F/P	P
IRIGM/EPM	F	F
OMT (1992)	P	P
UBC	P	NA
USFHWA	P	P
USACE	P	P

Notes: F - geotextile failed; P - geotextile passed; NA - criterion is not applicable, F/P - failed or passed (see text for comments) and NA/F - Not applicable or failed (see text for comments).

From the results presented in Tables 1 and 5 it can be observed that the permeability coefficient of the exhumed geotextile samples is of the order of 25 times the soil permeability coefficient, which satisfies current permeability criteria such as the ones presented by Carroll (1983), Giroud (1982) and Christopher and Holtz (1985)

3.4 Microscopic investigations of exhumed geotextile samples

The exhumed geotextile samples were observed under optical and electronic microscopes and photographs of some of the specimens are presented in Figures 5 to 8. In general it could be observed that the geotextile was in good conditions with the sample taken from the side wall of the drain with a greater degree of clogging but still mantaining a large amount of its openings free from soil particles, as shown in Figure 5. This is reasonable since water flow is more (or only) significant along the sides of the drain. Figure 6 shows that the grains retained in the geotextile were formed by clusters of soil particles, as commented earlier in this work. Figure 7 shows a detail of one of these clusters. These results emphasyses the difficulty related to the choice of appropriate soil particle diameters to use in filter criteria for residual soils. Figure 8 shows that clay particles or clusters were also found bonded to individual geotextile fibers. Some level of damage of the geotextile fibers could be identified and may have been caused during drain construction or by the action of microorganisms. Figures 5 to 8 show that after 10 years of existence the geotextile layer is in good operational condition.

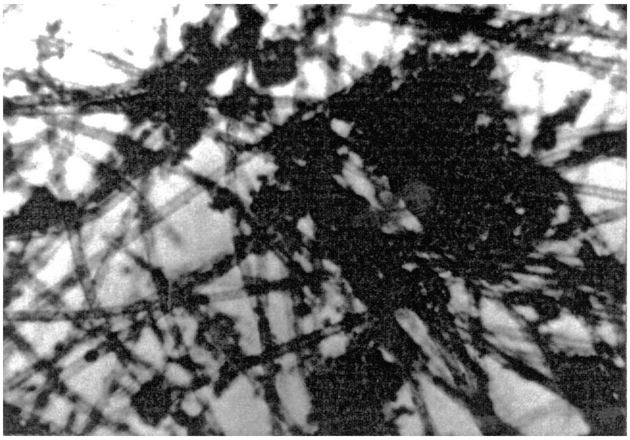

Figure 5. General view of the geotextile openings.

4. CONCLUSIONS

This work investigated the condition of a 10 years old geotextile drain in a residual sandy soil from quatzite. Clogging of granular drains in contact with this soil is common and nonwoven geotextiles have been successfully used as alternatives for granular drains. The main conclusions of the present work are summarised below:

. The geotextile was able to retain the fines from the residual soil and the enveloped gravel material in the drain was very clean in contrast to the contamined gravel material in regions where geotextile layers were not used.

. Geotextile permeability tests suggest a 70% loss of the original permeability under field conditions for the drain investigated. The permeability loss observed in a laboratory filtration test was significantly greater than in the field which was probably due to the soil-geotextile system in the laboratory having been subjected to more severe conditions than the ones found in the field. The destruction of soil clusters and the consequent intensity of suffusion is also likely to be dependent of the gradient of flow.

. The investigation of the condition of the geotextile pores after 10 years of operation showed that a large amount of free pores is still available.

. Geotextile filter design for soils formed by clusters of particles is a complex task. The results presented in this work shows that the acceptance or not of a geotextile filter by current criteria or the applicability of some criteria can be even dependent of the procedure adopted in the grain size analysis of the soil. Soil chemical and mineralogical analises are useful tools for the understanding of long term behaviour of geotextile drains in tropical soils. In spite of the encouraging results obtained in the present work, further research is required for a better understanding on the behaviour of geotextile filters in tropical soils.

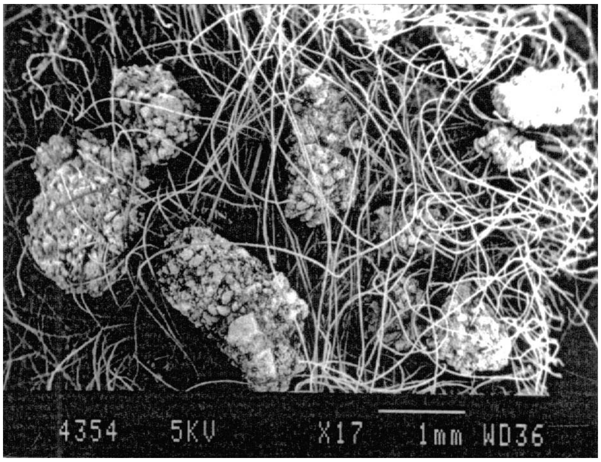

Figure 6. Clusters of particles retained in the geotextile.

ACKNOWLEDGEMENTS

The authors are indebted to the following institutions that helped to make this work possible: Federal District Highway Department, University of Brasília, CAPES - Brazilian Ministry of Education and Rhodia-Ster. Dr. Cristina Brandão and Prof. Elliot W. Kitajima, from the

University of Brasilia, gave important contributions to the chemical and microcopic analyses performed, respectively.

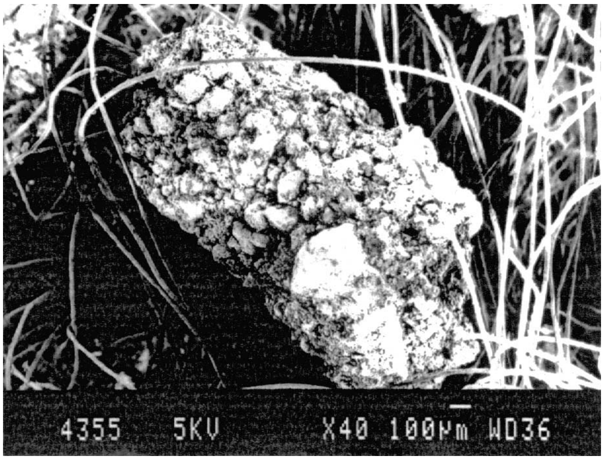

Figure 7. Detail of a cluster of particles.

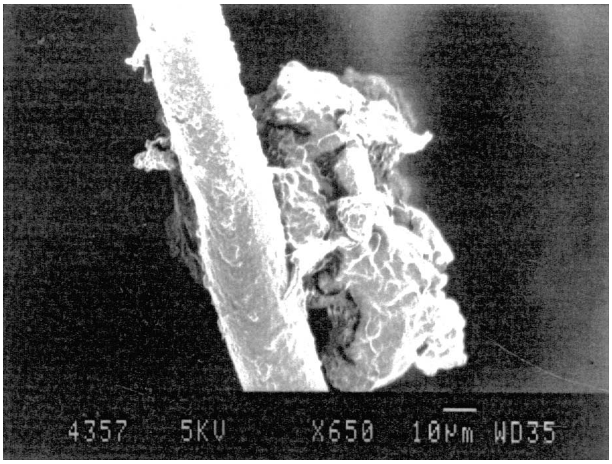

Figure 8. Fine particles bonded to a geotextile fiber.

REFERENCES

ASTM (1991) "*ASTM Standards on Geosynthetics*", 2nd Edition, Philadelphia, PA, USA, 104 p.

Calhoun, C.C. (1972) "Development of Design Criteria and Acceptance Specifications for Plastic Filter Cloths", *Technical Report S-72-7*, US Army Corps of Engineers, Waterways Experimental Station, Vicksburg, USA.

Carroll, R.G. (1983) "Geotextile Filter Criteria", *Transportation Research Record 916*, USA, pp. 46-53.

CFGG (1986) "*Geotextiles Manual*", Comité Français sur les Géotextiles et Geomembranes, Association Française de Normalisation, France, 64 p.

CGS (1992) "*Canadian Foundation Engineering Manual*", Canadian Geotechnical Society, 3rd Edition, Vancouver, BC, Canada.

Christopher, B.R. and Holtz, R.D. (1985) "*Geotextile Engineering Manual*", U.S. Federal Highway Administration, Report FHWA-TS-86/203, 1044p.

Faure, Y. Gourc, J.P., Brochier, P. and Rollin, A. (1986) "Soil-Geotextile Interaction in Filter Systems", *3rd International Conference on Geotextiles*, Vienna, Austria, Vol. 2, pp. 671-676.

Gardoni, M.G. (1995) "Evaluation of the Applicability of Laboratory Tests and Filter Criteria for the Use of Geotextile Drains in the Federal District", *MSc Thesis*, University of Brasília, Brazil (in Portuguese), 177 p.

Giroud, J.P. (1982) "Filter Criteria for Geotextiles", *2nd International Conference on Geotextiles*, Las Vegas, USA, Vol. 1, pp. 103-108.

Fannin, R.J., Vaid, Y.P. and Shi, Y.C. (1994) "Filtration Behaviour of Nonwoven Geotextiles", *Canadian Geotechnical Journal*, 31, pp. 555-563.

Mlynarek, J., Lafleur, J. and Lewnadowski, J.B. (1990). "Field Study on Long Term Geotextile Filter Performance", *4th International Conference on Geotextiles, Geomembranes and Related Products*, The Hague, The Netherlands, Vol.1, pp. 259-262.

OMT (1992) "Material Specification for Geotextiles", *Ontario Provincial Standard Specification 1860*, Ontario Ministry of Transportation, Canada.

USACE (1977) "Civil Works Construction Specification for Plastic Filter Fabric", United States Army Corps of Engineers, *Construction Guide Specification No. CW-00215*, Washington, DC, USA.

Effect of Cavities Between Soil and Geotextile Filter on Permeability

Prof. Dr. Erol Güler
Professor, Department of Civil Engineering, Boğazici University, Turkey

Emir Baran
Former M.Sc. Student, Turkey

ABSTRACT: During the placement of the geotextile filter, some free space can be left between the in-situ soil and the filter fabric. There is the possibility that the soil particles that separate from the soil matrix will accumulate on the surface of the filter geotextile and create an impermeable layer, which is called blinding. The aim of this study was to observe whether such blinding process really occurs. This was investigated by preparing samples with cavities of cylindrical shape. The diameters and the heights of the cavities varied. Two types of geotextiles, one of them needle-punched and the other spun-bonded, that are most commonly used as filters were used in the tests. Permeability tests conducted on the samples revealed that the presence of cavities did not cause any reduction in the permeability for the given clay and two geotextiles that have been used, compared to the permeability of the samples without cavities.

KEYWORDS: Blinding, Geotextile, Filtration, Permeability

1 INTRODUCTION

Geotextiles used for filtration and related applications should have similar functional criteria to those of aggregate filters. The fabric to soil system should permit free liquid flow across the plane of the fabric without clogging while preventing the escape of soil particles. There are several modes of failure that need to be considered in the design of a geotextile filter. The design for filtration, retention and long term clogging properties of geotextile filters has been studied by many researchers.(Giroud, 1982, Luettich et. al.,1994) Another possibility of failure is blinding. During the placement of the geotextile filter, some free space can be left between the in-situ soil and the filter fabric. There is the possibility that the soil particles that separate from the soil matrix will accumulate on the surface of the filter geotextile and create an impermeable layer. The aim of this study (Baran, 1996) was to observe whether such blinding process really occurs. This was investigated by preparing samples with cavities of cylindrical shape. The diameters and the heights of the cavities varied. Two types of geotextiles that are most commonly used as filters were used in the tests. One of the geotextiles was a needle-punched and the other a spun-bonded geotextile. Hydraulic conductivity tests were conducted on samples prepared with cavities.

2 METHODOLOGY

A mixture of kaolinite and bentonite clay was used in the tests. The percentages of kaolinite and bentonite were 75% and 25% respectively. Geotechnical properties of the clay mixture used in this study are given in Table 1.

In each sample, the geotextile filter was placed over gravel, and the soil sample with a cavity was placed over the geotextile. The gravel used was a uniform sized gravel passing No. 4 sieve.

Table 1. Geotechnical properties of clay

Properties	Values
Dry unit weight(kN/m^3)	15.2
Optimum water content(%)	23
Specific gravity	2.69
Activity	0.29
Smaller than 2 μm	47.1
Liquid limit(%)	85
Plastic limit(%)	25
Plasticity index(%)	60

Two types of geotextiles were used in all tests. The first one was nonwoven, needle-punched and the other one was nonwoven, spun bonded. The basic characteristics of the geotextiles used are listed in Table 2 and 3.

Table 2. Properties of spun-bonded geotextile

Properties	Test Method	Unit	Values
Unit weight	ASTM D3776	g/m^2	68
Thickness under 2 kPa pressure	ASTM D 1777	mm	0.36
Tensile strip test	BS/6906/1	kN/m	3.3
Permeability	EMPA/ITF	m/s	25E-04

The clay samples were prepared in an air-dried condition as a powder and mixed with each other properly before adding water to it. Then water was gradually added to the samples until the desired water content was reached. The samples prepared were allowed to sit for 24 hours to allow for the moisture to distribute evenly. All the samples were compacted at two percent dry of optimum. The compaction was conducted according to Standard Proctor compaction method as outlined in ASTM Standard D 698-78, Method A.

Table 3. Properties of needle-punched geotextile

Properties	Test Method	Unit	Values
Unit weight	ASTM D3776	g/m^2	95
Thickness under 2 kPa pressure	ASTM D 1777	mm	1.0
Tensile strip test	ASTM D 4595	kN/m	5.9
Permeability vertical under pressure 2 kN/m2	Franzius Inst. 10 cm water head	cm/s	0.5
Permeability vertical under pressure 200 kN/m2	Franzius Inst. 10 cm water head	cm/s	0.06

In preparation of samples which had cavities, special mold-bases as shown in Figure 1a, were laid down at the base of the compaction mold. Different mold bases with varying heights and diameters were used.

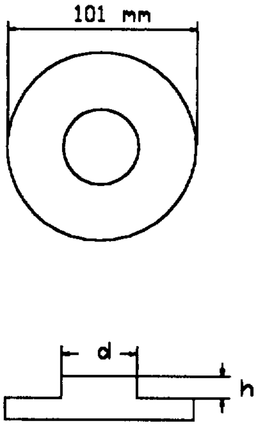

(a)

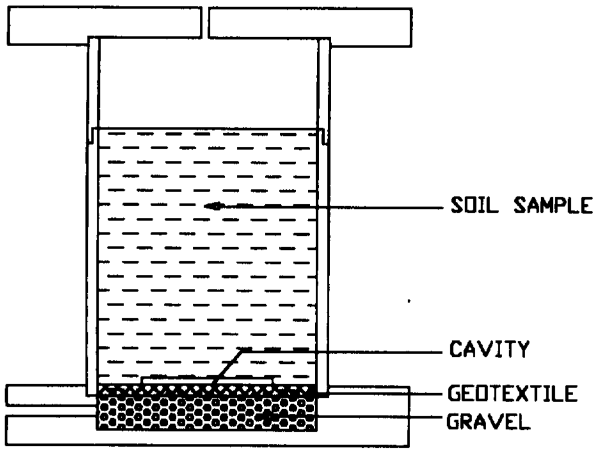

(b)

Figure 1. a)Special mold bases used to form cavities, b) Cross-section of a typical test sample

The chosen heights and diameters of the cavities were as follows: mold bases with height (h) of four mm and with height of six mm; For each height of cavity, there were three different diameters (d), twenty, forty and sixty mm.

After compaction, the mold bases under the samples were removed carefully leaving the cavities in the sample. The samples were placed over geotextile which was laid over a gravel layer because in a subsurface drainage installation, the downstream side of the geotextile is usually supported by gravel or rock. Cross section of a typical test sample is shown in Figure 1b.

Falling head permeability tests were conducted on the specimens in the molds in which they were compacted. Hydraulic head was on the average 135 cm. Measurements of the permeability tests were continued until permeability values reached an equilibrium condition.

3 TEST RESULTS

Permeability tests which were conducted on the samples which did not have a cavity, are given in Table 3.

Table 3. Result of permeability tests on samples without cavities

Sample type	Permeability (cm/s)
Soil only	5.14×10^{-8}
Soil with spun-bonded geotextile	5.58×10^{-8}
Soil with needle-punched geotextile	7.83×10^{-8}

The results of the tests with varying cavity geometry and type of geotextile used are given in Table 4 and Table 5.

Table 4. Result of permeability tests on samples with spun-bonded geotextile, Permeability(cm/s)

Diameter (mm)	20	40	60
Height (mm)			
4	6.80×10^{-8}	9.03×10^{-8}	8.55×10^{-8}
6	8.48×10^{-8}	1.07×10^{-7}	9.77×10^{-8} 1.06×10^{-7}

Table 5. Result of permeability tests on samples with needle punched geotextile, Permeability(cm/s)

Diameter (mm)	20	40	60
Height (mm)			
4	8.35×10^{-8}	9.74×10^{-8}	9.55×10^{-8}
6	$9.8.3 \times 10^{-8}$	1.10×10^{-7}	1.31×10^{-8} 1.38×10^{-7}

Permeability test results versus surface area of the cavities can be seen in Figure 2 for spun-bonded geotextiles and in Figure 3 for needle punched geotextiles. Surface area is described as the surface through which the water leaves the soil and enters the cavity. Therefore, the surface area is calculated as the sum of the circular section plus the peripheral area of the cylindrical cavity. For spun-bonded geotextiles, increasing the diameter, increased the permeability value slightly. Further increase in diameter of the cavity did not result in further increases, instead a slight decrease was observed. Increasing the height of the cavity resulted in higher permeabilities for all diameters. When needle punched geotextiles were used, increasing the diameter revealed similar results with those of spun-bonded geotexiles when cavity height was 0.4 cm. However, increasing the cavity diameter further caused an increase in permeability for the cavity height of 0.6 cm.

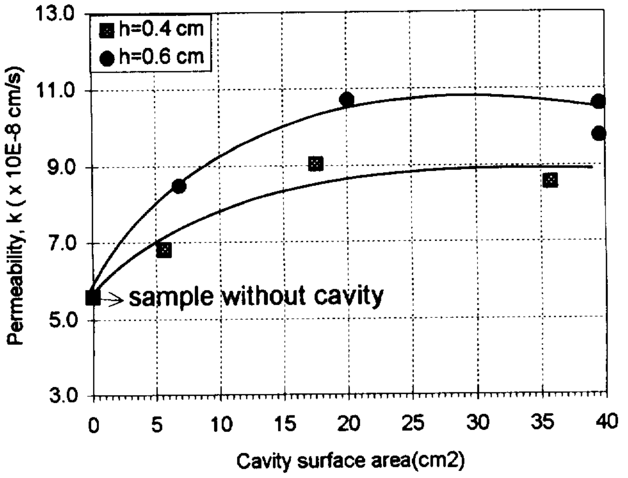

Figure 2. Permeability versus cavity surface area for spun bonded geotextiles

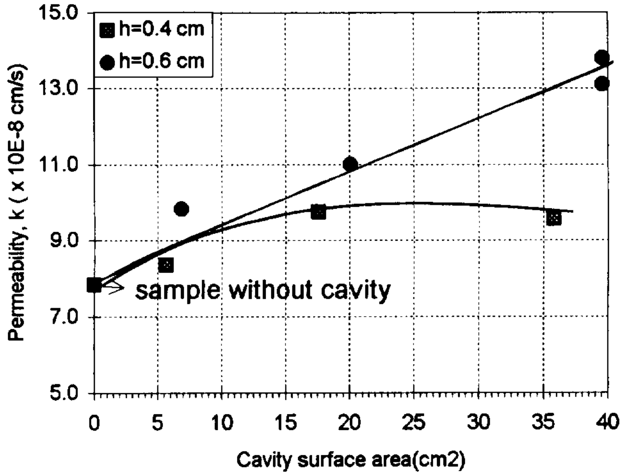

Figure 3. Permeability versus cavity surface area for needle punched geotextiles

Permeability results for both types of geotextiles were also plotted against the volume of the cavity. The permeability results versus volume of the cavities are shown in Figures 4 and 5 for spun-bonded and needle-punched geotextiles respectively. Similar conclusions can be drawn from these figures.

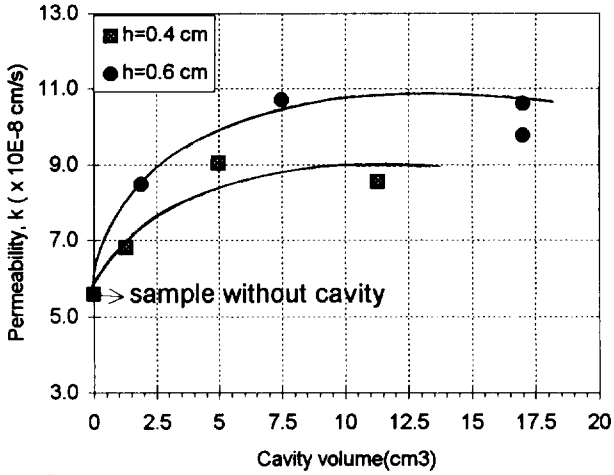

Figure 4. Permeability versus cavity volume for spun bonded geotextiles

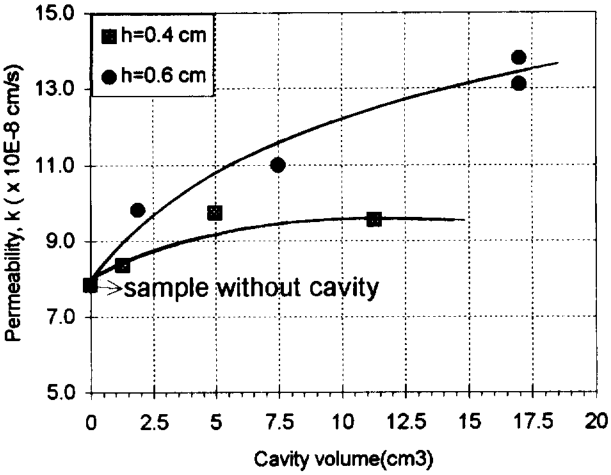

Figure 5. Permeability versus cavity volume for needle punched geotextiles

4 CONCLUSIONS

Permeability tests conducted on the samples revealed that the presence of cavities did not cause any reduction in the permeability for the given clay and the two types of geotextile that have been used compared to the permeability of the samples without cavities. A slight increase of the permeability was observed for smaller sized cavities. It was determined that the increase in the height of the cavity causes consistently an increase in the permeability. An initial increase in the permeability was measured with an increase in the diameter. For spun bonded geotextiles, increasing the size of the cavity causes an increase in the permeability for up to a maximum permeability level. Increasing the size of cavity beyond this point slightly decreases the maximum permeability value. For neddle punchedgeotextiles, the trend is similar for the cavity height of 0.4 cm. However, for a cavity height of 0.6 cm this reversal in behaviour is not observed and a further increase in permeability is measured with increasing cavity size. This indicates that the danger of blinding is even less for neddle punched geotextiles, for the given cavity sizes.

REFERENCES

ASTM (1989) *American Society for Testing Materials*, Annual Book for ASTM, Easton, March, 1989.

Baran, E.B. (1996) Effect of Cavities Between Soil and Geotextile on Permeability, *Master Thesis*, Boðaziçi University.

Giroud, J. P.(1982) "Separation Criteria for Geotextiles," *Proceeding of Second International Conference on Geotextiles*, Las Vegas, Vol.1, pp. 103-108

Luettich, S. M., J. P. Giroud, and R. C. Bachus (1994) *Geotextile Filter Design Guide*, Georgia,

Theoretical Basis for the Development of a Two-Layer Geotextile Filter

J.P. Giroud
Senior Principal, GeoSyntec Consultants, 621 N.W. 53rd Street, Suite 650, Boca Raton, Florida, USA

P. Delmas
Technical Director Polyfelt Group, Bidim Geosynthetics, 9 rue Marcel Paul, Bezons, France

O. Artières
Project Leader, Bidim Geosynthetics, 9 rue Marcel Paul, Bezons, France

ABSTRACT: This paper presents a description of the structure of nonwoven geotextiles, including the constriction size distribution curve and the opening size distribution curve, and a theoretical model that leads to a minimal required number of constrictions to ensure homogeneous opening size of the geotextile. Then, an analysis of the mechanism of filtration is presented, which quantifies the probability for a particle to be retained by (on or in) a nonwoven geotextile filter or to pass through the filter. This analysis shows that a needle-punched nonwoven geotextile filter having the minimal required number of constrictions is preferable to a thicker nonwoven geotextile filter. This leads to the concept of a two-layer geotextile filter where filtration is provided by a layer of needle-punched nonwoven material constructed with fine fibers and mechanical properties are provided by a layer of needle-punched nonwoven material constructed with coarse fibers.

KEYWORDS: Geotextiles, Nonwoven, Filtration, Opening size, Theory.

1 INTRODUCTION

Ever since geotextiles have been used as filters, filter thickness has been a subject of discussion. This paper sheds some light on the subject while providing a theoretical basis for the development of a two-layer geotextile filter. In Section 2, an analysis of the structure of nonwoven geotextiles shows that the opening size of nonwoven geotextile filters decreases with increasing thicknesses of geotextiles made from the same nonwoven material. In Section 3, an analysis of the mechanism of filtration shows that the probability for a particle to be retained by a geotextile filter depends on the thickness of the geotextile. It is concluded in Section 4 that a relatively thin needle-punched geotextile filter is desirable in many practical cases. However, a thin geotextile filter may not have the required mechanical properties to withstand mechanical damage and to resist deformations that could alter its opening size. To that end, a two-layer filter has been developed. This filter associates two layers of needle-punched nonwoven material: a layer constructed with fine fibers and having a thickness selected to provide optimal filtration characteristics; and a layer constructed with coarse fibers providing the required mechanical properties.

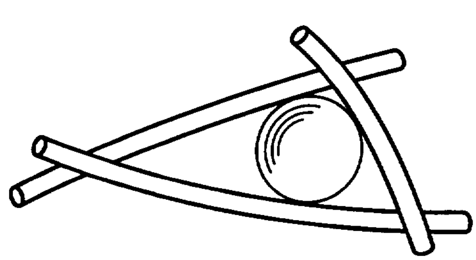

Figure 1. Constriction size.

2 STRUCTURE OF NONWOVEN FILTERS

2.1 Basic Definitions

2.1.1 Constrictions

To pass through a nonwoven geotextile filter, a particle must pass between fibers. A constriction is a passage delimitated by three or more fibers which are nearly, but not necessarily exactly, in the same plane. The size of a constriction can be defined as the diameter of the sphere which can just pass through the constriction (Figure 1). A constriction is different from a pore. Whereas a constriction is strictly defined, a pore is a loosely defined portion of the pore volume, i.e. the volume located between the fibers.

2.1.2 Constriction Size Distribution Curve

If a block of nonwoven material is considered (i.e. a three-dimensional sample, not a quasi two-dimensional sample such as a geotextile), and if this block is large enough to be representative, it contains a representative set of the constrictions which exist in the considered nonwoven material. This set of constrictions is represented by a constriction size distribution curve (Figure 2, Curve C).

The constriction size distribution curve is an intrinsic characteristic of the nonwoven material. Therefore, it is related to parameters that characterize the nonwoven material (e.g. the porosity, n, and the fiber diameter, d_f), but it is not related to parameters that depends on the geotextile, such as the geotextile thickness. Constriction sizes range from C_0, the size of the smallest constriction in the considered nonwoven material, to C_{100}, the size of the

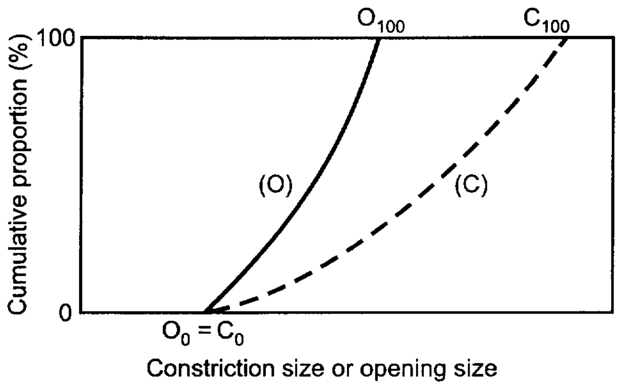

Figure 2. Constriction size distribution curve (C) and opening size distribution curve (O) for a nonwoven geotextile.

largest constriction in the considered nonwoven material; C_{100} is such that 100% of the constrictions in the considered nonwoven material are smaller than or equal to C_{100}.

One could argue that the size of the smallest constriction is $C_0 = 0$ because there is always the possibility that three fibers will meet at the same point, thus delimitating a passage with a zero size. However, from the viewpoint of filtration, constrictions with a size that is zero or very small should not be considered because a particle that meets such a constriction will not be stopped; instead, it will be diverted laterally. (The particles do not have to follow a straight path, and they naturally select the path of least resistance.)

2.1.3 Filtration Path

A soil particle that travels in a nonwoven geotextile filter follows a certain filtration path (Figure 3). A filtration path is tortuous, but its general direction is approximately perpendicular to the plane of the geotextile. As it travels along a filtration path, a particle passes through constrictions until it meets a constriction which is smaller

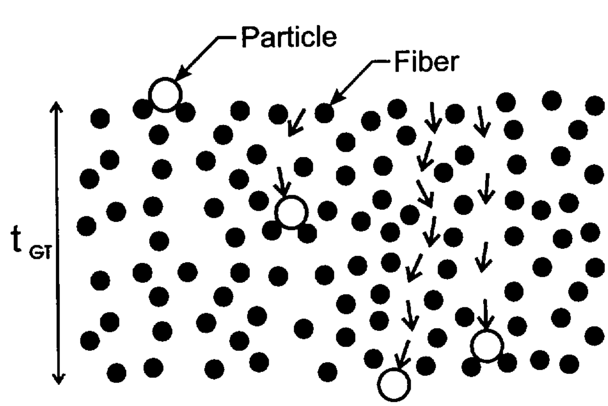

Figure 3. Filtration paths (t_{GT} = geotextile thickness).

than it is. Unless it diverts the particle, this constriction stops the particle. The level at which a particle is stopped depends on the filtration path (Figure 3): this is an important consideration in the analysis of the filtration mechanism. Of course, if the considered particle is not stopped by a constriction, it passes through the geotextile.

2.1.4 Opening Size

In each filtration path, there is a constriction that is smaller than the others. This constriction plays an essential role: it determines the size of the largest particle that can pass through the geotextile following the considered filtration path. This constriction is called the *controlling constriction* of the considered path, a terminology proposed by Kenney et al. (1985) for sand filters. In a given filtration path, the size of the controlling constriction is the *opening size* of the filtration path; therefore, the opening size of a filtration path is the size of the largest particle which can travel through the geotextile filter following this filtration path.

2.1.5 Opening Size Distribution Curve

In a nonwoven geotextile filter, there are many filtration paths, and these paths are all different. A given particle can be stopped in a certain filtration path, but it may pass through the filter if it follows another path. Each filtration path is characterized by its opening size. Therefore, a geotextile filter is characterized by an opening size distribution curve (Figure 2, Curve O). The size of the openings of a nonwoven geotextile (i.e. the sizes of the openings of the various filtration paths of the geotextile) range from O_0, the size of the smallest opening in the considered nonwoven geotextile, to O_{100}, the size of the largest opening in the considered nonwoven geotextile. It will be shown in Section 2.2.4 that O_0 is equal to C_0; O_{100} is such that 100% of the filtration paths in the considered geotextile have openings that are smaller than or equal to O_{100}. In other words, 100% of the openings of a geotextile are smaller than or equal to O_{100}. The opening size distribution curve is a characteristic of the geotextile and, in particular, the largest opening, O_{100}, is a characteristic of the geotextile, called the *opening size of the geotextile*. The opening size of a geotextile is the size of the largest particle that can pass through the geotextile provided it migrates individually through the geotextile and it is not attracted electrostatically or otherwise to the geotextile fibers.

2.2 Relationship Between Constrictions and Openings

2.2.1 Influence of the Thickness of a Nonwoven Filter

The constriction size distribution curve is an intrinsic characteristic of the material that constitutes a geotextile whereas the opening size distribution curve is a characteristic of the geotextile. The relationship between the constriction size distribution curve of the material that constitutes a geotextile and the opening size distribution curve of this geotextile depends on the thickness of the geotextile. To establish the relationship between these two types of curves, three nonwoven geotextiles with different thicknesses are considered. These three geotextiles are assumed to be made with the same nonwoven material (i.e. a material characterized by a given fiber diameter, a given porosity, and a given type of fiber arrangement).

Two extreme cases will be considered first, the case of a nonwoven geotextile with a zero thickness (Section 2.2.2) and the case of a nonwoven geotextile with an infinite thickness (Section 2.2.3); then the case of a nonwoven geotextile with a finite thickness will be considered (Section 2.2.4).

2.2.2 Infinitely Thin Nonwoven Geotextile

In a hypothetical infinitely thin nonwoven geotextile, each filtration path has only one constriction. Therefore, the opening size of each filtration path is equal to the size of the unique constriction of this filtration path. As a result, in the case of a hypothetical infinitely thin nonwoven geotextile, the opening size distribution curve is identical to the constriction size distribution curve (Figure 4, Curve 4).

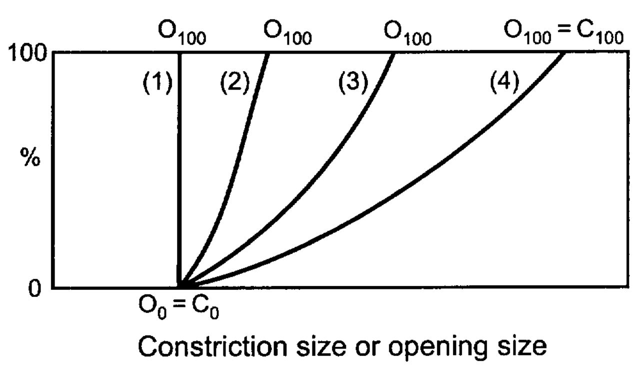

Figure 4. Opening size distribution curves for four geotextiles made from the same nonwoven material, but having different thicknesses: (1) infinitely thick, (2) thick, (3) thin, and (4) infinitely thin. (Curve 4 is also the constriction size distribution curve for the four geotextiles.)

2.2.3 Infinitely Thick Nonwoven Geotextile

In a hypothetical infinitely thick nonwoven geotextile, each filtration path contains an infinite number of constrictions. Therefore, in this case, there is a 100% probability that all constriction sizes are present in each filtration path. Thus, each filtration path contains the smallest constriction, C_0. When a filtration path contains the smallest constriction, this constriction is the controlling constriction. Therefore, in a hypothetical infinitely thick nonwoven geotextile, all filtration paths have the same controlling constriction, hence the same opening size ($O_0 = O_n = O_{100} = C_0$, where $0 < n < 100$). As a result, the opening size distribution curve of this geotextile is a vertical line (Figure 4, Curve 1). In other words, in a hypothetical infinitely thick nonwoven geotextile, all filtration paths have the same opening size, which is the opening size of the geotextile and which is equal to the smallest constriction size.

2.2.4 Nonwoven Geotextile Having a Finite Thickness

The case of a nonwoven geotextile having a finite thickness is considered. Elementary calculations show that, in typical nonwoven geotextiles, the number of filtration paths is greater than $1000/cm^2$. Therefore, if the considered specimen is large enough to be representative, it contains a very large (quasi infinite) number of filtration paths. The probability that at least one filtration path contains the smallest constriction is virtually 100%. When a filtration path contains the smallest constriction, C_0, this constriction is the controlling constriction, i.e. the opening size of the filtration path. A filtration path which has an opening size equal to the size of the smallest constriction is, of course, a filtration path that has the smallest opening size. Therefore, $O_0 = C_0$ (Figure 2).

In a given filtration path, the number of constrictions, in the case of a typical nonwoven geotextile, is not very large (for example, between 10 and 50, as indicated in Section 2.3.3). Therefore, the probability that the smallest constriction is present in all filtration paths is smaller than 100%. As a result, a certain number of filtration paths have a controlling constriction (i.e. an opening size) greater than C_0. Therefore, $O_n > C_0$.

The largest constriction size is C_{100}; therefore, the largest *possible* opening size is C_{100}. However, for a filtration path to have such an opening size, would require that all the constrictions of this filtration path be equal to C_{100}. But, in a given filtration path, the probability that all the constrictions are identical is virtually zero. Therefore, the maximal opening size that a filtration path may have (i.e. the opening size of the geotextile) is smaller than the maximal constriction size. Therefore, $O_{100} < C_{100}$.

The relationship, demonstrated above, between the constriction size distribution curve and the opening size distribution curve of a nonwoven geotextile having a finite thickness is illustrated in Figure 2. The opening size distribution curves of two nonwoven geotextiles with a finite thickness are shown in Figure 4: Curve 2 for a relatively thick geotextile and Curve 3 for a relatively thin geotextile. In Figure 4, it is important to note that Curve 4, which is the opening size distribution curve for the hypothetical infinitely thin nonwoven geotextile, is also the constriction size distribution curve for all four nonwoven geotextiles made with the same nonwoven material.

2.3 Theoretical Model of Nonwoven Geotextile Filters

2.3.1 Description of Chart

A theoretical model of the structure of nonwoven geotextiles (Giroud 1996) made it possible to develop a chart (Figure 5) that provides relationships between the following parameters: the geotextile opening size, O_{100}, the thickness of the geotextile, t_{GT}, the diameter of the fibers, d_f, and the porosity of the geotextile, n (solid curves for a given value of the porosity, and dashed curves for a given value of $\mu_{GT}/(\rho_f\ d_f)$ where μ_{GT} = geotextile mass per unit area, ρ_f = fiber density, and d_f = fiber diameter). This chart is in good agreement with the results of numerous tests performed on needle-punched (and some heat-bonded) nonwoven geotextile filters (Giroud 1996). The chart also gives an approximate value of the average number of constrictions, m, that a particle traveling through a nonwoven geotextile filter can be expected to pass through (dotted curves in Figure 5).

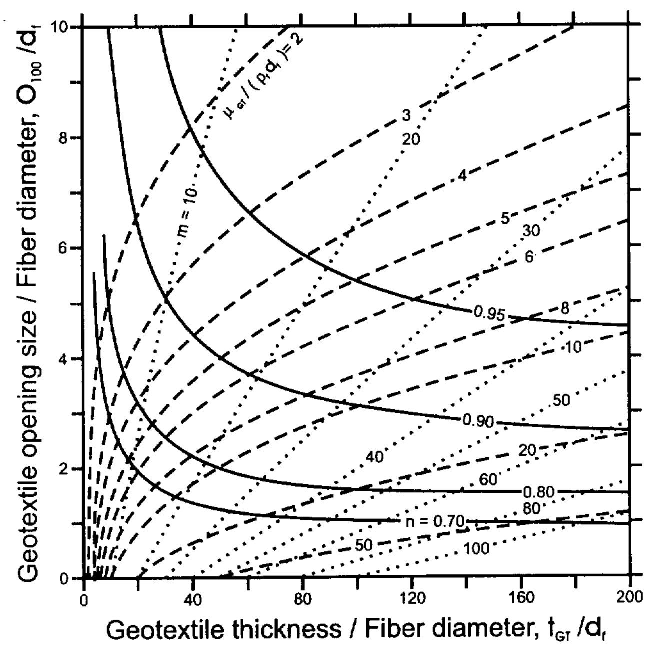

Figure 5. Chart giving three relationships between the geotextile opening size/fiber diameter ratio and the geotextile thickness/fiber diameter ratio for nonwoven geotextile filters.

2.3.2 Size of Constrictions

The chart in Figure 5 shows that, for a given nonwoven material characterized by its porosity, n, the opening sizes of geotextiles having different thicknesses made with this nonwoven material decrease for increasing thicknesses (solid curves) and tend to reach an asymptote as the geotextile thickness (and the geotextile mass per unit area) tend toward infinity. The horizontal asymptotes of the solid curves in Figure 5 correspond to the case of the hypothetical infinitely thick nonwoven geotextile used in the demonstrations presented in Section 2.2.3. Therefore, the geotextile opening size that corresponds to the horizontal asymptotes in Figure 5 is a theoretical value of the smallest opening size, O_0, and the smallest constriction size, C_0 ($O_0 = C_0$, as demonstrated in Section 2.2.4). On the other hand, the chart does not provide information on the size of the largest constrictions (C_{100}) because the theoretical model used to establish the chart presented in Figure 5 is not valid for extremely small values of the geotextile thickness/fiber diameter ratio (e.g. $t_{GT} / d_f < 10$); in other words, the chart presented in Figure 5 cannot represent the case of the hypothetical infinitely thin nonwoven geotextile discussed in Section 2.2.2.

2.3.3 Influence of the Number of Constrictions

In Section 2.2, the parameter used to compare geotextiles was the geotextile thickness. This was appropriate because the geotextiles considered had the same porosity and fiber diameter. In Sections 2.3.3 and 2.3.5, it will be seen that the appropriate parameter to compare nonwoven geotextiles having different porosities and/or fiber diameters is the number of constrictions.

The difference $O_{100} - O_0$ between the geotextile opening size, O_{100} (i.e. the size of the largest opening of the geotextile), and the value of the asymptote of the solid curves in Figure 5, O_0 (i.e. the size of the smallest opening of the geotextile), characterizes the homogeneity of the geotextile filter with respect to opening size: a small value of $O_{100} - O_0$ indicates an homogeneous geotextile, whereas a large value indicates an heterogeneous geotextile. The chart in Figure 5 shows that, for less than approximately 15 constrictions (m < 15), $O_{100} - O_0$ is large, whereas, when the number of constrictions is greater than approximately 25 to 30, $O_{100} - O_0$ is small and does not significantly decrease with increasing geotextile thicknesses. Therefore, it may be *qualitatively* said that: (i) to avoid using an heterogeneous geotextile filter, the number of constrictions should be greater than 15; and (ii) in cases where a very homogenous geotextile filter is required, the number of constrictions should be greater than approximately 25-30.

A very homogenous filter is required in cases, such as bank protection systems, where a large amount of particles must pass through the filter to ensure filtration while minimizing the risk of clogging. Indeed, in these cases, if the range of opening sizes of the filter is large, there is a high probability that the filter will stop some particles smaller than the geotextile opening size, O_{100}.

An attempt to *quantitatively* determine the required value of the number of constrictions consisted of performing the four following calculations (not shown here, but to be published elsewhere): (i) the derivative of $(O_{100} - O_0) / d_f$ with respect to t_{GT} / d_f ; (ii) the derivative of $(O_{100} - O_0) / d_f$ with respect to $\mu_{GT} / (\rho_f d_f)$; (iii) the ratio $(O_{100} - O_0) / d_f$; and (iv) the ratio $(O_{100} - O_0) / O_0$. These four calculations gave four relationships between the geotextile porosity and the minimal values required for the number of constrictions, m, to ensure that $O_{100} - O_0$ does not vary significantly as a function of the considered parameter, i.e. t_{GT} / d_f, $\mu_{GT} / (\rho_f d_f)$, d_f, or O_0. A parametric study, based on these four relationships, showed that the required minimal number of constrictions is of the order of 15 to 40 depending on the geotextile porosity and the considered parameter, with numbers of constrictions equal to or greater than approximately 25-30 being required to obtain a very homogeneous filter.

2.3.4 Influence of Geotextile Porosity

The chart presented in Figure 5 shows that the porosity of the nonwoven *material* has a large influence on the geotextile opening size. Nonwoven *materials* that have the same porosity and fiber arrangement are said to have the same structure. They are represented by a curve n = constant in Figure 5. Nonwoven *materials* that have the same structure differ only by the diameter of the fibers; and their constriction sizes are proportional to the fiber diameter. Thus, for nonwoven *geotextiles* made with nonwoven *materials* that have the same structure, the constriction size distribution curves: (i) are proportional to the fiber diameter; and (ii) consequently, in the traditional semi-logarithmic axes, are derived from one another by translations. Nonwoven *geotextiles* that have the same structure differ in general by their thickness; these geotextiles have the same constriction size distribution curve but different opening size distribution curves.

A parametric study, based on the theoretical model described in Section 2.3, showed that the geotextile porosity has a significant influence on the opening size values that can be achieved. The usually required opening sizes (e.g. 70 to 200 μm) can be provided economically (i.e. using relatively fine fibers and relatively small masses per unit area) by a nonwoven geotextile that has the minimal number of constrictions mentioned in Section 2.3.3 (i.e. 25-30) if the geotextile porosity is in the 0.85 to 0.95 range, which is typical for needle-punched nonwoven geotextiles, whereas nonwoven geotextiles with porosities smaller than 0.7 would require very coarse fibers and/or very large masses per unit area to have the usually required opening sizes while meeting the above minimal number of constrictions. The parametric study also showed that, with the typical porosities of needle-punched nonwoven geotextiles, it is possible to obtain geotextile opening sizes of the order of 80 μm by using fibers having a diameter of 25 μm, and of the order of 150 μm or more by using fibers having a greater diameter (e.g. 30 to 50 μm).

2.3.5 Importance of Constrictions

A parametric study, based on the theoretical model described in Section 2.3, showed that nonwoven geotextiles having the same number of constrictions and the same opening size (O_{100}) have approximately the same opening size distribution curve regardless of the values of the geotextile porosity and fiber diameter (provided, of course, that the appropriate relationship exists between porosity and fiber diameter to achieve the given O_{100}). This important finding shows that the number of constrictions is the most significant parameter for comparing geotextile filters. Also, when two nonwoven geotextiles have approximately the same opening size distribution curve, they have approximately the same constriction size distribution curve because approximately identical cumulative probability curves (i.e. the opening size distribution curves) must be based on approximately identical statistical sets (i.e. the constrictions).

3 ANALYSIS OF THE FILTRATION MECHANISM

3.1 Filtration Probabilities

Consider the two curves defined in Section 2.1, the constriction size distribution curve (which characterizes the material of which the geotextile is made) and the opening size distribution curve (which characterizes the geotextile). Both curves are cumulative probability curves. Thus, the constriction size distribution curve gives the probability, P_C, that a particle of size d will be retained at the surface of the geotextile and, correlatively, the probability, $1 - P_C$, that the particle will not be retained at the surface of the geotextile (Figure 6). The particles which are not retained at the surface of the geotextile either are retained in the geotextile or pass through the geotextile, and the opening size distribution curve gives the probabilities related to these two possibilities: the opening size distribution curve gives the probability, P_O, that a particle will be retained by (on or in) the geotextile and, correlatively, the probability $1 - P_O$ that a particle will not be retained, i.e. will pass through the geotextile (Figure 6). Thus, the following probabilities can be defined: probability that a particle will pass through the geotextile, $P_{PASS} = 1 - P_O$; probability that a particle will be retained in the geotextile, $P_{IN} = P_O - P_C$; probability that a particle will be retained on the geotextile, $P_{ON} = P_C$; and probability that a particle will be retained by (on or in) the geotextile, $P_{RETAIN} = P_O = P_{ON} + P_{IN}$.

Four situations can be considered depending on the size, d, of a particle relative to the extremities of the two curves (O_0, O_{100}, C_0 and C_{100}): (i) if $d > C_{100}$, the particle is retained at the surface of the geotextile because, in this case, there is no constriction larger than d ($P_{RETAIN} = P_{ON} = 1 = 100\%$, $P_{PASS} = 0$); (ii) if $O_{100} < d < C_{100}$, the particle cannot pass

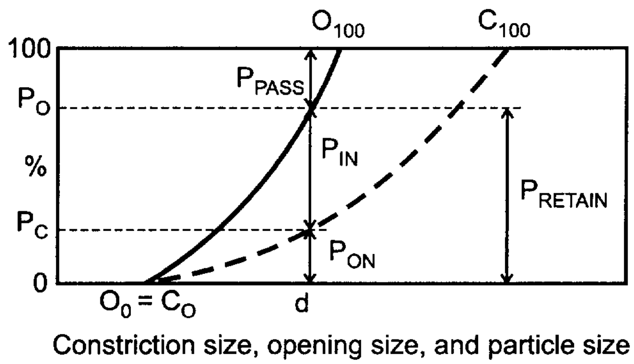

Figure 6. Probability that a particle will pass through a geotextile or will be retained in or on the geotextile.

through the geotextile because there is no filtration path with an opening size greater than d, and the particle either moves into the geotextile until it meets a constriction that stops or it remains at the surface of the geotextile if it happens that the constriction that stops it is at the geotextile surface ($P_{RETAIN} = P_{ON} + P_{IN} = 1 = 100\%$, $P_{PASS} = 0$); (iii) if $O_0 < d < O_{100}$, the particle has all of three possibilities, it can be retained in or on the geotextile or it can pass through the geotextile ($P_{ON} + P_{IN} + P_{PASS} = 1 = 100\%$); and (iv) if $d < O_0$, the particle passes through the geotextile ($P_{RETAIN} = 0$, $P_{PASS} = 1 = 100\%$).

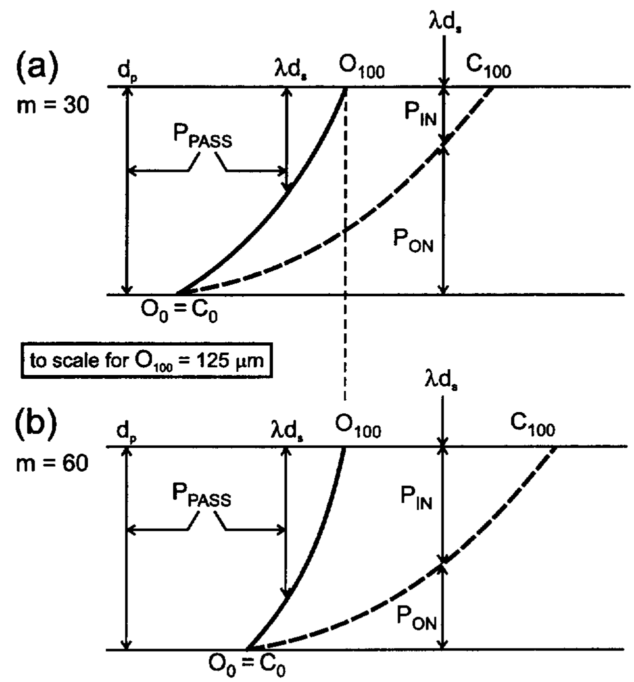

Figure 7. Probabilities of retention of two particles, one being a skeleton particle of size, d_s, the other being a fine particle of size, d_p, by two nonwoven geotextile filters having the same opening size, O_{100}, and having: (a) 30 constrictions ; (b) 60 constrictions.

3.2 Influence of Number of Constrictions on Filtration

In Section 2.3.3, it was shown that a minimal number of constrictions of 25-30 was required to ensure that the geotextile filter is very homogenous. The filtration analysis that follows shows that a greater number of constrictions may be more detrimental than beneficial.

The probabilities indicated in Section 3.1 and illustrated in Figure 6 can be used to compare the mode of particle retention by different geotextiles. Retention is a complex mechanism that includes the *retention* of skeleton particles and the *non-retention* of fine particles (Giroud 1996). Therefore, two particles will be considered: a skeleton particle of size d_s, which should be retained (Section 3.2), and a fine particle of size d_p, which should not be retained (Section 3.3). As indicated by Giroud (1996), skeleton particles are retained by a filter if the filter opening size is equal to or less than λd_s, where λ is a factor greater than one that accounts for particle bridging (hence a "factored size", λd_s, for the skeleton particles).

Two nonwoven geotextiles with the same opening size, O_{100}, are compared in Figure 7. This is a typical situation faced by a designer who has to make a choice between two apparently equivalent geotextile filters. These two geotextiles are assumed to have different opening size distribution curves and, consequently, they have different values of O_0 and $O_{100} - O_0$. Therefore, they have different numbers of constrictions, according to Section 2.3.3. The geotextile represented in Figure 7a has 30 constrictions, i.e. a number of constrictions sufficient to ensure that the geotextile filter is very homogeneous (see Section 2.3.3), whereas the geotextile represented in Figure 7b has 60 constrictions. These two geotextiles, having a different O_0, have different constriction size distribution curves. Combining the demonstrations presented in Sections 2.3.4 and 2.3.5 shows that the two constriction size distribution curves must be derived from one another by translation in the traditional semi-logarithmic axes. It is seen in Figure 7 that a particle of size d_s such that its factored size is greater than the geotextile opening size ($\lambda d_s > O_{100}$), as should be the case if the filter is properly designed, is: (i) more likely to be retained *on* the geotextile in the case of a nonwoven geotextile filter having 30 constrictions than in the case of a nonwoven geotextile filter having a greater number of constrictions; and (ii) correlatively more likely to be retained *in* the geotextile in the case of a nonwoven geotextile filter having 60 constrictions than in the case of a nonwoven geotextile filter having 30 constrictions. Skeleton particles move less and, therefore, the skeleton structure is less disturbed if more particles are retained *on* than *in* the geotextile filter (see Section 2.1.3 on the level at which a particle is stopped). Also, if, as a result of a design error or an unexpected variation of the soil characteristics, the skeleton particle factored size is smaller than the filter opening size ($\lambda d_s < O_{100}$), Figure 7 shows that less skeleton particles pass through the geotextile filter in the case of the filter having 30 constrictions than in the case of the filter having more constrictions.

From the above analysis, it appears that a nonwoven geotextile filter having 30 constrictions is preferable to a nonwoven geotextile filter having more constrictions because: (i) in the normal case where the soil skeleton particle factored sizes are greater than the geotextile opening size, the nonwoven geotextile filter having 30 constrictions retains soil skeleton particles with less disturbance of the skeleton structure than a nonwoven geotextile filter having more constrictions; and (ii) in the case where (as a result of a design error or an unexpected variation of the soil characteristics) the soil skeleton particle factored sizes are smaller than the geotextile opening size, the nonwoven geotextile filter having 30 constrictions is more likely to retain skeleton particles than a nonwoven geotextile filter having more constrictions.

3.3 Influence of Porosity and Fiber Diameter

As pointed out at the beginning of Section 3.2, it is important not only to retain the skeleton particles, but also *not to retain* the fine particles that must pass through the filter to prevent clogging. To that end, the smallest geotextile opening size, O_0, must be larger than a minimal value which can be determined as follows.

According to Mitchell (1970), grout particles flow easily through a soil being grouted if they are smaller than 1/25 times the d_{15} of the soil, i.e. smaller than 1/5 times the size of openings between the soil particles, since openings in granular materials are approximately equal to $d_{15}/5$ according to Kenney et al. (1985). This may be adapted to geotextile filters as follows. The soil particles most likely to cause filter clogging are the particles that may exhibit cohesion and may, therefore, adhere to fibers or to other particles. Particles that may exhibit cohesion are the particles smaller than approximately 5 µm. Therefore, O_0 should be greater than approximately 25 µm.

A parametric study based on the model presented in Section 2.3 showed that O_0 significantly depends on the geotextile porosity and fiber diameter and that, for usual values of needle-punched nonwoven geotextile porosity and fiber diameter, O_0 is always significantly greater than 25 µm. Therefore, the typical particles likely to cause clogging should pass easily through usual needle-punched nonwoven geotextile filters. Thus, it appears that the *non-retention* of fine particles is a criterion that is easily met by usual needle-punched nonwoven geotextile filters.

In conclusion, the comparison between two needle-punched nonwoven geotextile filters should be made essentially on the basis of the *retention* of the skeleton particles and not on the basis of the *non-retention* of fine particles. This approach is used in Section 3.4.

3.4 Retention of a Non-Uniform Soil

The method illustrated in Figure 7 can be extended to the case where the size of the skeleton particles ranges within two known limits (non-uniform soil). This case is illustrated in Figure 8, which shows that the various retention probabilities are proportional to areas delimitated by the constriction size distribution curve and the opening size distribution curve. Figure 8 leads to the same conclusions as Figure 7: (i) in the case where all of the skeleton particles are greater than the opening size of the filter ($d_s > O_{100}$), the skeleton particles are more likely to be retained *on* a nonwoven geotextile having 30 constrictions than *on* a nonwoven geotextile having more constrictions; and (ii) in the case where the range of skeleton particles includes sizes that are smaller than the opening size of the filter ($d_s < O_{100}$), the amount of skeleton particles likely to pass through a nonwoven geotextile filter having 30 constrictions is smaller than through a nonwoven geotextile filter having more constrictions. Essentially, Figure 8 shows that a nonwoven geotextile filter having 30 constrictions is more reliable than a nonwoven geotextile filter having more constrictions because it is less sensitive to variations of the soil particle size distribution curve.

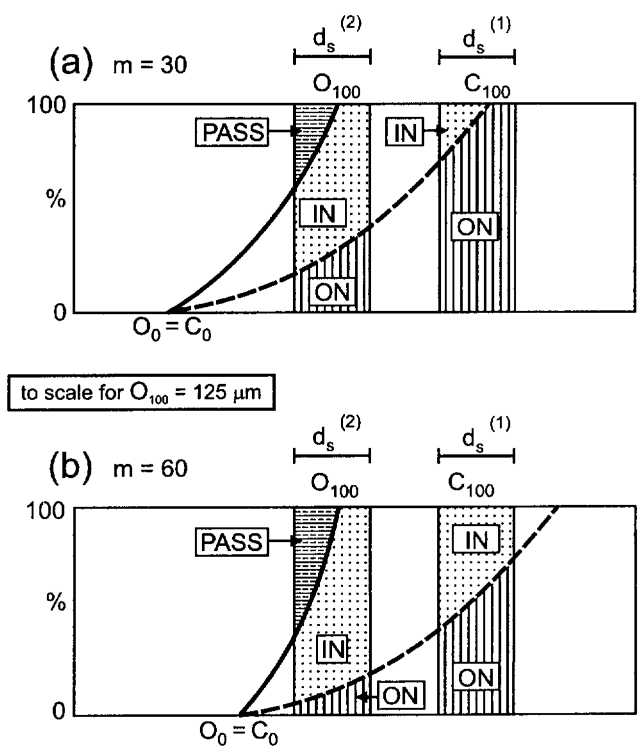

Figure 8. Probabilities of retention of skeleton particles by two nonwoven geotextiles having the same opening size, O_{100}, but having different numbers of constrictions : (a) m = 30; (b) m = 60. Two soils are considered: (1) all of the skeleton particles are larger than O_{100} ; (2) some of the skeleton particles are smaller than O_{100}.

4 TWO-LAYER GEOTEXTILE FILTER

4.1 Concept of Two-Layer Filter

Based on the analyses and discussions presented in Sections 2 and 3, a needle-punched nonwoven geotextile filter having approximately 25 to 30 constrictions is recommended for applications where a very homogenous filter is required. However, while such a geotextile can provide adequate filtration performance, it may not have the required mechanical properties to withstand mechanical damage and to resist deformations that could alter its opening size. Based on these considerations, a series of two-layer filters has been developed. These filters associate two layers of needle-punched nonwoven material: a functional layer constructed with fine fibers and having the required thickness to provide approximately 25 to 30 constrictions for optimal filtration characteristics; and a protective layer constructed with coarse fibers providing the required mechanical properties to protect the layer of fine fibers. For example, in one of the filters of the series, the fiber diameter is 25 μm for the fine fibers and 50 μm for the coarse fibers, each of the two layers having a mass per unit area of 200 g/m^2, hence a total mass per unit area of 400 g/m^2 for the two-layer nonwoven geotextile filter.

4.2 Opening Size of a Two-Layer Geotextile Filter

To minimize the risk of clogging, particles that pass through the layer of fine fibers should pass easily through the layer of coarse fibers. To that end, the opening size of the layer of coarse fibers must be significantly larger than the opening size of the layer of fine fibers. If this condition is met, only the layer of fine fibers must be considered when filter criteria are used, i.e. there is no need for special filter criteria for two-layer geotextile filters if there is a large difference of opening sizes between the two layers; the relationship between the opening sizes of the two layers depends on several parameters (such as porosity, thickness, and fiber diameter) and it is necessary to check on a case-by-case basis that the opening size of the layer of coarse fibers is much larger than the opening size of the layer of fine fibers. This can be done using the chart presented in Figure 5. For example, in the case of the two-layer geotextile filter described in Section 4.1, the following values are obtained: (i) for a fine fiber layer having a mass per unit area of 200 g/m^2, a fiber diameter of 25 μm and a porosity of 0.87: number of constrictions, 25; thickness, 1.7 mm; and opening size, 70 μm; and (ii) for a coarse fiber layer having a mass per unit area of 200 g/m^2, a fiber diameter of 50 μm and a porosity of 0.87: thickness, 1.7 mm; and opening size, 190 μm (the number of constrictions is irrelevant for the coarse fiber layer). It appears that, for the considered two-layer geotextile, there is a large difference between the opening sizes of the two layers.

5 CONCLUSION

This paper shows that the performance of nonwoven geotextile filters is significantly influenced by the porosity of the nonwoven material and the thickness of the geotextile. Both parameters govern the number of constrictions, i.e. the number of passages between fibers that a particle has to go through. An analysis of the structure of nonwoven geotextiles (Section 2) shows that a number of constrictions equal to or greater than approximately 25 to 30 should ensure homogeneity of the filtration characteristics. An analysis of the filtration mechanism (Section 3) shows that the probabilities for soil particles to be retained by, or to pass through, a geotextile filter can be derived from a comparison of the constriction size distribution curve of the geotextile material and the opening size distribution curve of the geotextile. The analysis shows that, in the practical situations reviewed, a better performance may be expected from a nonwoven geotextile filter with approximately 25-30 constrictions than from a nonwoven geotextile filter with more constrictions. These considerations led to the development of two-layer nonwoven geotextile filters. However, in addition to providing the theoretical basis for the development of two-layer filters, this paper shows that considerable information is now available regarding the structure of nonwoven geotextiles and the understanding of filtration mechanisms in geotextiles. In particular, this paper shows that, to analyse filtration mechanisms, it is necessary to use the entire opening size distribution curve, and not only the geotextile opening size, and that it is also necessary to use the constriction size distribution curve. This should open up the way to new filter design methods.

ACKNOWLEDGMENTS

The authors express their gratitude to K.L. Soderman for his comments, and to K. Holcomb and S.L. Berdy for their assistance in the preparation of this paper.

REFERENCES

Giroud, J.P., 1996, "Granular Filters and Geotextile Filters", *Proceedings of GeoFilters '96*, Lafleur, J. and Rollin, A.L., Editors, Montréal, Canada, May 1996, pp. 565-680.

Kenney, T.C., Chahal, R., Chiu, E., Ofoegbu, G.I., Omange, G.N. and Ume, C.A., 1985, "Controlling Constriction Sizes of Granular Filters", *Canadian Geotechnical Journal*, Vol. 22, No. 1, pp. 32-43.

Mitchell, J.K., 1970, "In-Place Treatment of Foundation Soils", *Journal of the Soil Mechanics and Foundation Division*, ASCE, Vol. 96, No. SM1, January 1970, pp. 73-110.

Aquatextiles: Use of Nonwoven Geotextiles for Filtration in a Municipal Water Treatment Plant

E. A. Richards
Professor, Department of Human Ecology, University of Alberta, Edmonton, Alberta, Canada T6G 2N1

J. D. Scott and D. W. Smith.
Professors, Department of Civil and Environmental Engineering, University of Alberta, Edmonton, Alberta, Canada T6G 2G7

ABSTRACT: Particle removal in municipal water treatment involves adsorption, sedimentation and filtration. The particles vary from materials in true solution to coarse suspensions and range in size from colloidal materials to coarse particles. This research explores the use of nonwoven geotextiles to enhance a pretreatment, screening procedure prior to rapid sand filtration. Laboratory and filed tests were conducted to determine long term filtration efficiencies for a polypropylene, needlefelt fabric at a municipal water treatment plant.

Removal efficiency of particles was determined by particle counting. Scanning electron microscopy was used to elucidate the filtration process. A variety of capture phenomena are involved for suspended particles less than 20 μm: entrapment, surface attraction and aggregation. This research shows that a nonwoven fabric with openings of 300 μm can successfully remove particles less than 10 μm. This innovative work represents new technology and is an opportunity for new markets for traditional needlefelt and new geotextiles. In this application these textiles would be better named aquatextiles.

KEYWORDS: Water Treatment, Filtration, Geotextiles, Aquatextiles, Nonwoven Fabrics, Environmental Engineering.

1 INTRODUCTION

Since their inception in the early 1970's geotextiles have become widely used in geotechnical applications. New markets for geosynthetics have concentrated on third generation: textiles designed for specific installations. Use of woven and nonwoven geotextiles has increased in what have now become traditional applications. This research project was designed to study new uses for conventional geotextiles in water treatment engineering rather than in geotechnical engineering. Innovative applications could open new markets for standard and new geotextile fabrics.

The objective of this research was to explore the possibility of using geotextile materials in filtration operations in municipal water treatment. Geotextiles have been used successfully in subsurface drainage applications since 1970 and it appeared possible to transfer that technology to the area of water treatment. Geotextiles appear to be promising filter media due to the variety of fibers and fabric constructions available commercially.

Liquid-particle separation in potable water treatment involves a wide range of techniques broadly divided into filtration and sedimentation. The main purposes of separation are to decrease waterborne disease through reduction in the number of harmful microorganisms and to increase aesthetics through reduction of suspended solids. Filtration in water treatment differs markedly from subsurface filtration/drainage applications in that the concentration of suspended particles is low and the volume of water flowing through a filter is very high.

The research project involved four components: development of a laboratory protocol for using textiles as a water filtration medium, testing a variety of geotextiles as possible media choices, development of a long term, field testing protocol and field testing at a municipal water treatment plant. The objective of this paper is to report the results of field testing where geotextiles were used for particulate removal at a municipal water treatment plant.

2 MATERIALS AND METHODS

2.1 Screening Studies

In the initial laboratory evaluation of potential fabrics a filtration device was designed which consisted of a simple filter apparatus with a constant pressure drop (Richards *et al.*, 1997). The particulate suspension used was the test dust for the American National Standard/NSF International Standard for Drinking Water Treatment Units at a concentration of 10 mg/L Eleven polypropylene geotextiles were tested in the laboratory and six fabrics were selected for additional laboratory testing at a water treatment plant. One fabric was chosen for further testing and the filtration device was modified to meet the demands of long term, field testing (Figure 1). The apparatus consisted of a peristaltic pump set to give a constant flow, the filtering device, a surge tank and a constant pressure drop tank. Change in pressure was measured with a float device in the surge tank, which was connected to a

Lakewood datalogger. The filtration device consisted of an enclosed glass funnel with exit ports for air bubbles. The fabric sample was placed at the center of the funnel, resting on a wire mesh.

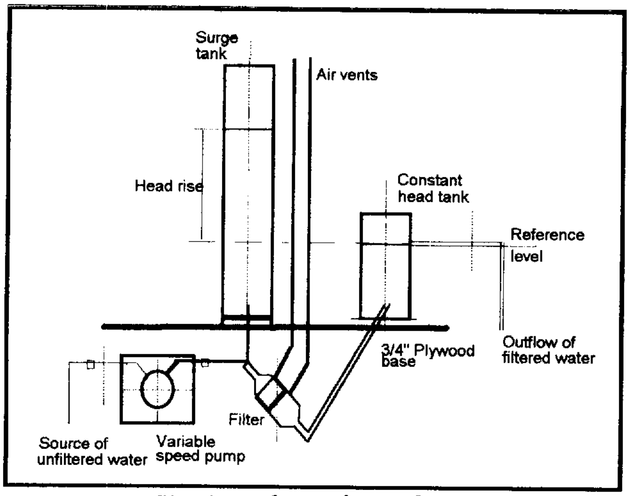

Figure 1. Profile view of experimental equipment for field testing in a municipal water treatment plant.

2.2 Fabric

The fabric selected for long term testing was a needlepunched, nonwoven, polypropylene fabric. The fabric mass and thickness as measured in the laboratory were 457 g/m^2 and 4.14 mm under a load of 2 kPa. The manufacturer's specification states a permittivity of 0.7 sec^{-1} at a flow rate of 34 L/(m^2 s) and an apparent opening size of 300 μm. This is a relatively thick, standard goetextile which is commonly used for underground drainage applications.

2.3 Experimental Procedure

The treatment steps at the Rossdale Water Treatment Plant located on the Saskatchewan River follow a standard procedure for municipal water purification (Figure 2). A coarse screening to remove large debris is followed by alum/polymer flocculation and coagulation to remove suspended particles. The water is softened with lime and the calcium carbonate precipitate over 20 μm in size settles through tube settlers in a still basin. There are additions of carbon dioxide to adjust the pH after softening, of chlorine for disinfection and of fluorine prior to final settling in the contactor basin. Filtration through a sand filter is the final treatment step prior to distribution to the city.

For this experimental program the influent was taken from the beginning of the contactor basin, after the addition of carbon dioxide, chlorine and fluorine. Of interest in this research were the particles in the water after softening, predominantly calcium carbonate, with sizes 20 μm or less, not including submicron sized particles. The influent was pumped from the still basin to the equipment, in excess of that needed for the testing, to keep the velocity of the influent constant at 10 m3/(m2/hr). Testing was conducted from October to December in 1996 at the Aqualta Rossdale Water Treatment Plant in Edmonton, Alberta, Canada.

2.4 Influent Characteristics

The influent remained relatively constant with respect to the distribution of particle sizes, from 1 μm up to and including 20 μm, but varied with respect to the number of particles from day to day and within a given experiment. During the testing period the total number of particles/mL varied from 2,090 to 20,370. The distribution of particles showed a peak at the five μm size, with the number of 15 and 20 μm particles remaining relatively constant. During each run of 6 to 11 hours there would be a change in influent over time with one or two peak periods. There was no consistency for the time during the day for the peaksand they did not relate to plant operations. Figures 3 illustrates the change in influent over time for Run 30.

2.5 Removal

Filter performance is measured by effluent water quality. Removal efficiency, expressed by percent removal for the number of particles of a given size, was determined by particle counting with an HIAC/ROYCO Model 8000A particle counter. Particles less than 20 μm were

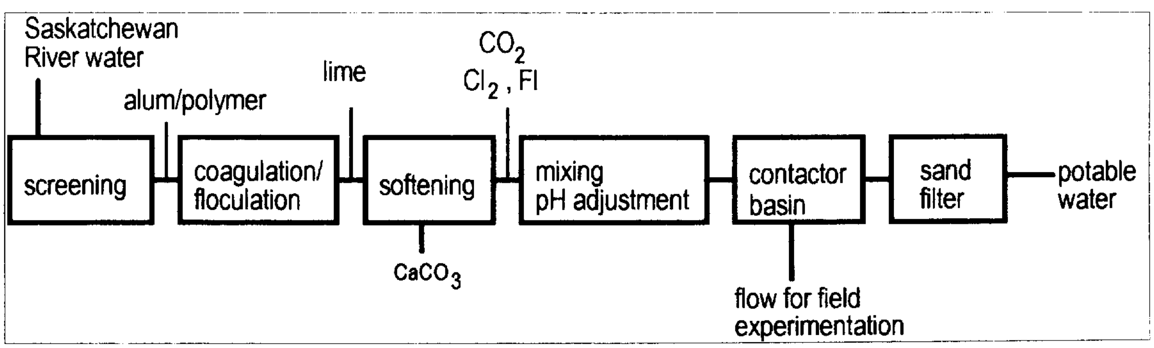

Figure 2. Steps in the municipal water treatment process at the Aqualta Rossdale Water Treatment Plant, Edmonton, Alberta,

counted. Four and five μm particle removals were of particular interest as the *Cryptosporidium parvum* cyst which causes Cryptosporidiosis (diarrhea) is about 4 μm in diameter.

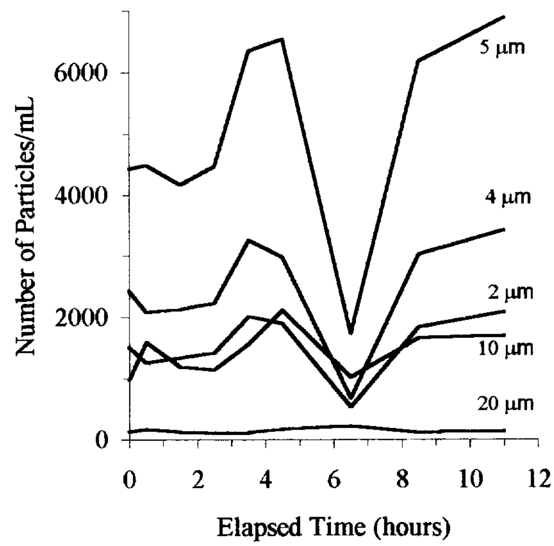

Figure 3. Change in influent particle size over time, Run 30, December 12, 1996.

3 FIELD TEST RESULTS

3.1 Removal

Removal of particles varied with time. For each experimental run there was an initial period of adjustment, followed by an increase in removal to a peak of removal efficiency, and then declining removal. The time of peak removal for different runs varied between 0.5 to 3.5 hours (Figure 4).

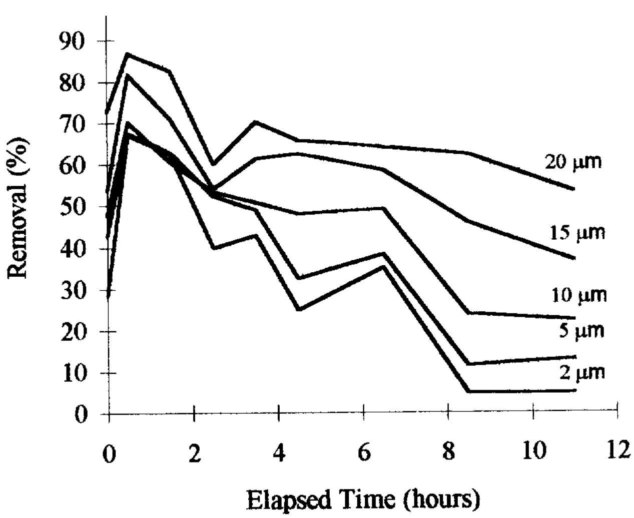

Figure 4. Removal efficiency over time showing the periods of initial adjustment, peak removal and declining removal for one layer of fabric, Run 30.

Examination of removal curves for all runs shows a similar pattern. The removal pattern is not smooth but shows a zigzag shape, especially after 4.5 hours. It appears that when the particulate loading on the filter reaches a critical level, particles detach from the fibers. The fabric is then able to capture particles more efficiently with a subsequent increase in removal efficiency. When the fabric is again unable to hold more particles the particles are detached. However, gradually the removal efficiency of the filter decreases with time. Varying the thickness of the filter layer by using additional layers of fabric increased the removal efficiency slightly.

3.2 Headloss

There was an increase in headloss with time as shown in Figure 5. As the number of layers of fabric increased, the headloss increased. An examination of the patterns of increased head required to maintain a constant flow velocity showed variations between runs as well as with the number of layers of fabric. An examination of headloss increase with the cumulative number of particles captured showed a consistent pattern. The cumulative number of 2 to 5 μm sized particles increased and then levelled off. The cumulative number of particles over 10 μm continued to increase with time. When this data is compared to the patterns of headloss it is the larger particles, the 10 to 20 μm particles, which determine headloss.

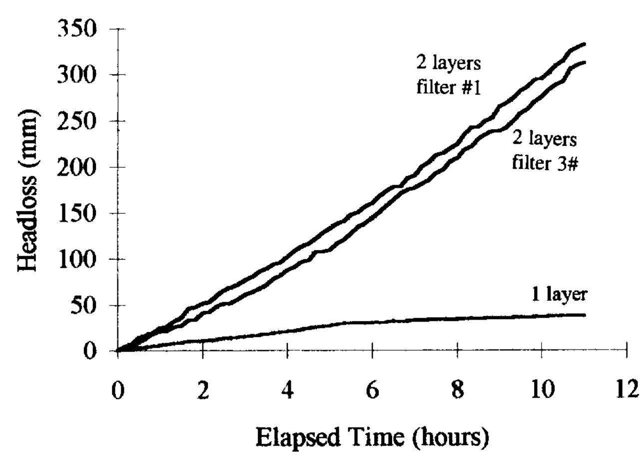

Figure 5: Pattern of headloss with one and two layers of fabric for concurrent tests, Run 30.

3.3 Scanning Electron Microscope

An Hitachi 2-2500 scanning electron microscope was used to examine fabric specimens after filtration. Examination of the photomicrographs showed an increasing number of particles captured with time (Figure 6). At the end of a filtration run the fabrics were loaded with calcium carbonate particles which were attached to the surface of the fibers. Cracks or roughness on the surface of the fibers also served as anchoring points for the calcium carbonate. As time increased an aggregation of small particles was observed.

4 DISCUSSION

While particle counting is a useful technique for measuring filtration efficiency it is the SEM analysis which elucidates the capture phenomena. SEM analysis shows a variety of removal phenomena of the suspended particles. It is postulated that the transport mechanisms of interception, inertia and sedimentation occur. The attachment mechanisms involve surface attraction between the calcium carbonate and the polypropylene fibers. In addition there appears to be entrapment of the calcium carbonate between adjacent fibers and aggregation of the particles on the fibers and between adjacent fibers. Detachment mechanisms were thought to be the result of particle shearing and scour due to an increase in interstitial fluid velocity.

The retention of particles less than 10 μm by nonwoven fabrics suggests that these fabrics could be used to enhance traditional water treatment practices when the influent contains suspended particles. While ideally a filter medium would remove all 4 and 5 μm sized particles to ensure removal of the *Cryptosporidium parvum* cysts, removal of 40% of this sized particles puts a decreased load on the sand filter. By placing a needlefelt fabric upstream of a sand filter the filtration run of the sand filter can be extended, thus increasing run length and efficiency.

5 CONCLUSIONS

1. Nonwoven geotextiles show sufficient removal performance, for limited time periods, to be of interest as a potential medium for removal of 2 to 10 micron particles in water treatment applications. It is suggested that these textiles be termed aquatextiles, rather than geotextiles.
2. The removal over time of 2 to 10 micron particles is a function of the particle size. There appears to be a limit to the amount of particles that a nonwoven fabric can hold that is specific to each particle size. Near this limit the retention of particles becomes some what unstable.
3. A polypropylene fabric with an apparent opening size of 300 microns effectively captured 2 to 20 micron particles. The influence of fabric structure and fiber composition on removal will be a promising area of filtration research.
4. Increasing the thickness of the fabric layer through using two layers of fabric increased particulate removal.
5. The use of nonwoven textiles in water treatment filtration applications will offer new markets for traditional geotextile fabrics as will as an opportunity to develop new fabrics with better capture properties.

ACKNOWLEDGEMENTS

The authors wish to thank: Mr. Riyaz Shariff and the operators at the Aqualta Rossdale Water Treatment Plant, Edmonton, Alberta; Dr. Ming Chen, University of Alberta, for his supervision of the electron microscope work; and Mr. J. Dobroseilski of AMOCO Fabrics and Fibers Company for supplying the experimental fabrics.

REFERENCES

Richards, E. A., Smith, D. W. and. Scott, J. D. (1997) Use of textile materials to enhance water treatment operations. 1997 CSCE/ASCE Environmental Engineering Conference, Edmonton, Alberta, 1695-1706.

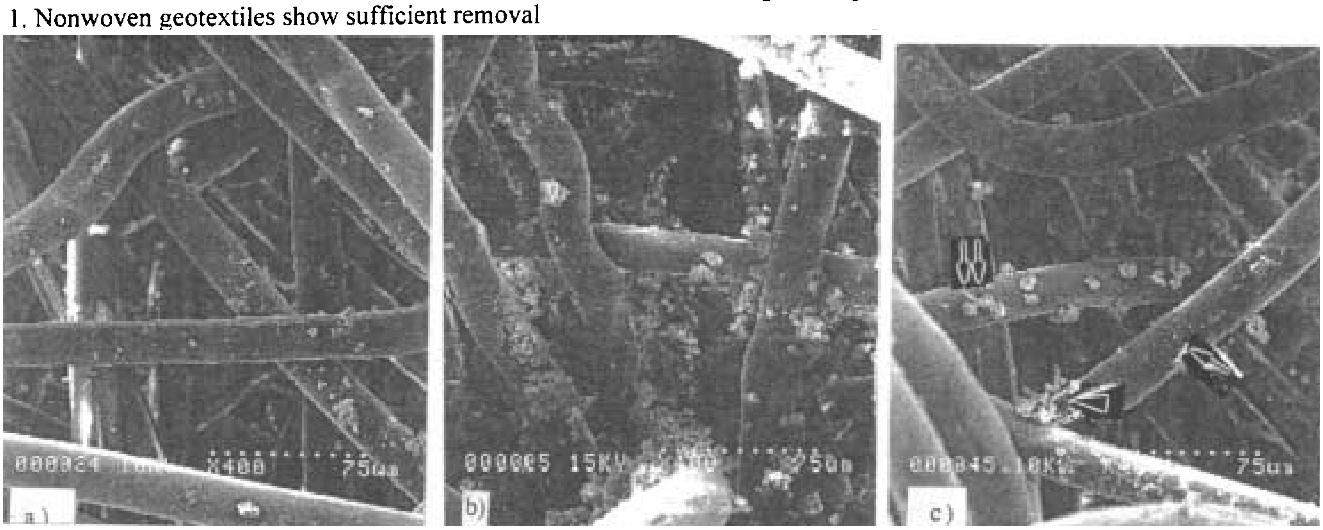

Figure 6. Scanning electron photomicrographs. Various times of capture of calcium carbonate particles a) 1.0 hour (Run 29), b) 10.75 hours (end, Run 29). c) Capture phenomena of surface attachment →, entrapment ➨, and aggregation ⇛.

Turbulence and dynamics in the falling head test

Adam Bezuijen
Sen. Consultant, Delft Geotechnics, Delft, the Netherlands.

ABSTRACT: The falling head test is elaborated theoretically. A closed form solution is presented for the course of the head loss in time during such a test, neglecting the contribution of inertia. Furthermore the influence of the mass of the oscillating water column is investigated. The governing equations are presented. Simulations with these equations show good agreement with the results of measurements. The results of calculations show that dynamics can have a distinct influence on the result of the test. Not only if oscillations are observed in the head loss over the geotextile, but also if only a monotone descending head loss is found in the test.

KEYWORDS: Laboratory tests, Permeability, Falling head test, Forchheimer, Inertia effects.

1 INTRODUCTION

A falling head test can be performed quicker than a constant head test. Electronic data acquisition equipment is necessary for the falling head test, but the price for this equipment decreases every year. Inter laboratory tests have shown that comparable results can be obtained with both tests. Both tests are incorporated in the CEN-Norm "Water flow capacity perpendicular to the plane, without load" prEN 12040 of the TC189 "Geotextiles" (CEN, 1955). It therefore can be expected that the falling head test will be used more and more in the future.

The principle of the falling head test is shown in Figure 1. A geotextile is placed in a U-shaped tube with a valve. The valve is closed before the test and there is a difference in water level in both sides of the tube. At the beginning of the test the valve is opened and the water starts to flow. Continuous monitoring of the pressure, with the pressure gauge shown, allows to monitor the water level in the tubes as a function of time, from which the head loss over the geotextile can be calculated. The water flow capacity of the geotextile tested on is determined by the head loss over the geotextile and the flow through the geotextile.

Evaluation of the results of a falling head test is nowadays automated by means of a computer program, in which the permittivity at a certain head loss is calculated from the measured head loss and its rate of decrease. In this paper a different approach is followed. The differential equation that governs the flow in a falling head test is solved analytically, assuming the Forchheimer flow equation. Using this formula the parameters in the flow equation are determined by non-linear regression.

2 THEORY

2.1 Turbulence

Using the Forchheimer relation and neglecting dynamic terms, the relation between head loss and specific discharge can be written as:

$$h = a_h q + b_h q^2 \tag{1}$$

Where h is the head loss, q the specific discharge and a_h and b_h are coefficients determining the permittivity of the geotextile with dimensions of *s* and s^2/m respectively.

In a falling head test there is a relation between the change in head loss and the specific discharge:

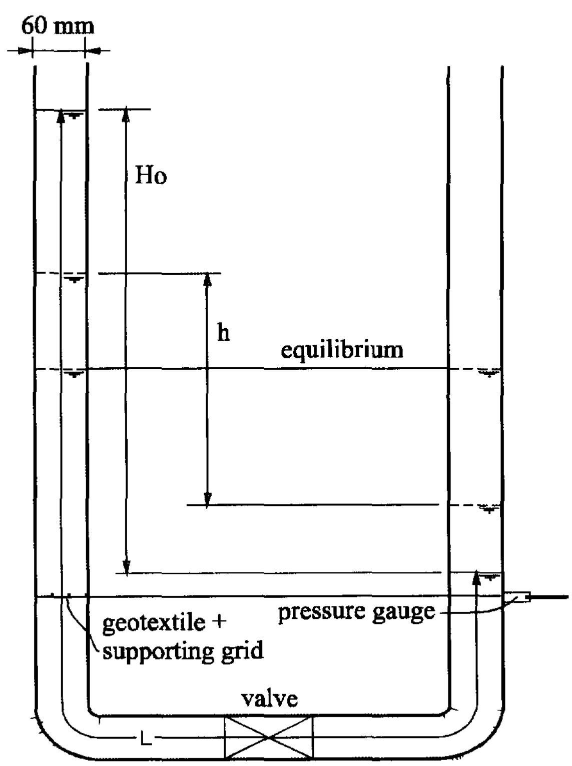

Figure 1: Sketch of a falling head apparatus.

$$q = -\alpha \frac{dh}{dt} \tag{2}$$

α depends on the geometry of the falling head apparatus. For the normal apparatus with two equal tubes, as shown in Figure 1, $\alpha=0.5$. If there is a constant head at the down flow side (this is the case if there would be no tube right from the valve in Figure 1), $\alpha = 1$. Inserting equation (2) in (1) and rearranging leads to the following differential equation:

$$\alpha^2 b_h (\frac{dh}{dt})^2 - \alpha a_h (\frac{dh}{dt}) - h = 0 \tag{3}$$

Since $\frac{dh}{dt} < 0$ (it is a *falling* head test), this can also be written as:

$$\frac{dh}{dt} = \frac{1-\sqrt{1+4b_h h / a_h^2}}{2\alpha b_h / a_h} \tag{4}$$

Substituting

$$z = 1 - \sqrt{1+4b_h h / a_h^2} \tag{5}$$

the differential equation reads:

$$dz - \frac{1}{z}dz = \frac{dt}{\alpha a_h} \tag{6}$$

Taking at $t = 0$, $z = z_0$, and calculating z_0 from (5), assuming that $h=H_0$ at $t=0$, (6) leads to:

$$\frac{t}{\alpha a_h} = z - z_0 - \ln\frac{z}{z_0} \tag{7}$$

Substituting back equation (4) leads to the final relation between t and h:

$$t = \alpha a_h \left[\sqrt{1+4\frac{b_h H_0}{a_h^2}} - \sqrt{1+4\frac{b_h h}{a_h^2}} - \ln\left(\frac{\sqrt{1+4\frac{b_h h}{a_h^2}}-1}{\sqrt{1+4\frac{b_h H_0}{a_h^2}}-1} \right) \right] \tag{8}$$

Figure 2 shows the result of a comparison between measurements on a relatively impermeable geotextile (the influence of dynamics in the test was expected to be small) and a calculation using Equation (8), in which a_h and b_h were obtained by non-linear regression on the measurement data, showing almost perfect agreement.

2.2 Dynamic effects

If the geotextile is very permeable, the inertia of the water column cannot be neglected. The head loss not only contributes to overcome the flow resistance in the geotextile, but also contributes to accelerate or decelerate the water column. An extreme example is the falling head test on a circular plate as was performed in the CEN round robin test (Dierickx, 1995), but it was also found in some permeable geotextiles, see Figure 3. To describe the results of

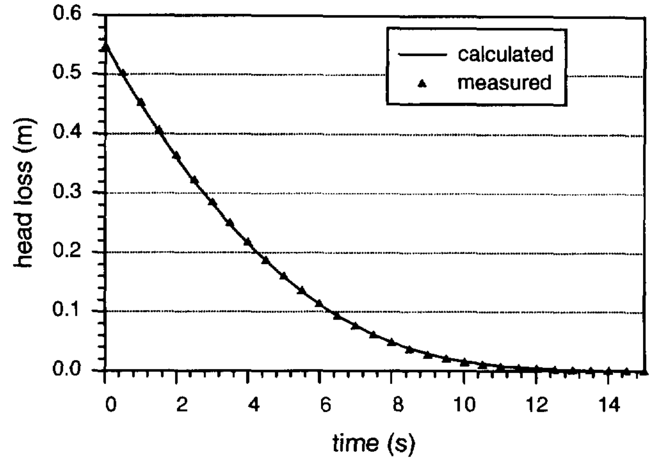

Figure 2: Falling head test on a less permeable geotextile (G2, see Section 2.2) and fit using Equation (8), a_h=2.44 s, b_h=148 s^2/m.

such tests equation (1) was extended with a term that includes inertia of the water column in the falling head apparatus. Taking this into account equation (1) reads:

$$h = a_h q + b_h |q| q + \frac{L}{g}\frac{dq}{dt} \tag{9}$$

The absolute sign is now necessary because the possibility of flow reversal. Using (2), (9) can be written as:

$$\alpha^2 b_h^* (\frac{dh}{dt})^2 - \alpha a_h (\frac{dh}{dt}) - \alpha \frac{L}{g}\frac{d^2h}{dt^2} = h \tag{10}$$

Where $b_h^* = b_h$ if $q > 0$ and $b_h^* = -b_h$ if $q < 0$. In this way the absolute sign in equation (9) is incorporated.
This equation was solved using an explicit finite difference scheme, using the following approximations:

$$\frac{dh}{dt} \approx \frac{h_{i+1} - h_i}{\Delta t} \quad \text{and} \quad \frac{d^2h}{dt^2} \approx \frac{h_{i+1} - 2h_i + h_{i-1}}{\Delta t^2} \tag{11}$$

Where h_i is the head loss at time step i and Δt is the time increment between 2 time steps. Inserting (11) in (10), h_{i+1} can be written as:

$$h_{i+1} = \frac{-B + \sqrt{B^2 - 4AC}}{2A} \tag{12}$$

with:

$$A = \alpha^2 \frac{b_h^*}{\Delta t^2}$$

$$B = -\alpha \left[2\alpha (\frac{b_h^*}{\Delta t})^2 h_i + \frac{a_h}{\Delta t} + \frac{L}{g\Delta t^2} \right] \tag{13}$$

$$C = (\alpha \frac{a_h}{\Delta t} + \alpha^2 \frac{b_h^*}{\Delta t^2} h_i - 1) h_i + \alpha \frac{L}{g\Delta t^2}(2h_i - h_{i-1})$$

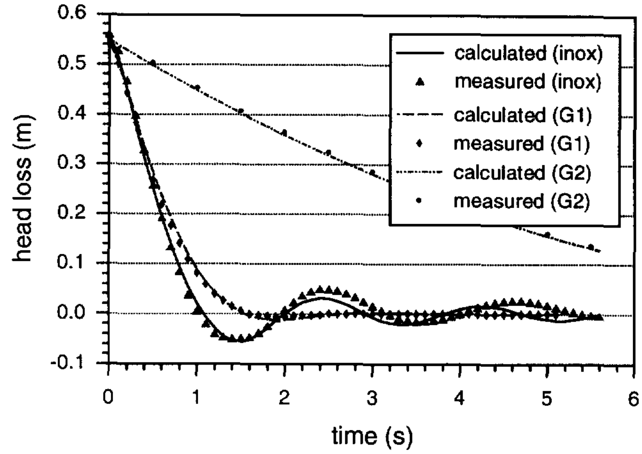

Figure 3: Measured and calculated piezometric head for a perforated plate (inox) and two different geotextiles.

Using these equations it is also possible to simulate the measured head loss in a falling head test as a function of time also for very permeable material quite accurately, see Figure 3. This figure shows measurements and calculations for 3 different geotextiles: The perforated plate used in the CEN tests and two geotextiles with different permeability. UCO (Terrasafe) 4000, which will be referred to as G1, a needle punched slightly head bonded nonwoven with a thickness of approximately 3.8 mm and Lotrak 16/15, referred to as G2, a woven geotextile (tape/tape) with a thickness of approximately 0.5 mm. The permeability of G2 is clearly less than that of G1. The whole curve of G2 is shown in Figure 2.

3 INFLUENCE DYNAMICS ON PARAMETERS

In the CEN norm “Water flow capacity normal to the plane, without load”, prEN 12040, dynamics is not taken into account. Time t=0 is the time the valve is completely opened and the first time dh/dt=0 is taken as the end of the test. The permeability of the geotextile is determined in this part of the curve, assuming that the difference in the head loss is zero when dh/dt=0, see Figure 4, which is a modified version from the figure in the norm. Figure 3 shows that the head loss can be less than zero due to dynamics. If this is the case, the curve is shifted along the Y-axis before the evaluation, to obtain a head loss of zero at dh/dt=0.

Taking one value for the parameters a_h and b_h in equations (12) and (13), it is possible to calculate the influence of dynamics by changing the length L of the water in the tube. The larger this length the larger the influence of dynamics. The CEN procedure described above and the non-linear regression technique can be used to obtain values for a'_h and b'_h (the accents indicate that the parameters are determined in a different way) using the solution without dynamics, Equation (8). If the CEN procedure is correct, then a'_h and b'_h should be equal to the input values for a_h and b_h.

This procedure was performed for the 3 different values of a_h and b_h, describing the permeability of the materials mentioned before. Table 1 shows the results of this procedure.

Table 1: Calculated values of the Forchheimer coefficients a_h (s) and b_h (s^2/m) and the velocity (VI) (m/s) and head loss (HI) (m) index. See also text.

	Perf. Plate				G1			G2		
L (m)	1.6 D	0	1.6	3	1.6 D	0	1.6	1.6 D	0	1.6
a_h, a'_h	0.01	0.0	0.0	0.0	0.65	0.63	0.16	2.4	2.3	2.2
b_h, b'_h	3.5	3.4	3.6	3.6	2.8	2.8	4.6	148	148	151
VI ($*10^{-3}$)	120	120	120	120	61	62	88	12	12	12
HI ($*10^{-3}$)	1.6	1.4	1.5	1.5	14	14	5.0	108	106	105

The column with D presents the parameters a_h and b_h used in the calculation including dynamics (equations (12) and (13)), resulting in the fits of Figure 3. When values for a_h and b_h were found, calculations were run with the same a_h and b_h for various lengths of the water column L (0, 1.6 and for the perforated plate also 3 m). The results of those calculations were used as an input for determination of a'_h and b'_h (presented in the columns with L = 0, 1.6 and 3 m without D). The method described in prEN 12040 has been used to obtain the part of the curve appropriate for calculations and Equation (8) and non-linear regression to obtain the parameters a'_h and b'_h. For the theoretical case L=0 (in reality the length of the column must always have a certain length, but this value is used to exclude the last term in equation (9)) there is no influence of dynamics. In that case the parameters a'_h and b'_h should be the same as a_h and b_h used in the dynamic calculation (D). In this case the procedure is just a check of the accuracy of both solutions. If L has a realistic length, there can be deviations. The calculation with L=1.6 m shows the influence of dynamics on the result of the test for the equipment used. The values for a'_h and b'_h mentioned for L=1.6 m are the values that will be found using the procedure of prEN 12040, thus

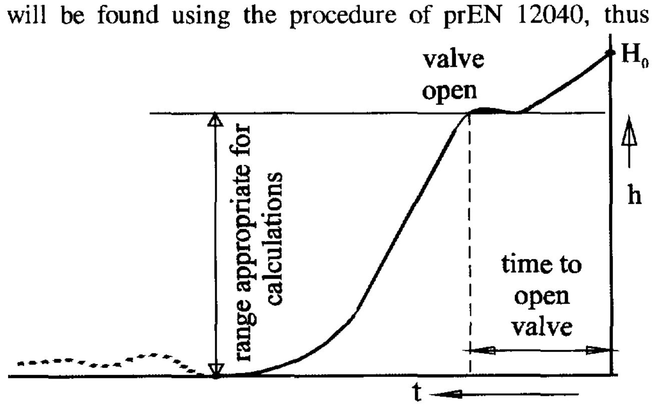

Figure 4: Sketch from prEN 12040 (modified) to calculate the water flow capacity.

neglecting dynamics.

The procedure of prEN12040 was slightly changed. The time the valve is completely opened is never known exactly and therefore the part of the curve with the steepest gradient is taken as the beginning of the test. In case the results are influenced by dynamics, this is a bit later than the moment the valve is open. A difference of approximately 0.3 s was found in the tests.

4 DISCUSSION ON THE RESULTS

Table 1 shows that the parameters used in the numerical calculations are in close agreement with a'_h and b'_h when the numerical results for L=0 are fitted with equation (8). This means that without dynamic effects both solutions correspond to each other, as could be expected. Small deviations occur due to the finite differences used in the numerical method. The small value of a_h, used to simulate the behaviour of the perforated plate, could not be found when the result of the numerical calculation with L= 0 was used to obtain a'_h. The influence of such a small value of a_h can be found in the damping of the oscillations (for time>2 s in Figure 3), but is negligible in the first part of the curve, where turbulent flow is dominant.

The results of the non-linear regression on the numerical simulations with a finite length L (and therefore influenced by dynamics), result in different values of a'_h and b'_h compared with the results for L=0. Remarkably the difference is only small in case the parameters for the perforated plate are used, but significant for geotextile G1 and still perceptible for the much less permeable geotextile G2. The parameters a'_h and b'_h differ considerably from a_h and b_h for G1. It is known that slight changes in the results of falling head tests can lead to relatively large changes in the parameters a_h and b_h (Bezuijen et al. 1994). However, also the velocity index and head index differ significantly. For G1 the This means that the procedure as suggested in prEN 12040 will not lead to the right values of a_h and b_h when there is an influence of dynamics. If dynamics has an influence, the flow capacity of the material is overestimated. Neglecting dynamics for geotextile G1 leads to a velocity index VI that is 30 % too high and to a head loss index that is 180 % too low.

For geotextile G2 the influence is only small. However, simulations has shown that for geotextiles with a velocity index of 34 mm/s, dynamics has still a considerable influence for an apparatus with a length of 1.6 m water column. For such a geotextile there will be hardly any overshoot in the head loss below zero, as is still present in geotextile G1 (see Figure 3). Neglecting dynamics for a geotextile with a velocity index of 34 mm/s leads to a VI that is 14% too high and a HI that is 47 % too high.

From this it can be concluded that is not sufficient to look at overshoot in the head loss to determine whether or not dynamic effects have an influence. The influence depends on the apparatus, but is significant (errors of more than 14 % and up to 180%) for the apparatus shown in Figure 1, with a water column of 1.6 m length, when the head loss reaches values close to zero between 1.5 and 4 seconds.

5 CONCLUSIONS

This study has led to the following conclusions:

1. The results of a falling head test on geotextiles can be described with Equations (12) and (13). In case dynamic effects can be neglected Equation (8) can be used.
2. The procedure as presented in prEN 12040 to deal with dynamic effects that occur in a falling head test on permeable geotextiles can lead to inaccurate results, even if no overshoot is visible in the head loss versus time plot. Considerable errors (from 14 % up to 180 %) were found when the head loss reaches values close to zero between 1.5 and 4 seconds.
3. The error found when using the procedure of prEN 12040 was largest in the head loss index.
4. It is advised to include the influence of dynamics in the interpretation of a falling head test when relatively permeable geotextiles are tested, or to use a constant head test.
5. More tests are needed to determine the entire range where dynamics has an influence.

ACKNOWLEDGEMENT

I would like to thank Dr. W. Dierickx of the Belgian Research Station for Agricultural Engineering for providing the measurement data and for stimulating discussion.

REFERENCES

Bezuijen A., Köhler H.-J. and Abromeit H.-U. (1994) "Geotextile permeability as a function of temperature", *5th Int. Conf. on Geotextiles, Geomembranes and Related products*, Singapore, 5 - 9 September, pp 655-658.

Dierickx W. (1995) "Research and Intercomparison Tests Necessary for the Harmonisation of Standards on Geotextiles, Task 4: Water Permeability Intercomparison". EC Measurement and Testing Project 0169, Document 0169/4/6, November.

CEN (1995) *Geotextiles and geotextile-related products - Determination of the water permeability characteristics normal to the plane, without load.* PrEN 12040:1995, July.

Factors Affecting Hydraulic Transmissivity of Geocomposite Drain Systems

Nader S. Rad
Laboratory Director, GeoSyntec Consultants, Geomechanics and Environmental Laboratory, Alpharetta, Georgia, USA

Cuneyt Gokmen
Program Manager, GeoSyntec Consultants, Geomechanics and Environmental Laboratory, Alpharetta, Georgia, USA

James M. Stalcup
Operation Manager, GeoSyntec Consultants, Geomechanics and Environmental Laboratory, Alpharetta, Georgia, USA

ABSTRACT: Effects of various testing parameters on the hydraulic transmissivity of geocomposite drain systems commonly used in leak detection and leachate collection systems of modern landfills are investigated. A laboratory testing program was performed utilizing different geonet, geotextile, geomembrane and geosynthetic clay liner (GCL) products. The test results indicate that, the configuration of the geocomposite system, the intensity and the duration of the sustained vertical stress, and the hydraulic gradient can strongly influence the hydraulic transmissivity of a geocomposite drain.

KEYWORDS: drainage, geonets, geocomposite, transmissivity, laboratory testing

1 INTRODUCTION

Modern landfill liner-system design commonly includes leak detection and leachate collection systems, which often consist of a geonet sandwiched between two geotextile layers, or between a geotextile and a geomembrane layer (both configuration herein are referred to as geocomposite drains). Hydraulic transmissivity of a geocomposite drain is known to be affected by various factors including: (i) physical characteristics of the geonet, geotextile, and when applicable, geomembrane components, (ii) the intensity and duration of the applied vertical stress, (iii) the hydraulic gradient, and (iv) presence of an overlying geosynthetic clay liner (GCL). The effects of these parameters on the hydraulic transmissivity of geocomposite drains were studied with a laboratory testing program utilizing different geonet, geotextile, geomembrane and GCL products in various geocomposite drain configurations.

2 TEST EQUIPMENT AND SETUP

The constant head hydraulic transmissivity test method described by the American Society for Testing and Materials (ASTM) test standard D 4716 was utilized in the testing program. A simplified schematic diagram of the test equipment and setup is presented in Figure 1. Referring to the figure, hydraulic transmissivity is calculated utilizing the following equation:

$$\theta = \frac{Q}{B \times (h/L)} \qquad (1)$$

where, θ is the hydraulic transmissivity (m^2/s), Q is the volume of discharged fluid per unit time (m^3/s), L is the length of the specimen (m), B is the width of the specimen (m), and h is the difference in the total head across the specimen (m). The hydraulic gradient is equal to the ratio of h to L.

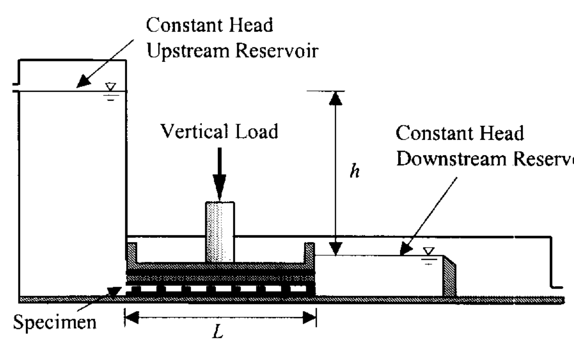

Figure 1. Schematic diagram of the test equipment and setup.

3 TEST MATERIALS

One geomembrane, two different geonets, three different geotextiles and one GCL product were used in the testing program. Table 1 provides general information on each product.

4 TEST SPECIMEN CONFIGURATION

Referring to Figure 2, the following test specimen configurations were used:

Table 1. Test material general information.

Test Material			
Designation	Type	Trade Name	Remarks
GM	Geomembrane	Gundline HD	High density polyethylene, smooth, t=1.5 mm
GN1	Geonet	Tensar NS140551	Polyethylene, t=5.0 mm, θ=1E-3 m^2/s @ σ= 720 kPa and i=1.0
GN2	Geonet	NSC PN 3000	Polyethylene, t=5.0 mm, θ=1E-3 m^2/s @ σ= 720 kPa and i=1.0
GT1	Geotextile	LINQ Typar 3601	Polypropylene, nonwoven, M_A=203 g/m^2, AOS=0.1 mm, and ψ=0.1 s^{-1}
GT2	Geotextile	Amoco 4557	Polypropylene, nonwoven, M_A=407 g/m^2, AOS=0.15 mm, and ψ=1.1 s^{-1}
GT3	Geotextile	Polyfelt TS750-Reg	Polypropylene, nonwoven, M_A=349 g/m^2, AOS=0.15 mm, and ψ=1.3 s^{-1}
GCL	GCL	Claymax	Primary backing: Amoco 4034, polypropylene, woven, M_A=98 g/m^2 Secondary backing: Chicopee (a very thin woven geotextile)

t: thickness (mm), M_A: mass per unit area (g/m^2), AOS: apparent opening size (mm), ψ: permittivity (s^{-1}), σ: vertical stress (kPa), and i: hydraulic gradient (-)

Configuration I - a geonet sandwiched between two geomembranes to evaluate the baseline hydraulic transmissivity of the geonet.

Configuration II - a composite of a geotextile and a geonet sandwiched between two geomembranes to evaluate the effects of a single geotextile layer over the geonet on its transmissivity.

Configuration III - a GCL placed over the geotextile component of a geocomposite drain (secondary backing against the geotextile) to evaluate the effects of an overlying GCL on the transmissivity of a geocomposite drain.

Configuration IV - a GCL directly placed over a geonet (primary backing directly against the geonet) to evaluate the effects of an overlying GCL on the transmissivity of a geonet.

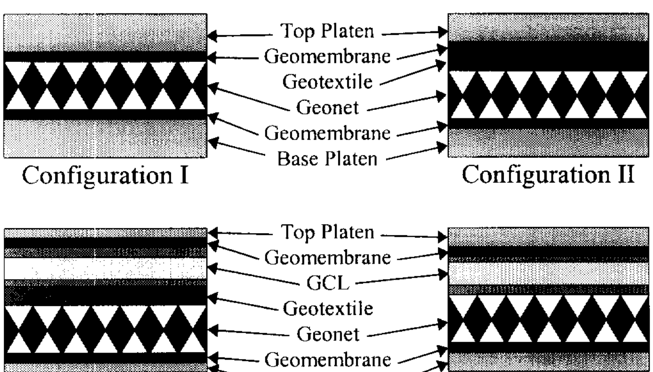

Figure 2. Schematic diagram of four different test configurations.

5 TESTING PROGRAM

Nine transmissivity tests were performed, as presented in Table 2. The tests were performed utilizing vertical stresses ranging from 24 to 766 kPa and hydraulic gradients ranging from 0.1 to 0.5. These boundaries were selected to encompass commonly encountered field conditions. Test duration (i.e., the period of applied vertical stress) varied from several days in the case of Tests 1 through 7 to approximately 120 days in the case of Tests 8 and 9.

Table 2. Summary of laboratory testing program.

Test	Config.	Test configuration (from top to bottom)							
		top							bottom
No.	No.	GM	GCL	GT1	GT2	GT3	GN1	GN2	GM
1	I	x						x	x
2	II	x		x				x	x
3	II	x		x			x		x
4	II	x			x		x		x
5	II	x				x	x		x
6	III	x	x	x			x		x
7	III	x	x			x	x		x
8	III	x	x	x				x	x
9	IV	x	x					x	x

6 TEST RESULTS

The test results are graphically presented in Figures 3 to 7. The results and the observations made during the tests are summarized in the following paragraphs.

Hydraulic gradient - Referring to Figures 3, 5 and 6, it appears that higher hydraulic gradients result in lower measured transmissivity values. This suggests that as the hydraulic gradient increases the flow regime becomes turbulent and Darcy's law may not be fully applicable (Williams, et al., 1984 and Cancelli, et al., 1987).

Geotextile - Referring to Figure 3 (a), it appears that presence of a geotextile over a geonet reduces its transmissivity. This is likely due to penetration of the overlying geotextile into the geonet channels (Williams, et al., 1984 and Koerner, 1990).

As illustrated in Figure 3 (b), the type of the overlying geotextile may have a significant impact on the hydraulic transmissivity of a geocomposite drain. For the geonets and geotextiles used in this investigation, the test results indicate that the hydraulic transmissivity may decrease by approximately half an order of magnitude when the heaviest/thickest geotextile is used.

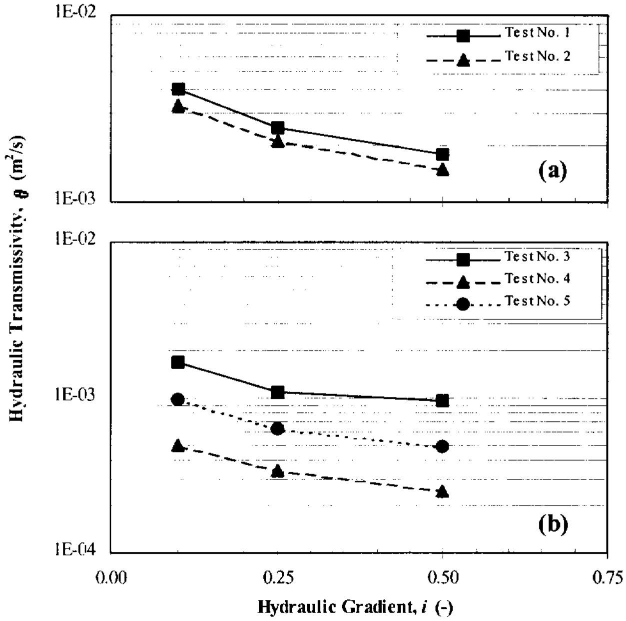

Figure 3. Effect of geotextile on transmissivity of geocomposite drains (σ=766 kPa).

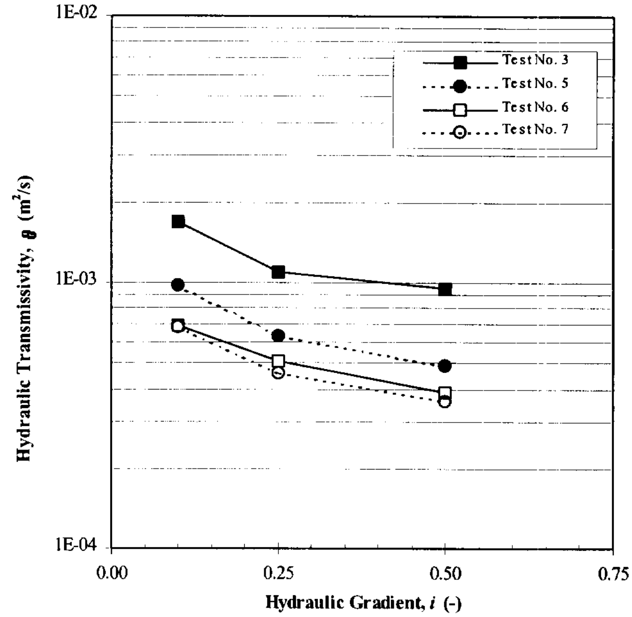

Figure 5. Effect of GCL on transmissivity of geocomposite drains with various geotextiles (σ=766 kPa).

Vertical Stress - The effect of the vertical stress on the transmissivity of geocomposite drains is depicted in Figure 4. Referring to the figure, hydraulic transmissivity decreases as the vertical stress increases. The decrease in the hydraulic transmissivity is likely due to: (i) compression of the geonet ribs, and (ii) increasing penetration of the overlying geotextile into the net (Williams, et al., 1984 and Fannin and Choy, 1995). As presented in the figure, for the geotextiles and geonets used in this investigation the

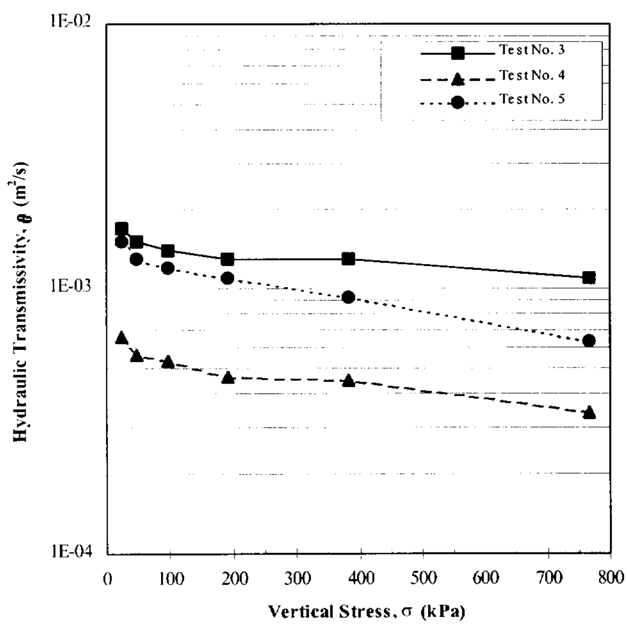

Figure 4. Effect of vertical stress and geotextile on the transmissivity of the geocomposite drains (i=0.25).

transmissivity may decrease by 30 to 60% as the vertical stress increases from 24 to 766 kPa. In general, the heavier/thicker the geotextile the stronger the decrease in the overall transmissivity of the geocomposite drains.

GCL - As illustrated in Figures 5 and 6, presence of an overlying GCL may reduce the transmissivity of a geocomposite drain by 30 to 70 %. Referring to Figure 5, the effect of GCL on the transmissivity is generally dependent on the type of geotextile used to separate the GCL from the geonet. For the materials used in this investigation, the reduction in the transmissivity was less when a heavier/thicker geotextile was used. It should be noted, however, that this observation contradict the results presented in Figure 3 (b). Thus, more research in this area is needed before a final conclusion can be drawn.

As presented in Figure 6, direct placement of a GCL on a geonet results in approximately an order of magnitude reduction in its transmissivity. Notwithstanding the transmissivity reduction, direct placement of GCL on a geonet may be an economical approach for some landfill designs. It should be noted, however, that the geotextile backing of the GCL placed against the geonet should have appropriate mechanical and physical properties to: (i) withstand potential damage under the applied vertical stress and construction activities, and (ii) limit migration of bentonite from the GCL into the geonet.

Duration of vertical stress - The effects of the duration of sustained vertical stress on transmissivity of geocomposite drains are presented in Figure 7. Referring to the figure, the transmissivity of a geocomposite drain decreases as the duration of the applied vertical stress increases. For the geocomposite drains and test duration used in this

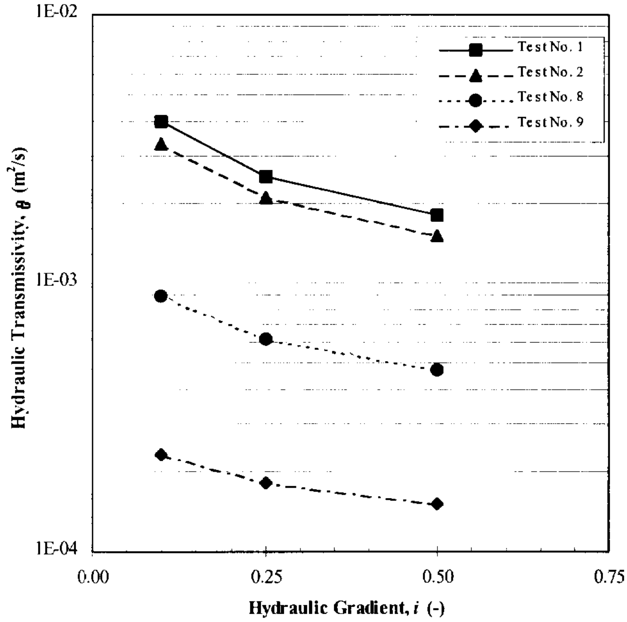

Figure 6. Effect of GCL on transmissivity of geocomposite drains with or without geotextile (σ=766 kPa).

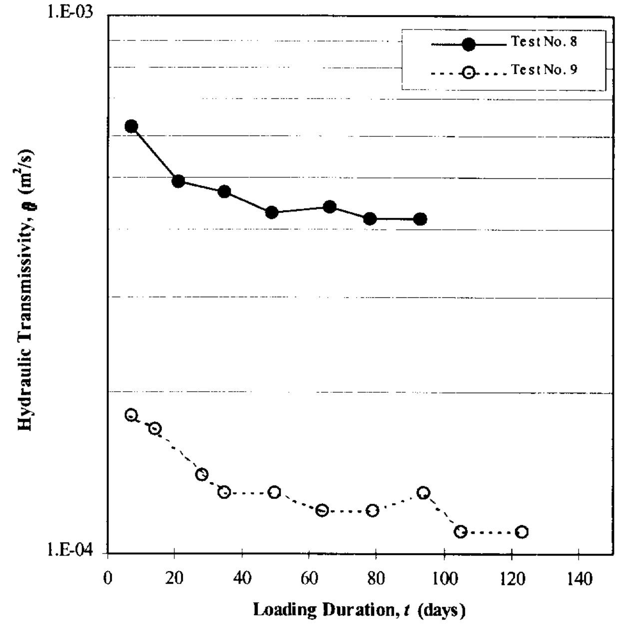

Figure 7. Long-term effect of applied vetical stress on the transmissivity (σ=766 kPa, i=0.25).

investigation most of the reduction occurred in the first 50 to 60 days. The maximum transmissivity reduction was approximately 30 to 40%. The observed decrease in the transmissivity is likely due to: (i) creeping of the geonet ribs (Smith and Kraemer, 1987), and (ii) creeping of the overlying geotextile into the geonet channels.

7 CONCLUSION

The purpose of this investigation was to evaluate the effect(s) of various parameters on the hydraulic transmissivity of geonets and geocomposite drains. Based on the results obtained in this study the following conclusions can be drawn:

(i) the higher the hydraulic gradient the lower the hydraulic transmissivity value;

(ii) the higher the vertical load the lower the hydraulic transmissivity value;

(iii) an overlying geotextile may reduce the hydraulic transmissivity of a geonet due to possible penetration of the geotextile into the geonet channels;

(iv) the physical and mechanical properties of the material(s) used in a geocomposite drain affect its overall transmissivity;

(v) direct placement of a GCL on a geonet may strongly reduce its overall hydraulic transmissivity due to penetration of GCL and possible migration of its bentonite component into the geonet channels;

(vi) presence of a layer of geotextile between the GCL and the geonet reduces the GCL effect on the transmissivity of the geonet; and

(vii) long-term application of vertical stress may reduce hydraulic transmissivity of a geocomposite drain.

The authors recommend that the actual design configurations be simulated, as closely as possible, in the laboratory to determine representative field hydraulic transmissivity values.

REFERENCES

ASTM (1993) *Annual Book of ASTM Standards, Volume 04.08,* Philadelphia, PA, 1470 p.

Cancelli, A., Cazzuffi, D. and Rimoldi, P. (1987) "Geocomposite Drainage Systems: Mechanical Properties and Discharge Capacity Evaluation", *Geosynthetics '87*, IFAI, Vol. 2, New Orleans, LA, pp. 393-404.

Fannin, R. J. and Choy H.W. (1995) "Factors Influencing the Long-Term Flow Capacity of Geonets", Geosynthetics '95, IFAI, Nashville, TN, pp. 267-280.

Koerner, R.M. (1990) *Designing with Geosynthetics,* Second Edition, Prentice Hall, Englewood Cliffs, N.J., 652 p.

Smith, A.D. and Kraemer, S.R. (1987) "Creep of Geocomposite Drains", *Geosynthetics '87*, IFAI, Vol. 2, New Orleans, LA, pp. 422-433.

Williams, N., Giroud, J.P., and Bonaparte, R. (1984) "Properties of Plastic Nets for Liquid and Gas Drainage Associated with Geomembranes", Proceedings of the International Conference on Geomembranes, Vol. II, Denver, CO, pp. 399-404.

Comparison of transmissivity tests DIN-ASTM-CEN

J. Müller-Rochholz
Professor, Department of Civil Engineering, Fachhochschule Münster, Labor für Baustoffe, Münster, Germany

Z. Bronstein
Institut für textile Bau-und Umwelttechnik , Greven, Germany

ABSTRACT: Working on harmonising tests, there were 3 different test available. They differ in specimen size, lateral pressure material, water input to specimen. These standards were tested in comparison on a set of identical materials with different hydraulic gradients. The results are given in plots flow us hydraulic.

KEYWORDS: Hydraulic transmissivity, In-plane flow, Drainage capacity, Drainage, Transmissivity

1 INTRODUCTION

World wide trade needs generally accepted technical values for the products traded. The work on international standards in the International Standard Organisation ISO is accelerated in the geosynthetic area by the Vienna-contract, which states a common speed and a mutual acceptance of standards between ISO and the Comité Européenne de Normalisation CEN. For drainage applications of geosynthetics the drainage capacity is the design parameter. This property may be tested by prEN ISO 12958 November 1995 or ASTM D 4716-87 or an old German Proposed made by Franzius Institute (DIN 60500 T7). This comparison included 10 Materials and the 3 standardised methods.

2 DEFINITIONS

In-plane water flow capacity: The volumetric in plane rate of water per unit width of the GTX or GRP, at defined gradients and loads, in a direction parallel to the plane of the prodact.

Transmissivity θ: The in-plane water flow capacity of the GTX or GRP under laminar conditions at a hydraulic gradient of unity.

Hydraulic gradient Δh: Ratio of the head loss in the GTX or GRP to the distance between two mesasuring points.

3 TEST METHODS

The 3 methods described in

- prEN ISO 12958 November 1995
- ASTM D 4716-87
- Franzius Institute method
-

are synoptic shown in fig. 1, 2 and 3.

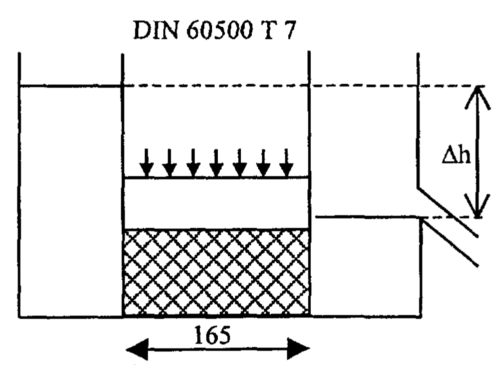

specimen size	
L x W (mm)	165 x 100
pressures (kPa)	2-200
hydr. gradient i=Δh/l	1
pressure platen	hard, plane

Figure 1: Schematic sketch of test condition DIN 60500 T7

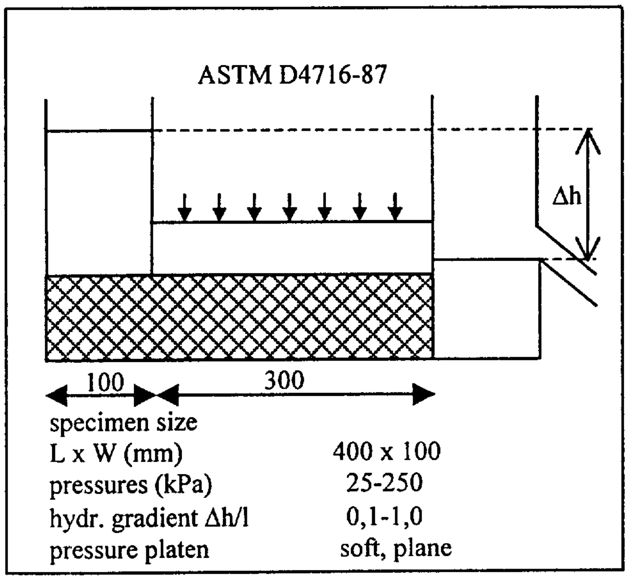

Figure 2: Schematic sketch of test condition ASTM D4716-87

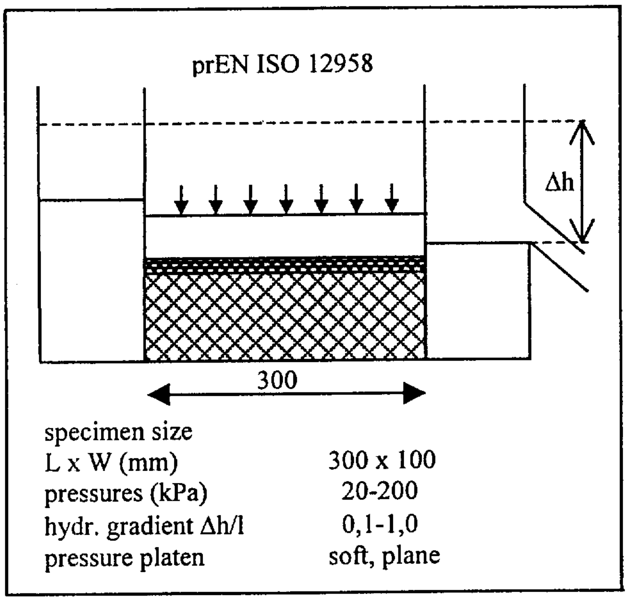

Figure 3: Schematic sketch of test condition prEN ISO 12958

The differences are specimen size, water input direction to specimen, kind of confining plate material.

3 MATERIALS TESTED

A wide set of materials covering typical products for drainage application were tested, the generic description is given hereunder.

		Number of Materials
-Random wire mats	-	4
-Oriented wire mats	-	1
-extruded geonet	-	2
-Cuspated sheet	-	1
-nowowen composite	-	1
-PE foam-particle	-	1

4 RESULTS

The results of comparison tests are given in figures 4 to 8.

Influence of pressure on drainage materials

The generic products show different behaviour, the lines of flow vs stress drop rapidly for random wire products, show less decrease for oriented wires and again less for geonet and cuspated film type products. Be aware that the flow axis is scaled differently, the flow at 2 kPa for wire products is very high.

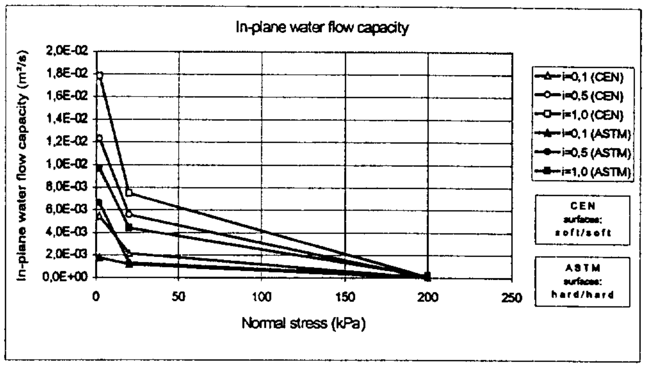

Figure 4: Oriented PA wire between nonwowens (Sterz, Breuer 1995, Ehler, Rohde 1995)

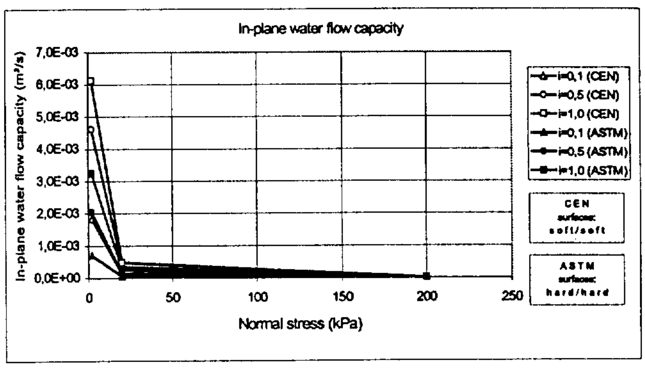

Figure 5: Random PP wire between nonwowens (Sterz, Breuer 1995, Ehler, Rohde 1995)

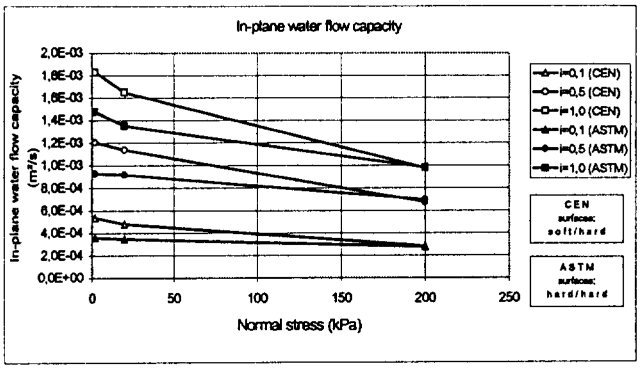

Figure 6: Extruded geonet with nonwowen
(Sterz, Breuer 1995, Ehler, Rohde 1995)

Influence of hard/soft platen

The soft (cellular rubber) platen of CEN simulating soft soil pressure on the geotextile filter leads to a strong decrease of the curves (see fig 7) by confining the flow section.

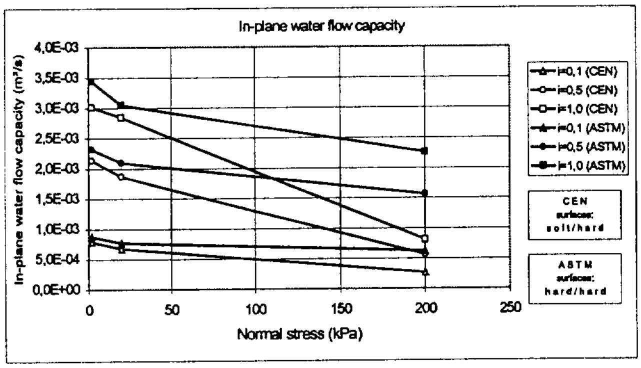

Figure 7: Cuspated sheet with nonwowen
(Sterz, Breuer 1995, Ehler, Rohde 1995)

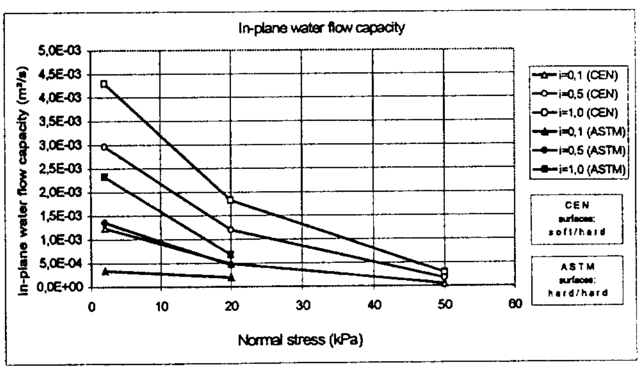

Figure 8: PE foam-particles with nonwowen cover
(Sterz, Breuer 1995, Ehler, Rohde 1995)

Influence of gradient

The dependence from gradient is not always linear (see fig 9), so if a value measured at a gradient not equal to 1 is than calculated for Transmissivity at gradient 1, the mistake is significant.

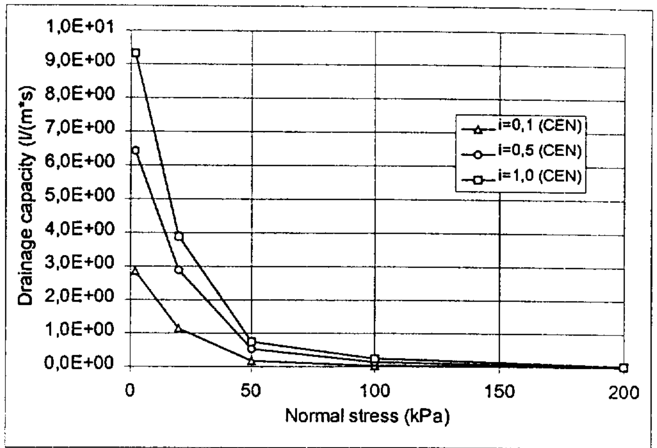

Figure 9: PE foam-particles with nonwoven

Influence of test method

From the curves given in fig 4 .. 8 tables were derived, giving the comparative values for the 3 standard methods for 3 materials (see table 1, 2, 3). Roughly evaluated the test according to ISO and CEN leads to product specific correlation values, a factor, valid for all materials is not extractable.

σ kPa	θ (CEN) m²/s	θ (ASTM) m²/s	θ (Franzius) m²/s
2	0,0208	-	0,1100
20	0,0013	0,0006	0,0120
200	0,0002	0,0001	0,0047

Table 1. Random wire mat (Sterz, Breuer 1995)

σ kPa	θ (CEN) m²/s	θ (ASTM) m²/s	θ (Franzius) m²/s
2	0,0050	-	0,0216
20	0,0003	0,0004	0,0024
200	< 0,0001	< 0,0001	< 0,0001

Table 2. Random wire mat between nonwowen (Sterz, Breuer 1995)

σ kPa	θ (CEN) m^2/s	θ (ASTM) m^2/s	θ (Franzius) m^2/s
2	0,0009	-	0,0063
20	0,0007	0,0014	0,0049
200	< 0,0001	0,0001	0,0009

Table 3. Extruded geonet with nonwowen (Sterz, Breuer 1995)

REFERENCES

Draft prEN ISO 12958 (CEN)
Geotextile and, geotextile-related Products-Determination of WaterFlow Capacity in their Plane
European Committee for Standardization.

ASTM D 4716-87
Standard test Method for Constant Head Hydraulic Transmissivity (In-Plane Flow) of Geotextile and geotextile-related Products
ASTM Committee D-35.

D. Sterz, W. Breuer
Transmissivity of difference drainage materials by CEN-test
Fachhochschule Münster, Münster, Germany 1995

E. Ehler, I. Rohde
Transmissivity of difference drainage materials by ASTM D4716-87
Fachhochschule Münster, Münster, Germany 1995

The Optimization Analysis Between Processing Parameters and Physical Properties of Geocomposites Composed of Multi-layered Nonwovens

H.Y. Jeon
Associate Professor, Department of Textile Engineering, Chonnam National University, Kwangju, Korea

J.Y. Kim
Research Associate, Department of Textile and Apparel Technology and Management, North Carolina State University, Raligh, NC, USA

ABSTRACT: The geocomposites of needle punched(NB) and spunbonded(SB) nonwovens having reinforcement and drainage functions were manufactured by thermal bonding method. The physical properties (e.g. tensile, tear and bursting strength, permittivity) of these multi-layered nonwovens were varied by processing parameters - temperatures, pressures, bonding periods etc. - in manufacturing by thermal bonding method. Therefore, it is very meaningful to optimize the processing parameters and physical properties of the geocomposites by thermal bonding method. An algorithm has been developed to optimize the process of the geocomposites using an artificial neural network (ANN). The geocomposites were employed to examine the effects of manufacturing methods on the analysis results and the neural network simulations have been applied to predict the changes of the nonwovens performances by varying the processing parameters.

KEYWORD: Multi-layered nonwovens, Thermal bonding method, Processing parameters, Optimization analysis.

1 INTRODUCTION

The function of nonwoven geotextiles are reinforcement, seperation, filteration, drainage and liquid barrier (Ingold 1994; Koerner 1994). Multi-layered nonwovens as a kind of geocomposites are manufactured by needle punching or thermal bonding to develop the above one or two functions of geotextile (Lünenschloss and Albrecht 1981; Gourc, Faure, Rollin and LeFlear 1982). Especially, in the case of application to thermal bonding to manufacture geocomposites (multi-layered nonwovens), the processing parameters e.g. temperature, pressure, time etc, were affected by the physical properties of geocomposites. From this view, it is very reasonable that the optimization analysis is applicated to examine the deviations and correalations between these parameters.

Process optimization is one of the most important topics in modern non-woven research because it directly influences many physical properties of the thermal bonded nonwoven geocomposite. It has been known that there exist very complicated interaction between processing parameters and material properties. The popular regression approaches always neglects some significant interactions between processing parameters in order to simplify the model and often have some difficulty in finding a reliable multivariable nonlinear model which must be considered as a model.

Very recently, the feed-forward multi-layered neural network approach has been widely used in many areas of engineering and science (Hornik 1989). Commonly, the neural networks can be employed in order to analyze some of the most complex non-linear system. The recent theoretical work has proven that neural networks can be successfully applied to express most classes of continuous functions with bounded inputs and outputs with any specified precision (Sharpe 1994).

In this paper, a neural network algorithm for optimizing the correlations between physical properties and processing parameters of multi-layered nonwovens to be manufactured at the different processing conditions was used and the optimum condition of these was derived from analytical results.

2 EXPERIMENTAL

2.1 Manufacturing of Geocomposites

Spunbonded(SB) nonwoven($18 g/m^2$) of polypropylene filament(7d) and needle punched(NB) nonwoven ($163 g/m^2$) of polypropylene staple fiber (12d) were used as raw materials for geocomposites composed of multi-layered nonwovens. A special designed thermal bonding apparatus was used to bind geocomposites and the plate which are available to heat and press was adapted to thermal bonding apparatus.

2.1.1 The processing conditions

Processing conditions of thermal bonding for manufacturing geocomposites composed of multi-layered nonwovens are as follows:

(1) Temperatures: 180 ~ 190 ℃ (at 2 ℃ intervals)
(2) Pressures: 4, 5, 6 kgf/m^2
(3) Times: 2, 3, 4 seconds

2.1.2 Types of geocomposites

The following types of geocomposites were manufactured at the above conditions:

(1) NP-thermal bonded
(2) NP/SB
(3) NP/NP
(4) SB/NP/SB

2.2 Physical Properties

Physical properties of multi-layered nonwovens were estimated in accordance with the following ASTM methods:

(1) Tensile strength for MD (machine direction) and CD (cross direction)- ASTM D 4632-91
(1) Tear strength - ASTM D 4533-91
(2) Bursting strength - ASTM D 3786
(3) Permittivity - ASTM D 4491-92

3 NEURAL NETWORK

In this paper, the feedforward back propagation algorithm is applied to model manufacturing process of non-woven materials. A basic multi-layer neural network structure is shown in Figure 1 depicting the hidden layer, and output layer.

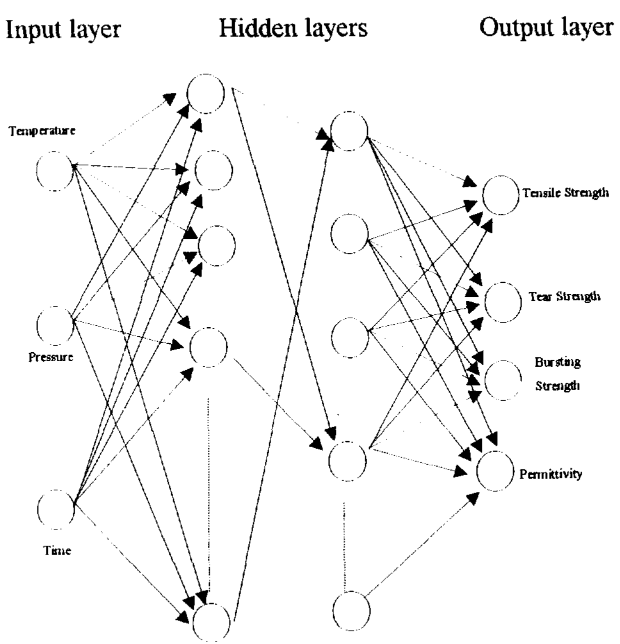

Figure 1. Architecture of a neural network having two layers.

This neural network has one input layer, one output layer, and any number of hidden layers. Each network consists of nodes (neurons). The input layer of the neural network takes information from the outside world and sends it to the nodes in the hidden layers. Similarly, the output layer of the neural network transmits the processed information to the external world.

To apply an m-variate signal input to a one-layer neural network consisting of n neurons each having m weights, we multiply an m-variate vector X (x_1, x_2, ... x_{m-1}, 1) with the (nxm)-variate weight matrix W. The result is an n-variate net input vector s (s_1, s_2, ... s_n). Then, we can show how each component s_j is calculated for layer 1:

$$s_j = \sum_{i=1}^{n} w_{ji} v_i + b_j = w_j T \cdot v + b_j \ , j=1,2,\ldots..k \qquad (1)$$

The index j spans the n neurons, while i spans the m weights in the jth neuron. The number of weights in the neuron is one of more than the number of input variables, x_i; the remaining one input variable is the bias, which is always equal to 1.

The quantity s_j is processed by an activation function to give the output o_j of the jth neuron:

$$o_j = f(s_j) \qquad (2)$$

The input consists of process variables such as pressure, temperature and processing time. The network output are predicted values of physical properties at possible process conditions. The network training is performed using the nonlinear least square methods. The error at the output neuron can be defined as

$$E = \frac{1}{2}(t_k - o_k)^2 \qquad (3)$$

where t_k is the target value of the output neuron. The backpropagation algorithms make use of the gradient descent methods for minimizing E. The error signal defined by

$$\delta_j = -\frac{\partial E}{\partial o_j} \qquad (4)$$

leads to the result of general delta rule

$$\Delta w_{ji} = \eta \delta_j o_i \qquad (5)$$

where η is an adaptation gain and δ_j is computed based on whether or not neuron j is in the output layer. If neuron j is one of the output neurons, then

$$\delta_j = (t - o_j) o_j (1 - o_j) \tag{6}$$

On the other hand, if neuron is not in the output layer,

$$\delta_j = o_j (1 - o_j) \sum_i \delta_i w_{ji} \tag{7}$$

For a fast convergence, the momentum with gain α will be introduced by following equation:

$$\Delta w_{ji}(k+1) = \eta \delta_j o_i + \alpha \Delta w_{ji}(k), \tag{8}$$

(, where k is the iteration step.)

4 RESULTS AND DISCUSSION

The feedforward back propagation algorithm based on the generalized delta rule and the minimum mean squared error (MSE) principle were used for the data sets. In a feedforward network, the processing units can be divided into several layers: input layer, hidden layers and output layer. The input components consist of process variables such as pressure, temperature and processing time which are considered to be the important parameters. Outputs of the network are the predicted physical properties at the given process condition. The number of units in the hidden layers were set to be 16 following a series of optimization experiments. The networks have been used for training hundreds of experimental data sets, namely, pairs of process conditions and physical properties of different multi-layered nonwovens produced by varying the process conditions.

The prediction results are shown in Figures 2-5. As shown in the figures, several physical properties were predicted quite well with small errors. Figure 2 shows predicted permittivity at different process conditions. From this, it is known that a high permittivity value can be obtained when geocomposites are made at 180°C . Same tendency like this is observed for short processing time and lower temperature ranges. But in very high pressure and long processing time, the property is deteriorated significantly below unacceptable region. Figure 3 shows effect of process condition on tear strength of nonwovens. It was clearly seen that process time affects significantly the tear strength in such a way that longer process time enhances the tear strength over whole temperature regions investigated. But pressure effect is really negative, that is, high pressure caused the decrease of tear strength of nonwovens. Tensile strength difference and burst strength of geocomposites represented in Figure 4 and Figure 5, show the same tendency of the case of tear strength. In Figure 4, tensile strength difference between MD and CD doesn't depend on processing conditions except for 190℃. Using a simulation model, we tried to find some optimal process conditions which optimize several physical properties in such a way that permittivity, tensile, tear strengths are maximized and tensile strength difference is minimized. From this, it is known that the optimum condition is found to be 182°C, 3sec and 4.9 kgf/cm^2, respectively.

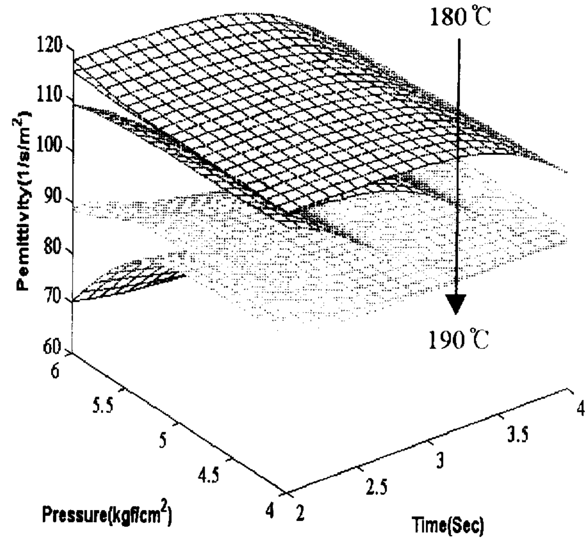

Figure 2. Prediction of permittivity using neural network.

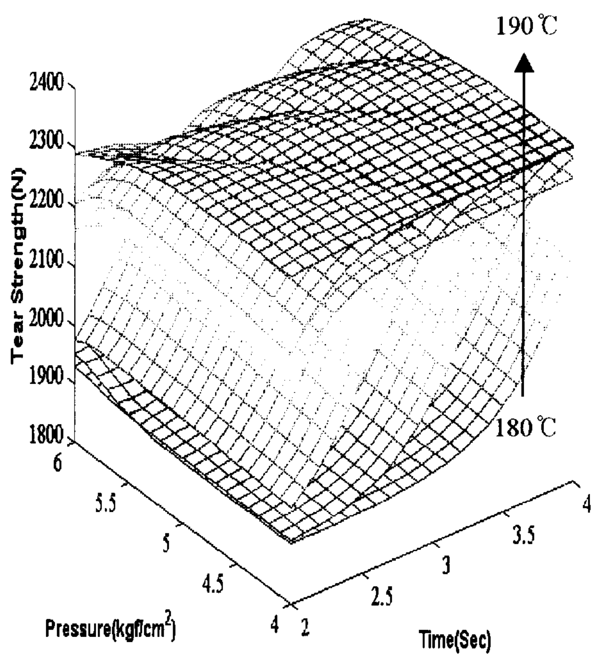

Figure 3. Prediction of tear strength using neural network.

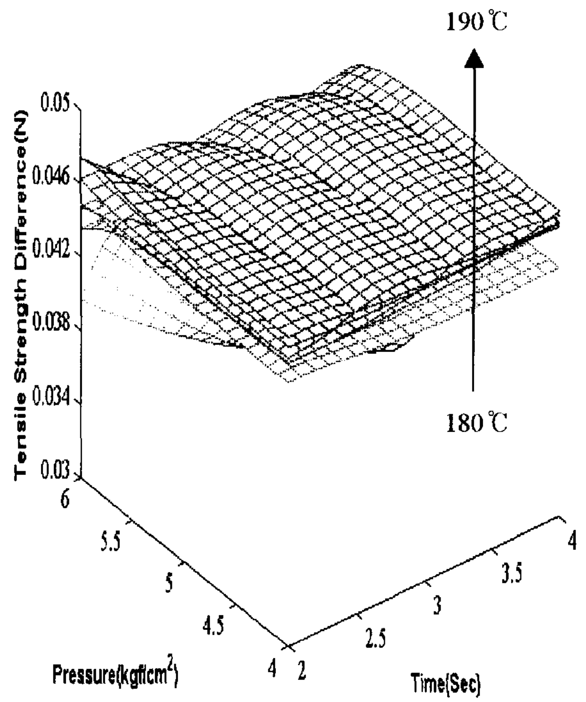

Figure 4. Prediction of tensile strength difference.

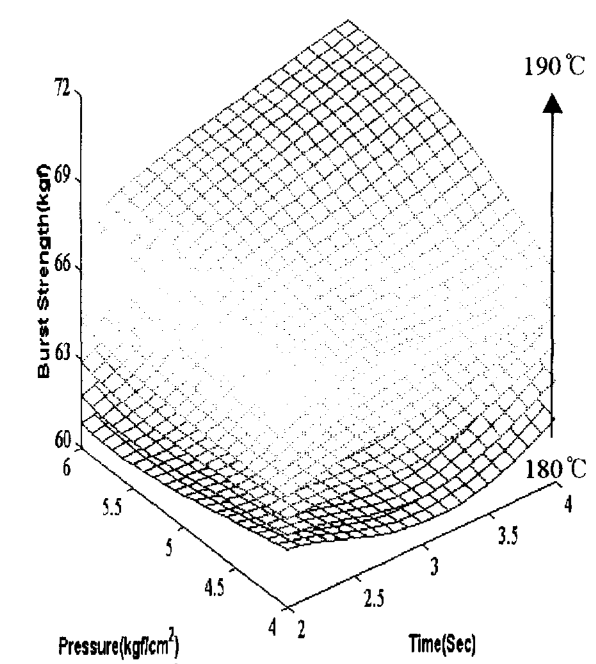

Figure 5. Prediction of burst strength using neural network.

5 CONCLUSION

The optimization analysis by neural network were used to examine the relations between processing parameters and physical properties of multi-layered nonwovens. Using this tool, we developed an algorithm for optimization of the geocomposite performances without a significant loss of physical properties. The simulated response surfaces were found to be highly effective in predicting the qualities of resulting geocomposites without actually producing them.

REFERENCES

Lünenschloss, J. and Albrecht, W. (1981) *Nonwoven Bonded Fabrics*, John & Sons, New York, pp. 178-313.

Gourc, J.P., Faure, Y., Rollin, A., and LeFlear, J. (1982) "Standard Tests of Permitivity and Application of Datcy's Formula", *Proc. 2nd Int. Conf. Geotextiles*, Las Vegas, NV, IFAI, Vol. 1, pp. 149-154.

Masounave, J., Rollin, A., and Denis, R. (1981) "Prediction of Permeability of Nonwoven Geotextiles from Morphometry Analysis", *J. Microscopy*, 121 (1), pp. 99-110.

Ingold, T.S. (1994) *The Geotextiles and Geomembranes Manual*, Elsevier Advanced Technology, Oxford, pp. 154-246.

Koerner, R.M. (1994) *Designing with Geosynthetics*, Prentice Hall, Englewood Cliffs, pp. 67-327.

ASTM Committee D-35 (1995) *ASTM Standards on Geosynthetics*, 4th ed.

Booth, J.E. (1968) *Principle of Textile Testing*, London: Newnes-Butterworths Publ.

Morton, W.E. and Heart, J.W. (1975) *Physical Properties of Textile Fibers*, New York: John wiley & Sons.

McGown, A., Andrawes, K.Z. and Kabir, M.H. (1982) "Load-Extension Testing of Geotextiles Confined in Soil." *Proc. 2nd Intl. Conf. Geotextiles*, Las Vegas, NV, IFAI, pp. 793-796.

Bhat, N. and McAvoy, T.J. (1989) "Use of Neural Nets for Dynamic Modeling and Control of Chemical Process Systems", *in Proc. 1989 American Control Conf.* pp. 1342-1347.

Hornik, K. (1989) "Multilayer Feedforward Networks are Universal Approximators", *Neural Networks*, vol.2, no. 5, pp. 359-366.

Sharpe, R.N., Mo-yeun Chow, Brigg S. and Windingland L. (1994) "A Methodology Using Fuzzy Logic to Optimize Feedforward Artificial Neural Network Configurations", *IEEE Transactions on Systems*, Man and Cybernetics, Vol.24, No.5.

Rustom, R., and Weggel, J. R (1993) "A Study of Erosion Control System: Experimental Result", *Proc. Intl. Erosion Control Assoc.*, Indianapolis

Theisen, M. S. (1992) "The Role of Geosynthetics in Erosion and Sediment Control: An Overview," *Journal of Geotextiles and Geomembranes*, Vol. 11

Static and Cyclic Behaviour of Sand Reinforced by Mesh Elements

J.C. Morel
Research Scientist, Ecole Nationale des Travaux Publics de l'Etat, Lyons, France

J.P. Gourc,
Professor, Lirigm, University Joseph Fourier, Grenoble, France

ABSTRACT: The technique involving micro-reinforcement of sand by mesh elements is used for surface soil layers that are likely to be subjected to cyclic loading conditions. Based on the triaxial test, a comparative study of reinforced and non-reinforced sand is carried out. The behaviour of the sand is enhanced by the presence of the micro-reinforcement elements: under low cyclic loading, the reinforced soil has a higher elasticity; under high cyclic loading, the mesh elements take up the load and the compressive strength is improved.

KEYWORDS: Micro-reinforcement, Triaxial test, Cyclic loading.

1. INTRODUCTION

This research paper concerns the change in behaviour of a sand when it is reinforced with small polypropylene mesh elements with external dimensions of 100 mm x 50 mm. Each individual mesh is a 10 mmx10 mm square. This type of reinforcement was designed by Mercer (Mercer et al., 1984) and optimised by Hytiris (Hytiris, 1986). The basic concept is the same as that of short-fibre reinforcement. However, the structure of the grid changes the implementation procedure and behaviour.

This type of reinforced sand has been the subject of a number of studies at the Lirigm, using the large shear box (Morel et al., 1997), and the biaxial compression test (Gourc et al., 1994, Morel et al., 1996) in plane strain conditions. The additional study presented here relates mainly to the behaviour of this material under cyclic compression using a triaxial testing apparatus.

Reinforced soils are reputed to have improved resistance to dynamic loading and fatigue compared to the same non-reinforced soils. Moreover, one of the main applications of this type of reinforcement concerns the surface layers subjected to repeated loading, for example as a result of traffic (this type of reinforcement can be used for unpaved roads). A comparative study of a sand with and without mesh elements would therefore seem to be of interest, especially as Lirigm was able to provide a high-performance triaxial test apparatus for cyclic loading.

Note that, in the case of the surface layer application, the reinforcing inclusions are required not only to improve the bearing capacity of the layer, but also to preserve its permeability, especially as this layer often serves as a draining layer. The compressibility under cyclic loading must therefore be reduced by the presence of the mesh elements.

2. EXPERIMENTAL CONDITIONS

The cyclic triaxial test apparatus at the Lirigm (Billet et al., 1990) can be used to test cylindrical samples of 70 mm diameter circular cross-section. The slenderness ratio (ratio of height to diameter) chosen here is equal to 1.9. The apparatus enables both the axial stress σ_1 and the lateral stress σ_3 to be cyclically slaved. During the tests described here, only σ_1 will vary cyclically. The cyclic loading is sinusoidal with time (frequency of 0.5 Hz in this case). This apparatus has already been successfully used to study the liquefaction of geotextile-reinforced sand (Billet et al., 1994; Richa, 1992; Vercueil et al., 1997). The lateral confining stress is kept constant at 100 kPa in all the tests presented.

The sand used for these tests has already been studied on numerous occasions at the University of Grenoble. It is known as Hostun RF sand, a siliceous sand of mean diameter $D_{50} = 0.35$ mm and uniformity coefficient $C_u = 1.7$. The grain density is $\rho = 2.7$ Mg/m^3.

Triaxial "static" compression tests were conducted for a unit weight value of 15 kN/m^3, corresponding respectively to void ratios of $e = 0.73$ and 0.66. All the "cyclic" compression tests were performed for $e = 0.73$, corresponding to a relative density $D_r = 56\%$.

The proportion of mesh elements added to the sand is characterised by the "reinforcement density, d_m" which, in %, is equal to the ratio of weight of mesh element with respect to the weight of the sand. It has been shown elsewhere (Gourc et al., 1994), that $d_m = 0.4\%$ was the reinforcement density providing the best compromise between:

- the favourable effect of the increase in number of mesh elements, implying a greater quantity of mesh elements subjected to tensile stress and thus improved overall strength of the reinforced soil,

- the unfavourable effect of the increase in number of mesh elements, involving disarrangement of the sand grains and thus a reduction in sand strength.

All the tests presented are for a value of d_m = 0.4%. The sand - mesh elements mixture is made after having moistened the sand (sand water content w = 10%) in order to obtain isotropic distribution of the inclusions. To make allowance for the scale of the test sample, the meshes are cut into 50 mm x 25 mm elements, without any asperities to avoid piercing the test sample membrane.

3. BIAXIAL TRIAXIAL COMPARISON (STATIC)

The Lirigm biaxial compression prototype testing apparatus can be used to perform tests in plane strain state (Gourc et al., 1994) but, with its present set-up, it cannot be used for cyclic compression tests. As a previous publication by the same authors described a study of mesh-element reinforcement based essentially on the biaxial apparatus, it seemed of interest to compare triaxial test results with biaxial test results, under the same "static" compression conditions. The test sample for the biaxial test was 340 mm long in the main vertical compression direction, 150 mm wide and 60 mm thick. Another experimental difference is that the biaxial test samples have lubrication on the ends whereas the triaxial samples do not.

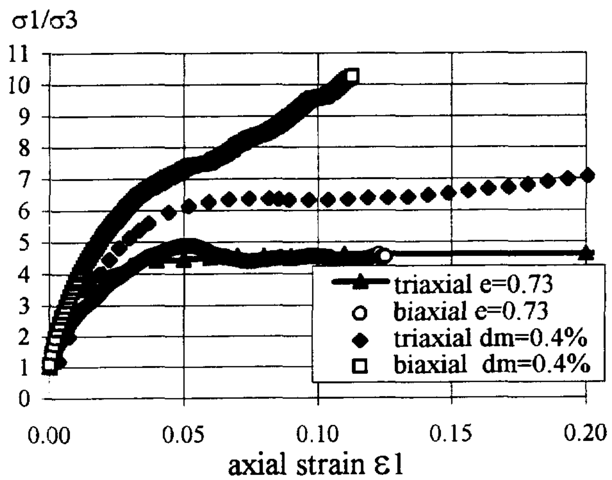

Figure 1 : Comparison of « static » tests, triaxial and biaxial tests

Lee (1970) and subsequently other authors showed on a non-reinforced sand that the angle of friction in the biaxial test is greater than the angle of friction in the triaxial test. This fact is confirmed by the tests described here.

Figure 1 compares the results obtained at Lirigm for a non-reinforced or reinforced (d_m = 0.4%) sand, presenting conventionally σ_1/σ_3 as a function of axial strain ε_1. The test is performed for an axial compression rate of 2 mm/min. In actual fact, this presentation can be justified only in the small strain range. For large strains, localised failure occurs and the mechanism involved is a block-on-block sliding mechanism (Desrues et al., 1985), as shown on photo 1 for a reinforced sand sample at the end of the test. In such cases it is more proper to present σ_1/σ_3 as a function of axial displacement: the curves obtained in biaxial and triaxial tests have much closer slopes in the large strain domain.

Generally speaking, the ductility of reinforced sand is clearly apparent. For the large strains reached, very few of the mesh elements had failed.

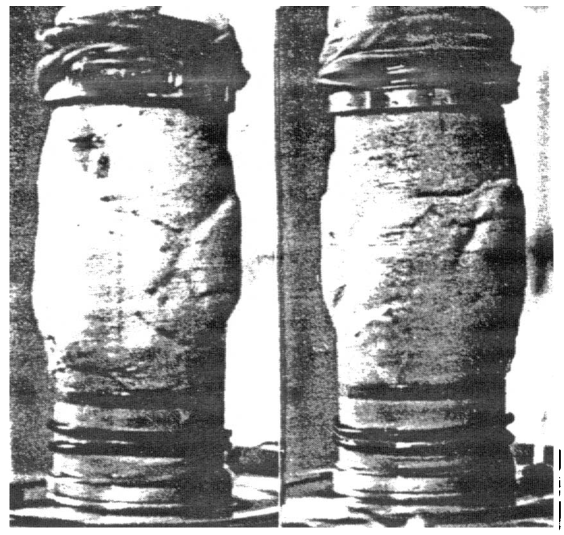

Photo 1 : Reinforced sand sample after failure at a « static » triaxial test.

4. BEHAVIOUR UNDER CYCLIC LOADING

The test procedure is similar in all cases:

- the confining pressure is kept constant (100 kPa),
- the first stage of the test ("static") corresponds to an increase in the deviatoric stress (σ_1 - σ_3) of 200 kPa/min.
- the second stage of the test corresponds to 500 cycles of 0.5 Hz frequency and 100 kPa amplitude from the initial value of the pre-defined deviatoric stress,
- the third stage of the test ("static") corresponds to the continued crushing of the test sample at a vertical displacement rate of 9.6 mm/min.

Figure 2 shows the change in axial settlement of the test sample during the cyclic loading stage, for three initial values of the deviatoric stress : 100 kPa, 200 kPa and 500 kPa. The behaviour of non-reinforced and reinforced sand is compared, except for the 500 kPa initial deviatoric stress because the non-reinforced sand failed for a deviatoric stress of 350 kPa under "static" conditions.

- Settlement on initial loading (N = 1) systematically reaches a greater value for the non-reinforced sand.
- The increase in vertical displacement with the number of cycles is also systematically higher for the non-reinforced sand.

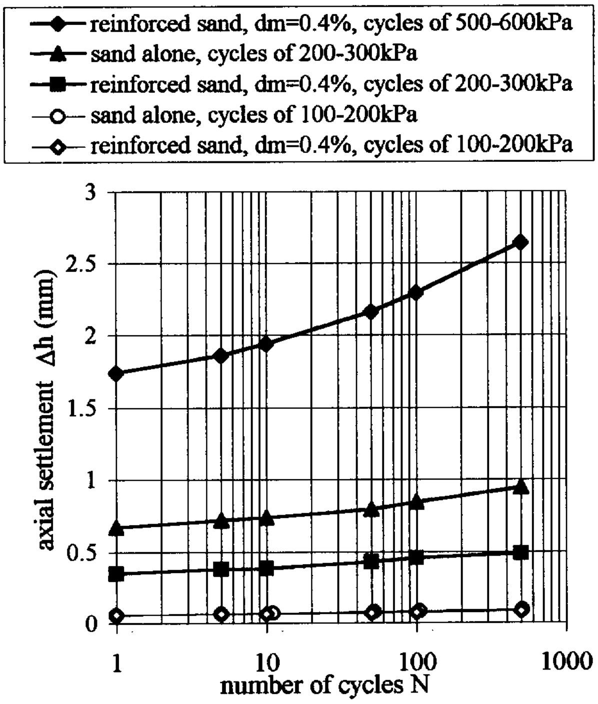

Figure 2: Cyclic loading stage: variation in vertical displacements as a function of number of cycles.

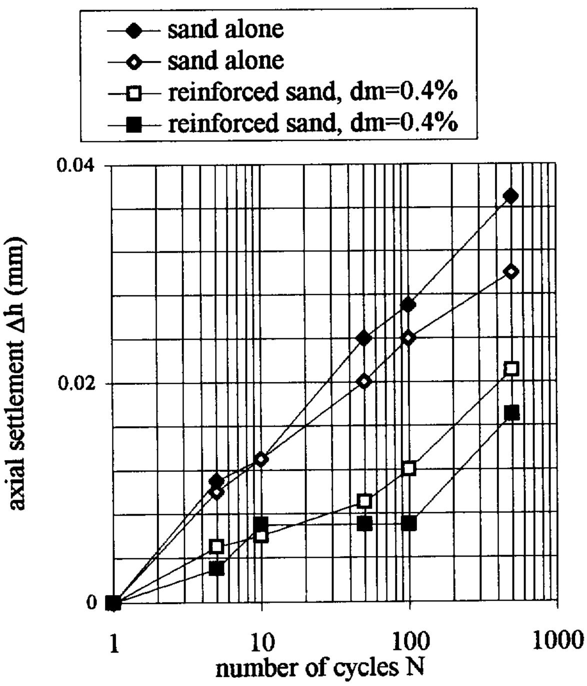

Figure 3: Cyclic loading stage (0-100kPa): variation in vertical displacements as a function of number of cycles, as from an initial loading of 100kPa

- A soil is generally considered to show acceptable behaviour under cyclic loading if the relationship between vertical displacement and log N is linear. In this case, it was found that this law is not obeyed for the non-reinforced sand (200-300 kPa) nor for the reinforced sand (500-600 kPa). The samples show a clear deviation from elastic behaviour.

The cyclic loading domain (0-100 kPa) is interesting because it corresponds to a possible range of use (surface layer) of this type of reinforcement. Both the reinforced sand and the non-reinforced sand are a long way from their failure state. Figure 3 adopts the same presentation as figure 2, except that the displacement under initial loading (N = 1) is not taken into account. The displacement scale is obviously different from that in figure 2. Two tests performed under the identical conditions are presented on the same graph, thereby showing the good repeatability of this relatively difficult type of test.

Vertical displacement for the reinforced sand is halved but, more surprisingly, the variation is no longer linear for values of N greater than 100 cycles.

5. INFLUENCE OF CYCLIC LOADING ON STATIC BEHAVIOUR

Figure 4 compares the behaviour of non-reinforced and reinforced test samples under triaxial compression with and without transient cyclic loading of 500 cycles between 200 and 300 kPa: for the reinforced sand, it is found that the test curves with or without transient cyclic loading coincide after the cyclic loading stage as if the material had somehow "forgotten" its loading history.

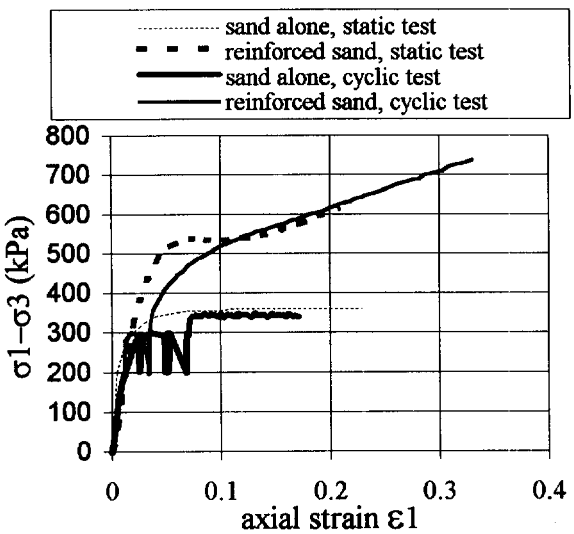

Figure 4: Comparative overall behaviour with and without transient cyclic loading (500 cycles) for reinforced or non-reinforced sand.

Figure 5 concerns only the reinforced sand and it is found that, contrary to the previous case, the cycles (500-600 kPa) well beyond the strength limit of the non-reinforced sand, have an effect on the post-cycle strength : the strength of the sand is increased through cyclic loading which has no doubt contributed to the mesh elements taking up the tensile stress. In a real-life situation, this could doubtless be obtained by controlled compacting.

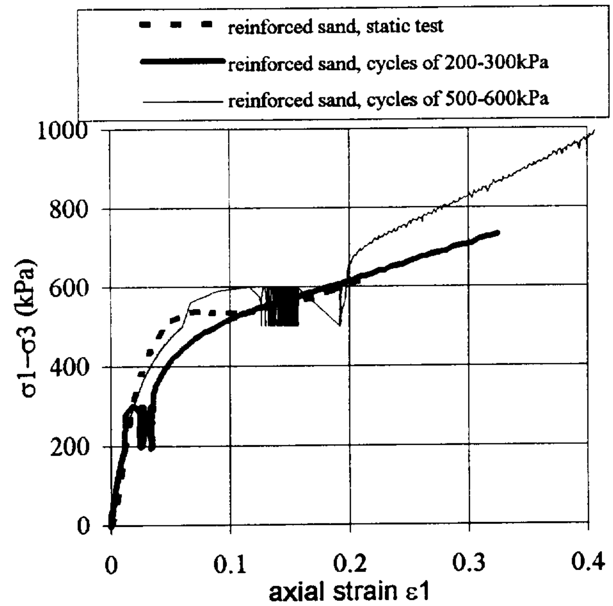

Figure 5: Comparative overall behaviour with and without transient cyclic loading (500 cycles) for reinforced sand.

6. INFLUENCE OF MESH-ELEMENT ORIENTATION

In the triaxial compression test, the direction of maximum strain is horizontal. The preferential orientation of the reinforcing inclusions should increase their efficiency. To verify this, a series of tests was conducted (fig. 6) in which the mesh elements are no longer placed randomly but in regularly spaced horizontal layers. In this case as well, the behaviour was compared for cases with and without cyclic loading. The reinforcement density ($d_m = 0.4\%$) is the same for the mesh elements oriented horizontally or randomly.

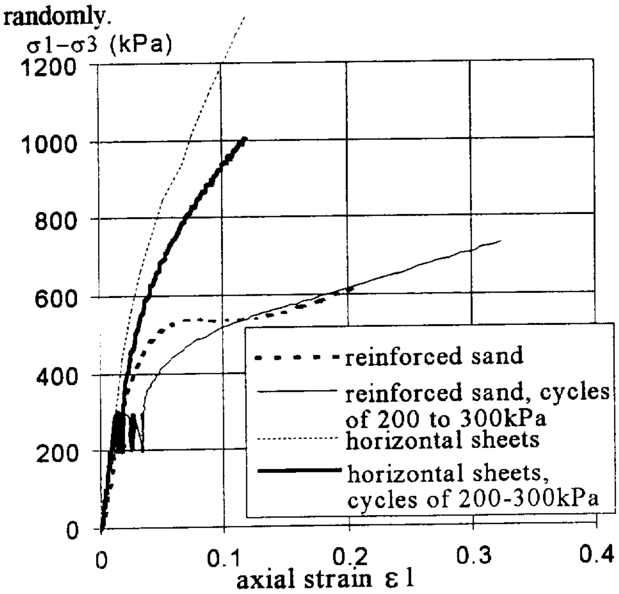

Figure 6: Comparative overall behaviour with and without transient cyclic loading (500 cycles) for horizontally or randomly reinforced sand.

For a given axial strain ε_1, the deviatoric stress is notably higher for the sample with mesh elements arranged horizontally. The strain values obtained under cyclic loading conditions are also much lower for horizontal mesh elements. However, the tests were not continued long enough to obtain sufficient strain values to achieve a possible coincidence of the curves corresponding to the tests with or without cyclic loading.

7. CONCLUSIONS

Triaxial compression tests under cyclic loading conditions were undertaken and show that reinforcement using mesh elements is a high-performance method, not only under "static" loading but also under «"cyclic" loading conditions. These observations should be used to improve their implementation procedures (pretensioning on compaction) and to find new applications.

8. REFERENCES

Billet, P., Cordary, D., Gourc, J.P. (1990) "Compression biaxiale d'un composite sol-géotextile", *Symposium Textile Composites in Building Construction*, Lyon, pp. 215-227

Billet, P., Cordary, D., Richa, B. (1994) "Laboratory study of sand liquefaction by the insertion of geosynthetics", *5th Int. Conference on Geosynthetics*, Singapore, pp. 537-540

Desrues, J., Lanier, J., Stutz, P. (1985) "Localization of the deformation in tests on sand sample", *Engineering Fracture Mechanics*, Vol. 21, pp. 909-921

Gourc, J.P., Morel, J.C. (1994) "Biaxial compression test on soil micro-reinforced by mesh-elements", *5th Int. Conference on Geosynthetics*, Singapore, pp. 365-368

Hytiris, N. (1986) "A new method of soil stabilization", *P.h.d.*, University of strathchyde, Scotland

Lee, K.L. (1970) "Comparison of plane strain and triaxial test on sand", *Journal of Soil Mechanics, ASCE*, May, pp. 901-921

Mercer, F.B., Andrawes, K.Z., Mc Gown, A., Hytiris, N. (1984) "A new method of soil stabilization", *Symposium on Polymer grid reinforcement in civil engineering"*, London, paper 8-1

Morel, J.C., Gourc, J.P. (1996) "Reinforced soil failure : Analysis at the biaxial compression test", *Int. Symposium on Earth Reinforcement*, Balkema, Fukuoka, pp. 111-116

Morel, J.C., Gourc, J.P. (1997) "Mechanical behaviour of sand reinforced by mesh elements", *Geosynthetics International*, Vol. 4, N° 5

Richa, B. (1992) "Étude au triaxial dynamique de la liquefaction des sols renforcés par géotextiles", *Thesis Dr University J.F. Grenoble*

Vercueil, D., Billet, P., Cordary, D. (1997) "Study of the liquefaction resistance of a saturated sand reinforced with geosynthetics", *Soil dynamics and earthquake engineering Journal*, (in press)

Stabilization of Earth Slopes with Fiber Reinforcement

Garry H. Gregory
Vice President - Senior Geotechnical Consultant, Fugro South, Inc., Fort Worth, Texas, USA

David S. Chill
Business Manager – Geofibers Business Unit, Synthetic Industries, Inc., Chattanooga, Tennessee, USA

ABSTRACT: The use of fiber reinforcement (geofibers) for stabilization of earth slopes was investigated by laboratory testing of non-reinforced and fiber-reinforced clay soils in the direct shear and triaxial shear apparatus. Fiber contents included 0.2 and 0.25 percent by dry weight for this study. The test results show increases in maximum shear stress (τ') at failure in the range of 20 to 50 percent for the fiber-reinforced specimens. Slope stability analyses were performed for a highway interchange embankment in Beaumont, Texas, USA, which had experienced repeated slope failures. The stability analyses produced an increase in calculated factor of safety from essentially one (imminent failure) for the non-reinforced case, to above 1.5 for the fiber-reinforced case. The slope was repaired with fiber-reinforced soil at a dosage rate of 0.25 percent, and has performed well to date.

KEYWORDS: Geofibers, Micro-reinforcement, Slope Stabilization, Earth slopes, Factor of Safety

1 INTRODUCTION

The use of geofibers for earth slope reinforcement has attracted significant interest in the past five years. Geofibers consist of relatively small fiber inclusions, distributed as an additive throughout the soil mass in the reinforced zone. Accordingly, the geofibers may be categorized as micro-reinforcement. Planar or continuous-sheet reinforcement elements, such as geotextiles and geogrids, are placed at discrete locations (usually horizontally) within the soil mass, with non-reinforced soil intervals between. Planar materials may be categorized as macro-reinforcement. Geosynthetic macro-reinforcement materials provide an effective solution to a wide variety of slope reinforcement problems, but have limitations in applications where the required anchorage zone is not available due to obstructions, as illustrated in Figures 1(a) and 1(b). Micro-reinforcement materials do not have these limitations since they reinforce the entire soil mass as a soil additive. The large anchorage zone is not required, and it is only necessary to extend the fiber-reinforced zone approximately 0.3 to 0.6 meters beyond the critical failure surface as illustrated in Figure 1(c). Therefore, micro-reinforcement geofibers can provide ideal solutions to slope stability conditions which previously were not practical with geosynthetics. The geofibers used in this study consisted of fibrillated polypropylene (FIBERGRIDS®, Synthetic Industries, Chattanooga, Tennessee, USA) in nominal 25 mm and 50 mm lengths.

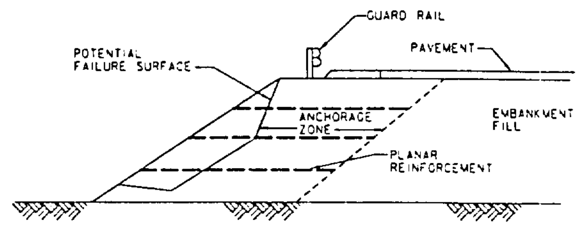

(a) anchorage-zone limitations from highway obstructions

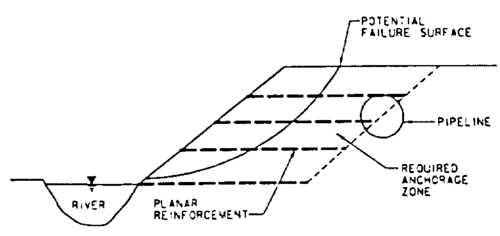

(b) anchorage-zone limitations from pipeline obstructions

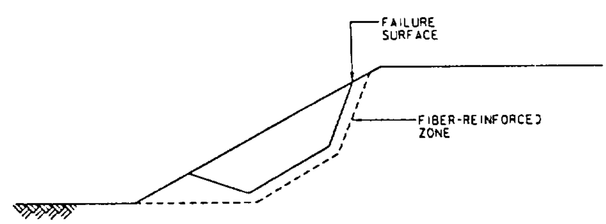

(c) large anchorage zone not required for geofibers

Figure 1. Anchorage-zone limitations of planar reinforcement compared to reinforced zone for geofibers.

2 BEAUMONT SLOPE

2.1 Project Description

The highway interchange embankment (Beaumont slope) is located at the intersection of U.S. Highway 69 and F.M. 347 in Beaumont, Texas, USA. The embankment is approximately 6 m in height at the tallest section, and has a slope ratio of 2.5 horizontal to 1 vertical (2.5H:1V) at the steepest section.

The fill soil in the slopes consists of a brown clay with some sand, gravel, and shells. The embankment soil has a liquid limit of 50, and a plastic limit of 17, with 68 percent passing the US No. 200 sieve. The material classifies as fat clay (CH), in accordance with ASTM D 2487. The embankment slopes on the northeast and northwest quadrants of this intersection had experienced repeated slope failures over the years. The failure-surface geometry typically consisted of a near-vertical scarp near the slope crest, a central failure surface about 1.5 to 2 m deep parallel to the slope, with an exit point about 1 to 1.5 m above the toe. These failures were typically repaired by excavating the failed areas and recompacting the same soil back into the slope without the use of soil additives or reinforcement. In the fall of 1995 both the northeast and northwest slopes had failed again. The northeast slope was repaired as previously described, without reinforcement or additives. The northwest slope was repaired with geofibers reinforcement. The laboratory testing program, slope stability analyses, and slope repair details are presented in subsequent sections.

2.2 Conceptual Model

A conceptual model was developed of the slope failure mechanism for use in planning the laboratory testing program and slope stability analyses. Embankment slopes of clay soils, with height ranges of 6 to 10 m and slope ratios in the range of 2.5H:1V to 3H:1V, often experience shallow failures within a few years after construction. The compacted soils initially have relatively high shear strength values throughout, and may have a significant level of preconsolidation stress induced by the compaction process.

Slope stability analyses using the "as compacted" shear strength properties do not predict the shallow failures. From these analyses, it is apparent that the initial as-compacted shear strengths deteriorate with time in the shallow zone. The strength loss is caused by a number of factors such as desiccation, shrink-swell, water infiltration, and down-hill creep. The principal author has investigated a large number of shallow slope failures in clay soils. The loss of shear strength is not uniform throughout the shallow zone. Three distinct soil zones are usually present, consisting of a weak zone along the failure surface, a weathered zone above the failure surface, and the relatively undisturbed zone below the failure surface. The actual failure surface may be less than 10 mm thick in many cases. The material in the thin failure zone is usually of a soft, paste-like consistency, with a high moisture content. This zone has obviously lost the preconsolidation stress induced during the compaction process, and has degraded to a normally-consolidated condition at the shallow overburden pressure. Consequently, under effective-stress conditions, the soil in the failure zone will have $c' = 0$. The principal author has found similar thin, paste-like weak zones paralleling the surface at depths of about 1.5 to 2 m in adjacent embankments which had not experienced slope failures, but which later failed. Accordingly, it is believed that the weak normally-consolidated zone is created prior to actual failure by the weathering processes previously discussed, and by stress concentrations at the base of the weathered zone due to down-hill creep. The weathered soil in the zone above the failure surface generally contains many desiccation cracks and secondary weathering features, and the soil mass in this zone has a substantially lower shear strength than when initially compacted. However, this zone may still retain some long-term cohesion, and will exhibit a higher mass shear strength than the failure zone. The embankment soil below the failure surface in the deeper zone may remain relatively undisturbed and retain most or all of its initial shear strength. The laboratory testing program and slope stability analyses were performed in a manner consistent with the three distinct soil zones.

3 LABORATORY TESTING PROGRAM

3.1 Sample Preparation and Testing

The laboratory testing program included non-reinforced (control) and fiber-reinforced soil specimens. The direct shear tests were performed as consolidated-drained (CD) tests, and included nominal 100-mm and 300-mm square specimens, and the ICU triaxial tests were performed on nominal 70 mm-diameter by 150 mm-length specimens. The direct shear tests included specimens prepared by standard compaction methods (95 percent ASTM D 698), and slurry-processed normally-consolidated (SPNC) specimens. All triaxial tests for this study were performed on specimens prepared by standard compaction methods. A consolidation test was also performed on a compacted specimen of the Beaumont clay, to determine the preconsolidation stress induced by the compaction process. The preconsolidation value was used in interpreting the direct shear test results.

The SPNC specimens were prepared by blending the soil in a mixer with sufficient water to form a thick slurry. The slurry was then partially consolidated in a 150-mm diameter CBR apparatus under approximately 70 percent of the normal stress to be used in the direct shear device. Following a consolidation period of about 24 hours, the sample reached a thick paste-like consistency, at which time it was removed from the CBR apparatus and trimmed into a 100-mm square shear box for testing. The remainder of the consolidation stage was completed in the direct shear machine, with the final consolidation stress equal to the normal stress to be used during the shear test. The normal stress range was selected to represent conditions along the actual failure surface in the slope. This procedure assured that the specimen would be normally consolidated during the test, to model the condition along the actual failure surface. Standard-compaction specimens were prepared using a controlled weight-volume relationship and static compaction techniques. The reinforced specimens were prepared by mixing the fibers and soil in a heavy-duty 19-liter mixer. Detailed descriptions of the sample preparation methods are available in a design guide for fiber-reinforced slopes (Gregory 1996).

3.2 Test Results

A total of 86 direct shear specimens and 32 triaxial shear specimens of clay soils were tested for this study. Twenty - one of the direct shear specimens were tested in the 300 mm square shear device, and the remainder were tested in the 100 mm square shear device. Twenty of the direct shear specimens and 12 of the triaxial shear specimens were performed for the Beaumont slope project. The remainder of the tests were performed for other slope projects or for research purposes.

Direct shear test results performed on 12 specimens of the Beaumont clay are presented on shear stress-normal stress plots in Figure 2. These tests were performed in a 100 mm square by 30 mm deep shear box. The geofibers were 25 mm in length for the reinforced specimens. The strain rate was 0.0076 mm/minute for all direct shear tests.

Figure 2 contains results for 8 specimens prepared with standard compaction methods. Figure 2 (a) was plotted using a bilinear fit. The first three points on each envelope have normal stress values below the preconsolidation stress induced by compaction (P_{cc}), and the fourth point is above the P_{cc} value. Clay soils during shearing, with normal stresses below the preconsolidation stress, may exhibit significant effective cohesion (c'), while those with normal stress values above the preconsolidation value exhibit $c' = 0$ (Gregory and Doane, 1996). Accordingly, the strength envelopes in Figure 2(a) were fit with a bilinear line to obtain shear strength parameters in both the preconsolidated and normally consolidated (NC) ranges of normal stress. The test results show an increase of approximately 35 percent in c' for the reinforced specimens compared to the non-reinforced.

Increases in ϕ' were 15 and 27 percent, respectively, for the preconsolidated and NC ranges of normal stress.

Figure 2(b) contains results performed on 6 specimens prepared by SPNC methods. The results in this figure were plotted with a linear fit since all specimens were normally consolidated during the tests. These results show an increase in ϕ' of 33 percent for the reinforced specimens compared to the non-reinforced. Triaxial shear test results performed on 6 specimens of the Beaumont clay are presented in Figure 3. These specimens were prepared using standard compaction methods, and were performed as ICU tests, with pore-pressure measurements. A strain rate of 0.015 mm/minute was used for these tests.

Figure 3(a) contains the results of three non-reinforced specimens plotted on a mohr-coulomb shear stress-normal stress diagram. Figure 3(b) contains the results of three specimens reinforced with 0.25 percent, 25 mm-long fibers. The test results on the specimens reinforced with 25 mm-long fibers in Figure 3(b) show an increase in ϕ' of 16.5 percent, and an increase in c' of 8.5 percent, when compared to the control test results.

Four mechanisms are believed to be involved in the increased shear strength of fiber-reinforced soil. These mechanisms are : (1) friction between individual fibers and the surrounding soil, (2) adhesion between individual fibers and the surrounding soil, in soils exhibiting significant cohesion properties, (3) micro-bearing capacity of the soil mobilized during pull-out resistance of looped fibers crossing the shear plane, and (4) increased localized normal stress in the soil across the shear surface resulting from the pull-out resistance of the fibers during shearing of the soil. The individual interaction and contribution of these mechanisms to the apparent increase in shear strength is complex and difficult to determine accurately. However, the combined effects, including any synergistic effects, is relatively easy to determine by conducting shear strength tests on both non-reinforced and reinforced specimens, as was performed for this study.

A summary of average direct shear and triaxial shear test results from all specimens tested during this study is presented in Table 1.

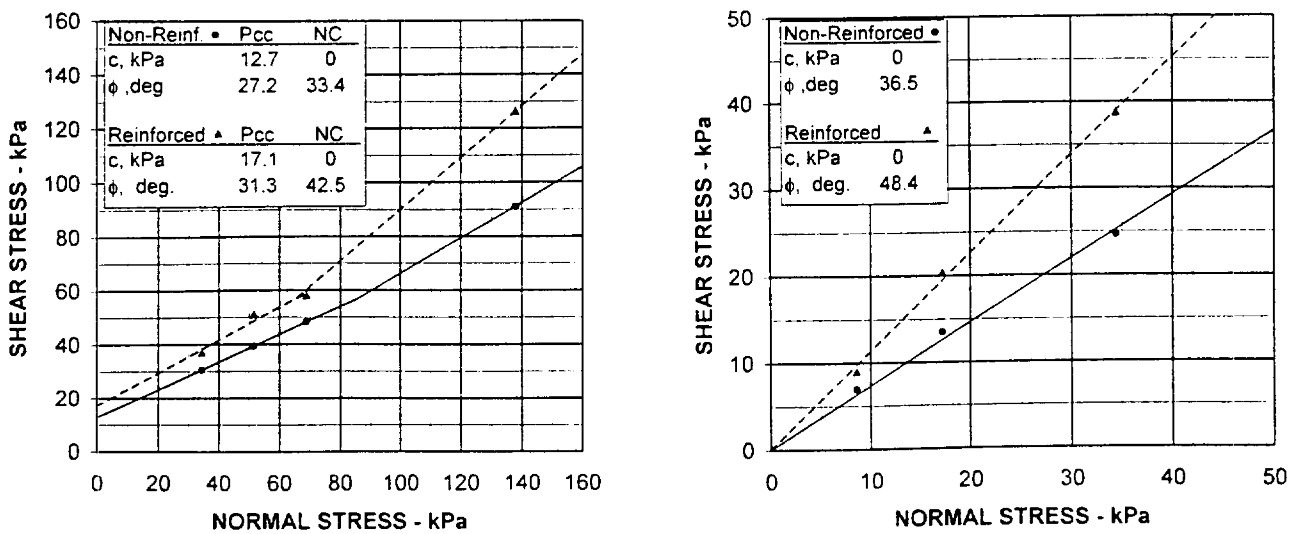

(a) Standard Compaction

(b) SPNC Preparation

Figure 2. Direct shear test results on 100 mm Specimens.

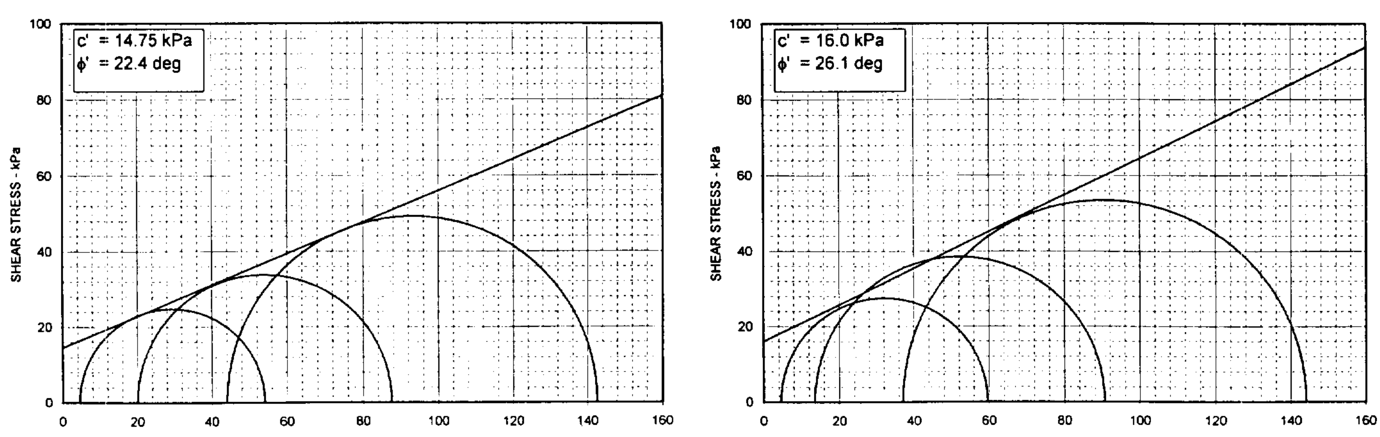

(a) Non-reinforced Specimens

(b) Reinforced Specimens

Figure 3. Triaxial test results on 70mm diameter specimens.

Table 1. Summary of Direct Shear and Triaxial Shear Test Results (Average values, including 0.2 and 0.25 % fibers)

Test Description	Number of Specimens	ϕ' (Deg.)	c' (kPa)
Direct Shear – 100mm Non-Reinforced	25	32.6	6.6
Direct Shear – 100mm Reinforced – 25mm Fibers	40	38.0	10.0
Direct Shear – 300mm Non-Reinforced	6	27.7	3.1
Direct Shear – 300mm Reinforced – 25mm Fibers	9	27.3	6.7
Direct Shear – 300mm Reinforced – 50mm Fibers	6	22.8	9.5
Triaxial Shear Non-Reinforced	9	22.0	14.8
Triaxial Shear Reinforced – 25mm Fibers	16	24.4	15.9
Triaxial Shear Reinforced – 50mm Fibers	7	30.8	15.4

It should be understood that the results in Table 1 are average values, based upon a range of fat clay (CH) and lean clay (CL) soils tested for this study. The averages for the direct shear tests in the 100mm device show increases of approximately 17 percent and 52 percent in ϕ' and c', respectively, for the reinforced specimens. The averages for the direct shear tests in the 300mm device show essentially the same ϕ' values, and an increase in c' values of 116 percent for the specimens reinforced with 25mm fibers. The average results from the 300mm direct shear device also show a decrease of 21 percent in ϕ' values and an increase of 206 percent in c' values for the specimens reinforced with 50mm fibers. The triaxial shear test average results show an increase in ϕ' values of 11 percent and an increase in c' values of 7 percent for the specimens reinforced with 25mm fibers. The average triaxial results with the 50mm fibers show an increase of 40 percent in ϕ' values, and an increase of 4 percent in c' values. In all cases where one shear strength parameter increased only a small amount or decreased slightly, the other parameter increased by a relatively large amount. Averaging the results in Table 1 for all clay types tested resulted in considerably more scatter than was observed for each individual soil type tested.

4 SLOPE STABILITY ANALYSES

4.1 Slope Geometry

The geometry of the existing slope, slide geometry, and subsurface stratigraphy were obtained from observations and measurements in the field, and from existing data and a new soil boring provided by the Texas Department of Transportation (TxDOT).

4.2 Soil Parameters

The soil parameters were obtained from the laboratory test results, adjusted in accordance with local practice. The unit weight values for the in situ soils were obtained from thin-wall tube samples taken from the boring. The unit weight values of the compacted soils were taken as 95 percent of maximum density as determined by ASTM D 698. Soil shear-strength parameters selected for the analyses are presented in Table 2. The labels and soil type numbers match those on the graphical output sheets from the computer analyses, presented in subsequent sections. The unit weight values are not included in Table 2, in order to conserve space. Unit weight values of 18.9 and 20.9 KN/m^3 were used for moist and saturated unit weights, respectively.

4.3 Analysis Methodology

Slope stability analyses of the Beaumont slope were performed using the computer program GSTABL7, an enhanced version of PCSTABL6 (Humphrey and Holtz, 1986), modified by the principal author. The limit equilibrium method, using a sliding-block search routine and the Modified Janbu method (Janbu 1954, 1973), was used in the analyses.

Table 2. Soil Parameters Selected for the Stability Analyses

Label	Soil type No.	c' (kPa)	ϕ' (Degrees)
Analysis of Initial Failure (Non-Reinforced)			
Surface-CH clay	1	9.3	24
Shoulder-CH clay	2	9.3	24
Weak-CH clay (failure surface)	3	0.0	32
Fill-CH clay	4	11.1	24
Base-CH clay	5	11.1	24
Deep-CH clay	6	11.1	24
Analysis of Repaired Slope (Fiber-Reinforced)			
Surface-CH clay	1	10.2	24
Shoulder-CH clay	2	10.2	24
Weak-CH clay (failure surface)	3	0.0	42
Fill-CH clay	4	11.1	24
Base-CH clay	5	11.1	24
Deep-CH clay	6	11.1	24

The shear strength of the failure surface zone (Weak-CH clay) was obtained from the direct shear test results on the SPNC specimens. The shear strength of the undisturbed embankment fill (Fill-CH clay) below the failure surface and in the protected shoulder of the roadway was obtained from the direct shear test results on the specimens prepared with standard compaction methods. In accordance with local practice and experience with similar soils, the ϕ' and c' values obtained in the tests were reduced by approximately 12 percent for use in the analyses, to account for uncertainties in stratigraphic distribution and construction quality control.

The shear strength of the surficial soil in the weathered zone (Surface-CH clay) above the failure surface cannot be obtained readily with laboratory tests. Samples taken from this zone will not be representative of the desiccation cracks and secondary weathering features throughout the soil mass. However, the apparent shear strength of the weathered zone may be obtained by computer analyses, using the known data.

The shear strength values of the failure-surface and undisturbed-fill zones are known from laboratory test results. The geometry of the failure surface is known from observations and measurements in the field, following failure. It is also known that the stability factor of safety (resisting forces and moments divided by the driving forces and moments) for the slope at the time of failure was one or slightly below one. Therefore, stability analyses of the failed slope can be performed with the known shear strengths of the failure-surface and undisturbed fill zones, and an initial estimate of the mass shear strength parameters in the weathered zone. An iterative analysis can then be performed by changing the estimated shear strength

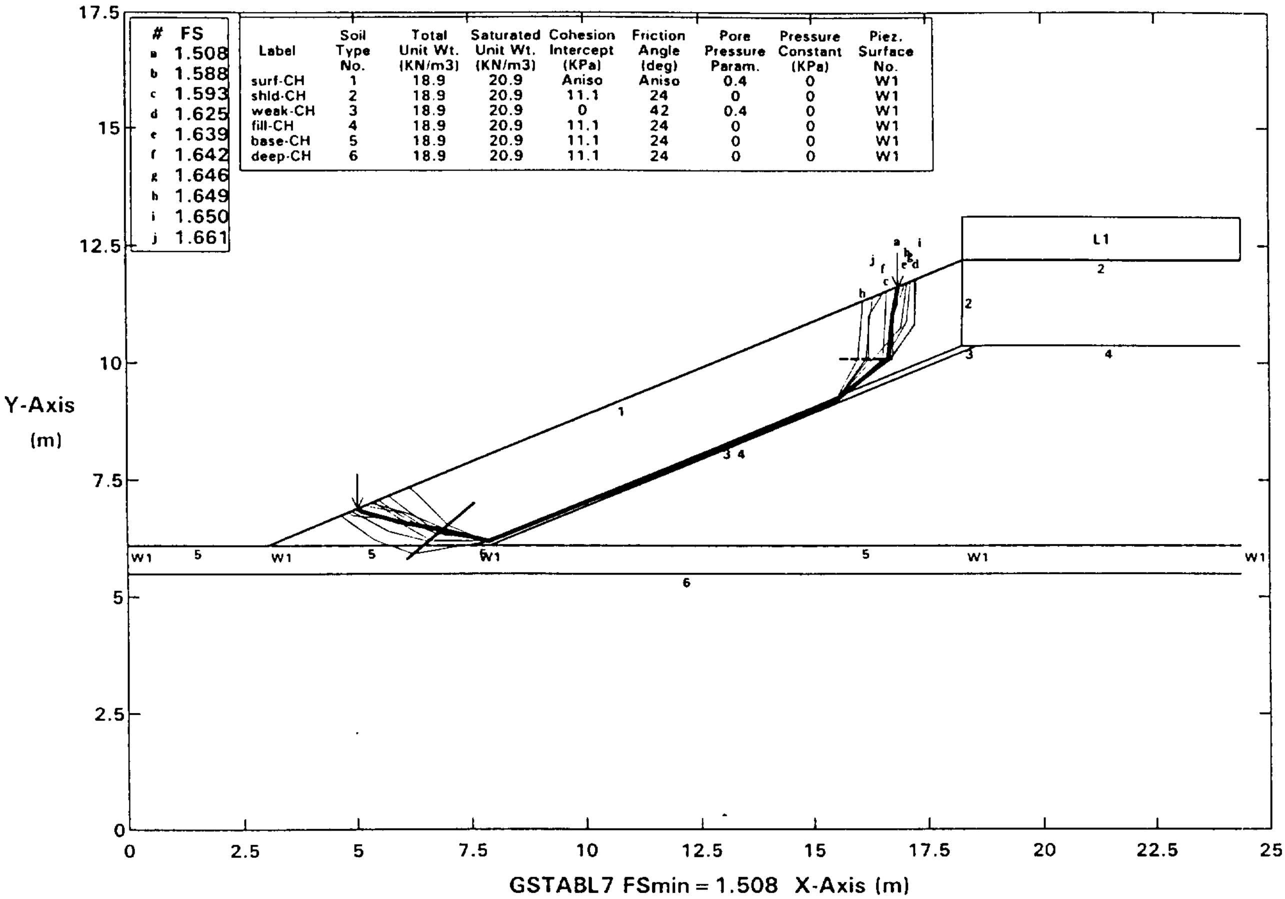

Figure 4. Graphical Computer output for the fiber-reinforced slope analysis.

parameters in each successive run until the calculated factor of safety converges to one or slightly below one. The changes in strength parameters can generally be applied uniformly to both ϕ' and c'. It has been found from experience that a good initial estimate of the shear strength parameters for the weathered zone is approximately 50 percent of those of the undisturbed fill zone.

The mass shear strength of the fiber-reinforced weathered zone may be determined as follows. Assume that the ratio of the shear strength of the reinforced weathered zone to the shear strength of the fiber-reinforced laboratory specimens, is the same as the ratio of the shear strength of the non-reinforced weathered zone to the shear strength of the non-reinforced laboratory specimens. The shear strength of the non-reinforced weathered zone to be used in the ratio comparisons is the value determined in the iterative analyses discussed previously. This approach provides rational values of shear strength parameters in all soil zones, for both the initial failure condition and fiber-reinforced slope condition.

The stability analyses were performed using the sliding-block search routine by forcing the trial failure surfaces to pass through the failure zone parallel to the slope, while allowing the trial surfaces to exit near the upper and lower ends of the slope in a more random manner. The weathered zone was assigned anisotropic properties in the analyses, with zero shear strength within zones plus or minus 10 degrees from vertical, to model tension cracks. The failure-surface zone was modeled as 150 mm thick for convenience in the analyses, although it is much thinner in the actual slope. For each analysis run, 110 trial failure surfaces were evaluated. The results of the slope stability analysis for the fiber-reinforced slope are presented in Figure 4 for illustration purposes. The initial failure analysis is not shown to conserve space. The 10 most critical (with respect to calculated factor of safety) trial failure surfaces are plotted in the figure. The most critical trial failure surface is shown with the heavy line. The failure surfaces are labeled with lower case letters, in ascending order of calculated factor of safety. The soil types are numbered below each boundary. The highway traffic loading at the top of the slope was included as a uniformly distributed load with an intensity of 9.6 kPa, and is shown on the figure by the designation L1. The ground-water surface detected in the boring is shown near the toe elevation with the designation w1. The ground-water surface and soil zones below the failure-surface zone were not used in the shallow failure analyses, but were used in a deep-seated global analysis performed for this slope, but not included in this study.

The slope stability analyses show an increase in calculated factor of safety from 1.007 (imminent failure) for the initial failure to 1.508 for the repaired, fiber-reinforced slope. This is an increase in calculated factor of safety of approximately 50 percent due to the geofiber inclusion.

5 CONSTRUCTION AND PERFORMANCE

5.1 Construction

The slope was repaired in late November of 1995 in general accordance with the assumptions made in the analyses. The area was prepared by excavating the failed area approximately 0.6 m below the primary failure surface. The excavated soil was spread in approximately 200 mm-thick loose lifts prior to compaction. Geofibers were spread at the calculated dosage rate of 0.25 percent by dry weight of soil, and each lift was processed and the 25 mm-length fibers mixed into the soil with a minimum of three passes of a roto-till pulverizing mixer of the type commonly used in lime-subgrade stabilization. Each lift was compacted to approximately 95 percent of maximum dry density at a moisture in the general range of optimum to 5 percentage points wet of optimum in accordance with ASTM D 698. The fill was placed in essentially horizontal lifts.

5.2 Performance

The fiber-reinforced northwest slope has performed well to date. No additional signs of movement have been observed. The northeast slope at the same interchange was repaired without fiber reinforcement approximately six weeks prior to the northwest slope. The non-reinforced slope has again failed.

6 ADDITIONAL PROJECTS

The authors have been involved in more than 10 slope projects on which geofibers were utilized for slope repair and stabilization. These projects have included roadway embankments, pipeline embankments adjacent to rivers or creeks, and an earth-fill dam. One of the pipeline projects involved the use of geofibers for deep-seated stability, as well as shallow stability. The oldest installation of geofibers on these projects was completed approximately six years ago. Most of the other projects were completed within the past three years. These installations have performed well. A detailed discussion of these projects is not possible due to space limitations.

7 CONCLUSIONS

The use of geofibers for earth slope reinforcement was investigated by laboratory testing of non-reinforced and fiber-reinforced specimens of compacted clay soils. A highway embankment slope in Beaumont, Texas, USA, was used as the primary case study. Extensive slope stability analyses were performed for the initial failure and fiber-reinforced slope conditions. The factor of safety was increased from essentially one at the initial failure condition, to approximately 1.5 for the repaired slope using the same soil reinforced with geofibers.

Increases in effective shear strength (τ') in the range of 20 to 50 percent due to geofibers inclusion were observed for this study, based upon ϕ' and c' increases from laboratory tests and the slope geometries considered. Similar increases in shear–strength parameters using fiber reinforcement have been reported by other researchers (Maher and Ho 1994, Alwahab and Al-Ourna 1995, Nataraj and McManis 1997). Additional research and development of analysis methods for the reinforcement mechanisms and influence of fiber properties are needed. Ranjan, et al (1996) performed a study of these influences and proposed a model for analysis of fiber-reinforced cohesionless soils.

Based upon the results of this study, observation of actual installations of fiber-reinforced slopes, and research performed by others, the geofibers are a viable and cost effective method for slope repair using micro-reinforcement where macro-reinforcement elements may not be practical due to space limitations for the anchorage zone. The geofibers can provide solutions to an entire class of slope problems which were not previously practical with geosynthetics.

Additional research is desirable using a broader range of fiber lengths and soil types. Standardization of laboratory testing and analysis methods is needed. Additional case histories are needed, and are expected to occur at an accelerated rate due to the increased use of geofibers.

REFERENCES

Alwahab, R.M., and Al-Ourna, H.H., 1995. "Fiber Reinforced Cohesive Soils for Application in Compacted Earth Structures," *Geosynthetics '95 Conference Proceedings*, Nashville, Tennessee, USA.

Gregory, G.H., Fugro-McClelland, (Southwest), Inc., and Synthetic Industries, *Design Guide for Fiber-Reinforced Soil Slopes*, Version 1.0, October 1, 1996.

Gregory, G.H., and M.L. Doane, 1996. "Shear Strength of Fill With Direct Shear Device," *Proceedings of the Texas Section Fall Meeting*, Geotechnical Session, ASCE, San Antonio, TX, pp. 101-110.

Humphrey, D.N., and Holtz, R.D., Purdue University, Users Manual for STABL6, with *Reinforcing Layer Option,* JHRP86/18, October 1986.

Janbu, N., 1954. "Application of Composite Slip Surface for Stability Analysis," *European Conference on Stability of Earth Slopes,* Stockholm, Sweden.

Janbu, N., 1973. "Slope Stability Computation," *Embankment-Dam Engineering, Casagrande Volume,* Edited by R.C. Hirschfeld and S.J. Poulos, John Wiley & Sons, New York, pp. 47-86.

Maher, M.H., and Ho, Y.C., "Mechanical Properties of Kaolinite/Fiber Soil Composite," *American Society of Civil Engineers*, Journal of the Geotechnical Engineering Division, Volume 120, No. 8, August, 1994.

Nataraj, M.S., and McManis, K.L., 1997. "Strength and Deformation Properties of Soils Reinforced with Fibrillated Fibers," *Geosynthetics International*, Vol. 4, No. 1, pp. 65-79.

Ranjan, Gopal, Vasan, R.M., and Charan, H.D., "Probabilistic Analysis of Randomly Distributed Fiber-Reinforced Soil," *American Society of Civil Engineers, Journal of Geotechnical Engineering Division*, Vol. 122, No. 6, June 1996.

Effect of Geotextile Reinforcement on the Stress-Strain and Volumetric Behavior of Sand

A.K. Ashmawy
Assistant Professor, Department of Civil and Environmental Engineering, University of South Florida, Tampa, Florida, USA.

P.L. Bourdeau
Associate Professor, School of Civil Engineering, Purdue University, West Lafayette, Indiana, USA.

ABSTRACT: Geosynthetic-reinforced soils exhibit a significant increase in strength compared with unreinforced soils. In this study, triaxial test results for a sand reinforced with horizontal geotextile inclusions and subjected to both monotonic and cyclic loading are presented. The influence of the inclusions on the stress-strain and volumetric behavior is investigated. It is shown that a large increase in deviator strength is attained when reinforcement is used. An increase in ductility is also observed, and is essentially due to the blocking of development and propagation of the shear band within the specimen. When subjected to cyclic loading, the reinforced sand accumulates less axial deformation than the unreinforced sand. Even though the unreinforced soil is contractive, a reduction in potential for volume change is introduced by the geotextile reinforcement. It is demonstrated that this reduction in volume change potential is mainly due to the increase in confinement.

KEYWORDS: Geotextiles, Reinforcement, Cyclic, Shear strength, Deformation.

1. INTRODUCTION

Over the past few decades, a large number of geosynthetic-reinforced earth structures, such as retaining walls, have been constructed worldwide. In order to better understand the reinforcement mechanisms acting in large-scale reinforced soil structures, it is necessary to first evaluate such mechanisms at the small-scale in a controlled laboratory environment. So far, three reinforcement mechanisms have been identified in the literature, namely passive or pullout anchorage, membrane action, and confinement enhancement (Ashmawy and Bourdeau 1995). Confinement enhancement has been attributed to the mobilization of shear stresses along the soil-geosynthetic interface, thereby reducing the lateral spread of the soil, as illustrated in Figure 1.

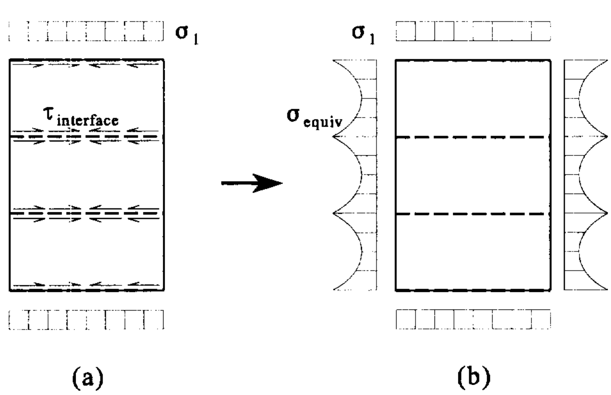

Figure 1. Confinement enhancement mechanism (a) interface shear stresses ; (b) equivalent confining pressure.

Most of the earlier experimental studies have focused on assessing the confinement enhancement mechanism under monotonic loading conditions. For example, Ingold and Miller (1983) investigated the confinement enhancement mechanism with the aid of radiographic analysis on clay specimens reinforced with plastic porous discs. The influence of the permeability of the reinforcement was examined in a study by Fabian and Fourie (1986) who tested high and low permeability inclusions. Ling and Tatsuoka (1994) conducted plane strain tests on a silty clay reinforced with three types of geosynthetics, to simulate the response of retaining walls.

Analytical models were proposed by Ingold and Miller (1983) and Chandrasekaran et al. (1989) to estimate the increase in monotonic strength of axisymmetric soil specimens reinforced with horizontal discs. In the latter model, the increase in strength is essentially expressed as a function of reinforcement spacing and specimen diameter. In both models, assumptions need to be made concerning the amount of shear stress mobilization along the reinforcement-soil interface.

One of the few studies dealing with the influence of confinement enhancement on the cyclic response of sand was conducted by Madani at al. (1979). The reinforcement material consisted of horizontal discs of aluminum foil, equally spaced along the triaxial specimen. It was concluded that the cyclic response of the reinforced sand essentially depends on the reinforcement spacing. In the present study, drained monotonic and cyclic triaxial tests are performed on sand reinforced with horizontal discs of woven and nonwoven geotextiles. The main purpose of the study is to compare the performance of the specimens under monotonic and cyclic loading conditions, and to evaluate, experimentally, the contribution of confinement enhancement to the monotonic strength and to the deformability of the reinforced sand under cyclic loading.

2. TESTING PROGRAM

The tests were performed on a commercially available "Concrete Sand" reinforced with horizontal discs of woven and nonwoven geotextiles. The properties of the sand and the geotextiles are listed in Table 1 and 2, respectively.

Table 1. Properties of Concrete Sand.

Maximum unit weight	18.8 kN/m^3
Minimum unit weight	15.5 kN/m^3
Coefficient of uniformity	3.6
Coefficient of curvature	1.5
Specific gravity	2.65

Table 2. Properties of geotextiles.

Classification	Woven	Nonwoven
Product name	Stabilenka 200	Typar 3801
Mass/unit area[a]	450 g/m^2	261 g/m^2
Tensile strength[b]	220 kN/m	20 kN/m
Stiffness at 10% strain[b]	2000 kN/m	120 kN/m

[a] ASTM D3776
[b] ASTM D 4595

The 71 mm diameter sand specimens were moist-tamped at six layers, each 28.3 mm high. A target dry unit weight of 16.5 kN/m^3 was selected, corresponding to a relative density of 35%. In general, sands do not exhibit contractive behavior in axial compression except at very loose states or at high confining pressures. Consequently, dilation was observed for the unreinforced sand specimens tested under both undrained and drained conditions. Based on drained and undrained monotonic tests on the unreinforced sand, the effective angle of internal friction, ϕ' was found to be 37°, within the effective confining stress range of 0 to 400 kPa.

The reinforcement was placed between the moist-tamped layers. In total, five horizontal discs of geotextile were equally spaced at 28.3 mm along each specimen. In addition, geotextile discs were placed at both specimen ends. The specimens were then saturated by flowing de-aired water and back-pressuring.

The testing program is outlined in Table 3. All tests were performed at a confining pressure of 50 kPa. It is believed that such low stress levels are typical in reinforced soil applications, such as small retaining walls and embankments. For the cyclic tests, a deviator cyclic stress amplitude corresponding to 80% of the monotonic strength of the unreinforced soil was selected. Axial load and volume change were measured during the displacement-controlled monotonic tests, while axial deformation was recorded as a function of number of cycles during the load-controlled cyclic tests.

Table 3. Outline of the testing program.

Test	Loading mode	Geotextile
U-UR	Monotonic undrained	None (unreinforced)
M-UR	Monotonic drained	None (unreinforced)
M-NW	Monotonic drained	Nonwoven
C-UR	Cyclic drained	None (unreinforced)
C-NW	Cyclic drained	Nonwoven
C-WV	Cyclic drained	Woven

3. EXPERIMENTAL RESULTS

The monotonic test results indicate, as expected, a significant increase in terms of strength when the geotextile reinforcement is used. As shown in Figure 2a, the failure strength of the reinforced sand under drained conditions is approximately four times greater than that of the unreinforced. Although the initial stiffness is almost the same for both cases, the reinforced specimen exhibited less brittle behavior and reached its maximum strength at a much higher strain level. From the volume change versus axial strain plot in Figure 2b, it is concluded that the presence of geotextile reinforcement also reduces the potential of volume change.

Unreinforced undrained and drained, and reinforced drained stress paths are plotted in Figure 3, where $p=\frac{1}{2}(\sigma_1+\sigma_3)$, $p'=\frac{1}{2}(\sigma'_1+\sigma'_3)$, and $q=\frac{1}{2}(\sigma_1-\sigma_3)$. In the unreinforced undrained case, the stress path is distinctly traveling along the failure envelope beyond a mean effective stress of approximately 100 kPa. The strength increase introduced due to the presence of the reinforcement can be interpreted as an increase in the effective angle of internal friction (ϕ'). The apparent effective friction angle of the reinforced soil is 62°. An apparent increase in ϕ' of 25° was therefore introduced by the nonwoven geotextile reinforcement.

Plots of cumulative axial and volumetric strain versus number of cycles are presented in figure 4. It is interesting to note the cyclic volume change response. Although the sand was dilative during monotonic loading, its cyclic behavior is purely contractive. This is attributed to the fact that, unlike monotonic loading, cyclic loading allows for a gradual rearrangement of particle packing, thereby causing continuous changes in soil structure as a function of loading

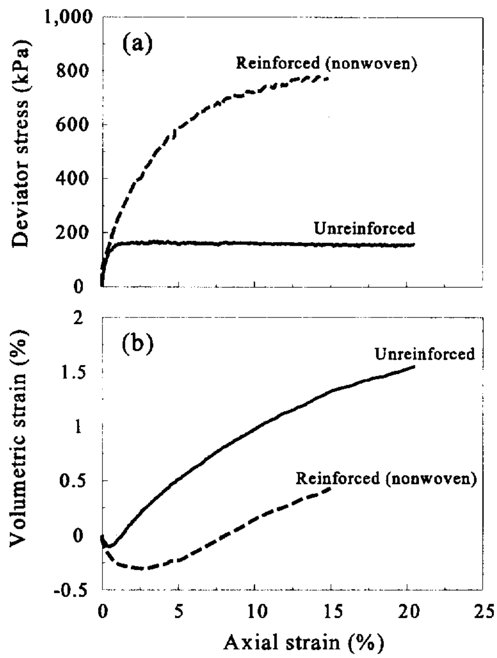

Figure 2. (a) Stress-strain and (b) volumetric response of unreinforced and reinforced concrete sand.

cycles. From a conceptual standpoint, if the amplitude of cyclic loading is not large enough to cause dilation during a given loading cycle, the volume will either remain unchanged, or more likely will slightly increase.

As shown in Figure 4, the use of geotextile reinforcement caused the rate and magnitude of cumulative axial strains to decrease. Also the tendency of the material to change its volume is smaller. This decease in volume change tendency or potential is attributed to the enhanced lateral confinement provided by the geotextile reinforcement. The woven geotextile provided better reinforcement than the nonwoven. Although no tests were performed to characterize the sand-geotextile interface properties, it is believed that, because of its geometry, the woven geotextile pore size matches better the soil particle size.

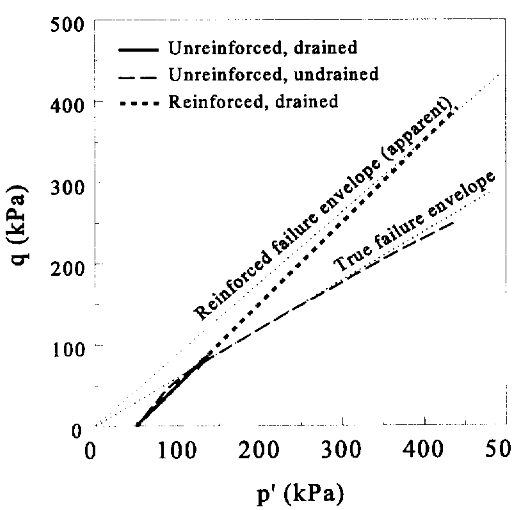

Figure 3. Stress paths and failure envelopes for unreinforced and reinforced specimens.

4. DISCUSSION

As mentioned earlier, the presence of the reinforcement during monotonic loading causes the sand to have a lower tendency for volume change under both drained and undrained conditions. In Figure 1, the mobilized frictional stresses along the interface act toward reducing the lateral or radial spreading of the material.

In the cyclic case, however, the sand is contractive rather than dilative, which may lead one to believe that the use of the reinforcement would be ineffective. It is difficult to understand the role of the reinforcement in this case without looking at the change in average area rather than volume, versus number of cycles. The plot shown in Figure 5 demonstrates that although the volume of all the specimens decreases with increasing number of cycles, the area does not. For the unreinforced case, the area of the specimen continuously increases, albeit at a decreasing rate, even at a high number of cycles. This outward radial spreading of the material, accompanied by the reduction in volume due to cyclic loading, causes a rapid increase in cumulative axial strains.

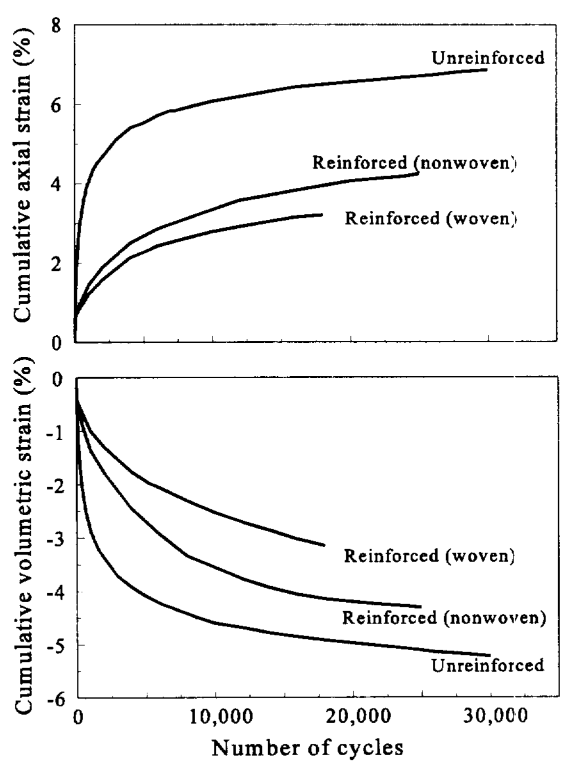

Figure 4. Variation in axial and volumetric strain as a function of number of cycles.

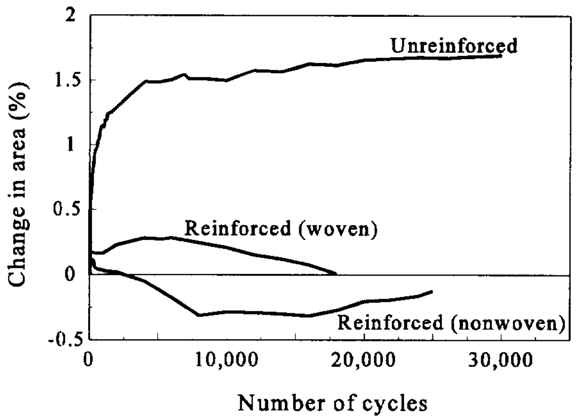

Figure 5. Change in specimen area as a function of number of cycles for the unreinforced and reinforced cases.

When geotextile reinforcement is used, the confinement enhancement causes a reduction in this radial spreading. After a very small initial increase in area during the first few cycles, the area of the specimen barely changes. Although a slight decrease of approximately 10 mm^3 was measured beyond a certain point for the nonwoven-reinforced specimens, this does not seem to be logically possible and is essentially due to the low resolution of the volume change measurement system. A significant difference in change in area is, however, evident when the response of the reinforced specimens is compared with that of the unreinforced specimen. The additional enhanced confinement, physically reflected in the smaller change in area, causes an increase in the average effective confining stress within the soil, therefore reducing its tendency for volume change.

5. CONCLUSIONS

Monotonic and cyclic drained triaxial tests were performed on unreinforced and reinforced sand specimens. The reinforcement consisted of geotextile discs, both woven and nonwoven, placed horizontally at equal spacing along the specimens. The experimental results indicate that the presence of the reinforcement resulted in a significant increase in monotonic shear strength of the soil and a reduction in its cyclic deformability. The volume change potential decreased in both the monotonic and cyclic cases when reinforcement was used, regardless of the tendency for contraction or dilation of the unreinforced soil. Under both monotonic and cyclic loading, the reduction in volume change was attributed to the equivalent confinement enhancement introduced by the geotextile reinforcement. The confinement enhancement mechanism was verified experimentally by monitoring the change in average specimen area during loading.

ACKNOWLEDGMENTS

Financial support was provided by the Swiss Federal Department of Transportation, Communication, and Energy, Grant No. OFR 2/92. The geotextile specimens were supplied by Reemay, Inc., and by the Nicolon Corporation. Additional support was supplied by the School of Civil Engineering at Purdue University.

REFERENCES

Ashmawy, A.K. (1995) "Analysis and Modeling of the Response of Geotextile-Reinforced Soil to Monotonic and Cyclic Loading", Ph.D. Thesis, Purdue University, West Lafayette, Indiana, USA, 268 pp.

Ashmawy, A.K., and Bourdeau, P.L. (1995) "Geosynthetic-Reinforced Soils Under Repeated Loading: A Review and Comparative Design Study", *Geosynthetic International*, Vol. 2, No. 4, pp. 643-678.

Chandrasekaran, B., Broms, B., and Wong, K.S. (1989) "Strength of Fabric Reinforced Sand under Axisymmetric Loading", *Geotextiles and Geomembranes*, Vol. 8, pp. 293-310.

Fabian, K., and Fourie, A. (1986) "Performance of Geotextile-Reinforced Clay Samples in Undrained Triaxial Tests", *Geotextiles and Geomembranes*, Vol. 4, pp. 53-63.

Ingold, T.S., and Miller, K.S. (1983) "Drained Axisymmetric Loading of Reinforced Clay", *Journal of Geotechnical Engineering*, ASCE, Vol. 109, No. 7, pp. 883-898.

Ling, H.I., and Tatsuoka, F. (1994) "Performance of Anisotropic Geosynthetic-Reinforced Cohesive Soil Mass", *Journal of Geotechnical Engineering*, ASCE, Vol. 120, No. 7, pp. 1166-1184.

Madani, C., Long, N.T., and Legeay, G. (1979) "Comportement Dynamique de la Terre Armée à l'Appareil Triaxial", *Compte Rendu*, Colloque International sur le Renforcement des Sols, Paris, France, Vol. 1, pp. 83-88. (in French)

Numerical Simulation of Dynamic Behavior of Soil with Reinforcement

R.H. CHEN
Professor, Institute of Civil Engineering, National Taiwan University, R.O.C.

T.C. CHEN
Ph.D. Candidate, Institute of Civil Engineering, National Taiwan University, R.O.C.

ABSTRACT: Dynamic tests on soils with reinforcement are generally time consuming and expensive. Numerical simulation is another approach to improve the understanding of the dynamic behavior of reinforced soils. The numerical simulation of dynamic triaxial tests presented in this paper considers the reinforced soil a homogenous material with transversely isotropic property. The reinforcement is polyethylene sheets, representing the stiff reinforcement. For the purpose of comparison, laboratory tests are performed as well. As the results show, there is agreement between the simulation and the testing results.

KEYWORDS: Reinforced soil, Numerical simulation, Dynamic triaxial test.

1 INTRODUCTION

The property tests of reinforced soils are generally difficult to perform, because of difficulty preparing reinforced specimen and estimating representative specimen size. Moreover, due to lack of instruments and devices and the high operational skill needed, performing dynamic triaxial tests is not common. However, numerical simulation is another approach that may be used to improve our understanding of the dynamic behavior of reinforced soils. In this paper the numerical simulation is studied. Firstly, the reinforced soil is considered as a homogenous composite with nonlinear (or piece-wise linear) anisotropic elasticity constitutive properties. The cyclic loading and boundary conditions are similar to those of real tests. Numerical methods are used to evaluate the performance of this equivalent composite. For comparison, a series of dynamic triaxial tests are performed as well.

2 LITERATURE REVIEW

In numerically simulation of reinforced soils, two methods generally used, i.e., the separated method and the equivalent homogenous method. The former represents each component of reinforced soil, soil and reinforcement, are represented by different mathematical elements. The latter considers, from a macroscopic view, reinforced soil as a homogenous medium. The advantage of the separated method is that the interaction between soil and reinforcements as well as the internal forces of reinforcements can be found. However, it requires more complex parameters in numerical simulation, such as the material properties of both soil and reinforcements. Additionally, the interaction model between soil and reinforcements is needed and plays a very important role, yet an acceptable model has not been developed.

The homogenized approach employs the composite concept with anisotropic mechanical theory to characterize the complex behavior of reinforced soils. Lesniewska (1996) pointed out that, to use this method the structure should be at least in accordance with mechanically homogeneity.

In homogenous methods, the reinforced soil can be simulated as an anisotropic homogenous medium by distributing the strength or the stiffness of reinforcements upon that of the soil element from a weighted viewpoint (Romstad et al. 1976; Sawicki 1983; De Buhan et al. 1989; Wu 1989; White and Holtz 1992). Among the anisotropic models, orthotropic and transversely isotropic models are most commonly used. In an equivalent homogenous method, Harrison and Gerrad (1972) considered the soil reinforced by non-extensible strips as an equivalent homogenous material in elastic condition. The stress-strain relation of reinforced soil is assumed cross-anisotropic elastic, and elastic constants were derived. However, the nonlinear property of reinforced soils was not considered.

3 NUMERICAL MODELING

3.1 Constitutive Relation

There are several considerations important in simulation. The composite concept is used to homogenize the reinforced soils into an equivalent homogenous medium with the transversely isotropic model to characterize reinforced soil. Since the stress-strain relation of soil is nonlinear, the soil behavior is simulated by a hyperbolic model. A plane strain condition is considered as well, because of considering real structures situation.

The scheme of soil and the reinforcement as well as the equivalent homogenous element are shown in Figure 1. Both the soil and the reinforcement are assumed isotropic.

In short, the constitutive model is derived and formulated as follows, according to the force equilibrium, strain compatibility, and anisotropy elasticity.

$$E_h = \frac{(A+B)^2 - (\nu_r A + \nu_s B)^2}{A+B}$$

$$\frac{1}{E_v} = \frac{1}{E_r}(\eta_r - 2\nu_r C) + \frac{1}{E_s}(\eta_s - 2\nu_s D) + \frac{2(C+D)}{\frac{E_r C}{\nu_r} + \frac{E_s D}{\nu_s}}$$

$$\nu_{hh} = \frac{\nu_r A + \nu_s B}{A+B}$$

$$\nu_{hv} = \frac{(1-\nu_r)A + (1-\nu_s)B}{A+B}\left[C+D\right]$$

$$\frac{1}{G_{vh}} = \eta_r \frac{2(1+\nu_r)}{E_r} + \eta_s \frac{2(1+\nu_s)}{E_s}$$

$$A = \frac{\eta_r E_r}{1-\nu_r^2}; \quad B = \frac{\eta_s E_s}{1-\nu_s^2}; \quad C = \frac{\eta_r \nu_r}{1-\nu_r}; \quad D = \frac{\eta_s \nu_s}{1-\nu_s}$$

$$E_s = E_{si}\left(1 - \frac{E_{si}\varepsilon}{(\sigma_1 - \sigma_3)_{ult} + E_{si}\varepsilon}\right)^2; \quad E_{si} = K_s Pa\left(\frac{\sigma_m}{Pa}\right)^{ns}$$

where

E_h : tangent modulus of the composite in horizontal direction
E_v : tangent modulus of the composite in vertical direction
ν_{hh} : Poisson's ratio of the composite that characterizes the transverse strain in horizontal direction due to the horizontal stress.
ν_{hv} : Poisson's ratio of the composite that characterizes the transverse strain in horizontal direction due to the vertical stress.
G_{vh}: shear modulus of the composite in vertical direction
E_r : tangent modulus of the reinforcement
ν_r : Poisson's ratio of the reinforcement
η_r : volumetric ratio of the reinforcement
E_s : tangent modulus of the soil
ν_s : Poisson's ratio of the soil
η_s : volumetric ratio of the soil
E_{si} : initial tangent modulus of the soil
K_s: soil constant
ns: soil constant
σ_m: mean stress
ε : strain
Pa: atmospheric pressure

3.2 Analysis Procedure

The FLAC computer program (1993) was used in the numerical analysis. The analytical procedure is shown in Figure 2. The constitutive law of the above formulae is introduced into numerical model by the FISH function of FLAC. Basically, FLAC code solves the fundamental governing equations of a continuum by an explicit finite difference method, thus the stress-deformation relation of a continuum is found. The step starts from the input of soil and reinforcement properties. The input of material properties and parameters shown in Table 1 are adopted from soil and reinforcement testing, according to ATSM standard, individually. In addition, Table 2 lists the initial tangent moduli of the soil tested for hyperbolic model (Duncan and Chang 1970). The reinforcement is polyethylene sheet and is considered to be linear elastic in small strain conditions. The next step is generating the numerical grid and the boundary conditions. After completing this step, the remaining operations will be executed by the program until the result is found.

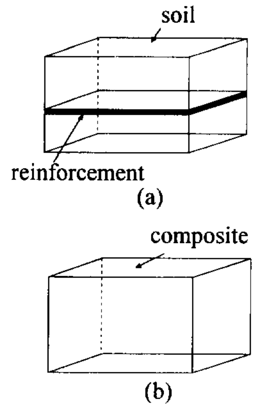

Figure 1. Schematic of (a) reinforced soil element, (b) equivalent composite.

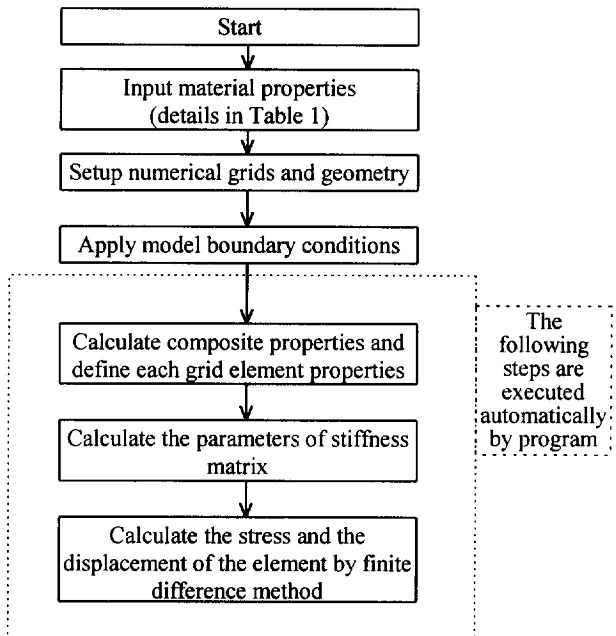

Figure 2. Numerical simulation procedure.

3.3 Dynamic Triaxial Test and Numerical Simulation Model

For qualitative comparison and simplicity, a series of

Table 1. Input parameters.

Property (unit)	Reinforcement	Soil
Poisson's ratio ν_r	0.32	
Volumetric ratio η_r	0.03	
Young's modulus (MPa)	2171	
Poisson's ratio ν_s		0.3
Volumetric ratio η_s		0.97
Material constant K_s		858.62
Material constant ns		1.95
Yield stress (kPa)*		$(\sigma_1 - \sigma_3)_f$

*Yield stress is calculated from the Mohr-Coulomb model.

Table 2. The initial tangent modulus of soil.

Confining pressure (kPa)	Initial tangent modulus (MPa)
50	189.69
75	260.02
100	303.66

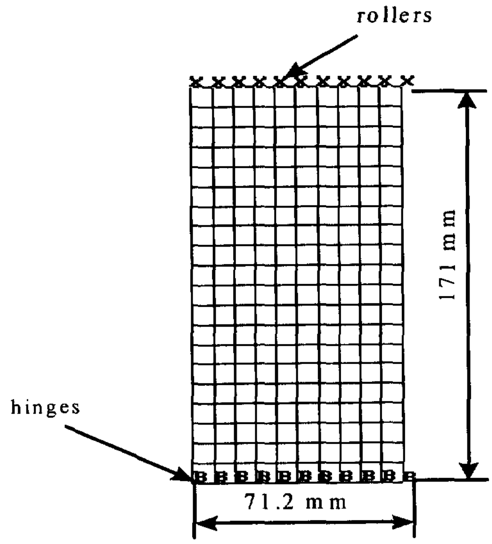

Figure 3. Numerical grid and boundary conditions of the specimen.

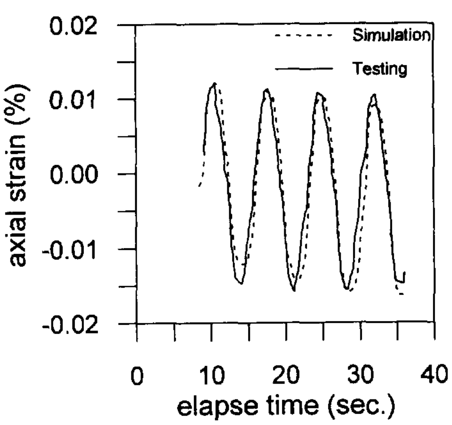

Figure 4. Axial strain versus elapsed time under 50 kPa confining pressure.

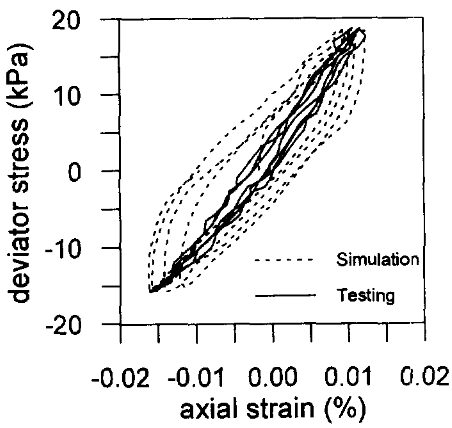

Figure 5. Deviator stress versus axial strain under 50 kPa confining pressure.

commonly used dynamic triaxial tests on reinforced soils are performed. This is because plane strain tests are rarely available in practice. The dynamic triaxial testing equipment is designed by Chan and Mulilis (U.C. Berkeley), and a cyclic loading and stress controlling device was used. The test methods are briefly mentioned below.

The soil is C109 Ottawa Sand, which consists primarily of rounded quartz particles. It is prepared with a relative density of 73%. The specimen is 71.2 mm in diameter, 171 mm in height. Three, equally spaced, horizontal layers of polyethylene sheet reinforcement were placed in the specimen. The polyethylene sheet is 68 mm in diameter and 0.2 mm thick. The Young's modulus and the tensile strength are 2171 MPa and 7.78 kN/m respectively, according to ASTM D4595-86 testing specification. Two different confining pressures 50 kPa and 75 kPa are applied.

In accordance with the test situation, the numerical model of the specimen is arranged as shown in Figure 3. Hinges are set at the bottom and rollers are set at the top of the core, respectively. The loading process used in the numerical analysis is similar to the testing procedure.

4 RESULTS AND DISCUSSION

The comparison between testing and simulation results are shown in Figures 4 to 7. Figures 4 and 5 are for confining pressure equal to 50 kPa, and Figures 6 to 7 are for confining pressure equal to 75 kPa. In the figures, the dashed lines and solid lines stand for the simulation and test results, respectively.

Figure 4 shows that both the results appear a slightly viscous characteristic. The axial strain of numeric

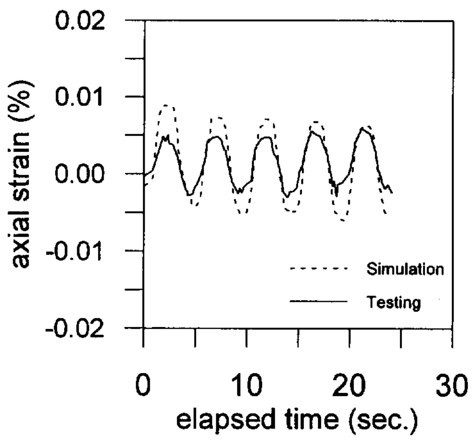

Figure 6. Axial strain versus elapsed time under 75 kPa confining pressure.

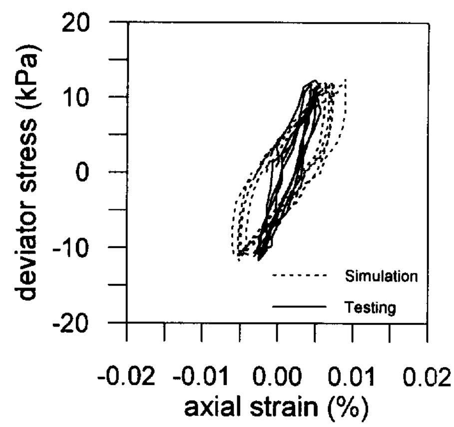

Figure 7. Deviator stress versus axial strain under 75kPa confining pressure.

simulation decayed with time, with each cycle of loading, and the hysteresis loops enlarged, shown in Figure 5. In contrast, the result from the testing maintained the same loop size than the simulation result. This is because the numerical model has introduced nonlinear properties of soil, and the viscous characteristic of reinforced soil is considered in this study. Thus, the simulation result shows the hysteresis behavior. It is noticed that the testing curve seems to be a little twist, this is because the curve is plotted from the raw testing data without regression. Except for the viscous influence, the amplitude and trajectory of axial strain in Figure 4 and the slopes of stress and strain in Figure 5 show good agreement.

In Figures 6 and 7, because the confining pressure increases, both average slopes of solid and dashed lines are larger than those in Figures 4 and 5. The hysteresis loops in Figure 7 are also more condensed than those in Figure 5. This means that the energy dissipation under higher confining pressure is less than under lower confining pressure for each cycle of applied load. The other evidence of this, finding in Figure 6, is the trajectory of the solid lines does not decay. The paths of both lines coincide but slightly differ in the maximum amplitude. This difference is due to testing device, non-uniformity in the cross sectional area of the specimen, imperfect homogeneity of a specimen, and not exactly plane strain condition of testing. However, the result of the simulation is reasonable. From the figures shown above, there is agreement between the simulation and the testing results.

5 CONCLUSION

This study attempts to characterize reinforced soils under cyclic loading by an equivalent homogenous approach. The reinforced soil is considered as a composite by employing the transversely isotropic properties and nonlinear stress-strain relations. Comparison of results from dynamic triaxial tests and numerical simulation show that there is agreement between the two.

REFERENCES

De Buhan, P., Mangiavacchi, R., Nova, R., Pellegrini, G., and Salencon, J. (1989) "Yield Design of Reinforced Earth Walls by a Homogenization Method", *Geotechnique*, Vol. 39, No. 2, pp. 189-201.

Duncan, J.M. and Chang, C.Y. (1970) "Nonlinear Analysis of Stress and Strain in Soils", *Journal of Soil Mechanics and Foundations*, ASCE, Vol. 96, pp. 1629-1653.

FLAC program (1993) Itasca Consulting Group, Inc.

Lesniewska, D. (1996) "Classification of Reinforced soil Structures Based on Their Possible Failure Mode", *Proceedings of the International Symposium on Earth Reinforcement*, Fukuoka, Japan, pp. 401-406.

Harrison, W.J. and Gerrard, C.M. (1972) "Elastic Theory Applied to Reinforced Earth", *Journal of Soil Mechanics and Foundations,* ASCE, Vol. 98, pp. 1325-1345.

Romstad, K.M., Herrmann, L.R., and Shen, C.K. (1976) "Integrated Study of Reinforced Earth - I: Theoretical Formulation", *Journal of Geotechnical Engineering*, ASCE, Vol. 102, pp. 457-471.

Sawicki, A. (1983) "Plastic Limit Behavior of Reinforced Earth", *Journal of Geotechnical Engineering*, ASCE, Vol. 109, pp. 1000-1005.

Wu, T.H. (1989) "Behavior of Soil - Geotextile Composites and Its Application to Finite Element Analysis", *Geosynthetics '89*, San Diego, USA, pp. 365-372.

White, D.M. and Holtz, R.D. (1992) "Seismic Analysis of Reinforced Slope - A Review", *Proceedings of the International Symposium on Earth Reinforcement Practice,* Fukuoka, Japan, pp. 311-316.

Rail Transport Support Upgradation - Potential Evaluation of Innovative Geosynthetics

V.K. Jain
Executive Director,Geotechnical Engg., Research, Designs & Standards Organisation, Ministry of Railways, Manak Nagar, Lucknow-226011, India.

A. Azeem
Geotechnical Research Engineer, Research, Designs & Standards Oganisation, Ministry of Railways, Manak Nagar, Lucknow-226011, India.

ABSTRACT: Indian Railways have recorded manifold increase in traffic levels, speeds and axle loads in recent decades. Since the track formation was initially constructed to cater for a very low level of traffic, speed and axle load, the increase in structural demand on old formations have lead to severe failures. The paper examines the factors governing stability of subgrades, reviews the practice/methodologies of its design and strengthening. It also gives details and findings of field trials using low strength, low modulus geotextiles and geomeshes. Based on model studies, the potential of high strength, high modulus bi-oriented geogrids is established which is under evaluation through field trials.

KEYWORDS: Geogrids, Geotextiles, Model tests, Rail Road Applications, Reinforcement.

1 INTRODUCTION

On Indian Railways, manifold increase in traffic level, speed and axle loads have been recorded in the recent decades.

Parameter	Year 1950	Year 1996	Projected (2000)
Traffic level (Gross Million Tonne)	100	400	500
Speed (Kmph)	75	140	160
Axle Load (tonne)	14	20.32	25

Most of this increase is on core routes known as golden quadrilateral of approx. length 11500 Kms. With liberalisation, Indian economy is growing at a targeted rate of 6 to 7% per year and railway traffic is expected to increase by 8 to 9%. As majority of track subgrades were initially constructed to cater for a very low level of traffic, axle loads and speeds, the manifold increase in traffic levels have placed a much greater level of structural demand on the existing track support. This has resulted in several subgrade failures. As on March 97, 750 Km of track is under permanent speed restriction due to weak subgrade. In addition, temporary speed restrictions are imposed during monsoons for about 500 Km. This results in slow down of trains, loss of carrying capacity and greater maintenance inputs.
Conventional method of subgrade improvement is replacement of poor subgrade with granular material. In most of the locations, the depth of replacement is worked out to be 70cm and above. This is difficult to implement in field due to high volume of traffic and lack of track possession. This depth can be reduced by 30 to 40% if granular material is reinforced with one layer of high strength high modulus bi-oriented geogrids. With reduced depth, the work can be executed under running traffic conditions without needing track possession.

2 METHODOLODY OF TRACK SUB-STRUCTURE DESIGN

Till recently, track subgrade designs were largely based on empirical approaches. Collaborated studies were carried out to assess the state of stresses inside the subgrade and to evolve a rational methodology for its design. Its main features are :

i) The graphs have been developed for induced stresses for different modular ratios (ratio of elastic modulus of subgrade to elastic modulus of soil), depth of construction and axle load. A graph for 25t axle load is placed as Fig.1. (Yudhbir et- al,1993)
ii) Undisturbed soil samples are collected from the site and are tested on Dynamic Triaxial Apparatus simulating field loading in laboratory to assess its threshold strength.
iii) The depth of subgrade construction is designed on the principle that induced stresses on the soil should be less than its threshold strength.

3 SUBGRADE STABILIZATION TRIALS USING INNOVATIVE GEOTEXTILES.

Based on extensive literature studies, tentative specifications for geotextiles to be used for stabilization of subgrade were formulated (Table-1). Trial laying of geotextiles conforming to the above specifications were undertaken on a problematic fine grained subgrade needing excessive maintenance inputs on a double line track. Geotextile was placed under a ballast cushion of 250mm, sandwiched between two nominal sand layers of thickness 50mm each. The post-treatment observations revealed that the upward migration of fines was checked by geotextile, however, the fabric continued to deform and eventually ruptured under outer rail seat (Fig.2). The study revealed that light weight, low modulus non-woven geotextiles are only effective in controlling upward migration of fines but could not contribute in arresting the shear failures.

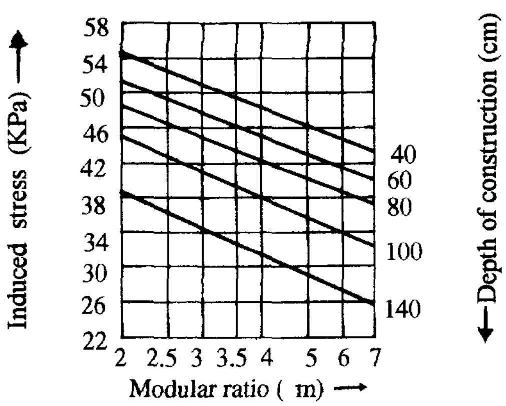

Figure 1. Induced Stresses at Subgrade(Yudhbir et- al,1993)

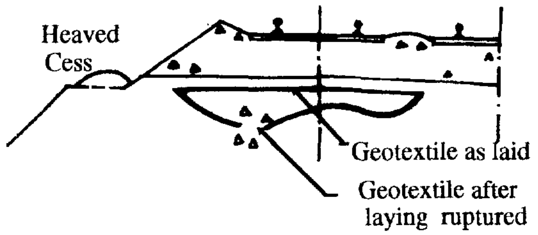

Figure 2. Subgrade Stabilization Trial using Geotextiles.

It was then decided to use available varieties of low strength, low modulus unoriented unstretched geomeshes (Netlon - India Grade CE 121, CE 131) in the similar fashion on problematic subgrades failing in shear on a single line track. Similar to geotextiles, this geomesh also continued to deform under passage of traffic and eventually ruptured near the rail seats (Fig.3).

Field trials using low modulus geotextiles as well as geomeshes amply demonstrated their limitations in preventing subgrade shear failures. The potential of high strength high modulus bi-oriented geogrids was thereafter evaluated.

Table 1. Specifications of Geotextile for Track Stabilizations

Parameters	Specifications
1. Composition	Polypropylene/Polyester. (Polyester to be used only in non-alkaline environment. Coloured fabric be preferred being more resistant to ultra Violet).
2. Mode of Manufacture	Non-woven, Needle punched
3. Denier	4 to 10.
4. Thickness (Under Surcharge pressure of 2 KPa)	3.00 mm and above.
5. Weight	400 gm/m^2
6. Tensile strength (By cut strip test 200 x 50mm)	Min. 60 Kg.
7. Elongation at break (By cut strip test 200 x 50mm)	40% to 100%
8. Pore size	Max. 120 micron.
9. Equivalent\ Opening Size (EOS) 0_{90}	40 to 75 micron.

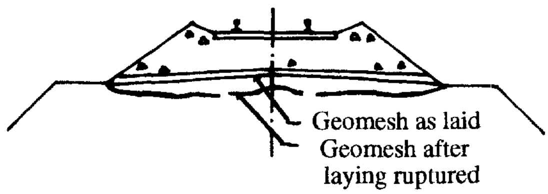

Figure 3. Subgrade Stabilisation trial using Geomesh.

4 MODEL STUDIES

Model studies were carried out in the laboratory using a large size metal box 300 mm x 300 mm x 200 mm. The mould was filled with non-cohesive sub-ballast material conforming to Indian Railways specifications and compacted to desired density (90% of MDD). The test conditions included the following :

i) Sub-ballast material only (unreinforced),
ii) Sub-ballast with one layer of biaxially oriented geogrid (Tenax LBO 301) placed at the mid-height.

iii) Sub-ballast with two layers of biaxially oriented geogrid (Tenax LBO 301) placed at heights 1/3rd and 2/3rd respectively.

The relevant properties of biaxially oriented geogrid Tenax LBO 301 are as follows :

	MD	TD
• Peak Tensile Strength (KN/m)	19.5	31.6
• Yield Point Elongation (%)	16.0	11.0
• Aperture Size (mm)	30	40
• Unit Weight (gm/m^2)	350	

The vertical load was applied through a square steel plate 125 mm x 125 mm size.

The ratio of mould dimension to footing dimension was 5.76 and its influence on test results are considered as marginal only.

The observations included recording of incremental vertical load and corresponding vertical deformations at the four corners of the box. The load deformation characteristics for the three test conditions are shown in Fig.4 which reveal the following :

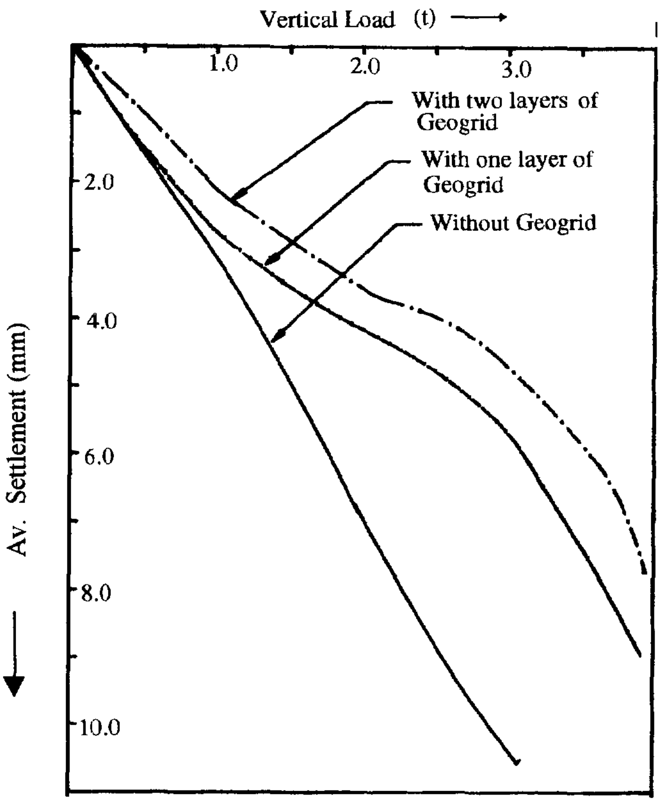

Figure 4. Model Studies – Load Deformation Curves with & without reinforcements

* In all cases, settlement increased with increasing load. Settlement was maximum for unreinforced conditions.

* Runaway deformations were noted at a vertical load of 3 tonnes in case of unreinforced sub-ballast and at 4 tonnes in case of reinforced sub-ballast.

* When compared with unreinforced conditions at a vertical load of 3t. the percentage decrease in deformation was 46% in case of single layer reinforcement and 54% in case of double layer reinforcement.

* Under these test conditions, the modulus of elasticity is worked out to be 63 MPa for unreinforced condition and 111 MPa for single layer reinforced condition.

This data have been used for design of subgrade thickness for a case study on Cuttack-Bhadrak Section.

5 CASE STUDY

Cuttack-Bhadrak Section is a vital main line railway track between Howrah-Madras and connects Paradeep Port with Talcher-Shalimar. Maximum permissible speed of the section is 105 Kmph. A speed restriction of 30 and 50 Kmph is imposed on the stretch from Km 389/1 to 392/15 Dn line during rainy and dry seasons respectively due to weak subgrade. To strengthen the weak formation, detailed field investigations including testing of undisturbed and disturbed soil samples from site were undertaken by RDSO. The undisturbed soil samples have been tested in a Dynamic Triaxial Apparatus for confining pressure of 20 KPa (equivalent to a depth of 90 cm) and 35 KPa (equivalent to a depth of 180cm). With these values, a graph has been plotted between depth of construction and threshold strength of the soil. (Fig.5)

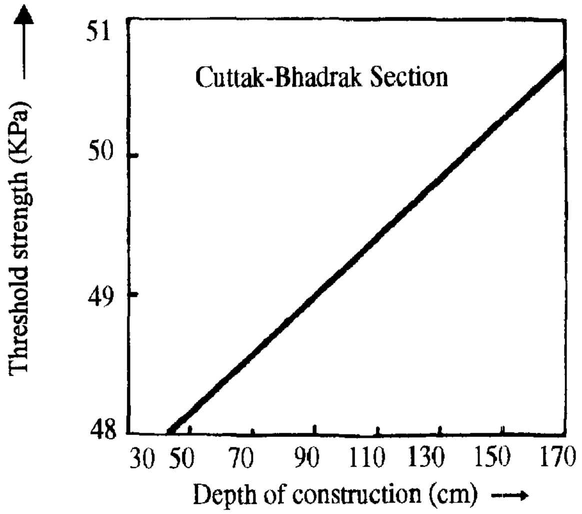

Figure 5. Threshold strength Vs Depth of Construction.

The depth of construction is worked out to be 75 cm (25 cm ballast + 50 cm sub-ballast). This depth is reduced to 55cm (25cm ballast and 30cm sub-ballast) by reinforcing sub-ballast with one layer of bi-oriented geogrid. Sample calculation is presented in Appendix-I.

With the use of geogrid reinforcement, the depth of sub-ballast is reduced from 50cm to 30cm, resulting in a saving of 40%. The most important feature of this design is that while interposing a sub-ballast of 50cm thickness requires track possession, no track possession is required for interposing 30cm thick sub-ballast layer. Since this is a core route, track possession is difficult. Therefore, provision of reinforcement will help in executing the work under running traffic.

6 CONCLUSION

Maintenance of railway subgrade is important due to manyfold increase in traffic levels, speeds and axle loads. Induced stresses in the subgrade should be less than threshold strength of the soil.
Strengthening of weak formation is required to be done under running traffic without track possession due to heavy traffic.
Soil is poor in tension. Provision of reinforcement will enhance the soil modulus.
Low strength low modulus geotextiles and geomeshes are not suitable for subgrade stabilisation.
High strength high modulus bi-oriented geogrid is more suitable for formation rehabilitation. One layer of geogrid reinforcement will reduce the sub-ballast thickness by about 40%.
Further studies would be needed to work out optimum modulus and strength characteristics of geogrid and sub-ballast characteristics for achieving higher economies, especially where depth of sub-ballast worked out is higher than 70cm.

REFERENCES

RDSO (1989) "State of the Art - Use of Geotextiles in Rail Track Foundation" *Civil Engineering Report No.C-261*, Manak Nagar, Lucknow.

Singh, P.P. (1995) "Use of Geosynthetics in Railway formations to improve bearing capacity of subgrade soils". *Dissertation submitted for MS Degree*, BITS, Pilani, India.

Yudhbir et-al (1993) "A Rational Approach to the Development of Design Methodology for Railway Formations" *Final Report*, IIT/Kanpur.

Appendix-I

Computations for depth of sub-structure

Eb = Young's Modulus of ballast
Esb = Young's Modulus of subballast
Es = Young's Modulus of soil
db = Depth of ballast
dsb = Depth of subballast
dt = Total depth of construction

Case-I - Without geogrid reinforcement:

db = 25cm
dsb = 50cm
dt = db + dsb = 75cm

Eb =130 MPa,
Esb = 63 MPa (from model test)
Es = 40 MPa

$$Eeq = \frac{Eb \times db + Esb \times dsb}{db + dsb} = 85.33$$

$$\text{Modular ratio, } m = \frac{Eeq}{Es} = \frac{85.33}{40} = 2.13$$

For dt = 75cm, Induced stress = 48.2 KPa (from Fig.1)
Threshold strength of soil = 48.7 KPa (from Fig.5)
Hence safe.

Case-II – Using one layer of geogrid reinforcement LBO-301:

db = 25cm
dsb = 30cm
dt = db+dsb = 55 cm

Eb = 130 MPa
Esb = 111 MPa (from model test)
Es = 40 MPa
Eeq = 119.63 & m =2.99 (computed as in Case I above)

For dt = 55cm, Induced stress = 48 KPa (from Fig.1)
Threshold strength of soil = 48.3 KPa (from Fig.5)
Hence safe.

The Use of Geotextiles for the Construction of the European High Speed Train Network

Frans De Meerleer
Director - TEXION. Commercial Consultants to LYS-FABRICS, Belgium.

Frank Donckers
General Manager Business Unit Raw Materials - IDEAL GROUP, LYS-FABRICS, Belgium.

ABSTRACT: The construction of a network of high speed trains in Europe involves the use of geotextiles for many applications. The Authors describe the general uses of geosynthetics in railway sub-ballast and construction applications, but point out those aspects where geotextiles play a particular part in assisting in the extreme environment of high speed train earthworks. The paper goes on to describe some actual applications where the main network has used geotextiles and outlines some of the difficulties involved in their specification, particularly bearing in mind the European decision to not standardise on geotextile classifications between Member Countries.

1 THE USE OF GEOTEXTILES TO ASSIST WITH SUBGRADE PROBLEMS

It has long been recognised that subgrade pumping beneath railways is a problem that can be ameliorated by the use of a geotextile at the ballast/subgrade interface. (Refs.1 & 2) The design difficulty has always been how to know which type of geotextile is the most suitable. With time, experienced railtrack engineers came to the opinion that low permeability and fine pore size were the preferable criteria for railways. The function of a geotextile beneath a railway is fundamentally different from that beneath a temporary access road or a permanent highway. The essential differences are a) that the ballast used to provide sleeper support is very coarse, uniform and angular, b) the regular repetition of the vibration from the axles can set up sympathetic resonant harmonic oscillations in the soil and c) the rail track system feeds a unique long distance wave of both negative and positive pressure into the ground ahead of the train itself.

The geotextile improves the structural integrity of the track and reduces the need for maintenance. It is generally considered (as shown in Fig.1), that the shedding of precipitation, caused by the fine pore size of the textile, is of particular benefit to the structural integrity of the track, whereas the filtration objective of the textile in preventing the upward migration of fines is of prime relevance to the maintenance requirements.

The new high speed train lines are multi-track systems (as opposed to low speed single track lines often encountered in developing countries), so maintenance is not such a critical problem as structural integrity. Therefore, in considering the geotextile requirements for this purpose, prevention of degradation of the subgrade is the main consideration. This logic has led to the conclusion that fine pore size and puncture resistance of the textile are the most important requirements. However, these properties can be found in a variety of different textiles including both woven and nonwoven types. Naturally, lightweight nonwovens are not suitable for this purpose since they can be damaged too easily. However, the heavy grades of needlepunched and woven tape textiles have been selected for sub-ballast separation.

The European Union has made substantial progress with regard to the standardisation of design approach for all civil and structural engineering matters including geosynthetics. However, there has been the positive decision not to standardise the classification of geosynthetics for particular purposes. This appears to have been a pragmatic decision which holds the situation as at present, based upon different national, commercial and experience considerations for the utilisation of these products. No doubt this will have to be addressed in due course, but at the moment it leads to apparent anomalies in pan-European projects such as the high speed train system. Where the lines cross a national border, it has proved necessary to employ a different material because of different national preferences, experiences and classification systems, even though the ground conditions on each side of the border may be identical. The Authors feel that this should not be viewed as a failure of the concept of the European Union, but an indication of how difficult and time consuming it is to join together and blend a large number of sophisticated developed countries.

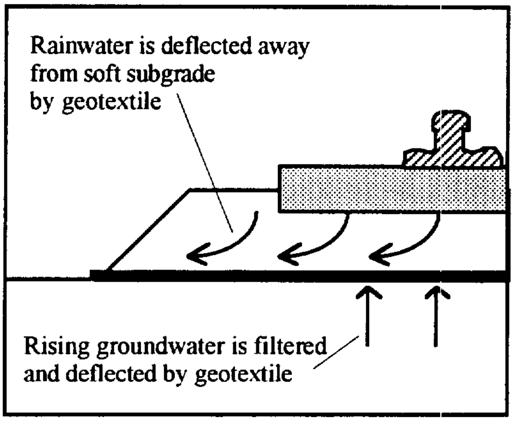

Fig.1. Rainfall shedding and pumping prevention by highly impermeable geotextile.

For, example, the Belgian Railways (N.M.B.S.) prefers to use nonwovens for this purpose, whilst the German Railways (D.B.) prefers woven tape products.
These filtration and drainage applications at sub-ballast level are particularly important in areas of cuttings, where water tables are high.

In addition to the prevention of contamination and saturation that a sub-ballast textile can provide, in high speed track conditions consideration must be given to the fundamental role of stress absorption. As can be seen in Fig.2 (Ref.3), although vertical stress is absorbed by the ballast layer, there is still a considerable amount of vertical stress remaining at the base of the ballast, to be passed down into the relatively soft subgrade. In embankment situations, where the subgrade is a pre-specified and pre-compacted material, and where drainage may be good, this stress may be absorbed adequately. However, a strong geotextile at this horizon can absorb stress and reduce the impinged load onto the subgrade. By reducing lateral shear stresses in the subgrade, the textile will help to increase its overall bearing capacity. Cohesive soils under shear exhibit a lower bearing capacity than those that are not. Under these circumstances - which include soft subgrades, wet subgrades and high speed train environments, it could be considered advantageous to choose stiffer woven products rather than nonwovens.

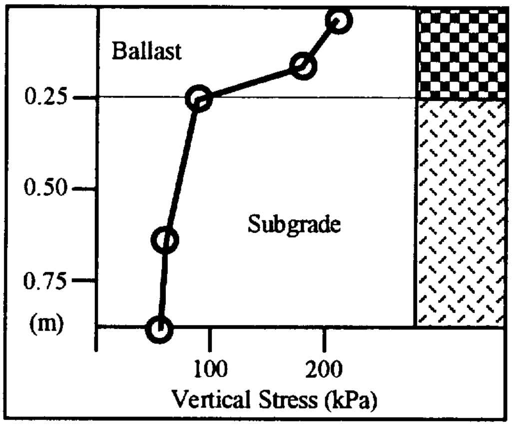

Fig.2. Typical variation of stress vertically beneath a rail line without the benefit of a geotextile (Ref.3).

The critically important contribution of a geotextile is shown in Fig.3 (Ref.4) which shows the typical results of a series of cyclical triaxial test in which the shear stress on the soil sample is continuously varied to simulate the passage of a high speed train.

Note that in this case, when the shear stress imposed on the soil exceeded $65kN/m^2$, the soil rapidly deteriorated with increasing induced strain until failure was reached at only 10,000 cycles. Below a shear of $65kN/m^2$, the soil stabilised up to and beyond one million cycles. The impact of reducing shear on performance and maintenance cannot therefore be overstated. A high strength geotextile can contribute significantly to this providing that it has adequate durability (abrasion resistance and polymer longevity). There are doubts expressed about the potential longevity of woven slit film textiles, for example.

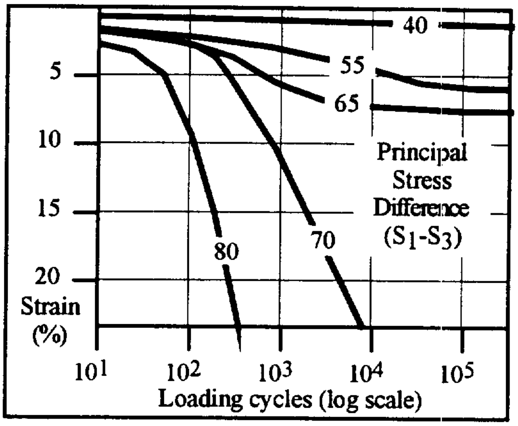

Fig.3. Effect of shear stress on cyclically induced cumulative strain in a soil without the benefit of geotextile (Ref.4).

2 GEOTEXTILES AS DRAINAGE COMPONENTS BENEATH NEW EMBANKMENTS

It is common to use geotextiles as separators at the base of new embankments. As mentioned previously, since in the case of high speed trains, structural stability is of paramount importance, the European system has commonly included the use of geotextiles as elementary separators at the base of embankments not only to act as construction aids, ensuring the highest level of integrity for the structure, but also as components in drainage elements, thus ensuring the reduction of water levels in the basal zones of the embankments. Especially where embankments are relatively more permeable than the underlying formation material, the use of low permeability geosynthetic textiles can lead to a reduction in received precipitation water in much the same way as is achieved beneath the ballast layer itself.

Once more, in this application, there have proved to be national differences, with the French Railways (S.N.F.C.) using woven geotextiles and immediately across the border, the Belgian Railways using nonwovens.

3 GEOTEXTILES AS REINFORCING COMPONENTS BENEATH NEW EMBANKMENTS

Even more so than highway embankments, high speed rail embankments are subject to potential lateral slope failures. The front of a high speed train is preceded by a force wave within the rail and sleeper system which actively pushes down on the soil before the train arrives, followed by a continuously high surcharge load during the train passage. To counteract this effect, geotextiles are used in the sloping sides of banks as reinforcement layers and in particular, they are used as horizontal reinforcing layers at the basal horizon of embankments, to protect against slip circle failure. Not only are the dynamic forces greater with high speed trains, but as can be seen in Table 1, (Ref.5.) rail and sleeper weights also increase directly as the train speed increases. Although relatively small, this must also be taken into account in the slope design.

Axle wt. Tonnes	Speed Km/hr	Rail Wt. Kg/m
35	50	57
35	140	65
35	200	70

Table 1. Typical rail weights

It is interesting to note that although overall slope load is increased, the use of heavier weight rails reduces the direct shear loading of the ballast and sub-soil system. For example, increasing the rail weight from 48 to 68 kg/m diminishes soil shear stress by 20%.

The need for structural integrity is generated principally by the need for consistent and even track alignment both vertically and horizontally. Deformation levels that might be tolerated for ordinary railway trains are not permissible on high speed tracks.

South of Brussels, the Belgian Railways have employed the traditional high strength polyester woven geotextiles as the basal reinforcement layer for their sector of the European Network leading to Paris. This was not the usual standard reinforcing detail, but at the location of the River Zenne, the existing track structure had to be widened as well as refurbished to take the high speed traffic. The Zenne was running parallel to the old railway track and the widening involved displacing the river laterally to construct the new extension.

The cross section of this location is shown in Fig.4., where it can be seen that geotextiles were used to contain the entire fill body that infilled the old river bed and channel. The river was accommodated in a newly constructed canal built away from the new high speed track. Naturally, geotextiles were used in the banks of the canal as well, for erosion protection.

One of the interesting principles of the European High Speed Train Network is that the stations were to be located in the centre of cities to provide true accessibility for the public. In practice, this meant that existing main line stations were to be upgraded for the new high speed trains.

This led to a problem experienced by the Japanese in the construction of their high speed inter-city trains - lack of space. In order to widen the track zone in city areas, it has become necessary to utilise reinforced soil technology as the most modern, cost-effective method of construction. Not only is reinforced soil construction cost-effective, but it is also environmentally friendly, permitting the adoption of a number of green grass and vegetated face finishes.

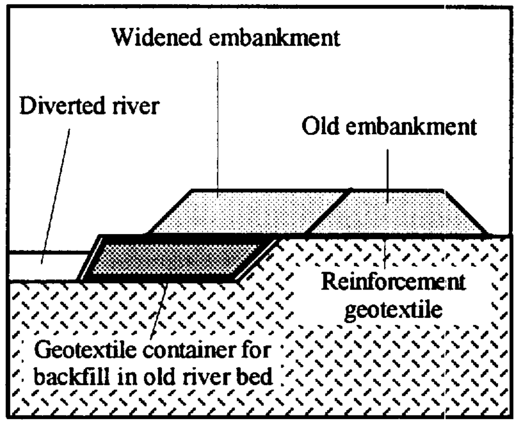

Fig.4. Widening of the Belgium - Paris sector parallel to the River Zenne.

The Japanese experience with earthquakes has highlighted the benefits of reinforced soil structures in areas of vibration. During recent major earthquakes, reinforced soil structures were invariable, the only ones left standing. In the light of these results, it is not surprising that reinforced soil should be adopted to support high speed train lines which are a major source of vibration.

4 GEOTEXTILES IN THE CONSTRUCTION OF HIGH SPEED BRIDGES AND RAIL FLY-OVERS

The impermeability of bridge decks and fly-overs was a major concern for the Network designers. As a result of considerable technical input and research, a number of special composite geotextiles were developed impregnated with bitumen.

The geotextiles themselves were composite heavy nonwoven needlepunched (1500 g/m2) and strong woven (100 kN/m) which offered a cost-effective and reliable solution. Although well proven in laboratory testing, it is interesting to await the outcome of several years of real use to evaluate the results. Their use is shown in Fig.5.

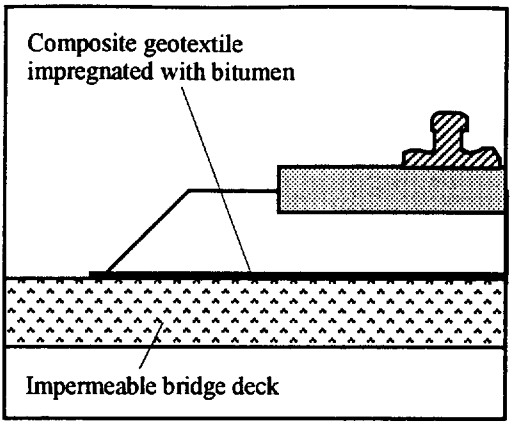

Fig.5. Location of bitumen impregnated composite between ballast and bridge decking.

5 LIFE EXPECTANCY OF GEOTEXTILES IN HIGH SPEED RAILWAY SYSTEMS

It is interesting to note that the life expectancy requirements of geotextiles in high speed designs varies depending upon where the textile is situated in the design. For example, the basal reinforcing geotextiles used to prevent slip circle failure should be designed to last in excess of 100 years, whereas, the sub-ballast textiles could be designed for less. The reasons for the less stringent requirements for the sub-ballast textile are that in addition to the ballast layer experiencing unavoidable deformations and in addition to potential frequent replacement of textiles during ballast maintenance, the predicted life of the concrete sleepers will, in any event, only be some 40 to 50 years, thus necessitating a major upper level refurbishment at that interval period. A longer planned life expectancy for the textile at this level would therefore not be cost effective.

Note: The Authors wish to acknowledge that the opinions expressed herein are their personal opinions and do not represent the views of their respective organisations.

References.

1. Membranes in Ground Engineering by P.R.Rankilor., Published by Wiley. 1981.
2. Designing with Geosynthetics by R.M.Koerner. Published by Wiley. 1986, (p159).
3. Track Geotechnology and Substructure Management. E.T.Selig and J.M.Waters. Published by Thomas Telford Services Ltd. U.K., 1994.
4. Design of Conventional Railtrack Foundations by D.L.Heath et al. Proceedings Inst.Civ.Eng. Vol. 51. Feb.1972.
5. Civil Engineer's Reference Book (4th Edition) edited by L.S.Blake, Published by Butterworths. U.K. 1989.

Geosynthetic System for the Facing of Bovilla Dam

P. Sembenelli
Geotechnical Consultant and Managing Director, SC Sembenelli Consulting, Milan, Italy

G. Sembenelli
Geotechnical Consultant, SC Sembenelli Consulting, Milan, Italy

A. M. Scuero
Technical Director, Carpi Group, Arona, Italy

ABSTRACT: Bovilla Dam is currently the highest embankment dam incorporating a polymer (PVC) geomembrane installed within a system of geosynthetics, to provide the necessary waterproofing to the top 58 m of an 81 m high structure. Bovilla dam is the last of several such dams, of increasing height, designed and built in the last decade, along the lines set forth since the pioneering projects of 1959 - 1960. The position of the waterproofing system is on the upstream face of the dam, the waterproofing element is a 3 mm thick, plasticized and stabilised PVC geomembrane and the geosynthetic system is protected with a facing of cast-in-place, concrete slabs.

KEYWORDS: Dam, Geocomposites, Geomembranes, Protective cushioning, Seepage control

1 INTRODUCTION

Bovilla Dam, across Terkuze river in Albania, was originally designed as a concrete faced, gravel fill. It was not possible to reconstruct the basis for selecting a 1V/1.6H slope typical for rockfill but definitely steep for a sand-and-gravel fill. The design of the facing was developed around 1994 along the earliest schemes for such facings: a grid of concrete beams run under both the vertical and the horizontal joints of the facing slabs. The thickness of the slabs was about 0.5 m. The reinforcing of beams and slabs was quite complex and even more so was the system of the copper and PVC waterstops.

During the construction of the embankment, mostly built with alluvial gravel-and-sand, gullying of the upstream face by rainfalls developed. Attempts to reconstitute the face and recompact the fill gave unsatisfactory results. A growing concern for the end quality of the concrete facing and a compelling need to reduce both construction cost and time, suggested to look for alternate facing solutions.

A geosynthetic system essentially based on PVC geomembrane and geotextiles, finally proved to be a solution compatible with the fill materials, applicable notwithstanding of the slope of the face, requiring a much shorter placement time and nearly halving the cost of the design solution.

Late in 1994 the change in design was decided and design of the new facing system started. Placement of the bedding and drainage layer started in mid 1995 and was completed by the end of the year. Placement of the geosynthetic system started in May 1996 and was carried out in 3 parts: centre, left and right. The left and right parts were placed only after grouting of the foundation rock along the side beam was completed. For this reason placement of the 3 parts was not continuous. Placement of the geosynthetic system was completed in September and the waterproofing protection completed in November 1996. Figure 1 shows the upstream slope of Bovilla dam when placement of the waterproofing and protection were in progress. The net time required for the placement of the geosynthetic system was 30 days with an average placement rate of 300 m2/day. The net time required to place the concrete protection was 100 days with an average placement rate of 90 m2/day.

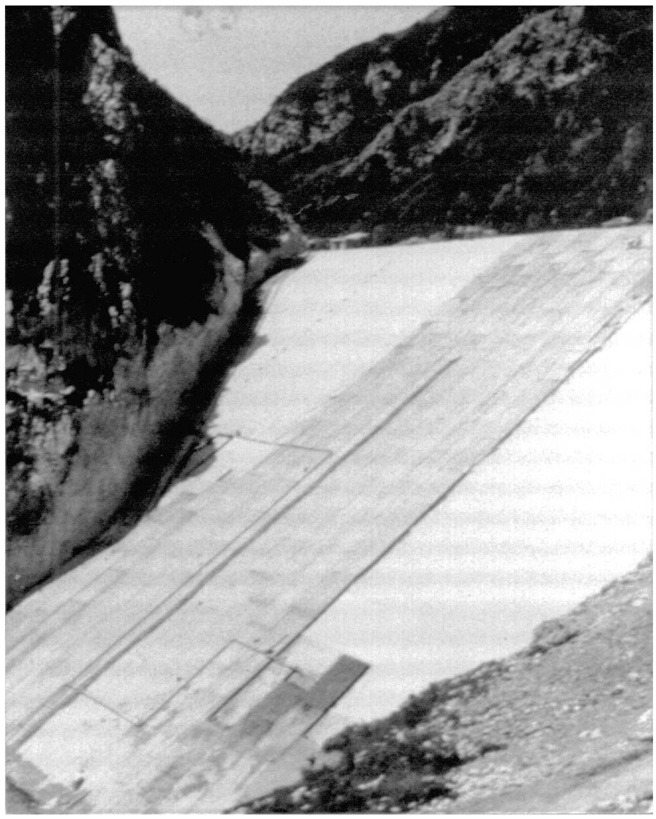

Figure 1. Upstream slope of Bovilla dam in 1996. Protection has been completed in the centre part of the face.

The cost of the waterproofing system, including bedding, geosynthetics system, peripheral seal and concrete facing was on the order of 160 US$/m2, in 1996 costs. All geosynthetics were imported from Italy and placement was directed by expatriate personnel.

2 THE FORERUNNERS OF TODAYS DAMS

The first synthetic material tested as a waterproofing element was Butyl Rubber RI (Sabetta dam 1959) soon followed by Polyvinyl chloride PVC (Dobsina Dam 1960 and Terzaghi dam 1962). Low density polyethylene LDPE was used for the first time in 1964 (Toktogul cofferdam).

In later years the preferred choice became PVC in Europe and high density Polyethylene HDPE in the USA. According to a list of 83 earth and rock dams, major reservoirs and cofferdams waterproofed with geomembranes, prepared by the Senior Author, 54 structures have been built in Europe, 10 in Australasia, 5 in Africa and 14 in the Americas. PVC has been used on 33 known cases of the total. In Europe PVC has been used on 24 cases and in the Americas on 3 cases only. Waterproofings for high dams were mostly based on PVC. The Authors believe that part of PVC's success is due to the easily installed and well-performing welds possible with this polymer.

During the pioneering period, design practice developed along 2 lines: -i) thin geomembranes (< 0.5 mm) and -ii) thick geomembranes (> 1.0 mm). Thin geomembranes were selected mainly based on seepage loss considerations overlooking the possibility of damage during placement. Practical difficulties in welding very thin geomembranes, suggested using glued joints and often such geomembranes have been installed using folded connections. Negative experiences were the result of this type of design (Sembenelli 1995). Thick geomembranes and welded connections were adopted as a result of considering proper placement and welding as relevant requirements.

The selection of PVC and HDPE allowed production of continuous, high quality welds. Hot-air welding with hand-held blowers, soon evolved into machine welding by hot air and hot points. As a result of attention to the quality of the seams, the senior Author developed, in the early 70s the double track seam which made possible testing of the entire seams' length.

Bovilla is the latest example of more than 70 cofferdams, large reservoirs and dams designed along the concepts developed in Italy since Sabetta. The Italian practice always adopted thick geomembranes to provide extra strength against handling and placement damages and to allow high quality, controlled welds. Soon after the pioneering examples based on Butyl rubber RI and Chlorosulphonated polyethylene CSPE, Italian practice adopted PVC as the polymer. Quite early geocomposites consisting of a PVC geomembrane + a Polyethylene terephthalate PETP nonwoven geotextile were substituted for plain PVC sheets. Multi-layer geocomposites, incorporating a diffused reinforcement were developed and applied along this line of thinking.

The design of Bovilla dam was based on the experience gained with large scale testing, in designing and in supervising construction of several dams in Italy and abroad. Possibly the most significant experience related to the type of geocomposite adopted is Alpe Gera Dam (174 m high). The protection with cast in place concrete slabs was successfully adopted at Jibiya Dam (Sembenelli 1990). The peripheral connection was perfected in the application of geomembrane waterproofings on several concrete dams like Pracana Dam.

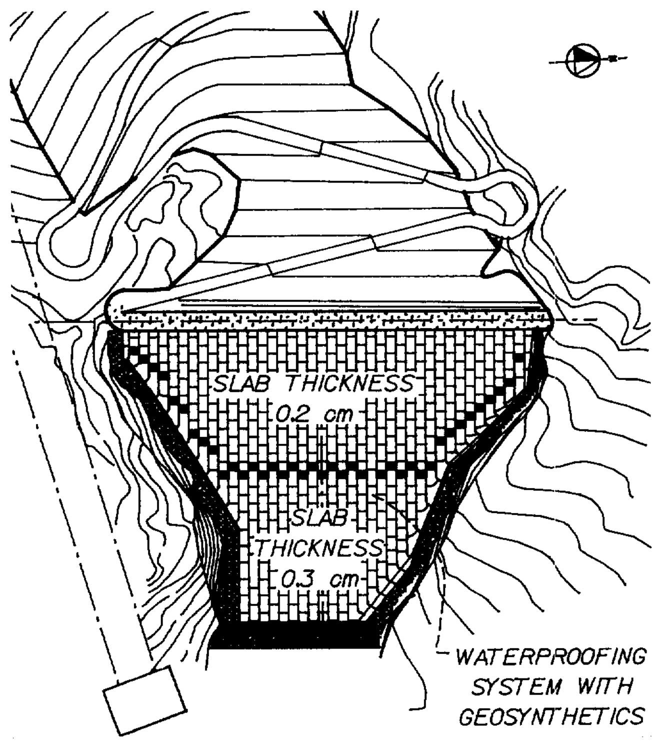

Figure 2. The plan of Bovilla dam with waterproofing based on a geosynthetic system and a cast-in-place concrete slab as a protection.

3 THE EMBANKMENT OF BOVILLA

The dam, as shown in Figure 2, is placed in a narrow, winding gorge cut through a ridge of limestone rock just downstream from a tectonic contact with a schist formation. The relatively soft schists have been eroded and the limestone forms a long and high wall at the South-West end of the reservoir. A diversion tunnel has been cut through the limestone of the left bank. The limestone is heavily karstified and a large spring exists under the right abutment of the dam. Except for the excavation required to set the side beam, no excavation was carried out on the abutments. A deep, karstic niche was backfilled with concrete prior to filling against it.

At the upstream toe of the dam, river bottom rock was reached some 10 m below riverbed and the channel was filled with a concrete plug. The plug was raised some 15 m above riverbed elevation thus creating a gravity toe block nearly 25 m high. Figure 3 shows the cross section of Bovilla.

In order to condition the riverbed materials under the future fill, the rock on the sides of the gorge was demolished to a distance sufficient to permit the transit of construction equipment. Rock fragments covered by clean,

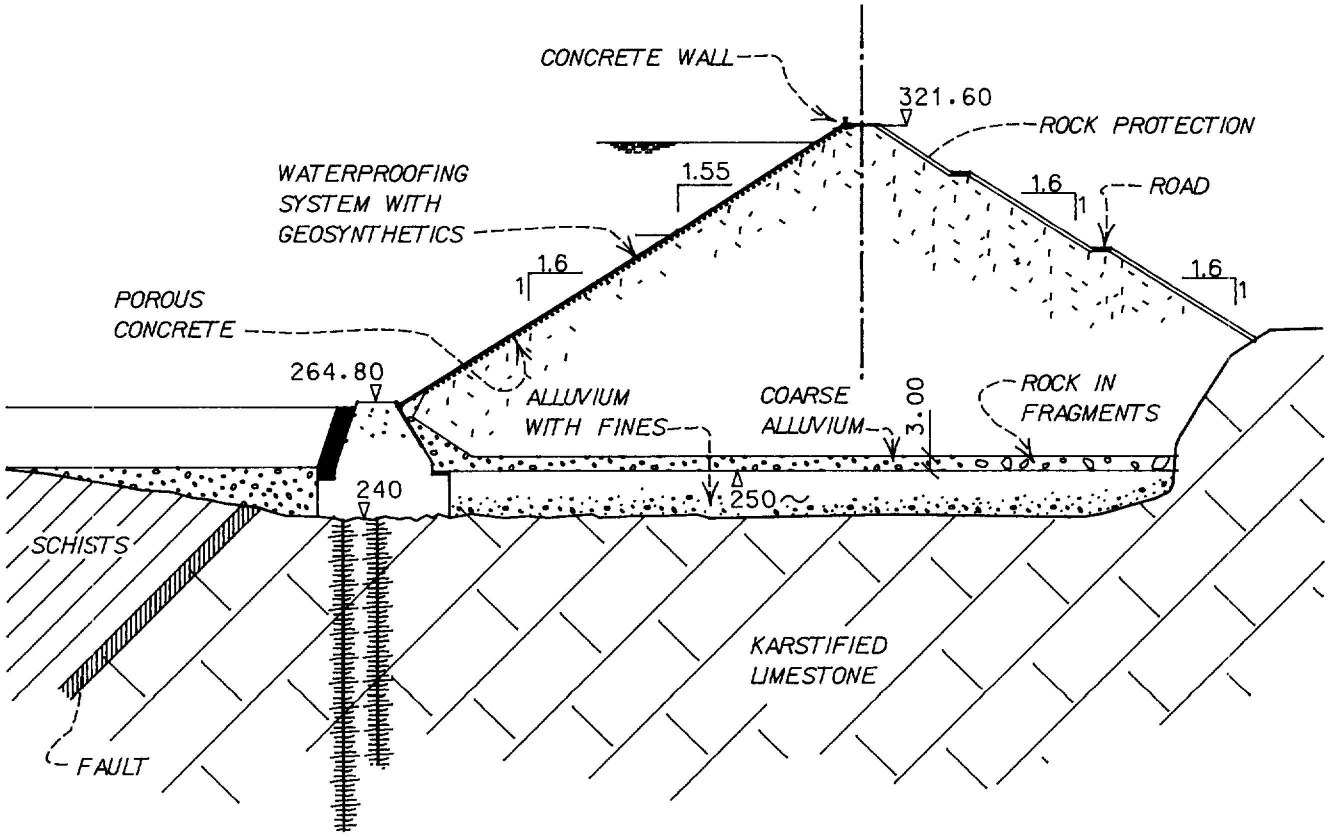

Figure 3. Main cross section of Bovilla dam on the Terkuze river. The maximum height of the dam is 81 m and the geosynthetic system has been applied over the top 57 m. The crest length of the dam is about 140 m.

coarse gravel were leveled and compacted in the riverbed channel thus creating an efficient bottom drain.

A substantial deposit of alluvial materials existed in the expanse of the reservoir and the embankment was filled with borrow-run sand-and-gravel. The alluvium is well graded and contains a certain amount of fines so that the permeability of the compacted embankment is quite low and certainly not uniform. The high percentage of fines was hindering proper compaction near the slope and favoured gullying along the compacted face. Difficulties experienced at properly filling and forming the face, suggested placing the centre and downstream parts of the fill only, while a proper solution was worked out. Hence the lower 40 m of the embankment were built in 2 separate stages which increased the potential for non uniform settlement of the face, under hydrostatic loads.

The rock line for the side beam was designed so as to obtain a profile in the plane of the face as regular as feasible. Fairly extensive excavations were necessary at given locations to smooth corners and to eliminate overhangs. The rock bench where the side beam had to be set, was designed with a gentle inward slope.

To eliminate gullying by rainwaters and to provide a free-draining, strong and uniform support to the waterproofing system, a sand-free, low-cement concrete was adopted which could be placed to produce a smooth surface. The specified aggregate size was 15 - 25 mm with Cu $<$ 2 and the cement just enough to hold the grains together. Laboratory tests carried out on the cemented granular bedding proved that its coefficient of permeability was $k > 1$ cm/s. The cemented granular bedding was placed from the top of the fill, as the fill was raised, in 2 m high bands, smoothed and compacted with a vibratory plate mounted on the arm of an excavator.

The thickness of the free-draining bedding layer was increased all along the periphery to widen the length of the contact between the drain and the abutment rock, with the aim of improving the collection of any seepage underpassing the side beam.

The toe block and side beam, part of the original design, had been cast as an unreinforced concrete block sitting over the abutment rock. As part of the design of the geosynthetic facing, the abutment surface, immediately below the side beam, was modified so as to avoid too steep as well as too flat profiles at the contact with the embankment. This was obtained by trimming the rock in excess or by concrete castings, where the abutment's rock was dipping too steeply.

A second stage reinforced concrete slab was placed over the surface of the side beam to reduce the danger of concentrated seepage in the concrete, which could eventually bypass the peripheral connection. Low pressure contact grouting was applied systematically to the concrete-to-concrete and concrete-to-rock joints trough holes drilled from the face of the side beam.

As an additional measure against short circuit seepage, the surface of the side beam's concrete, immediately above the geomembrane-to-concrete connection line, was treated with epoxy resins to fill honeycombs and hair cracks.

4 THE WATERPROOFING SYSTEM

The waterproofing system of Bovilla dam was based on the previous designs of similar dams (Sembenelli and Amigò 1996) and on experiences and studies regarding seepage flow through holed geomembranes. The choice of a geocomposite was dictated by the benefits provided by a geotextile backing, particularly if intimately connected to the geomembrane, in reducing the level of losses and in avoiding channelized flow under the liner (Fukuoka 1986).

The basis for selecting a geocomposite developed by the special Contractor CARPI was the proven performance of the liner under water heads far greater than that expected at Bovilla although, most of the precedents available were concrete or masonry dams (Scuero 1997). Other geosynthetics, like HDPE, would require finding adequate solutions to accept a more than tenfold larger coefficient of thermal expansion. A thermally stable geosynthetic makes much easier welding and protection with light weight slabs.

The waterproofing system, shown in Figure 4, consists of a 3 mm geomembrane coupled to a 700 g/m2 geotextile. The geomembrane is a monolayer PVC (polyvinyl chloride) extruded from a straight-head extruder. The geotextile is a nonwoven, needle punched, continuous filament, PP (polypropylene) fibre. The coupling is obtained by calendering the geotextile on the hot PVC sheet as it leaves the extruder. A selvedge of 50 mm is left on one side, for proper longitudinal welding of adjacent rolls. The geocomposite is produced in 2.05 m wide rolls of indefinite length.

Large scale loading tests were conducted on a high capacity cell. The support was the granular bedding, on 1 to 1 scale, and the maximum test pressure was 900 kPa i.e. 50 % in excess of the maximum expected water pressure on the face. Each test consisted of 3 loading-unloading cycles, with a first loading bench at 500 kPa, 24 hours of sustained load at 900 kPa and 6 hours recovery time in unloaded conditions in between cycles. The profile of the geocomposite under maximum load was obtained.

Another set of tests were carried out as shown in Figure 5 to simulate a collapse of the granular bedding surface. A sharp edge, vertical sided hole 0.3 m in diameter and 0.2 m deep was created under the geomembrane and a water pressure equal to 150 % of the full reservoir load was applied. The geocomposite stretched into the hole beyond the failure strain of the geotextile backing (about 34 % as determined with large scale burst tests) but the PVC geomembrane did not burst. The geotextile teared at an early stage of the test but, being on the underside of the geomembrane, its failure could not be observed in detail.

The geocomposite was factory cut to the exact lengths assigned by the design to each roll so that placement could be faster and more accurate, all horizontal seams could be eliminated, and wastage kept below 1 %.

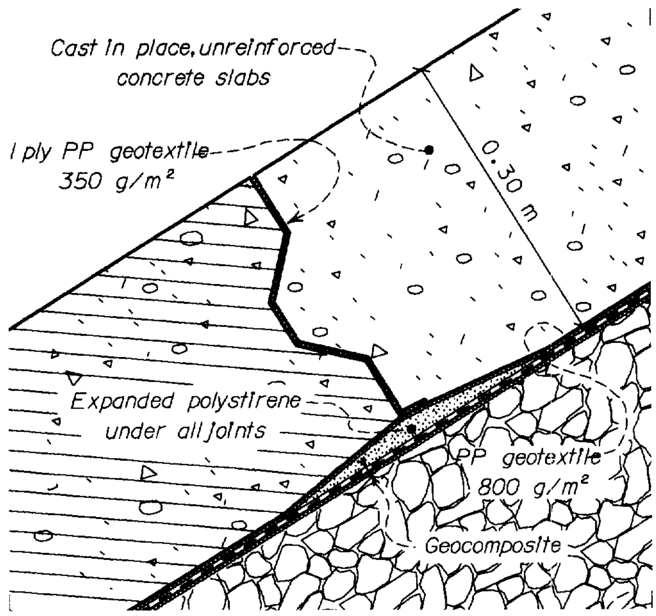

Figure 4. Cross section of the waterproofing system used at Bovilla dam.

Each roll of geocomposite was carried to the crest, unloaded and fastened to the concrete beam running along the upstream edge, with a tie down system (bolts and nuts). The roll was hence winched downslope and manually guided to its final position. The friction angle between geotextile and granular bedding was measured in the laboratory and proven to be 38°, about 20% larger than the slope angle. Hence a substantial grip developed between geotextile and granular bedding, enough to support the full dead weight of the geocomposite.

The geocomposite was ballasted against wind actions with strings of sand bags supported with ropes. The distance between ballast strings was about 6 m.

In spite of the ballast, however, a light but sustained wind circulating through the voids of the bedding layer, cut the frictional resistance to nearly zero and the full roll length ended hanging from the top beam. The geocomposite stretched about 0.5 % and some readjusting cuts had to be made at the toe of the slope.

The geocomposite was welded with butt welds 30 mm wide. Welds were all made with hot air equipment and about 50 % of the welding was manual. All welds were inspected and tested with a blade.

The design of the periphery of the geocomposite was such as to allow sharp, differential settlements of the fill with respect to the tie-down line. A reserve length of geocomposite was provided, sandwiched between anti-grip sheets of HDPE and nonwoven geotextile.

A geomembrane strip (without geotextile backing) was used to form the peripheral connection along the block toe and side beam. The connection was of the tie down type (bolts and nuts) with a prior application of a flattening polymer paste and soft rubber gasket. The tie down was obtained with embedded 10 mm bolts spaced 0.2 m and an 8 mm stainless steel flat profile and nuts. Each nut was closed with a dynamometric wrench.

A detailed inspection of the geomembrane surface and a detailed approval procedure was specified prior to covering the geocomposite with the geotextile. This operation was deliberately done just before starting the casting operations so as to minimise the possibility that undetected damages could happen to the geomembrane while covered.

One of the key checks of the inspection was aimed at assessing the conditions of the supporting layer. Loose stones or other small objects accidentally entrapped under the geocomposite were located. A rule was set to decide when the characteristics of the geomembrane would not permit draping the foreign object, given its dimensions or shape. In such cases the geocomposite was slit open and the object removed. The cut was hence repaired by superimposing a piece of geomembrane.

5 THE PROTECTION OF THE GEOMEMBRANE

In many dams exposed geomembranes have been adopted with success and have proved their adequacy to a lasting service (Amigò 1994). Protection of the geomembrane is often avoided to allow inspection and easy maintenance while the presence of a protective layer may forbid checks and hinder repairs.

Protection also adds to the cost of the dam and may sometimes require an investment comparable to that of the waterproofing system itself. Timewise, protection requires, in general, construction times which are longer then those needed to place, weld and test the waterproofing system itself. The decision to protect the geosynthetic system needs therefore to be justified and, in general, light solutions are preferable to heavy ones.

The rationale for deciding to protect the facing of Bovilla was based on several reasons: the steepness of the gorge and the consequent danger of falling rocks, which would damage the waterproofing system, the steepness of the face reducing to nearly zero the possibility of supporting the geosynthetic system by friction and, finally, the remoteness of the site and the fear that the geosynthetics could be vandalised.

Cast in place, unreinforced concrete slabs were selected as protection. The thickness of the slabs was 0.3 m in the lower parts of the facing where the length of the free standing slab exceeds 100 m and was reduced to 0.2 m over the upper 50 m of the face. A nonwoven, needle punched, continuous fibre, PP (polypropylene) filament geotextile 800 g/m2 was placed over the geocomposite to work as a decoupling layer, as well as a protection to the geomembrane against mechanical damage during concreting operations. The PP geotextile proved to work efficiently also as a light reinforcement to the slab (Sembenelli 1996).

Shear tests carried out on a large sample of the geocomposite resting on the granular bedding and covered with the specified geotextile, enabled the measurement of the actual friction at the geomembrane-to-geotextile interface. Tests proved that a friction angle of 22 ° was the maximum that could be relied upon. This angle is 70 % of the slope angle. Therefore a substantial portion of the

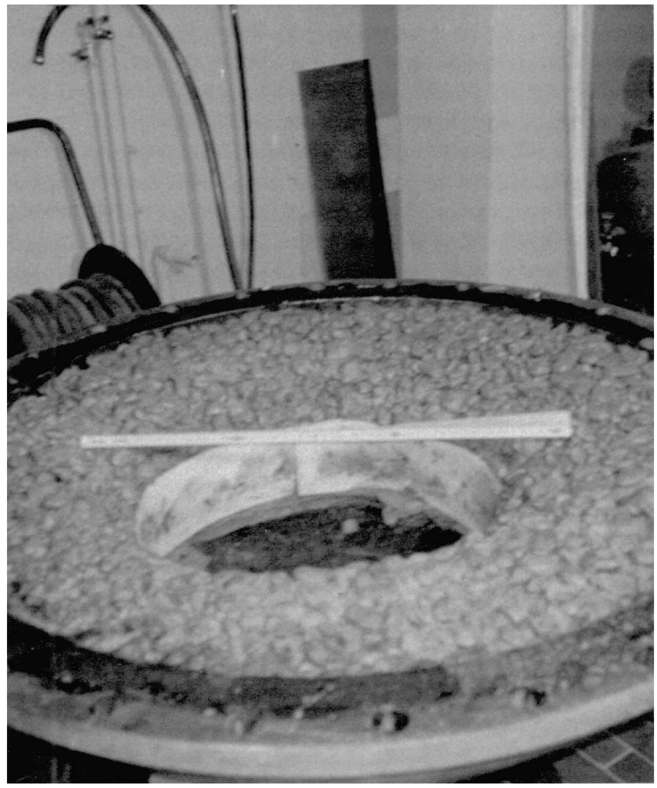

Figure 5. Large scale survivability test of the geomembrane simulating a collapsed hole in the bedding layer. The test was carried out in a high pressure vessel under 1.5 the maximum reservoir pressure. The granular support used in the testing chamber is the actual bedding placed on the dam.

protective slabs dead weight will have to be taken by the toe block. A reduction coefficient must be applied to the geotextile-to-support friction angle to account for the effects of construction and with related vibrations.

The joint pattern was based on continuous vertical and staggered horizontal joints. Shear keys were created along the sides of all slabs so as to block them, both ways. At horizontal joints, where appreciable angular deformations were considered likely to occur, through-going dowels were provided. Horizontal joints have the only purpose of allowing angular deformations to copy the deformed profile of the embankment facing, under full hydrostatic load. Horizontal joints are therefore obtained with the interposition of 1 ply of 350 g/m2 geotextile. Vertical joints are assigned the key function of relieving any uplift pressure existing under the slabs upon draw down. A 3 ply packing of geotextile is therefore provided along them all. While along all horizontal joints the geotextile undergoes a substantial compression, negligible forces compress the geotextile interface along vertical joints. The in-plane permeability of the geotextile remains hence close to that of the material under a nominal normal stress. Slabs were cast in successive horizontal rows which allows halving the required length of forms as shown in Figure 6. The surface finish required for the slabs was obtained by straight-edge and trowel.

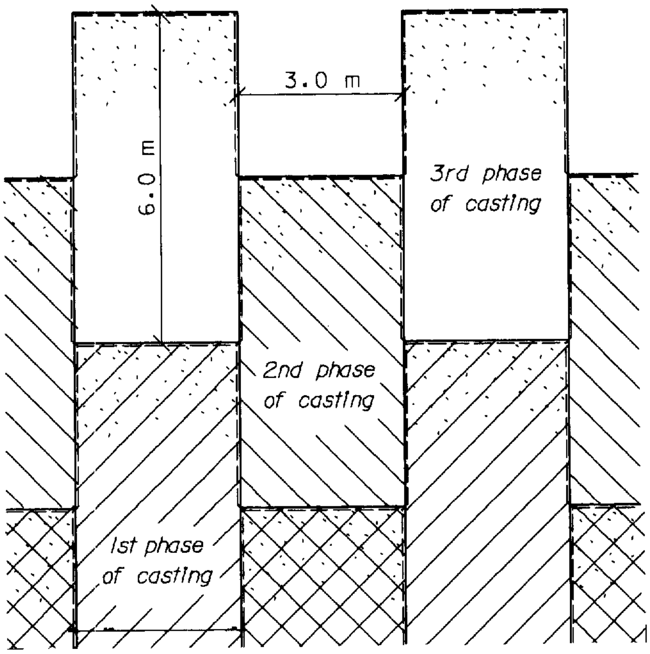

Figure 6. Joint pattern of the slabs forming the protection at Bovilla dam and casting sequence.

Each vertical slab rests, with most of its weight, against the toe block or against the side beam. Proper thickening and reinforcement of the concrete section was hence introduced so as to keep the compressive stresses at the contact, within acceptable limits (the maximum compressive stress is on the order of 800 kPa). The design was developed so as to make each slab self-supporting. Several sections exist, along the side beam, where the contact line between the slab and the beam dips steeper than the concrete-to-concrete friction angle (assumed as 35 °). Along such sections, the profile of the side beam was shaped in a jig-saw manner so as to prevent side way slippage of the slab foot.

An offset in the toe block profile locates the contact line between block and protection so that it stays off the vertical of the peripheral connection to ensure that the inevitable settlement of the edge of the facing slabs, with respect to the toe of the block, would not damage the connection. A styrofoam cap placed over the profile and the nuts, in its turn enclosed in a pocket of uniform sand, was added for the same purpose as shown in Figure 7.

Protection was placed from the bottom upward in 3 sections. The centre portion first was placed and, later, the 2 sides. The reasons for such unusual placement (which resulted in an increased length of side forms and in some complication in welding a geocomposite placed long before, to a newly laid one) were a need for drilling and grouting works along the side beam which could not be completed on time. Figure 8 shows the protection slabs during casting.

No personnel traffic was allowed on the geocomposite and/or on the geotextile. The Contractor thus selected to

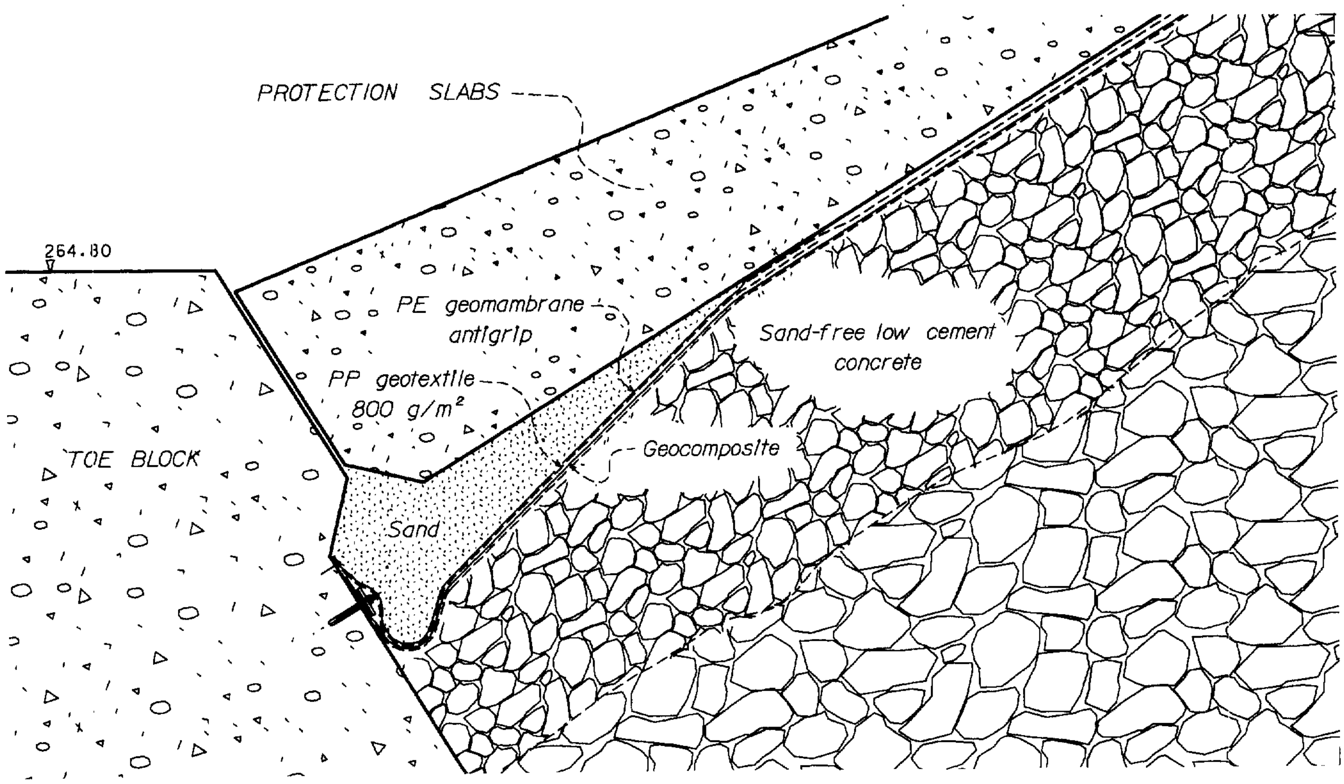

Figure 7. Connection between the waterproofing system and the toe block. A similar connection is used along the side beam.

serve the casting front from the toe of the dam. All walkways were arranged over the completed slabs and concrete was pumped to the placement zone.

A precast wave wall was part of the design of the crest of the dam. The precast elements were conceived so as to provide an early protection of the geocomposite from possible damage produced by falling objects.

6 THE MONITORING OF THE FACE

Monitoring localised water losses through the geomembrane is the main goal for a dam such as Bovilla. A diffused monitoring is possible today but still waiting further testing and certainly a costly measure. An overall monitoring system was hence selected which consisted of 3 open piezometers installed on the surface of the free draining bedding, immediately under the waterproofing system. The piezometer tips were limited to the lowest 2 m of the facing and piezometers pipes were of such diameter as to allow inserting a remote control electric pore pressure transducer at any later time in the future for continuous readings.

The size and distribution of the settlements of the face are of paramount importance for a waterproofing system based on geosynthetics. To survey settlements induced by the hydrostatic load, a lattice of reference points has been set into the concrete of the protecting slabs. Such points can be surveyed again when the reservoir is lowered and will make it possible to know the permanent deflection of the facing. Measuring the maximum inward deflection of a 110 m long face, while the reservoir pressure is on, is more complex and was not considered practicable at Bovilla. No post-loading readings are available so far.

7 CONCLUSIONS

Several successful dams in operation since 30 or more years prove that waterproofing earth and rock dams with geosynthetics is a viable and durable solution.

There has been a remarkable evolution as far as the type of the polymers most used in dams. Recent cases point to plasticized and stabilised PVC as the most widely used polymer nowadays.

Dams up to 60 m have been commissioned and all indications point to the adequacy of geosynthetics to build dams up to 100 m in height or even more. To the increasing height of dams (and acting water heads) Designers have answered with progressively more sophisticated "waterproofing systems" incorporating several layers of different geosynthetics. A similar evolution has taken place in welds, details of periphery, protections and QC procedures.

Specific testing and design procedures have been developed and are now available for a responsible design and a performing construction.

Monitoring equipments for the waterproofing system are becoming more and more sophisticated and tailored to suit modern solutions and needs.

It is not difficult to foresee that an array of geosynthetics will be more and more present in the dams of the future.

Figure 8. Close up of the cast-in-place, unreinforced concrete slab protection adopted at Bovilla dam.

REFERENCES

Amigò, R. and Aguiar E. (1994) *Manual para el Diseño, Construccion y Explotacion de Embalses Impermeabilizados con Geomembranas*, Consejería de Agricultura y Alimentación - Gobierno de Canarias

Fanelli, G., Squero, A., Vaschetti, L. G. (1995) "PVC Membrane Protects Italy's Highest Dam", *Water Power & Dam Construction*, November 1995, pp. 20-23

Fukuoka, M. (1986) "Large Scale Permeability Test for Geomembrane-Subgrade System", *Third International Conference on Geotextiles*, Vienna, Austria, Vol.III, pp.917-922

Scuero, A. M. and Vaschetti, G. L. (1996) "Geomembranes for Masonry and Concrete Dams: State of the Art Report", *Geosynthetics: Applications, Design and Construction - First European Geosynthetics Conference*, BALKEMA, Maastricht, Netherlands, pp.889-896

Sembenelli, P. (1990) "Engineering Geosynthetics in Design and Construction of Jibiya Dam", *Fourth International Conference on Geotextiles, Geomembranes and Related Products*, BALKEMA, The Hague, Netherlands, Vol. 2, pp. 419-424

Sembenelli, P. (1994) "Geosynthetics in Embankment Dams", *Geotechnical Engineering Emerging Trends in Design and Practice*, OXFORD & IBH, New Delhi, India, pp. 279-304

Sembenelli, P. (1995) "Lessons Learned from the Failure of Artik Dam", *Geosynthetics: Lessons Learned from Failures - Short Course Handout*, IFAI, Nashville, Tennessee, USA, (in print)

Sembenelli, P. and Amigò, R. (1996) "Geomembranes for Earth and Rock Dams: State of the Art Report", *Geosynthetics: Applications, Design and Construction - First European Geosynthetics Conference*, BALKEMA, Maastricht, Netherlands, pp. 877-888

SC - SEMBENELLI CONSULTING (1997) "Earth and Rock Dams with Synthetic Geomembranes as Waterproofing Elements - List and main data" - *Unpublished*

Long Term Performance of Exposed Geomembranes on Dams in Italian Alps

Daniele Cazzuffi
ENEL Ricerca - Polo Idraulico e Strutturale, Milano, Italy

ABSTRACT: The paper presents the more recent results of an experimental program related to the behaviour vs. time of PVC geomembranes and PVC-PET geocomposites applied for rehabilitation of different types of dams owned by ENEL on the Alps. In particular, the behaviour vs. time of geosynthetics has been studied for the masonry dams of Lago Miller and Camposecco and for the concrete dams of Lago Nero, Piano Barbellino, Cignana and Pantano d'Avio. The considered geosynthetics are without any external protection and the related dams are in the West and Central regions of Alps at an elevation of more than 1,800 m above the sea level. The laboratory tests, carried out at the Special Materials and Geosynthetics Laboratories of ENEL Ricerca in Milano, allowed to determine the following characteristics: plasticizer content, hardness Shore A, tensile and water vapour transmission properties. According to the first observation programs and laboratory tests, the considered geosynthetics exhibit generally a satisfactory behaviour vs. time.

KEYWORDS: Dams, Geomembranes, Geocomposites, Laboratory Tests, Performance Evaluation.

1 INTRODUCTION

The first complete application of a PVC geomembrane at an old dam on the Alps was carried out in Italy in 1976 at the 11 m-high Lago Miller masonry dam, built between 1925 and 1926. Significant leakage led to the installation of a 2.0 mm-thick PVC geomembrane.

The geomembrane is also unprotected, so that it is exposed to the action of ice and ultra violet rays, particularly important as Lago Miller dam is located at an elevation of 2,170 m (Cazzuffi, 1987).

Another Italian installation of a PVC geomembrane for dam maintenance purposes was in 1980/1981 at the Lago Nero concrete dam. This 40 m-high structure was built from 1924 to 1929. A 2.0 mm-thick PVC geomembrane was placed without any external protection.

The 2.5 m-wide PVC geomembrane sheets were applied using a unique system, now patented by the firm Carpi, which allowed for continuous fastening along the vertical lines and also horizontal prestressing of the geomembrane itself.

A polyester needle-punched staple filament nonwoven geotextile (with a mass per unit area of 350 g/m^2) was thermobonded in factory to the geomembrane, thus forming a geocomposite before application on site (Monari, 1984).

Other applications of PVC geomembranes to vertical upstream facings of old Italian concrete or masonry dams were performed more recently with very similar techniques. In the applications to Cignana and Piano Barbellino concrete dams, the stainless steel ribs are embedded in an extra layer of concrete placed on the upstream facing.

The maintenance of the Piano Barbellino dam was finished in 1987 (Photo 1): the geocomposite was constituted with a PVC geomembrane of 2 mm thickness and a PET geotextile of 1.5 mm thickness (Scuero, 1989). Differently, the maintenance of the Cignana dam was achieved in 1988 and the geocomposite was constituted with a PVC geomembrane of 2.5 mm thickness and a PET geotextile of a 1.5 mm thickness.

Similar geosynthetic was applied in 1991-1992 on the cellular gravity concrete dam of Pantano d'Avio (Photo 2), 63 m height and built in the Fifties at the very remarkable elevation of 2,378 m (Cazzuffi, 1996).

Moreover, a PVC-PET geocomposite (with a geomembrane 2.5 mm thick) was applied in 1993 to the vertical upstream facing of Camposecco masonry dam (Photo 3), 27 m height and built in the Twenties at the considerable elevation of 2,337 m (Scuero and Vaschetti, 1996).

Table 1 summarises the characteristics of the 6 dams discussed in this communication (Lago Miller, Lago Nero, Piano Barbellino, Cignana, Pantano d'Avio and Camposecco), while Fig. 1 shows their location.

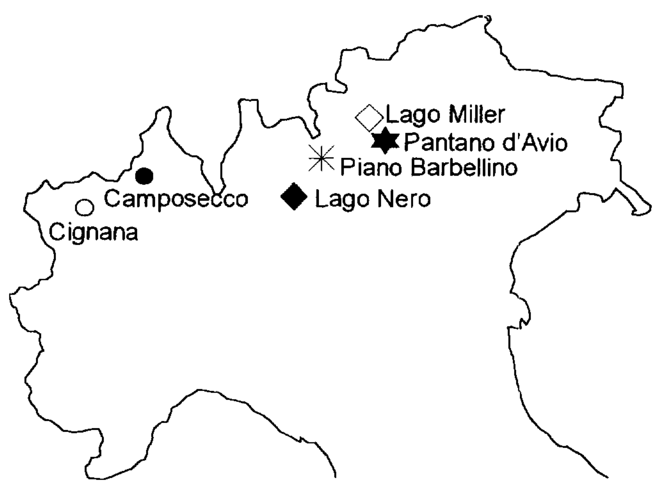

Figure 1. Location map of Italian dams on the Alps considered in the present paper.

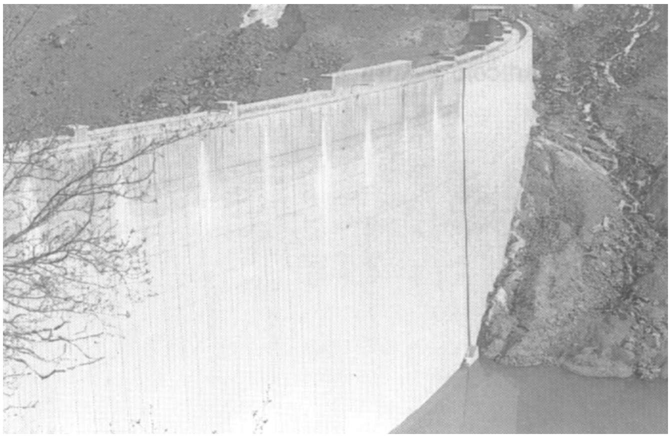

Photo 1. Piano Barbellino dam.

Photo 2. Pantano d'Avio dam.

2 OBSERVATION PROGRAM AND LABORATORY TESTS

During the recent observations (since 1995), different samples of geosynthetics were taken on the different dams, mainly on the upper part, exposed to weathering.

Only for the Pantano d'Avio dam (Photo 2) and for the third year sampling (Photo 4), samples were taken at the water level area submitted to the tidal range (dry and wetting zone).

The laboratory tests were carried out at the Special Materials and Geosynthetics Laboratories of ENEL Ricerca in Milano.

Among the different laboratory tests performed on the different geomembrane samples, the more relevant were as following:

- plasticizer content (according to ISO 6424);
- hardness Shore A (according to ISO R 868);
- tensile properties (according to ISO 527);
- water vapour transmission test (according to ASTM E 96).

For the geocomposite samples, the tests were performed only on the PVC geomembrane: the PET geotextile layer was taken away in laboratory, with the same methodology described also by Cazzuffi (1995).

Tests results on reference samples were only available for the Pantano d'Avio and Camposecco dams. Considering that the PVC geomembranes were produced by the same manufacturer, it was decided to use the same scale to show the results on all the samples taken on the different dams; the evolution of the properties vs. time since application is presented in Figure 2.

Table 1. List of dams considered in the paper (in chronological order according to geosynthetic application).

Dam	Lago Miller	Lago Nero	Piano Barbellino	Cignana	Pantano d'Avio	Camposecco
Type	M	C	C	C	CC	M
Height (m)	11.00	45.50	69.00	58.00	63.00	27.00
End of construction	1926	1929	1931	1928	1956	1930
Elevation (m)	2,170	2,024	1,868	2,158	2,378	2,337
Orientation	E	NW	E	W	S	NW
Slope (H/V)	Vertical	Vertical	Vertical	Vertical	0.5/1.0	Vertical
GM thickness (mm)	2.0	2.0	2.0	2.5	2.0	2.5
GM area (m^2)	1,500	4,000	6,000	8,250	17,000	4,800
GM application	1976	1980/1	1987	1988	1991/2	1993
Legend	M: Masonry dam C: Concrete dam CC: Cellular gravity concrete dam GM: Geomembrane			E: East W: West S: South NW: North West		

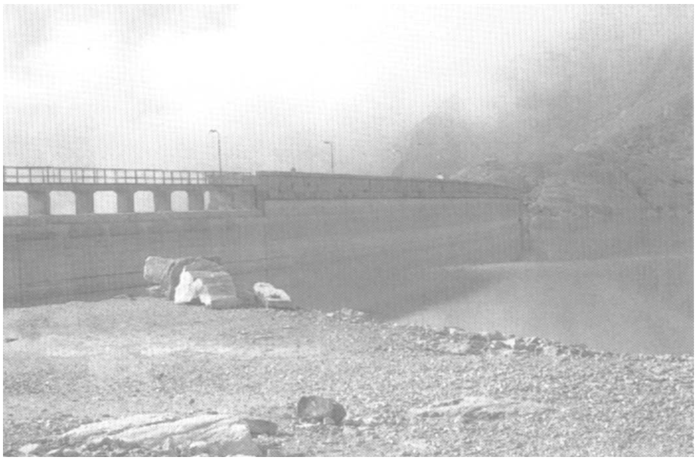

Photo 3. Camposecco dam.

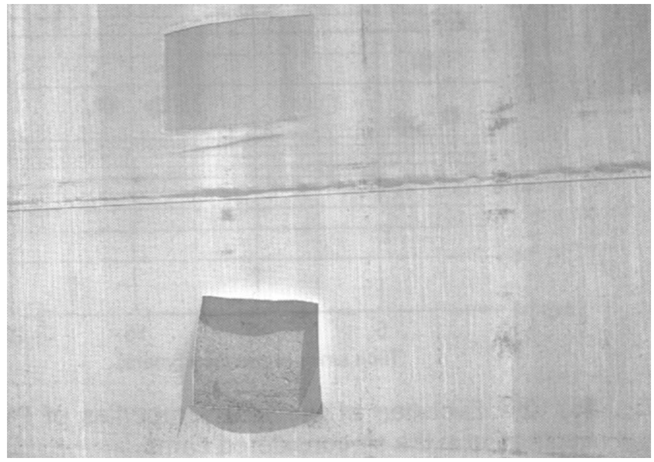

Photo 4. Location of the geomembrane sample exhumed in 1995 at Pantano d'Avio dam after 3 years since application.

3 CONCLUSIONS

The main results achieved by this extensive experimental program are as following:

- the PVC geomembranes exhibit generally a satisfactory behaviour vs. time;
- the plasticizer content exhibits a small decrease vs. time, even if it remains very high, for example about 28% after 19 years since application in Lago Miller dam;
- correspondingly, the hardness Shore A exhibits a certain tendance to limited increase, i.e. the geomembranes seem to be subjected to become a little bit more rigid;
- the results of the tensile properties confirm the above mentioned trend, i.e. the tensile strengths (both in longitudinal and transversal directions) generally tend to increase, while the corresponding strains tend to be subjected to limited decrease, thus forming a more rigid product;
- the water vapour transmission test results have been reported to permeability coefficient values according to the equations proposed by Giroud (1984) even if recently these equations have been questioned in literature (see, for example, Eloy-Giorny et al., 1996); in any case, being in this experimental study more interested to the comparative results than to the absolute values, it's important to remark that the permeability coefficient is quite constant vs. time, ranging from 2×10^{-13} m/s to 1×10^{-13} m/s.

Based on these results, similar rehabilitation systems of dams may be generalised, considering that a particular attention has to be taken into account during all phases of design and geosynthetic installation.

Finally, considering the lack of protection, survey and regular control during time of the geomembrane characteristics seem to be necessary.

Particular attention should be paid when geomembranes are exposed to South orientation, thus receiving the most of UV radiations.

REFERENCES

Cazzuffi, D. (1987) "The Use of Geomembranes in Italian Dams", *Water Power and Dam Construction*, Vol. 39 (3), pp. 17-21.

Cazzuffi, D. (1995) "Experimental Study on the Behaviour vs. Time of Different Geosynthetics Used in Canals Owned by Enel", *Proceedings Rencontres 95*, Beaune, France, Vol. 2, pp. 9-15.

Cazzuffi, D. (1996) "Réhabilitation de Barrages en Maçonnerie ou en Béton a l'Aide de Géomembranes: l'Expérience Italienne", *Comptes Rendus du Colloque Technique "Les géotextiles et les géomembranes dans les barrages"*, Paris, France, pp. 14.1-14.12.

Eloy-Giorni, C., Pelte, T., Pierson, P., and Margrita, R. (1996) "Water Diffusion Through Geomembranes Under Hydraulic Pressure", *Geosynthetics International*, Vol. 3, No. 6, pp. 741-769.

Giroud, J.P. (1984) "Impermeability: The Myth and a Rational Approach", *Proceedings International Conference on Geomembranes*, Denver, CO, USA, Vol. 1, pp. 157-162.

Monari, F. (1984) "Waterproof Covering for the Upstream of the Lago Nero Dam", *Proceedings International Conference on Geomembranes*, Denver, CO, USA, Vol. 1, pp. 105-110.

Scuero, A.M. (1989) "Waterproofing of the Upstream Face of Existing Concrete Dams with a PVC Geomembrane", *Proceedings Int. Conference on Uprating and Refurbishing Hydro Power Plants (II)*, Zurich, Switzerland, pp. 291-303.

Scuero, A.M., and Vaschetti, G.L. (1996) "Geomembranes for Masonry and Concrete Dams: State of the Art Report", *Proceedings of the First European Geosynthetics Conference EuroGeo 1*, Balkema, Maastricht, Netherlands, pp. 889-896.

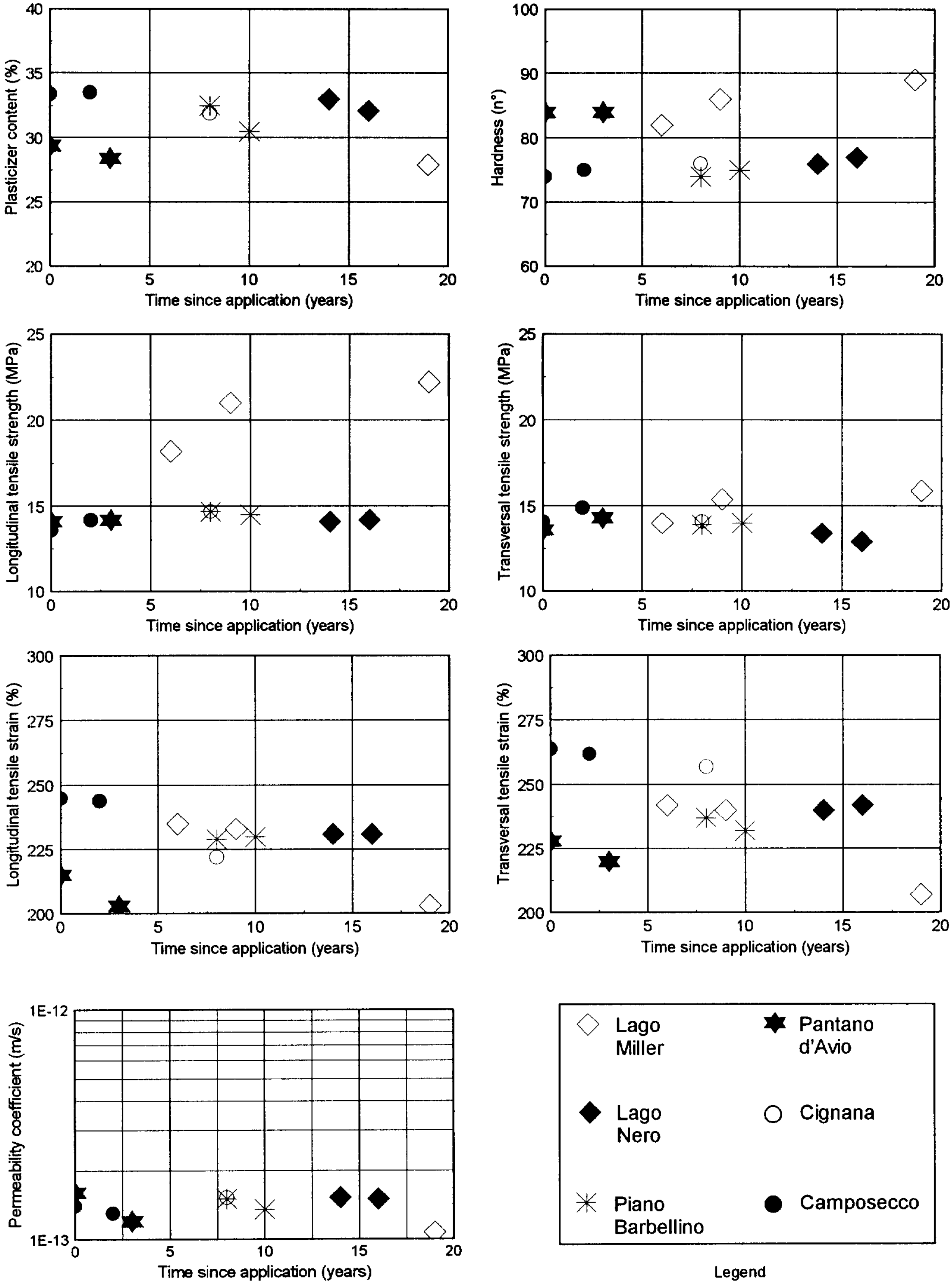

Figure 2 - Evolution of the main properties of PVC geomembranes vs time, after different years of application in the six considered dams (Lago Miller, Lago Nero, Piano Barbellino, Pantano d'Avio, Cignana and Camposecco).

A Sail-Shaped Dam Made of High-strength Composite Geomembrane

Jiang Kun'e and Yuan Lixin
Research Institute of Water Resources and Hydropower, Liaoning Province, P. R. China

ABSTRACT: This paper recommends the design and construction of a membrane dam, also known as sail-shaped dam, made of high-strength composite geomembrane. The bottom edge of the dam is anchored onto the concrete base plate, and the top edge is hung on a cable across the river. The dam height may be regulated by changing the length of cable, even to flatten it to the base plate when discharging the flow. This new type of hydraulic flexible dam has an artistic profile and a distinctive style. The cost of this dam is also less than any other types of gate or dam with the same height. To date, two sail-shaped dams have been built on non-gated spillways of reservoir in our province and have made the most of the water projects.

KEYWORDS: Dams, Geomembranes, Composite materials

1 INTRODUCTION

The membrane dam, also known as sail-shaped dam, is a low-head water retaining structure made of high-strength composite geomembrane. The bottom and two side edges are anchored on a concrete base plate and side wall respectively, and the topedge is hung on cable across the river, the two ends of which are twined around winches located on both banks. The dam height may be regulated by changing the length of cable, raising the water level for irrigation or power generation, or flattening the dam on the river bed for discharging flood or navigation. When it is installed on a non-gated spillway of a reservoir, it can increase the common storage to make the most of the water project.

Building hydraulic flexible structures with geosynthetics is an initiative work. It is necessary to meet the requirements of strength , impermeability, and durability, as well as the frost-resistance if the structure is located in a cold region. Through a series of laboratory and field tests, we have selected polypropylene woven geotextile coated with ethylene vinyl acetate copolymers(EVA) to serve as the dam material to build sail-shaped dams on the spillways of Heiyushan reservoir (Fushun city) and Lanshan reservoir (Changtu county) in Liaoning province in 1996 and early 1997 respectively. The Lanshan sail-shaped dam has three continuous spans of 15m each, the two existing bridge piers are taken as the supports of cable transferring the cables to the winches by pulleys, so as to move the three spans synchronously. This type of structure is easy to construct, simple and convenient to operate, making it unnecessary to install pipelines and inflat/ deflat equipment. threrfore the cost of this system is the lowest as compared with other types of closed hydraulic flexible structures with the same height.

2 WORKING CONDITIONS AND DESIGN CALCULATION

2.1 Calculation of Configuration of Membrane

During the process of water-retaining, the membrane is subjected to tensile stress only when the water pressure is applied on it, no compressive stress and bending moment occur. and no stress in the direction of the dam axis, as it is long enough in compared with the height of dam. Therefore it is considered as two-dimensional problem.

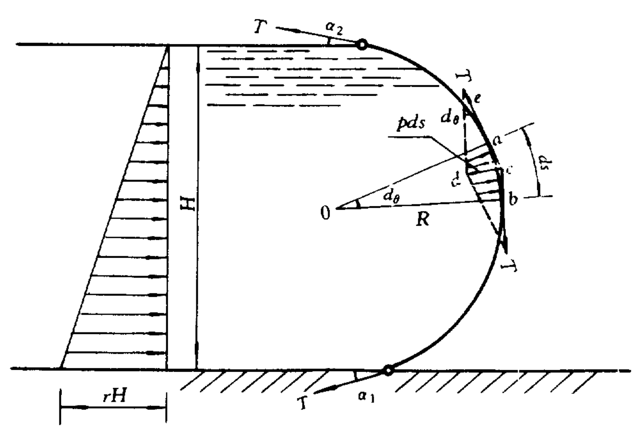

Fig. 1 Calculating sketch of membrane dam

When the water depth on the upstream side of membrane dam is H, and no water on the downstream side. The total upstream water pressure is $P=\frac{1}{2}\gamma H^2$, where γ = unit weight of water = 1 t/ m^3. From the equilibrium of all horizontal forces, we have:

$$T=\frac{\gamma H^2}{2(\cos\alpha_1+\cos\alpha_2)} \quad (1)$$

in which: T = tangental tension of the membrane. In Fig.1, considering ds is very small, $\overset{\frown}{ds}=ab$. $\Delta abo \backsim \Delta ecd$, then

$$\frac{R}{ab}=\frac{T}{cd} \quad \text{or} \quad \frac{R}{ds}=\frac{T}{pds}$$

where p = unit water pressure at that point, and R = radius of curvature. Therefore

$$R=\frac{T}{p} \quad (2)$$

Using above relationship, we can compute the geometric configuration of the membrane simply by diagrammatic method, the error of which will not exceed 5%, so it can meet the practical requirement. In the diagrammatic method, the upstream water depth is divided into a number of equal divisions, and the average unit water pressure of each division is computed, and the radius of curvature is calculated by Eq.2. Join circular arcs of each division together, to form finally the whole configuration of the membrane dam.

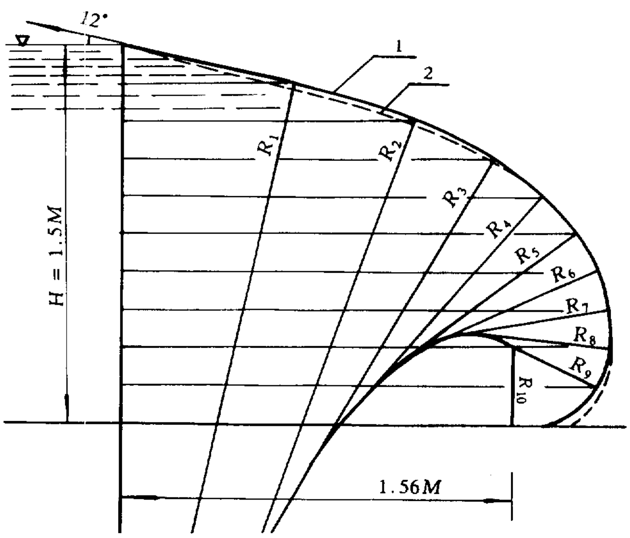

Fig.2 Determine configuration of membrane dam by diagrammatic method: 1-computed curve, 2-Tested curve by hydraulic model study.

Now, we take the membrane dam of the spillway at Heiyushan reservoir as an example: H = 1.50m, $\alpha_1=0^\circ, \alpha_2=12^\circ$, We have

$$T=\frac{\gamma H^2}{2(\cos\alpha_1+\cos\alpha_2)}=\frac{1\times1.50^2}{2(1+0.978)}=0.569 \text{ tf/m or}$$

5.69 KN/m

Ten equal divisions are made for H, the radius of curvature of the first division is

$$R_1=\frac{T}{p_1}=\frac{5.69}{\frac{1}{2}(0+1.5)}=7.58\text{m}$$

Similarly, for the second division

$$R_2=\frac{5.69}{\frac{1}{2}(1.5+3.0)}=2.53\text{m}$$

The rest may be done in the same way. The configuration is drawn as in Fig.2. From which, the total length of membrane is 3. 05m, and the horizontal distance between anchor and crest is 1.56m.

2.2 Calculation of Cables

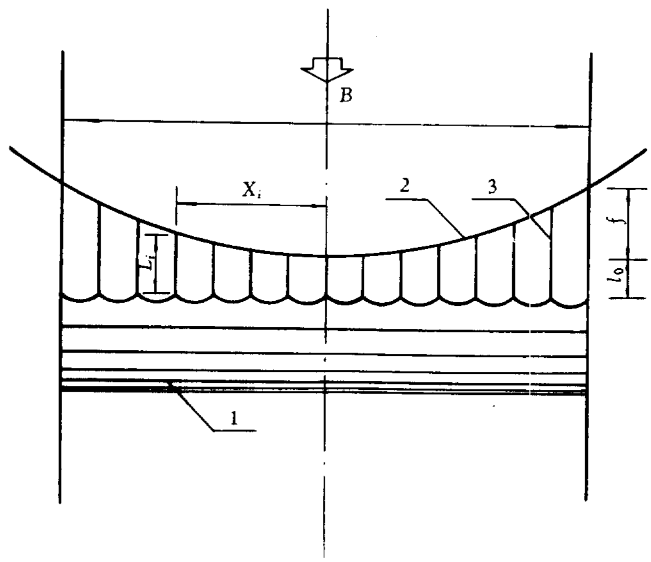

Fig. 3 Layout plan of membrane dam: 1-dam, 2-main cable, 3-secondary cables

The layout plan of the membrane dam is shown in Fig.3. The main cable is a river crossing cable, and the secondary cables are used to tie the membrane dam onto the main cable. The spacing of which depends on the strength of membrane and the junction points. If the spacing is 1m, the tensile stress of each secondary cable is T = 5.69 KN . The maximum tensile stress of the main cable may be computed by the following formula:

$$S_{max}=\frac{TB^2}{8f}\sqrt{1+16\frac{f^2}{B^2}} \quad (3)$$

Table 1. Test results of high strength composite geomembrane for sail-shaped dam.

Item	Unit	Amount	Remark
Weight	g/m^2	975	
Total thickness	mm	1.2	
Thickness of EVA coater	mm	2×0.3	
Tensile strength(warp)	KN/m	42.6	Refer to ASTM D-1682
(weft)	KN/m	38.7	
Elongation (warp)	%	7.05	Refer to ASTM D-1682
(weft)	%	8.43	
Tearing strength	KN	1.04	Refer to ASTM D-1117-80
puncture strength	MPa	1.7	Refer to ASTM D-3780
Fatigue test	Times	100000	strength kept unchanged
Grab test	KN	11.0	Width of clamp = 30cm The tensile strength of the joint between membrane and cable.
Freez-thaw test	—	—	After 428 freezing-thawing cycles, tensile strength reduced by 24.5%.

In this example, we have

$$S_{max} = \frac{5.69\times15^2}{8\times5}\sqrt{1+16\frac{5^2}{15^2}} = 53.34\ \text{KN}$$

If the curvilinear equation of main cable is

$$y = \frac{fx^2}{(\frac{B}{2})^2} = \frac{5x^2}{(\frac{15}{2})^2} = 0.0889x^2$$

$$(\frac{dy}{dx})^2 = 0.0316x^2$$

The length of the main cable

$$L = 2\int_0^{B/2}\sqrt{1+(\frac{dy}{dx})^2}dx = 2\int_0^{7.5}\sqrt{1+0.0316x^2}dx$$

$$= 2\left[\frac{x}{2}\sqrt{1+0.0316x^2} + \frac{1}{2\sqrt{0.0316}}\cdot\ln\left(x\sqrt{0.0316}+\sqrt{1+0.0316x^2}\right)\right]_0^{7.5}$$

$$= 2\times9.34 = 18.68\text{m}$$

The length of the secondary cable may be computed by following formula:

$$L_i = \frac{fx_i^2}{(\frac{B}{2})^2} + L_0 \qquad (4)$$

In which: L_i = Length of the cable at point i,
L_0 = Length of the cable at center of span,
x_i = Distance from center of span to point i.

If $L_0 = 1.0$m, Therefore:

$$L_1 = \frac{5\times1^2}{(\frac{15}{2})^2} + 1 = 1.089\ \text{m}$$

$$L_2 = \frac{5\times2^2}{(\frac{15}{2})^2} + 1 = 1.356\ \text{m}$$

The rest may be done in the same way.

In order to check the reliability of the results computed by approximate methods, we have conducted hydraulic model study (1: 5). It is indicated that the results are basically coincidence.

3 SELECTION OF MATERIAL

The sail-shaped dam is a hydraulic flexible structure exposed to the air and sunlight, or soaked in water over a long period of time, so that the flexible material must have sufficient tensile strength, watertightness, durability, tearing strength, flexibility, fatigue strength, and frost-resistance, etc. For this reason, after qualitative tests on several polymeric materials, we have decided to use polypropylene woven geotextile as the skeleton of composite geomembrane, and coated with ethylene vinyl acetate copolymers (EVA) adding an age-inhibiting agent. It is also required that the geotextile must be treated, so as to provide high cohesiveness with EVA. According to the concrete working condition of sail-shaped dam, we have conducted various tests of physical and mechanical properties of processed material. The results are listed in Table 1.

An appropriate factor of safety should be considered in design of a sail-shaped dam, because of error in calculation, nonuniformity of skeleton material, loss of strength during operation, as well as the safety demand according to importance of the project, which is usually in the range of 3 to 5. The factor of safety of the two dams described in this paper are 6.8 and 11.1.

4 JOINT OF THE MEMBRANES

Due to the limitation of the width of the geomembrane, it is necessary to piece together by lap joint. We have sewn up with polyamide fibre thread(density of stitches 2 ~ 3mm). The holes of needle are sealed by thermo-bonding EVA pieces of the same thickness to prevent from leakage. The test results of lap length and number of stitching rows effect on shearing strength are shown in Table 2.

Table 2. Test results of shearing stress of lap joint

Lap length (mm)	Number of stitching row	shearing strength (KN/m)
80	2	28.3
80	3	37.5
80	4	38.9

80mm lap length and 3-row stitches are adopted

5 ANCHORAGE

The anchorage of a membrane dam on the concrete base plate or side wall is composed of built-in bolts (spacing 20cm), steel plate, pipe and channel. To punch bolt holes in the membrane is unnecessary. The pull-out resistance test was conducted before installation. The detail of anchorage is shown in Fig.4

6 CONCLUSION

It is an attempt to use high-strength composite geomembrane to build low-head water-retaining structures, in order to open up the application of geosynthetics. Through careful design and experimental study, it is indicated that the properties of this special material can meet the requirement of working conditions of the dam. So far, two sail-shaped membrane dams, 1.17m and 1.5m high, 15m and 3 × 15m span, have been built on spillways of reservoirs in our province. This simple type of structure with low engineering cost is a large benefit to the projects. Practice has proven that they are successful. However, the field observation is still taking place. At present, the height of the dam is limited by the strength of material. In order to acquire still greater results, it is necessary to take up effective measures to develop geosynthetics with higher strengths, to improve the lap joints, and to reduce wrinkles on the dam, so as to make the structure more perfect and safe.

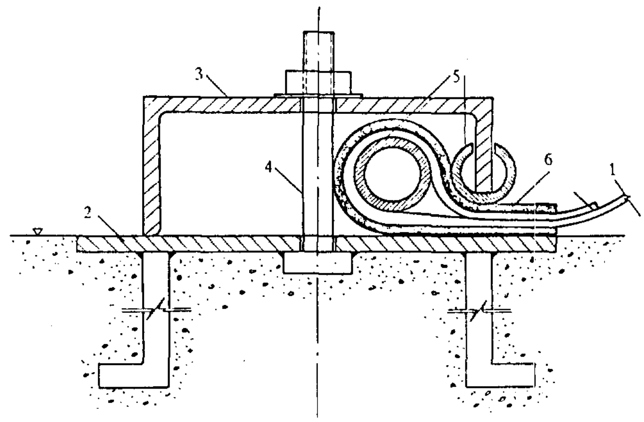

Fig. 4 Anchorage: 1-membrane, 2-steel plate, 3-channel, 4-built-in stainless steel bolt, 5-steel pipe, 6-rubber plate

REFERENCES

B . E. Sergeev, et al, (1984) *"Hydraulic Flexible structures"*, COLOS, Moscow, USSR. (in Russian). pp. 9-38.

Design Institute of Lanzhou Municiple Engineering (1979), "Design of Rubber Membrane Dams", *Proceedings of National Conference on Standardization of Dam Bag and Technical Exchange of Rubber Dams*, Benxi City, Liaoning Province, PRC. PP. 300 – 319

Use of a Synthetic Rubber Sheet for Surface Lining of Upper Pond at Seawater Pumped-Storage Power Plant

H.Shimizu
Director, Okinawa Seawater Pumped-Storage Project Construction Office, Electric Power Development Co., Ltd., Okinawa, Japan

Y.Ikeguchi
Deputy Manager, Okinawa Seawater Pumped-Storage Project Construction Office, Electric Power Development Co., Ltd., Okinawa, Japan

ABSTRACT: This paper presents a new technology for dam surfacing based on the use of rubber sheet which will be used in the construction of the world's first seawater pumped-storage power plant. The plant, presently under construction on Okinawa Main Island, is planned and financed by the Ministry of International Trade and Industry (MITI), Japan, with the Electric Power Development Co., Ltd. (EPDC), under a consignment contract with MITI, being in charge of surveys, research, designs and supervision of the construction. In designing this pilot plant, the sheet foundation design, the sheet anchoring method, selection of the sheet material, structural designs, and leakage water detection and dewatering system have been newly developed in consideration of the requirements imposed on a seawater pumped-storage power plant. This paper presents the design concept, construction work, the method and outcome of the quality management and observed behavior of sheets during typhoon conditions.

KEYWORDS: Construction, Dams, Design, Geomembranes, Pond Liners

1 INTRODUCTION

The objective of this plant is to develop seawater pumped-storage power generation technology for commercial use. The technology will be validated through a 5-year test operation and its application technology established accordingly.

The plant's upper pond is located on a plateau at approximately 150m elevation on the Pacific coast of Okinawa Main Island. The ocean is directly utilized as the lower pond. Power is generated at a maximum 30MW output at a powerhouse installed approximately 150m underground. As seawater is employed, a synthetic rubber sheet is used for the surface lining of the upper pond. Various new materials and new construction methods are also employed, including fiberglass reinforced plastic for the penstock. The seawater resistance and durability of each structure will be verified accordingly.

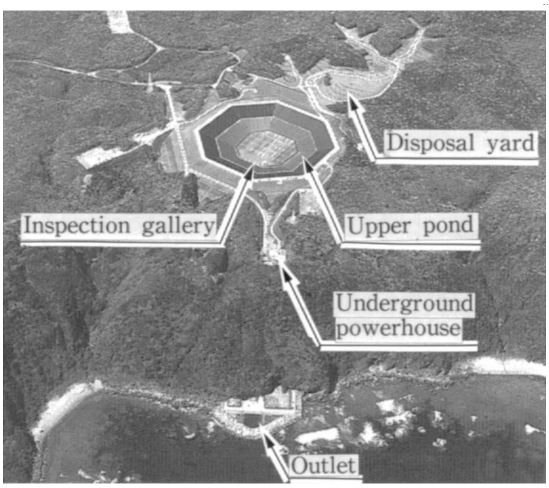

Photograph 1. Panoramic view of the plant.

As a complicated configuration would provide difficulties in surface lining installation, the upper pond is designed with a layout of maximum possible simplicity. To improve workability, the dam body is an octagonal mortise earth fill dam. The slope is 1:2.5 (v:h) considering the stability of the embankment. Excluding the transition layer, the overall embankment volume is approximately 420,000m^3. As shown in Figure 1, the surface lining is formed with a sheet anchor (filling concrete included), a transition layer (sheet foundation with crushed rock), and a lining sheet (main sheet, cushion fabric, cover sheet, etc.). The surface area of the sheet lining is approximately 53,000m^2. Started in November, 1994, the surface lining work was completed in February, 1996.

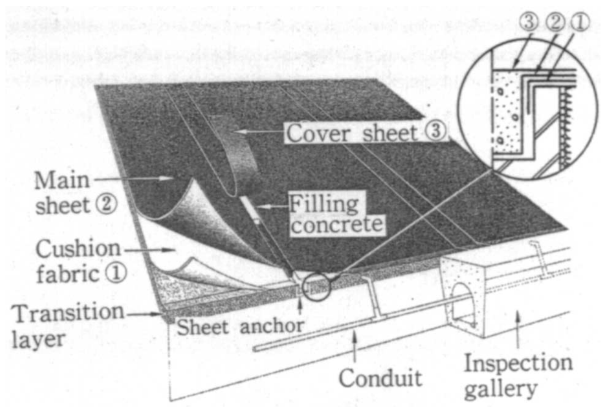

Figure 1. Structure of sheet lining.

2. SELECTION OF UPPER POND SURFACE LINING

2.1 Surface Lining Structure

The following conditions are required for the plant's surface lining.

1. The lining materials are required to have virtually zero-permeability to provide a barrier preventing seawater leakage into the natural ground.
2. The surface lining is required to maintain impervious sealing performance against repetitive water level fluctuation.

Although it was possible to consider a concrete, asphalt or sheet lining as the surface lining, the sheet lining was finally selected for the following reasons. It is made of materials which provide a much lower permeability than concrete or asphaltic linings. Concrete lining has joints which present weak points in terms of the watertight integrity of the lining structure overall. Sheet lining construction costs are also lower than those for concrete or asphaltic linings.

In sheet lining structures, the sheet surface can either be exposed or protected by earth materials or concrete. Here, an exposed structure was selected as it permits easy repair in the event of sheet damage while assuring high reliability subject to appropriate maintenance inspection.

2.2 Sheet Materials

The following conditions are required for the plant's sheet materials.

1. As an exposed sheet lining structure was selected for the pumped-storage pond, the water level of which may be frequently changed, and with the plant located in sub-tropical Okinawa, sheet materials which provided less temperature sensitivity are suitable for the plant's sheet lining. (Temperature sensitivity shows extents of physical properties changes such as an ultimate elongation and a tensile strength caused by temperature change.)
2. Since the surface lining must be resistant to repetitive cyclic load and its structure must ensure impervious sealing performance in the location in which the intake and inspection gallery adjoin the structure, the sheet materials are more suitable due to their superior elongation and flexibility.

Table 1. Characteristics of the sheet materials.

Materials	EPDM	PVC	HDPVC	HDPE
Ultimate elongation(%)	450	300	400	700
Tensile strength(N/cm^2)	750	1632	1423	2957
Temperature sensitivity				
at high temperature	L.S.	S.	S.	S.
at low temperature	L.S.	S.	L.S.	S.

Notes: Values in table are minimum values of the standard sheets. L.S. and S. denote less sensitive and sensitive.

Synthetic rubber (EPDM), soft polyvinyl chloride (PVC), high density soft polyvinyl chloride (HDPVC: specially developed PVC for improvement of the physical properties and feeling (like rubber) with increase of PVC molecular weight and the addition of plasticizer), or high density polyethylene (HDPE) are generally employed for the surface lining of sheet linings. The characteristics of the sheet materials are compared in Table 1. EPDM was selected after studies and comparisons of the material performance and workability of these materials. Since HDPE provides a low elongation at yield (although its ultimate elongation is high.), HDPE was judged less suitable for the plant's sheet materials.

An outdoor exposure test near the site, bacteria proof test, seawater resistance test, and marine organism deposit test were carried out on the EPDM sheet used in this plant to determine its characteristics under near-real conditions. The long term durability of the EPDM sheet was confirmed.

3. DESIGN OF SUBGRADE FOR SURFACE LINING

The requirements for the subgrade of a rubber sheet lining for a seawater pumped-storage upper pond, are listed below:

1. It must provide a surface sufficiently hard to support the sheet, and ensure sufficient slope stability.
2. It drains the spring water from the natural ground, thereby dispersing the pore water pressure on the back of the sheet.
3. In the event of sheet failure, it diverts leakage water downward, finally leading to the inspection gallery built around the pond bottom, thereby preventing infiltration of seawater into the natural ground. (A dam body with a permeability coefficient in the order of $10^{-4} \sim 10^{-6}$cm/s has very low permeability.)
4. The residual air behind the sheet should be exhausted, because such air may inflate the sheet like a balloon when water is filled, or the negative pressure created by strong wind may pull the sheet up.

A crusher run with a maximum particle size of 20mm was selected from a number of materials meeting the above requirements in terms of water permeability and air porosity, with due consideration given to economy and seismic stability. The layer thickness was designed at 50cm. In this project, this crusher run foundation is termed the 'transition layer' as it is an intermediate transition layer between the dam body and the sheet lining.

4. DESIGN OF SHEET ANCHOR

4.1 Study of Sheet Anchoring Method

An exposed surface lining is used in this plant. In this structure, on-site adherence works may present structural weakness. For this reason, the concrete block anchoring method was adopted in order to alleviate on-site adhering works. In this method, the on-site sheet adhesions are embedded into specially designed U-shaped concrete blocks with filling concrete. No sheet-edge bonding work is performed on-site except for the cover sheets that provide an impervious lining over the anchoring works. As this anchor method is sufficiently heavy and wraps the sheet completely, it prevents wind damage experienced by anchoring by flat bar or by wrapping into buried pipe. Also, with the sheet surrounded by the sheet anchor, a sheet failure would not extend beyond the surrounding area.

4.2 Sheet Anchor Block Design

The following functions are required for the sheet anchor.

1. It must anchor the lining sheet firmly.
2. The main sheet surface must not adhere on site.
3. Its configurations and weight must be durable against sheet deformation resulting from an earthquake or a strong wind such as a typhoon.
4. It must provide an effective exhaust capability.

The U-shaped precast concrete blocks provide the functions given in 1, 2 and 3. To include the function described in 4, therefore, a precast unit with built-in PVC tubes was designed, as shown in Figure 2. One of the main reasons for designing a concrete block with built-in PVC tubes was that it requires less filtration installation area than the method which uses a buried perforated tube to prevent clogging of fine particles during stone crushing, thereby significantly reducing the risk of fine particle loss due to filter failure. Another reason was that it prevents the risk of sheet break due to subsidence of the transition layer caused by a tube break resulting from uneven settling of the transition layer. The exhaust tube also promotes drainage of leaked water in the event of sheet failure. A patent application for this type of sheet anchor structure has been filed.

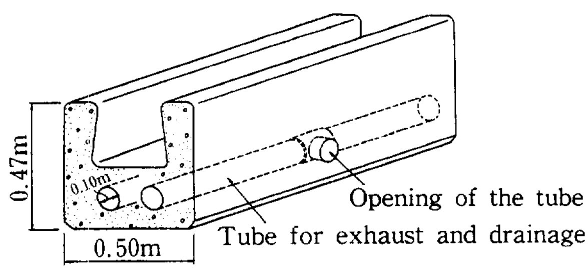

Figure 2. Anchor block.

4.3 Study of the Sheet Anchor Interval

According to this principle which is to eliminate on-site adhesion work on the exposed side of the sheet, the interval in the horizontal direction of sheet anchors was selected so that this would be as large as possible in reference to the maximum width of a sheet capable of being manufactured and transported to the construction site. This synthetic sheet is usually manufactured in 1.2 m wide belts which are joined at the manufacturer's plant into a single wide sheet. Considering the restrictions in the sheet transportation and the handling / fabricating limitations at the manufacturer's plant, the lateral interval of the anchor works was taken as 8.5m for slopes and 17m at the pond bottom.

For the interval in the slope direction, the sheet conditions during a strong wind such as a typhoon were considered. Strong wind induces negative pressure on the sheet surface. If air enters under the sheet, the sheet swells to maintain the balance of the inside and outside pressure. In this case, the sheet anchor intervals in the slope direction were determined considering the relationship between the sheet deformation (swell height) and the anchor intervals in the slope direction. Regarding sheet deformation, a rectangular rubber sheet sample was anchored at its four sides and caused to swell with compressed air supplied from behind. In addition to this model experiment, numerical analysis was conducted with a finite element method (code name; ABAQUS) that permits the handling of super-elasticity materials such as rubber sheet. Where the aspect ratio (ratio of short side to long side at the sheet anchored area) was 1:2 and 1:5, the model test showed no significant difference in deformation under the same pressure. This analysis also indicated no significant difference in sheet deformation where the aspect ratio was larger than 1:2. The test indicated that deformation does not exceed a maximum 28% increase. It is, therefore, unnecessary to install a sheet anchor in the horizontal direction on the slope when the anchor intervals in the sheet horizontal direction are controlled. Consequently, the sheet anchor in the horizontal direction on the slope is located at the crest of the pond, berm, and at the toe of the slope.

4.4 Sheet Anchor Stability Against Sheet Swell

Sheet swelling due to strong wind induces tensile stress in the sheet and causes the sheet anchor to lift. In this case, sheet anchor stability was studied using the sheet deformation calculation model shown in Figure 3. The results of the study were compared with those of the previously described model test and it was confirmed that the values derived from the model test and the two-dimensional calculation model matched.

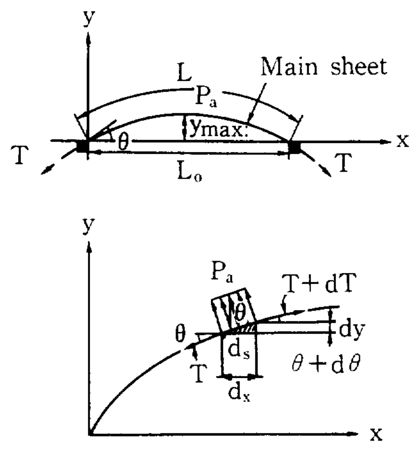

Figure 3. Sheet deformation calculation model.

The calculation method is outlined below. The negative pressure on the sheet, P_a, can be determined from equation (1).

$$P_a = \frac{\gamma_a}{2g} Cv^2 \tag{1}$$

where: γ_a = weight of air unit volume; C = coefficient of wind force; v = wind velocity; and g = gravitational acceleration. The mechanical equilibrium of forces is expressed in equations (2) and (3).

$$T\sin\theta = P_a\, ds\cos\theta + (T + dT)\sin(\theta + d\theta) \quad (2)$$

$$T\cos\theta + P_a\, ds\sin\theta = (T + dT)\cos(\theta + d\theta) \quad (3)$$

where: T = tensile force induced in sheet; and θ = swell angle. Relation of $T = f(v, \theta, L_o)$ and $L = f(v, \theta, L_o)$ is led from the equations (1) through (3). Also, the length of the sheet after swelling, L, can be determined from equation (4).

$$L = \frac{\sigma_t}{E} L_0 + L_0 \quad (4)$$

where: σ_t = tensile stress (T/A) induced in sheet; A = cross area of sheet; and E = elasticity coefficient of EPDM sheet. Substituting the relative equation between E and σ_t obtained from the model experiment for Equation (4), leads to another equation, i.e., $L = f(v, \theta, L_o)$ due to the relation $T = f(v, \theta, L_o)$. Therefore, iteration the calculations for the unknown v and θ until L obtained from the two equations match, the sheet deformation (deflection angle, swell height, and distortion) and the induced stress in response to the optional wind velocity can be calculated.

Assuming a sheet anchor interval of 8.5m and a deformation reaching the limit of $\theta = 90^{\circ}$ (semicircle), the mean wind velocity, distortion, and tensile stress were calculated from the above equations. Consequently, the sheet distortion becomes 57.1% and the tensile stress 118N/cm^2 at approximately 43m/s wind velocity. These are sufficiently below the standard values of the main sheet (EPDM) shown in Table 2. The force toward the upper sheet anchor is determined from the tensile stress induced in the sheet is 4,710N/m, which is less than the sheet anchor weight of 5,370N/m. Assuming a sheet swell, the sheet anchor would therefore not be lifted.

5. DESIGN OF LINING SHEET

5.1 Member Structure and Lining Sheet Material

As described, the major lining sheet members for this plant are the main sheet, cushion fabric, and cover sheet. The functions and materials of each member are described hereafter.

5.1.1 Main sheet

The main sheet is a trunk member of the lining sheet and inhibits seawater leakage. As the lining sheet of this plant is exposed, to improve its ozone resistance the proportion of EPDM in the rubber content is higher at a minimum of 70%.

The basic specifications are shown in Table 2. The thickness is established by considering the strength, resistance to irregularities, and workability. No special conversion of the plant production line was necessary for the 2.0mm thick EPDM sheet. The ultimate elongation is determined by considering the partial deformation. Since the sheet used in the plant was improved to reduce the tension set, its tensile strength exceeds that of the standard sheet (750N/cm^2).

Table 2. Basic specifications of the main sheet.

Thickness (mm)	2.0～2.3
Ultimate elongation in tensile shear test (%)	450 or more
Tensile strength in tensile shear test (N/cm^2)	981 or more

Sheets joined and widened at the manufacturer's plant are used for the main sheet. To minimize irregularities in the adhering surface of the cover sheet by reducing the number of joints wrapped in the sheet anchor, the main sheet is joined in the slope direction. The tensile strength of the joints is greater than that of the original sheet. A test was performed to check its impervious sealing performance. The results confirmed there would be no air suction due to negative pressure. According to records regarding agricultural ponds, it is clear that with no water leakage through the joints, therefore, it provides the necessary high reliability.

5.1.2 Cushion fabric

The cushion fabric prevents small irregularities and protrusion onto the surface of the transition layer and concrete from affecting the sheet. It protects the sheet from the edges of the crushed stone and concrete. It also prevents sheet failure due to local deformation as it makes the sheets installed surface smooth, thereby completely distributing sheet distortion to prevent local deformation of the base. (Elongation ratio in proportion to the same deformation is reduced.)

Long-fiber non-woven spun bonded fabric is generally used as the lining sheet cushion material. Compared with polyester and polypropylene, polyester was selected for the raw materials of the cushion materials, because of its excellent heat resistance and for water-proof performance. A repetitive hydraulic resistance test was carried out for the on-site sheet adhesions of which the base was a 20mm diameter simple grain material, assuming a loss of fine particles from the transition layer. Consequently, a minimum of 800g/m^2 is taken as the standard value of weight (mass per unit area).

5.1.3 Cover sheet

The cover sheet provides an impervious sealing performance of the sheet anchor concrete surface which can become a weak point due to crack formation, etc. (The sheet anchor fixes the sheet mechanically. Its structure is dynamically stable. It does not, however, provide a water impervious seal.) Its material and specifications are the same as those of the main sheet.

5.2 Cover Sheet Adhesion Method

The adhering areas of the main and cover sheets are exposed. As this is the most important area for the water impervious seal of the surface lining, an adhesive tape (self-curing adhesive isobutylene-isoprene rubber tape) was used. The adhesive tape prevents condensation due to the adhesive when the sheet is cooled. Condensation can occur due to the heat of vaporization associated with the adhesive's organic solvent. The isobutylene-isoprene rubber adhesive is initially combined with a curing agent. As this tape cures slowly, it eliminates any extra work required such as brushing, and results in a homogeneous adhesion surface.

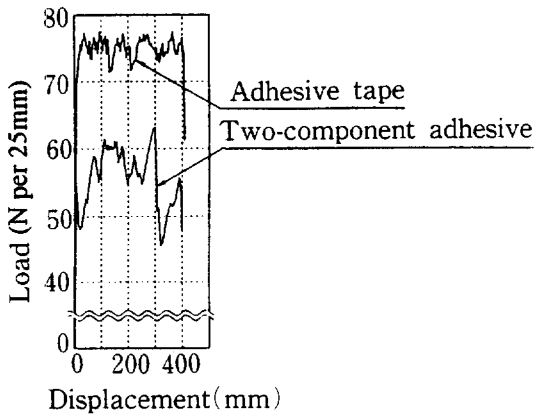

Figure 4. 180° peel test results

A 180° peel test was conducted on the adhering rubber sheet both after using a two-component adhesive and the adhesive tape. (Accelerated curing was used for test pieces at high temperature so that they provide the final adhesive strength.) The test results are shown in Figure 4. The peel strength of the adhesive tape is greater than that of the two-component adhesive. Here, the most important factor is that the adhesive tape shows smaller fluctuations in adhesive strength on peeling. Consequently, the adhesive tape ensures a higher water impervious seal. Adhesion with this tape prevents the formation of water leak routes.

6. QUALITY CONTROL IN SURFACE LINING INSTALLATION

6.1 Transition Layer Works

Stable quality is expected in the transition layer works since all materials are purchased from an existing crushing plant for concrete and road-base materials. In compaction, the finished density and surface conditions may, however, vary and quality control is, therefore, most important. The control standards were developed for precise quality control including a compaction method specifying the compaction equipment, spread depth, and tamping frequencies / times.

The control standards were developed based on the following basic conditions.

1. The material grain size shall be appropriate. The material shall be dynamically stable. Its structure shall also be stable in terms of the soil hydrology.
2. Compaction shall be sufficient.
3. The surface shall be smooth and dense.

The focal control points for the materials, compaction and surface finishing are grain distribution, dry density and flatness respectively. The controlled value of the field density was set at 1.92 t/m^3, 70% of the relative density, in reference to the compaction test data for the material containing natural water. This value was shown to provide sufficient strength for the embankment slope stability under the natural water content or saturation (postulating sheet failure) according to the triaxial compression test (CD test), and was selected with due consideration to its workability. Regarding the site density test method, the RI (radioisotope) method was used mainly as it allows measurement on the slope and is a simple method. The water replacement method was used in addition in the flat area and in the bottom of the crest and berm.

The quality control test showed that the values satisfied the control standards in all works (Table 3). The on-site permeability test also showed sufficient permeability for the transition layer. The site test conducted after compaction by the tamping method used in the actual installation showed that in the case of a minimum 10^{-2}cm/s permeability coefficient, the transition layer performance of the residual air exhaust under the sheet was assured, with an air permeability coefficient in the order of 10^{0}cm/s.

Table 3. Quality control test results of transition layer.

Items	Spec.	Ave.	Max.	Min.
Dry density (t/m^3)	≧1.92	2.03	2.37	1.92
Permeability Coefficient (cm/s)	—	0.27	1.50	0.014

6.2 Lining Sheet Installation

For the lining sheet installation, control standards were developed to specify the installation conditions based on the temperature, humidity, wind velocity, etc., control method for the adhering area of the cover sheet, adhesion width of each member, and the adhesion location in detail.

Regarding the material quality, an inspection was conducted on all points of the basic specifications every 1,000m^2. The rubber sheet quality may vary depending on the quality control in the raw material mixture process, pressure in the curing process, and the temperature control accuracy.

The cover sheet is the only member providing an impervious seal to the on-site sheet adhesions and thus requires a highly reliable adhesion. Quality control includes visual inspection and confirmation by touch to check for adhesion defects. Inspection with an inspection spatula confirmed no partial gaps remained not to adhere at the edges of the adhering areas. A negative pressure test was conducted throughout the adhering area. (Apply soapy water to the adhering area, depressurize at a minimum 0.51MPa over 10 seconds and check for foaming.)

Table 4. Quality control test results of adhesion work.

Items	180° peel strength (N per 25mm)	Tensile shear strength (N per 25mm)	
Curing period	7 days	7 days	3 months
Spec.	24.5 or more	196 or more	392 or more
Max.	80.4	503	631
Min.	29.1	314	405
Ave.	55.0	434	509

Test pieces produced under the same conditions were cured for 7 days, and the 180° peel strength and tensile shear strength were measured. The tests confirmed a stable adhering surface had been formed. The tensile shear strength was re-evaluated after a 3-month curing period and it was confirmed that the adhering area provided a strength equivalent to that of the main sheet. The test results are shown in Table 4.

7. OUTLINE OF WATER LEAK DETECTION AND DEWATERING SYSTEM

The system leads water leaking from the sheet to the inspection gallery (height=2.0m, width=2.0m) through the transition layer or PVC tube built into the sheet anchor. Since the groundwater from the drain hole on the ground is also led to the inspection gallery, it would be possible for the seawater and the fresh water to mix. To prevent such mixture, a pipe is installed from each conduit to each drain pit directly to collect the water. The leakage from the sheet only is pumped back to the upper pond. The groundwater is discharged to a nearby stream through a drainage tunnel. The seawater is, therefore, not discharged to the outside but returned to the upper pond and discharged back into the ocean after power generation. As the fresh water is discharged to the stream, the system is ecologically friendly.

Leakage from the sheet is detected by a salt analyzer (electronic conductivity measuring unit) and the fluctuation in the volume of leakage are measured by flow meter. Both instruments are installed on the conduit. To divide the slope into 55 and the bottom into 9 sections, a transparent conduit (acrylic) was installed to facilitate visual verification of the leakage locations in each section.

8. LINING SHEET BEHAVIOR UNDER STRONG WIND

Photograph 2. Sheet swell behavior in strong wind

In 1996, five typhoons approached Okinawa Main Island and provided opportunities to observe sheet swell behavior. When typhoon No.12 (Maximum instantaneous velocity; 49m/s, 10min. mean velocity; maximum 28m/s) approached in August, the water detection / dewatering system piping, etc., had not been completed. Air was able to enter the sheet without restriction through the built-in sheet anchor tube. Consequently, a maximum sheet swelling of approximately 1.5m height took place (10min. mean velocity; maximum 18m/s, Photograph 2). The lining condition after the typhoon approach, was checked by visual inspection when it was confirmed that there were no problems such as sheet failure, and almost no residual sheet distortion or transition layer interruption.

Although typhoon No.21 approached in September, with an equal wind velocity, sheet swelling was controlled to approximately 1/3 by cutting off the air supply from the built-in sheet anchor tube. Since the crest road was paved, it was reasonable to assume that air inflow from the crest into the transition layer would be effectively prevented, thereby further controlling sheet swelling.

9. CONCLUSIONS

Following the completion of the lining in February, 1996, fresh water (rainfall and groundwater pumped up from the underground powerhouse) has been stored in the upper pond since June, 1996, to protect the lining sheet and to eliminate residual air from behind the sheet prior to the actual operation of the plant. No water leakage has occurred. This sheet lining has complete technically and has become the main development toward the realization of the world's first seawater pumped-storage power plant. Also, it raised the sealing confidence in the sheet lining used in agricultural ponds etc.

The paper presents the following suggestions for future projects with the rubber sheet lining for better technology.

1. Further improvement in the adhesion performance for on-site sheet adhesions is needed to enable application in ponds with larger water depths.
2. Transition layer material has been developed for low cost performance and better workability to meet the necessary functional performance.
3. Minimizing the 'human factor' in lining sheet installation would improve work stability and efficiency.
4. Where this lining is applied to store fresh water, the lining performance can be dropped to some degree compared with seawater storage. Cost reduction resulting from a more streamlined design will be the subject of a future project.

ACKNOWLEDGMENTS

The writers wish to express their sincere gratitude to the members of MITI and all those concerned for their excellent cooperation and kind guidance.

REFERENCE

Takimoto,J. and Onoi,Y. (1997) "A Rubber Surface Pond on Strongly Weathered Rock Foundations for the Seawater Pumped-storage Power Plant", ICOLD Congress, 1997 Q.73, R.32, pp479-498.

A Scheme of Using Geosynthetics to Treat Cracks on A Reservoir Blanket

Z.Y. Liu
Director, Technical Inquiry Committee of Water Conservancy Bureau of Hebei Province, China

ABSTRACT: A reservoir in the Hebei province of China has been in operation since 1961.A natural cohesive soil layer was used as the horizontal impervious blanket for the auxiliary dam. Cracks often occurred on the blanket and in the foundation of the dam during the operation. A scheme of using geosynthetics to treat the cracks was proposed. The scheme is composed of three reaches, namely, the anti-seepage reach , the drainage reach and the dam slope reach. Geomembrane, geomembrane-geotextile composite, and geopipes were used. A series of tests were made. The methods of testing and design will be presented in this paper.

KEYWORDS: Blanket, Cracks, Geocomposite, Design scheme.

1 INTRODUCTION

Huangbizhuang Reservoir in the Hebei Province of China was constructed from 1958 to 1961 with a catchment area of 23400 km^2 and a capacity of 1.21 billion cu. m. It has an auxiliary dam with a length of 7000 m and a maximum height of 19.2 m. The overburden layer of the foundation is composed of cohesive soil , sand, gravel and cobbles. The cohesive soil layer with thickness of 3~10 m was used as natural horizontal impervious blanket. A lot of cracks occurred on several parts of the blanket after storage of water for more than 35 years due to the unequal settlement of the soil layer under the water and dam load. The cracks were traditionally treated by digging ditches and backfilled with cohesive soil or by grouting with mud or cement. All of these measures had very little effect. In recent years some cracks were found under the dam and might extend in the foundation as far as the downstream side of the dam. It was found after exploration and excavation that most cracks on the blanket had silted up and those under the dam were mostly kept empty. It was generally considered that the cracks on the blanket would do little harm to the reservoir but those under the dam might cause seepage failure in the foundation .In order to refrain the water in the reservoir from flowing directly into the cracks under the dam and on the blanket near the dam, a scheme of using geosynthetics to treat the cracks was proposed. The whole work consists of a series of laboratory tests and a conceptual design. Geomembranes, geotextiles and geopipes were used in the scheme.

2 TESTS OF HYDRAULIC TRANSMISSIVITY OF THE SPACE BETWEEN THE GEOMEMBRANE AND THE SOIL

2.1 Test Equipment and Samples

2.1.1 Test box

A box with size of 2.5 m × 0.5m × 1.0 m is made of steel and divided into two stories. The height of each story is 0.5 m. Flange plates and rubber water-tight seal were used to prevent the leakage of water between stories. Inlet and outlet pressure gauges were installed as shown in Figure 1.

2.1.2 Properties of geosynthetics and soil sample .

Two types of geosynthetics were used in the tests. One is PVC geomembrane with a thickness of 0.6 mm, and the other is geomembrane-geotextile composite composed of 0.45 mm PVC geomembrane and 210 g/m^2 needle-punched non-woven geotextile. Their properties are presented in Table 1.

Three kinds of soil samples were excavated from the blanket of the reservoir. Their properties are presented in Table 2.

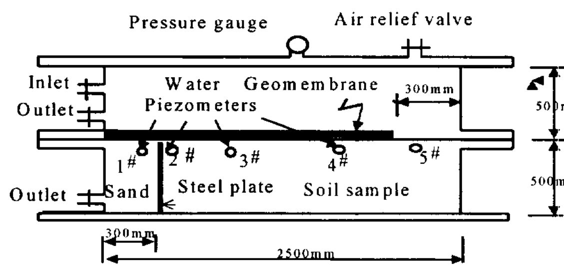

Figure 1. Test box.

Table 1. Properties of geosynthetics.

Types of geosynthetics	Thickness of geomembrane (mm)	Weight of geotextile (g/m^2)	Stripe tensile strength (KN/m)	Elongation at break (%)
PVC geomembrane	0.6	——	9.49	282
PVC geomembrane-geotextile composite	0.45	210	12.44	83

Table 2. Properties of soil samples.

Soil samples	γ_d (KN/m^3)	Distribution of grain size (%) 0.25~0.1 mm	0.1~0.05 mm	0.05~0.005 mm	<0.005 mm	Coefficient of permeability (cm/s)
No.1	15.2	10.5	39.5	44.9	5.1	7.09×10^{-5}
No.2	15.0		6.5	63.0	30.5	2.63×10^{-5}
No.3	14.4	1.0	34.0	61.9	3.1	9.23×10^{-5}

2.2 Test Procedures

A mixture of three kinds of soil samples was used in the tests with a thickness of 0.5 m and dry density $\gamma_d = 15$ KN/m^3. A sand drain with a width of 30 cm was placed at the outlet end of the box. A steel plate was welded on the front and back sides of the box to separate the sand drain from the soil sample. Geomembrane was put on the soil surface with a 30 cm gap to allow the water flowing into the geomembrane-soil interface. Glue was used to prevent leakage along the inner faces of the box. Four piezometers were put under the geomembrane with 1# on the sand and 2#, 3#, 4# on the soil. Another piezometer, 5# was put outside the geomembrane. Some pore pressure cells were buried in the soil sample. The detailed layout is shown in Fig. 1. The soil sample was pre-saturated. Water was supplied with varied heads of 1m, 3m, 6m and 9m. Each head was kept for 4 to 14 days until the discharge of the interface flow through the space between the geomembrane and the soil becoming stable. From the records of the pore pressure cells buried in the soil sample, the seepage water through the soil body was quite small and could be neglected.

2.3 Test Results and Interpretation

Eight tests were carried out from 1994 to 1995. The discharge of the interface flow, and the readings of the piezometers were recorded. The hydraulic gradients I between the piezometers were calculated and the hydraulic transmissivity θ of each segment between every two piezometers can be calculated by the following equation:

$$\theta = \frac{Q}{BI}$$

where: θ = hydraulic transmissivity of the space between geomembrane and soil (m^2/s); Q = discharge of interface flow (m^3/s); B = width of the box (m); I = hydraulic gradient between two piezometers, $I=\Delta H/L$; L = distance between two piezometers(m); ΔH = water heads difference between two piezometers(m).

The results of one of the tests, Test No.1, for example, in which 0.6 mm PVC geomembrane was used, are given in Table 3.

Table 3. Results of Test No.1.

Water head	Duration	Discharge	Reading of piezometers					Calculated results of each segment									
								5#~4#, l=0.38m		4#~3#, l=1.0m		3#~2#, l=0.50m		2#~1#, l=0.05m		5#~1#, l=1.93m	
H (m)	(days)	(10^6m^3/s)	5#	4#	3#	2#	1#	ΔH (m)	θ (10^{-6}m^3/s)	ΔH (m)	θ (10^{-6}m^3/s)	ΔH (m)	θ (10^{-6}m^3/s)	ΔH (m)	θ (10^{-6}m^3/s)	ΔH (m)	θ (10^{-6}m^3/s)
1.0	5	0.013	0.90	0.51	—	0.11	0.02	0.39	0.032					0.09	0.018	0.88	0.071
3.0	4	0.042	2.80	2.14	0.89	0.75	0.04	0.66	0.060	1.25	0.084	0.14	0.30	0.71	0.007	2.76	0.073
6.0	4	0.11	6.10	4.90	2.35	1.75	0.05	1.20	0.087	2.55	0.108	0.60	0.23	1.70	0.008	6.05	0.088
9.0	14	0.197	9.00	7.95	4.75	3.30	0.04	1.05	0.178	3.20	0.154	1.45	0.17	3.26	0.007	8.96	0.106

The above table shows that the values of transmissivity θ vary significantly for different water heads at different positions along the interface. The factors affecting the values of θ are : ①, the difference of water pressures above and below the geomembrane, ②, the water pressure acting on the soil surface , and ③, the head loss at the inlet and outlet of the interface. We can see that the values of θ in the case of lower water heads (H=3 m and H=6 m) at the inlet segment (between 5# and 4# piezometers) are smaller than those at the middle segments (between 4# and 3# piezometers, and 3# and 2# piezometers), which might be caused by the head loss at the inlet. But in the case of higher water head (H=9m), θ at the inlet segment becomes larger, which might be caused by the larger settlement of the soil body under higher water pressure and a larger space between the geomembrane and the soil being formed.

On the other hand, all the values of θ at the outlet segment (between 2# and 1# piezometers) are smaller than those at other segments because the geomembrane at the outlet segment was subjected to a large pressure difference which made a large deformation of the geomembrane while the soil sample was subjected to a very small water pressure which made very little settlement of the soil body. Hence the interface space between the geomembrane and the soil is very small in this segment. At other segments the values of θ vary with the water heads which made different deformations of the geomembrane and the soil sample and affected the transmissivity of the interface space between the geomembrane and the soil.

3 PERMEABILITY OF GEOMEMBRANES

The permeability of geomembranes can be determined by the WVT (Water Vapor Transmission) test method suggested by ASTM E96.

Haxo (1984) carried out a series of tests for different kinds of Polymeric membranes. The values of WVT can be converted into coefficients of permeability K by the following equation(after Lord and Koerner):

$$k = \frac{WVT}{S\left(R_1 - R_2\right) \times 1.175 \times 10^{10}} \Delta l$$

where: k = coefficient of geomembrane(cm/s); WVT = Water Vapor Transmission(g/m^2, day); S = the saturation vapor pressure at test temperature(mm of mercury), S = 32mm at 20℃; R_1 = the relative humidity within the test cup, R_1 = 1.0 in Haxo's test; R_2 = the relative humidity outside the test cup, R_2 = 0.2 in Haxo's test; Δl = thickness of the membrane (mm).

The WVT test results and the corresponding values of k of PVC membrane are presented in Table 4

Table 4. Values of WVT and k of PVC membrane.

Thickness of PVC membrane(mm)	WVT(g/m^2,day)	k(cm/s)
0.28	4.42	4×10^{-12}
0.51	2.97	5×10^{-12}
0.76	1.94	5×10^{-12}
0.79	1.85	5×10^{-12}

Hence the value k of PVC membrane ranges from 4 to 5×10^{-12}cm/s.

4 DESIGN SCHEME

4.1 General Description

The width of the geocomposite on the blanket is 100 m, where cracks generally occurred and that on the dam slope is 70 m determined by the high water level. The Scheme is composed of three reaches on the cross-section, namely, the anti-seepage reach, the drainage reach, and the dam-slope reach. A single layer of 0.5 mm geomembrane with a length of 50m is put on the blanket of the anti-seepage reach, a composite made of 0.5mm geomembrane and 250g/m² needle-punched geotextile with a length of 50m on the drainage reach and a composite of geotextile-geomembrane-geotextile with a length of about 70m on the dam slope. A drainage system is provided to keep low water pressure under the geomembrane and geocomposite on the blanket. It consists of nine longitudinal drainage pipes at intervals of 10m, one transversal drainage pipe, a collecting well and a sump pump to collect and pump out seepage water. The layout is shown in Figure 2.

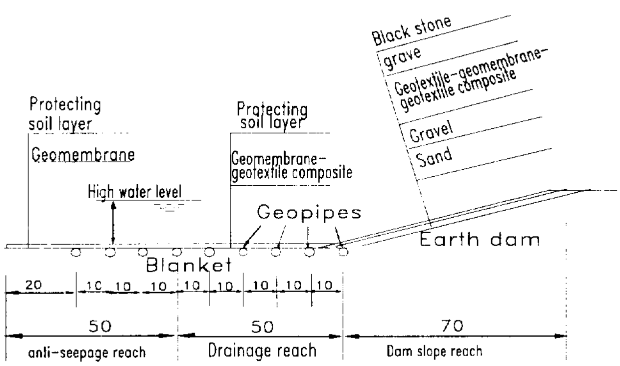

Figure 2. Cross-section of design scheme.

4.2 Pressure Heads under the Geomembrane between Pipes.

4.2.1 The water head equation under the geomembrane between two pipes (Figure 3)

Let the distance between any two pipes be 2L, set the origin at the mid-point of the interval between two pipes. Let y be the pressure head under the geomembrane at a distance x from the origin. The depth of water is 18m. The quantity of water permeating through the geomembrane will be

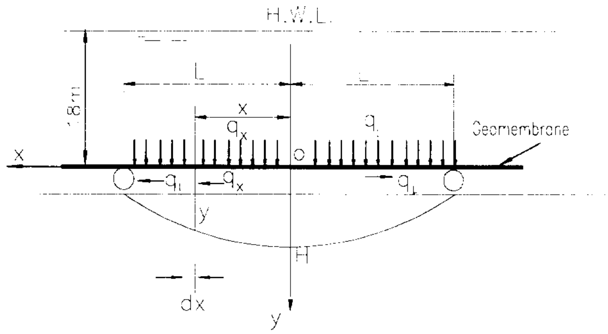

Figure 3. The curve of water head between two pipes

$$q = kIA = kIl \text{ per unit width} \tag{1}$$

where: q = quantity of water permeating through the geomembrane; l = length of permeating area, here l = dx, q = dq (m^3/s per unit width); k = permeability of geomembrane, k = 5×10^{-14}m/s; I = hydraulic gradient, I $=\Delta H/t$, ΔH= difference of pressure head above and below the geomembrane, ΔH = 18-y; t = thickness of geomembrane, t = 5×10^{-4}m

Substituting into eq.(1), we get: $dq=10^{-10}(18-y)dx$

The quantity of water permeating through the geomembrane from the origin O to a distance x will be $q_x = \int_0^x dq$, or

$$q_x = 10^{-10}\int_0^x (18-y)dx \tag{2}$$

The interface discharge through the space between the geomembrane and the soil will be

$$q = I\theta \tag{3}$$

where: q = interface discharge (m^3/s per unit width), at a distance x from the origin, q = q_x I = hydraulic gradient, here I = dy/dx; θ = transmissivity of the space. Hence

$$q_x = \frac{dy}{dx}\theta \tag{4}$$

Suppose the water pressure head y varies curvilinearly with x and the equation of the curve is

$$y=ax^2+bx+c \tag{5}$$

The boundary conditions are: ① x = 0, y = H where H is the max. head at the origin; ② x = L, y = 0 because there is a drainage pipe at a distance L from the origin; ③ x = 0, dy/dx = 0, because at the origin no water would seep in opposite directions, and q = dy/dx θ = 0, therefore dy/dx = 0, substituting them into eq.(5) we get the pressure head equation

$$y= -\frac{H}{L^2}x^2+H \tag{6}$$

4.2.2 The maximum head under the geomembrane between two pipes.

Substituting eq.(6) into (2)

$$q_x= \int_0^x 10^{-10}\left\{18-\left(\frac{H}{L^2}x^2+H\right)\right\}dx=10^{-10}\left(18x+\frac{1}{3}\frac{H}{L^2}x^3-Hx\right) \tag{7}$$

which must be equal to the quantity of interface discharge represented by eq.(4), into which substituting eq.(6) we get

$$q_x=\frac{dy}{dx}\theta = \frac{d}{dx}\left(-\frac{H}{L^2}x^2+H\right)\theta=-\frac{2Hx}{L^2}\theta \tag{8}$$

Balancing eq.(7) and (8)

$$10^{-10}\left(18x+\frac{1}{3}\frac{H}{L^2}x^3-Hx\right)=-\frac{2Hx}{L^2}\theta$$

we get the max. head at the origin

$$H=\frac{18x}{x-\frac{1}{3}\frac{x^3}{L^2}-\frac{2x}{L^2}\theta\times 10^{10}} \tag{9}$$

In the anti-seepage reach, L = 10/2 = 5 m, θ = 0.155×10^{-6} m^2/s, substituting into eq.(9) we get the max. head H = −0.146 m.

In the drainage reach, L = 5m, θ = 0.35×10^{-6} m^2/s, substituting into eq.(9) we get the max. head H = −0.064 m

4.2.3 Quantity of water flowing into pipes due to seepage and permeation.

By using equations (1) and (3) the quantity of water flowing into different longitudinal pipes at different positions could be estimated as shown in table 5.

Table 5. Quantity of water flowing into pipes.

Position of pipe	Quantity of water ($10^{-8}m^3/s$ per unit width)
The upstream pipe	16.7
Pipe in anti-seepage and drainage reach	1.8
Pipe at dam foot	7.2

4.2.4 Quantity of water flowing through the defects of the geomembrane.

In the design of a drainage system a defect of one hole with size of 1 cm^2 per 4000 m^2 of the geomembrane would be considered (Giroud, 1989). Accordingly the quantity of water flowing through the defect would be estimated by $q=\mu A\sqrt{2gh}$, where: μ=discharge coefficient = 0.65; A = area of hole = 1cm^2; h = 18 m. After substitution we get q= 1.22 $\times 10^3$ m^3/s per 4000 m^2. The total length of three reaches of the geomembrane is about 170 m, hence 4000 m^2 corresponds to a width of 4000/170 = 23.5 m. The quantity of water flowing through the defects per unit width will be

q_6 =1.22$\times 10^3$/23.5 = 5.2$\times 10^5$ m^3/s (per unit width)

CONCLUSIONS

1. Cracks often occur in the foundation and on the blanket of an earth dam if it is built on a soil foundation and lined with a horizontal soil blanket. From economic and safety points of view the use of geosynthetics to treat the cracks might be more effective and appropriate than other measures. A scheme composed of three reaches, the anti-seepage reach, the drainage reach and the dam-slope reach, is recommended.

2. A drainage system must be provided to keep a low water pressure under the geomembrane. High water pressure under the geomembrane must be avoided because it might cause splitting action on the cracks, seepage failure of the soil foundation and rupture of the geomembrane during storage of water or rapid falling of water level. In this scheme there might be a high water pressure under the upstream part of the geomembrane (from the end to the first pipe), but it is quite far from the dam and would have little effect on the safety of the dam.

3. The functions of the geotextile affiliated with the geocomposite used in the drainage reach are to keep a further low water pressure under the geomembrane near the dam and to protect the geomembrane from being destroyed.

4. The quantity of water through the defects of the geomembrane is much greater than that due to seepage or permeation, anyway, it must be considered in the design of drainage pipes, and a certain factor of safety should be taken into account.

REFERENCE

Giroud,J.P. and Bonaparte R. (1989) "Leakage through Liners Constructed with Geomembranes –Part 1. Geomembrane Liners", *Geotextiles and Geomembranes*,Vol.1,No.1, Elsevier Science Publishers Ltd., U.K.p.64

Haxo, H.E. et.al. (1984) "Permeability of Polymeric Membrane Lining Materials" *Proceeding of International Conference on Geomembranes*. Denver, USA. pp.151 – 156.

Koerner, R.M. (1994) *Designing with Geosynthetics* (Third Edition) Prentice-Hall inc. New Jersey, USA. pp.432 – 433.

Installation Damage Field Tests on a Geomembrane and Waterproofing of the SELVET Dam

H. Girard
Cemagref, Groupement de Bordeaux, 50 - avenue de Verdun, 33612 - Cestas Cedex, France

D. Poulain
Cemagref, Groupement de Bordeaux, 50 - avenue de Verdun, 33612 - Cestas Cedex, France

C. Mine
PRODIREG, 20 - Avenue des Chevaliers Tireurs, 73000 - Chambéry, France

G. Potié
SIPLAST, 12 - rue Cabanis, 75680 - Paris Cedex 14, France

ABSTRACT : The SELVET dam, located in the center of France, at an altitude of 1050 meters, was completed during the summer of 1996. It is 18 meters high and, with a crest length of 250 meters, can store 600 000 m^3 for drinking water purposes. Its backfill in stony gravel is waterproofed by a bituminous geomembrane placed on the upstream face. The choice of this geomembrane was the result of tenders from the relevant companies ; the design of the support and protection layers of the geomembrane and the implementation conditions are presented. In particular, field tests were performed to simulate installation damage during construction : 6 different structures were tested to define the Geomembrane Lining System (GLS), the purpose being to use local materials with sharp stones. Results of laboratory puncture tests are also given.

KEYWORDS : Geomembrane, Dam, Installation damage field test, Bi-axial tensile test, Puncture test, Slope stability

1 PRESENTATION

The substratum is a permeable basalt. The initial solution consisted of an embankment dam, constructed with a 0/150 mm basaltic random rockfill together with a watertight seal provided by a central diaphragm wall inserted in a silty gravel transition core (0/50 mm). A grout curtain was necessary to waterproof the foundation.

In this case an alternative solution was adopted using an elastomeric bitumen geomembrane placed on the upstream face. This was more economical and allowed the work to be completed in a shorter time. Because the fill was entirely random rockfill (0/150 mm) and not affected by rainwater, dam construction could take place in the winter.

The choice of the geomembrane was the result of tenders from the relevant companies and was justified by its competitive price and its references in France for this type of dam. The support and protection layers of the geomembrane had to satisfy the usual economic objectives for dams of this nature and the specific technical constraints at this site (in particular, resistance to puncturing from any sharp stones found in the fill and to the thick ice during winter). The final specification depended on installation damage tests realised under actual site conditions (on-site vehicles running over the protective layer). The six different Geomembrane Lining System (GLS) tested ranged from a minimum GLS, where the geomembrane was laid directly on the basaltic random rockfill (with any especially large stones removed) to the most complex one which was carried out with a bitumen stabilised support layer and anti-puncturing geocomposites. The article describes these field tests and the results obtained from visual inspection and burst testing. These tests helped to determine the final choice for the GLS (figure 1). Its installation, together with the precautions taken and the stability calculations carried out are described in detail.

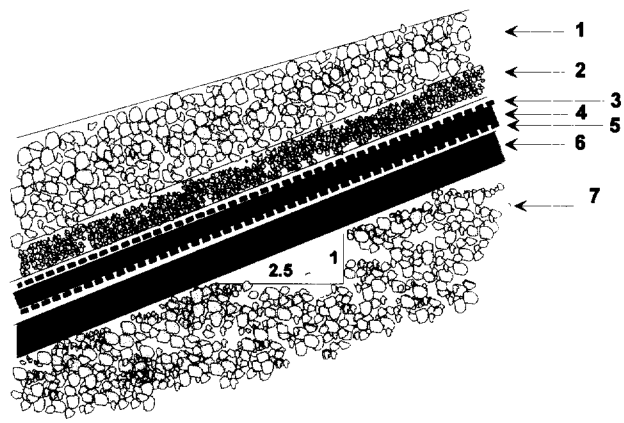

1 : 0 / 300 mm random rockfill (0.60 m to 1.40 m thick)
2 : 0 / 31.5 mm gravel (300 mm thick)
3 : Geocomposite (800 g/m²)
4 : Bituminous geomembrane (4 mm thick)
5 : Geocomposite (500 g/m²)
6 : Gravel - bitumen emulsion mix (150 mm thick)
7 : 0 / 100 mm random rockfill

Figure 1. Cross section of the Geomembrane Lining System

Complementary laboratory testing (puncture tests) was also performed for research purposes ; comparisons of the results of these tests were made with the results of the installation damage tests in the field.

2 ADVANTAGES OF A GEOMEMBRANE LINING SYSTEM (GLS)

2.1 Basic solution

A first study carried out in 1991 had evidenced that various types of dams could be considered for this site, namely in concrete (gravity dam), rock or earth. The geological and geotechnical surveys, continued in 1994 and 1995, evidenced that a flexible, backfill type dam was more suited to the context of the site than a concrete dam.

The materials available on the site consisted of :

- coarse 0/150 mm gravel, obtained by the blowing up of a basalt deposit situated on the right bank, providing large quantities of material ;
- 0/50 mm silty gravel in the bottom of the valley, but with an availability of only 30,000 m^3.

Given these conditions, the typical profile adopted as a basic solution for the backfill included the following zones :

- a pseudo central core, 5 metres wide, in silty gravel sealed by a diaphragm wall in extension of a grouting curtain previously made in the foundation ;
- upstream and downstream fill in coarse gravel.

2.2 Type of dam retained

After consulting relevant firms, this basic solution was finally abandoned in favour of a homogenous backfill, with upstream sealing by a geomembrane. This choice was based on the following :

- it proved to be more economical (cost lower by approximately 10%) ;
- it provided the opportunity for an easier, later intervention on the grouting curtain then situated at the upstream toe of the dam ;
- it proved to be time-saving, as the grouting curtain and the backfill could be carried out simultaneously ;
- the construction of the backfill, solely in 0/150 mm coarse gravel, is less sensitive to the vagaries of climate and could therefore be considered in winter ;
- maintenance of silty gravel at the bottom of the valley is propitious for the sealing of the basin ;
- there is currently a considerable corpus of experience in the use of geomembranes for sealing dams, including large dams (ICOLD, 1991).

3 DESIGN OF THE GLS

3.1 Constraints specific to the site

The Geomembrane Lining System (GLS) had to meet the economic objectives specific to this type of small dam and the technical constraints specific to the site, in particular the mechanical aggressivity of the local materials proposed for support and protection, and the risk of thick ice in winter.

This latter factor resulted in the recommendation of protecting the entire surface of the geomembrane. The coarse 0/100 mm gravel of the upstream part of the backfill on which the GLS was to be installed was obtained by blasting on one of the slopes of the pond. It consisted of sharp stones without any cohesion, given the close grading of 50/100 mm and the absence of fines. Moreover, for economic reasons, use of rockfill, also obtained by blasting of the on-site basalt to obtain a grading larger than that of the backfill, had to be used for the protection of the geomembrane.

The geomembrane adopted was that proposed by the company awarded the contract, namely an elastomeric bitumen geomembrane with appropriate characteristics and references for the dam to be built.

3.2 Field damage tests

In such a context, damage tests of the geomembrane had to be made under installation conditions (figure 2) to determine the transition layers to be implemented on each side of the geomembrane. In view of the nature of the support and protection layers, the implementation of the protective structure by machines driving over the surface probably represented the highest risks of damage for the geomembrane.

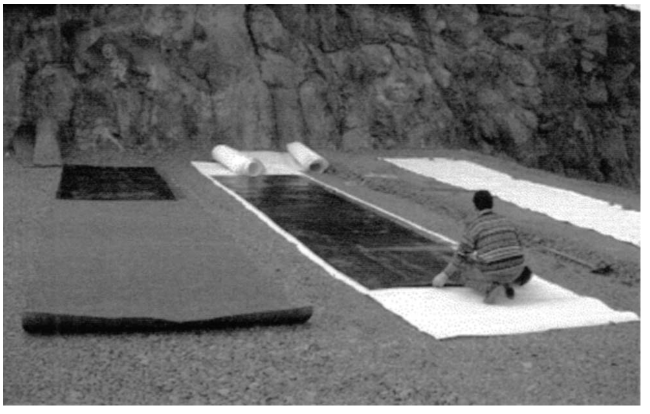

Figure 2. View of the installation of the geomembrane on a test area.

Six on site tests were thus prepared. The geosynthetic materials used for the tests and the retained GLS were as follows :

- TERANAP 431 TP Elastomeric Bitumen Geomembrane, called GMB in the rest of the text, 4 mm thick and with a mass per unit area of 4.8 kg/m² ;

Table 1 : Geomembrane Lining Systems tested

Test N°	Support layer (over backfill)	Support geosynthetic	Sealing	Protective geosynthetic	Transition layer (under rip-rap)
1	Silty gravel from the site	None	GMB	GTX1	0/80 mm basalt (20 cm thick)
2	0/80 mm basalt	GTX2	GMB	GTX1	0/80 mm basalt (20 cm thick)
3	0/80 mm basalt	GCP2	GMB	GTX2	0/80 mm basalt (20 cm thick)
4	0/80 mm basalt	GCP2	GMB	GCP2	0/80 mm basalt (20 cm thick)
5	0/80 mm basalt covered with 6/10 mm fine gravel	GCP2	GMB	GTX2	Crushed quarry gravel 0/31.5 mm (20 cm thick)
6	0/80 mm basalt covered with 6/10 mm fine gravel	GCP2	GMB	GCP2	0/80 mm basalt (20 cm thick)

- heat-bonded, non-woven TERRAM geotextiles, type T6 or T7, called GTX1 and GTX2, 1.6 mm thick (NF 38-012, under 2 kN/m^2) and with a respective mass per unit area of 280 and 330 g/m² (NF G 38-013) ;
- PRODRAIN 1-FT3 and 1-FT4 geocomposites, called anti-puncture geocomposites GCP1 and GCP2, with a mass per unit area of 500 and 800 g/m² respectively. They are composed of T3 (135 g/m² ; 0.9 mm) and T4 (190 g/m² ; 1.2 mm) geotextiles (same producer as T6 and T7, but thinner), with short textile fibers needle-punched on to them.

The lining systems tested were laid on the 0/150 mm coarse gravel backfill and topped with a 80 cm thick layer of 100/500 mm rip-rap, as described in Table 1.

The support layer was compacted in all the on site tests with a smooth, heavy vibrating roller, and the protection layers were positioned as work progressed by a loader driving over the rip-rap. The gravel placed above the geomembrane was compacted with a small tandem roller.

The tests were performed on a backfill installed for that purpose in the area of borrowed material, 15 m wide, with a 30 % slope, and 10 m long. Each test area was 2 m wide.

Two samples of 1 m² each of the geosynthetic materials installed were taken at random from each of the 6 tests. Analysis of the damage to the geomembrane included a detailed visual examination of the 12 samples and bi-axial tensile tests on the parts of each sample which appeared to have suffered the most damage.

Above all, the visual examination evidenced the following elements :

- severe damage on test No. 1, with punch marks over the entire surface, 8 of which came close to piercing ; more localized damage with nonetheless the presence of several impacts, close to piercing, in each of the tests Nos. 2, 3 and 4 (with one identified hole on test No. 2) ;
- the samples from tests Nos. 5 and 6 revealed only a few local, shallow punch marks.

3.3 Bi-axial tensile tests (Burst tests)

The bi-axial tensile tests were adopted to characterize, in the laboratory, the extent of the damage to the geomembrane. On the one hand, these tests integrated several parameters (tensile strength, deformability, leak detection, etc.) of particular interest in this case, and, on the other hand, were compatible with the short time-frame required by the site. Two samples were therefore cut from each of the 1 x 1 m panels taken from the site. These samples were taken from the areas which had visibly suffered the greatest damage (while avoiding the visually identified hole for which test would have been pointless).

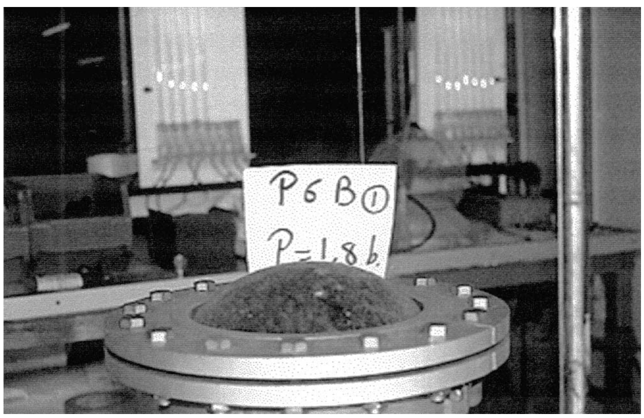

Figure 3. Bi-axial tensile test

The bi-axial tensile tests were performed on specimens with a diameter of 350 mm compressed by pressurised air with 200 mm diameter openings. The pressure was applied progressively in steps of 20 kPa, with a hold of 2 minutes between each step. Displacement was measured at the top of the geomembrane at the end of each step, and the burst pressure was recorded.

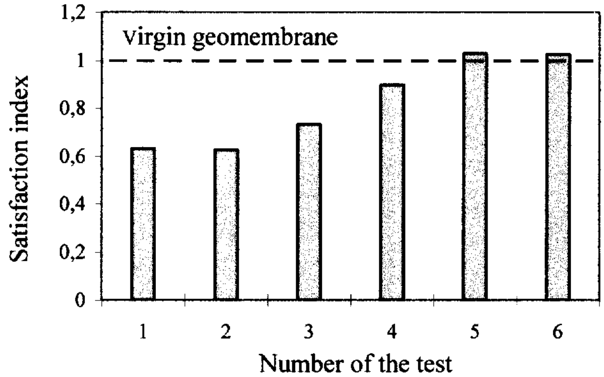

Figure 4. Summary of the bi-axial tensile tests for the 6 areas

The results of the tests were summarized in the form of a satisfaction index corresponding to the ratio between the mean of the displacements upon breakage recorded on the 4 samples from the same test area, and the mean of the displacements of 4 virgin samples. These values are shown in Figure 4.

Only the tests Nos. 5 and 6 gave a satisfaction index equal to 1, which confirmed the detailed visual examination of the geomembranes. Similar results were given by an equivalent index corresponding to the values of the bursting pressures.

3.4 Puncturing tests

These tests were performed after completion of the site, for research purposes, according to the French standard NF P 84-507, to determine the static puncturing resistance under the following conditions :

. opening diameter = 45 mm,
. punch diameter = 8 mm,
. puncturing speed = 50 mm/min,
. measurements : recording of the force applied and of the depth of the puncture.

For each GLS, 3 specimens were subjected to the test, whereas only one was taken for each geosynthetic tested.

The test was performed, of course, only on the geosynthetics. In that respect, it will be seen (Table 1) that test area No. 5 is the equivalent of test area No. 3 and test area No. 6 the equivalent of test area No. 4. The synthetic results shown in figure 5 correspond to the GLS of test areas 1 to 4. The GLS called « test area 7 » corresponds to the system implemented at the dam. For the static puncturing test, the geosynthetics were arranged as in the field :

. the smooth face of the geocomposite faced upwards (towards the punch) ;
. for the GCP1 and GCP2 geomembranes, the « short fibre » face was in contact with the geomembrane.

Examination of the results in figure 5 evidence a better behaviour for test areas 4 and 6, which correlates with the results of the in-situ test areas (observations and results of the bi-axial tensile tests). The result for test area 7 is close to that of test area 6 (GLS of similar constitution). On the other hand, test area 5, the behaviour of which in-situ was considered satisfactory, behaves less well under static puncturing, whereas the GTX2 (used in test area 5) has a resistance equal to or greater than the GCP1 and GCP2 (test areas 4, 6 and 7). This evidences that the short fibres play a significant part in improving puncturing resistance.

In summary, the puncturing test is a simple test which provides valuable information for the comparison of the different geosynthetics tested for the protection of the geomembrane. It is, however, an index test which fails to take account of the granular layers of the support and protection structures, and cannot therefore be used alone for the sizing of a GLS. In our case, the in situ tests evidenced that the better quality of the support implemented for test area 5 compensates for the use of a less effective protective geocomposite.

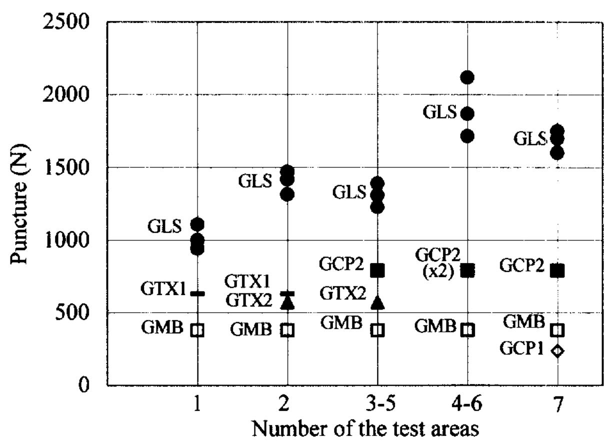

Figure 5. Summary results of the puncture tests

3.5 Description of the GLS adopted

Given the previously described on-site tests, it proved impossible to ensure a support layer solely with the on-site materials. At the very least, this layer had to be covered with fine gravel (tests Nos. 5 and 6). This solution, however, presented difficulties in implementation over a wide area (7,500 m²), due to the lack of cohesion of the gravel, which meant that the stones were likely to roll down the facing under the geomembrane upon its installation. To avoid this installation difficulty, the support layer was finally made of gravel mixed with a bitumen emulsion. Under such conditions, with an improved quality of the support, it was decided to replace the GCP2 geosynthetic support under the geomembrane by a lighter-weight geocomposite (GCP1). Furthermore, to protect the geomembrane, the safest components of tests were adopted : the anti-puncturing geocomposite (test No. 6) and the crushed quarry gravel (test No.5). The GLS thus obtained is shown in figure1.

3.6 Stability of the GLS

To avoid eventual tensioning of the geomembrane, this one was installed with the smooth face uppermost. In these conditions, the weakest interface of the GLS as far as slippage stability is concerned consists of the contact between the geomembrane and the upper geotextile. The friction angle (δ) was measured between these two elements of the GLS with an inclined plane test (Gourc et al.1996 ; Girard et al. 1994). This test consisted of installing the geosynthetics to be studied on a flat frame, hinged on one side. The geosynthetics are then subjected to a low vertical stress by means of a layer of soil placed on the upper geotextile, held in place by a mobile, freely sliding frame (not fixed to the flat frame). The flat frame is then raised until slippage occurs along the interface being studied. The slippage angle is then measured. In the case in hand, the geomembrane was fixed to the flat frame ; the upper geotextile was then loaded with 30 cm of 0/31.5 mm gravel as used on the site. Slippage of the geotextile was obtained at values of 22 and 24 degrees (2 tests). A conservative value of 22° was taken in the calculations for the friction angle between the smooth face of the geomembrane and the upper geotextile.

The first stability calculation was performed taking account of a constant protection thickness equal to 1 metre, made up of a 30 cm layer of 0/31.5 mm gravel topped by 70 cm of random rockfill taken from the site. The mechanical characteristics adopted for these materials are c=0 (zero cohesion) and $\varphi = 45°$. Furthermore, given the high permeability of these materials, it can be considered that when the dam is empty the protection layer is never saturated.

The calculations were performed according to the hypotheses defined above taking the highest profile of the upstream face. In this section, the total height of the slope is 17 m, with a slope of 1 / 2.5. The stability analysis is performed with the dam empty, by the blocks method (Soong and Koerner, 1996).

The safety coefficient thus obtained is equal to 1.22. This was considered too low, and to improve slippage safety the protection layer was therefore increased to 1.40 m at the foot of the slope and reduced to 0.60 m at the top. The calculations made with this variable thickness produced a slightly higher safety coefficient of 1.32. A calculation performed using the ETAGE software (Soyez et al. 1990) developed by the Central Civil Engineering Laboratory (LCPC) produced the same result. We subsequently verified that slippage safety was also ensured during the filling of the dam ; in this case, the minimum coefficient obtained was equal to 1.20 at the beginning of the filling.

This profile with a variable thickness, as described above, was thus adopted for protection. The increase in the toe trench made it possible to increase considerably the slippage safety, which is thus ensured without taking account of tensile stress that can be absorbed by the upper geotextile (GCP2) anchored at the top of the slope.

4 IMPLEMENTATION OF THE GLS ADOPTED

A transition area (0/100 mm) was installed between the body of the backfill (0/150 mm) and the emulsioned gravel, over a width of 3 metres, following completion of the grouting curtain at the toe of the upstream face. Its surface, parallel to the slope, was reworked with an excavator, and carefully finished by hand, to eliminate all of the larger pieces. The gravel-bitumen emulsion mix (0/14 mm) layer, 15 cm thick, was laid on the slope with a crawler-mounted loader and spread with a rake. Compacting was performed along the slope with a tandem roller anchored to the top of the slope, and the final surface then brushed.

The anti-puncturing geocomposite was then unrolled over the slope working downwards from the crest. The 2 m wide sections were sewn together. The geomembrane, delivered to the site in 4 m rolls, was unrolled downwards from the crest, the roll being hung from a hoisting tackle mounted on a shovel loader. The smooth face of the geomembrane was laid uppermost to avoid tensile stresses from settlement of the protection layer. A detailed pattern lay-out enabled the sections to be adapted to the length of the slope to avoid transverse joints.

Figure 6. Installation of the geomembrane

Geomembrane sections were joined with a blow-torch, with a 20 cm overlap. The project manager performed a visual inspection of all the seams.

The connection of the geomembrane to the grouting curtain at the foot of the slope was an important factor for sealing of the dam. The solution adopted consisted of lowering the geomembrane into a trench filled with concrete with the addition of bentonite (150 kg cement, 400 l with 10% of bentonite, 950 kg of 0/3 mm sand and 500 kg of 8/14 mm gravel). This trench was cut in the basalt with a trencher to a depth of 1 m along the centre line of the grouting curtain, then filled in 2 phases. The concrete was poured into the dam side part of the trench (using shuttering) to obtain a smooth vertical face. The geomembrane was then installed, and the upstream part of the trench filled. To improve the sealing of this sensitive transition area, an overlap strip of the same geomembrane (1 m wide) was then installed and seamed with the main geomembrane on one side and with the concrete (upstream part of the trench) on the other side. The geomembrane was anchored to the crest by a classic trench filled with gravel.

Figure 7. Installation of the protective layer of the GLS

The protection layer was installed as work progressed from the foot of the slope using a loader and a crawler-mounted shovel loader, after the installation of the top pierce-proof geocomposite. The two machines moved over the full thickness of the protection layer (gravel layer plus random rockfill) to restrict stresses on the geomembrane and to take advantage of the stability of the random rockfill resting at the foot of the slope up against a support fill.

5 CONCLUSION

The dam was built between October 1995 and August 1996, the backfill being completed during the winter. The installation of the GLS was performed without any particular difficulty between April and July 1996. The dam was filled in early 1997.

The damage on site installation tests made it possible to define a GLS adapted to the specific conditions of the dam with, in particular, the use of rip-rap taken from the site to form the protection layer.

The comparison between the results of the installation field tests (observations and bi-axial tensile tests) and laboratory puncture tests gave interesting information about the use of the latter.

ACKNOWLEDGMENTS

We should like to thank the Viadène SIAEP, owner of the Selvet dam, the DDAF of Aveyron department and MERLIN consulting engineers, project managers who enabled us to complete this study and participated in the design and the construction of the GLS.

REFERENCES

Comité Français des Géotextiles et Géomembranes (CFGG), 1991 - *Recommandations générales pour la réalisation d'étanchéités par géomembranes*, 47 pp.

Girard, H., Berroir, G., Gourc, J.P. and Mathieu, G. (1994) "Frictional behaviour of geosynthetics and slope stability of lining systems", *Fifth International Conference on Geotextiles, Geomembranes and Related Products*, Singapore, volume 1, pp. 339-342.

Girard, H., Lefranc, M. and Tisserand, C. (1996) "Waterproofing and rehabilitation of dams by geomembranes in France", *First European Geosynthetics Conference, Geosynthetics : applications, design and construction, EUROGEO 1*, Maastricht, Netherlands, pp. 945-952.

Giroud, J.P., (1992) "Geosynthetics in dams : two decades of experience", *Geotechnical Fabrics Report*, 10 (5), 6-9 and 10 (6), 22-28.

Gourc, J.P., Lalarakotoson, S., Müller- Rochholz, H. and Bronstein, Z. (1996) "Friction measurement by direct shearing or tilting process - Development of a European standard", *First European Geosynthetics Conference, Geosynthetics : applications, design and construction, EUROGEO 1*, Maastricht, Netherlands, pp. 945-952.

International Commission on Large Dams (ICOLD), 1991, *Watertight geomembranes for dams : state of the art*, Bull. 78, 140 pp.

Soong, T.E. and Koerner, R.M. (1996) "Seepage induced slope instability", *Geotextiles and Geomembranes*, Vol. 14, pp. 425-445.

Soyez,.B., Delmas, Ph., Herr, Ch. And Berche, J.C. (1990) "Computer evaluation of the stability of composite liners", *Fourth International Conference on Geotextiles, Geomembranes and Related Products*, The Hague, Netherlands, Volume 1, pp. 517-522.

BITUMEN GEOMEMBRANES IN IRRIGATION - CASE HISTORIES FROM A RANGE OF CLIMATES

B. Breul
Colas S.A., Direction Recherche et Développement, 92653 Boulogne Billancourt, France

R. Herment
Société des Pétroles Shell, Direction Bitumes, 92563 Rueil Malmaison, France

ABSTRACT: Bitumen was in use 5000 years ago for irrigation works that are still in good condition. Today, bituminous geomembranes are providing efficient, durable waterproof linings to irrigation canals, ponds and reservoirs throughout the world. They are either fluid-applied or delivered in rolls 4 metres wide. A survey of twenty irrigation dams around 10m high built between 1973 and 1983 in France with unprotected geomembrane facings found them performing well after 10-20 years service. Linings to a reservoir at Goudel in Niger and canals cut in laterite near Niamey have demonstrated their suitability in tropical climates. In North Africa, the Gulf States, Singapore, India and New Zealand, 5m-wide bituminous geomembranes have been in use on irrigation canals for some ten years and are still performing satisfactorily. In the USA, leaky areas on a large concrete-lined canal were stopped with an SBS bitumen-based geomembrane available in 4m widths in France.

KEYWORDS: Aging, Canal Liners, Case Study, Dams, Embankment, Geomembranes, Bitumen

1 INTRODUCTION

Five thousand years ago, crude petroleum was only accessible where it emerged from deep fissures in the ground. The heavy residue contained a high percentage of bitumen, which the ancients, especially in the Middle East, used for its waterproofing properties. Since those early times, it has been used to build and repair wells, reservoirs, canals and baths and consolidate irrigation canal embankments. Many of these constructions are still in good condition.

Bitumen emerged as a standard 20th century waterproofing material in civil and water engineering in the form of bituminous concrete, asphalt and bituminous geomembranes. The last-mentioned are lightweight materials that are easy to lay and repair, with waterproofing properties that make them ideal for irrigation works. They may take one of three forms:

◆ Bitumen can be sprayed onto a geotextile in situ (ISBGs)

◆ They may be prepared (prefabricated) in the factory and delivered to site in rolls (PBGs)

◆ An impervious asphalt may be laid on the canal or reservoir floor with the membrane confined to the sloping sides.

2 BITUMINOUS GEOMEMBRANE FOR IRRIGATION WORKS

The material underlying the lining must be free from grass an other organic matter, and well drained if it is not naturally impervious. Gas collection wells are also needed if there is a risk of fermentation. It must be stable, smooth, with no sharp stones, and compacted to at least 90% Proctor optimum.

Although not always necessary, a protective covering should be added if the geomembrane is exposed to uplift pressures, wind suction, severe sunlight, impact, ice, debris, animals or wilful damage. It usually consists of unprocessed natural material although stabilisation with cement or bitumen reduces the thickness required.

Bituminous geomembranes, 3.3mm to 5.6mm thick with a density of 1.15, are three times heavier than polymer geomembranes, and therefore less affected by wind action.

3 EXAMPLES OF IN SITU BITUMINOUS GEOMEMBRANES

3.1. France

In situ bituminous geomembranes (ISBGs) were used in France in the early sixties under railway track and for renovating old roads; the ballast and top foundation courses respectively were removed to a depth of up to 800mm and the bituminous membrane was sprayed in two 3-5mm coats with a glass fleece or non-woven polyester geotextile in between, before covering with new material. The membrane isolates the overlying material from contaminated groundwater and shields the foundation from percolating surface runoff.

This approach was used again on the Huningue (1962) and Nord (1966) ship canals. It usefully reduces leakage through the canal floor. It must be protected on the banks against erosion and wave action.

When water reservoirs began to be lined in the seventies, it was found necessary to design special reinforcing arrangements to control root damage.

The choice of bitumen grade is governed by air temperatures at the site, altitude and exposure to sunlight. The bitumen is sprayed from a tanker through a spraybar at the rear or extending out to one side, horizontally or at an angle when spraying slopes. The geotextile is normally unrolled after the first coat has been sprayed.

The first application of an ISBG to a mountain reservoir 1800m asl in the French Alps was followed by several coastal reservoirs near Toulon with capacities ranging from 3000 m^3 to 40,000 m^3, where the membrane was laid on pervious material and protected with 8cm of lean concrete.

Surface protection is not always necessary. Two small rockfill dams, 4-13m high, were built in 1973 and 1975 in southern France, each faced with an ISBG exposed to direct sunlight. The agricultural ministry's research institute CEMAGREF monitored the performance of the facings and reported the appearance of only one tear at the crest after eight years, which remained unchanged over the following seven years. A strip of geotextile that had not been impregnated with bitumen and had aged was easily repaired. The other dam showed no flaws after more than 20 years.

Use of ISBGs was slowed in France because the country's dense road network accessible to heavy trucks favoured prefabricated bituminous geomembranes, but they are an excellent answer for narrow inaccessible sites and for covering large flat areas.

3.2 USA

There has been a special ISBG working group within ASTM committee D35-10 since 1996.

3.2.1. Irrigation Canals

The United States has a very extensive irrigation canal system and the US Bureau of Reclamation has issued tables correlating canal size and capacity, slopes, fill material and thickness.

3.2.2. Reservoirs

American engineers use ISBGs to line large reservoirs with capacities in excess of 1 Mm^3.

At Oakland, the ISBG is covered with 100mm of concrete and lies on a foundation of 10cm of dense and porous asphalt.

Engineers and scientists at the Department of Energy's Hanford site in Washington have developed a maintenance-free waste-site surface barrier made from natural materials that will last for 1000 years. They monitor a 5-acre prototype constructed in 1993 over a decommissioned wastewater disposal facility. There is a multi-layer barrier of various natural materials (sand, gravel, clay, etc.) 4.50 metres thick. In addition, an ISBG was laid on 150mm of asphalt.

4 PREFABRICATED BITUMINOUS GEO-MEMBRANE RESERVOIR LININGS

A few interesting examples are described in the following.

4.1. France: Embankments Less than 18m High

Seventeen water reservoirs impounded by rockfill embankments have been monitored by CEMAGREF over the last twenty years. Only four linings had protective coverings and all the underlying rockfill was free-draining. Reported damage was minor, consisting of a single case of a PBG being punctured by sharp stones underneath, one tear by vandals, and one section of seam that separated. The three spots were quickly repaired in a durable manner.

The only reported damage on the other embankments was minor damage to seams from plant roots, which was easily repaired. Mud curling was observed on the PBG without surface protection although it had no effect on watertightness and the process always stopped at the geotextile.

There are many other geomembrane linings ranging from 1500 m^2 to 10,000 m^2 in area all over France that have been giving complete satisfaction for the last twenty years.

4.2 France: Large Irrigation Works

Ospedal dam, 26m high, with a 5000 m^2 PBG facing laid on porous asphalt and a geotextile and protected with interlocking pavings, was built in Corsica in 1978 and remains in excellent condition, as evidenced by 19 years of periodic inspection.

In 1976, an irrigation reservoir was built at Gap in southern France with a 25,000 m^2 PBG facing, and Ortolo rockfill dam in Corsica was completed with a similar 6800 m^2 facing. Problems were experienced with the poorly compacted soil when first filling the Gap reservoir. A tear in the geomembrane where it joined a concrete pipe allowed leakage to wash away material from the embankment, but it was easily repaired.

The Ortolo facing was laid on a elaborate base (25-30mm ballast impregnated with 3 kg/m^2 bitumen emulsion and 100mm cold laid asphalt) plus a geotextile. The protective covering was geotextile plus 140mm in situ fibre reinforced concrete (polypropylene fibre, length 30mm, weight 1kg/m^3). All seams were 100% tested with an automatic ultrasound tester. The quality of construction enabled the structure to withstand exceptional floods successfully.

4.3. Reservoirs in Hot Climates

From 1981 to 1983, large jobs ranging in size from 50,000 m^2 to 80,000 m^2 were completed in Saudi Arabia at Hail, Riyadh, Taif and Dorman at the Royal Palace. They included many ornamental ponds.

At Goudel near Niamey, a river water storage reservoir was lined with 4500 m^2 of PBG in 1981 and remains in good condition apart from some tears at junctions with concrete structures.

In 1989 at Palma, Majorca, 22,500 m^2 of PBG was used to line an aeration lagoon.

In 1991, reservoirs in the gulf of Marrakech had 90,000 m^2 of elastomeric bitumen PBG laid directly on the sand, without any protective covering.

In the same period, large reservoirs were lined with 30,000 m^2 PBG in Abu Dhabi.

In 1996, 110,000 m^2 of PBG was used at a settling pond in Nigeria.

All these prefabricated bituminous geomembranes performed well with respect to sunlight and temperatures in these hot climates.

5. CANALS

5.1. France

PBGs are used extensively for lining irrigation ditches and canals. Tests performed after fifteen years service near Le Mans revealed that PBGs covered with soil and grassed, were ageing well. They performed valuable service in controlling leakage from critical canal sections in the Freyssinet system. The largest job was the 260,000 m^2 of elastomeric bitumen PBG lining to the Nieffer canal near Mulhouse.

5.2. Very Hot Climates in Africa and Asia

Prefabricated bituminous geomembranes were effective in the construction of Ishagi canal, Iraq, in 1981 and the Mines d'Or canal at Poula in Burkina Faso. They also successfully repaired the 64,000 m^2 of leaking concrete lining to the Tanorga irrigation canal in 1985, and controlled leakage over 22,000 m^2 of Tungabhadia canal in India in 1987. A geotextile underlay and slate gravel protective covering were provided for the Mines d'Or canal PBG.

5.3. North America

Two of three leaking sections of the Caspa District canal in Wyoming, USA, were repaired with 9000 m^2 and 60,000 m^2 elastomeric bitumen PBG in 1992 and 1994 respectively. The third, slightly larger (80,000 m^2) section was repaired in 1995 by the canal operator's own employees.

When the West canal in Oklahoma was leaking in 152 places, PBG repairs to an 800m section restored irrigation supplies to 120 ha of farmland.

California has the densest canal system in the USA, and PBG has been used extensively to repair earth and concrete-lined canals.

Two water treatment ponds covering 75,000 m^2 and 6.50m deep, lined with elastomeric bitumen PBG, lost only 1 litre per square metre per day as against the design criterion of not more than 20 litres.

5.4. Special Problems in Livestock Farming Areas in Developing countries

Near Niamey in Niger, canals cut into the laterite were lined with 20,000 m^2 of PBG in 1991, and six years later, it was observed that:

◆ Canals in vegetable-growing areas were in good condition.

◆ Canals in livestock farming areas had been damaged at cattle crossings.

◆ Local residents had purposely torn the geomembrane in places to take water. It is also said that bituminous geomembrane material is popular for re-soling shoes.

This means that special measures are needed to combat damage of animal and human origin, such as fencing, thorn hedges, concrete cattle crossings and more water offtakes.

In Niger as in many other places, special care is needed when joining geomembrane to concrete, and should include firm cold jointing, double membrane thickness and clamp bars.

6. CONCLUSION

Laying bituminous geomembranes, with or without surface protection, is such a simple job that it can be successfully performed in many countries with standard tools and trained local labour, to build and repair irrigation canals and reservoirs. The examples described also illustrate that bituminous geomembranes are easy to repair, retain their waterproofing properties over time and age well.

The choice between in situ and prefabricated alternatives or combining bituminous geomembranes with asphalt is governed by local cost factors, since all three approaches have proved their worth.

7. ACKNOWLEDGEMENTS

Thanks are due to Messrs Siplast and Hypofors for permission to quote details of their jobs.

REFERENCES

Van Asbeck, W.F. (1962). *Bitumen in Hydraulic Engineering*, Vol 1, pp1-3

Sheel France brochure. La membrane bitume enterré, Nov 1974

Dunglas, J., Lelu, V. and Chaigne, P. Revêtement de canaux di'irrigation par béton bitumineux étanche ou membrane bitume enterré. *Revue Eau et aménagement de la région provençale*. No.14, July 1977

Alonso, Degoutte and Girard (1990). Result of Seventeen Years of Using Geomembranes in Dams and Basins. *Proc. 4th Int. Conf. On Geotextiless, Geomembranes and Related Products*. The Hague

Wing, N.R. and Gee, G.W. (1994). Quest for the Perfect Cap. *Civil Engineering*. Nov. 1994

Tisserand, C (1983). Un grand bassin à membrane non protégée. *Colloque Etanchéité superficiel*. Paris (CEMAGREF issue)

ICOLD. Bulletin No. 38 Use of Thin Membranes on Fill Dams

Bianchi, C., Rocca Serra, C. and Girollet, J (1979). Utilisation d'un revêtement mince pour l'étanchéité d'un barrage de plus de 20 mètres de hauteur. Communication C11. *Proc. 13th ICOLD Congress*. New Delhi 1979

Breul, B. and Herment, R (1997). Bituminous Geomembrane Waterproof Lining to Manes Storage Reservoir. *Proc. Rencontres 97 Congress*, Reims 1997

Shell Bitumes newsletter *Le Liant* No. 14, May 1996. Le barrage d'Ortolo

Shell Bitumes newsletter *Le Liant* No. 14, May 1996. Les géomembranes bitumineuses conquièrent l'Amérique

Colétanche bituminous geomembrane

being laid at Ortolo dam

Reservoir lined with Colétanche

at Goudel, Niger

Canal lined with Colétanche

near Niamey, Niger

Caspa Alcova, Wyoming (USA)

Caspa Alcova, Wyoming (USA)

Irrigation Canal, California (USA)

Altus, Oklahoma (USA)

Construction Technology of Geotextile Mattresses for Bank Protection of Liaohe River, Liaoning Province, P. R. China

Wang Dianwu,
Research Institute of Water Resources and Hydropower, Liaoning Province

Wang Xiaobai
Management Office of Agricultural Development Projects Using World Bank Loan, Liaoning Province

ABSTRACT: Since early 1980's, the exprimental study of application of geotextiles to the bank protection of Liaohe river in our province has been caried on . We have innovafed in construction technology, featuring the cold region in our country, such as sinking geotextile mattresses on/under the ice cover, and on a boat / floating bridge, etc. This paper briefs these construction methods, the properties of geotextiles in use for mattresses and the design principles are also provided.

KEYWORDS: Geotextiles, Embankments, Erosion control, Construction

1 INTRODUCTION

To handle dangerous section of a dike has always been the crux to river training works. Since last decade or so, geotextile mattresses have been used in such sections along the trunk of Liaohe river. According to the statistics, a total of 2 million sqm or more geotextiles were used in some 150 bank protection works. It has saved a great deal of investement and about 150 thousand tons of twig as compared with traditional fascine bundles and riprap works, which is corresponding to protecting thousands hectares of rapid growth forest, that is beneficial not only to ecological environment, but also to saving expense of transportation, as the total weight of 2 million sqm of geotextiles is only 300-500 tons, which is far less than that of twig. When the GT mattresses are used, the most appropriate construction method may be chosen, and the work efficiency could be increased by 50% or more , the quality of project and operating results may be guaranteed as well.

2 MANUFACTURE AND WEIGHT OF GEOTEXTILE MATTRESSES

2.1 Material of Geotextile Mattress

Five kinds of polypropylene woven geotextiles were used mainly in bank protection of Liaohe river. The main properties of GT are shown in table 1.

As seen by Table 1, the mechanical properties of the five kinds of GT can all meet the engineering requirement, but in consideration of that the larger the opening size, the lower the cost, so that, under the permissible filter condiftion, we choose the GT with opening size as large as possible.

According to laboratory filter test, field erosion test and analysis on engineering practice for these five kinds of geotextile, the design criterion of filter is taken as:

$$O_{90} \leqslant Ad_{90} \tag{1}$$

In which, the coefficient A is 10 for clay and loam; 2~5 for sandy loam and sand.

2.2 Determination of the Size of GT Mattress

Transversal (normal to the stream) length of the GT mattress is composed of two parts, i. e. the above-water part and under-water part. The transversal length of the above-water part is determined similar to the normal bank protection, and that of the under-water part will be calculated in reference to the thalweg if the main flow of the river is near the bank; or in reference to maximum eroding depth if the thalweg is far from the bank.

The transversal length of under-water GT mattress calculated with thalweg is:

$$L = L_1 + L_2 + L_3 \tag{2}$$

Where: L = total length of under-water GT mattress (m); L_1 = length of mattress required for connecting to that of above-water part and for anchoring (m); $L_2 = S_1S_2\ \sqrt{X^2+H^2}$, in which: S_1 and S_2 are coefficients of wrinkle and contraction under-water respectively. The actual measurement values for Liaohe river are S_1 = 1. 4 and S_2 = 1. 05; X = horizontal distance between thalweg and water surface on the bank during low water level(m); H = depth of water at thalweg during low water level (m); L_3 = overlength beyond the thalweg, or $L_3 = K_0 h\sqrt{1+m_0^2}$; in which: K_0 = safety factor; m_0 =

Table 1. Properties of GT used in the Bank Protection of Liaohe River

Polypropylene woven GT	Weight (g/sqm)	Thickness (mm)	Tensile strength (N/5cm)		Elongation per unit length(%)		Equivalent opening size O_{90}(mm)	Permeability (cm/s)
			warp	weft	warp	weft		
A	100	2.0	496	408	26.0	20.0	0.70	6.84×10^{-4}
B	110	2.5	511	666	28.6	25.0	0.72	3.57×10^{-3}
C	103	2.1	584	526	13.0	17.5	0.15	
D			540	480	15.3	13.8	0.66	
E			392	357	19.5	17.5	0.33	

stable slope rate under-water; h = maximum eroding depth(m).

If transversal length of under-water GT mattress is calculated with maximum eroding depth, the total length of it will be:

$$L = L_1 + L_2' \qquad (3)$$

where: L_1 is the same as in Eq. (2); $L_2' = K_0 h \sqrt{1+m_0^2}(H_m + H_{max})$. in which: H_m = mean depth during low water level(m); $H_{max} = H_m(2B/R_m + 1)$. in which: B = width of river corresponding to the bed forming discharge (m); and R_m = radius of curvature at river bend(m); and H_m = mean depth before erosion at the section in question.

The longitudinal length (in the direction of stream) of GT mattress was adopted 20 ~ 50m for on/under ice cover construction. and 10~20m for on boat/raft construction in Liaoning Province.

The dimension of GT mattress for base protection of spur /longitudinal dike may be computed by following formula:

$$L = l + m_1 h + l_0 + a \qquad (4)$$

$$B = b + 2m_2 h + 2l_0 + a \qquad (5)$$

In which: L and B = length of mattress parallel and perpendicular to the axis of dike, respectively, (m), m_1 and m_2 = end slope and side slope of dike, respectively, l = length of dike(m), b = top width of dike (m), $l_0 = K_0\sqrt{1+m_0^2}\, h_s$, where: h_s = depth of local erosion around the dike (m), which may be calculated by formula or determined by experiment, the actual measruement value for Liaohe river is h_s = 1.1~2.8m, K_0 and m_0 are the same as in Eq.(2). a = additional length including wrinkle and contraction under-water(m).

2.3 Manufacture of Geotexile Mattress

The four edges around the GT mattress and every 0.50~0.60m in the transversal direction should fold up and sew into a sleeve--like pipe for penetrating nylon rope to act as reinforcements.

Now the factories can produce the GT mattress according to designed size and disposition of reinforcements.

2.4 Geotextile Mattress Weight

The types of weight for GT mattress are as follows:

1. precast concrete blocks put on sides of the mattress, and arranged in checkers inside the mattress, dump additional stone within the checkers make the mean weight up to 1.2kN/m², and 1.6kN/m² for side one.
2. Put willow or oak twig bundles on two-layer GT mattress to form 1.0×1.0m checkers with riprap within it. The weight of which may be 3.7~5.6 kN/m².
3. Earth pillow weight, this is a bag made of coated woven geoitextile, filled with earth in situ, then sewn up. The length of which used in Liaohe river is 5 ~ 10m, 0.30 ~ 0.40m in diameter and single weight 10~20kN.
4. Put gabions, 0.30~0.60m in diameter, on edges of GT mattress; and arranged in checkers on it. Then dump riprap within checkers for 0.30 ~0.50m thick.
5. Combined weight of gabion, riprap, and earth pillow. The gabions are used for side weight and an additional weight of gabions at 10 ~ 20m spacing. The riprap or earth pillows are placed between the gabions. The weight is about 1.0~2.0kN/m²

3 CONSTRUCTION TECHNOLOGY

3.1 Sinking Mattresses on Ice Cover

The construction period in our province is usually from the last ten days of December to the first ten days of March the following year.

Table 2. Field experimental results of ultimate bearing capacity of ice cover in Liaohe river area

	Freezing period				Thawing period			
Thickness of ice cover (cm)	10	20	30	40	10	20	30	40
Bearing capacity (kN/m^2)	5.60	9.20	14.66	20.00	2.40	4.00	4.95	5.80

Figure 1. Sinking mattresses on ice cover

Dig an ice pit according to the size of GT mattress, construction period, designed weight and bearing capacity of ice cover.

The field experimental results of ultimate bearing capacity of ice cover for various thicknesses during freezing and thawing periods in Liaohe river area are listed in Table 2.

Place the GT mattress into the ice pit, the adjacent mattresses should be lapped or sewn on.

The weight should be put firstly on the downstream side of mattress, then extended progressively from upstream to downstream. When the weight reaches designed amount, the mattress body will sink itself uniformly within a short time.

With regard to the construction of GT mattress for base protection of spur /longitudinal dike, it should be done during thawing period when the bearing capacity of ice cover is greater, or determined in accordance with the law of thawing ice cover in local area, weight of dike, and loading of construcfion. To ensure safety for construction and shorten the time of construction as far as possible. The procedures are as follows: positioning on ice surface, spreading GT mattresses, putting weight on it, and building dike according to designed shape preliminarily. The dike deformed as soon as the thaw of river, to build again the dike to design section after thawing is basically stable.

3.2 Sinking GT Mattress Under Ice Cover

To dig through two longitudinal ice trenches, one near the bank and the other on the midstream side of the mattress, and two transversal ice trenches at upstream and downstream ends. The trenches should not meet each other, they are used to pull mattress under ice cover. and to dump weight through them.

Figure 2. Sinking GT mattress under ice cover

Fold up the first GT mattress longitudinally and keep downstream end of it on the surface. Put the folded mattress on the upstream side of the first transversal ice trench.

Tie the upstream end of mattress to the piles driven through ice to the river bed, and hold down it on the ice cover with earth pillow.

Tie polyethylene (PE) ropes on each corner of downstream end of mattress(which is on the top of folded mattress), then throw the ropes into water through transversal ice trench and draw out from longitudinal ice trench(on the midstream side) by means of a stalk-hook. Then the mattress will follow the ropes passing through the water under ice cover, and be drawn out and put on the ice cover. The next mattress should then be sewn to the former. The rest may be done by the same way.

Throw the ropes into water through that longitudinal ice trench and draw out from another longitudinal ice trench(on the bank side). Pull the ropes to place the GT mattress (which floats on the water under ice cover), then fix it to bank and midstream ice surface. Finally, to give weight through transversal and longitudinal trenches on it. The mattress will sink onto the river bed.

3.3 Sinking GT Mattress on Boat/Raft

During bank protection construction period in

Liaoning province(the low water level period), the depth of water in the river is usually not more than 1.0m, and the velocity is about 0.5 ~ 1.5m/s. In practice, a realistic measure of sinking GT mattress by sliding it off while drawing the ropes in on the boat has been used. The main procedures of construction are as follows:

Positioning the two sides of GT mattress by transit or surveying rods, drive a pile on river bank and drop an anchor in river to fix steel rope used for guiding the boat to pull the GT mattress.

Place the GT mattress on the regulated slope of the bank, put and fix the precast concrete blcoks on it. A steel pipe is installed on the front edge of the mattress. The PE ropes(16mm in diameter) spaced 2 ~3m centers are tied on the steel pipe and the boat.

The boat moves along the steel rope and pull the mattress with the PE ropes, the mattress will be developed gradually under the water until it reaches desired position.

Then, dump additional weight on the mattress from the boat.

3.4 Sinking GT Mattress on a Floating Bridge

The floating bridege is made up of raft or boat located near the river bank. The length of which should be longer than the transversal length(normal to the stream)of GT mattress. The loading capacity must be more than the total weight of earth pillows, gabions, and workers. The position of the floating bridge is held by steel or PE ropes to an anchor.

The procedure of sinking mattress is as follows:

Carry the processed GT mattress onto the floating bridge, which is rolled in transversal direction.

Make a sinking pillow (earth pillow or gabion) which is as long as the transversal length of mattress and wrapped up by the upstream end of the mattress, then sewn up with nylon thread.

Throw the GT mattress into the water as soon as the sinking pillow is completed. The rolled mattress will be opened up gradually and spread over the water surface under the floating bridge depending on dynamic force of flow.

Fasten the longitudinal reinforcement of mattress to the wooden piles on the bank to prevent the mattress from sliding to river bed while it is sinking. The drift is that the mattress travels downstream with the current during it sinks to the river bed. It is necessary to determine the drift by field experiment in advance, as the position of floating bridge used for sinking next GT mattress is related to this value and length of lapping joint of the two mattresses.

Put transversal side weight (earth pillow or gabion)onto the end of the mattress from the boat, and then dump bulk weight on it.

3.5 Placing GT Mattress Under Water

The discharge before flood season is very small on the upstream reaches of Liaohe river, even zero in some reaches. These cases would occur in medium and small sized rivers, During such period of time, the construction of GT mattress may be done simply by manpower. In this method, the mattresses should be constructed the same way as in sinking it on boat described above, then pull into place by standing in shallow water or opposite bank, or placing GT mattresses directly onto the river bed when the water depth is less than 1.0m, and then put the weight on it.

4 CONCLUSION

Through experimental study and engineering practice, some construction methods for placing GT mattresses in seasonal rivers in cold region have been developed. The method should be chosen in accordance with local conditions. However, practice has indicated that sinking GT mattress on ice cover is an optimal method for bank protection of frost-prone rivers in cold regions, because the construction on ice cover has following advantages:

1. Making mattresses, positioning, sinking mattresses, and placing weight will be more accurate, and easier to control the quality of construction.
2. The boat/raft and anchores are unnecessary for construction on ice cover, In addition, it is convenient to transport.
3. High efficiency, so as to shorten construction period and to save the cost of project.
4. Farmers are often employed in construction of bank protection work in China. The period from ice thawing till flood is the busy season in farming, while the winter is slack season, so that the labour force will be optimized

REFERENCES

Wang Dianwu (1994) "Construction Technology of Geotextile Mattresses for Bank Protection" *Proceedings of Symposium on Rock and Soil Mechanics and its Application* Held by Chinese Young Scholars, Science Publisher, Wuhan, Hubei Province, P.R.China. pp.502~506.

Wang DianWu (1994) "Filter Criteria of woven Geotextiles for Protective Works" *Proceedings of Fifth International Conference on Geotextiles, Geomembranes and Related prodocts,* Singapore, 5-9 September 1994 Vol. 2 pp.763~766.

A New Structure for Protecting the Banks of Waterways

J. Yan

Research Engineer, Hydraulic Engineering Department , Nanjing Hydraulic Research Institute , Nanjing 210029, P. R. China.

ABSTRACT: This paper describes a new type of reinforcement for steep-faced embankment by roughened woven geotextile for protecting the bank of waterways. First , the authors have developed a new type of roughened woven geotextile , and have studied the engineering properties of roughened woven geotextile for reinforcing the soil body (fractional coefficient between geotextile and clay about 0.4) . In this paper, the coupling calculation and analysis of stress-seepage for the soil body of embankment have been performed by finite element method for determining the design factors of this structure and laying disposition of the geotextile, at the same time the action of reinforcement materials on the stability of soil embankment have been considered . Finally, the paper describes a case of bank protection in a fourth-grade waterway. In comparison to the common type of bank protection engineering, the structure proposed in this paper have advantages of rapid construction, low cost, and high safety.

KEYWORDS: Waterway, Revetment , Friction, Woven Fabrics, Design.

1 INTRODUCTION

The purposes of bank revetment of waterways are primarily protect direct erosion and attack of shipping wave. Geotextile was usually put to use as geotextile soft caisson etc. in waterways in the past . But wrap-around reinforcement steep-faced embankment was applied to roads and railways etc. . We probes into applying wrap-around reinforcement steep-faced revetment in waterways in this paper, and proves its feasibility from selecting reinforcement materials and designing reinforcement embankment and analyzing states of stress-strain of embankment, calculating stability of embankment. Finally , the paper describes a case of bank revetment in a fourth-grade waterway, and it have success preliminarily .

2 ROUGHENED WOVEN GEOTEXTILE

We have researched and developed a new type of roughened woven geotextile (PP) for fitting the need of engineering, and have carried out the permeability characteristics testing, and engineering properties testing of woven geotextile in the laboratory, its properties are shown in table 1.

Table 1. Properties of woven geotextile (PP)

Test project		Unit	Measured value	Test method
Weight per unit		g/m^2	290	GB/T 13762-92
Strip tensile	T	kN/m	55.2	ASTM D4595
	W		52.2	
Trapezoidal tear	T	kN	1.78	GB/T 13762-92
	W		1.60	
Permeability		cm/s	1.49×10^{-3}	NHRI-89
Frictional angle	μ_1	°	21.9	Sample Size $200\times200mm^2$
	μ_2		30.0	

Notes: μ_1 = frictional angle between geotextile and loam (°) ; μ_2 = frictional angle both geotextiles (°) , GB/T = National Trial Standard of China , NHRI = Nanjing Hydraulic Research Institute .

3 DESIGN OF WRAP-AROUND REINFORCEMENT EMBANKMENT

When designing wrap-around reinforcement steep-faced embankment, we primarily take into account several aspects, such as high of embankment, length of embankment, gradient of embankment, loads of embankment, geological conditions of ground, and characteristics of reinforcement materials and soil-filled . And define the rational position of reinforcement material in the soil-filled, the required reinforcement length, the vertical spacing , and the fold-over length.

We adopt to traditional way " Limit equilibrium concepts" and design wrap-around reinforcement steep-faced embankment. Design ways in detail reference "Geotextiles" (N.W.M.John,1987) , but we take into account simultaneously water pressure in course of designing in waterways .

4 SEEPAGE-STRESS COUPLING CALCULATION

In fact, the stress within the body of the embankment will change the porosity of the fill, thus changing the permeability of the fill through the embankment body and affecting the distribution of seepage forces. In turn, seepage flow affects seepage forces and thereby influences the distribution of stress in the revetment. This indicates the need to simultaneously consider the interaction between stress fields and seepage fields. Seepage-Stress Coupling Calculation can give states of stress and strain during construction and using in reinforcement and the different positions of embankment body. the reinforcement will be rational used .

4.1 Mathematical Modeling

4.1.1 Seepage-Stress Coupling

The equations which represent the coupled seepage and strain in an embankment body are based on the Biot consolidation theory , stress equilibrium , a hyperbolic constitutive model for soil (Duncan and Zhang, 1970 ; Duncan etc. ,1980) , and stress equilibrium and continuity of pore fluid (Zhu and Shen , 1990) . These equations can be expressed in the following matrix form:

$$\left.\begin{array}{l} [k][\Delta u]+\rho g[Q][h]^{n+1}=[\Delta F_1]-[Q][h]^n \\ [Q][\Delta u]+([s]+[R]\Delta t)[h]^{n+1}=[\Delta F_2]\Delta t-[s][h]^n \end{array}\right\} \qquad (1)$$

Where: $[k]$ = stiffness matrix ; $[\Delta F_1]$ = load increment matrix per unit volume ; $[\Delta F_2]$ = constant matrix solved using know value of hydraulic head ; $[Q]$ = coupled seepage-stress matrix ; $[s]$ = compression coefficient matrix of fluid ; $[h]$ = hydraulic head matrix ; $[R]$ = permeability matrix ; and $[\Delta u]$ = displacement increment matrix .

4.1.2 Modeling Reinforcement Geotextile

Tensile loads can be expected to develop in the geotextile as a result of deformations in the embankment body , One approach to model the relationship between load and strain is to assume a simple linear elastic model described by the following stiffness matrix :

$$k=\frac{AE}{l_e}\begin{bmatrix} \alpha^2 & \alpha\beta & -\alpha^2 & -\alpha\beta \\ \alpha\beta & \beta^2 & -\alpha\beta & -\beta^2 \\ -\alpha^2 & -\alpha\beta & \alpha^2 & \alpha\beta \\ -\alpha\beta & -\beta^2 & \alpha\beta & \beta^2 \end{bmatrix} \qquad (2)$$

Where: l_e = length of linear element ; A = cross-sectional area of the linear element ; $\alpha = \cos\theta$; $\beta = \sin\theta$; θ = orientation of the composite liner ; and E = elastic modulus of the reinforcement geotextile composite .

5 The INTERNAL STABILITY OF REINFORCEMENT EMBANKMENT

There are a number of methods the model the internal stability of a slip surface in a steep-faced embankment. We adopt to the circular slip analysis methods of Bishop in which the tensile forces induced in the geotextile are assumed to generated an additional tensile power (Ingold.I.S,1992) .

When calculating the geotextile vertical spacing , it should be assured that the tensile force acting on each geotextile layer does not exceeding the design tensile strength of the geotextile for that layer (N.W.M. John,1987) .

6 ANALYTICAL EXAMPLE

6.1 Background

An example illustrating the application of these theories is taken from Zha-Jia-Su shipping line , it is a fourth-grade waterway, its typical cross-section and design results are shown in Fig 1 .

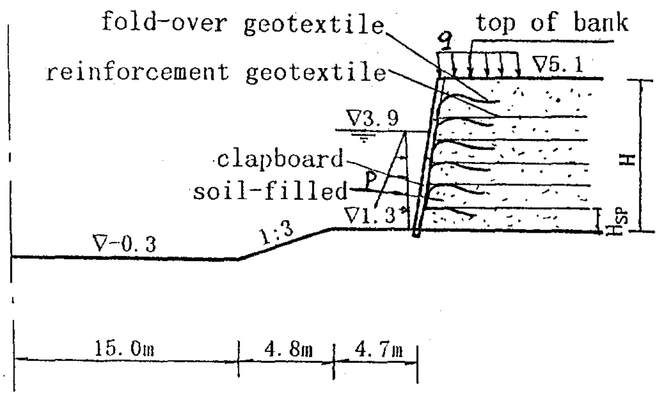

Fig 1. Zha-Jia-Su shipping line typical section and design results

6.2 Design of the Wrap-around Reinforcement Embankment Section

We Adopt to " Limit Equilibrium Concepts " and design the wrap-around reinforcement embankment in the Zha-Jia-Su shipping line. The design parameters in this example are summarized in table 2. , and design results are shown in table 3. .

Table 2. Design parameters for this example

H	H_w	γ	μ_1	μ_2	ϕ'	Ta
3.8	4.2	19.3	21.9	30.0	24.0	52.2

Notes: H = height of embankment (m) ; H_w = height of water level in waterway (m) ; γ = unit weight of soil-filled (kN/m^3) ; ϕ' = internal fractional angle (°) ; Ta = allowance tensile in the reinforcement geotextile (kN/m) .

Table 3. Design results for this example

H	β_1	L	H_{sp}	L_f
3.8	80.0	4.0	0.6	1.5

Notes: β_1 = slope of embankment to the horizontal (°) ; L = reinforcement length (m) ; H_{sp} = vertical spacing of the reinforcement geotextile (m) ; L_f = the fold-over length (m) .

6.3 Seepage-Stress Coupling Calculation

6.3.1 Calculation Parameters and Conditions

In the case of seepage-stress coupling calculation of Zha-Jia-Su shipping line , the material parameters in this example are shown in table 4 and 5 . The construction of embankment is divided six grades , each grade height of construction is 0.6 m , time of construction is six days , in addition to add two grades to fill water in waterway , so there are eight grades in calculation . In this example the calculations were based on 812 four-nod isoparametric elements with 884 nodes .

Table 4. Seepage parameters for example calculations

H_{up}	H_{down}	k_s	k_g
3.90	2.20	7.0×10^{-6}	1.49×10^{-3}

Notes: H_{up} = The design water level (m) ; H_{down} = the low water level (m) ; k_s = permeability of soil-filled (cm/s) ; k_g = permeability of geotextile (cm/s).

Table 5. Soil-filled parameters for coupled calculations

R_f	K	m	r	k_b	k_{ur}	c	ϕ
0.80	125	0.45	0.4	200	400	0.25	21.0

6.3.2 Calculation Results

The soil-filled is homogeneous clays , and the geotextile permeability coefficient is much more than that of soil-filled , the isotonic lines is well-distributed in seepage zone, so the figures of contour lines of water head are omitted.

Since the geotextile liner is flexible and its deforms with the embankment , when tensile stress are developed in the embankment , they will be partially transmitted to the geotextile that in turn will mobilize tensile force . These tensile forces can then be expected to modify the distribution of stress and strain in the body of embankment . The calculation results using period of embankment are shown in Fig 2 .

Fig 2 (a) and (b) show the distribution of major and minor principal stress of seepage-stress coupling calculation , the maximum values of them is respectively 7.85

kPa and 5.36 kPa , major and minor principal stress in

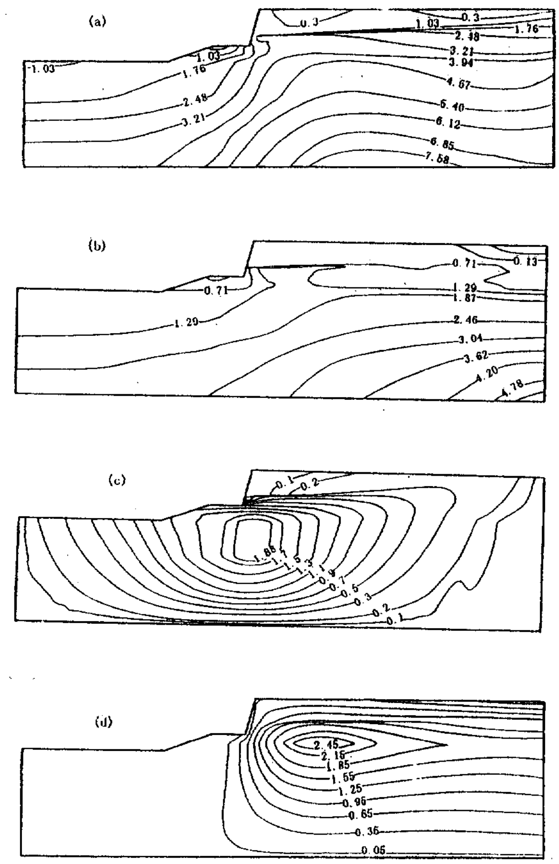

Fig. 2. The calculation results . (a) Contour lines of equal major principal stress (kPa) ; (b) Contour lines of equal minor principal stress (kPa) ; (c) Contour lines of horizontal displacement (cm) ; (d) Contour lines of vertical displacement (cm) .

reinforcement is respectively 3.24kPa and 1.66kPa, both of them are much less than *Ta* (allowance tensile in the reinforcement geotextile) , but both of major and minor principal stress have a phenomenon of stress centralization in one-third height of reinforcement embankment , it indicted that it should lay the reinforcement in this position. Fig 2 (c) and (d) summarize horizontal and vertical dis-placement for seepage-stress coupling calculation , both of them are small , the maximum value of them is respectively 2.10cm and 2.74cm , the tensile stress which the deformation generated would not break off the reinforcement geotextile .

6.4 Stability Analysis

We Adopt to above theories to calculate the stability safety factor of embankment, including two kinds of reinforcement and non-reinforcement , the safety factor of each kind is respective 2.12 and 1.82 . Obviously ,the safety factor of reinforcement is larger than that of non-reinforcement , and the safety factor of reinforcement is satisfied with the civil engineering specification of China .

7 CONCLUSIONS

We prove the feasibility of using roughened woven geotextile to wrap-around reinforce embankments in a fourth-grade waterway . The seepage-stress coupled calculations and analyses show that woven geotextile can ensures that the reinforcement was laid the rational position and the less horizontal and vertical displacement of the embankment , stability calculations show that the reinforcement can increase the stability of embankment . some studies in this aspect are being performed to improve design methods and assess level and show advantages of this way.

REFERENCES

Zhu . B , and Shen .Z , 1990 , " Calculations in soil mechanics ", Shanghai scientific and technological press , Shanghai ,China ,(in Chinese)

T. Tao , D .F. Li and J . Yan ,1995 , " Calculation of coupled stress and seepage for dams with a geotextile /geomembrane composite liner" ,Geosynthetics International. P707~721 .

The initial design of transform engineering of Zha-Jia-Su shipping line , Chapter 1 , introduction of design , ZheJiang province ,China ,1993. (in Chinese).

Alternative Design and Construction of an Under Seawater Road Tunnel Using Geosynthetics in Greece

A. Kollios
Dr. Civil Engineer, Edafomichaniki Ltd, Athens, Greece

ABSTRACT: The construction of a 2,7 km length road tunnel and its approaches for the junction of two caps was designed with a net off - shore length of 700 m below sea - bed level. An extensive geological and geotechnical campaign was performed for the complexed foundation design. At this context an alternative water - proofing design concerning the immerged part of the tunnel sections was performed involving a special geomembrane type with hangers, that obviously offered a cost - effective solution and was approved for construction by the project Owner.

KEYWORDS: Case - Study, Design - by - Function, Geomembranes, Tunnel Construction.

1 INTRODUCTION

On the written instruction of a European contracting Joint - Venture, a detailed geological and geotechnical campaign was carried out as the basis for the detailed foundation design of an immerged tube tunnel crossing the Preveza - Aktion sea strait at the area of Western Greece. The investigations included geological mapping of the approaches to the tunnel and geotechnical drilling boreholes, both on-shore and off-shore, aiming at the determination of a detailed longitudinal geological soil section along the tunnel axis. The contractual design referred to separate tunnel sections as a girder box of 12,0 m width and 7,5 m effective height, incorporating base and roof slabs and side walls of 1,0 m thickness each. The immerged tunnel sections were to be placed immediately below sea-bed level and the maximum seawater height was approximately 26,0 m. Each tunnel section referring to the immerged part had a length of 135,0 m and was to be preconstructed on a dry dock, then by floating to reach the specific placement location.

The stratigraphy along the immerged tunnel axis presented the following geotechnical formations:

I. The upper geological unit referred to rather loose, contemporary sea deposits involving grey silty sands and silts, with lenses and pockets of soft brown clays, extending to an average depth of 15 - 22 m below sea - bed level, being significantly deeper at the center part of the strait (reaching 40 m depth).
II. The lower formation consisted of plioplistocene hard marls with intercalations of dense sandy and gravely layers.

The tunnel immerged sections were designed to be founded by means of stone columns used for sub-soil improvement, in order to minimize the expected large settlements of the initially very loose alluvial deposits. The girder box section was originally designed to bear a 6-mm thick metal plate placed within the bottom slab, acting as a water-proofing element of the sensible tunnel section. An alternative design involving the use of geomembranes was then proposed to the contracting group, replacing successfully the metal plate and offering an interesting solution to the emerged problems. The geomembrane proposal was adopted and is actually under application of the project, to be finished by the end of the year 1998.

2 GEOMEMBRANE DESIGN

Water proofing of underground road tunnels under important hydrostatic pressures by geosynthetics involves the determination of the most involved property for geomembranes, the thickness of the liner. This property is directly related to the resistance to tear, to the puncture resistance and to the impact damage resistance. In fact a linear and sometimes exponential increase in resistance to the above mentioned actions is related to the geomembrane thickness increase.

In order to determine the minimum necessary operational geomembrane thickness, a rough estimate of the stress - strain conditions applied on the contractual girder box structure was performed using simple static analysis by a finite element method. The results of this analysis allowed the determination of the most critical vertical stress applied on the geomembrane (Figure 1).

For the calculation, it was assumed that each preconstructed section of the tunnel was separately isolated by the proposed system, since the in-between joints were to be sealed by the contractually foreseen system of water stops.

The initial design of the minimum necessary function thickness of the geomembrane to be applied at the bottom of the tunnel sections refered to the determination of a cost-effective safety factor F considered as the ratio of the minimum necessary thickness to the allowable design thickness. This factor of safety F ranged from F=1,5 to 5,0 depending on the polymere type, the special construction conditions of the project, the method and the effectiveness of the quality control of the water - proofing system. The design of the allowable thickness of the liner was based upon the deformations to occur to the geomembrane during the construction and the life - time of the project. These deformations would mainly be construction deformations that would directly influence the relative displacements of the geomembrane during placement, since the presence of stone piles assured for a practically non - deformable foundation interface.

The allowable thickness design was performed according to R.M. Koerner, 1990 theoretical principles and the results were plotted at the following Figure 2.

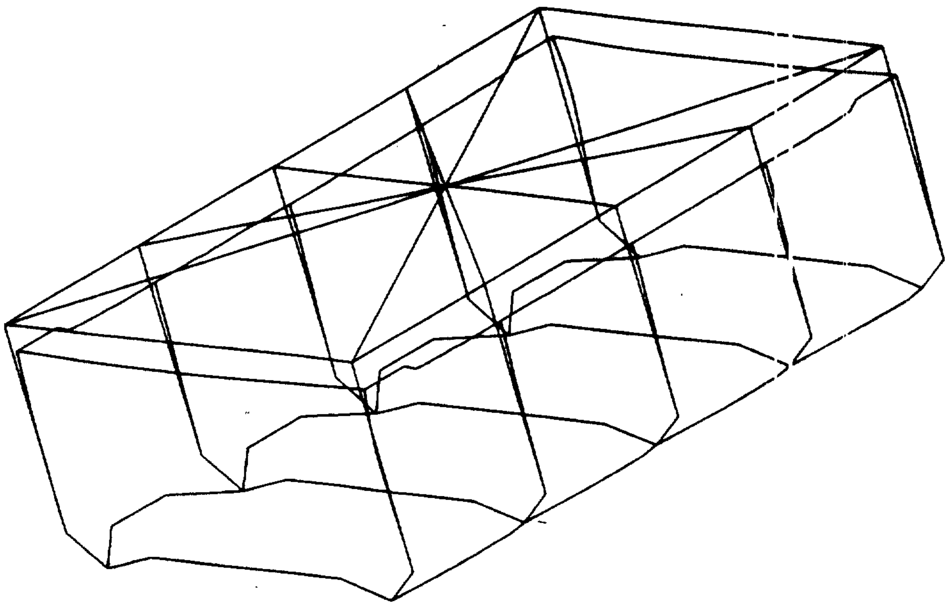

Figure 1. Indicative results of initial and deformed mesh of a typical tunnel section.

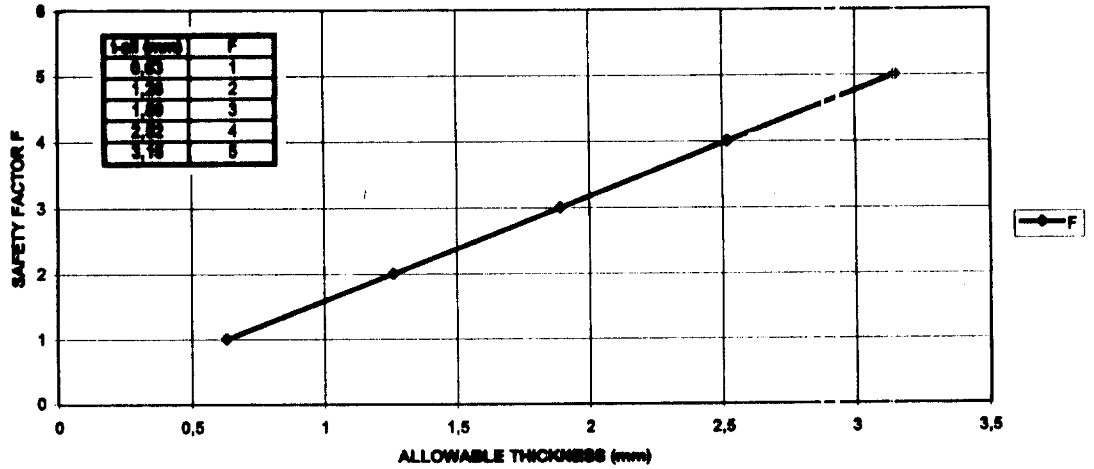

Figure 2. Correlation of the allowable thickness of the liner to the design safety factor

Based upon the final results, the alternative design for geomembrane selection proposed:

a. A high density polyethylene geomembrane with a minimum thickness of 2,5 mm, corresponding to a safety factor of $F_1 = 4$, or
b. A low density polyethylene geomembrane with a minimum thickness of 1,5 mm, corresponding to a safety factor of $F_2 = 2$.

All calculations were performed according to Eurocode 7, taking into consideration a seismic factor of a=0,30. g. As deduced by the analysis, the maximal vertical stress applied on the bottom geomembrane was calculated at the level of 300 KPa approximately.

3 CONSTRUCTION PROPOSALS

3.1 General Considerations

The main factor of concrete desintegration in saline water is the influence of remaining chlorides within the concrete mass that create reinforcement corrosion. To avoid any such risks at the bottom of each tunnel section, the proposed use of a geomembrane, according to the design presented above, placed at the lower part of the concrete slab, exactly replacing the metal plate of 6 mm thickness initially planned, offers an interesting and rather cost-effective solution. In addition to that, water-proofing of also the walls and the roof of each section might also be adopted by the contractor, in conjunction with a high quality concrete mix, adequate for sea-water tunnelling purposes. The technical advantages of the proposal were evident in terms of quality control during construction, provided that the main geosynthetic placement rules would be completely respected.

3.2 Construction Details

The geomembrane to replace the metal plate of 6 mm should be placed exactly at the same location, as contractually foreseen, i.e. at the lower limit of the concrete slab. For doing so, special conditions and care involved the following points:

a. In order to assure a perfect adhesion of the geomembrane to the concrete slab (so that no detachment during construction and navigation of the sections occurred), the geomembrane should present the special section indicated at Figure 3.
   For this section, values of D , d and H were such to assure for a perfect adhesion and that no lateral displacement of the geomembrane to the lower part of the slab might occur. The design called for D = H = 10 -20 mm and d = 5 - 10 mm.
b. The lower interface of the geomembrane would be in contact with the specially constructed bases placed on the stone - piles levelled surface. Those specially constructed bases should be covered by plastic materials (such as teflon, thin plastic sheets) that did not need to present any life - time performance, but they should be applied only for the moment of placement. In this way, during placement, any wrong movement of the tunnel section would not transduce any secondary harmful friction of the membrane to the foundation bases (because of the protection provided).

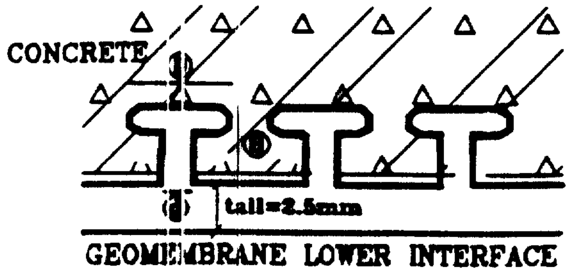

Figure 3. Special section of geomembrane to assure adhesion to the concrete slab.

c. The remaining space between the foundation bases and the lower interface of the geomembrane should be filled with cement grout under pressure, according to the contractual specifications. Therefore, a life - time protection of the geomembrane was assured.
d. Concreting of the slab over the geomembrane should be carefully executed, especially where the reinforcement is placed, so as not to create any short of dammage due to scratches on the geomembrane.

In order to combine a complete waterproofing of all the design section of the tunnel according to the specifications used for geomembranes in underground constructions, the geomembrane protection of the bottom slab might also be placed over a 20 cm thick concrete base that would extend all around the section of the bottom, the walls and the roof of the section (outer girder box). This alternative proposal was not finally accepted and the contractually imposed water - proofing system was applied on site (sprayed polyourethane).

4 CONCLUSIONS

The use of a special type of geomembrane allowed a most interesting alternative solution for water proofing the bottom slab of an under sea-water road tunnel, actually under construction, replacing the contractually foreseen metal plate and offering an important cost benefit (estimated at the level of 10% approximately over the total foundation cost). The existing geomembranes installation experience (mostly acquired during construction of multiple store - garages below ground level and the underground tube train and stations at the broader Athens area) combined with the strictly applied supervision, create the assurance for obtaining the most efficient water-proofing method for the final stage of function of the project, which is set to be fully realised by the end of 1998.

ACKNOWLEDGMENTS

The author would like to thank Mr. S. Papaspyrou of Edafomichaniki Ltd for his review of the original manuscript as well as the site engineers Mr. S. Zafiratos and G. Kilimis from the contracting group for their help concerning the follow-up of the project. Special thanks are also due to Mr. G. Dernikos, project manager at the time of issue of the present alternative proposal for his directive ideas.

REFERENCES

EDAFOMICHANIKI LTD (1994-1995) Geological and Geotechnical Investigations for Aktion - Preveza Junction, Athens, Greece.

GEOFELT m.b.H (1994) Tunnelliner Information Data Sheets - Agruflex.

Koerner, R.M. (1990) *Designing with Geosynthetics*, Second Edition, USA, pages 410-413.

Kollios, A. (1995) *Waterproofing by Geosynthetics Alternative Proposal* - Aktion Preveza Junction - Preliminary Design and Specifications, Athens, Greece.

POLYFELT Ges.m.b.H (1994) High Density Geomembranes - Polyline data sheet and specifications.

Application and Testing of Geotextiles in Deep-draft Quays

Fengwu Liang
Senior Engineer, China Nanshan Development (Group) Incorporation, Shenzhen, China

ABSTRACT: Eight berths capable of taking ships up to 25000 DWT and 50000 DWT respectively were completed in Shenzhen port, in 1985 and 1995 separately. The berths are deep-draft quays in 11, in 12.5 and in 13.1 meters, behind which woven geotextiles were successfully placed as filters for trial. The durability of the geotextile requires further investigations since it was the first time that geotextiles were used in a large quantity in quay construction, instead of the conventional Crushed-stone filter courses. A blind shaft was built at one end of the quays. Field investigations and observation, a research institute has been commissioned to carry out the observation and investigation for ten successive years. In the shaft, synthetic bags, filled with the same quarry-run fills were placed at three different locations as the filter layers, i.e. underwater, intertidal zone and above water level.

KEYWORDS: Case Study, Geotextiles, Design, Walls, Filtration

1 THE CHANGES OF THE FILTER COURSES IN GRAVITY TYPE BLOCK QUAY

In a conventional gravity type block quay, the bulkhead wall is often a kind of retaining concrete block wall in a concrete stair type or gravity type. The block size is designed based on the lifting capacity of the crane held by the contractor. A large crushed stone riprap prism as filter courses is often used to keep the fills from leaking through the joints between the blocks to the front of the quay(Fig. 1). The quantity of works for construction of the quay is divided roughly into following parts:

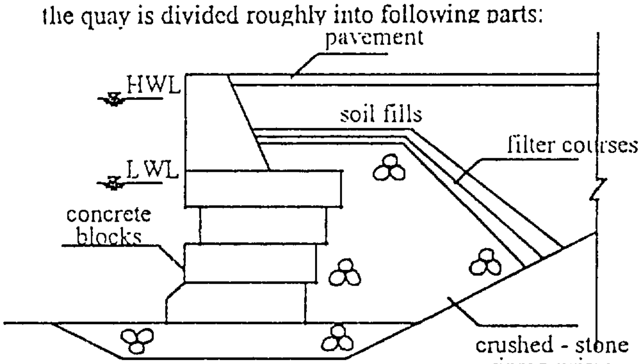

Fig 1. A Conventional Gravity Type Block

The two main factors inflecting the cost and the construction period are item 2 and item 3. Usually , 20 percent of total cost and 50 percent of whole construction period will be spent on item 3. As new type construction materials are springing up in the wake of development in science and technology, scientist , after several decades hard work, eventually found out a new effective structure of gravity type quay to replace the conventional one. Eight berths each with . capability of taking ships varying from 10,000 DWT to 50,000 DWT, had been successively built in Shenzhen China during the 10 years from 1985 to 1995. The structure of the quays was reformed not only on its blocks size but also on its filter courses by replacing crushed-stone riprap with woven synthetic fabrics. As a result of the reformation , the construction works were simplified enomorously.

2 DESIGN OF THE FILTER COURSE IN BLOCK QUAYS

A gravity type solid-filled block quay, of good durability and flexibility to working loads as its advantages, is made up of many blocks which form many joints cross and down over the back of the blocks. In order to keep fills from leaking through the joints into the port, a reliable crushed-stone riprap filters should be built. If we want to adopt woven fabrics instead of crushed-stone riprap as filters, we need to reduce the number of joints, and to make the distribution of joints regular. According to our many years experience, a reinforced concrete hollow block in large size , which simplifies the distribution of joints , has been used in a deep-draft quay for 25,000 DWT in Chiwan harbour. The woven fabrics as filter courses were first time adopt in deep-draft quay with overall height 15m and draft 11m. As local soil and rock materials are easily accessible, it is convenient to unguarded quarry run rocks from Chiwan area as fills behind the hollow block quays. Closed H type reinforced concrete hollow blocks, weighing 200 t each, were designed for the quays. On top of the blocks are hollow relieving platforms with wave absorbing chambers. The longitudinal length of the hollow block along the quay is 3.5 m , and the width of the relieving platform which sits directly on top of the block is the same as that of the block, with no alternate joint between the two, thus leaving a vertical through joint every 3.5 m behind the quay. To facilitate placing synthetic fabrics and cut down their consumption, an independent strip of synthetic fabric was placed at every joint and the strip had a 1.00 m overlap on each side of the joint over the back of the blocks. Since the overall height of the block was about 10.00 m, the levelled foundation bed for the blocks would surely develop some irregularity, thus the joints between installed blocks would be far larger than the stipulated 5 cm in the construction code. Therefore, the largest allowable joint width was stipulated to be 10 cm -15 cm in the design. However, to prevent differential settlement of blocks causing excessive tension in the synthetic fabric strips, the designed width of the synthetic fabric strips was 25 cm.

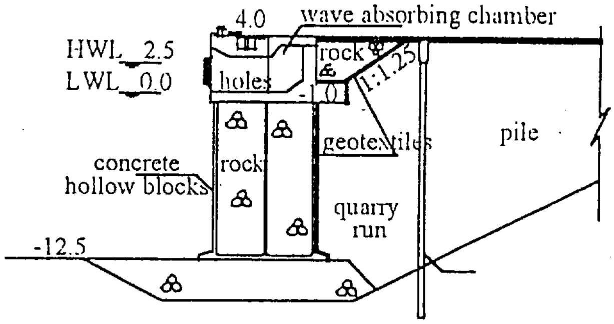

Fig 2. A Sectional View of A Gravity Type Hollow Block Quay with Wave Absorbing Chambers (Unit: m)

Synthetic fabric strip locking latch seat were embedded in the back walls of the blocks beside the joint. .In order to lock the fabric to the back of the blocks, prepared holes were placed on the synthetic fabric strips in line with the position of the locking latch seat: To minimise difficulties of underwater operations, the connection of the locking latch seat and bolts with the synthetic fabric strips should be as simple as possible. The structure of a locking device is shown in Fig. 2.

Three types of woven synthetic fabric strips were designed and used at the cross section of the quays.
Type A: woven synthetic fabric strips of 2.25m x 12.00 m were used behind the hollow blocks.
Type B: woven synthetic fabric strips of 2.25 m x 4.50 m were placed on the cantilever extension of the relieving platforms.
Type C: woven synthetic fabric strips of 4.50 m wide were used beneath the stone prism placed behind the wave absorbing chambers to eliminate residual wave energy. The geotextiles were placed continuously with an overlap of 1.00 m.

As shown in Fig. 2c, loops were arranged both at the top end of type A and at the lower end of Type B to prevent soil grains from being washed out locally. The total consumption of geotextiles used for the 264m long berth accommodating ships up to 25000 DWT is 12000 m^2.

In 1988 and 1995, 6 light weight gravity type quays each capable of taking ships up to 50,000 DWT were successively contructed in Chiwan Harbqur and Mawan Harbour. This further developed and extended the application of Woven fabrics in deep-draft quays and make their section more economical and reasonable.

The light weight gravity type quay is a new type structure, specially designed for uneven distribution of geology, with bent structure upper and hollow blocks underwater. The combination of the upper bent with the railway can make over-water fills as a slope. This greatly releases the fills pressure upon the vertical bulkhead wall, and make filter courses set only behind the blocks for underwater all year long while the protection of filter courses for the over-water fills is unnecessary.

As is well known, the perfect way to extend the woven fabrics service life is to shelter it from ultraviolet radiation. The light weight gravity type block quay in Chiwan, with its double ribbed upper bent, is an ideal method resolving this problem, with each hollow block weight under the relieving platforms within the crane lifting capacity 500 Ton. Joints are set every 7 metres covered with woven fabrics. The permeable bent and slope type bank protection are constructed above the relieving platforms. Thus, it not only provide a stable berthing condition, but also, due to the riprap being replaced and with no worry about the penetration through the stone and damage to filter course, simplifies the construction of stake foundation under the crane railway. And also, with the fills pressure and weight reduced, the pressure on the ground is released enormously. The woven fabrics make the construction easier and faster and cut down the cost by replacing the complicated crushed-stone filter courses. The quay, built with lower cost and higher quality using new materials and new technology, and with the tangled ground treatment problem resolved, was awarded a national silver medal on its perfect designing.

3 SELECTION AND PROTECTION OF WOVEN GEOTEXTILES

The woven geotextiles used as filters behind the quays should have the following properties:
1. Good in soil retention property and that in separating water and soil;
2. High water permeability to protect woven synthetic fabrics from being blocked up to form a detrimental water head;
3. Sufficient strength: tensile strength, impact strength, tear and puncture resistance;
4. Sufficient durability: good ultraviolet resistance, chemical corrosion resistance and sea water resistance.

The durability of geotextiles should not be affected by moulds eating rats and termites and by atmospheric temperature.

A new woven synthetic bag factory in Chiwan, manufacturing woven synthetic bags for chemical fertiliser, was completed and put into production at the time when the designs were completed. A research institute was then commissioned to carry out various tests for the physic-mechanical and chemical properties of the synthetic textile produced in the factory. It was finally decided to use the synthetics produced in this factory instead of the originally selected T7W7 woven geotextiles.

The main features of the woven geotextiles manufactured in this factory are as follows:
Longitudinal strength 2.5t/m
Latitudinal strength 2.5t/m
Impact resisting strength: Crushed when placed on concrete floor and stone of 30 kg dropped from a height of 2.00 m.
Chemical composition polypropylene
Unit weight 190g/m2

Permeability: No evident water head was observed during flume tests under sea flood and ebb condition simulated.

Laboratory tests showed that, no change in the tensile strength of the synthetic fabric was observed when the synthetic fabric was exposed to corrosive media of acid, alkali, salt and sea water. The resistance of the fabric against moulds was stable and their properties were also stable when they were subjected to oxygen blasting in normal atmospheric temperature: and no loss of weight was observed. From the outer appearance of the fabric, the colour, lustre and softness remained the same as that before the test. It was smooth surfaced, transparent and no abnormality had been observed in the texture of the fabric.

As the strength of the synthetic fabrics couldn't meet the designed requirements, it was decided to use two layers of the synthetic textile at each joint.
Since anti-ageing agent was added to the polypropylene fabric, the synthetic fabric had a poor ultraviolet resistance. Practice proved that the textile would soon become brittle when they were exposed to sunshine. To prevent the textile from being exposed to sunshine, it is requested that the ocessed synthetic fabric strips should first be stored in dark rooms and then placed at night time or in cloudy days whenever it is possible, in order to prevent geotextile from being damaged by the dumping of rocks, a Φ =2mm wire netting with grids of 3×3cm was placed against the textile behind the quays as protection. A layer of rubble stone was riprapped over the geotextile on the slope and then larger stones were placed.

4 IMPORTANT REMARKS

Woven synthetic fabrics used as filters should first possess a porosity matching the permeability of the backfills so as to ensure an unimpeded drainage and the geotextile should not be liable to blocking. As a matter of fact, the permeability of commonly used woven synthetic fabric is usually higher than that of the adjacent soils. However, special attention should be payed to the gradual blockage of pores of geotextiles during their service.

A filter course is not formed by geotextiles themselves but formed when fine particles in the fills behind the fabric are washed off through the pores of the fabric and the remaining coarse grains form arch type structures around the pores while the soil beyond forms another granular filter course with different graded grains. The further away the soils is from the geotextile, the lower the permeability of soils becomes. A new natural filter course is thus formed, behind which are natural soils, and. after such a natural filter is formed, soil grains will not be washed off any more as the soils behind it becomes stable (Fig. 3). Therefore, geotextiles don't work directly as a filter but help backfills forming a

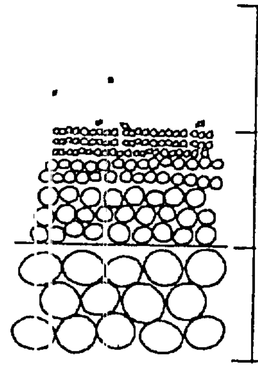

Fig 3. Forming Process of A Filter Course

stable natural filter course. Proper selection of woven or non-woven synthetic fabrics according to the permeability requirement of a structure and the grain sizes of the fills is of great importance to a stable and effective filter course. The backfills for marine ports usually consist of rather coarse grains. Though the backfills are influenced by the complex alternating currents and waves during flood and ebb and the arch type structures behind the geotextiles are sometimes liable to failure The squeezing action of the fills behind the geotextiles can generally keep the natural filter course stable and the pores and draining passages are not liable to salutation and blockage.

Geotextiles suitable should meet the requirements as follows:
(1) For natural soils when the weight of soil particles passing sieves with a screen size of 0.074mm (U.S. standard sieve #200)
Accounts for less than 50% of the total weight;
D85(soil)/EOS (geotextile) ≥ 1 (EOS: The effective pore size)
(2) For soils other than above mentioned soil:
Eos (geotextile) <0.211mm (U.S.standard sieve #70)
But, when D85 <0.074mm, it is not advisable to use geotextiles.
(3) Geotextiles with EOS smaller than 0.149mm (U.S. standard sieve #100) should not be used as they are liable to blocking.
(4) Within the limits stipulated in the criterion, geotextiles with larger pores should be used.

The above requirements only apply to specified soils and steady flow, and the influence of soil density has not been taken into account. However, those requirements can be considered properly in the case of soft and loose soils.

When geotextiles are used in quay structures, the following requirements have also to be followed.
(1) The permeability (K) of geotextiles should be greater than 10 K of soils, where K is the permeability parameter.
(2) the slope ratio should be less than 3 so as to prevent the geotextile from blocking and corresponding tests should be carried out.
(3) Unstable geotextiles or geotextiles with poor ultraviolet resistance should not be exposed to direct sunshine for more than 5 d.

5 LABORATORY TEST AND SITE OBSERVATION

In the national harbour engineering code, the service life of a gravity type quay should be more than 50 years. The polypropylene woven fabrics , instead of crushed-stone riprap, are applied in a quay structure for the first time. Its durability requires further investigation and observation. Some scientific research institutions have been commissioned to study the loss of its tensile strength and weight, and the changes of its outer appearance by submerging the fabrics into an acid liquid made up of artificial sea water and lactate for 6 month. In the middle of the quay ,an observation well in which 2 series of samples, one series of soil and the other plate, were laid on both the place beneath low water and well ground to observe behavior of the fabrics in a long term of 10 years.

The results from both laboratory and observation are shown in Fig. 4:

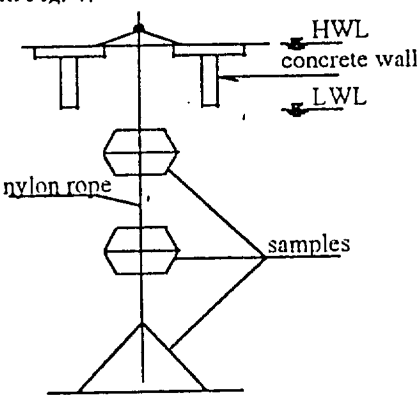

Fig 4. Samples Installation
View on Testing Ground

The results from both laboratory and observation are shown in Fig 5.

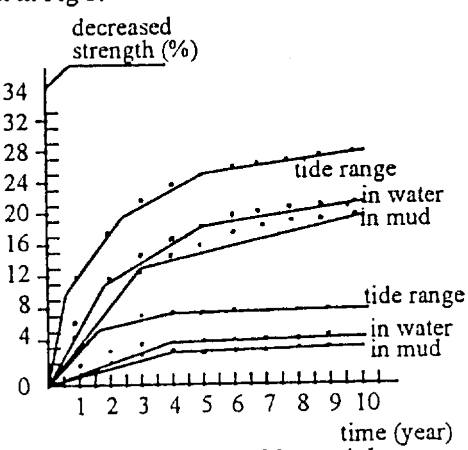

Fig 5. Relative Curve of Strength Loss
and Exposing Period

From the above results , we can see:

1. In the laboratory test the polypropylene woven fabrics are not sensitive to sea water, acid, alkali, and bacterial erosion at all.
2. The 10 years' observation demonstrates that the polypropylene woven fabrics corrosion and erosion by nature sea water and mud is not serious.
3. In the water level changing area , due to the contact of fabrics with f l s , the fabrics tensile strength decreased by 33.5 percent of which, by 26.5 percent in the first 3 years , and by 7 percent in the later 7 years in a slow decreasing rate. Under the low water level area, the tensile strength of the polypropylene woven fabrics decreased by 23.5 percent of which, 18 percent in the first 3 years and 5.5 percent in the later 7 years. The tensile strength-time diagram shows that the curve rate is more and more even at the time of 10 years later. By extension of the curve , we can calculate that the tensile strength of over water woven fabrics will have decreased by 50 percent while that of under water by 40 percent by the time in 50 years.
4. The above results also show that woven fabrics filter course and the concrete block with 50 years service life in gravity quays can match very well. When a type of anti-ageing woven fabrics with a longer durability are applied, the service life of a gravity quay is usually more than 70 years if it locates in a no accidents environment , especially in a no ice environment.
5. Woven fabrics filter course in a gravity quay should be set under water as fully as possible to shelter it from damage of the atmosphere and sunshine to extend its service life.

6 ECONOMIC BENEFITS

The economic benefits of woven synthetic fabrics used as filters for the quay for 25000 DWT ships in Chiwan Port are given in Table 1 as compared with that of filter drains and riprap prism filter course.

From the table, it can be seen that the filter course comprising synthetic fabrics produce a remarkable economic benefit which saved investment by 74% compared with the crushed-stone filter drains and by 76.1% compared with the riprap prism with crushed stone filter course and construction period is cut down by 1 to 4 times when geotextiles are used as a filter. Thanks to the using of geotextiles which are very easy to handle, the two hollow block deep-water quays were completed in just) months in spite of the complicated joints handled at the two ends of the quays, the time consuming bag-bond concreting on the riprapped rock foundation bed and the special requirement for wave absorbing chambers on the upper part of the quay. Both quays have therefore been evaluated as excellent projects by the relevant authorities.

REFERENCE:

1. Benhai Wei, and Len Jan (1997), "Total Report on Polypropylene Woven Fabric Performance Test in Chiwan Harbor" p5-9, Nanjing Hydraulic Research Institute, P.R.China
2. Benhai Wei (1989), "Report on Polypropylene Woven Fabric Performance Test in Chiwan Harbor" p4-7, Nanjing Hydraulic Research Institute, P.R.China

Jute Geotextiles

U. Datta & P.K. Chatterjee
Indian Jute Industries' Research Association (IJIRA), 17 Taratola Road, Calcutta 700088, India.

B. Chottopadhyay & A. Ghosh
Civil Engineering Department, B.E. College (Deemed University), Howrah 711103 India.

ABSTRACT: A heavy duty open mesh woven jute fabric is perhaps the first geotextile, which has been in use for protection of slopes from erosion by rain and wind in Europe and America since early fifties. Lighter fabrics have been developed and their performance has been evaluated under various soil and climatic conditions. The results reveal that the fabrics reduce soil loss by about 90% and comparable with the performance of the existing product.
Woven jute fabrics for separation and filtration have been developed and found to be cost effective in river bank protection work replacing conventional granular filter. In this application the fabrics need chemical treatment for enhancement of durability. After successful trials under different soil and river conditions, the treated fabrics are being commercially used. Similarly treated fabrics have also been tried for construction of roads on soft soil as separator and found to be cost effective with encouraging results.
Jute non-wovens have been found suitable for filtration and drainage.

KEYWORDS: Erosion Control, Filtration, Separation, Embankments, Geotextiles

1 INTRODUCTION

Jute as a geotextile material is well known in Europe and America for protection of slopes from erosion by rain and wind. A heavy duty open mesh woven fabric in the name of Soil Saver/Geojute/Anti-Wash has been in use since fifties and the jute producing countries have been exporting the item since then. The demand of the product went upto as high as 100 M m^2 . In mid-sixties, when concept and application of geotextiles started, other natural and synthetic materials entered in this field of application. At present global demand of natural geotextiles is about 86.6 M m^2 - a recent survey reveals. Among the products, straw based products claim about 60% of the market, while jute and coir together claim about 37% and the rest 3% by others like wood-wool, synthetic etc. (Rickson et al. 1996). It has been reported that the decline in the demand of jute is due to nonavailability of the product in the market because of the fact that a few mills produce the product, which requires special type of processing equipment. For involvement of more number of mills in supply of the product, two products have been developed in consultation with the experts in this field. The products are of different open areas and their performance has been studied extensively. The results of the studies have been discussed in this paper.

The synthetic geotextiles are very expensive in the third world countries and so its application is limited. The civil engineers of the countries are looking for low cost alternatives for geotechnical constructions. Jute being one of the cheap fibres having good strength, structural stability, abrasion resistance etc. its properties for civil engineering applications have been evaluated by many workers (Thomson 1985, Kabir 1988, Aziz 1991) and found to be useful for specific applications. A prefabricated fibre drain using jute fabric and coir rope was developed for consolidation of silty subsoil and used commercially in Singapore (Ramaswamy et al. 1984). Treated Jute Geotextiles for separation and filtration developed by IJIRA was used for protection of bank of the river Hooghly at Nayachar, opposite to Haldia Port (Datta et al 1990, Sanyal et al. 1993). The product is being used by the engineers of Irrigation & Waterways Directorate, Govt. of West Bengal for river bank protection work after extensive trials under various conditions of soil and river under their control. Results of the trials have been discussed here.

Similar fabrics were tried for construction of roads on soft soil as separator and encouraging results were reported. Jute nonwovens were also tried for construction of unpaved roads as well as for filtration and drainage of roads . The results are satisfactory (Rao et al. 1996).

2 FABRICS FOR CONTROL OF SURFACE SOIL EROSION

A heavy duty open mesh jute fabric is perhaps the first natural geotextile used in this field of application scientifically in early fifties in Europe and America. The fabric is made of thick yarns of 5 mm diameter, which requires special type of machinery for processing. Ludlow Jute Mills, an American firm in India set up a separate plant in their mills for manufacture of the product and developed special machinery in collaboration with a jute machine manufacturer. Other mills also entered into the business to cater to the demand of the product. But from mid-sixties with the advent of other geotextiles of natural and synthetic origin in this field with the concept and application of geotextiles, its demand gradually declined to the present level. A recent market survey of the product revealed that nonavailability of the product in the market was one of the reasons for decline of demand. The experts suggested products, which could be produced by any mill having conventional jute processing machinery. For the purpose, IJIRA developed two varieties of Jute Mesh (JM) type I&II and tested the properties and performance in India and abroad. The specifications of the products including Soil Saver have been furnished in Table 1 below.

Table 1 Specification of Jute Geotextiles for Control of Surface Soil Erosion.

Jute Geotextiles	Weight (g/m^2)	Yarn diameter (mm) Warp	Yarn diameter (mm) Weft	No. of threads/dm Warp	No. of threads/dm Weft	Width (Cm)
Soil Saver	500	5	5	6.5	4.5	122
Jute Mesh						
Type I	400	2	3	34	15	122
Type II	300	3	3	12	11	122

2.1 Properties

The physical properties of the materials tested by Soil Management Division, Silsoe College, U.K. and IJIRA are given in Table 2 along with the properties of the products available in the market for similar application.

Table 2 Physical properties of Jute and other geotextiles for Control of Surface Soil Erosion.

	WOVEN				NON WOVEN	
Properties	Soil Saver	Jute Mesh Type I	Jute Mesh Type II	Coir	Straw based	Synthetic
Weight (g/m^2)	500	400	300	700	250	450
Thickness (mm)	5	3	3	4	8.5	18
Coverage (%)	55	60	40	60	100	85
Tensile Strength (KN/m)						
Warp	20	16	12	25	-	3.2
Weft	9.5	6	11	12	-	-
Water holding capacity(%)	600	500	400	280	700	90

2.2 Functions

When installed they act in two ways - 1. Arrest movement of soil particles, seeds and nutrients on the surface of the soil and 2. Help fast growth of vegetation, which covers the surface with a canopy of living mass as well as reinforces the soil with roots, protecting the surface from erosion by rain and wind permanently.

2.3 Trials and Results

The functional performance of Soil Saver is well known to the users for more than four decades; however, that of the new products has been studied by Silsoe College in UK and Tea Research Association as well as the Directorate of Forests, Govt. of West Bengal, in India in collaboration with IJIRA. Silsoe College studied the performance and compared it with the others while Tea Research Association studied soil loss of the hillocks of Cachar district in Assam, after plantation of tea using Jute Mesh Type I & II and compared it with that of bare plots. Forest Directorate used Soil Saver for protection of hill slopes in the district of Darjeeling in West Bengal through vegetation. The results of Silsoe College are shown graphically in Figure 1 & 2, while those carried out by Tea Research Association in Figure 3. The comparison of vegetation densities on treated and untreated areas of Darjeeling is given in Table 3. Vegetation density was measured six months after installation.

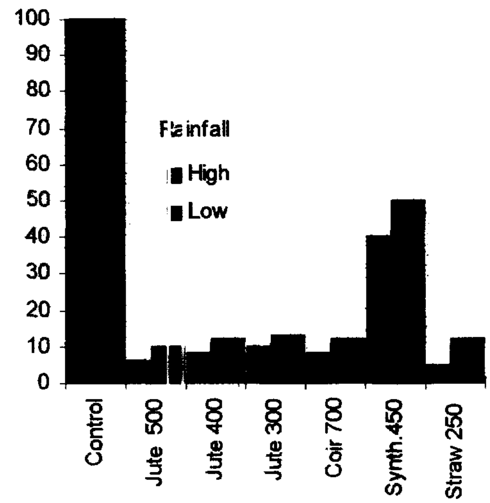

Figure 1 Soil loss (%) for different geotextiles treatment under different rainfall (Soil - Sandy loam)

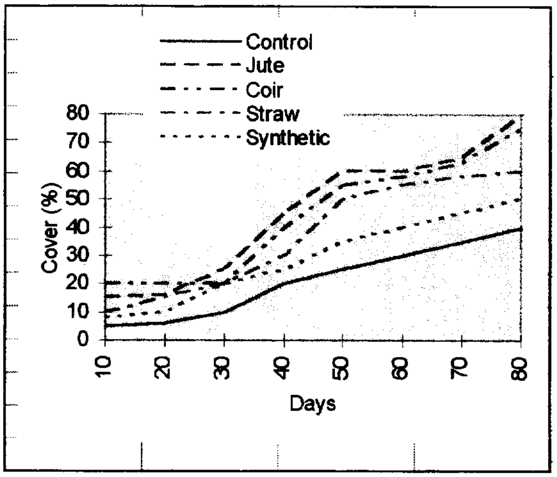

Figure 2 Vegetation cover (%) under different geotextiles with time (Soil-Sandy loam).

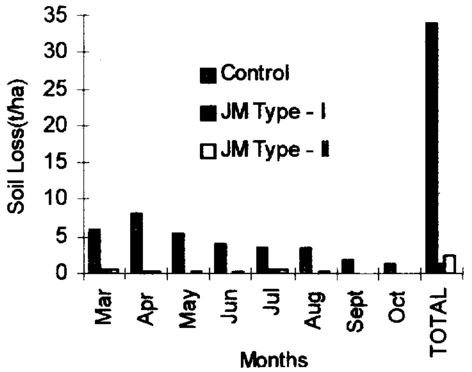

Figure 3 Soil loss under treatment of Jute Mesh Type I & II in different months of rainy season (Total rainfall - 2304 mm, Soil composition - Sand : 73%, Silt : 18% and Clay : 9%)

Table 3 Vegetation densities of treated and untreated areas

Plant species	Slope (60-65)° Treated	Slope (60-65)° untreated	Slope (30-45)° Treated	Slope (30-45)° untreated
Chipley	43	48	27	11
Kash* Vimsing	45	21	58	30
Patay	5	1	2	-
Guelo	1	1	17	1
Unio	9	12	12	2
Banmara	4	6	12	7
Amlisho	5	6	-	2
Kalimontey	10	-	-	6
Bansho	43	-	-	-
Raikhaney	-	2	6	1
Bhakatey	-	-	5	-
Total	165	97	139	60

* Planted; Plant species (local names)
Soil composition - Sandy loam mixed with small stones; Rain fall - above 3000 mm.

2.4 Selection of Fabrics

Selection of suitable fabric depends on the site conditions like gradient of the slope, intensity of rain fall, wind velocity and soil composition.

2.5 Installation

It is very easy to install. Any unskilled person can lay after training at site After cleaning the surface and making it as smooth as possible the fabrics are laid after anchoring at the top of a slope and rolling down to the bottom, where it is anchored again and cut. The layers are to be overlapped by 10 cm side by side. The over laps are fixed with the surface with the help of iron pegs of suitable size or living pegs made of tree branches, which may grow with time at intervals of one metre. End to end overlapping should be 15 cm and fixed with the ground keeping the finishing end on the top and starting end under. After installation, seeds of suitable plant/bush/legume may be spread over the treated area. Sapling/tree cutting may also be planted through the open areas if necessary. The treated area should be restricted from stamping and grazing till vegetation takes firm roots. Damage caused by chance should be repaired immediately placing fresh fabric on it and fixing it with the ground.

2.6 Discussion

It is evident from the above results that Soil Saver as well as the fabrics of Type I & II are capable of reducing soil loss by around 90%, inspite of its less coverage compared to nonwovens as well as cover the surface with vegetation within three months. It is due to the fact that it is highly flexible, which increases by about 25% when wet. So, after first shower, it can establish intimate contact with soil surface reducing soil loss significantly. Moreover, it can absorb water to the extent of four to six times of its weight and helps reduce run off velocity considerably. The water is released in dry spell creating a moist atmosphere, which helps vegetation to grow fast. Apart from these properties jute has good insulation property, which again helps control the extremes of temperature for healthy growth of vegetation. After a period of one and a half years to two years it looses its strength while the biomass, which remains on the surface is not toxic, but increases water permeability of the soil.

3 FABRICS FOR SEPARATION AND FILTRATION

Development of such fabrics was initiated by Calcutta Port Trust in late eighties, when the trust was searching for low cost fabrics for protection of bank of the river Hooghly opposite to Haldia, a riverine port in EasternIndia. Erosion of the bank was creating navigation problem for big ships. As synthetic geotextile for river bank protection is expensive in India, the Calcutta Port Trust approached IJIRA to develop fabrics for the purpose with specific properties like pore size, water permeability and durability for a reasonable period till siltation starts. For the purpose a twill woven fabric was designed and developed and treated with rot resistant chemicals and bitumen to enhance durability. Bitumen treatment was developed so that it maintains the pores of the fabric for filtration and water permeability across the plane of the fabric. The enhancement of durability of the fabric was measured in laboratory using standard methods IS:1623-1992 (BIS Hand Book 1996). The test results are given in Table 4.

Table 4 Results of Soil Burial Test

Incubation period (Week)	Loss in strength (%)		
		Treated	
	Control	Rot resistant chemicals	Rot resistant + Bitumen
3	90	5	2
6	100	50	20
9	-	90	50
12	-	100	80

A pilot trial on the bank observed strength loss around 30% after a year, when siltation was to the extent of 30 cm on the lower part of the bank. The engineers accepted the fabric for the bank protection work, and applied it commercially for protection of the bank to a stretch of 1.5 Km in 1992. The specification of the fabric is shown in Table 5.

Table 5 Specification of Jute Geotextile for Separation and Filtration

Physical properties		
Weight (g/m^2)	-	760
No. of threads/dm Warp	-	102
No. of threads/dm Weft	-	47
Thickness (mm)	-	3
Weight after bitumen treatment (g/m^2)		1200
Width (cm)	-	76
Pore size (O_{90}) micron	-	150
Mechanical Properties		
Strength (KN/m) Warp	-	20 (Min.)
Weft	-	20(Min.)
Elongation(%) Warp	-	5
Weft	-	10
Puncture Resistance (Kg/cm^2)		40
Hydraulic Properties		
Water permeability (L m^2/Sec.) at water column of 10 cm.		20

3.1 Further Trials

Directorate of Irrigation and Waterways, Govt. of West Bengal wanted to replace the conventional filter material for river bank protection work by geotextile due to the fact that quality filter material is not always available particularly in remote areas. They tried jute geotextile (filter) for protection of the banks of the Padma at Hasanpur, embankment of the river Phulahar at Ramayanpur as well as the banks of the river Hooghly at Barrackpore. Sundarban Development Board, Govt. of West Bengal has also used the material for protection of the approach road connecting a jetty constructed in a river subject to high tidal action in Patharpratima. The object of the trials was to compare its performance with that of conventional granular filter material. The above projects were completed in June'95, July'96, February '97 and August '96 respectively following the approved designs of the respective divisions. In these designs only the filter materials were replaced by Jute Geotextile (filter). The Civil Engineering Department of B.E. College tested soil of the sites and made necessary adjustment in the design for proper anchorage of the fabrics with overlapping. B.E. College is also monitoring the sites at regular intervals of time to assess the condition of the structures.

3.2 River Characteristics and Soil Composition of the Sites

3.2.1 Hasanpur

The Padma is a unidirectional river carrying about 30,000 cumec. of water during peak period July to October. From November water recedes and becomes stagnant during March to June. Right bank of the river at Hasanpur was subject to erosion. The bank was regraded to a slope of 2:1. The fabrics were anchored in a trench of 0.5m x 0.5m at the top and at the bottom it was anchored under a sausage of size 1 m x 3 m made of boulders of size 0.45m. A rip rap layer was placed on the fabric with two layers of boulders. The soil composition of the site is cited below.

Whitish grey sandy SILT (Sand - 30%, Silt-59% and Clay - 11%).

3.2.2 Ramayanpur

The river Phulahar becomes active from June to October, when it erodes its banks and sometimes causes flood. The embankment at Ramayanpur protects the villages and agricultural land nearby from the flood water. For protection of the embankment the project work was carried out to a stretch of 400 m, which is on a bend of the river and subject to erosion. The fabrics were anchored at the top in a trench of 0.5m x 0.5 m and at the bottom it was anchored under an apron of size 8m x1m made of boulders of size 0.45 m. Two layers of boulder were placed on the fabrics as rip-rap. Soil composition of the site is given below.

Sandy grey SILT with little clay (Sand - 29%, Silt - 63% and Clay - 8%). Standard Proctor Test, OMC(%) - 12.4 , γd Max (Mg/m^3) - 1.7

3.2.3 Barrackpore

The Hooghly is a tidal river. In August-September the tidal waves rise upto 3 m when the river is full of water. The site is a bathing place, which was damaged with the time. Bank length of 20 m was repaired using Jute Filter on the slope after repairing. Jute Filter was laid on the slope with proper anchorage at the top and bottom and cement mortar blocks of size 0.5m x 0.5m x 0.10m were placed on the filter fabric. The soil composition of the site is given below.

Grey clayey SILT (Sand - 4.5%, Silt - 82% and Clay - 13.5%). LL-30.5, PL-19.5; Bulk density (Mg/m^3) - 1.94, Water content (%) - 31, UC Strength (KN/m^2) - 0.66.

3.2.4 Patharpratima

A jetty was constructed in the river Matla in Sundarban for water transport for benefit of the people of the area. The river is a tidal one and the tidal actions are severe in the spring (August-September). For protection of the approach road to the jetty, on the slopes of the road Jute Filter was applied with proper anchoring and brick blocks of size 0.5 m x 0.5mx0.25m were placed on the fabrics. The soil composition of the site is highlighted below.

Grey clayey SILT with little sand (Sand - 0.4%, Silt - 78.6% and Clay - 21%) LL - 33.8, PL - 17.6, Standard Proctor Test, OMC(%) - 20.5, γd Max (Mg/m^3) - 1.7.

3.3 Inspection Results

Hasanpur - No subsidence on the rip-rap on Jute Filter, while subsidence upto 15 cm was observed at places of that on the conventional filter materials after the flood of '95

Ramayanpur - No damage was observed after the severe flood in October'96

Barrackpore - It has been completed recently and it is too early to comment on it.

Patharpratima - No sign of displacement of the blocks is visible after seven months of tidal actions on the slopes.

3.4 Discussion

In bank protection work normally 150 mm thick layer of ballast of size 10 mm to 15 mm is used as filter, which does not function properly on all types of soil particularly on silty soft soil, as observed in Hasanpur bank protection work, which developed subsidence of the rip-rap structure at places. One of the disadvantages of granular filter is - it is difficult to maintain uniform thickness of the ballast over the length and breath of the area under treatment, particularly when it is spread manually. Moreover, it is difficult to procure quality filter material in remote areas like Sunderban, where the Jetties constructed using available filter are damaged frequently under the tidal action of the rivers of the region.

The filter fabric is cheaper than the conventional filter material. Moreover, procurement and installation are very easy. Only care is to be taken during installation so that it is not ruptured. If it is damaged by chance, it may be repaired placing a piece of material on the damaged portion. It is a renewable resource and available in plenty. It is very cheap in comparison to synthetic geotextiles particularly in the third world countries.

After the above trials and realising the advantages, the Directorate has decided to apply the material commercially for bank protection work under their control and requisitioned materials for protection of both banks of a canal under Tista Barrage Project in Jalpaiguri to a stretch of 1.2 Km. The work will be completed by June, 1997. Further material for protection of bank of the river Mahananda is under negotiation.

Engineers sometimes expressed doubt about durability of the structures using Jute Geotextiles. In this context, it may be mentioned that the bank length of the Hooghly at Haldia treated in 1992 with Jute Geotextile is still in a good shape. It implies that though the strength of the fabric is not there the biomass which remains is acting as a filter or a natural filter has developed in the soil adjacent to the fabric and is working.

The fabric for separation and filtration has also been applied for construction of roads on soft soil by Kakinada Municipality in Andhra Pradesh in India. The site was a reclaimed area in the port of Kakinada, which is an important port in South India. The road was made for moving trucks carrying cargo materials to port godowns. In this application width was increased by stitching the fabrics side by side. Construction of the road was designed by Central Road Research Institute, Delhi.

After one year the condition of the road satisfied the authorities, who has decided to increase the road length using similar fabric.

4 CONCLUSION

Jute geotextiles are very cheap in comparison to synthetic geotextiles particularly in the third world countries and may find a big outlet. The jute producing countries may utilise their spare capacities of sacking product lines for the purpose with some modifications in machinery and structure of the fabrics to suit the requirements of geotextiles. Durability may be enhanced by chemical treatments in specific applications like bank protection work, road construction etc. While for protection of surface soil through establishment of vegetation, short durability is an advantage since the fabric becomes superfluous after growth of vegetation.

In India application of geotextiles is in an experimental stage and it is the right time to explore the ideas of application of Jute geotextiles to the practicing engineers in their respective fields. For the purpose, the Ministry of Textiles, Govt. of India and United Nations Development Programme (UNDP) have come forward to assist a project on development of Jute geotextiles for specific end uses under the leadership of the Indian Jute Mills Association. A number of Research and Development organizations and educational institutions are working in the project in their respective fields of expertise.

Object of geotextiles is to reduce cost of construction with good serviceability. In this context, Jute geotextiles have been found to be effective for protection of slopes, river bank protection, consolidation of silty sub-soil as well as roads on soft soil.

ACKNOWLEDGEMENTS

The authors are grateful to the Ministry of Textiles, Govt. of India and UNDP for funding the project activities. They are also grateful to the Indian Jute Mills Association, Calcutta for monitoring the project activities efficiently.

The authors acknowledge with thanks the co-operation extended by the engineers of Irrigation & Waterways Directorate, Forests Directorate, Sundarban Development Board, Govt. of West Bengal for application of Jute Geotextiles.

Thanks are also due to the managements of the jute mills, who supplied materials as per specification and helped during development of the products as well as chemical treatments.

Thanks are due to the colleagues of the authors, who helped the project work directly and indirectly and also to the Directors of the institutions for their permission to present the paper.

REFERENCES

Aziz, M.A. and Ramaswamy, S.D. (1991), "Properties of Jute Geotextiles for Civil Engineering Applications", *Text. Trends* Vol. 33 No. 12, PP. 29-40.

Barooah, A.K. and Borbarah, B.C.(1997),*Use of Biodegradable Jute Geotextiles for Integrated Soil & Crop management in Tea (Part I)- Soil Conservation progress Report for 1995 & 96,* Tea Research Association, Tocklai Experimental Station, Jorhat, Assam, India.

BIS (1996), *Bureau of Indian Standards Hand Book,* Testing Jute Fabrics for resistance to attack by micro-organism (2nd revision), Bureau of Indian Standards, New Delhi, India

Datta, U, Ghosh, S.N., Chatterjee, P.K., Krishnan, R.S. (1990), "Jute Geotextiles" , Proc. *National Seminar on Jute R&D*, Delhi, April, PP 144-150.

Kabir, M.H., Abedin, M.Z., Zakaria, M. and Saha, P. G. (1988), "Use of Jute Fabric as Soil Filter", Proc. *1st. Indian Geotextiles Conf.*, Bombay, Vol. 1, PP.G 15-23.

Rao, P.J., Bindumadhav, Babu, G.L.S., Pathak, D.N. and Shah, A. J. (1996), "Use of Jute Geotextiles as Separator in Pavements - A case study", Proc. *National Seminar on Jute based Geotextiles*, New Delhi, PP.14-24

Ramaswamy, S.D. and Aziz, M.A.(1984), "Jute fabric upon Coir grid matting for Stabilisation", Proc. *Int. Conf. on Road Development*, Paris, PP 775-779.

Rickson, R.J. and Loveday, A. D.(1996), "Technical Specification and Market Study of Potentially improtant Jute Geotextile Products", Presented in *IJO Jute-Geotextile Conf.*, Dhaka, Bengladesh, Sept.'96.

Sanyal, T. and Chakraborty, K.(1993), "Application of a Bitumenised Jute Textile in Bank Protection work in the Hooghly Estuary", *Geotextile & Geomembranes* Vol 13, PP 127-132.

Thomson, J. (1985), "Jute Holds ground", *Textile Horizons,* Sept., PP. 28-29.

ABRASION PROPERTIES OF GEOTEXTILES SUBJECT TO DYNAMIC LOADING

W.S.Alexander
Business Development Manager, Amoco Australia

ABSTRACT: In many civil engineering applications geotextiles are subjected to dynamic loadings. These applications include use as a filter fabric beneath rock beaching, (rip-rap), and particularly in marine or tidal applications, which are subject to storm events. Also, to a lesser extent, dynamic loadings occur in railway and logging haul road applications.
This paper reviews the performance of commonly used geotextiles in these applications by exhuming geotextiles from a range of projects after a number of years. A testing program was undertaken to compare properties of geotextiles. Simple testing of geotextiles was carried out in mechanical agitators as well as r actual marine environment. The properties of a range of geotextiles, spun-bond, heat-bonded, continuous filament and staple-fibre non-wovens were compared before and after testing to establish the relative abrasion resistance of different geotextiles subjected to dynamic loading.

KEY WORDS: abrasion, geotextiles, case study, dynamic mechanical analysis testing

1 INTRODUCTION

Abrasion resistance is not widely considered an important characteristic of geotextiles. The proof of this statement is borne out by the lack of any abrasion performance parameters in commonly used geotextile specifications around the world. In civil engineering applications for geotextiles such as sub-soil drainage, roadway separation and liner protection abrasion is a secondary consideration. There are, however, applications where abrasion resistance is important to the long-term performance of the geotextile. These applications include the use of geotextiles as filters behind rock revetments as well as, to a lesser extent, in dynamic loading situations such as in railway track applications (ref.1) and unsealed haul roads.

2 EXISTING ABRASION TESTS

The ASTM currently has one standardised abrasion test for geotextiles, D4886, "Standard Test Method for Abrasion Resistance of Geotextiles (Sand Paper/ Sliding Block Method)". This test is, however, not widely used for the reasons already stated that abrasion is not widely accepted as being important as well as the general view that these tests are very severe and not a fair reflection of the actual abrasion mechanism in a given engineering application. It is difficult to specify what level of abrasion resistance is appropriate, according to D4886, for a given situation. Australian geotextile standards do not address the issue of abrasion although Austroads (ref.2) describe abrasion as " significant where there is repeated loading such as below rip-rap in shore protection or during placement of the first lift on an embankment/pavement when construction equipment must operate on a thin layer "

In Germany the BAW rotating drum test has been used for some years to carry out abrasion testing of geotextiles. The author is not aware of further details of this test.

Two other standard textile abrasion tests, the Stolle and the Taber Abrasion test are, likewise, considered severe and inappropriate for testing geotextiles. Other abrasion tests have been put forward by Gray (ref.3) and Dine (ref.4), however these are not known to be widely used.

3 REVETMENT APPLICATIONS

Failures of geotextiles in revetment applications have been observed at La Canau, France 1985 and at Somers, Australia 1990. Storm events cause severe turbulent wave action, which has been shown to unravel and damage geotextiles. At Somers a non-woven, needle-punched, continuous-filament polyester geotextile failed after being subjected to wave action over only a few days. A replacement non-woven needle-punched, staple-fibre polyester geotextile was found to perform adequately when used in the same environment. Existing abrasion tests only consider the mechanical abrasion of geotextiles, caused by rock particles abrading the geotextile. Geotextiles should, ideally, be well secured by secondary armour rock however, in practice, when subjected to wave action there is some small movement of the geotextile. In some cases the geotextile will only be secured by large discrete rock units and relatively large movements of the geotextile between these rocks will occur. The structure of the geotextile must be adequate to prevent unravelling of the geotextile from this hydraulic loading as well as be resistant to mechanical abrasion caused by rubbing of the geotextile on rock.

4 HYDRAULIC TESTING

Because of the difficulties of field testing geotextiles subject to wave action in a foreshore environment a simple test was devised to replicate the effects of dynamic wave action on geotextiles.

Geotextiles tested were 3 different commercially available Australian geotextiles, which are commonly used in revetment works. Each geotextile was a non-woven (NW), needle-punched (NP) type. Fibre type was either staple-fibre (SF) or continuous-filament (CF) and polymer was either polypropylene (PP) or polyester (PET). Samples of geotextile were placed in a domestic washing machine and agitated for given periods of time. (See Fig 1) Each agitation cycle was 12 minutes long and samples were tested for 4 and 8 cycles. The samples were visually inspected and Mass, Grab Tensile Strength and Mullens Burst Pressure were measured before and after testing. The results are detailed in Tables 1 and 2, and Fig 2 below:

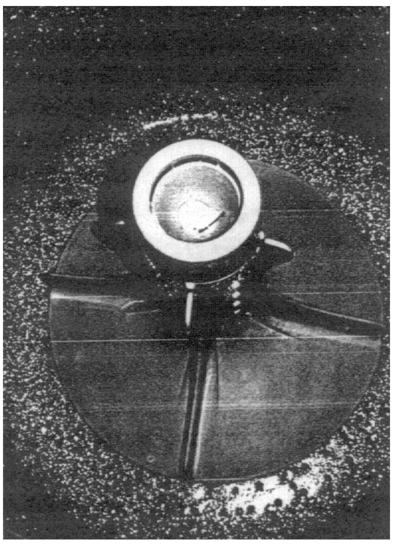

Fig 1. Photo of Washing Machine Agitator

Table 1. Sample description

A	NW, NP, SF, PP
B	NW, NP, SF, PET
C	NW, NP, CF, PET

Table 2. Test Results

	Mass (gsm)			Grab (N)			Mullens (kPa)		
	B*	4	8	B*	4	8	B*	4	8
A	275	275	275	872	829	829	3500	3400	3400
B	298	298	298	550	550	550	2425	2425	2425
C	265	255	255	1100	1100	890	3300	3300	3300

* Before

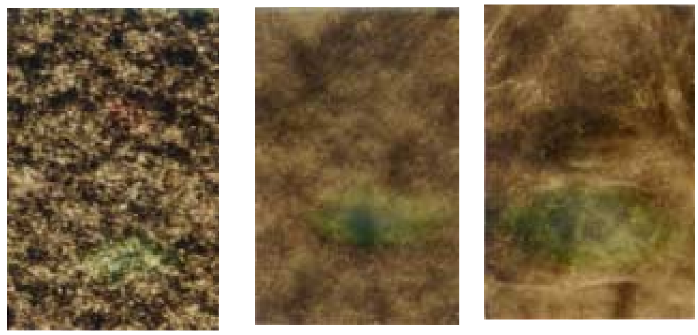

Sample A SampleB Sample C

Fig. 2 Visual appearance of samples after testing (8 cycles)

5 DISCUSSION OF RESULTS

From the above results it is clear that all geotextiles are subject to damage due to wave action, to varying degrees according to the type of structure of the geotextile. Visual inspection showed severe "fluffing" of samples B and C after 8 cycles (96 minutes in agitator). The structure of the geotextiles had begun to unravel. After 8 cycles sample C had virtually disintegrated. This appears to be due to sample C's lightly needled nature compared to the other more heavily needled staple-fibre fabrics. However, sample A showed little change in its visual appearance, even after 8 cycles, which may be explained by its tightly needled staple-fibre structure. The mechanical properties of each sample were affected to varying degrees. The mullens burst for each was largely unaffected. The grab tensile results for sample A showed a 5% reduction and for sample C showed a 20% reduction, which is a significant reduction and may indicate general strength reduction. Further mechanical strength testing of the sample is needed, such as wide strip tensile strength, trapezoidal tear strength and drop cone test, to determine if the mechanical properties are more broadly affected.

5.1 Limitations of Results

This test should be seen as a useful index test to compare performance of different types of geotextiles. It is also useful to give broad guidance as to a geotextile's suitability for use in this type of application. The severe damage to sample C in this test closely replicates the damage sustained to this fabric at the Somers site and so gives a fair reflection of the damage that may occur in revetment applications. Because of the difficulty of replicating actual field conditions, ie coastal marine environment subject to tidal action, in the laboratory, it is difficult to more accurately co-relate these results to field conditions and to standardise the test to set minimum acceptable performance limits. It is recognised that this testing regime is very severe and may not be appropriate to test abrasion of geotextiles in other applications such as roading or rail track. This test method only replicates turbulent wave action and does not take into account the mechanical abrasion of rock and soil particles rubbing against the geotextile. One improvement to the method would be to include rock particles in the agitator to help model field conditions more accurately. To this end testing has been conducted by others in Australia using a modified form of the LA Abrasion test, although the results have not been published. In this test, samples of fabric are fixed to the internal walls of a drum, which is filled with water and rocks. The drum is then rotated and the fabric samples are tested for the effects of water borne abrasion. The German BAW rotating drum test may also address this issue.

5.2 Recommendations

From this testing it would not be recommended to use geotextile C in revetment applications in marine applications due to the disintegration of the fabric's structure after 8 cycles in the test. The reduction in grab tensile may indicate a broad reduction in the strength properties of the geotextile.

5.3 Further Testing

Because of the limited nature of this project it is required to conduct further extensive testing to determine the reproduceability of the test method. Variables such as length of time of testing and addition of, and type of, rock samples need to be investigated.

6 CONCLUSIONS

The following conclusions were made based on this testing:

- abrasion is an important consideration in some engineering applications of geotextiles, such as revetment and rail track situations.
- abrasion is inadequately treated by current standard tests
- dynamic wave action causes stresses, other than mechanical abrasion, to occur in the geotextile
- a simple agitation test, using a domestic washing machine, was found to be a useful index test to compare performance of different geotextiles as well as to give broad assessment of suitability of geotextile for application
- field experience, together with agitator testing, show that some lightly needled continuous-filament non-wovens are not suitable for use in revetment applications in tidal environments
- The results of this testing together with field experience, indicate that staple-fibre non-woven geotextiles are most suitable for use in this application.

ACKNOWLEDGEMENTS

The writer would like to thank Mr. G. Byrne of Vantree Pty Ltd for his assistance.

REFERENCES

Raymond, G. (1982) "Geotextiles for Railroad Bed Rehabilitation" *Second International Conference on Geotextiles*, Las Vegas, USA. pp.479-484

AUSTROADS, (1990) *Guide to Geotextiles* pp.53

Gray, C.G. (1982) "Abrasion Resistance of Geotextile Fabrics" *Second International Conference on Geotextiles*, Las Vegas, USA. pp.817-821

Van Dine.D., Raymond, G. and Williams, S.E.(1982) "An Evaluation of Abrasion Tests for Geotextiles" *Second International Conference on Geotextiles*, Las Vegas, USA. pp. 811-816

STABILITY CRITERIA FOR GEOSYSTEMS - AN OVERVIEW -

Krystian W. Pilarczyk
Manager R&D, Rijkswaterstaat, Hydraulic Engineering Division, Delft, The Netherlands, Fax +31-15-2611361

Mark Klein Breteler
Project Manager, Delft Hydraulics, The Netherlands

Theo Stoutjesdijk
Project Manager, Delft Geotechnics, The Netherlands

ABSTRACT: Geotextile systems such as bags, mattresses, tubes and containers filled with sand or mortar can be a good and often cheaper alternative for more traditional materials/systems as rock, concrete units or asphalt. These new systems were applied successfully in a number of countries and they deserve to be applied on a larger scale. Because of low price and easy construction these systems can be a good alternative for coastal protection and coastal structures in developing countries. The main obstacle in their application is however the lack of proper design criteria.
An overview is presented on stability criteria of the existing geosystems and their limitations.

KEYWORDS: Geomattresses, Geobags, Geotubes, Design

1 INTRODUCTION

Various structures/systems can be of use in hydraulic and coastal engineering, from traditional rubble or concrete systems to more novel methods as geosystems and others. Within the scope of the research on the stability of rock and block revetments, much knowledge has been developed about the possible failure mechanisms and methodology on development of stability criteria under current and wave load (CUR/RWS, 1995a,b). Until recently, no or unsatisfactory design tools were available for a number of other (open) types of revetment and geosystems. This is why the design methodology for block revetments has recently been extended in applicability by means of a desk-study for a number of geosystems, such as sandbags and sand- and mortar-filled mattresses and tubes/containers. Also other stability aspects, such as soil-mechanical stability and residual strength were taken under consideration.

Geotextile systems utilize a high strength synthetic fabric as a form for casting large units by filling them by sand or mortar, or as curtains collecting sand. At this moment there is a relative large number of products of this type on the market provided by some specialistic companies all over the world. Mattresses are mainly applied as slope and bed protection. Bags are also suitable for slope protection and retaining walls or toe protection but the main application is construction of groins, perched beaches and offshore breakwaters. The tubes and containers are mainly applicable for construction of groins, perched beaches and offshore breakwaters. They can form an individual structure conforming functional requirements for the project or as a component of the main structure. In general, the sand-filled structure can be used as: temporary structures to learn the natural interactions/responses, permanent structures at locations with relatively low wave attack ($H < 1.5$m), or submerged structures where direct wave forces are reduced. The mortar-filled systems can resist much higher wave and current loading and, if necessary, can be interconnected by bars or by creating a special interlocking shape.
The main advantages of these systems in comparison with more traditional methods are: a reduction in work volume, a reduction in execution time, a reduction in cost, a use of local materials, a low-skilled labour requirement and possibility of using of locally available equipment.

This paper aims at giving a summary of the increased knowledge, especially that concerning the stability criteria for sand- and mortar-filled mattresses, bags and geotubes that have been made available.

2 STABILITY CRITERIA

2.1 Wave-load stability

There are two practical design methods available: the black-box model and the analytical model. In both cases, the final form of the design method can be presented as a critical relation of the load compared to strength, depending on the type of wave attack. For revetments, the basic form of this relation is:

$$\left(\frac{H_s}{\Delta D}\right)_{cr} = \frac{A}{\xi_{op}^{2/3}} \text{ with maximum } \left(\frac{H_s}{\Delta D}\right)_{cr} = 8.0 \quad (1)$$

In which: A = revetment (stability) factor (-), H_s = significant wave height (m), $\Delta = \rho_s/\rho_w-1$ = relative density (-), ρ_s = density of the protection material, ρ_w = density of water (kg/m^3), D = thickness of the top layer (m), and ξ_{op} = breaker parameter (-). For porous top layers, such as sand mattresses and gabions, the relative density of the top layer must be determined, including the water-filled pores:

$$\Delta_m = (1 - n) \cdot \Delta \quad (2)$$

In which: Δ_m = relative density including pores (-) and n = porosity of the top layer material (-).
The breaker parameter is defined as follows:

$$\xi_{op} = \frac{\tan\alpha}{\sqrt{H_s/L_{op}}} \quad (3)$$

In which: α = slope angle (°), $L_{op} = 1.56\ T_p^2$ = deep-water wavelength at the peak period (m), and T_p = wave period at the peak of the spectrum (s).

The advantage of this black-box design formula is its simplicity. The disadvantage, however, is that the value of A is known only very roughly for many types of structures.

The analytical model is based on the theory for placed stone revetments on a granular filter. In this calculation model, a large number of physical aspects are taken into account. In short, in the analytical model nearly all physical parameters that are relevant to the stability have been incorporated in the "leakage length" factor. The final result of the analytical model may, for that matter, again be presented as a relation such as Eq. 1 where A = f(Λ). For systems on a filter layer, the leakage length is given as:

$$\Lambda = \sqrt{\frac{b_f D k_f}{k'}} \quad (4)$$

with: Λ = leakage length (m), b_f = thickness of the filter layer (m), k_f = permeability of the filter or subsoil (m/s), and k' = permeability of the top layer (m/s).
With a system without a filter layer (a system placed directly on sand or clay) the permeability of the subsoil (eventually with gullies/surface channels) is filled in. For the thickness of the filter layer it is examined to which depth changes at the surface affect the subsoil. One can fill in 0.3 m for sand and 0.03 m for clay. The values for D and Δ depend on the type of revetment. When schematically representing a block on a geotextile on a gully on sand, the block should be regarded as the top layer and the combination of the geotextile and the small gully as the filter layer. The leakage length can be calculated using:

$$\Lambda = \sqrt{\frac{(k_f d_g + k_g T_g)D}{k'}} \quad (5)$$

with: k_f = permeability of the filter layer (gully) (m/s), d_g = gully depth (m), k_g = permeability of the geotextile (m/s), T_g = thickness of the geotextile (m), D = thickness of the top layer (m), and k' = permeability of the top layer (m/s).

To be able to apply the design method for placed stone revetments under wave load to other systems, the following items may be adapted:

- the revetment parameter A;
- the (representative) strength parameters Δ and D;
- the design wave height H_s;
- the (representative) leakage length Λ;
- the increase factor Γ on the strength.

Only suchlike adaptations are presented in this summarizing paper. The basic formulas of the analytical model are given in (CUR/ RWS, 1995a).

2.2 Flow-load stability

Severe flow attack may in practice occur on revetments, such as with flow over a steep slope and flow attack near many kinds of structures (downstream of sills, gates, discharge structures and the like). At these structures, the flow is often specifically determined by the geometry and the boundary conditions. With flow over a steep slope, such as on the downstream slope of a over-flow dam or dike, the situation is less ambiguous.

When the flow velocity is known well, or can be calculated reasonably accurately, Pilarczyk's relation (1990) is applicable:

$$\Delta D = 0.035\ \frac{\Phi}{\Psi}\ \frac{K_T K_h}{K_s}\ \frac{u_{cr}^2}{2g} \quad (6)$$

in which: Δ = relative density (-), D = characteristic dimension (m), g = acceleration of gravity (g=9.81 m/s^2), u_{cr} = critical vertically-averaged flow velocity (m/s),

Φ = stability parameter (-), Ψ = critical Shields parameter (-), K_T = turbulence factor (-), K_h = depth parameter (-), and K_s = slope parameter (-).

* The stability parameter Φ depends on the application. Some guide values are given below.

	Continuous toplayer	Edges and transitions
Riprap and placed blocks	1.0	1.5
Mattresses, gabions, and washed-in blocks	0.5	0.75

* With the critical Shields parameter Ψ the type of material can be taken into account. Some guide values are given below.

Revetment type:	Ψ (-)
riprap	0.035
loose, placed blocks	0.05
blockmats	0.07
gabions	0.07
sand and concrete mattresses	0.07

* The degree of turbulence can be taken into account with the turbulence factor K_T. Some guide values for K_T are given below.

Situation:	K_T (-)
Normal turbulence:	1.0
Increased turbulence (i.e. river bends)	1.5
Heavy turbulence (i.e. hydraulic jump)	2.0
Load due to water (screw) jet:	3.0 to 4.0

* With the depth parameter K_h, the water depth is taken into account, which is necessary to translate the depth-averaged flow velocity into the flow velocity just above the revetment. The depth parameter also depends on the measure of development of the flow profile and the roughness of the revetment. The recommended formulas can be found in (Pilarczyk, 1990, Klein Breteler, 1996). The following indicative values for the water depth h > 2 m are given below:

developed profile : $K_h = 0.2$
nondeveloped profile : $K_h = 0.4$

For shallow water and rough flow ($h/k_s<5$): $K_h = 1.0$;

h = water depth (m) and k_s = equivalent roughness according to Nikuradse (m); $k_s \approx 0.05$ m for mattresses.

* Slope parameter K_s. The stability of revetment elements also depends on the gradient under which the revetment is applied, in relation to the angle of internal friction of the revetment. This effect on the stability is taken into account with the slope parameter K_s, which is defined as follows:

$$K_s = \sqrt{1 - \left(\frac{\sin\alpha}{\sin\theta}\right)^2} \tag{7}$$

with: θ = angle of internal friction of the revetment material (°) (about 90° for concrete mattresses and 30 to 40°for sand-filled systems) and α = transversal slope of the bank (°).

With a downward flow along a steep slope it is difficult to determine or predict the flow velocity exactly, because the flow is very irregular (high turbulence, inclusion of air as a result of which the water level cannot be determined very well, etcetera). One is confronted with this when dimensioning the revetment of (the crest and) the inner slope of a dike in the case of flooding. In that case a design formula based on the discharge is preferable (Klein Breteler, 1996).

2.3 Soil-Mechanical Stability

The water movement on a revetment structures can also affect the subsoil, especially when this consists of sand. This effect is treated within the framework of the soil-mechanical aspects and can be of importance to the stability of the structure.

There are three aspects that will be discussed within the framework of soil-mechanical aspects:

- elastic storage;
- softening (liquefaction);
- drop in the water level.

These aspects and the accompanying damage mechanisms en design methods are discussed in detail below. Background information can be found CUR/RWS (1995a).

Elastic storage in the subsoil is connected with the permeability and stiffness of the grain skeleton and the compressibility of the pore water (the mixture of water and air in the pores of the grain skeleton). Because of these characteristics, wave pressures on the top layer are passed on delayed and damped to the subsoil of the revetment construction and to deeper layers (as seen perpendicular to the slope) of the subsoil.

This phenomenon takes place over a larger distance or depth as the grain skeleton and the pore water are stiffer. If the subsoil is soft or the pore water more compressible (because of the presence of small air bubbles) the compressibility of the system increases and large damping of the water pressures over a short distance may occur. Because of this, alternately water undertension and overtension may develop in the subsoil and corresponding to this an increasing and decreasing grain pressure.

Elastic storage can lead to the following damage mechanisms:

- lifting of the top layer;
- sliding of the top layer;
- sliding of the subsoil.

For the stability of the top layer, elastic storage could particularly be of importance if the top layer is placed directly on the subsoil without there being small gullies under the top layer and, if the permeability of the top layer is (locally) less than that of the subsoil. These conditions imply that the leakage-length approach according to the analytical model for the stability under wave load cannot be applied.

The stability of the subsoil may be jeopardized if, because of elastic storage, the grain tension decreases so strongly that insufficient sheer stress can be absorbed in the subsoil to prevent sliding. The design method with regard to the different damage mechanisms connected with elastic storage are presented in the form of design diagrams. In these diagrams the permissible wave height is plotted against the thickness of the top layer and the slope gradient. If the revetment construction consists of a top layer on a filter layer, the thickness of the filter layer may in these diagrams be partially or completely (depending on the type of revetment) added to the thickness of the top layer.

Also through cyclic generation of water tension, water overtensions may occur in the subsoil, but with impermeable top layers also directly under the top layer. In sand, these watertensions can be calculated using the MCYCLE program developed by Delft Geotechnics. As the top layer becomes more impermeable, the water tension manifests itself closer to the surface of the slope. In the case of a very permeable top layer this is exactly the opposite. Softening (liquefaction) can be defined as follows:
A cyclic variable load causes compaction to occur in a layer of sand. This leads to a decrease in the pore space. The water in the pores is subjected to pressure and will want to run off. At first, water overtension occurs. This causes a decrease in the contact pressure between the grains and with this the resistance to sliding. Finally, the water overtension might become so large that the contact pressure between the grains falls away completely. This is called softening or liquefaction.

The difference between liquefaction and elastic storage is that with liquefaction, water overtension is connected with a plastic deformation of a grain skeleton instead of an elastic deformation. Water overtension through softening occurs when the grain skeleton deforms plastically to a denser packing. From which follows that the dangers connected with liquefaction are smaller as the subsoil is compacted better during construction.

With regard to liquefaction, the following design rules are suggested for constructions with a reasonably compacted subsoil:

- With a top layer on sand there is no danger of liquefaction, if:
  - the slope gradient is gentler than or equal to 1:3,
  - the slope gradient is gentler than 1:2 and the wave height H_s is smaller than 2 m, or
  - the slope gradient is gentler than 1:2 and the subsoil is well-compacted.
- With a top layer on clay there is no danger of liquefaction.
- With a top layer on a granular filter there is generally no danger of liquefaction.

In these design rules hardly any distinction is made between types of revetment.

Through a drop in the water level a difference in the rise over the top layer may occur. A drop in the water level may occur as a result of tide or a ship passing through a waterway or canal. As with packed stone revetments, this is only a problem if any possible filter layer and the top layer are sanded up and because of this obtain a low permeability.

No calculations need to be made on this phenomenon if applies:

$$\frac{\Lambda \sin\alpha}{2} \leq \Delta D \cos\alpha \tag{8}$$

in which: Λ = leakage length (m), α = slope angle (°), Δ = (representative) relative density of the top layer (-), D = (representative) thickness of the top layer (m).

3 TYPES OF STRUCTURES

3.1 Concrete Mattresses

Characteristic of concrete mattresses are the two geotextiles with concrete or cement between them. The geotextiles can be connected to each other in many patterns, which results in each mattress system having its own appearance and properties. An example is given in Figure 1.

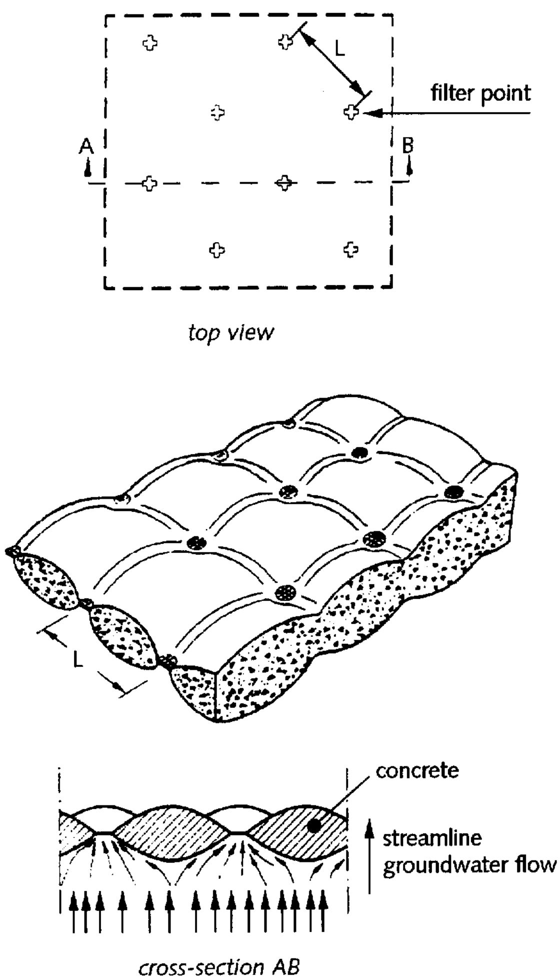

Figure 1 Example of concrete mattress

The permeability of the mattress is one of the factors that determine the stability. It is found that the permeability given by the suppliers is often the permeability of the geotextile, or of the so-called Filter Points. In both cases, the permeability of the whole mattress is much smaller.
A high permeability of the mattress ensures that any possible pressure build-up under the mattress can flow away, as a result of which the differential pressures across the mattress remain smaller. The stability is therefore the largest with a large mattress permeability. In the long term, however, pollution of the Filter Points or the clogging of the geotextile can cause a decrease in the permeability.

3.1.1 Design rules with regard to wave load

In the design rules for concrete mattresses with regard to wave load the calculation of the leakage length is adapted. This consideration, which is closely related to a consideration in accordance with the analytical model, results in a design formula in the form of the black-box formula.

During wave attack, the mattress will be exposed to a differential pressure which is directed upwards, as also is the case with packed stone revetments. This takes place the moment the wave has drawn back, just before the wave impact. Just as with packed stone revetments, the leakage length for this differential pressure is the most important construction-descriptive parameter. The leakage length (Λ) can be calculated using Eqs. 4 or 5. The values of the leakage length may vary from about 0.5 to 10 m depending on the type (permeability) of the mattress, the permeability and thickness of the filter, and the presence of cavities under the mattress.

The failure mechanism of the concrete mattress is probably as follows:

- First, cavities under the mattress will form as a result of uneven subsidence of the subsoil. The mattress is rigid and spans the cavities.
- With large spans, wave impacts may cause the concrete to crack and the spans to collapse. This results in a mattress consisting of concrete slabs which are coupled by means of the geotextile.
- With sufficiently high waves, an upward pressure difference over the mattress will occur during wave run-down, which lifts the mattress.
- The pumping action of these movements will cause the subsoil to migrate, as a result of which an S-profile will form and the revetment will collapse completely.

The value of stability factor A in the design formula of the black-box model (Eq. 1) depends on the leakage length and the subsoil: A = 2 to 4. A permeable mattress on sand has a medium-sized or small leakage length and then the value of A is 3 to 4. A low-permeable mattress on a filter has a large leakage length and therefore an A-value of 2 to 3 (Figure 2). For the determination of the leakage length, one is referred to the analytical model.

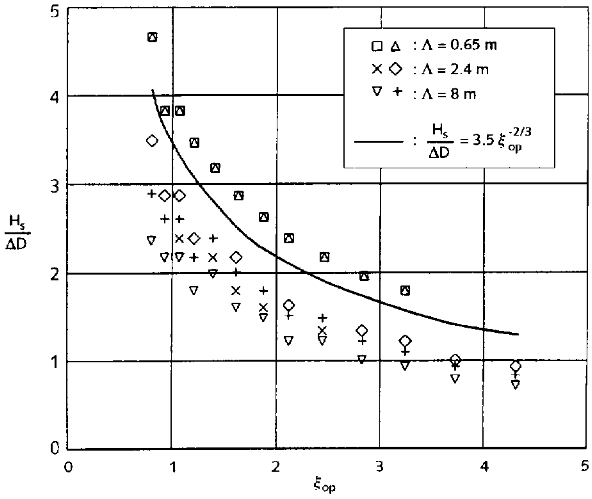

Figure 2 Calculation results for concrete mattresses

The representative relative density Δ follows from the standard definition. For the representative thickness D, the average thickness should be filled in.

It can be concluded that, compared to the available data in literature, the derived stability relations give a safe estimation of the stability. Because the relations have not been verified sufficiently yet, it is not recommended to decrease the existing safety.

In the long run, the permeability of the top layer may diminish as a result of accretion and silting-up. This will have a negative effect on the stability, especially with systems with a leakage length smaller than approximately 2 m. If the leakage length is larger than 2 m, the effect of the permeability of the top layer on the stability is rather small.

3.1.2 Design rules with regard to flow load

A number of characteristic values for the critical flow velocity for concrete mattresses is given below.

Thickness	on slope	on bottom
50 mm	2.7 m/s	3.3 m/s
100 mm	3.9 m/s	4.7 m/s
200 mm	5.5 m/s	6.4 m/s

For the application of the design formula (Eq. 6), guide values for the constants are given in Section 2.2. For the representative thickness D, one should fill in the average thickness of the top layer.

3.1.3 Design rules with regard to soil-mechanical stability

The flow through a concrete mattress is concentrated in the Filter Points. The permeability of the systems filled with concrete lies approximately between $1 \cdot 10^{-4}$ and $5 \cdot 10^{-3}$ m/s. A concrete mattress is less flexible than a sand mattress and does not connect to the subsoil as well as a sand mattress. In contrast with sand mattresses, it is assumed that only the sliding of the whole mattress can occur and not just part of it.

* Elastic storage

With regard to elastic storage, the following design example for a wave height H = 1 m and a slope 1 on 3 is given. The required thickness of the mattress on sand for various failure mechanisms and wave steepnees (S_{op}) is equal to:

Failure type	S_{op} = 0.03	S_{op} = 0.05
Lifting of toplayer	0.35 m	0.25 m
Partial sliding toplayer	0.80 m	0.60 m
Sliding of toplayer	0.30 m	0.25 m
Sliding of subsoil	0.55 m	0.40 m

Concrete mattresses are mostly stiff and anchored at the top. Therefore, not the sliding and/or uplifting of the toplayer but the sliding of the subsoil is the most dangerous (for H = 1m, the required thickness is 0.55m).

If the systems are placed on a filter, one can take into account an increase in the stability with regard to elastic storage. For the total thickness of a concrete mattress on a filter, $D + b/\Delta_t$ can be filled in, where b is the thickness of the filter.

* Liquefaction

The design rules with regard to liquefaction do not differ from those presented in Section 2.3.

3.2 Sand Mattresses

A sand mattress consists of two geotextiles attached onto each other, between which sand is interposed. This way, a mattress is formed of sausages lying next to each other which run from the top to the bottom of the slope and which are interconnected. The lower geotextile is usually flat and the upper geotextile lies on top of it, in arches.

* Construction/design/repair

The edges and connections of sand mattresses are vulnerable and must therefore be finished carefully. Mattresses lying next to each other can be sown together and the ends can be secured with for example ground anchors.

In actual practice, mattresses are not only threatened by the hydraulic load. The possibility of vandalism occurring, limits sand mattresses to being applied in places where unauthorized persons do not have access to. The system is also vulnerable to collision, (drifting) ice, floating bulky refuse, sunlight and chemical degradation.

* Stability

Sand mattresses cannot be used when the significant wave height H_s is larger than 1.0 m (max. 1.5 m in case of properly compacted subsoil). Unfortunately, not much research has been conducted into the stability of sand mattresses. Besides Pilarczyk's design formula (1990), a small-scale model investigation, a desk study and a prototype experiment have been found. Based on these, the following value for A in the design formula (Eq. 1) is recommended according to the black-box model: A = 4 to 5. In this formula the relative density including pores Δ_m should be filled in for the representative relative density. For the representative thickness D of the mattress, the average thickness should be filled in:

$$100\%\ \text{filled} \quad : \quad \frac{D}{D_d} = 0.7 \text{ to } 0.8$$

$$90\%\ \text{filled} \quad : \quad \frac{D}{D_d} = 0.6 \text{ to } 0.7$$

with: D = average thickness of the mattress (m) and D_d = maximum diameter of the sausages (m).

Above a flow velocity of 1.5 m/s (max. 2 m/s), the sand in the mattresses is no longer internally stable. The design formula on stability against currents is given in section 2.2.

A sand mattress is relatively flexible and connects closely to the subsoil. The geotechnical design criteria are similar to those for the concrete mattresses.

3.3 Geobags and geotubes

Geobags or tubes can be filled with sand, gravel or concrete. The bags may have different shapes and sizes, varying from the well-known sandbags for emergency dikes to large flat shapes or elongated "sausages" (see Figure 3). The most common use for sandbags in hydraulic engineering is for temporary structures. The reasons why sandbags are not or hardly used for permanent structures are as follows:

- the resistance against flow load and wave load is relatively small;
- because the geosystems are prone to vandalism and the effect of sunlight, for example, the durability is relatively small;
- good design formulas are lacking;
- a construction made of sandbags looks ugly.

Major advantages of sandbags as construction material are the low costs and the simple processing. Uses for sand- or cement-filled bags are, among other things:

- revetments of relatively gentle slopes;
- temporary toe constructions in places where in due course vegetation should develop;
- (temporary) training walls/groins;
- temporary or permanent offshore breakwaters;
- temporary dikes surrounding dredged material containment areas.

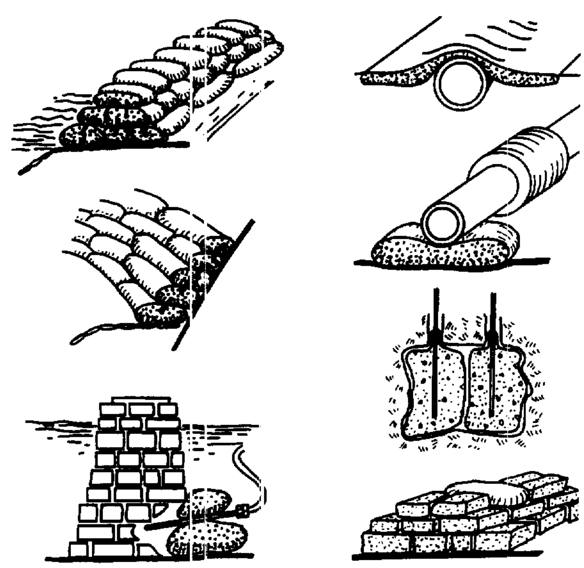

Figure 3 Application of geobags and containers

Because sand is easy to use and cheap, it is extremely suitable for temporary structures. Above a flow velocity of 1.5 to 2 m/s, the sandbags cannot be used for permanent applications because the sand is no longer internally stable.

Sandbags can be placed as follows:

1. *As a blanket*: One or two layers of bags placed directly on the slope. An "interlocking" problem arises if the bags are filled completely. The bags are then too round. A solution is not to fill the bags completely, so that the sides flatten out somewhat, as a result of which the contact area becomes larger.
2. *As a stack*: Bags stacked up in the shape of a pyramid. The bags lie half overlapping with the long side parallel to the shoreline.

When installing geosystems, one should see to it that this does not take place on a rough foundation. Sharp elements may easily damage the casing of the element. Geosystems must not be filled completely. With a fill ratio of approximately 75% an optimum stability of the elements is reached. A sound soil protection is necessary if gravel (sand) sausages are used in circumstances where they are under attack of flow or waves.

Background information on geobags can be found in Pilarczyk (1995) and Wouters (1995).

New developments concern the large hydraulically filled geotubes and hydraulically or mechanically filled geocontainers (in combination with a split barge). Information on these systems can be found in Leshchinsky (1995), Pilarczyk (1996,1997) and Den Adel et al (1996).

3.3.1 Design rules with regard to wave load

The stability relation of sand, gravel or cement bags which are used as protection elements on a slope appears to deviate somewhat from the formula according to the black-box model. For regular waves the recommended formula is as follows:

$$\left(\frac{H}{\Delta D}\right)_{cr} = \frac{3.5}{\sqrt{\xi_o}} \tag{9}$$

In which Δ is the relative density if the pores are completely filled with water (Δ_m). The representative thickness D is the average thickness of the top layer, measured perpendicularly to the slope.

If this stability relation is combined with the relation found between H_s and H, (significant wave height with irregular waves and the wave height with regular waves) this results in the following stability relation:

$$\left(\frac{H_s}{\Delta D}\right)_{cr} = \frac{2.5}{\sqrt{\xi_{op}}} \tag{10}$$

For concrete sausages (tubes) used as a protection element on the crest of a low or underwater breakwater, it is found that the following stability relation for regular waves can be used:

$$\left(\frac{H}{\Delta b}\right)_{cr} = 3.2\left(\frac{H}{L_0}\right)^{1/3} \tag{11}$$

In which b is the width of the sausage. Should two sausages be connected, the widths of both sausages together can be filled in for b.

If the sausage is placed with its longitudinal direction perpendicularly to the axis of the breakwater, the following stability relation applies:

$$\left(\frac{H}{\Delta l}\right)_{cr} = 1.0 \tag{12}$$

In which l is the length of the sausage.

3.3.2 Other design rules

Stability against current should be treated according to the rules given in Section 2.2.
The soil-mechanical stability should be treated according to the criteria mentioned in Section 2.3.

4 CONCLUSIONS

The geotextile systems can be a good and mostly cheaper alternative for more traditional materials/systems. These new systems deserve to be applied on a larger scale.
Information presented on the stability criteria will be of help in preparing the preliminary alternative designs with geosystems. However, there are still many uncertainties in the existing design methods. Therefore, further improvement of design methods and more practical experience at various loading conditions is still needed.

REFERENCES:

CUR/RWS, 1995a. Design Manual for Pitched Slope Protection. CUR report 155. A.A. Balkema.

CUR/RWS, 1995b. Manual on the use of rock in hydraulic engineering. CUR report 169. A.A. Balkema.

Den Adel, H., Hendrikse C.H., and Pilarczyk, K.W., 1996, Design and application of geotubes and geocontainers, Proceedings of the 1st European Geosynthetics Conference (EuroGeo), Maastricht.

Klein Breteler, M., 1996, Alternative open slope revetments, in Dutch), Delft Hydraulics, H1930.

Leshchinsky, Dov, and Leshchinsky, Ora, 1995, Geosynthetic Confined Pressurized Slurry (GeoCops): Supplement Notes for Version 1.0, May 1995 (Copyright Nicolon US and US Army Corps of Engineers).

Pilarczyk, K.W. (ed.), 1990. Design of seawalls and dikes - including overview of revetments, in: Coastal Protection, A.A. Balkema (Publisher).

Pilarczyk, K.W., 1995, Novel systems in coastal engineering; geotextile systems and other methods, Rijkswaterstaat, Delft.

Pilarczyk, K.W., 1996, Geosystems in hydraulic and coastal engineering - An overview, Proceedings of the 1st European Geosynthetics Conference (EuroGeo), Maastricht, A.A. Balkema (Publisher).

Pilarczyk, K.W., 1997, Application and design aspects of geocontainers, *Geosynthetics '97*, Long Beach, CA.

Pilarczyk, K.W. and Zeidler, R.B., 1996, Offshore breakwaters and shore evolution control, A.A. Balkema Publisher, Rotterdam.

Stoutjesdijk, T., 1996, Geotechnical aspects of alternative systems (in Dutch), Delft Geotechnics, H1930.

Wouters, J., 1995, Stabiliteit van geosystemen (Stability of geosystems, in Dutch), Delft Hydraulics, H1930.

Evaluation of Geosynthetic Fabric Containers to Contain Contaminated Dredged Sediment

Horace Moo-Young
Department of Civil and Environmental Engineering, Lehigh University, Bethlehem, PA, USA

Tommy Meyers
Environmental Engineering Division, Waterways Experiments Station, Vicksburg, MS, USA

Dan Townsend
Department of Civil Engineering, Louisiana State University, Baton Rouge, LA, USA

ABSTRACT: Recent changes in environmental regulations to protect the water column have prohibited the open water disposal of dredged sediment from the New York Harbor. As a result, the New York Harbor will lose about a foot of depth each year if the contaminated sediments are not dredged. Because of the restrictions and perceived political problems with dredging and open water disposal of the contaminated materials, the New York Port Authority investigated the use of geosynthetic fabric containers (GFC) to reduce the movement of contaminated sediments outside of the boundary of the disposal site and to decrease the impact of the sediment on the water column. This laboratory study investigates the migration of fines and contaminants through GFCs. Contaminated sediment was characterized for the physical and chemical properties. Laboratory filtration tests were conducted on the contaminated sediment and GFC configurations to determine the amount of total suspended solids that would be released to the water column.

KEYWORDS: Geotextiles, Filtration, Hazardous Containment, Apparent Opening Size

1 INTRODUCTION

The New York Harbor is a major industrial port on the East Coast of the U.S. where 4,500 ships carry $60 billion per year worth of goods. River borne silts are sifting into the harbor's shipping channels and reduce the depth of the harbor. New York and New Jersey Port Authority continuously dredges to maintain channel depths for cargo ships and tankers. From 1990 to 1994, the average amount of dredged material was approximately 4.3 million cubic yards (5.6 million m^3). Dredged material was disposed in the Atlantic Ocean, a few miles east of the Jersey Shore at the New York Bight Dredged Material Disposal Site. Recent changes in environmental regulations have restricted open water disposal of the sediment due to contamination. These restrictions on dredging have decreased the average amount of sediment dredged by 70% to 1.3 million cubic yards (1.7 million m^3) in 1996. As a result, the New York Harbor will lose about a foot of depth each year if contaminated sediments are not dredged. Decreases in the harbor depth will have a severe impact, as larger cargo ships will dock at deeper ports.

Containing the contaminated sediment in a geosynthetic fabric container (GFC) for placement from split hull barges is one alternative that can reduce the movement of contaminated sediments outside the boundary of the disposal site and decrease the impact on the water column. After placement of the sediment, the opening of the GFC is closed, transported to an aquatic disposal site where it is then released from the barge. When properly constructed, GFCs have performed well as hydraulic and geotechnical structures. Numerous projects have shown the beneficial uses of GFCs for dikes in shallow and deep-water energy (Fowler and Sprague, 1994; Risco, 1995).

This paper reports the findings on a laboratory study of the GFC performance with respect to the migration of fines and contaminants. In this study, laboratory filtration tests were conducted to provide information on the release of fines through GFCs.

2 MATERIALS

2.1 Dredged Sediment

Sediment (Category III by U.S. Army Corps of Engineers, New York District (CENAN) classification) from New York Harbor was used in this study. The sediment was mixed in a 250-gallon (1 m^3) tank for three hours. Samples of the mixed sediment were collected for geotechnical and chemical analysis.

Three samples of the contaminated dredged sediment were analyzed for polycyclic aromatic hydrocarbons (PAHs), NH_4, Total Organic Carbon, Arsenic, Cadmium, Chromium, Copper, Iron, Manganese, Lead, Mercury and Zinc. Table 1 summarizes the standard procedures, detection limits, and chemical analysis on the sediment.

According to American Society for Testing and Materials (ASTM) designation D-2487, the sediment classifies as a sandy clay (CH). The initial water content (ASTM procedure D-2974) of the sediment was 207%, and the specific gravity (ASTM procedure D-854) of the sediment was 2.57. Consolidation tests were performed on sediment according to ASTM procedure D-2435 method A, and test results showed that the sediment was highly compressible with a compression index of 1.2.

2.2 Geosynthetics

A geosynthetic fabric container (GFC) is constructed by sewing one or more layers of geotextiles together to form a container that will support and contain a measured amount of saturated material. A woven polyester geotextile (fabric A) was used as the strength layer in the GFC. Four polypropylene nonwoven needle punched geotextiles were tested as potential filter layers for the GFC: fabric B (4 ounce/yd^2), fabric C (8 ounce/yd^2), fabric D (12 ounce/yd^2) and fabric E (16 ounce/yd^2). Physical and hydraulic properties of the geotextiles were determined using ASTM procedures and are shown in Table 2. Geotextiles in this study meet the recommended soil retention criteria which requires the apparent opening size (AOS) to be less than two to three times the soil particle size for which 85% of the total soil is finer (AOS < 2 or 3 d_{85} where d_{85} = 0.185 mm).

Table 1 Chemical analysis of sediment

Chemical	Procedure	Detection Limits sediment mg/kg	Average mg/kg
NH_4	EPA-600-350.1 EPA-CRL #324	N/A	198
TOC	SM-5310 EPA-CE-81-1	1	53,000
Chromium	SW-846-7191	0.1	182
Copper	SW-846-7211	0.1	641
Iron	SW-846-6010	1.5	35400
Manganese	SW-846-6010	0.5	330
Mercury	SW-846-7471	0.2	2.05
Lead	SW-846-7421	0.1	429
Arsenic	SW-846-7060	0.5	20.3
Cadmium	SW-846-7131	0.01	12.4
Zinc	SW-846-6010	0.7	931
PAH	N/A	N/A	90.84

3 METHODS

3.1 Pressure Filtration Test

Bench top filtration tests were conducted to obtain information on the release of fines from geosynthetic fabrics of varying AOS. The filtration procedure described in this method simulates the migration of fines through a GFC. A vacuum pressure is applied to a filter media to separate liquids from solids. During a dredging operation, cake formation occurs after the GFC is filled with the sediment and is caused by self-weight consolidation. Cake formation also occurs after placement of the GFC in the disposal facility and is caused by consolidation under a hydrostatic pressure.

3.2 Apparatus

A Millipore Hazardous Waste Filtration System was used to conduct the pressure filtration tests, and this pressure filtration device is also used for the Toxicity Characteristic Leaching Procedure (TCLP) in hazardous waste testing (U.S. Environmental Protection Agency (EPA), 1982). The geosynthetic fabric was placed on a filter holder that was able to withstand pressures up to 100 psi (690 kPa). Five GFC configurations were tested: A, A + B, A + C, A + D, and A + E.

Three filtration tests were conducted on each fabric configuration at applied pressures of 5 psi (34.5 kPa) and 10 psi (69 kPa). Pressure was applied to the inlet of the filtration device using a compressed nitrogen cylinder. A relief valve on top of the chamber was used to adjust the pressure. A 250 ml graduated cylinder was used to measure the volume of filtrate.

Table 2. Geotextile properties

Fabric Properties	Units	A	B	C	D	E
Thickness	mm	NP	1.8	2.7	3.7	4.7
	(mils)		70	105	145	185
Mass per unit area	g/m^2	339	136	271	406	542
Permittivity	sec-1	NP	2.0	1.26	0.75	0.571
Apparent Opening Size	mm	0.25	0.21	0.21	0.15	0.15
	(US Sieve)	60	70	70	100	100

Note: NP-Not provided by manufacturer

3.3 Procedure

The geosynthetic fabric and filter chamber were initially weighed. The filter was then washed with deionized water, allowed to drip dry, and placed on the filter holder. The lower portion of the filtration apparatus was assembled, and to reduce the potential for migration of fines at the edges, the filter fabric slightly overlapped the filter holder. Approximately 500 grams of the sediment was weighed and placed into the filtration device, whereby the slurry was allowed to settle before running the test. The top plate was placed on top of the chamber and sealed. Silicone grease was used to reduce the loss of pressure between the chamber and the upper and lower plates. Pressure from the nitrogen cylinder was gradually applied on top of the sample, until the desired pressure was achieved. The volume of the filtrate was measured using a 250-ml beaker and recorded with respect to time. Tests were conducted until the pressure began to decrease, and no more filtrate passed through the filter. When consolidation of the sediment at the applied pressure was completed, the filter cake ruptured which caused a decrease in the applied pressure.

Total suspended solids (TSS) tests were conducted on the filtrate in the graduate cylinder using the Standard Method for Water and Wastewater procedure at 209F. The filtration apparatus was disassembled, and the filtered cake was weighed. The final water content of the filtered cake was obtained using ASTM procedure D-2216. Thirty filtration tests were conducted on the contaminated sediment from the New York Harbor; three replications were conducted for the five fabric configurations at filtration pressures of 5 (34.5 kPa) and 10 psi (69 kPa).

4 RESULTS

Initial and final TSS data indicate that there is low migration of the fines through the various filter configurations. Table 3 shows the filtration test results for tests conducted at 5 psi (34.5 kPa). The filtering efficiency was determined by comparing the final TSS of the filtrate to the initial TSS of the contaminated sediment as shown in equation 1 (Henry and Hunnewell, 1995; Christopher and Holtz, 1985).

$$FE = \frac{TSSinitial - TSSfinal}{TSSinitial} X\ 100 \qquad (1)$$

where FE = Filtering Efficiency, %
$TSS_{initial}$ = intial TSS, mg/l
TSS_{final} = final TSS, mg/l

For the filtration tests conducted on the various fabric configurations, the initial water content ranged from 180-200%. The fabric configurations reduced the TSS migrating to the water column by an average factor of 1000. In all tests, the water flow through the fabric and sediment slowed with time. Initial and final TSS data indicate that there is low migration of the fines through the various filter configurations.

Figure 1 plots the TSS and fabric weight relationships for the filtration tests conducted at 5 psi (34.5 psi) with a minimum TSS concentration occurring at fabric D. Fabric E showed a sharp increase in TSS compared to fabric D. The TSS and fabric weight relationship at 10 psi (69 kPa) has a minimum TSS occurring at fabric D. These data indicate that fabric D has the lowest TSS concentration passing through the material.

Figure 2 plots the apparent opening size and total suspended solids relationship for tests conducted at 5 psi (34.5 kPa) and 10 psi (69 kPa). As the apparent opening size decreases, the total suspended solids concentration decreases.

5 SUMMARY AND CONCLUSION

The feasibility of using GFCs to contain contaminated sediment from the New York Harbor was studied. Laboratory filtration tests were conducted to determine the flow rate of suspended solids through a GFC system. Filtration testing provided an index test to determine the migration of fines through the fabrics. From these tests, it was shown that GFCs provide adequate filtration for dredge sediment. Utilizing the GFCs to contain contaminated dredged sediment will reduce the migration of fines in an open water disposal facility.

Table 3 Filtration test data at 5 psi (34.5 kPa)

Fabric Tested	Final Water Content (%)	Initial TSS (g/l)	Final TSS (mg/l)	Average Flow (ml/min)	TSS Filtering Efficiency (%)
A	121	433.3	64.3	0.78	99.98
A + B	132.6	425.8	44.3	0.73	99.99
A + C	126	438.9	33.9	0.69	99.99
A + D	121	442.9	28.5	.68	99.99
A + E	112.7	448	68.4	0.87	99.98

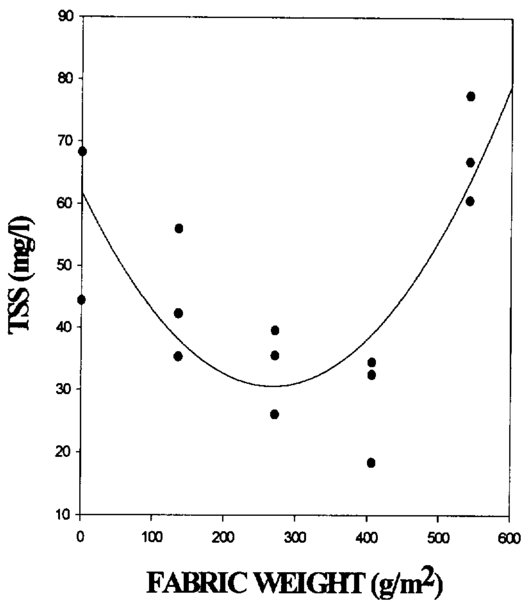

Figure 1. TSS and fabric weight relationship for filtration test at 5 psi (34.5 kPa).

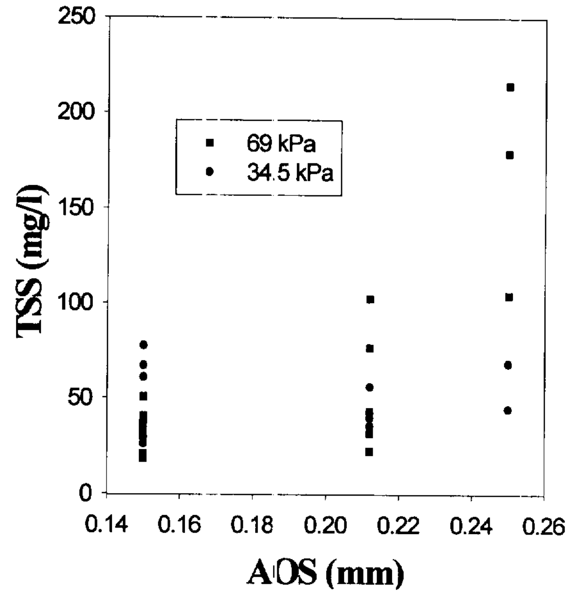

Figure 2. Relationship between TSS and AOS for filtration tests at 5 (34.5 kPa) and 10 (69 kPa) psi.

ACKNOWLEDGEMENT

The Nicolon Corporation in Norcross, Georgia provided the geosynthetic fabrics for fine migration analysis. The authors would also like to thank the New York and New Jersey Port Authority for their support on the project.

REFERENCES

Christopher, B.R. and Holtz, R.D. (1985). "Geotextile Engineering Manual", FHWA-TS-86-203. Washington, D.C., Federal Highway Adminstration.

Fowler, J., Sprague, C.J., and Toups, D. (1994). "Dredged material-Filled Geotextile Containers, *Environmental Effects of Dredging Technical Notes*, U.S. Army Waterways Experiments Station, Vicksburg, MS.

Henry, K.S. and Hunnewell, S.T. (1995). "Silt Fence Testing for Eagle River Flats Dredging", *Cold Regions Research and Engineering Laboratory, Report 95-27*. Hanover, NH.

Risko, A.J. (1995). "Memorandum for the Record, FY 95 Marina Del Ray Detailed Project Summary," *U.S. Army Engineer District*, Los Angeles, Los Angeles, CA.

U.S. Environmental Protection Agency. (1982). "Test Methods for Evaluating Solid Waste," SW-846, 2nd ed., Office of Solid Waste and Emergency Response, Washington, D.C.

Infrared Thermography of Damage in Geosynthetics

M.P. Luong
Professor, CNRS-LMS, Ecole Polytechnique, F-91128 Palaiseau, France

M. Khay
Civil Engineer, CETE Centre d'Expérimentation Routière, F-76121 Grand Quevilly, France

ABSTRACT: This paper aims to illustrate the use of quantitative infrared thermography as a nondestructive, noncontact, and real-time technique to detect the intrinsic dissipation that depicts the physical processes of damage and the mechanisms of geosynthetics failure. The parameter investigated in this experimental work is heat generation due to the energy dissipated by geosynthetics subject to tensile loading, up to failure. This experimental technique subsequently proposes a durability threshold, a loading limit beyond which geosynthetics fail.

KEYWORDS: Failure, Laboratory Tests, Materials Tests, Mechanical Properties, Tensile Strength.

1 INTRODUCTION

The use of geosynthetics in geotechnical engineering has been steadily increasing these last decades. It was initiated primarily by the manufacturers who sensed the need, developed, and marketed the products. The range of applications of geotextiles (Giroud 1980) is enormous: (i) filtration, drainage, earth dams, canals, coastal works, bank and shore protection, and in erosion prevention and control systems; (ii) stabilization of landslides, parking lots, paved and unpaved roads, roadways, and railroads on soft subgrades; and (iii) reinforcement of retaining structures, earth and waste slopes, and embankments. Geosynthetics (geotextiles, geogrids and geomembranes) can also be used together in a geocomposite system to provide multiple functions. Common applications of geocomposites are in hazardous waste containment systems and as prefabricated drainage layers. With the rapid recent growth in the use of these materials, civil engineers often have difficulty obtaining reliable mechanical characteristics for design, specifications, and construction with geosynthetics.

This paper emphasizes the application of infrared thermography to detect the occurrence of damage and to examine the mechanism and process of geosynthetics failure. Subsequently it proposes a limit of dissipative stability, defined as a drastic change in the rate of intrinsic dissipation.

2 THERMOGRAPHY BACKGROUND

Damage theories rely on assumed discontinuous phenomena at the microscopic scale. At the macroscopic scale, damage parameters, considered as internal variables, are introduced according to the following main approaches: i) effective stress introducing a scalar continuous variable; ii) plasticity formalism suggesting phenomenological constitutive models that are widely used in engineering applications; and iii) micromechanics using micro- and macroscale relationships

Understanding damage requires making a clear distinction between the physical damage, the process of damage, and the manifestation of damage. This experimental work is based on the assumption that intrinsic dissipation and damage present the same evolution under loading up to failure as they occur in traditional strength tests.

The development of the thermo-visco-elastic-plasticity equations requires three types of basic assumptions (Dillon 1963, Kratochvil & Dillon 1969), leading to the following coupled thermomechanical equation:

$$\rho\, C_v \dot{T} = K\nabla^2 T - (\beta : \overset{4}{D} : \dot{E}^e)T + S : \dot{E}^I + r_0$$

where $\overset{4}{D}$ denotes the fourth-order elasticity tensor,
C_v ($J.kg^{-1}.K^{-1}$: Joule per kilogram per degree Kelvin) the specific heat at constant deformation and
K ($W.m^{-1}.K^{-1}$: Watt per metre per degree Kelvin) the thermal conductivity.

This equation shows the potential applications of the infrared scanning technique in diverse engineering domains (detection of fluid leakages, nondestructive testing using thermal conduction phenomena, elastic stress measurements, and localization of dissipative phenomena). The detected temperature change, resulting from four quite different phenomena, must be correctly discriminated by particular test conditions and/or specific data reduction. This is the main difficulty when interpreting the thermal images obtained from experiments under the usual conditions.

Infrared thermography is a convenient technique for producing heat pictures from the invisible radiant energy emitted from stationary or moving objects at any distance and without surface contact or any perturbation of the actual surface temperature of the objects viewed. The temperature rise ahead of a fatigue crack has been measured and thus proved using an infrared thermographic camera by Attermo & Östberg (1971). Attempts to measure and characterize the heat generated during the cyclic straining of composite materials have also been made. The scanning infrared camera was used to visualize the surface-temperature field on steel and fiberglass-epoxy composite samples (Charles *et al.* 1975) during fatigue tests.

A scanning camera, analogous to a television camera, utilizes an infrared detector in a sophisticated electronics system. It detects radiated energy and converts it into a detailed real-time thermal picture in a video system either in color or monochromatically. Response times are shorter than one microsecond. Temperature differences in the heat patterns are discernible instantly and are represented by several hues. The quantity of energy W ($W.m^{-2}.\mu m^{-1}$), emitted as infrared radiation, is a function of the temperature and emissivity of the specimen. The higher the temperature, the more important the emitted energy. Differences of radiated energy correspond to differences of temperature. The infrared scanner unit in use comprises:

i.- a set of infrared lenses which focuses the electromagnetic energy, radiating from the object being scanned, into the vertical prism,

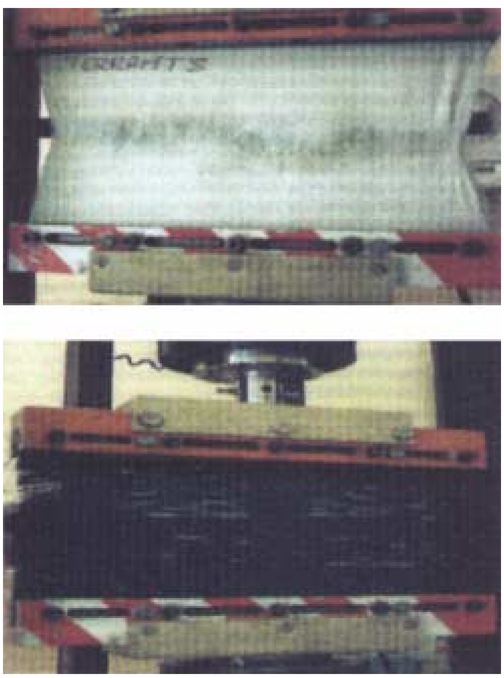

Figure 1 - 1D-tension tests on standardized specimens of various geosynthetics.

ii.- an electro-optical mechanism which discriminates the field of view in 10^4 pixels by means of two rotating vertical (180 rpm) and horizontal (18,000 rpm) prisms with a scanning rate of 25 fields per second,

iii.- a set of relay optics containing a selectable aperture unit and a filter cassette unit which focuses the output from the horizontal prism onto a single-element point detector, located in the wall of a Dewar chamber,

iv.- a photovoltaic SW short-wave infrared detector composed of Indium Antimonide InSb which produces an electronic signal output varying in proportion to the radiation from the object within the spectral response 3.5 μm to 5.6 μm,

v.- a liquid nitrogen Dewar which maintains the InSb detector at a temperature of -196 °C allowing a very short response time of about one microsecond, and

vi.- an electronic control with preamplifier that produces a video signal on the display screen.

The received radiation has a nonlinear relation with the object temperature, can be affected by atmosphere damping, and includes reflected radiation from the object's surrounding. In consequence, calibration and correction procedures have to be applied. Knowing the temperature of the reference, the view-field temperature can then be calculated with a sensitivity of 0.1 °C at 20 °C. This infrared device is used to scan the following tests on geosynthetics.

3 TENSILE TESTING ON GEOSYNTHETICS

When reinforcing materials are deposited in embankments or slope, not only the deformation conditions of soil, but also the direction of reinforcing materials in soil influences the functions and effects of reinforcing materials. A geotextile may be subjected to various tensile loadings all over its life. The most common cases are caused by local irregularities of soil layer upon which it is placed. Rocks, stones, cracks or settlements in soil mass are frequent, even with a meticulous control of the earthwork. A great number of different tensile tests exist nowadays (Figure 1). Nevertheless there still exists the need for a good understanding of the failure mechanisms in order to specify a test procedure on geotextiles (Fayoux & Loudière 1984, Rollin *et al.* 1984).

A tensile force is gradually applied by a tension hydraulic actuator to a geotextile specimen while its length L is measured. Generally the nominal stress is expressed by the force F divided by the width b_0 of the specimen and the strain ε is obtained by dividing the increment ΔL by the initial length L_0. Different types of tightening system have been devised for specimen gripping (Luong & Habib 1989).

Presently, most of the tensile characteristics (yield and failure, strain at yield and at failure) provided by laboratory tests - and so considered as references in civil engineering - are based on uniaxial standardized tensile tests such as AFNOR NFT 54102, DIN 53455 or ASTM D638. However the great influence of geosynthetic specimen geometry and of the applied strain rate has been shown in literature (Gourc *et al.* 1986, Hoekstra 1988, Steffen 1984, Van Leeuwen 1977). The scattering of results caused by the influence of the specimen geometry and the sliding of the jaws can be reduced by measuring the strain in the central part of the specimen where failure occurs. It complicates the test procedure and needs more expensive equipment. Furthermore, the narrowing in the central part of the specimen may be very prejudicial to the validity of the measured elongation: very large strains occur at failure in contrast to limited lateral strains in reality.

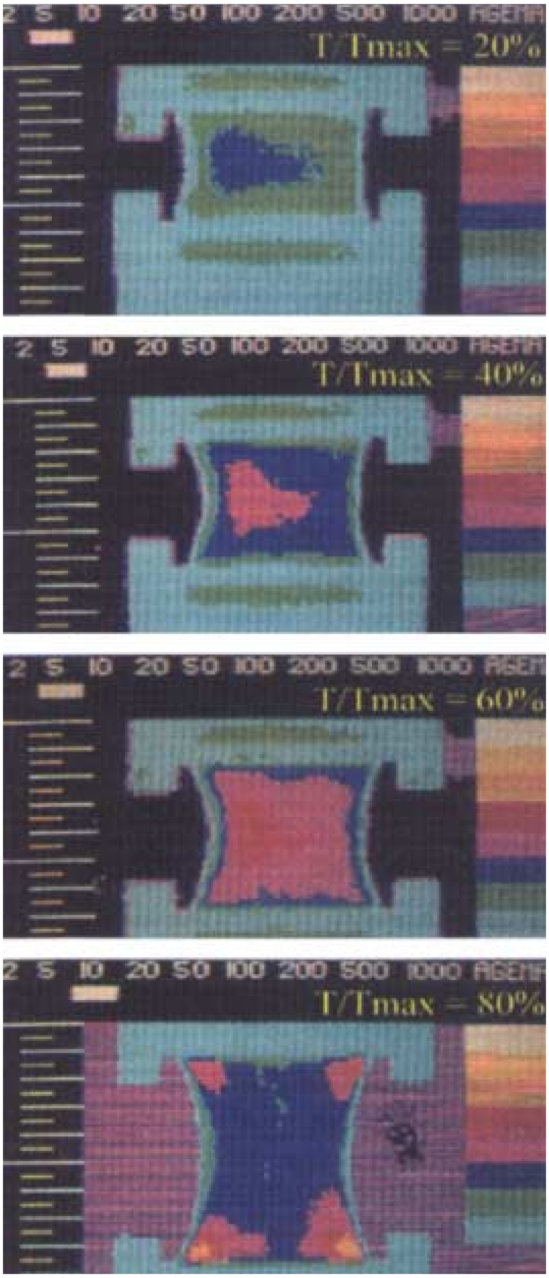

Figure 2 - Thermal images showing the failure process on a specimen of non-woven geotextile subject to 1D-tension test (0.5 °C for each color hue).

The principle of 2D-tension test is similar to the uniaxial tension test. The specimen is simultaneously loaded in two perpendicular directions with a 2D-tension frame. The lateral strain can be controlled, but in certain cases it would be closer to field conditions to maintain the deformation at the same value in the two dimensions. The stress-strain curves obtained in such test conditions would be particularly interesting for the designer. Unfortunately, in consideration to the ease of use and the cost of the required equipment, the generalization of the 2D-tension test seems to be not yet very realistic. The bursting test can be used as a more convenient alternative (Luong & Bernhard 1990).

The proposed parameter, investigated in strength tests on geosynthetics, is heat generation due to the energy dissipated by the material that has been loaded up to failure (Figure 2). The contribution of the plasticity term is revealed by the rapid evolution of the heat dissipation once the stable reversible domain has been exceeded.

Geotextiles are dense fiber assemblies, usually defined as those in which the mechanics is dominated by fiber deformation predicted from assembly deformation. Thanks to the heat dissipation of the textile at large stresses, infrared thermography provides a ready mean to evidence what happens when the fabric yields: a) the effect of slippage from fiber ends, or false ends where fiber paths curve back on themselves, b) the cause of yielding and failure of bonds, either bond breakage or slippage of fibers through bonds, and c) the relevance of the geometry of fiber paths and binder distribution.

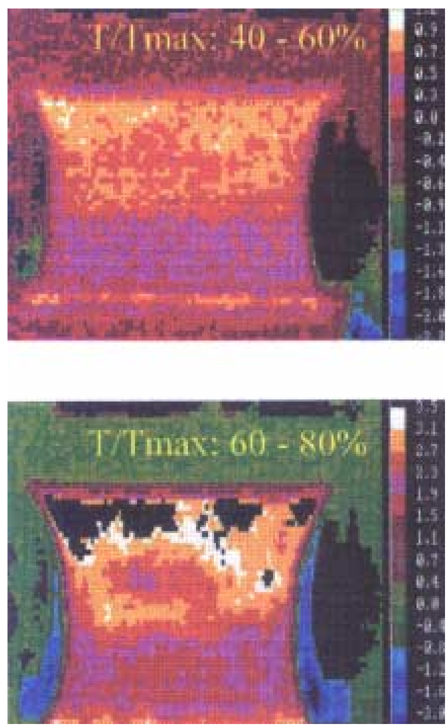

Figure 3 - Intrinsic dissipation evidencing the failure process on a specimen of non-woven geotextile subjected to 1D-tension test (Temperature scale is given in °C).

The infrared scanner device displays a ten-color calibrated surface-temperature picture of the specimen. Each color hue corresponds to 0.2 °C. A computer-aided thermography software allowed the data reduction of the thermal images that shows heat generation between two loading levels (Figure 3). These thermal images provided quantitative values of the intrinsic dissipation of geosynthetics specimens subject to loading up to failure. The same procedure has been applied for each load step. The manifestation of the damage mechanism is revealed by a break of the intrinsic dissipation regime of the loaded specimen. Experimental results have been summarized in Figure 4 where it can be seen how a threshold of dissipative stability is determined using a graphical procedure. This provides a simple way to define a durability threshold for the tested material.

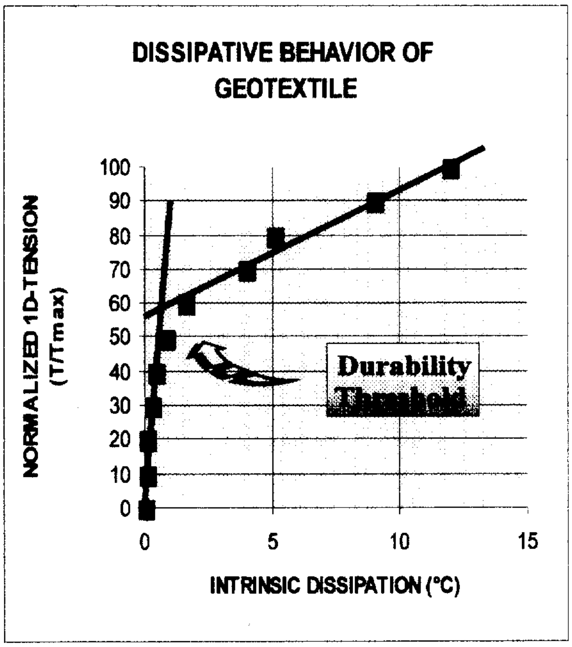

Figure 4 - Graphical determination of the durability threshold of a geotextile under tension.

4 CONCLUDING REMARKS

This work has demonstrated that the intrinsic dissipativity of geosynthetics subject to tensile loading is the most sensitive and accurate manifestation of damage occurrence. Owing to the thermomechanical coupling, this useful technique provides a nondestructive real-time test with no contact to observe the physical processes of geosynthetics degradation, to detect the occurrence of intrinsic dissipation, and to estimate the evolution of dissipative behavior. It thus provides a measure of the material damage and permits evaluation of the sharp limit of a low accumulation of damage beyond which the material leads quickly to failure.

Infrared thermography can be used for the validation of new testing methods on geosynthetics, the development of the mechanics of woven and non-woven geotextiles, particularly the relationships between the mechanical behavior of filaments and the fabric, and between the tensile strength as measured in various tests.

In addition the infrared thermographic analysis of geosynthetics under tension evidences the failure mechanisms of geosynthetics. Consequently it can be applied for the quality assessment and control of geosynthetics products.

REFERENCES

Attermo, R. & Östberg, C. (1971), "Measurements of the temperature rise ahead of a fatigue crack", *Int. J. Fract. Mech.*, 7, II, 122-124.

Charles, J.A., Appl, F.J. & Francis, J.E. (1975) "Using the scanning infrared camera in experimental fatigue studies", *Exp. Mech.*, 14(4), 133-138.

Dillon, O.W.Jr (1963) "Coupled thermoplasticity", *J. Mech. Phys. Solids*, 11, 21-23.

Fayoux, D. & Loudière, D. (1984) "The behaviour of geomembranes to the soil", *Int.Conf. Geomembranes*, Denver, 175-180.

Giroud, J.P. (1980) "Behaviour of geotextiles", *Mechanics of flexible fibre assemblies*, NATO ASI, E: Applied Sciences, 38, Sijthoff & Noordhoff.

Gourc, J.P., Leclerc B., Benneton, J.P., Druon, M., Puig, J. & Delorme, F. (1986) "Traction sur géomembrane: contribution à la définition d'un essai standardisé unique", *3rd Int. Conf. Geotextiles*, Vienna, 945-950.

Hoekstra, S.E. (1988) "Review of bursting experiments on geomembranes", *RILEM TC103 MHG Meeting*, Montréal, 18 pages.

Kratochvil, J. & Dillon, O.W. (1969) "Thermodynamics of elastic-plastic materials as a theory with internal state variables", *J. Appl. Phys*, 40, 3207-3218.

Luong, M.P. & Habib, P. (1989) "Thermographie infrarouge d'un géotextile non tissé soumis à la traction", *Materials and Structures / Matériaux et Constructions*, 22, 53-59.

Luong, M.P. & Bernhard, C. (1990) "Bursting test: validation by 2D-tension test and infrared thermography", *4th Int. Conf. Geotextiles and Geomembranes*, May 28 - June 01, The Hague, The Netherlands, Balkema G.Den Hoedt, 573-578.

Rollin A., Lafleur J., Marcotte M., Dascal O. & Akber Z. (1984) "Selection criteria for the use of geomembranes to the soil", *Int. Conf. Geomembranes*, Denver, 493-499.

Steffen H. (1984) "Report on 2D stress-strain behaviour of geomembrane with and without friction", *Int. Conf. Geomembranes*, Denver 181-185.

Van Leeuwen J.H. (1977) 'New methods of determining the stress-strain behaviour of woven and non woven fabrics in the laboratory and in practice", *Int. Conf. Use of Fabrics in Geotechnics*, Paris, II 299-304.

Influence of Reinforcement Damage on the Pull-out Resistance of Geogrids

M.L. Lopes
Assistant Professor, Department of Civil Engineering, University of Porto, Porto, Portugal

T. Ayele
Ph.D. Student, Department of Geological Engineering, University of Bratislava, Bratislava, Slovakia

ABSTRACT: This paper studies the influence of reinforcement damage on the soil-reinforcement interaction mechanism by analyzing the results of pull-out tests carried out with pre-damaged reinforcements and a granular soil. The reinforcement tested was HDPE uniaxial geogrid and the soil was a well graded very gravelly sand. Testing equipment is described and soil and reinforcement materials are characterized physically and mechanically. To study the influence of reinforcement damage on its interaction mechanism with the soil, five different configurations of reinforcement damage and two different values of confinement stress were used. The role of damage configuration and of confinement stress on the pull-out behaviour of damaged geogrids is discussed. Finally, some general conclusions are put forward.

KEYWORDS: Geogrids, Damage, Interaction, Pull-out test, Pull-out resistance.

1 INTRODUCTION

Geosynthetics can be damaged during handling, placement, and construction operations, if enough care is not taken. The degree of reinforcement damage (extension, severity, and type) that can occur during those operations depends also on the types of machinery, soil, and reinforcement used.

Published field and laboratory test results generally consider reinforcement damage in terms of reduction in tensile and burst strength, grab, puncture and tear resistance, and number of holes per square meter (Razaqpur et al. 1993). Lately, some studies have been carried out accounting for reinforcement damage in terms of long term behaviour of geosynthetics (using creep tests for the assessment of damage) (Esteves, 1996).

However, when geogrids are used as soil reinforcement, particularly in walls and slopes, in addition to the short and long term tensile resistance requirements, the pull-out resistance must be sufficient to inhibit the failure by lack of pull-out resistance. To study the influence of a certain amount of damage on the pull-out behaviour of a high density polyethylene (HDPE) uniaxial geogrid, five different types of damage were simulated in the laboratory and the damaged specimens were tested in a pull-out apparatus. The influence of confinement stress on the pull-out behaviour of the damaged specimens was studied by carrying out tests under two different levels of confinement stress.

2 EQUIPMENT AND MATERIALS

The pull-out box used to study soil-geogrid interaction has internal dimensions of 1.53 m length, 1.00 m width, and 0.80 m height (Figures 1 and 2). The reduction of the influence of the top boundary on the pull-out resistance of the reinforcement and the uniform distribution of the applied vertical stresses are achieved by placing over the top of the soil a smooth neoprene slab having a thickness of 0.025 m. To reduce the influence of the front wall on that resistance, a steel sleeve is used which extended 0.20 m inside the box. The pull-out force, obtained by a hydraulic system, is transmitted to the specimen by a clamp (Figure 3). The confinement stress is applied by placing ten small hydraulic cylindrical masses on the top of the box (Figure 2 and 4). The pull-out force and the confinement stress are measured by load cells (Figures 3 and 4). The frontal displacement and the displacements along the length of the reinforcement are measured by six linear potentiometers (Figure 2).

The soil used in the tests is granular as illustrated by the particle size distribution curve shown in Figure 5. The sand had a maximum and minimum dry unit weights of 18.9 kN/m^3 and 16.1 kN/m^3, respectively. The dry unit weight of the sand used in the tests was 17.5 kN/m^3. The friction angles, defined by direct shear tests, for this unit weight and the two confinement stresses (24.1 kPa and 48.4 kPa) used in the pull-out tests were 37 ° and 35.2 °, respectively, being zero the cohesion of the soil. The geogrid tested was a HDPE uniaxial geogrid with a tensile strength of 55 kN/m. Each specimen had 0.33 m width and 0.96 m confined length at the beginning of the test and was positioned at the middle of 0.60 m height of sand. The constant displacement rate applied in the tests was 1.8 mm/min. Figure 6 shows the dimensions and the position of the points of measurement of the displacements along the reinforcement for the undamaged specimen. Either, the dimensions and the position of the points of measurement, were the same for all specimens tested during the study.

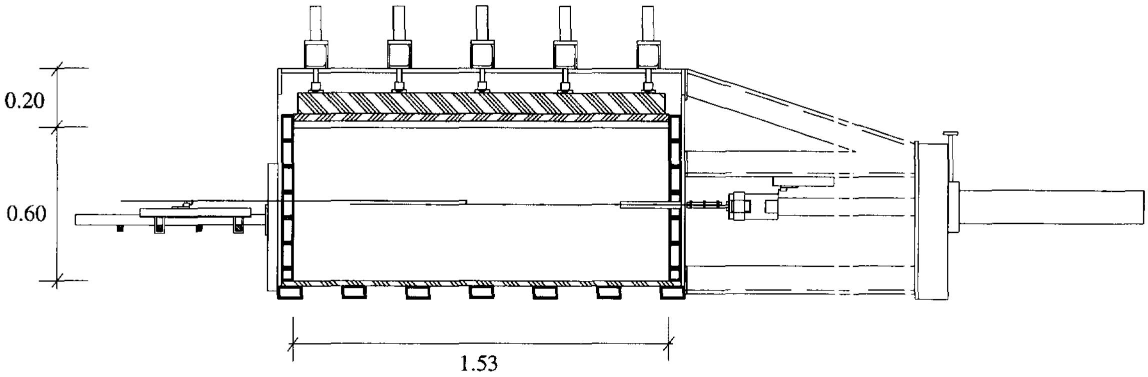

Figure 1. Pull-out box: schematic representation.

Figure 2. Pull-out apparatus - lateral view.

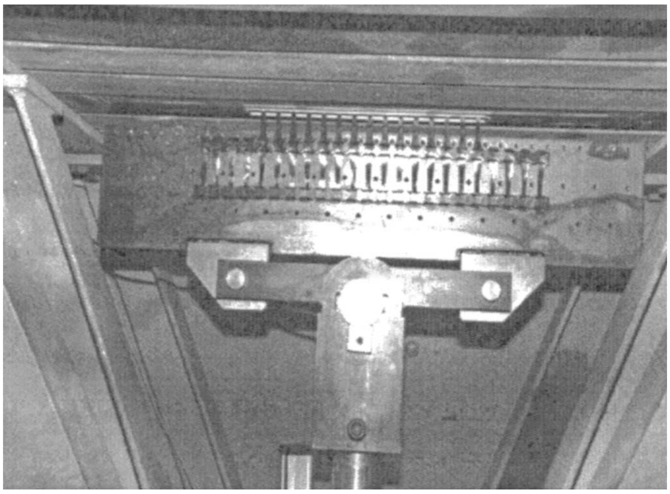

Figure 3. Clamp and load cell for measurement of pull-out force.

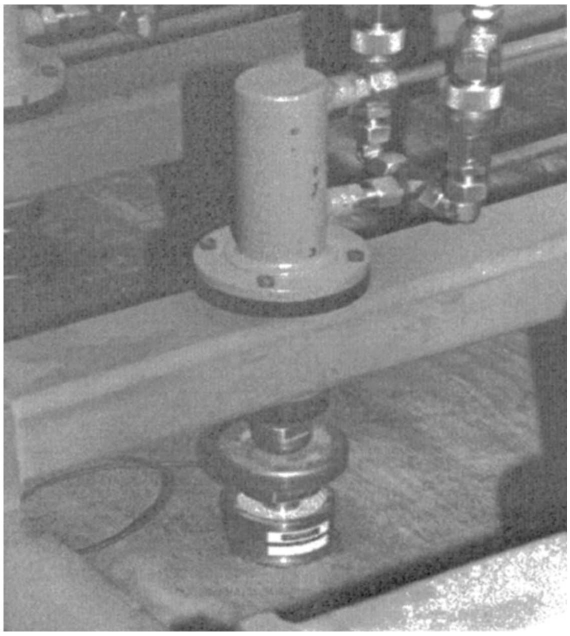

Figure 4. Confinement stress measurement system.

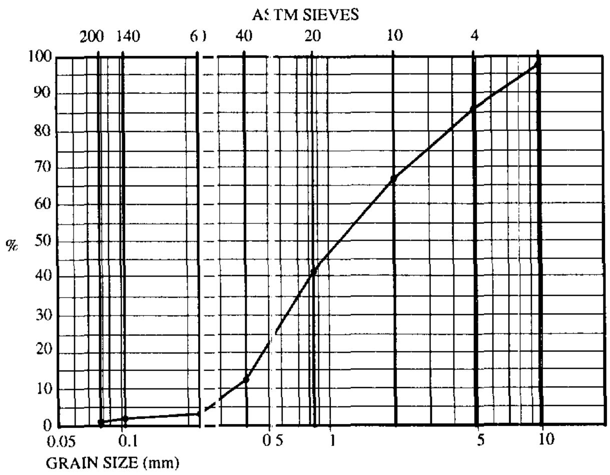

Figure 5. Granulometric curve of the soil.

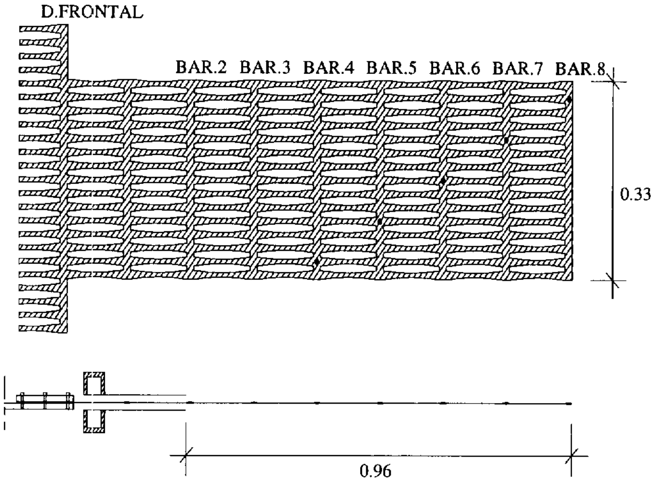

Figure 6. Undamaged specimen. Dimensions and position of the points of measurement of the displacements along the reinforcement.

3 ANALYSIS OF RESULTS

To study the influence of reinforcement damage on the pull-out behaviour of the geogrid, six pull-out tests were carried out for each confinement stress. One of the tests performed was with the undamaged geogrid (SPU) (Figure 6) and the others five with the damaged specimens. The various configuration of the damaged specimens (SP1, SP2, SP3, SP4, SP5) and the points of measurement of the displacements along the geogrid are presented in Figure 7. This figure represents only the confined geogrid at the beginning of the test.

The variation of the pull-out force with the front displacement of the reinforcement is presented in Figure 8 for specimens SPU, SP1 and SP5 under a confinement stress of 48.4 kPa. Specimens SP1 and SP5 had the same damage configuration (four ribs were cut adjacent to the mid-width of specimen), but its position along the length of the geogrid was different (SP1 at the middle and SP5 at the front). It can be seen that the pull-out behaviour of specimen SP5 is very similar to that of the undamaged specimen until failure occurs by lack of tensile strength (tensile failure) at a front displacement of 0.096 m. Specimen SP1 fails by lack of pull-out resistance (shear failure) at a front displacement of 0.142 m for a maximum pull-out force of 33.10 kN/m. The maximum pull-out force for the undamaged specimen (SPU) was 36.44 kN/m, at a front displacement of 0.087 m.

The displacements by strain along the geogrid measured in the tests with specimens SPU, SP1 and SP5 under a confinement stress of 48.4 kPa are present in Figure 9. It can be seen that the contribution of the posterior part of specimen SP5 for the pull-out resistance of its interface with the soil is zero. In fact, bars 6, 7 and 8 do not move during the test. The higher strain in the anterior part of the geogrid can be justified by the localization of the damage (just in the entrance of the sleeve). In fact, as the pull out of the geogrid starts the damaged zone goes inside the unconfined area of the sleeve, deforms more than the undamaged specimen and fails by lack of tensile strength before starting the mobilization of shear stresses in its interface with the soil in the posterior part of the geogrid. As the front part of specimen SP1 was not damaged, during pull-out all the geogrid length contributes for the pull-out resistance of its interface with the soil, failing when this maximum resistance is reached. Specimen SP1 shows lower displacements by strain in bar 6 than in bar 8. The reason is the position of the linear potentiometer in bar 6 (just in the back limit of the damaged area), showing a localized reduction in movements due to damage, suggesting the easier penetration of the soil grains in the larger apertures of the geogrid in the damaged area, with consequent local increase of the interlock mechanism.

Figures 10 and 11 present the results of the pull-out tests in terms of variation of the pull-out force with the front displacement of the reinforcement for confinement stresses of 48.4 kPa and 24.1 kPa, respectively, for an undamaged specimen (SPU) and four damaged specimens (SP1, SP2, SP3 and SP4) (see Figure 7). Table 1 shows, for the two confinement stresses considered, the maximum pull-out force measured for each specimen tested, and the ratio between this force and that measured for the undamaged specimen. Analogous presentation can be seen in Table 2 for the front displacement for the maximum pull-out force.

The influence of the confinement stress in the pull-out resistance of the geogrid is presented in Figure 12. This figure shows the displacements by strain along the undamaged specimen for the two values of the confinement stress used in the tests (48.4 kPa and 24.1 kPa). It can be concluded that the increase in the confinement stress leads to a significant increase in the pull-out resistance of the reinforcement, increasing the maximum pull-out force about 71 % when the confinement stress changes from 24.1 kPa to 48.4 kPa. This behaviour suggests the importance of the skin friction mechanism in the pull-out resistance of the geogrid tested.

Figures 10 and 11 and Table 1 suggest that the behaviour of damage type SP1 and SP2 is distinct from that of SP3 and SP4. In fact, for the less damaged specimens (SP1 and SP2) the failure occurs by lack of pull-out resistance, as in the undamaged specimen (SPU), and for the heavily damaged specimens (SP3 and SP4) the failure mode is lack of tensile strength. In damage type SP1 and SP2, although the extensibility of the reinforcement increases (see Table 2) its stiffness is enough to mobilize shear stresses all along its length. The maximum pull-out force is similar or even greater than that of the undamaged geogrid. The greater values obtained are, probably, due to the local increase in the dimensions of the geogrid with consequent easier penetration of the soil grains in it, leading to a local increase of passive thrust mobilization on the bearing members of the grid (see Figure 9, bar 6). Damage type SP3 and SP4 due to the strong reduction of reinforcement stiffness in the damaged zone inhibits the mobilization of shear stresses in the length of the geogrid located behind that zone.

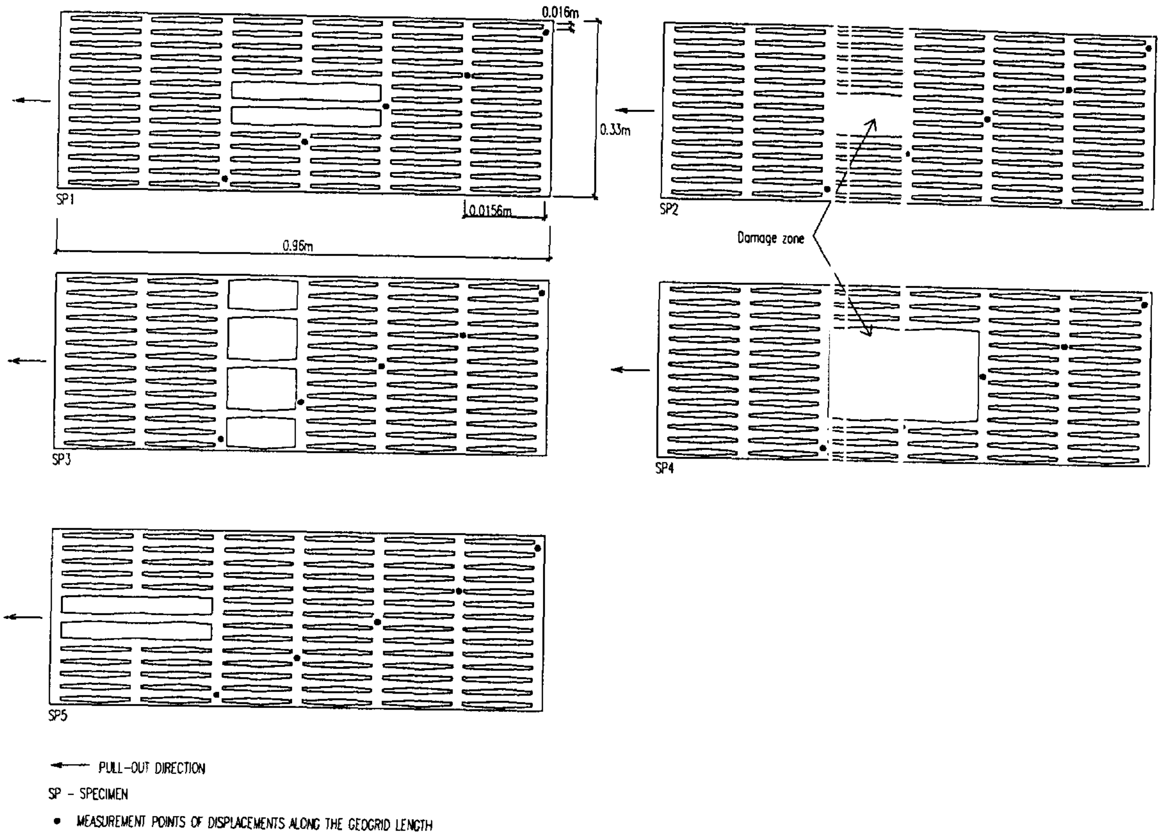

Figure 7. Geogrid damaged specimens.

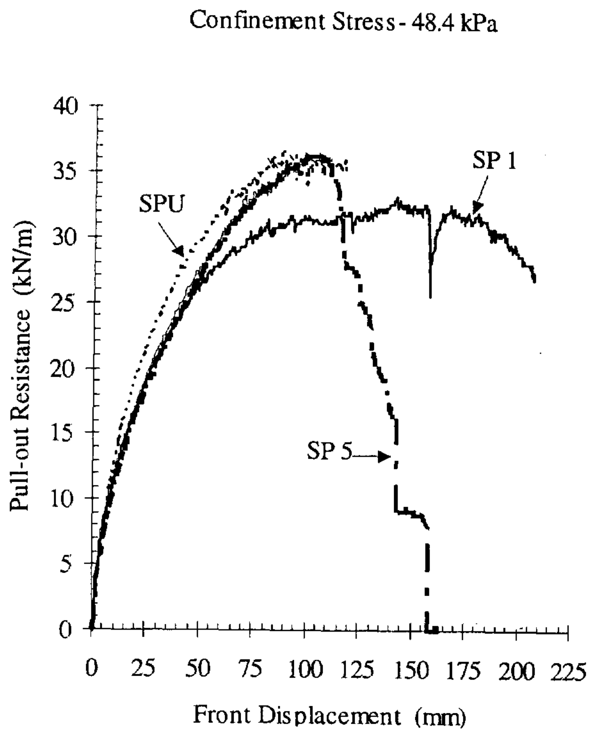

Figure 8. Influence of localization of damage along the length of the geogrid ($\sigma_{conf.}$=48.4 kPa).

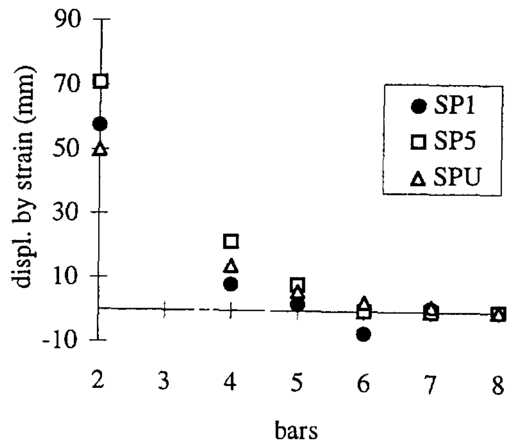

Figure 9. Displacements by strain along the geogrid (specimens SPU, SP1 and SP5, $\sigma_{conf.}$=48.4 kPa).

In these cases only the remaining length contributes for the pull-out resistance of the reinforcement and failure occurs by lack of tensile resistance in the unconfined area of the sleeve.

The front displacement for the maximum pull-out force when the geogrid fails by lack of pull-out resistance (specimens SPU, SP1 and SP2) increases with damage (see Table 2). This is, the geogrid becomes more extensible with damage. This behaviour is more clear under a confinement stress of 48.4 kPa. In fact, for relatively similar values of maximum pull-out forces, the front displacement is about 45% to 63% higher when the specimen is damaged. The increase of confinement stress leads to an increase in maximum pull-out force and in front displacement for the maximum pull-out force. However, for damage configuration SP3 the influence of confinement stress is almost negligible.

The influence of damage is more important for higher confinement stresses. In fact, the extensibility of the damaged reinforcements increases more significantly, decreasing the ratio between the maximum pull-out forces of damaged and undamaged specimens when the confinement stress increases (see Tables 1 and 2).

Table 1. Ratio between maximum pull-out forces.

Specimens	Confinement stress 24.1 kPa		Confinement stress 48.4 kPa	
	Maximum pull-out force, T (kN/m)	$T_{(damaged)}/T_{(undamaged)}$	Maximum pull-out force, T (kN/m)	$T_{(damaged)}/T_{(undamaged)}$
SPU	21.26	1.00	36.44	1.00
SP1	26.14	1.23	33.10	0.91
SP2	25.51	1.20	37.35	1.02
SP3	21.26 *	1.00	21.86 *	0.60
SP4	17.61 *	0.83	28.24 *	0.77
SP5	------	----	36,10 *	0.99

Note: * Tensile failure.

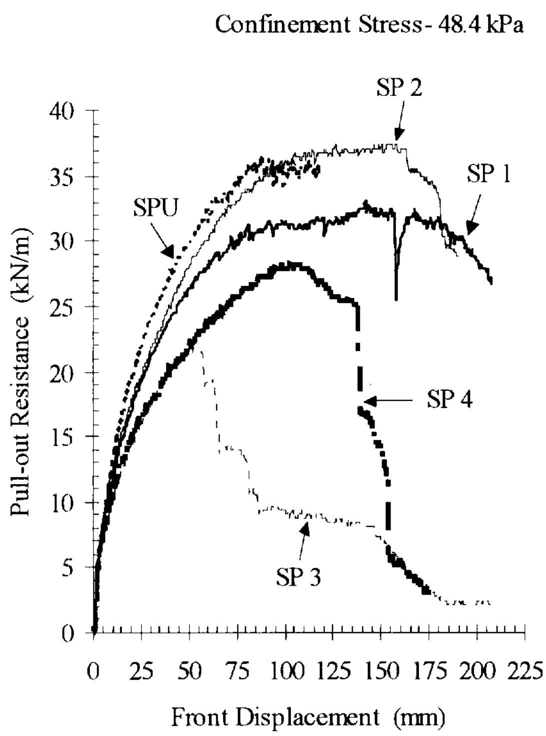

Figure 10. Influence of reinforcement damage on the pull-out behaviour of the geogrid for a confinement stress of 48.4 kPa.

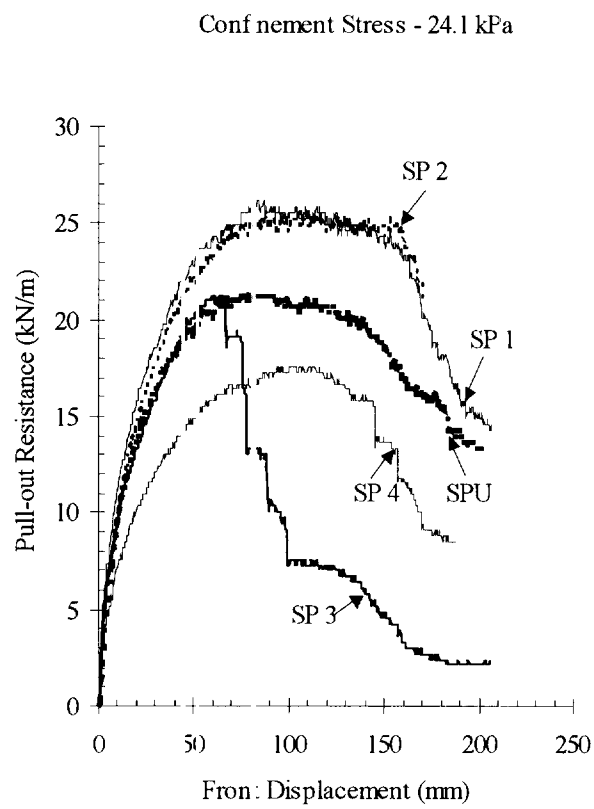

Figure 11. Influence of reinforcement damage on the pull-out behaviour of the geogrid for a confinement stress of 24.1 kPa.

Table 2. Front displacements for the maximum pull-out forces.

Specimens	Confinement stress 24.1 kPa		Confinement stress 48.4 kPa	
	Front displacement for the maximum pull-out force (m)		Front displacement for the maximum pull-out force (m)	
SPU	0.072	(1.00)	0.087	(1.00)
SP1	0.082	(1.14)	0.142	(1.63)
SP2	0.097	(1.35)	0.126	(1.45)
SP3	0.060 *	(0.83)	0.053 *	(0.61)
SP4	0.094 *	(1.31)	0.098 *	(1.13)
SP5	-------	--------	0.096 *	(1.10)

Notes: Values in parentheses () are the ratio between front displacements for the maximum pull-out force of damaged and undamaged specimens; and * means specimen tensile failure.

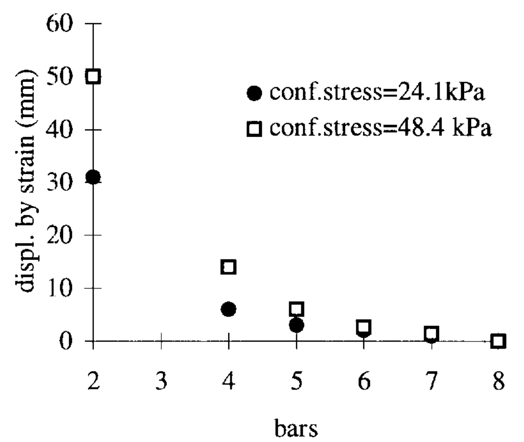

Figure 12. Influence of confinement stress on the displacements by strain along the geogrid (undamaged specimens).

4 CONCLUSIONS

The study of the influence of reinforcement damage on the pull-out behaviour of a HDPE uniaxial geogrid embedded in a well graded very gravelly sand leads to the following major conclusions:

1. The localization of the same configuration of damage along the length of the geogrid can affect its pull-out behaviour, leading to tensile failure of the reinforcement when its location is near the front.
2. The configuration of damage can lead to a distinct behaviour of the geogrid: small damage leads to pull-out failure; large damage leads to tensile failure.
3. In general, damage increases the displacement at failure, the geogrid becoming more extensible.
4. In general, the increase of confinement stress leads to the increase of the maximum pull-out force and of the front displacement at the maximum pull-out force.
5. The influence of the geogrid damage on its pull-out behaviour increases significantly as the confinement stress increases, increasing the geogrid extensibility and decreasing the ratio between maximum pull-out forces of damaged and undamaged specimens.

ACKNOWLEDGMENTS

The authors would like to express their thanks to the financial support of Program PRAXIS XXI and of FEDER, Research Project 3/3.1/CEG/2598/95.

REFERENCES

Esteves, S.A.C. (1996) "The Strength of Geosynthetics and Construction Damage Effects", *M.Phil. Thesis*, University of Strathclyde, Glasgow, UK, 288p.

Razaqpur, A.G., Bauer, G.E., Halim, A.O.A. and Zhao, Y. (1993) "Pullout Resistance and Load-Slip Response of Mechanically Damaged Geogrids", *Geosynthetic Soil Reinforcement Testing Procedures*, ASTM STP 1190, Philadelphia, USA pp.195-206.

Full-Scale Dynamic Tests on Geocomposites as Waterproof Layer and Reinforcement of the Surface of Embankment

J. ZHANG
Ph. D. Candidate, Department of Civil Engineering, University of Canterbury, Christchurch, New Zealand

D. Y. ZOU
Lecturer, Department of Civil Engineering, Southwest Jiaotong University, Sichuan, P. R. of China

ABSTRACT: The paper introduces the four groups of the full-scale dynamic tests which have been done to investigate the effects of the geosynthetic complex layers to behaviors of embankment. The results of system modulus, stresses, and settlements in the embankment for the tests are compared, some conclusions are obtained: the thickness of optimal complex layer is 100mm; special attention should be given to geosynthetics that is directly paid between subgrade surface and ballast. Because geosynthetics is used, mud stone can be used as fill in the embankment.

KEYWORD: Composite Material, Embankments, Railroad Applications, Separation

1 INTRODUCTION

Mud stone is a kind of poor quality soil that can not be used as filling in the embankment. The reason is that when the mud stone is saturated, its strength will be very low. However, railroad has to pass extensive mud stone areas. Hence, the soil will be improved to suit the design code. Comparing with soil improvement, geosynthetics is an economic method. When ground water, i. e., spring, is not present, geocomposites (geotextiles + geomembrances + geotextiles) not only prevent water above it into mud stone (Selig and Waters 1994), but also improve the stress state of the subgrade. Thus the disadvantage of mud stone can be overcome. When the geocomposites and subballast are used together, their functions will be used completely. However, in the geocomposites, geomembrance is very important to the design. Hence, It is necessary that the second subballast layer is inserted between subballast and subgrade. In this case, The thickness of geocomposites and the second subballast layer (the thickness is called complex thickness) (Fig. 1) is a key to an economic and safe design.

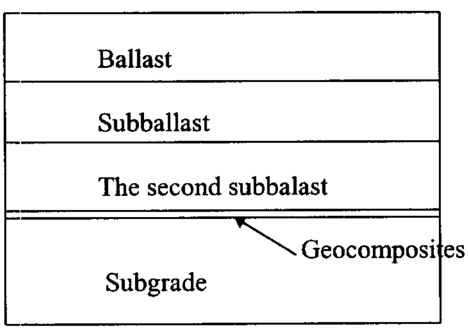

Figure 1. Confirmation of the embankment

For obtaining the optical complex thickness, four complex thicknesses were tested. Comparisons of the stresses, settlements and system moduli illustrate that the optical complex thickness should be 100mm. The thickness assures the functions of subballast and avoids the abrasion and attrition between geocomposites and big particles..

2 MODEL TEST

2.1 Model and Material

The tests take 1:1 model to simulate the subgrade, ballast, subballast, sleeper. The size of the model box is 2.5m by 0.9m by 2.3m and it is made by steel frame and thick hard woods. In the analysis, because subgrade, subballast, ballast and superstructures are symmetry, only one-half of its section is taken.

According to measuring pressures on sites which illustrate that a axial weight will be taken by the successive 5 sleepers (Cui et al. 1994), maximum static pressure on the sleeper under the train wheel is 42 KN. However, because of the effects of track, train characteristics, and operating condition, measuring pressures on sites were in the range 45 KN - 60 KN. In terms of the above analysis, the static loading 45 KN and the dynamic maximum loading amplitude 15 KN were taken.

Subgrade clay was got from the site. special gravity G_s= 2.67; liquid limit W_l=36; plastic limit W_p=23.1; plasticity index I_p=13.5; maximum dry density ρ_{dmax}=1.645g/cm^3; optimal water content W_{opt}=20.5. In the filling, density was controlled by 95% maximum dry density.

The ballast was 250 mm thick. The subballast was 200 mm thick(Cui et al 1994). The second subballast layer consists of sand and its thickness would be changed from 0 - 300mm.

The geocomposites consist of the two layers of non-woven geotextiles(Polyester) and a layer of geomembrance (PVC-Polyvinyl Chloride). Its weight is 600g/m^2 and thickness is about 2mm. Main parameters were measured in the factory. tensile strength, puncture strength, and permeatibility strength were 600 N/5CM, 1.5MPa, 0.5 MPa, respectively. Before the tests, the ones were measured again which were 657 N/5CM, 1.92 KN, 0.825MPa, respectively(average value). A number of tests confirmed the parameters had change slightly.

2.2 Test Procedure

2.2.1 Test Equipment

All tests were done by the servo-hydraulic system. In the system, there are a displacement gauge and a load cell on the loading head. They measure total settlement and pressure. In the subgrade, displacement gauges, earth pressure cells, and acceleration gauges are setup along various height and away the loading center figure 2.

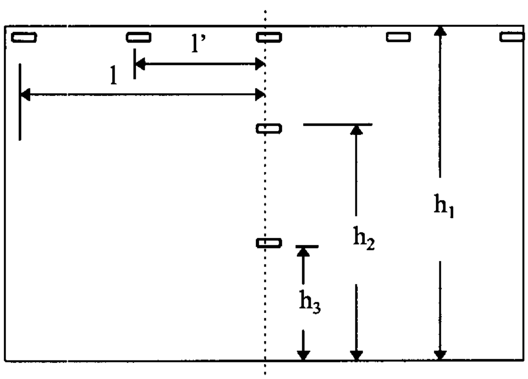

Figure 2. Location of instrument

2.2.2 Test Procedure

The test procedure should reflect situations on the site. Therefore, the thickness of the second subballast layer is a key factor, because it should spread stress from wheel load and prevent geomembrances from being punctured by big particles. At the same time, efficiency spreading stress by the second subballast layer was expected to be investigated. The four thicknesses of the second subballast layers which were 0mm, 100mm, 200mm, 300mm, respectively, were selected to the tests. According to different thickness, the location of some instruments were changed as followed: In model 1, the location of instruments were l=500mm, h1=850mm, h2=500mm, h3=200mm. In model 2, the location of instruments were l'=200mm, h1=750mm, h2=550mm, h3=350mm. In model 3, the locations of instruments were l'=200mm, h1=750mm, h2=550mm, h3=350mm. In model 4, the locations of instruments were l'=300mm, h1=75mm, h2=550mm, h3=350mm (l denotes distance from loading center; h denotes height from the bottom of box)

In the tests, the thickness and density of ballast and subgrade were the same. However, loading times would be changed according to the cases. The loading times of the model 1 and 2 were one million times, respectively. The loading times of the model 3 and 4 were 500 thousand times, respectively. The different loading times among the models were decided by the total settlement.

3 RESULTS

3.1 Comparisons of deformation loading modulus

Deformation loading modulus E_v denotes the ratio of the stress and strain in the static loading. It will reflect the stiffness of system of the embankment (including ballast, subballast, geocomposites, and subgrade). For the new constructed embankment, initial deformation is very important. Therefore, E_v is important factor. The larger E_v, the smaller the settlement and the higher the density.

To investigate the change of the deformation loading modulus after the dynamic tests, the E_v was measured before and after the tests based on load plate test. The result of the model 1 is shown in figure 3.

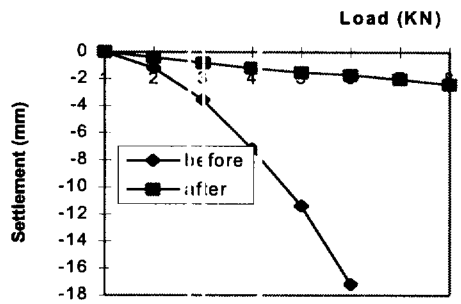

Figure 3. Relation between load and settlement before and after test in model 1

It denotes that the settlement of the embankment is clearly reduced after dynamic test, hence E_v increases greatly. The relation between the load and settlement is non-linear before test, but the relation becomes linear after test. Figure 4 reflects the relation between E_v and the thickness of the second subballast layer. The deformation loading modulus E_v of the four models are nearly the same before tests. However the E_v increases when the thickness of the second subballast layer increases from 0 to 200mm, but when the thickness of the one is equal to 300mm, its E_v has nearly no change. The results show that the thickness of the complex layer made by the second subballast layer and geocomposites will directly affect the stiffness and stability of the embankment and if the complex layer is too thick, its function will be reduced. The stress at the interface between geocomposites and the subgrade will directly affect the settlement of the embankment Five earth pressure cells were setup on the interface . Figure 5 gives results of model 1 and 2.

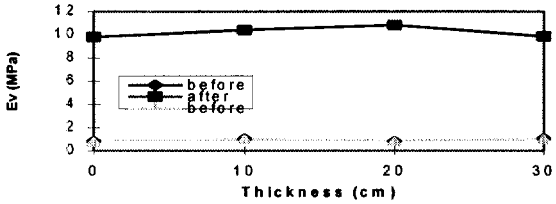

Figure 4. Relation between Ev and the thickness of complex layer

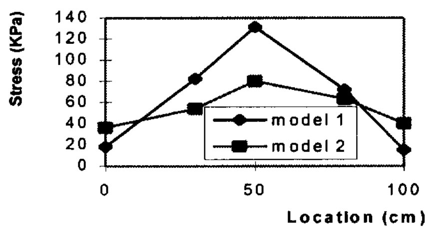

Figure 5. Stress of interface

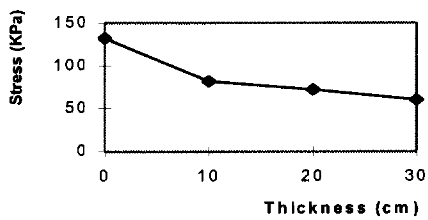

Figure 6. Relation between maximum stresses and thickness of complex layer

3.2 Stress at Interface Between Geocomposites and the Subgrade

These results show that the complex layer reduces the stress peak at the interface between the geocomposites and the subgrade. Figure 6 compares the maximum stress of the four tests which illustrate the complex layer has the function reducing stress, but the efficiency will gradually reduce as the thickness of the complex layer increases. Therefore, the optimum thickness of complex layer is very important in the embankment design.

3.3 Distributed Stresses Along the Depth

The distributed stresses along the depth of the embankment causes the settlement of the embankment. The complex layer reduces the stress at the interface between the complex layer and subgrade (figure 5), the layer also affects the distributed stresses. Figure 7 shows the results of the model 1 and 2. In the top of subgrade, the stresses in the model 1 are greater than the ones in the model 2. However, in the low part of subgrade, the stresses in the model 1 are smaller than the ones in the model 2. This result denotes that although the complex layer reduces the stresses at the interface, the stress attenuation along the depth of the embankment in the model 2 is slower than that in the model 1. Special attention should be given to a high speed train. Geocomposites which affects stresses in the embankment is very interesting. Figure 8 is the result in which stresses were measured above and below geocomposites. It efficiently reduce stresses below geocomposites and change the value of the stresses of distribution along the depth of embankment. At the 100mm range above and below geocomposites, the stresses are reduced by about 30%.

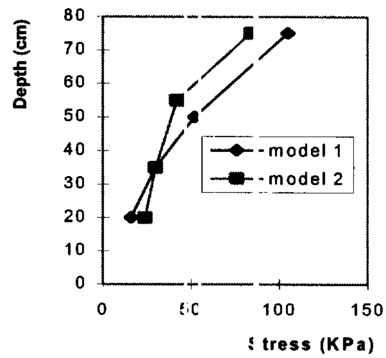

Figure 7. Distributed stress in model 1 and 2

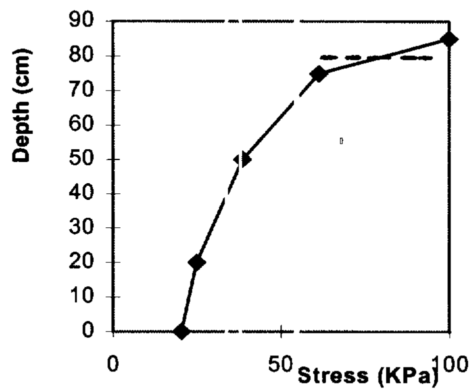

Figure 8. Effect of geocomposites on stress

3.4 Settlement of the Subgrade

The settlement of the surface of the subgrade will affect stability of the embankment and will increase cost of maintenance in the future and if settlement is greater, geocomposites will be in the dynamic extension state. Therefore, reducing settlement will be a key to the research. Figure 9 shows the results of settlement in the four models. These results illustrate that initial settlement is most part of total settlement, For example, initial settlement is 93% and 55% of the total settlement in the model 1 and 2, respectively. The result is conformable to stress analysis. Because the complex layer is on the surface of the subgrade, the settlement of subgrade is reduced greatly. If the settlement in various models compares with the settlement of the model 1, the percent at model 2, 3, 4 is

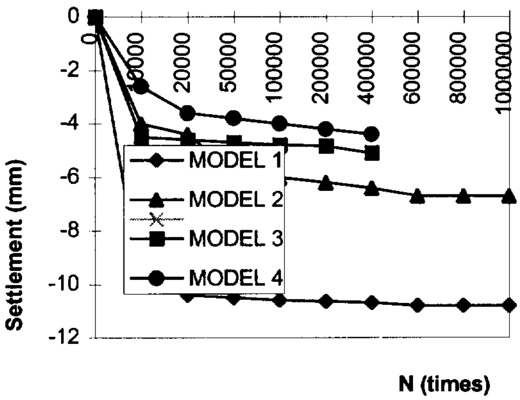

Figure 9. Surface settlement of embankment

37%, 52%, and 59%. The efficiency of the complex layer is very clear. Figure 10 shows settlement along the depth of

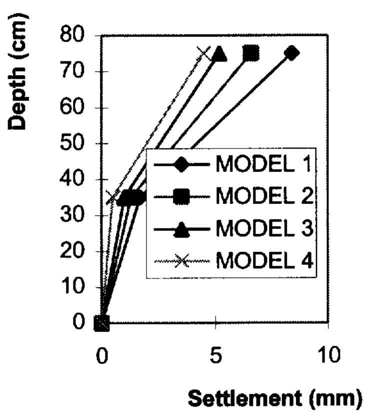

Figure 10. Distributed settlement along embankment

the embankment. The result shows that the settlement will reduce as the thickness of the complex layer increases. This is also conformable to the distributed stresses.

3.5 Situation of the Geosynthetics

After the four model tests, the geocomposites were checked by eyes and tests. In the model 1, the surface of the geocomposites is very rough. The reason is that big particles in the first subballast layer and ballast contact the surface of the geocomposites under dynamic loading. However, in the model 2, 3, 4, the surfaces of the geocomposites were still new after tests. The reason is that the second subballast layer separates big particles and geocomposites and avoids their contacts.

Comparing geocomposite properties before and after the tests, tensile strength, puncture strength, and tear strength were nearly the same. It illustrates that the geocomposite qualities are well and meet the need of the project.

4 CONCLUSIONS

According to the above analysis, some conclusions can be obtained:

1. The static system moduls will increase with the thickness of complex layer. However the efficiency of complex layer will gradually reduce as its thickness increases. Because complex layers are inserted between subgrade and ballast,the amplitude of dynamic stresses is reduced. It illustrates that complex layers have efficiency spreading stress.
2. With respect to the maximum stress in the model 1, the maximum stress in the model 2, 3, and 4 reduce 36%, 38%, and 39%, respectively. With respect to the settlement of subgrade surface in the model 1, the settlement of subgrade surface in the model 2, 3, and 4 reduce 37-%, 52%, and 59%. Compared to these results, in practice, the complex layer 100mm in model 2 is optimal thickness.
3. Compared to state of geocomposites after tests, if there is no the second subballast layer (in model 1), the surface of geocompositess become very rough, the reason is that big particles contact the surface of geocomposites under dynamic loading. If the case is taken, the geomem-brance in the geocomposites may be punctured out in the future. Therefore, attention must be given that geocomposites are directly paid between subgrade surface and the first subballast layer.

REFERENCES

Cui, Y., Zhang, J., and Chou, X. W. (1994) *An Investigation of Subgrade Stresses in Field tests,* Project Report for Department of China Railroad, Report, Department of Civil Engineering, Southwest Jiaotong University, China

Cui, Y., Zhang, J., and Chou, X. W. (1994) *Full-scall Dynamic Test on effect of loading frequence and subballast,* Project Report for Department of China Railroad, Report, Department of Civil Engineering, Southwest Jiaotong University, China

Selig, E. T. and Waters, J. M. (1994) *Track Geotechnology and Substructure Management,* Thomas Telford Publications, London, England

Performance Test to simulate Geotextile Puncture under dynamic cyclic Loading

G. Mannsbart
Technical Manager, Polyfelt Ges. m. b. H., Linz, Austria

H. Breymann
Head of Geotechnical Department, Testing and Research Institute for Civil Engineering, Salzburg, Austria

M. Moser
Head of Geotechnical Laboratory, Testing and Research Institute for Civil Engineering, Salzburg, Austria

ABSTRACT: Puncturing is one of the decisive stresses geotextiles are exposed to. For geotextiles used as separators under unpaved roads, the stress elongation behavior under dynamic puncture loading is of crucial importance. Dynamic and cyclic stresses caused by sharp edged aggregate have only been taken into account to a small amount in geotextile testing so far. On the basis of existing test methods (CBR-puncture according to EN 12236, Pyramid puncture according to ASTM 5494 and NFG 38019) a special test has been developed. The main modification is a cylic up-and-down movement of the pyramid piston, which is pushed slowly into the geotextile.
The deformation and the puncture force are continuously measured, and the envelope of the obtained curves is the main charcteristic of the geotextile behavior. Numerous test results have been obtained in the laboratory and will be cross-checked with the results from on-site trials. It is shown that needle punched nonwovens perform very well. This is attributed to the rupture resistance and to the resistance to tearability of the product. To be able to withstand the harsh installation stresses, geotextiles have to show a clearly defined force elongation behavior in the dynamic cyclic loading test.

KEYWORDS: Dynamic mechanical analysis, Geotextiles, Installation Damage, Puncture Resistance, Separation

1 INTRODUCTION

Still the most common use of geotextiles is in road and pavement construction. Geotextiles increase stability and improve the performance of the subgrade by reducing deformations and by increasing the bearing capacity of the soil. (Polyfelt; 1986)

The primary function is separation, but also filtration, drainage, and strengthenig of the soil may be regarded as secondary functions in road and pavement constrution. The geotextile must prevent the movement of fines from the subgrades into the sub-base course. To be able to fulfill this requirement, it is necessary that the geotextile withstands all stresses during the installation phase.

Stresses occurring during installation are critical in most of the cases and therefore are regarded as decisive for design. Installation stress is understood here as the sum of puncturing, burst, and abrasive forces which occur during placement of the sub-base material as well as during compaction and loading by construction traffic. To simulate the forces exerted on a geotextile by a single sharp edged grain of the fill, a dynamic cyclic loading test has been developed.

2 TEST DESCRIPTION OF THE CYCLIC PYRAMID PUNCTURE TEST

2.1 Test Setup

When considering international specification tendencies, that aim to guarantee the separation function of geotextiles, one finds the CBR puncture resistance, Mullen Burst strength, and tear strength as essential specification criteria. In only a few standard specifications unit weight is also listed as a requirement. Dynamic and cyclic stresses caused by sharp edged aggregate have only been taken into account to a small amount in geotextile testing so far. (Bräu; 1996).

To be able to simulate the puncturing forces on a geotextile separator, a specific test method has been developped on the basis of existing test methods (CBR-puncture according to EN 12236, Pyramid puncture according to ASTM 5494 and NFG 38019; Werner; 1986). The main modification is a cylic up-and-down movement of a pyramid-shaped piston, which is pushed slowly into the geotextile. By the use of this test the static and dynamic behavior of geotextiles under a pyramid load can be studied.

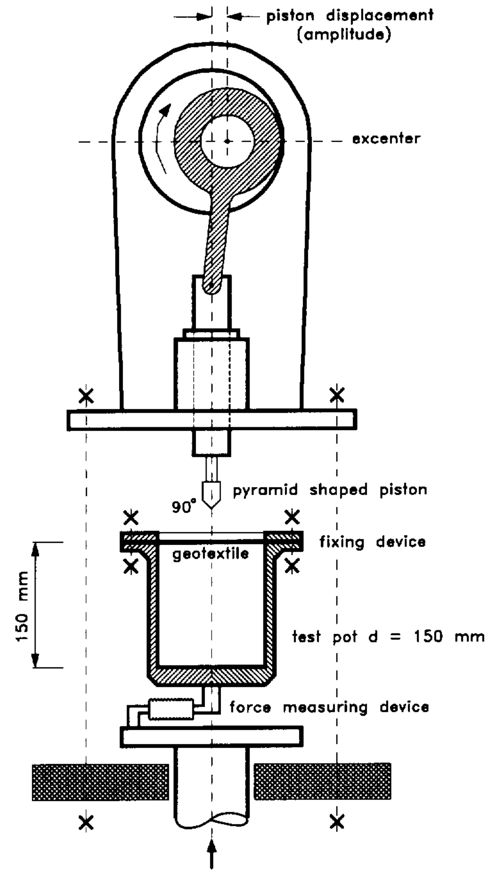

Figure 1: Scheme of the test device

The geotextile is positioned and fixed on a test pot. A pyramid shaped piston is used to simulate a sharp edged grain which exerts the stress during installation.
The test pot has an inner diameter of 150 mm and a height of 150 mm. The fixing device was made in accordance with EN ISO 12 236.
Dynamic and static forces acting on the test pot due to the movement of the pyramid were measured.
For the dynamic puncture, the maximum value of the loading cycle is registered.

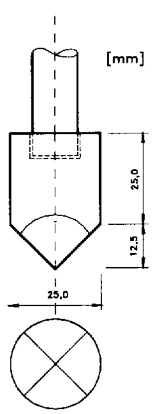

Figure 2: lay-out of the pyramid piston

2.2. Test Procedure

The test device offers the possibility to simulate both dynamic as well as static loading. Therefore, the test description is made in two parts.

2.2.1 Static Pyramid puncture test

In the static test, the piston is moved downward continuously until rupture occurs. The test is performed in analogy to EN ISO 12 236. Instead of the cylindrical piston with 50 mm diameter the pyramid according to ASTM D 5494 is used (see Fig. 2). The velocity of the (upward) movement of the pot is 10 ± 1 mm/min.

2.2.2 Dynamic Pyramid puncture test

In the dynamic test, the pyramid is exposed to cyclic up-and-down movement. The same 50-mm diameter cylindric piston and the pyramid peak according to ASTM D 5494 are used.
The pyramid is moved up and down vertically by the use of an eccenter (see Fig. 3). At the same time, the test pot with the fixed geotextile is moved upwards against the oscilating pyramid. The force-elongation behavior is recorded.
The oscilating movement is achieved by an excenter, which has an amplitude of ± 5 mm. The frequency of the vertical movement of the pyramid is 15 Hz.

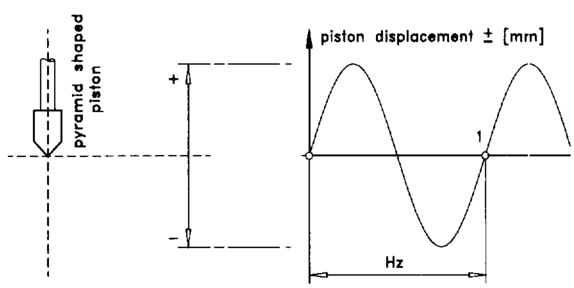

Figure 3: Principle of dynamic (cyclic) loading.

The stress for the dynamic test is characterized by the following parameters:

- vertical (upward) velocity of the pot (= velocity of the fixed geotextile) [mm/min]. The pot is moved upwards continuously by a special device with a velocity of 10 mm/min. The allowable tolerance is ±1mm/min.
- maximum vertical displacement of the pyramid during it's oscilating movement [mm]
- Frequency (strokes per second) for the movement of the pyramid [Hz]

For every type of geotextile at least five single tests (static, dynamic) at 23° ± 2°C should be performed. The mean values F_{stat}, F_{dyn} and the standard-deviation are calculated.

2.2.3. Test results

The static puncture force F_{stat} is the maximum value of the forces (in Newtons) measured during puncturing of the fixed geotextile specimen.

The dynamic puncture Force F_{dyn} is the maximum value of the dynamic forces (in Newtons) measured during puncturing of the fixed geotextile specimen. Here puncturing will be achieved by the superposition of the oscilating movement of the pyramid with the continuous upward movement of the pot.

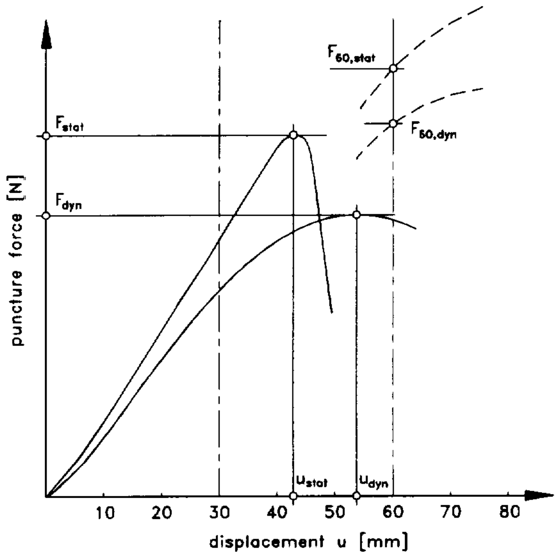

Figure 4: Graphical evaluation of the test results.

2.2.4 Boundary conditions

The test should be performed for at least 5 single specimens at 23° ± 2°. The curve of the force -elongation behavior is recorded.

The specimen has been prepared with a marking and cutting template and installed without any tension between the clamping rings.

The pot is fixed centered under the pyramid and the start-amplitude is fixed. For the start-amplitude of every test, the peak of the pyramid is lying without any tension on the surface of the fixed geotextile, and the pyramid has been set to the lowest point of the excenter.

The test is finished, if a decisive reduction of the puncture force is observed.

The evaluation is done according to the curves in Figure 4. The envelope curve of the arithmetic mean values is plotted.

The deformation has been determined by an electronic device in millimeters with an accuracy of ± 0.1 mm. The dynamic and the static puncture forces are given in Newtons. The maximum of the obtained values is considered the puncture force.

2.2.5 Test report

In the test report the values obtained (static and dynamic puncture force) as well as the standard-deviation and the coefficient of variation are stated. A graphic evaluation (force-displacement curve) similar to the one given in figure 4 is enclosed.

3 TEST RESULTS

Large series of tests have been performed on various types of products. Thermobonded as well as needlepunched staple fibers and continuous filament nonwovens have been examined.

Among the results which have been obtained, results from a typical range of products are presented in this paper. Results for different grades of a specific polypropylene continuous filament nonwoven geotextile are given. The specimens have been tested with respect to both their static and dynamic puncture resistances. The properties of these products are given in Table 1.

Table 1 Properties of tested products

	Type A	Type B	Type C
CBR test [N]	2300	3500	4200
Tens. Str. [kN/m]	13.5	21.5	26.5
Elongat. MD/CD	80% / 45%	80% / 45%	80% / 45%
Weight [g/m2]	200	315	400

At least 10 single tests have been performed for each of these grades. In Table 2 the mean values for the static puncture force (F-stat.) and the displacements at maximum load (Displ.-stat.) are given. Standard deviations and coefficients of variation obtained from these tests, are also shown in Table 2.

Table 2 Values obtained in the static puncture test

	Type A	Type B	Type C
F-stat. [N]	609.49	941.34	1285.20
Sdev	152.36	234.46	165.51
CVar	25	24.91	12.88
Displ.-stat.[mm]	42.8	42.90	47.60
Sdev	2.10	2.92	1.51
Cvar.	4.90	6.81	3.16

The graphical results for geotextile C are shown in Figure 5.

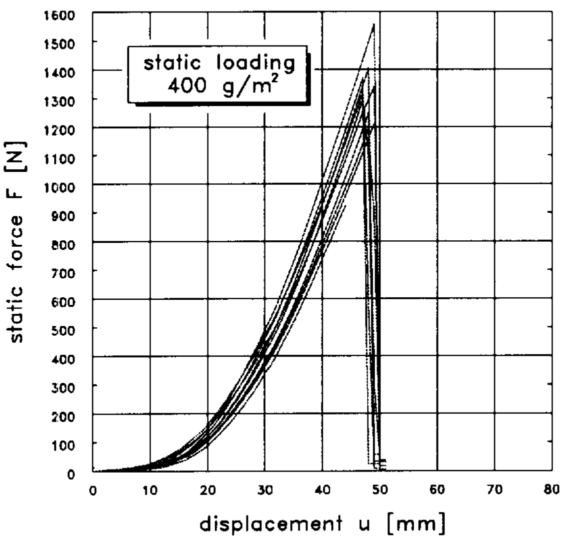

Figure 5: graphic results - static pyramid puncture test

In Table 3, the mean values for the dynamic puncture force (F-dyn.) and displacement at maximum load (Displ.-dyn.) are given along with their standard deviations and coefficients of variation.

Table 3 Values obtained by the dynamic puncture test.

	Type A	Type B	Type C
F-stat. [N]	511.95	780.40	955.27
Sdev	98.20	127.19	161.45
CVar	19.18	16.30	16.90
Displ.-stat.[mm]	45.20	41.10	50.50
Sdev	3.26	2.42	3.44
Cvar.	7.21	5.90	6.81

The graphical results for Geotextile C are shown in Figure 6.

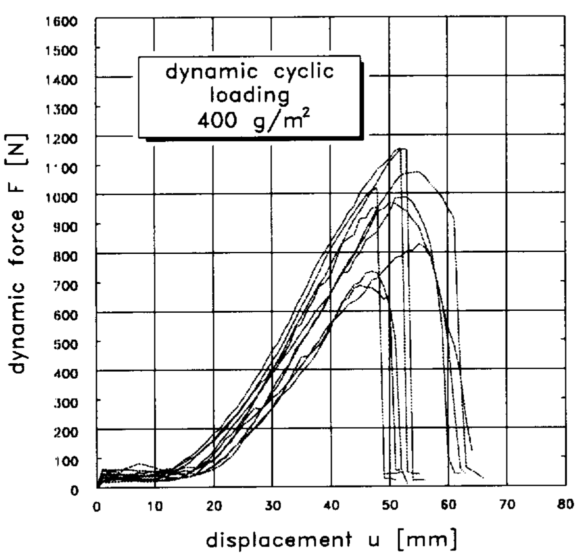

Figure 6: graphic results - dynamic pyramid puncture

4 ON SITE TESTS

To be able to show a correlation between laboratory and field tests, it is intended to perform onsite tests with sharp edged granular material on soft and weak subgrades.

For these tests sharp edged diabas granulate will be used and the performance of different geotextiles will be studied.

5 CONCLUSION AND OUTLOOK

By a newly developed test method it is possible to evaluate the performance of a geotextile under dynamic loading. The properties of a product can be described by its behavior under static and dynamic puncturing and the force-deformation behavior can be quantified. By the use of the described test, a clearer more performance-orientated specification can be made possible.

An analysis of the first series of tests has shown the following significant results:

- The values for dynamic puncturing are far below the ones for the static tests.
- The shape of the curve is similar for both the static and the dynamic tests. Differences can mainly be seen in the behavior after rupture; the static tests show a sudden decrease, whereas the dynamic tests show a slow decrease.
- Static as well as dynamic tests show a relation between performance and the weight per unit area for each product type. However, the manufacturing process is of decisive importance for the performance of the geotextile. Therfore weight alone is not an adequate parameter for specification and should (if necessary) only be used as identification parameter.

It seems necessary to continue testing both in the laboratory as well as on full scale trials on site.

6 REFERENCES

Werner, G. (1986) Design criteria for the separation function of Geotextiles, 3rd intl. conference on Geotextiles, Vienna, Austria; Vol 1 pp 71 - 75;

Bräu; (1996) Damage of Geotextiles during installation - Experience from real sites and research works, 1st European conference on geosynthetics, Maastricht, Netherlands, pp 145 - 150.

Polyfelt (1986) Design and practice, Technical manual for Polyfelt TS.

Author Index

Author Index

Author Index

Author Index

Subject Index

The pages listed indicate the first page of the paper in which the reference is found.

Subject Index

Subject Index

Subject Index